

Developing a Prism Qualification Test to Ensure Adequate Splitting Resistance in Pretensioned Concrete Railroad Ties

KSU-21-10

April 2021

Dr. Adrijana Savic, Civil Engineering, KSU

Dr. Robert J. Peterman, Civil Engineering, KSU

Dr. B. Terry Beck, Mechanical & Nuclear Engineering, KSU

Dr. Kyle A. Riding, Civil and Coastal Engineering, UF

Abstract

This report presents the results from research that evaluated the effect of wire indentation type, edge distance, and the strength of concrete at de-tensioning on longitudinal splitting in pretensioned concrete railroad ties. Four-wire pretensioned concrete prisms were cast with varying reinforcement types and edge distances and the resulting splitting crack lengths were carefully measured. Results showed that concrete edge distance was the most significant factor affecting longitudinal splitting cracks, with reinforcement indentation type also playing a key role. This work resulted in the successful development of a qualification test to ensure adequate splitting resistance in pre-tensioned concrete railroad ties. This test was formally adopted as section 4.2.4 in Chapter 30 of the 2021 AREMA Manual for Railway Engineering.

Corresponding Author: Dr. Robert J. Peterman (bob@ksu.edu)



U.S. Department of Transportation
Federal Railroad Administration

The contents of this report reflect the views of the authors, who are responsible for the facts and accuracy of the information presented herein. This document is disseminated in the interest of information exchange. The report is funded, partially or entirely, by a grant from the U.S. Department of Transportation's University Transportation Centers Program. However, the U.S. Government assumes no liability for the contents or use thereof.



METRIC/ENGLISH CONVERSION FACTORS

ENGLISH TO METRIC

LENGTH (APPROXIMATE)	
1 inch (in)	= 2.5 centimeters (cm)
1 foot (ft)	= 30 centimeters (cm)
1 yard (yd)	= 0.9 meter (m)
1 mile (mi)	= 1.6 kilometers (km)

AREA (APPROXIMATE)	
1 square inch (sq in, in ²)	= 6.5 square centimeters (cm ²)
1 square foot (sq ft, ft ²)	= 0.09 square meter (m ²)
1 square yard (sq yd, yd ²)	= 0.8 square meter (m ²)
1 square mile (sq mi, mi ²)	= 2.6 square kilometers (km ²)
1 acre = 0.4 hectare (he)	= 4,000 square meters (m ²)

MASS - WEIGHT (APPROXIMATE)	
1 ounce (oz)	= 28 grams (gm)
1 pound (lb)	= 0.45 kilogram (kg)
1 short ton = 2,000 pounds (lb)	= 0.9 tonne (t)

VOLUME (APPROXIMATE)	
1 teaspoon (tsp)	= 5 milliliters (ml)
1 tablespoon (tbsp)	= 15 milliliters (ml)
1 fluid ounce (fl oz)	= 30 milliliters (ml)
1 cup (c)	= 0.24 liter (l)
1 pint (pt)	= 0.47 liter (l)
1 quart (qt)	= 0.96 liter (l)
1 gallon (gal)	= 3.8 liters (l)
1 cubic foot (cu ft, ft ³)	= 0.03 cubic meter (m ³)
1 cubic yard (cu yd, yd ³)	= 0.76 cubic meter (m ³)

TEMPERATURE (EXACT)	
$[(x-32)(5/9)]$ °F	= y °C

METRIC TO ENGLISH

LENGTH (APPROXIMATE)	
1 millimeter (mm)	= 0.04 inch (in)
1 centimeter (cm)	= 0.4 inch (in)
1 meter (m)	= 3.3 feet (ft)
1 meter (m)	= 1.1 yards (yd)
1 kilometer (km)	= 0.6 mile (mi)

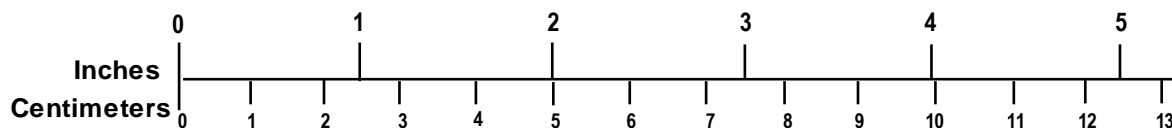
AREA (APPROXIMATE)	
1 square centimeter (cm ²)	= 0.16 square inch (sq in, in ²)
1 square meter (m ²)	= 1.2 square yards (sq yd, yd ²)
1 square kilometer (km ²)	= 0.4 square mile (sq mi, mi ²)
10,000 square meters (m ²)	= 1 hectare (ha) = 2.5 acres

MASS - WEIGHT (APPROXIMATE)	
1 gram (gm)	= 0.036 ounce (oz)
1 kilogram (kg)	= 2.2 pounds (lb)
1 tonne (t)	= 1,000 kilograms (kg)
	= 1.1 short tons

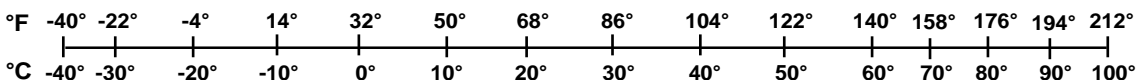
VOLUME (APPROXIMATE)	
1 milliliter (ml)	= 0.03 fluid ounce (fl oz)
1 liter (l)	= 2.1 pints (pt)
1 liter (l)	= 1.06 quarts (qt)
1 liter (l)	= 0.26 gallon (gal)
1 cubic meter (m ³)	= 36 cubic feet (cu ft, ft ³)
1 cubic meter (m ³)	= 1.3 cubic yards (cu yd, yd ³)

TEMPERATURE (EXACT)	
$[(9/5)y + 32]$ °C	= x °F

QUICK INCH - CENTIMETER LENGTH CONVERSION



QUICK FAHRENHEIT - CELSIUS TEMPERATURE CONVERSION



For more exact and or other conversion factors, see NIST Miscellaneous Publication 286, Units of Weights and Measures. Price \$2.50 SD Catalog No. C13 10286

Updated 6/17/98

Acknowledgements

The authors would like to thank the Federal Railroad Administration (FRA) for providing the majority of funding that made this research possible. The researchers would also like to thank Dr. Hailing Yu at the John A. Volpe National Transportation Systems Center for her valuable suggestions and parallel analysis work. Finally, the authors wish to thank the Precast/Prestressed Concrete Institute (PCI) for establishing an industry advisory panel to the project and also everyone who helped during this endeavor.

Contents

Illustrations v

Tables xviii

1.	Introduction	19
1.1	Background	19
1.2	Objectives	20
1.3	Overall Approach	20
1.4	Scope	20
1.5	Organization of the Report	21
2.	Literature Review	22
2.1	Bar-Concrete Interaction.....	22
2.2	History of Experimental, Analytical and Numerical research	23
3.	Material and Operation.....	35
3.1	Prestressing Wires	35
3.2	Reinforcement Storage	45
3.3	Concrete Materials and Mix Design.....	50
4.	Methodology.....	56
4.1	Experimental Facility and Prism Casting Procedure.....	56
4.2	Experimental Set-up	59
4.3	Casting Procedure of Prisms	62
4.4	Sure Cure System	63
4.5	Testing procedure and Transfer length Measurement	66
4.6	Assessment of Prism cracking	69
5.	Results	73
5.1	Transfer lengths and Prism Cracking-Mix#1	75
6.	Comparison Charts	99
6.1	Concrete Mixture-Mix#1	99
6.2.	Concrete Mixture-Mix#2	110
6.3.	Concrete Mixture-Mix#3	119
6.4.	Mix#1 versus Mix#2	123
6.5	Mix#1 versus Mix#2 versus Mix#3	133
7.	Proposed Qualification Test for Arema Manual for Railway Engineering	136
8.	Theoretical Lateral Stresses Due to Hoyer Effect	139
9.	Conclusions and Recommendations.....	142
9.1.	Conclusions.....	142
10.	References	144

Appendix A. Calculation of System Qualification Test Prism Parameters	148
Appendix B. Results	150
Abbreviations and Acronyms (sample)	277

Illustrations

Figure 1-1: Failed Prestressed Concrete Ties	19
Figure 2-1: Schematic Representation of Hoyer effect.....	32
Figure 3-1: Manufacture of Indented Wire using Rollers (Beck et al., 2019)	35
Figure 3-2: Manufacture of Prestressing Wire Indents (Beck at al., 2019)	36
Figure 3-3: Schematic of Indented Wire Measurement (Beck et al., 2019)	36
Figure 3-4: Wire Support and Traversing System (Beck et al., 2019)	37
Figure 3-5: Ideal Bilinear and Measured Strain Profile (Beck et al., 2019)	37
Figure 3-6: KEY 3D Wire Indent Geometrical Features (Beck et al., 2019)	38
Figure 3-7: WA Wire Type- Microscope Image and 3D Model (Haynes, 2015).....	40
Figure 3-8: WB Wire Type- Microscope Image and 3D Model (Haynes, 2015)	40
Figure 3-9: WE Wire Type- Microscope Image and 3D Model (Haynes, 2015)	41
Figure 3-10: WF Wire Type- Microscope Image and 3D Model (Haynes, 2015)	41
Figure 3-11: WG Wire Type-Microscope Image and 3D Model (Haynes, 2015).....	42
Figure 3-12: WH Wire Type-Microscope Image and 3D Model (Haynes, 2015).....	42
Figure 3-13: WI Wire Type- Microscope Image and 3D Model (Haynes, 2015)	43
Figure 3-14: WJ Wire Type- Microscope Image and 3D Model (Haynes, 2015)	43
Figure 3-15: WM Wire Type- Microscope Image and 3D Model (Haynes, 2015)	44
Figure 3-16: Photo of WP Wire Type.....	44
Figure 3-17: Photo of WQ Wire Type	45
Figure 3-18: Chemical used in Reinforcement Cleaning Process (Deoxidine 7310) (Arnold, 2013)	46
Figure 3-19: WG Wire Type Before (left) and after (right) Cleaning	47
Figure 3-20: Reinforcement Storage Rack (Bodapati, 2018)	47
Figure 3-21: Hypothesized Sidewall Concrete Crushing (Beck, 2019).....	48
Figure 3-22: Observed Crushed Concrete Residue-Left side of the WH Wire Type (Beck, 2019)	49
Figure 3-23: Observed Crushed Concrete Residue-Right side of the WH Wire Type	49
Figure 3-24: Observed Crushed Concrete Residue for Wire Type WG	50
Figure 3-25: Tucson Small Crushed Gravel Aggregate (CA3) used in the study	51
Figure 3-26: Tucson Large Crushed Gravel Aggregate (CA2) used in this study.....	51
Figure 3-27: Granite Aggregate (CA4) used in this study	52

Figure 3-28: Uncrushed Pea Gravel Aggregate (CA1) used in this study	52
Figure 3-29: Fine Aggregate (sand) used in this study	53
Figure 3-30: Concrete Mixer	55
Figure 4-1: Original Pre-tensioned Concrete Prism -1in Edge distance (Bodapati, 2018).....	56
Figure 4-2: Steel Frames (Savic, 2018)	57
Figure 4-3: Prisms with Different Cross Sections (Savic, 2018).....	59
Figure 4-4: Stages of Pre-tensioning.....	60
Figure 4-5: Load Cells at Dead End of Prestressing Bed	60
Figure 4-6: Prestressed Jacking arrangement at the Live End.....	60
Figure 4-7: Digital Display of Prestressing Forces Measured by Load cell	61
Figure 4-8: Adjusted Setup-Additional Chucks between First and Second Prism	61
Figure 4-9: Adjusted Setup-Dead End of the Prestressed Bed	62
Figure 4-10: Adjusted setup of Prestressed Bed	62
Figure 4-11: Casting the Prestressed Concrete Prisms	63
Figure 4-12: Twelve Concrete Cylinders under Temperature Control through Sure Cure Mini Controlling System	64
Figure 4-13: Typical Temperature (F) Plot of Prism and Cylinder Specimens.....	64
Figure 4-14: Making the Sure-Cure Cylinders	65
Figure 4-15: Testing the Cylinder Using Forney machine	65
Figure 4-16: Example of Measured Compressive strength of Cylinder	66
Figure 4-17: Laser Speckle Imaging System (Beck, 2010)	67
Figure 4-18: Overall Automated LSI Sensor Traversing System (Beck, 2010)	68
Figure 4-19: Measuring the Transfer Lengths (Savic, 2018).....	68
Figure 4-20: Traverse Control and LabVIEW Data Acquisition Interface (Beck, 2010).....	69
Figure 4-21: Example of Crack Assessment Form	70
Figure 4-22: Measuring Crack Width (Savic, 2018)	71
Figure 4-23: Example of Prisms and Observed Cracking ($\frac{1}{2}$ in edge distance)	71
Figure 4-24: Typical Picture of Observed Cracking Live and Dead end (Savic, 2018).....	72
Figure 5-1: Mix#1, 6000 psi, WA, $\frac{3}{4}$ in. Edge Distance-Longitudinal Strain Profile.....	75
Figure 5-2: Mix#1, 6000 psi, WA, $\frac{5}{8}$ in Edge Distance-Longitudinal Strain Profile.....	76
Figure 5-3: Mix#1, 6000 psi, WA, $\frac{1}{2}$ in Edge Distance-Longitudinal Strain Profile.....	76
Figure 5-4: Mix#1, 6000psi, WA-Observed Cracking (Live End).....	77
Figure 5-5: Mix#1, 6000psi, WA-Observed Cracking (Dead End).....	77

Figure 5-6: Mix#1, 6000psi, WA-Crack Area (in ²).....	77
Figure 5-7: Mix#1, 6000psi, WA-Crack Length (in).....	78
Figure 5-8: Mix#1, 6000psi, WA-Number of Cracks.....	78
Figure 5-9: Mix#1, 4500psi, WB-Observed Cracking (Dead End).....	79
Figure 5-10: Mix#1, 4500 psi, WB-Observed Cracking (Live End).....	79
Figure 5-11: Mix#1, 4500 psi, WB-Crack Area (in ²).....	80
Figure 5-12: Mix#1, 4500 psi, WB-Crack Length (in).....	80
Figure 5-13: Mix#1, 4500 psi, WB-Number of Cracks.....	80
Figure 5-14: Mix#1, 6000psi, WB-Observed Cracking (Dead end).....	81
Figure 5-15: Mix#1, 6000 psi, WB-Observed Cracking (Live end).....	81
Figure 5-16: Mix#1, 6000 psi, WB-Crack Area (in ²).....	82
Figure 5-17: Mix#1, 6000 psi, WB-Crack Length (in).....	82
Figure 5-18: Mix#1, 6000 psi, WB-Number of Cracks.....	83
Figure 5-19: Mix#1, 6000 psi, WB second time-Crack Area (in ²).....	83
Figure 5-20: Mix#1, 6000 psi, WB second time-Crack Length (in).....	84
Figure 5-21: Mix#1, 6000 psi, WB second time-Number of Cracks.....	84
Figure 5-22: Mix#1, 6000 psi, WB third time-Crack Area (in ²).....	85
Figure 5-23: Mix#1, 6000 psi, WB third time-Crack Length (in).....	85
Figure 5-24: Mix#1, 6000 psi, WB third time-Number of Cracks.....	86
Figure 5-25: Mix#1, 3500 psi, WE, ¾ in. Edge distance (Savic, 2018).....	87
Figure 5-26: Mix#1, 3500 psi, WE, ⅝ in. Edge distance (Savic, 2018).....	88
Figure 5-27: Mix#1, 3500 psi, WE, ½ in. Edge distance (Savic, 2018).....	89
Figure 5-28: Mix#1, 4500 psi, WE, ¾ in. Edge distance (Savic, 2018).....	90
Figure 5-29: Mix#1, 4500 psi, WE, ⅝ in. Edge distance (Savic, 2018).....	91
Figure 5-30: Mix#1, 4500 psi, WE, ½ in. Edge distance (Savic, 2018).....	92
Figure 5-31: Mix#1, 6000 psi, WE, ¾ in. Edge distance (Savic, 2018).....	93
Figure 5-32: Mix#1, 6000 psi, WE, ⅝ in. Edge distance (Savic, 2018).....	94
Figure 5-33: Mix#1, 6000 psi, WE, ½ in. Edge distance (Savic, 2018).....	95
Figure 5-34: Mix#1, 12000 psi (82.74MPa), WE, ¾ in. Edge distance- Live and Dead End.....	96
Figure 5-35: Mix#1, WE-Number of Cracks.....	97
Figure 5-36: Mix#1, WE-Crack Length (in).....	97
Figure 5-37: Mix#1, WE-Crack Area (in ²).....	98
Figure 6-1: Mix#1, 4500 psi, ½ in. Edge Distance-Crack Area (in ²).....	99

Figure 6-2: Mix#1, 4500 psi, $\frac{5}{8}$ in. Edge Distance-Crack Area (in ²)	100
Figure 6-3: Mix#1, 4500 psi, $\frac{3}{4}$ in. Edge Distance-Crack Area (in ²)	100
Figure 6-4: Mix#1, 4500 psi, $\frac{1}{2}$ in. Edge Distance-Crack Length (in)	101
Figure 6-5: Mix#1, 4500 psi, $\frac{5}{8}$ in. Edge Distance-Crack Length (in)	101
Figure 6-6: Mix#1, 4500 psi, $\frac{3}{4}$ in. Edge Distance-Crack Length (in)	102
Figure 6-7: Mix#1, 4500 psi, $\frac{3}{4}$ in. Edge Distance-Transfer Lengths (Dead and Live end)	102
Figure 6-8: Mix#1, 4500 psi-Number of Wires Ends with Splitting Cracks	103
Figure 6-9: Mix#1, 6000 psi, $\frac{1}{2}$ in. Edge Distance-Crack Area (in ²)	104
Figure 6-10: Mix#1, 6000 psi, $\frac{5}{8}$ in. Edge Distance-Crack Area (in ²)	104
Figure 6-11: Mix#1, 6000 psi, $\frac{3}{4}$ in. Edge Distance-Crack Area (in ²)	105
Figure 6-12: Mix#1, 6000 psi, $\frac{1}{2}$ in. Edge Distance-Crack Length (in)	106
Figure 6-13: Mix#1, 6000 psi, $\frac{5}{8}$ in. Edge Distance-Crack Length (in)	106
Figure 6-14: Mix#1, 6000 psi, $\frac{3}{4}$ in. Edge Distance-Crack Length (in)	107
Figure 6-15: Mix#1, 6000 psi-Number of Wires Ends with Splitting Cracks	108
Figure 6-16: Mix#1, 6000 psi-Transfer Lengths (Dead end and live end)	108
Figure 6-17: Mix#1-4500 psi vs 6000 psi	109
Figure 6-18: Mix#1-Total Crack Lengths-4500 psi vs 6000 psi	110
Figure 6-19: Mix#2, 4500 psi, $\frac{3}{4}$ in. Edge Distance-Crack Area (in ²)	111
Figure 6-20: Mix#2, 4500 psi, $\frac{5}{8}$ in. Edge Distance-Crack Area (in ²)	111
Figure 6-21: Mix#2, 4500 psi, $\frac{1}{2}$ in. Edge Distance-Crack Area (in ²)	112
Figure 6-22: Mix#2, 4500 psi, $\frac{3}{4}$ in. Edge Distance-Crack Length (in)	112
Figure 6-23: Mix#2, 4500 psi, $\frac{5}{8}$ in. Edge Distance-Crack Length (in)	113
Figure 6-24: Mix#2, 4500 psi, $\frac{1}{2}$ in. Edge Distance-Crack Length (in)	113
Figure 6-25: Mix#2, 4500 psi-Number of Wires Ends with Splitting Crack	114
Figure 6-26: Mix#2, 6000 psi, $\frac{3}{4}$ in. Edge Distance-Crack Area (in ²)	114
Figure 6-27: Mix#2, 6000 psi, $\frac{5}{8}$ in. Edge Distance-Crack Area (in ²)	115
Figure 6-28: Mix#2, 6000 psi, $\frac{1}{2}$ in. Edge Distance-Crack Area (in ²)	115
Figure 6-29: Mix#2, 6000 psi, $\frac{3}{4}$ in. Edge Distance-Crack Length (in)	116
Figure 6-30: Mix#2, 6000 psi, $\frac{5}{8}$ in. Edge Distance-Crack Length (in)	116
Figure 6-31: Mix#2, 6000 psi, $\frac{1}{2}$ in. Edge Distance-Crack Length (in)	117
Figure 6-32: Mix#2, 6000 psi-Number of Wires Ends with Splitting Cracks	117
Figure 6-33: Mix#2-4500 psi vs 6000 psi	118
Figure 6-34: Mix#2, Crack Lengths (in)-4500 psi vs 6000 psi	119

Figure 6-35: Mix#3, 4500 psi, $\frac{3}{4}$ in. Edge Distance-Crack Area (in ²)	120
Figure 6-36: Mix#3, 4500 psi, $\frac{5}{8}$ in. Edge Distance-Crack Area (in ²)	120
Figure 6-37: Mix#3, 4500 psi, $\frac{1}{2}$ in. Edge Distance-Crack Area (in ²)	121
Figure 6-38: Mix#3, 4500 psi, $\frac{3}{4}$ in. Edge Distance-Crack Length (in)	121
Figure 6-39: Mix#3, 4500 psi, $\frac{5}{8}$ in. Edge Distance-Crack Length (in)	122
Figure 6-40: Mix#3, 4500 psi, $\frac{1}{2}$ in. Edge Distance-Crack Length (in)	122
Figure 6-41: Number of Wires Ends with Splitting Cracks.....	123
Figure 6-42: Mix#1 vs Mix#2, 4500 psi, $\frac{3}{4}$ in. Edge Distance-Crack Area (in ²).....	124
Figure 6-43: Mix#1 vs Mix#2, 4500 psi, $\frac{5}{8}$ in. Edge Distance-Crack Area (in ²).....	124
Figure 6-44: Mix#1 vs Mix#2, 4500 psi, $\frac{1}{2}$ in. Edge Distance-Crack Area (in ²).....	125
Figure 6-45: Mix#1 vs Mix#2, 4500 psi, $\frac{3}{4}$ in. Edge Distance-Crack Length (in).....	125
Figure 6-46: Mix#1 vs Mix#2, 4500 psi, $\frac{5}{8}$ in. Edge Distance-Crack Length (in).....	126
Figure 6-47: Mix#1 vs Mix#2, 4500 psi, $\frac{1}{2}$ in. Edge Distance-Crack Length (in).....	126
Figure 6-48: Mix#1 vs Mix#2, 4500 psi, $\frac{3}{4}$ in. Edge Distance-Number of Wires Ends with Splitting Cracks.....	127
Figure 6-49: Mix#1 vs Mix#2, 4500 psi, $\frac{5}{8}$ in. Edge Distance-Number of Wires Ends with Splitting Cracks.....	127
Figure 6-50: Mix#1 vs Mix#2, 4500 psi, $\frac{1}{2}$ in. Edge Distance-Number of Wires Ends with Splitting Cracks.....	128
Figure 6-51: Mix#1 vs Mix#2, 6000 psi, $\frac{3}{4}$ in. Edge Distance-Crack Area (in ²).....	129
Figure 6-52: Mix#1 vs Mix#2, 6000 psi, $\frac{5}{8}$ in. Edge Distance-Crack Area (in ²).....	129
Figure 6-53: Mix#1 vs Mix#2, 6000 psi, $\frac{1}{2}$ in. Edge Distance-Crack Area (in ²).....	130
Figure 6-54: Mix#1 vs Mix#2, 6000 psi, $\frac{3}{4}$ in. Edge Distance-Crack Length (in).....	130
Figure 6-55: Mix#1 vs Mix#2, 6000 psi, $\frac{5}{8}$ in. Edge Distance-Crack Length (in).....	131
Figure 6-56: Mix#1 vs Mix#2, 6000 psi, $\frac{1}{2}$ in. Edge Distance-Crack Length (in).....	131
Figure 6-57: Mix#1 vs Mix#2, 6000 psi, $\frac{3}{4}$ in. Edge Distance-Number of Wires Ends with Splitting Cracks.....	132
Figure 6-58: Mix#1 vs Mix#2, 6000 psi, $\frac{5}{8}$ in. Edge Distance- Number of Wires Ends with Splitting Cracks.....	132
Figure 6-59: Mix#1 vs Mix#2, 6000 psi, $\frac{1}{2}$ in. Edge Distance-Number of Wires end With Splitting Cracks.....	133
Figure 6-60: Mix#1, Mix#2, Mix#3-Effect of Cover on End-Splitting.....	134
Figure 6-61: Mix#1 vs Mix#2 vs Mix#3-Crack Length (in).....	134
Figure 6-62: Mix#1 vs Mix#2 vs Mix#3-The Overall Crack Length (in)	135

Figure 8-1: Tangential Stress in Concrete (psi)	140
Figure 8-2: Prisms with Varying Cover and Release Strength (Based on # of Tendon Diameters)	141
Figure 10-1: Generic Tie Cross-Section	148
Figure 10-2: System Qualification Test Prism Cross-Section	149
Figure 10-3: Mix#1, 6000 psi, WA, $\frac{3}{4}$ in. Edge Distance-Longitudinal Strain Profile.....	150
Figure 10-4: Mix#1, 6000 psi, WA, $\frac{5}{8}$ in. Edge Distance-Longitudinal Strain Profile.....	151
Figure 10-5: Mix#1, 6000 psi, WA, $\frac{1}{2}$ in. Edge Distance-Longitudinal Strain Profile.....	151
Figure 10-6: Mix#1, 6000psi, WA-Observed Cracking (Live End).....	152
Figure 10-7 : Mix#1, 6000psi, WA-Observed Cracking (Dead End).....	152
Figure 10-8: Mix#1, 6000psi, WA-Crack Area (in ²).....	152
Figure 10-9: Mix#1, 6000psi, WA-Crack Length (in).....	153
Figure 10-10: Mix#1, 6000psi, WA-Number of Cracks	153
Figure 10-11: Mix#1, 4500psi, WB-Observed Cracking (Dead End)	154
Figure 10-12: Mix#1, 4500 psi, WB-Observed Cracking (Live End)	154
Figure 10-13: Mix#1, 4500 psi, WB-Crack Area (in ²)	155
Figure 10-14: Mix#1, 4500 psi, WB-Crack Length (in).....	155
Figure 10-15: Mix#1, 4500 psi, WB-Number of Cracks	156
Figure 10-16: Mix#1, 6000psi, WB-Observed Cracking (Dead end).....	156
Figure 10-17: Mix#1, 6000 psi, WB-Observed Cracking (Live end).....	157
Figure 10-18: Mix#1, 6000 psi, WB-Crack Area (in ²)	157
Figure 10-19: Mix#1, 6000 psi, WB-Crack Length (in).....	158
Figure 10-20: Mix#1, 6000 psi, WB-Number of Cracks	158
Figure 10-21: Mix#1, 6000 psi, WB second time-Crack Area (in ²).....	159
Figure 10-22: Mix#1, 6000 psi, WB second time-Crack Length (in).....	159
Figure 10-23: Mix#1, 6000 psi, WB third time-Crack Area (in ²)	160
Figure 10-24: Mix#1, 6000 psi, WB third time-Crack Length (in)	160
Figure 10-25: Mix#1, 4500 psi, WF, $\frac{3}{4}$ in. Edge Distance-Longitudinal Strain Profile.....	161
Figure 10-26: Mix#1, 4500psi, WF-Observed Cracking (Dead end)	162
Figure 10-27: Mix#1, 4500 psi-Observed Cracking (Live end)	162
Figure 10-28: Mix#1, 4500 psi, WF-Crack Area (in ²).....	162
Figure 10-29: Mix#1, 4500 psi, WF-Crack Length (in)	163
Figure 10-30: Mix#1, 4500 psi, WF-Number of Cracks	163

Figure 10-31: Mix#1, 6000 psi, WF, $\frac{3}{4}$ in. Edge Distance-Longitudinal Strain Profile.....	164
Figure 10-32: Mix#1, 6000 psi, WF-Observed Cracking (Dead End)	164
Figure 10-33: Mix#1, 6000 psi, WF-Observed Cracking (Live End).....	164
Figure 10-34: Mix#1, 6000 psi, WF-Crack Area (in ²).....	165
Figure 10-35: Mix#1, 6000 psi, WF-Crack Length (in)	165
Figure 10-36: Mix#1, 6000 psi, WF-Number of Cracks	166
Figure 10-37: Mix#1, 4500psi, WG-Observed Cracking (Dead end)	167
Figure 10-38: Mix#1, 4500 psi-Observed Cracking (Live end)	167
Figure 10-39: Mix#1, 4500 psi, WG-Crack Area (in ²).....	168
Figure 10-40: Mix#1, 4500 psi, WG-Crack Length (in).....	168
Figure 10-41: Mix#1, 4500 psi, WG-Number of Cracks.....	169
Figure 10-42: Mix#1, 4500 psi, WH-Observed Cracking (Dead End).....	170
Figure 10-43: Mix#1, 4500 psi, WH-Observed Cracking (Live End).....	170
Figure 10-44: Mix#1, 4500 psi, WH-Crack Area (in ²).....	171
Figure 10-45: Mix#1, 4500 psi, WH-Crack Length (in).....	171
Figure 10-46: Mix#1, 4500 psi, WH-Number of Cracks.....	172
Figure 10-47: Mix#1, 4500 psi, WI, $\frac{3}{4}$ in. Edge Distance-Longitudinal Strain Profile	173
Figure 10-48: Mix#1, 4500 psi, WI-Observed Cracking (Dead End)	173
Figure 10-49: Mix#1, 4500 psi, WI-Observed Cracking (Live End)	174
Figure 10-50: Mix#1, 4500 psi, WI-Crack Area (in ²)	174
Figure 10-51: Mix#1, 4500 psi, WI-Crack Length (in)	174
Figure 10-52: Mix#1, 4500 psi, WI-Number of Cracks	175
Figure 10-53: Mix#1, 6000 psi, WI, $\frac{3}{4}$ in. Edge Distance-Longitudinal Strain Profile	175
Figure 10-54: Mix#1, 6000 psi, WI-Observed Cracking (Dead end).....	176
Figure 10-55: Mix#1, 6000 psi, WI-Observed Cracking (Live end)	176
Figure 10-56: Mix#1, 6000 psi, WI-Crack Area (in ²)	177
Figure 10-57: Mix#1, 6000 psi, WI-Crack Length (in)	177
Figure 10-58: Mix#1, 6000 psi, WI-Number of Cracks	178
Figure 10-59: Mix#1, 4500 psi, WJ, $\frac{3}{4}$ in. Edge Distance-Longitudinal Strain Profile	179
Figure 10-60: Mix#1, 4500psi, WJ-Observed Cracking (Dead End).....	179
Figure 10-61: Mix#1, 4500psi, WJ-Observed Cracking (Live End)	180
Figure 10-62: Mix#1, 4500 psi, WJ-Crack Area (in ²)	180
Figure 10-63: Mix#1, 4500 psi, WJ-Crack Length (in)	181

Figure 10-64: Mix#1, 4500 psi, WJ-Number of Cracks	181
Figure 10-65: Mix#1, 6000 psi, WJ, $\frac{3}{4}$ in. Edge Distance-Longitudinal Strain Profile	182
Figure 10-66: Mix#1, 6000 psi, WJ-Observed Cracking (Dead end).....	182
Figure 10-67: Mix#1, 6000 psi, WJ-Observed Cracking (Live end).....	182
Figure 10-68: Mix#1, 6000 psi, WJ-Crack Area (in ²)	183
Figure 10-69: Mix#1, 6000 psi, WJ-Crack Length (in)	183
Figure 10-70: Mix#1, 6000 psi, WJ-Number of Cracks	184
Figure 10-71: Mix#1, 4500 psi, WM, $\frac{3}{4}$ in. Edge Distance-Longitudinal Strain Profile	185
Figure 10-72: Mix#1, 4500psi, WM-Observed Cracking (Dead End)	185
Figure 10-73: Mix#1, 4500 psi, WM-Observed Cracking (Live End)	186
Figure 10-74: Mix#1, 4500 psi, WM-Crack Area (in ²)	186
Figure 10-75: Mix#1, 4500 psi, WM-Crack Length (in)	187
Figure 10-76: Mix#1, 4500 psi, WM-Number of Cracks	187
Figure 10-77: Mix#1, 6000 psi, WM, $\frac{3}{4}$ in. Edge Distance-Longitudinal Strain Profile	188
Figure 10-78: Mix#1, 6000 psi, WM, $\frac{5}{8}$ in. Edge Distance-Longitudinal Strain Profile	188
Figure 10-79: Mix#1, 6000 psi, WM-Observed Cracking (Dead End)	189
Figure 10-80: Mix#1, 6000 psi, WM- Observed Cracking (Live End)	189
Figure 10-81: Mix#1, 6000 psi, WM-Crack Area (in ²)	189
Figure 10-82: Mix#1, 6000 psi, WM-Crack Length (in)	190
Figure 10-83: Mix#1, 6000 psi, WM-Number of Cracks	190
Figure 10-84: Mix#1, 4500 psi, WP, $\frac{3}{4}$ in. Edge Distance-Longitudinal Strain Profile.....	191
Figure 10-85: Mix#1, 4500 psi, WP-Observed Cracking (Dead End)	191
Figure 10-86: Mix#1, 4500 psi, WP-Observed Cracking (Live End).....	192
Figure 10-87: Mix#1, 4500 psi, WP-Crack Area (in ²).....	192
Figure 10-88: Mix#1, 4500 psi, WP-Crack Length (in.)	193
Figure 10-89: Mix#1, 4500 psi, WP-Number of Cracks	193
Figure 10-90: Mix#1, 6000 psi, WP, $\frac{3}{4}$ in. Edge Distance-Longitudinal Strain Profile.....	194
Figure 10-91: Mix#1, 6000 psi, WP-Observed Cracking (Dead End)	194
Figure 10-92: Mix#1, 6000 psi, WP-Observed Cracking (Live End).....	194
Figure 10-93: Mix#1, 6000 psi, WP-Crack Area (in ²).....	195
Figure 10-94: Mix#1, 6000 psi, WP-Crack Length (in)	195
Figure 10-95: Mix#1, 6000 psi, WP-Number of Cracks	196
Figure 10-96: Mix#1, 4500 psi, WQ, $\frac{3}{4}$ in. Edge Distance-Longitudinal Strain Profile.....	197

Figure 10-97: Mix#1, 4500 psi, WQ-Observed Cracking (Dead End).....	197
Figure 10-98: Mix#1, 4500 psi, WQ-Observed Cracking (Live End).....	198
Figure 10-99: Mix#1, 4500 psi, WQ-Crack Area (in ²).....	198
Figure 10-100: Mix#1, 4500 psi, WQ-Crack Length (in).....	199
Figure 10-101: Mix#1, 4500 psi, WQ- Number of Cracks.....	199
Figure 10-102: Mix#1, 6000 psi, WQ, ¾ in. Edge Distance-Longitudinal Strain Profile.....	200
Figure 10-103: Mix#1, 6000 psi, WQ, ⅝ in. Edge Distance-Longitudinal Strain Profile.....	200
Figure 10-104: Mix#1, 6000 psi, WQ- Observed Cracking (Dead End).....	200
Figure 10-105: Mix#1, 6000 psi, WQ-Observed Cracking (Live End).....	201
Figure 10-106: Mix#1, 6000 psi, WQ-Crack Area (in ²).....	201
Figure 10-107: Mix#1, 6000 psi, WQ-Crack Length (in).....	202
Figure 10-108: Mix#1, 6000 psi, WQ-Number of Cracks.....	202
Figure 10-109: Mix#2, 4500 psi, WB, ¾ in. Edge Distance-Longitudinal Strain Profile	203
Figure 10-110: Mix#2, 4500psi, WB-Observed Cracking (Dead End)	203
Figure 10-111: Mix#2, 4500 psi, WB-Observed Cracking (Live End)	204
Figure 10-112: Mix#2, 4500 psi, WB-Crack Area (in ²)	204
Figure 10-113: Mix#2, 4500 psi, WB-Crack Length (in).....	204
Figure 10-114: Mix#2, 4500 psi, WB-Number of cracks.....	205
Figure 10-115: Mix#2, 6000 psi, WB, ¾ in. Edge Distance-Longitudinal Strain Profile	205
Figure 10-116: Mix#2, 6000 psi, WB-Observed Cracking (Dead End)	206
Figure 10-117: Mix#2, 6000 psi, WB-Observed Cracking (Live End)	206
Figure 10-118: Mix#2, 6000 psi, WB-Crack Area (in ²)	207
Figure 10-119: Mix#2, 6000 psi, WB-Crack Length.....	207
Figure 10-120: Mix#2, 6000 psi, WB- Number of Cracks	208
Figure 10-121: Mix#2, 4500 psi, WF, ¾ in. Edge Distance-Longitudinal Strain Profile.....	209
Figure 10-122: Mix#2, 4500 psi, WF-Observed Cracking (Dead End)	209
Figure 10-123: Mix#2, 4500 psi, WF-Observed Cracking (Live End).....	210
Figure 10-124: Mix#2, 4500 psi, WF-Crack Area (in ²).....	210
Figure 10-125: Mix#2, 4500 psi, WF-Crack length (in).....	211
Figure 10-126: Mix#2, 4500 psi, WF-Number of Cracks	211
Figure 10-127: Mix#2, 6000 psi, WF, ¾ in. Edge Distance-Longitudinal Strain Profile.....	212
Figure 10-128: Mix#2, 6000 psi, WF-Observed Cracking (Dead End)	212
Figure 10-129: Mix#2, 6000 psi, WF-Crack Area (in ²).....	213

Figure 10-130: Mix#2, 6000 psi, WF-Crack-Length.....	213
Figure 10-131: Mix#2, 6000 psi, WF-Number of Cracks	214
Figure 10-132: Mix#2, 4500 psi, WG, $\frac{3}{4}$ in. Edge Distance-Longitudinal Strain Profile.....	215
Figure 10-133: Mix#2, 4500 psi, WG, $\frac{5}{8}$ in. Edge Distance-Longitudinal Strain Profile.....	216
Figure 10-134: Mix#2, 4500 psi, WG, $\frac{1}{2}$ in. Edge Distance-Longitudinal Strain Profile.....	216
Figure 10-135: Mix#2, 4500 psi, WG-Observed Cracking (Dead End).....	217
Figure 10-136: Mix#2, 4500 psi, WG-Observed Cracking (Live End).....	217
Figure 10-137: Mix#2, 4500 psi, WG-Crack Area (in ²).....	217
Figure 10-138: Mix#2, 4500 psi, WG-Crack Length (in).....	218
Figure 10-139: Mix#2, 4500 psi, WG-Number of Cracks.....	218
Figure 10-140: Mix#2, 4500 psi, WH-Observed Cracking (Dead End).....	219
Figure 10-141: Mix#2, 4500 psi, WH-Observed Cracking (Live End).....	219
Figure 10-142: Mix#2, 4500 psi, WH-Crack Area (in ²).....	220
Figure 10-143: Mix#2, 4500 psi, WH--Crack Length (in)	220
Figure 10-144: Mix#2, 4500 psi, WH-Number of Cracks.....	221
Figure 10-145: Mix#2, 4500 psi, WI, $\frac{3}{4}$ in. Edge Distance-Longitudinal Strain Profile	222
Figure 10-146: Mix#2, 4500 psi, WI-Observed Cracking (Dead End)	222
Figure 10-147: Mix#2, 4500 psi, WI-Observed Cracking (Live End)	223
Figure 10-148: Mix#2, 4500 psi, WI-Crack Area (in ²)	223
Figure 10-149: Mix#2, 4500 psi, WI-Crack Length (in)	224
Figure 10-150: Mix#2, 4500 psi, WI- Number of Cracks	224
Figure 10-151: Mix#2, 6000 psi, WI, $\frac{3}{4}$ in. Edge Distance-Longitudinal Strain Profile	225
Figure 10-152: Mix#2, 6000 psi, WI, $\frac{5}{8}$ in. Edge Distance-Longitudinal Strain Profile	225
Figure 10-153: Mix#2, 6000 psi, WI-Observed Cracking (Dead End)	226
Figure 10-154: Mix#2, 6000 psi, WI-Observed Cracking (Live End)	226
Figure 10-155: Mix#2, 6000 psi, WI- Crack Area (in ²)	226
Figure 10-156: Mix#2, 6000 psi, WI-Crack Length (in.)	227
Figure 10-157: Mix#2, 6000 psi, WI-Number of Cracks	227
Figure 10-158: Mix#2, 4500 psi, WJ, $\frac{3}{4}$ in. Edge Distance-Longitudinal Strain Profile	228
Figure 10-159: Mix#2, 4500 psi, WJ, $\frac{5}{8}$ in. Edge Distance-Longitudinal Strain Profile	228
Figure 10-160: Mix#2, 4500 psi, WJ-Observed Cracking (Dead End)	229
Figure 10-161: Mix#2, 4500 psi, WJ-Observed Cracking (Live End)	229
Figure 10-162: Mix#2, 4500 psi, WJ-Crack Area (in ²)	230

Figure 10-163: Mix#2, 4500 psi, WJ-Crack Length (in)	230
Figure 10-164: Mix#2, 4500 psi, WJ-Number of Cracks	231
Figure 10-165: Mix#2, 6000 psi, WJ, $\frac{3}{4}$ in. Edge Distance-Longitudinal Strain Profile	232
Figure 10-166: Mix#2, 6000 psi, WJ-Observed Cracking (Dead End)	232
Figure 10-167: Mix#2, 6000 psi, WJ-Observed Cracking (Live End)	233
Figure 10-168: Mix#2, 6000 psi, WJ-Crack Area (in ²)	233
Figure 10-169: Mix#2, 6000 psi, WJ-Crack Length (in)	234
Figure 10-170: Mix#2, 6000 psi, WJ-Number of Cracks	234
Figure 10-171: Mix#2, 6000 psi, WJ second time, $\frac{3}{4}$ in. Edge Distance- Longitudinal Strain Profile.....	235
Figure 10-172: Mix#2, 6000 psi, WJ second time, $\frac{5}{8}$ in. Edge Distance- Longitudinal Strain Profile.....	235
Figure 10-173: Mix#2, 6000 psi, WJ second time-Crack Area (in ²)	236
Figure 10-174: Mix#2, 6000 psi, WJ second time-Crack Length (in).....	236
Figure 10-175: Mix#2, 6000 psi, WJ second time-Number of Cracks.....	236
Figure 10-176: Mix#2, 4500 psi, WM, $\frac{3}{4}$ in. Edge Distance-Longitudinal Strain Profile	237
Figure 10-177: Mix#2, 4500 psi, WM, $\frac{5}{8}$ in. Edge Distance-Longitudinal Strain Profile	238
Figure 10-178: Mix#2, 4500 psi, WM-Observed Cracking (Dead End)	238
Figure 10-179: Mix#2, 4500 psi, WM-Observed Cracking (Live End)	238
Figure 10-180: Mix#2, 4500 psi, WM-Crack Area (in ²)	239
Figure 10-181: Mix#2, 4500 psi, WM-Crack Length.....	239
Figure 10-182: Mix#2, 4500 psi, WM-Number of Cracks	240
Figure 10-183: Mix#2, 6000 psi, WM, $\frac{3}{4}$ in. Edge Distance-Longitudinal Strain Profile	240
Figure 10-184: Mix#2, 6000 psi, WM, $\frac{5}{8}$ in. Edge Distance-Longitudinal Strain Profile	241
Figure 10-185: Mix#2, 6000 psi, WM-Observed Cracking (Dead End)	241
Figure 10-186: Mix#2, 6000 psi, WM-Observed Cracking (Live End)	242
Figure 10-187: Mix#2, 6000 psi, WM-Crack Area (in ²)	242
Figure 10-188: Mix#2, 6000 psi, WM-Crack Length (in).....	242
Figure 10-189: Mix#2, 6000 psi, WM-Number of Cracks	243
Figure 10-190: Mix#2, 4500 psi, WP, $\frac{3}{4}$ in. Edge Distance-Longitudinal Strain Profile.....	244
Figure 10-191: Mix#2, 4500 psi, WP, $\frac{5}{8}$ in. Edge Distance-Longitudinal Strain Profile.....	245
Figure 10-192: Mix#2, 4500 psi, WP-Observed Cracking (Dead End)	245
Figure 10-193: Mix#2, 4500 psi, WP-Observed Cracking (Live End).....	246

Figure 10-194: Mix#2, 4500 psi, WP-Crack Area (in ²).....	246
Figure 10-195: Mix#2, 4500 psi, WP-Crack Length (in)	247
Figure 10-196: Mix#2, 4500 psi, WP-Number of Cracks	247
Figure 10-197: Mix#2, 6000 psi, WP, ¾ in. Edge Distance-Longitudinal Strain Profile.....	248
Figure 10-198: Mix#2, 6000 psi, WP-Observed Cracking (Live End).....	248
Figure 10-199: Mix#2, 6000 psi, WP-Observed Cracking (Dead End)	249
Figure 10-200: Mix#2, 6000 psi, WP-Crack Area (in ²).....	249
Figure 10-201: Mix#2, 6000 psi, WP-Crack Length (in)	249
Figure 10-202: Mix#2, 6000 psi, WP-Number of Cracks	250
Figure 10-203: Mix#2, 4500 psi, WQ, ¾ in. Edge Distance-Longitudinal Strain Profile.....	251
Figure 10-204: Mix#2, 4500 psi, WQ, ⅝ in. Edge Distance-Longitudinal Strain Profile.....	251
Figure 10-205: Mix#2, 4500 psi, WQ-Observed Cracking (Live End).....	252
Figure 10-206: Mix#2, 4500 psi, WQ-Observed Cracking (Dead End).....	252
Figure 10-207: Mix#2, 4500 psi, WQ-Crack Area (in ²).....	252
Figure 10-208: Mix#2, 4500 psi, WQ-Crack Length (in).....	253
Figure 10-209: Mix#2, 4500 psi, WQ-Number of Cracks.....	253
Figure 10-210: Mix#2, 6000 psi, WQ, ¾ in. Edge Distance-Longitudinal Strain Profile.....	254
Figure 10-211: Mix#2, 6000 psi, WQ, ⅝ in. Edge Distance-Longitudinal Strain Profile.....	254
Figure 10-212: Mix#2, 6000 psi, WQ-Observed Cracking (Live End).....	255
Figure 10-213: Mix#2, 6000 psi, WQ-Observed Cracking (Dead End).....	255
Figure 10-214: Mix#2, 6000 psi, WQ-Crack Area (in ²).....	255
Figure 10-215: Mix#2, 6000 psi, WQ-Crack Length (in).....	256
Figure 10-216: Mix#2, 6000 psi, WQ-Number of Cracks.....	256
Figure 10-217: Mix#3, 4500 psi, WB-Observed Cracking (Live End)	257
Figure 10-218: Mix#3, 4500 psi, WB-Observed Cracking (Dead End)	257
Figure 10-219: Mix#3, 4500 psi, WB-Crack Area (in ²)	258
Figure 10-220: Mix#3, 4500 psi, WB-Crack Length (in).....	258
Figure 10-221: Mix#3, 4500 psi, WB-Number of Cracks	259
Figure 10-222: Mix#3, 4500 psi, WF-Observed Cracking (Dead End)	260
Figure 10-223: Mix#3, 4500 psi, WF-Observed Cracking (Live End).....	260
Figure 10-224: Mix#3, 4500 psi, WF-Crack Area (in ²).....	261
Figure 10-225: Mix#3, 4500 psi, WF-Crack Length (in)	261
Figure 10-226: Mix#3, 4500 psi, WF-Number of Cracks	261

Figure 10-227: Mix#3, 4500 psi, WI-Observed Cracking (Dead End)	263
Figure 10-228: Mix#3, 4500 psi, WI-Observed Cracking (Live End)	263
Figure 10-229: Mix#3, 4500 psi, WI-Crack Area (in ²)	264
Figure 10-230: Mix#3, 4500 psi, WI-Crack Length (in)	264
Figure 10-231: Mix#3, 4500 psi, WI-Number of Cracks	264
Figure 10-232: Mix#3, 4500 psi, WJ-Observed Cracking (Live End)	265
Figure 10-233: Mix#3, 4500 psi, WJ-Observed Cracking (Dead End)	265
Figure 10-234: Mix#3, 4500 psi, WJ-Crack Area (in ²)	266
Figure 10-235: Mix#3, 4500 psi, WJ-Crack Length (in)	266
Figure 10-236: Mix#3, 4500 psi, WJ-Number of Cracks	267
Figure 10-237: Mix#3, 4500 psi, WM, ¾ in. Edge distance- Longitudinal Strain Profile	268
Figure 10-238: Mix#3, 4500 psi, WM-Observed Cracking (Live End)	268
Figure 10-239: Mix#3, 4500 psi, WM-Observed Cracking (Dead End)	269
Figure 10-240: Mix#3, 4500 psi, WM-Crack Area (in ²)	269
Figure 10-241: Mix#3, 4500 psi, WM-Crack Length.....	269
Figure 10-242: Mix#3, 4500 psi, WM- Number of Cracks	270
Figure 10-243: Mix#3, 4500 psi, WP-Observed Cracking (Live End).....	271
Figure 10-244: Mix#3, 4500 psi, WP-Observed Cracking (Dead End)	271
Figure 10-245: Mix#3, 4500 psi, WP-Crack Area (in ²).....	272
Figure 10-246: Mix#3, 4500 psi, WP-Crack Length (in)	272
Figure 10-247: Mix#3, 4500 psi, WP-Number of Cracks	273
Figure 10-248: Mix#3, 4500 psi, WQ, ¾ in. Edge Distance-Longitudinal Strain Profile.....	274
Figure 10-249: Mix#3, 4500 psi, WQ, ⅝ in. Edge Distance-Longitudinal Strain Profile.....	274
Figure 10-250: Mix#3, 4500 psi, WQ-Observed Cracking (Live End).....	275
Figure 10-251: Mix#3, 4500 psi, WQ-Observed Cracking (Dead End).....	275
Figure 10-252: Mix#3, 4500 psi, WQ-Crack Area (in ²).....	275
Figure 10-253: Mix#3, 4500 psi, WQ-Crack Length	276
Figure 10-254: Mix#3, 4500 psi, WQ-Number of Cracks.....	276

Tables

Table 1: Summary Indented Wire Measurements (Beck, 2019).....	39
Table 2: Material properties of each reinforcement type (Bodapati, 2018).....	39
Table 3: Advanced indent geometrical features (Haynes, 2015).....	45
Table 4: Mix design #1	54
Table 5: Mix design #2	54
Table 6: Mix design #3	55
Table 7: Number of Prisms with Each Wire Type, Concrete Mixture, and Release Strength.....	74

1. Introduction

1.1 Background

Railroads in the United States (U.S.) today are still an emblem of innovation and the foundation of economic growth. The freight rail network is vital to the supply chain in the U.S. Its importance to the global economy reaches from rural America to urbanized metropolitan areas and ports of entry. The economical transport of goods, services, and people efficiently and safely by railroads has been described as vital, active, and aggressive to the economic growth of the U.S. (Cootner, 1963; Irani et al., 2016). Unlike other modes of transportation (trucking, automobiles, airplanes, etc.), the railroad builds and maintains its own track infrastructure (ballast, ties, rail, etc.), communications, and bridge/tunnel infrastructure to haul over 2.2 billion tons of freight each year over 140,500 miles of track (AAR, 2018).

Maintaining track structure is critical to the movement of trains, the rail tie is the part of an integral system transferring the rolling stock load to the subgrade as well as maintaining the proper gauge of the rail. Many railroads have transitioned from traditional wooden ties to concrete prestressed concrete ties on mainlines. However, similar to wooden ties, prestressed concrete ties are susceptible to wear and damage creating potentially unsafe conditions for trains.

A study supported by the Railway Tie Association (Hailing Yu, David Y. Jeong, 2014) indicated that the average number of damaged prestressed concrete ties since the 1970's was found to be between 7.9-9.2 % out of a sample of 29,000,000 concrete ties. This rate was higher in the period between the 1970's and 1980's, when approximately 22.2 % of the 7.4 million concrete ties installed were shown to have incurred damage. Figure 1-1 shows a poorly damaged prestressed tie in the field.



Figure 1-1: Failed Prestressed Concrete Ties

Damage to prestressed concrete ties is important to the concrete crosstie industry where incompatible conditions can result in longitudinal splitting that occurs and possible tie failure. A common reason for prestressed concrete tie failure is the failure of the bond between the steel and concrete within the end region of the tie where the prestress force is transferred into the tie through bond. This bond is vital for transferring the stresses between the two materials in any prestressed concrete member. The bond behavior between steel and concrete is affected by the

type of prestressing wire (specifically the wire geometry), the edge distance, the compressive strength of concrete and the type of concrete mixture used (Bodapati, 2018). The detailed physics of the bond behavior between steel and prestressed concrete is still largely unknown by the research community. Several studies have investigated the bond behavior between reinforcement concrete and wires (Tepfers, 1979, J.A.den Uijl, 1992, Bodapati, 2018).

1.2 Objectives

The primary objective of this research was to evaluate the impact of edge distance and compressive strength of concrete on longitudinal splitting between steel and concrete in prestressed ties utilizing different types of steel wire and concrete mixtures.

The secondary objective of this research was to determine the best parameters for prestressed concrete ties to prevent longitudinal splitting cracks along prestressing tendons. This is very important for prestressed manufacturers, and especially for the railroad crosstie industry because it can reduce failures in the field.

This work resulted in the successful development of a qualification test to ensure adequate splitting resistance in pre-tensioned concrete railroad ties.

1.3 Overall Approach

A study was conducted at Kansas State University to understand the effect of edge distance, indent type, the compressive release strength and concrete mixture on the longitudinal splitting behavior between steel and concrete. For the experimental testing three prisms with different cross sections were cast simultaneously in series. The tests presented here were conducted on pre-tensioned concrete prisms cast in steel frames. Four prestressing wires were symmetrically embedded into each concrete prism, resulting in a horizontal and vertical wire spacing of 2.0 in. The prisms were 59.5 in. long with square cross sections. The first prism was 3.5 x 3.5 in. with cover $\frac{3}{4}$ in, the second was 3.25 x 3.25 in. with cover $\frac{5}{8}$ in and the third prism in series was 3.0 x 3.0 in. with cover $\frac{1}{2}$ in. All prestressing wires used in these initial tests were 5.32 mm (0.21 in.) diameter and had different indentation types. The indent pattern variations of the wires included spiral, classical chevron shape, and the extreme case of smooth wire with no indentions. The wires were initially tensioned to 7000 lbs. and then gradually de-tensioned after reaching the desired compressive strength. The different compressive (release strength) strength levels tested included 3500 psi, 4500 psi, 6000 psi and extreme case of 12000 psi for one wire type. Three different concrete mixtures with a water-to-cementitious (w/c) ratio 0.32 were used for all castings except one test where a 0.38 w/c ratio was used. For compressive release strength 12000 psi a 0.26 w/c ratio was used, and desired strength was achieved after 6 days. Concrete-to-steel reinforcement ratios and mechanical properties of test prisms were representative of actual prestressed concrete crossties used in the railroad industry.

1.4 Scope

The experiments conducted at Kansas State University were designed to understand the effect of edge distance, indented wire type, release strength of concrete and type of concrete mixture on the longitudinal splitting between prestressing steel tendons and concrete. For these tests, steel frames were used, and three prisms with different cross sections were cast end-to-end. The

specimens each had square cross sections and similar wire spacing but had different thicknesses of edge distance. All test specimens had four wires arranged symmetrically in the specimen's cross section. Four prestressing wires were symmetrically embedded into each concrete prism, resulting in a common wire spacing of 2.0 in. The prisms were 59.5 in. long with square cross sections. The first prism was 3.5 x 3.5 in. with cover $\frac{3}{4}$ in. thickness of the edge distance, the second was 3.25 x 3.25 in. with $\frac{5}{8}$ in. thickness of the edge distance and the third prism in series was 3.0 x 3.0 in. with cover $\frac{1}{2}$ in. thickness of the edge distance. All prestressing wires used in these tests were of 5.32 mm (0.21 in.) diameter and were of different wire types. The indent pattern variations of the wire types included spiral, classical chevron shape, and the extreme case of smooth wire with no indentations. Each wire was pulled to 7000 lbs., and de-tensioned gradually when the compressive strength of the concrete reached prescribed values 3500 psi, 4500 psi or 6000 psi (all within ± 200 psi of the prescribed release strengths). For WE wire an extreme 12000 psi was also tested with a 0.26 w/c ratio and this extreme release strength was reached after six days. The measured values of compressive strengths were determined by testing 4 in. diameter x 8 in. long compression strength cylinders that were temperature match cured. Prisms had almost identical concrete-to steel reinforcement ratios and mechanical properties as prestressed concrete ties which were manufactured in the railroad industry.

1.5 Organization of the Report

This report is organized into ten chapter's Following Chapter 1, Chapter 2 includes a Literature review of related work conducted on prestressed concrete members in the past. Chapter 3 includes Material used in this research and description of prestressing operation. Chapter 4 includes Methods used for conducting the tests and experimental program. Chapter 5 includes Results of experimental tests using different type of mixtures. Chapter 6 presents Comparison charts. Chapter 7 includes Proposed Qualification Test for Arema manual. Chapter 8 presents Theoretical Lateral Stresses Due to Hoyer Effect. Conclusions and recommendations are presented in Chapter 9. Lastly, References are in Chapter 10.

2. Literature Review

The literature search focused on prestressed concrete tie splitting and/or cracking along with bond damage between wire and concrete. As stated previously, the detailed physics behind bond behavior between steel and prestressed concrete is still largely unknown. However, researchers investigated several analytical, numerical and experimental approaches as reported in this chapter.

2.1 Bar-Concrete Interaction

2.1.1 Bond of Reinforcement in Concrete: -State of the art FIB CEB-FIP

The basic characteristics associated with the bond between steel and concrete are detailed in a state-of-the art report by FIB CEB FIP (Task group Bond Models, 2000). This bond transferred the longitudinal force from the reinforcement to the concrete in the prestressed structure. This transfer produced a change in force in the reinforcing bar along its length. The displacement occurred between steel and concrete was a result of the difference between steel strains and concrete strains.

It was also found that interaction between the concrete and a bar subjected to a pull-out force could be divided into four different stages as described below.

Stage I (un-cracked concrete): In this stage bond stress was very low. Bond was assured by a chemical adhesion. In this stage, it was found that splitting did not occur. The presence of highly localized stresses arose close to lug tips. Micromechanical interaction which was the product of microscopically rough steel was also present in this stage concurrently with chemical adhesion. The relative displacement could be measured, and it consisted of two parts: the relative slip at the interface and the shear deformations in the concrete.

Stage II (first cracking): With increasing values of bond stress, the chemical adhesion broke down. In deformed bars, the lugs produced a bearing stress in the concrete and transverse micro-cracks. In this stage, tips of the lugs allow the bar to slip but the wedging action of the lugs were limited and there was no appearance of concrete splitting.

Stage III: For higher bond stress values, the longitudinal cracks (splitting cracks) start to spread radially. This related to the wedging action. The external component of the pressure was resisted by the hoop stresses in the surrounding concrete (Tepfers, 1979). As a result, the surrounding concrete produced a restriction action on the bar, with interlocking among the reinforcement bond strength and stiffness are thus guaranteed. This stage ended as soon as concrete splitting reached the outer surface of the concrete member. Bond failure, which depends on the extent of transverse confinement, could be present in this stage.

Stage IVa-This phase followed the breakage of the adhesive bond; force transfer was then provided primarily by friction alone.

Stage IVb-In this phase splitting cracks broke out through the whole cover and bar spacing. An adequate amount of transverse reinforcement could assure bond efficiency despite concrete splitting.

When end slip values started to increase, the bond strength reached a peak and then started to decrease. Additionally, the bond strength remained significant even at very large slip values (Gamborova et al. 1989, Gamborova and Rosati, 1996). Research concluded that bond behavior tended to become of the dry-friction type (Coulomb type).

Stage IVc- In this phase bond failure was caused by bar pull-out. The force transfer changes from bearing to friction and the shear resistance could be considered as a value for this transaction. Additionally, it was observed that continuing loading tends to decrease the bond stress were observed.

The bond between steel and concrete depends on a variety of parameters. Primary parameters which depend on the interaction between the reinforcing unit (e.g. wire, strand, and bar) and the concrete. There are other technological aspects which are important to the bond including: edge distance, clear space between the bars, the number of bar layers and bounded bars, casting direction, and bar position.

With a multi-wire strand that is commonly used in prestressed concrete structures, the bond-slip behavior can be studied using pull-out tests. If the anchorages are long, the reinforcement stresses are high. The Poisson effect has a significant influence on the bond stress when the steel is in the elastic range. When the external force (tensioning) has been released, the diameter of a pre-tensioned tendon increases. This leads to the appearance of increased radial stresses and contributes to the frictional bond resistance. When the steel stress is increased the bond resistance of a tendon is reduced. Consequently, two different bond situations can be considered: (1) transfer length region, push-in situation, and (2) flexural bond region, pull-out situation. In the region of transfer length, the steel stress decreases when the pre-tensioned tendon is released. This means the tendon diameter will increase and contribute to a greater bond connection. Under flexural loading this situation is completely different. The steel stress in a cracked section will be increased, and therefore, the tendon diameter will be reduced, and the bond resistance will be weaker.

Increasing loads can lead to transverse cracking and splitting. Physical and mechanical factors such as confining pressure, edge distance, transverse reinforcement and concrete toughness have also been considered important. Concrete toughness is usually characterized by crack adhesion. The type of interaction can determine the type of failure: pull-out failure or splitting failure. The bond failure is usually accompanied by the longitudinal splitting of the concrete surrounding the bar, and bond capacity vanishes when radial cracks get to the outer surface of the structural element.

For splitting failure, limit analyses models show that there is a critical crack extension, which maximizes the ultimate bond strength (Tepfers 1979 and 1982).

2.2 History of Experimental, Analytical and Numerical research

Bond behavior between concrete and steel has been the subject of previous research including: Gamborova and Rosati, Abrishami and Mitchell, Tepfers and Olson. However, limited research has been conducted to investigate prestressed concrete members.

In this field Abrishami and Mitchell (1996) performed an investigation to determine the bond stress-versus-slip response for pre-tensioned strand in concrete along the transfer and flexural

length. For this test method, they used seven cylinders. A prestressed concrete structure with seven-wire strands was tensioned to an initial force level P_o in a loading frame. At the moment when concrete achieved the desirable release strength, a pull-out test was performed.

In order to achieve small bond stress, tension was reduced using the small area and increment of force ΔP_o . In this phase the bond stress is given by equation:

$$u = (P_o - P_t) / (\pi d_b L) \quad 2-1$$

Where, P_o is the pre-tensioned force, P_t the top force in the strand and L is the embedment length.

This phase was repeated in small increments of loads to achieve the reduction at the top of the specimen. The relative slips were measured for each loading. This incremental loading was repeated until the entire bond-stresses-slip response was reached.

For this test, a concrete with a compressive strength of 25 MPa (3625 psi) was used at the time of testing which resulted in a 35 MPa (5075 psi) compressive strength after 28 days.

The specimens had dimensions of 150 mm (6 in.) in diameter by 300 mm (12 in.) in length. The prestressing steel diameters were 9.5 mm, 13 mm and 16 mm (3/8 in, 1/2 in. and 0.6 in.).

Out of all the bond failures which occurred by the pullout of the strand, only a few of them were caused by splitting. The stiffness of the bond stress-versus-slip response was greater in the transfer length region. In the phase after bond failure, the flexural bond length specimens showed a ductile response, additionally, the transfer length specimens showed brittle bond failure.

2.2.1 J.A. den Uijl

Den Uijl (1992) worked under the assumption that the bond associated with prestressed strand is based on dry friction. It was assumed that circumferential tensile stresses that make equilibrium with the radial compressive stresses may cause splitting cracks resulting in a reduction or complete loss of bond. Splitting action was analyzed experimentally and numerically, considering the softening behavior of concrete in tension and the position of the strands in the concrete cross section.

According to den Uijl (1992) two different stages could be considered for the bond behavior between steel and concrete. The first stage was adhesion and interlocking between concrete and the strand surface. This initial bond was broken with appearance of small relative displacements. In the second stage dry friction was the principal mechanism.

Den Uijl (1992) also investigated the effect of the bond situation on the bond capacity of strand. In a pull-out test, the strand was pre-tensioned before the concrete was casted. During the test, the bond force and strand displacement were measured when the concrete reached a desirable strength. All specimens were 100mm (4in) long cylinders with 103mm (4.05in) in diameter. For these tests, a 9.3 mm (0.37 in) diameter strand was used. The strand was in the vertical position and fixed, pre-tensioned as in the push-in tests. There were five series of tests consisting of four pull-out specimens, one series with four push-in specimens and one series with only four pull-out specimens.

For this study a consistent mixture of 350 kg/m³ (21.85 lbs/ft³) rapid hardening Portland cement with a 0.40 water-cement ratio was used for all castings. Round shaped graded river sand and

gravel with a maximum size of 8mm (0.31 in.) and an additive were used in these tests. The desirable strength of concrete was 55.4 MPa (8035 psi) and splitting tensile strength of 3.12 MPa (453 psi). These properties were recorded after 5 days. The tensile strength of wire was found to be 1950 MPa (282,824 psi).

The pull-out tests were conducted in two phases. During the first phase, the pull-out force was applied to the strand with the unloaded side fixed. During the second phase when slip reached the value of 2 (0.08 in) to 3mm (0.12 in), the specimen was unloaded, the anchor was removed, and the specimen was reloaded with the free end at the unloaded side. The results of the pull-out tests with fixed unloaded end were very sensitive to bond length variation. These results were obtained with a hanger stiffness of 30 KN/mm (171 lbs. /in.) (15 tests) and 165 KN/mm (942 lbs. /in.) (5 tests). For the push in tests, the hanger rod stiffness amounted to 37 KN/mm (211 lbs. /in.) (8tests), 72 KN/mm (411 lbs. /in.) (8 tests), 165 KN/mm (942 lbs. /in.) (2 tests) and 323 KN/mm (1844 lbs. /in.) (2 tests), and all push-in results were evaluated together.

For the strand in the push-in situation, the strand was considered as a circular bar and normal stresses were radially directed. Den Uijl (1992) concluded that radial compressive stresses made equilibrium with circumferential tensile stresses and radial compressive stresses first reached the tensile strength in the contact area. Consequently, radially directed micro-cracks occurred and the circumferential tensile stresses were redistributed. It was also noted that the maximum force occurred when the thick-walled cylinder around the strand was partly cracked.

The study reported higher radial stresses with regard to small edge distances and splitting was occurred in prisms. Furthermore, the average circumferential stress was equal to the tensile strength when the edge distance was increased.

In this research, the influence of the edge distance was given as the function of clear strand spacing. Additionally, it was also concluded that thick walled cylinder approach was useful for a single strand and it was not valid for multiple strand configurations.

2.2.2. R. Gustavson

Gustavson (2004) found that the bond response in prestressed concrete is determined by the ability of the strand to establish normal stresses at the strand concrete interface. The variation of normal stresses depends on the indentation and the helical strand.

Gustavson (2004) examined the response of the strand-concrete interface using the results from pull-through (PT) and push-in tests (PI). For this experiment three-wire and one wire were used. An adhesion, friction, and indentation were observed as the main parameters responsible for splitting failure.

The wires were either indented or had a smooth surface. Included were variations of the wire surface and concrete mix. Two different bond situations were observed. The first was simulated by pull-through tests, and the second by push-in tests. The pull-through tests were performed in three series using different strand and concrete properties. During the pull-in tests the same strand configurations were used but with different values of release concrete strength. The strand could rotate within the concrete. For this experiment, the PC strand EU 138/6, 3x3.0 mm (0.12x0.12 in.) with a nominal diameter of 6.5 mm (0.26 in.) was used.

All the specimens were cast in the laboratory, and the concrete was vibrated during the casting operation. Steel or plastic tubes were used as forms, with plastic tops and bottoms. These plastic tops and bottoms were removed before testing. A steel plate with a circular cavity was used as a frame, with a diameter of 50 mm (2 in.), and a thickness of 2 mm (0.08 in.). In this testing, strain gauges with a length of 10mm (0.4 in.) were used, to measure the tangential strains in the steel tube.

The first series of tests consisted of nine concrete specimens made with 6.5 mm (0.26 in.) diameter wire. The concrete compressive strength was 55 MPa (7977 psi), the modulus of elasticity was 33 GPa (478.6 ksi) and the fracture energy was 96 N/mm² (13924 lbs./in²).

The second phase was a study of the properties of the individual wire surface, the indentation, the geometry of the strand and the concrete properties. These parameters were variables that were changed during the test in order to find out how they affected the bond response. The concrete release strength in this phase was 45 MPa (6527 psi), whereas the concrete with silica additions was 57 MPa (8267 psi).

Sixteen different configurations of the strand-concrete interface were tested with two specimens of each configuration. In the third series, the viability of the tested configuration was observed, the strength of the concrete was 54 MPa (7832 psi) and the compressive strength of the concrete with silica additives was 78 MPa (11313 psi). Young's modulus of elasticity was 28 GPa (406.1 ksi) and 37GPa (536.7 ksi) for the concrete and the concrete with silica additives, respectively.

In PT tests, the strands did not have the prestress force and the deformation rate was 2.2 mm/min (0.09 in/min) during the whole test. The transducer was used for measuring the displacement of the strand, and a thin wire was used for measuring the rotation of the specimen displacement transducer.

For PI tests, the prestressed force in the strand was 28 KN (6294 lbs.), corresponding to a prestress of 1320 MPa (191.4 ksi). Concrete was cast 28 hours after the strand was prestressed. The deformation rate was 1mm/min (0.04 in/min) during the release stage. Two transducers were used for measuring the displacement of both the strand and the concrete surface.

This experimental research showed that in the case of pull-out failure the maximum bond capacity of strands was not influenced by the compressive strength of the concrete. The bond response in prestressed concrete was determined by the ability of the strand to establish normal stresses at the strand-concrete interface.

The variation of normal stresses depends on the indentation and the helical strand. The results showed the presence of two spatial wave patterns with different periods.

With this research, it was also concluded that adhesion was greatly increased by an increased micro-roughness of the strand surface. The adhesion capacity increased with the density of concrete mix. Friction, as the second parameter, strongly influenced the bond capacity. With increasing friction, the bond capacity after de-bonding was increased. The indentation was identified as a very important parameter. The indents caused a compressive stress in the direction normal to the strand-concrete interface which resulted in an increase in the occurrence of splitting failures.

2.2.3 J.C. Galvez, J.M. Benitez, B. Tork, M.J. Casati, D.A. Cendon

Galvez et al. (2011) presented analytical, experimental and numerical work based on observations of the bond-splitting process. For their analytical approach they used a thick walled linearly elastic cylinder method to predict the bond stress value and value of slip, resulting in an equation for transfer length. In their experiments they used specimens having a rectangular shape with one embedded prestressing wire and different thicknesses of edge distance.

During the test released load, displacement of the actuator, longitudinal shortening of concrete specimens, and crack opening displacement of the longitudinal cracks were recorded. The specimens with deep, shallow and tiny indentation of wire were observed. Splitting failure was observed on the specimens with the thinnest edge distance. The longitudinal shortening of the concrete prism decreased after splitting failure where the wire lost confinement. It was concluded that the critical released load which causes the splitting failure diminished with increased depth of the wire indentations. The deepest wire indentation had the best bond between wire and concrete, until the splitting failure. This was shown by a lower slippage of the wire at the end of the concrete prism (end-slip) and by a larger shortening of the specimen for equal released load.

For this experiment, EN-10138 Y 1770 C4 wires were used having a nominal diameter of 4 mm (0.16 in.) with $E=226$ GPa (32778529 psi) and $\epsilon_u=5.25$ %. Three types of indentation depths were used (shallow, medium and deep). A total of 27 specimens were made with wire embedded longitudinally in the specimen.

The dimensions of specimens were 400 mm (15.7 in.) in length, 60 mm (2.4 in.) in width with three different edge distances. All wires were tensioned to 17 KN (3822 lbs) before casting within stiff vertical frames. The prestressing force was applied monotonically up to the desired value. An extensometer was used for measuring the final prestressing stress. All specimens were cast horizontally in one layer in the ground steel molds. A vibrating table was used to make compact consistent concrete. Testing was conducted 28 days later.

The experiment was performed in two stages. During the first stage, the prestressing force was sent from the frame to the testing machine. On the second stage the prestressing force was transferred from testing machine to the concrete prism. During the experiment, the release strength of the prestressing force of the wire was controlled.

During the test released load, displacement of the actuator, longitudinal shortening of concrete specimens, wire concrete slip on the upper lower faces of the prismatic specimens, and crack opening displacement of the longitudinal cracks were recorded. The longitudinal shortening of the concrete prisms decreased after splitting failure when the wire lost confinement. It was concluded that the critical released load which caused the splitting failure diminished when the depth of the wire indentations increased. The deepest wire indentations were found to have the best bond between wire and concrete, until the splitting failure.

Galvez et al. (2012) also performed a numerical procedure which modeled the splitting of concrete caused by the radial pressure of the wire and the bond between concrete and steel. Their model was based on the cohesive crack approach with bond based on a plasticity formulation. The cohesive crack model is generally used as a model of the fracture of quasi-brittle materials. Hillerborg was the first who proposed this model in the late 1970s. The bond model was based on the interface interaction between concrete and steel.

The numerical procedure considered the possible failure of concrete by the splitting action of the wire. The bond model was incorporated into an interface finite element model. For simulation of the cracks, they used a cohesive crack model, and the model was run in software Abacus. Their numerical and experimental approach gave similar results.

2.2.4. Jose M. Benitez, Jaime C. Galvez

Benitez and Jaime Galvez (2011) developed an analytical model for simulating the bond between steel and concrete, in prestressed structures during the prestressing force release. With this model the bond stress was evaluated in the transfer length region, where bond stress is not constant, during the prestressing force release. This model was validated with experimental research using different type of wire indentations, and with specimens having different thicknesses of edge distance. This analytical model is based on Tepfer's (1979) proposal for reinforced concrete, and on the work of Van der Veen (1997) who modelled the thick-walled concrete ring to predict the cracking of the concrete on a cross-section. This analytical model allowed approximation of the radial and tangential stresses between wire and concrete, using Poisson's effect, confinement of the steel, the edge distance, and the mechanical properties of the materials.

For validating the results, the testing was performed with specimens which had one prestressing wire. The transfer length was experimentally evaluated in compliance with RILEM (Reunion Inetrnationale des Laboratoires et Experts des Materiaux, Systemes de Construction et Ouvrages) standard. According to these standards, the transfer length is defined as a distance from the end of the specimen where concrete strain was equal to zero to the section where strain became constant. With this model the concrete strain along the length of the wire during the prestressing force release can be predicted. And as a result, the value of transfer length can be found.

A rectangular concrete specimen with one single wire was placed in the prism longitudinally. The initially prestressing force was P_0 and the force at the end of the prism was given $P_0 - \Delta P$, where ΔP presents the released force. Wire develops tangential and normal stresses at the steel concrete interface. They observed a slice of prism with a $|dx|$ thickness, at a distance $|x|$ from the end of the prism. Using the force equilibrium, they got the equation:

$$\frac{\Delta \Delta \sigma_x}{\Delta_x} = - \frac{p_e}{A_s} \tau \quad 2-2$$

$\Delta \sigma_x$ is the wire stress variation between sections, p_e is the wire perimeter, A_s is the area of wire section and τ is the average tangential stress between wire and concrete.

The difference between the strains of both materials was used to get the equation for slip

$$\frac{d_s}{d_x} = \frac{\Delta \sigma_x}{E_s} - \frac{\sigma_c}{E_c} \quad 2-3$$

s is the slip between wire and concrete and dx is the slice thickness, E_s Young's modulus of elasticity of strain and E_c is the Young's modulus of elasticity of concrete, σ_c is the concrete normal stress at x section.

Force equilibrium was used to calculate concrete strains.

$$\sigma_c = \frac{A_s}{A_c} (\Delta\sigma_0 - \Delta\sigma_x) \quad 2-4$$

A_c is the net area of the concrete section.

The analogy of thick walled cylinder was used to consider the concrete confinement of the wire. R_I was the inner radius and R_2 was the outer radius. The minimum edge distance was expressed as $R_2 - R_I$. They assumed a linear elastic behavior of material with no occurrence of cracking. The circumferential and the radial stresses are σ_o and σ_r .

The circumferential strain for the steel is:

$$\epsilon'_\theta_s = \frac{\sigma\theta_s - \nu_s(\sigma_{rs} + \sigma_{zs})}{E_s} \quad 2-5$$

And for the concrete:

$$\epsilon'_\theta_c = \frac{\sigma\theta_c - \nu_c(\sigma_{rc} + \sigma_{zc})}{E_c} \quad 2-6$$

σ_r and σ_θ are the radial and hoop stresses and σ_z is the stress in the normal direction to the section.

Using the Tepfers equation, the tangential stress between steel and concrete at x distance from the end prism can be expressed as:

$$\tau = B_1 \Delta\sigma_x - B_2 \Delta\sigma_0 \quad 2-7$$

$$B_1 = \frac{\nu_s E_c + \frac{A_s}{A_c} \nu_c E_s}{\tan\alpha [(1 - \nu_s) E_c + (H + \nu_c) E_s]}$$

$$B_2 = \frac{\nu_s E_s \frac{A_s}{A_c}}{\tan\alpha [(1 - \nu_s) E_c + (H + \nu_c) E_s]} \quad 2-8$$

The tangential stresses between steel and concrete reach the certain limiting value and τ_{max} , which cannot be exceeded. The authors assumed, that once this critical value has been reached the tangential stress remains constant and equal to τ_{max} .

Slip steel-concrete is given by equations along the prism. The equations for two different zones were given $0 < x < x_{lim}$

$$s = \frac{((B_2 - B_1) \Delta\sigma_0 + \tau_{max})(\beta E_s A_s (\Delta\sigma_0 (B_2 - B_1) + \tau_{max}) + 2 \Delta\sigma_0 B_1)}{2 E_s B \tau_{max} B_1} \quad 2-9$$

$x > x_{lim}$

$$s = \left(A_s \Delta\sigma_0 \frac{B_2}{B_1} \beta - \frac{A_s \Delta\sigma_0}{A_c E_c} \right) \left(\frac{L}{2} - x_{lim} \right) - \frac{\tau_{max} \beta A_s}{B_1 B} \left(e^{(B_1 - B_2) \frac{\Delta\sigma_0}{\tau_{max}} - 1 - \frac{BL}{2}} - e^{(B_1 - B_2) \frac{\Delta\sigma_0}{\tau_{max}} - 1 - Bx_{lim}} \right) \quad 2-10$$

If the value of x along the τ stress has exceeded the τ_{max} it is noted as x_{lim} .

For this model, they used the experimental results of Galvez's (Galvez et al., 2009) experimental work. The research was focused to show the influence of edge distance and the indentation depth in the transfer length on normal and tangential stresses between steel and concrete during the prestressing force release. The experimental tests were given in the previous section. Both analytical and experimental results gave the similar results.

2.2.5. Joseph R. Holste, Mark Haynes, Robert J. Peterman, B. Terry Back, Chih-Hang John Wu

Holste et al. (2014) showed the influence of indentation of wires on bond behavior between steel and concrete for tests conducted at Kansas State University. The concrete specimens had different types of wires and for the pull-out test, wires were tensioned to 75 % of their ultimate capacity before casting. When concrete reached the maximum strength release of 4500 psi, the wires were gradually de-tensioned. Wire slip and force were measured during the de-tensioning procedure on each side of the specimen. Approximately 12 different wires with a diameter of 5.32 mm (0.21 in.) were used with different indentation including: smooth wire WA, a spiral patterned wire WE, four and two-dot indented wires (WK and WL), and eight chevron patterned indented wires (WB, WD, WF, WH, WI, WJ and WM). The concrete mixture consisted of Type-III cement, sand, 3/8 in. aggregate, water and admixture Type-F HRWR. The mix was consistent for every test. Materials were oven dried to remove any moisture.

A Frame with two I beams acting at the main supports was used for pull-out tests. Each wire was tested in three different locations. Three sets of channel section attached to I beams were used for recording. At the ends of the frame, S-type load cells were attached, and a wire chuck attached to the load cell. The wires were tensioned to 7000 lbs., and casting took place after that. All specimens had dimensions 2.5 in. height with a diameter of 2 in. When concrete reached the strength of 4500 psi, the wire was de-tensioned. The first testing was a specimen with a 4in. diameter, for this specimen there was no occurrence of splitting, so tests were continued with diameter of 2 in. The two in diameter specimen provided minimum cover concrete. Simultaneously with the specimen's, cylinders were cast to determine the compressive strength of concrete. All cylinders were temperature match cured using Sure Cure system. The difference in specimen's volume and cylinders volume led to use of a special cooling box to place the compressive cylinders in as they cured. When the compressive strength of concrete was reached, the specimens were tested. The linear variable differential transformers (LVDT's) were used to measure the amount the wire slipped in and out of the concrete. Load cell and LVDT measurements were recorded using a data acquisition system. The data acquisition system was set to scan 100 scans per second because the test was quasi static.

It was found that smooth wire WA during the test didn't cause splitting, WE (spiral wire) showed splitting, but this wire did not have indent and it was removed from testing, all the chevron wires caused the splitting during testing, but they exhibited different bond behavior. The authors concluded for chevron wires, that specimens seemed to split when the maximum bond force was achieved. They found the top and bottom slip values; the bottom values were found to provide the highest correlation with the geometrical measurements of the different indents. The top values showed correlation. The indent depth was the most important features for the bottom and top splitting. This experiment gave the results where the geometry of the indent pattern could

be used to determine at what slip value the reinforcement would cause a specimen to slip. The higher bonding wire patterns showed the lower slip value needed to split the specimen.

2.2.6. Matthew L. Arnold, Robert J. Peterman, Naga Narendra B. Bodapati, B.

Terry Beck, Chih-Hang (John) Wu

Arnold et al. (2013) investigated how the indentation of wire increases the bond performance between steel and concrete. The bond characteristics were determined by experimental tests conducted at Kansas State University. For these experiments low-relaxation steel wires were used for the pull-out tests. These tests served as quality control tests. All these wires were tested in original condition how they received, and they had different indent characteristics. All specimens were with 4in outer diameter tube with 8in length. The wires were 5.32 mm (0.21 in.) in diameter and were in the center of the tube and the sand-cement mortar was placed and allowed to cure. Mortar cubes with dimensions 2 in. x 2 in. were used to determine the compressive strength of the mortar. All specimens were tested when compressive strength of the mortar reached prescribed values of 4500 psi and 5000 psi. Each wire was tested six times, and six batches were made with 12 pullout specimens, one with each wire type.

During these pull-out tests, the wires (smooth type, chevron type, spiral type and diamond type) were loaded and simultaneously the slip of the wire was monitored and recorded. All force versus end-slip data were combined to obtain the average bond performance. All these results were then compared to transfer length measurements. It was found that there was correlation between the pullout tests and transfer length measurements.

The authors observed consistent pullout strength results when six different mortar batches were used, and these tests were found to have good correlation with the bond performance of the wires in pre-tensioned applications.

2.2.7. Vincent Briere, Kent A. Harries, Jarret Kasan, Charles Hager

Briere et al. (2013) evaluated the bond between pre-tensioned strands and concrete depends using three mechanism: adhesion between the steel surface and cement, friction and wedge action because of Hoyer effect (shown in Figure 2-1) and mechanical interlock between strand wires and concrete. The Hoyer effect can lead to the radial expansion depending on friction and mechanical wedge which also increase the mechanical interlock effect. The Hoyer effect also affects the transfer length. In prestressed concrete structures, the transfer of large prestressing forces can possibly lead to local cracking which relates to bursting stresses or splitting. This in turn relates to the transfer strand force through bond.

In the Hoyer effect when wire or strand is tensioned, the diameter decreases due to the Poisson effect. After de-tensioning, the wire and tendon attempt to return to their previous diameter, when radial forces develop along the concrete/tendon interface.

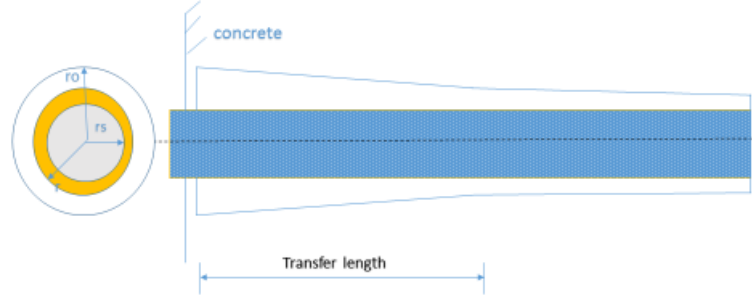


Figure 2-1: Schematic Representation of Hoyer effect

With radial expansion of the tendon prestress force is transferred to the concrete by exerting a force normal to the strand concrete interface. This enhances friction and develops wedge that enhancing the effectiveness of the normal force. The radial force is compressive, and circumferential stresses are perpendicular. Oh et al (2014) considered strand as a solid cylinder having an unstressed radius r_o and stressed radius of r_s . The radial pressure is obtained by the following equations:

$$p = \frac{r_o(1 - \nu_p f_{pz}/E_p) - r_s(1 - \nu_c f_{cz}/E_c)}{\frac{(1 - \nu_p)r_o}{E_p} + \left(\nu_c - \frac{r_s^2 + c^2}{r_s^2 - c^2}\right)r_s/E_c} \quad 2-11$$

$$f_{cz} = f_{pz} r_o^2 / c^2 \quad 2-12$$

$$r_s = r_o \left(1 - \frac{\nu_p f_{pi}}{E_p}\right) \quad 2-13$$

Where f_{pz} is the axial stress in prestressing strand at a distance z from the free end, f_{cz} is the axial stress in concrete at a distance z , c is the clear cover, ν_c and ν_p are the Poisson's coefficient of concrete and steel, respectively, E_c is the modulus of elasticity of concrete, E_p is the modulus of elasticity of steel, σ_θ and σ_r the circumferential and radial stress, respectively.

The radial and circumferential stresses are given as function of the radial distance using the following equations:

$$\sigma_r = \frac{-p\left(\frac{1}{c^2} - \frac{1}{r^2}\right)}{\left(\frac{1}{c^2} - \frac{1}{R^2}\right)} \quad 2-14$$

$$\sigma_\theta = \frac{-p\left(\frac{1}{c^2} + \frac{1}{r^2}\right)}{\left(\frac{1}{c^2} - \frac{1}{R^2}\right)} \quad 2-15$$

This study determined the empirical values for the dilation ratio ν_p . Five samples with strand diameters 12.7 mm (0.5 in.) and 15.2 mm (0.6 in.), respectively, and 1860 MPa (270 ksi) low relaxation prestressing strand were used. Each test included stressing the strand from zero up to 1488 MPa (215816.2 psi) or $0.8 \times f_{pu}$ in increments of $0.1 \times f_{pu}$. Each strand had ten repetitions, and first strand was unstressed. All tests were conducted in a self-reacting frame using a pair of

hydraulic arms. With hydraulic arms the load was applied to the strands, and strands were anchored by strand chucks

Electrical strain gages were used along with a modified clip gage extensometer, to measure the diametric strain of the strand. An extensometer was mounted to measure the change in diameter of the rings and strands. As a result, all specimens exhibited a significant axial strain offset following the first load cycle. Load repetitions exhibited small additional offsets. It was noticed that the dilation ratio of prestressing strand effects concrete cracking behavior and prestress force transfer behavior. The degree of dilation was shown to be affected by the prestressing steel geometry: single wire tendons were affected by Poisson's ration only and multi wire strands having a greater apparent dilation ratio.

2.2.8. Byung Hwan Oh, M. ASCE; Eui Sung Kim; and Young Cheol Choi

Hwan Oh et al. (2006) built upon the work (Balazs 1987) by building on a theory which investigated the transfer lengths. They proposed concrete-steel model in which the prestressing steel was considered as a solid cylinder and the surrounding concrete as a hollow cylinder. The cracking of concrete in a radial direction due to Hoyer's effect had been considered using an appropriate tensile-stress crack width relation. Simultaneously with analytical modeling, the experimental tests were conducted to measure the transfer lengths considering different variables such as concrete compressive strength, strand diameter, the edge distance and strand spacing. The experimental data and analytical approach gave similar results.

In summary, the literature review revealed that the transfer of prestressing force is a complex problem, and the value of transfer length is very important. According to all experimental testing's performed until recently, a lot of variables affect the value of transfer length. The main variables found have included the strand diameter, prestress intensity, the concrete strength and the edge distance. The proposed theory which was considered in this research considered the prestressing steel as a solid cylinder and the concrete as a hollow cylinder. The bond stress was expressed simply in terms of two variables, the coefficient of friction which was taken as 0.4 (Tepfers 1979, Janney 1954) and the interface pressure p which could be determined using the equation 2-16. Derivation of radial circumferential stresses were previously given in equation 2-14 and 2-15. With this analytical model an expression for the interface pressure was given as follows:

$$p = \frac{r_o \left(1 - \frac{\nu_p f_{pz}}{E_p} \right) - r_j \left(1 - \frac{\nu_c f_{cz}}{E_c} \right)}{\frac{(1 - \nu_p) r_o}{E_p} + \left[\nu_c - \frac{r_j^2 + c^2}{r_j^2 - c^2} \right] r_j / E_c} \quad 2-16$$

Where r_o is the initial diameter of steel before prestressing, r_j is the diameter of steel after prestressing, c is the edge distance, ν_c is the Poisson's coefficient of concrete, ν_p is Poisson's coefficient for wire, E_c is the modulus of elasticity of concrete, f_{pz} is the axial stress of concrete at distance z from the free end, and f_{pz} is the axial stress of prestressing steel at a distance z from the free end.

For Anisotropic analysis some modified properties are given, which are directly connected with number of radial cracks and average strain due to cracks. The value of the modulus of elasticity

is reduced and is given by following equation in which w is width of crack, and L is length of crack:

$$E_{\theta} = \frac{\sigma_{\theta}}{\frac{\sigma_{\theta}}{E_c} + \frac{w}{L}} \quad 2-17$$

Where σ_{θ} is the circumferential stress, w is the crack width and L is the crack spacing of radial cracks.

For fully cracked concrete cylinder, according to this analytical approach, the displacement of concrete after release of prestressing force is given by following equation:

$$u_c = c \left(\frac{f_{tr}}{E_{cr}} - \frac{\nu_c f_{cz}}{E_c} \right) \quad 2-18$$

Where $E_{cr} = E_{\theta}$ at the outer surface and f_{tr} is σ_{θ} at $r = c$.

The authors considered the effects of partial and full cracking due to pressure in obtaining the governing equation. A tensile stress-crack width relation was incorporated into this equation for the new value of modulus of elasticity. All equilibrium equations were given for each segment of a member in the longitudinal direction and the strain development curves. The authors obtained all transfer lengths from these strain profiles. The observed analytical approach gives the similar results to the experimental testing.

3. Material and Operation

3.1 Prestressing Wires

The geometry of the prestressing wire indents has been found to be a significant variable in the formation of longitudinal splitting cracks in pre-tensioned concrete railroad ties. Longitudinal splitting along prestressing tendons can result in severe splitting and complete tie failure in the field under normal train loading over time. Until recently, inspection of prestressing wire indent properties consisted of sampling indents from a small segment of wire. This resulted in very limited statistical information on the wire indent properties. To address this deficiency, a high resolution automated non-contact optical wire indent scanning system was developed at Kansas State University (Beck, 2019) for complete and rapid characterizing of all relevant indent geometrical parameters. The scanning system can measure large segments of wire to yield statistically significant samples of all relevant indent parameters. These parameters include: indent depth, indent width, indent sidewall angle, indent pitch and indent volume (Beck, 2019).

Indented wire is manufactured by pulling wire through a set of three rollers, oriented at 120 degrees apart. Each roller has contact teeth that indent the surface of the wire in a regular pattern. Figure 3-1 shows a typical set of indent rollers and Figure 3-2 shows the indent pattern generated on a section of indented wire. The resulting indent pattern comprises a variety of geometrical shapes (Beck et al., 2019).



Figure 3-1: Manufacture of Indented Wire using Rollers (Beck et al., 2019)

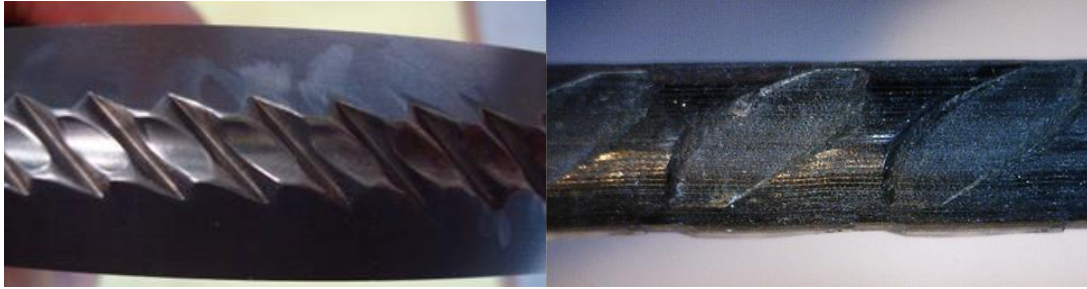


Figure 3-2: Manufacture of Prestressing Wire Indents (Beck et al., 2019)

As stated previously, a high-resolution automated non-contact optical wire indent profiling system was developed for completely and rapidly characterizing all relevant geometrical parameters. Figure 3-3 illustrates a schematic diagram showing the basic features and its operation. The system consisted of a commercially-available laser line scan module, which measured the profile shape of a “slice” along the longitudinal surface of the prestressing wire under testing.

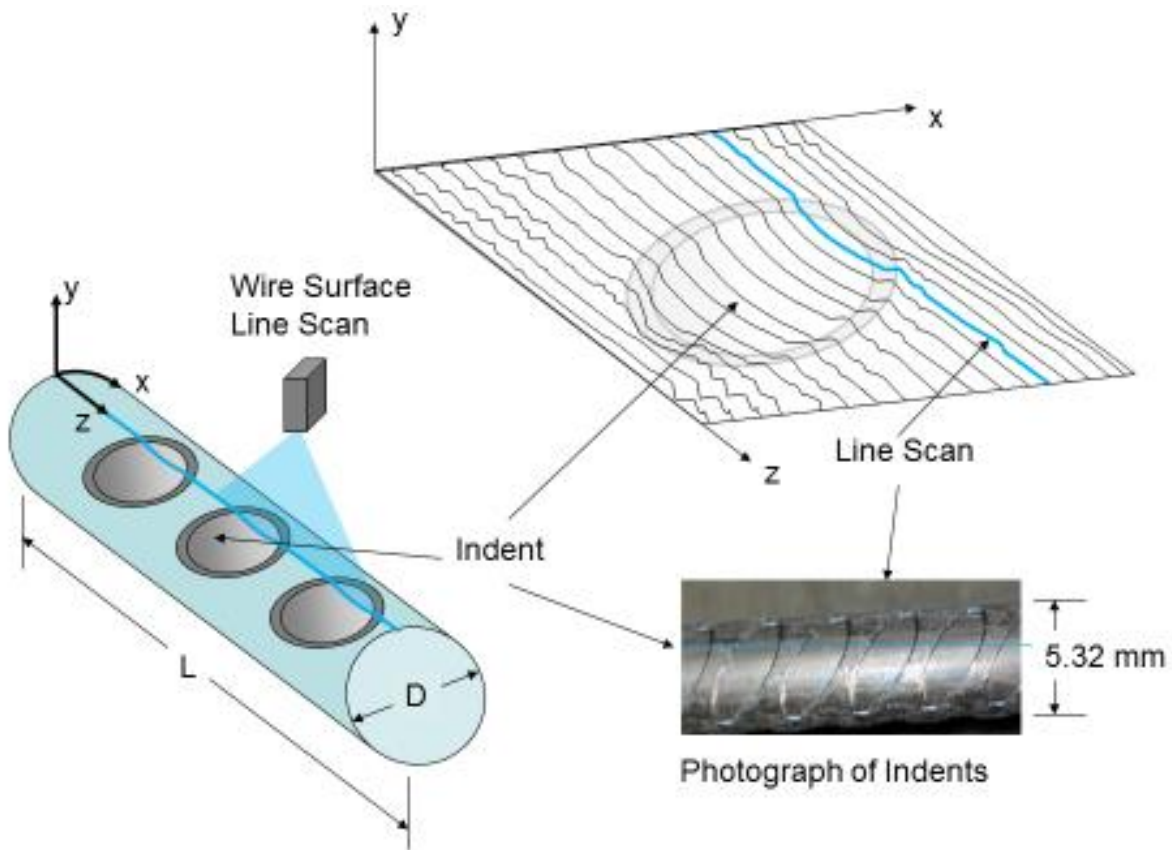


Figure 3-3: Schematic of Indented Wire Measurement (Beck et al., 2019)

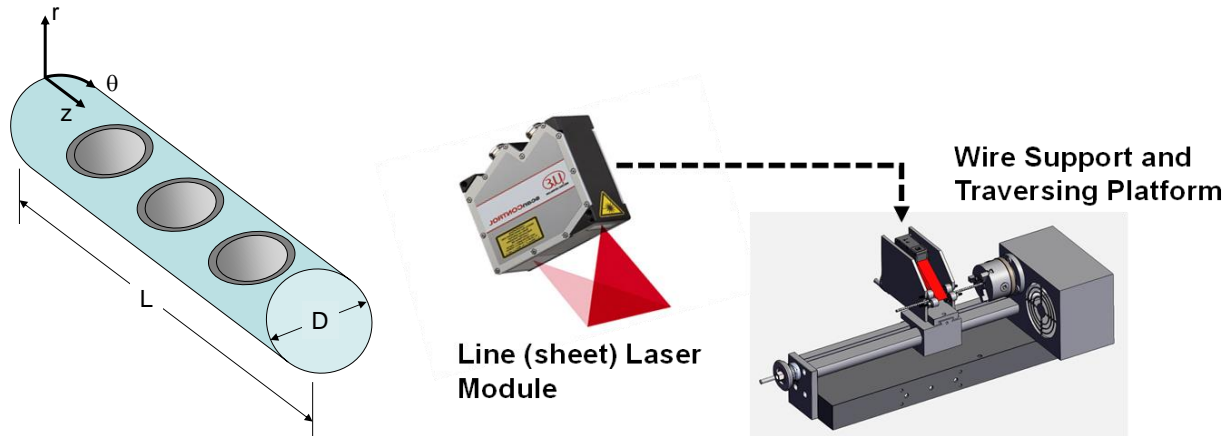


Figure 3-4: Wire Support and Traversing System (Beck et al., 2019)

Additionally, Figure 3-4 shows the traversing system which was designed to measure up to 36in. of indented wire length. The current light sheet system had a spatial resolution approximately an order of magnitude of only a few microns. Figure 3-5 shows a photograph of the overall LabVIEW based indent scanning system. A wide variety of indent shapes can be accommodated by the system.

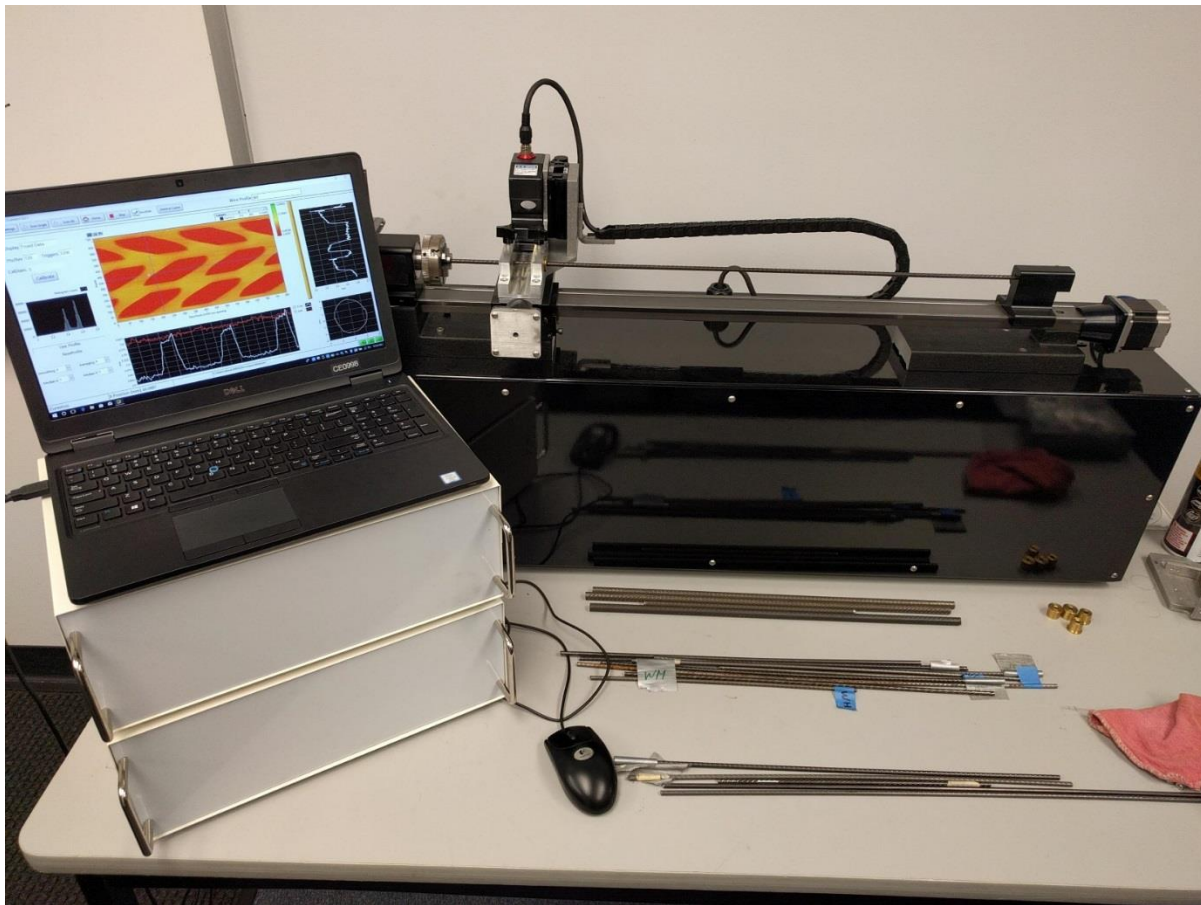


Figure 3-5: Ideal Bilinear and Measured Strain Profile (Beck et al., 2019)

For this study, features of interest that were recorded included: indent depth, indent volume, indent sidewall area, indent sidewall angle, indent length, indent pitch period, indent width, indent distance and indent orientation angle. Figure 3-6 shows graphically the indent features of interest.

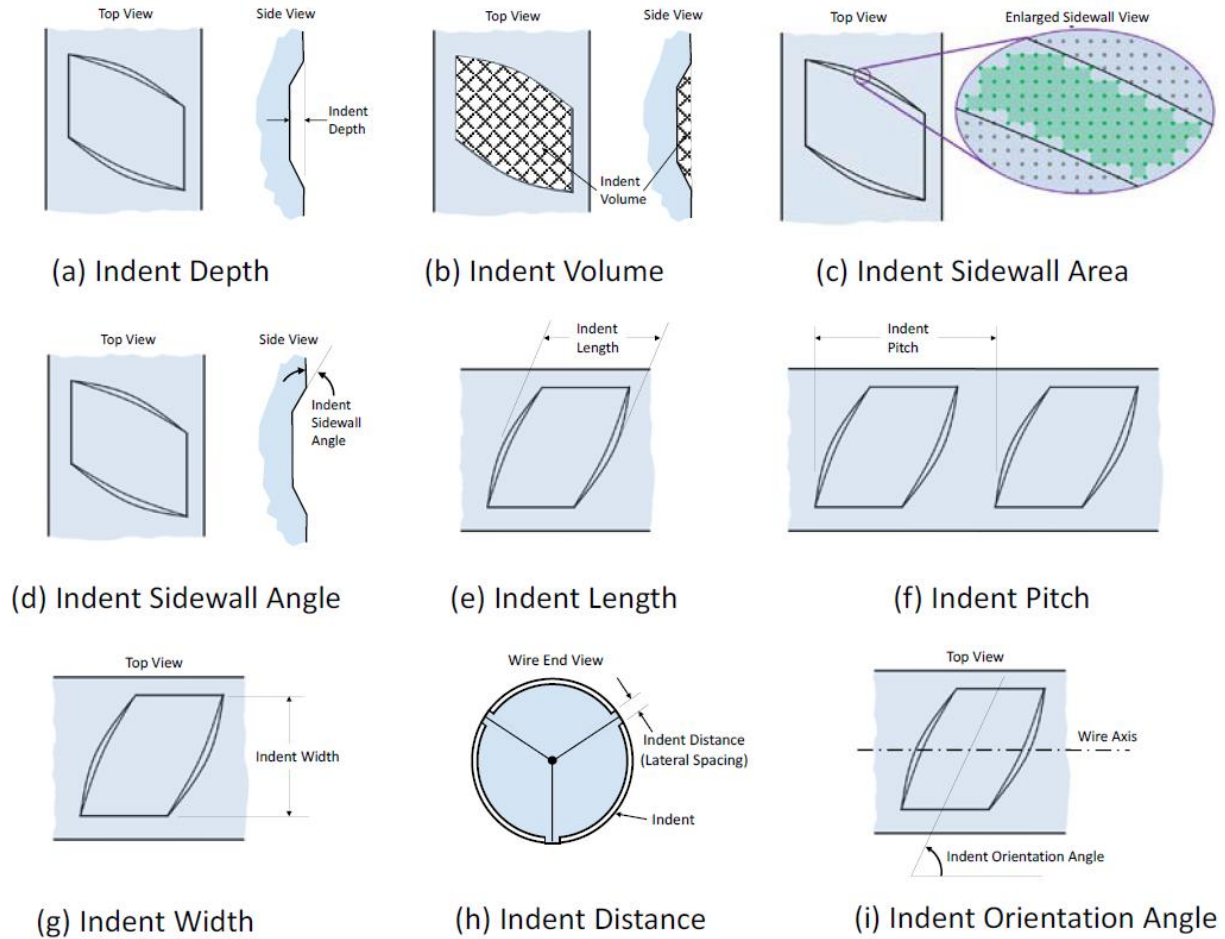


Figure 3-6: KEY 3D Wire Indent Geometrical Features (Beck et al., 2019)

Table 1 shows a summary of indent measurements for all wires used in this research.

Table 1: Summary Indented Wire Measurements (Beck, 2019)

	Average depth (mm)	Edge wall angle (degree)	Edge wall angle (rad)	Side wall area (mm ²)	Volume (mm ³)
WB	0.119	16.45	0.287	2.9217	1.696
WE	0.259	15.1	0.263		
WF	0.163	28.07	0.490	2.45201	2.446
WG	0.066	10.56	0.184	2.31676	0.760
WH	0.164	16.27	0.284	3.96131	2.154
WI	0.094	11.02	0.192	2.8498	1.102
WJ	0.123	11.52	0.201	3.63758	1.428
WM	0.101	16.41	0.286	2.06205	1.252
WP	0.117	29.00	0.506	1.80258	1.745
WQ	0.067	11.58	0.202	2.14883	0.776

For this research study different types of wires were used for each individual set of prisms. All wires test had a diameter of approximately 5.32 mm (0.21 in). Wires types were denoted using the following nomenclature: “WA”, “WB”, “WE”, “WF”, “WG”, “WH”, “WI”, “WJ”, “WM”, “WP” and “WQ”. All reinforcements were low-relaxation type at grade 270ksi steel. The indentation types tested included smooth, spiral, chevron and deep chevron. Material properties for each reinforcement type is given by the manufacturers and shown in Table 2 (Bodapati, 2018).

Table 2: Material properties of each reinforcement type (Bodapati, 2018)

	Indentation type, Diameter	Ultimate tensile force (lb.)	Ultimate Tensile Strength (ksi)	Cross-Sectional Area (in ²)	Modulus of Elasticity, E (ksi)
WA	Smooth, 5.32mm	10,184	293.5	0.0347	27,700
WB	Chevron, 5.32mm	9,712	281.7	0.0345	30,510
WE	Spiral, 5.32mm	9,258	268.6	0.0345	28,570
WF	Diamond, 5.32mm	9,280	269.2	0.0345	29,000
WG	Chevron, 5.32mm	9,376	271	0.0346	30,300
WH	Chevron, 5.32mm	9,438	271.2	0.0348	29,870
WI	Chevron, 5.32mm	9,389	279.5	0.0336	29,000
WJ	Chevron, 5.32mm	9,702	276.9	0.0350	28,600

Shown in Figure 3-7 to Figure 3-17 are microscope images of wire and an associated 3D CAD model (Haynes, 2015).

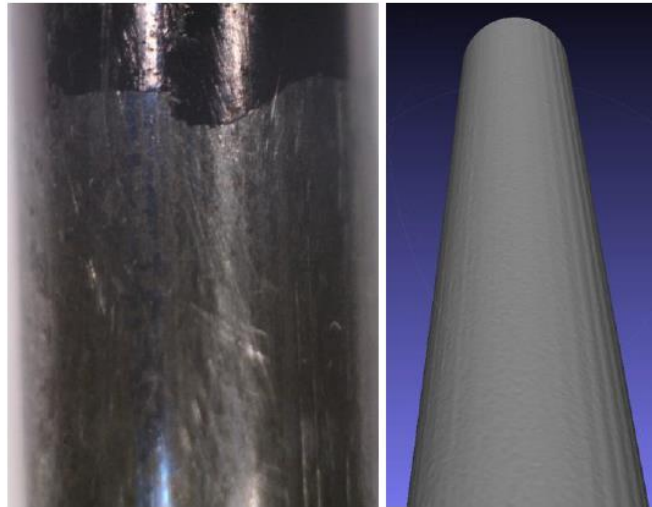


Figure 3-7: WA Wire Type- Microscope Image and 3D Model (Haynes, 2015)



Figure 3-8: WB Wire Type- Microscope Image and 3D Model (Haynes, 2015)

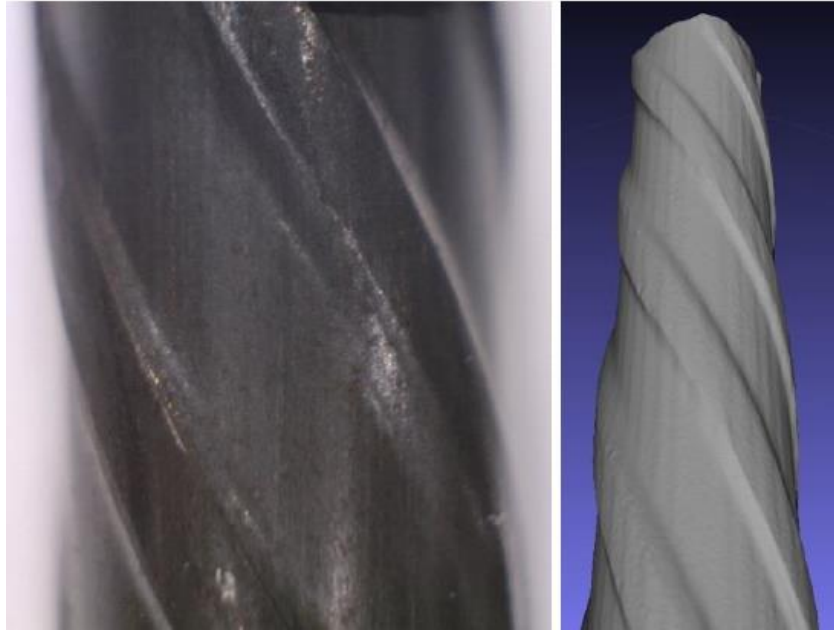


Figure 3-9: WE Wire Type- Microscope Image and 3D Model (Haynes, 2015)

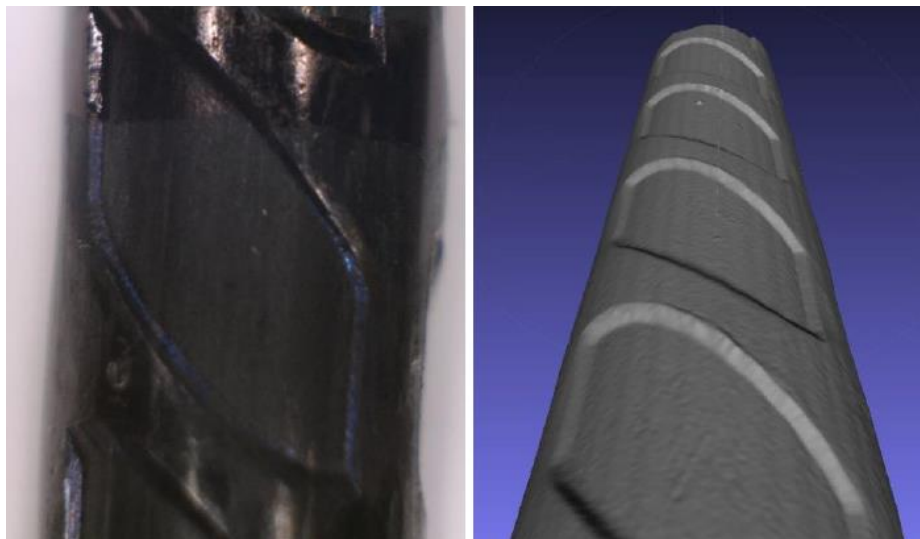


Figure 3-10: WF Wire Type- Microscope Image and 3D Model (Haynes, 2015)



Figure 3-11: WG Wire Type-Microscope Image and 3D Model (Haynes, 2015)



Figure 3-12: WH Wire Type-Microscope Image and 3D Model (Haynes, 2015)



Figure 3-13: WI Wire Type- Microscope Image and 3D Model (Haynes, 2015)



Figure 3-14: WJ Wire Type- Microscope Image and 3D Model (Haynes, 2015)



Figure 3-15: WM Wire Type- Microscope Image and 3D Model (Haynes, 2015)



Figure 3-16: Photo of WP Wire Type



Figure 3-17: Photo of WQ Wire Type

Table 3 shows advanced indent geometrical features for each wire sample which include: the indent projected surface area (PSA), the indent volumetric void (VV), the indent surface area (TFSA), and the indent edge wall surface area (EdgeTFSA). All these parameters were found to have strong correlations to the transfer length created by wire (Haynes, 2015).

Table 3: Advanced indent geometrical features (Haynes, 2015)

	PSA (mm ²)		VV (mm ³)		TFSA (mm ²)		EdgeTFSA (mm ²)	
	Avg.	Std. Dev.	Avg.	Std. Dev.	Avg.	Std. Dev.	Avg.	Std. Dev.
WB	17.58	1.02	2.69	0.58	16.62	1.08	1.72	0.17
WF	16.97	2.44	3.46	0.72	17.25	0.24	1.90	0.10
WG	13.50	1.40	1.26	0.08	12.41	1.02	0.65	0.15
WH	16.92	0.77	2.85	0.04	16.71	0.71	3.16	0.02
WI	14.26	0.02	1.70	0.21	13.76	0.15	2.23	0.32
WJ	16.0	1.13	2.30	0.13	14.65	1.14	2.39	0.97

3.2 Reinforcement Storage

All wires used in this study were stored in separate polyvinyl chloride (PVC) tubes having a length of 25 ft. The tubes were 3in in diameter. Silica-based desiccant packets were placed in the PVC tubes to prevent rusting and preserve the reinforcements “as-received” surface condition for testing. These 25 ft pieces were then cut into shorter lengths approximately 223 in. for testing. Wires WG and WH used in these tests were extracted from existing prisms. The length of these wires was approximately 63 in. After removing from original prisms, WG and

WH type wires were then cleaned using the following procedure as described in a study by Arnold (2013):

1. Rinse with water from a hose with a spray nozzle;
2. Spray with Deoxidine 7310 and water solution and scrub steel surface by hand;
3. Rinse with water from a hose with a spray nozzle;
4. Spray with Deoxidine 7310 and water solution and let the sample sit approximately 15 seconds;
5. Scrub steel surface using a brass brush for approximately 30 seconds;
6. Rinse with water from a hose with a spray nozzle;
7. Dry steel specimen with clean cloth; and
8. Stand specimen with clean cloth.



Figure 3-18: Chemical used in Reinforcement Cleaning Process (Deoxidine 7310) (Arnold, 2013)



Figure 3-19: WG Wire Type Before (left) and after (right) Cleaning

Figure 3-18 and Figure 3-19 show the material used for cleaning the wires and give us the visual effect of cleaning process. Figure 3-20 shows the reinforcement storage rack that was used for this study. Since all of the wires denoted as WG and WH were used in previously described testing, for this study all samples were extracted from existing prisms. A procedure was performed using a machine for compressive testing. All wires which were extracted from existing prisms had a length of approximately 63 in.



Figure 3-20: Reinforcement Storage Rack (Bodapati, 2018)

After extracting the wires from the existing prisms, it was observed that the indents typically contained residual along one side of the indent at each wire end (Figure 3-21). Upon further inspection it was noticed that the concrete appeared to have been crushed, and that the side of the indents that contained the concrete was different at opposite ends.

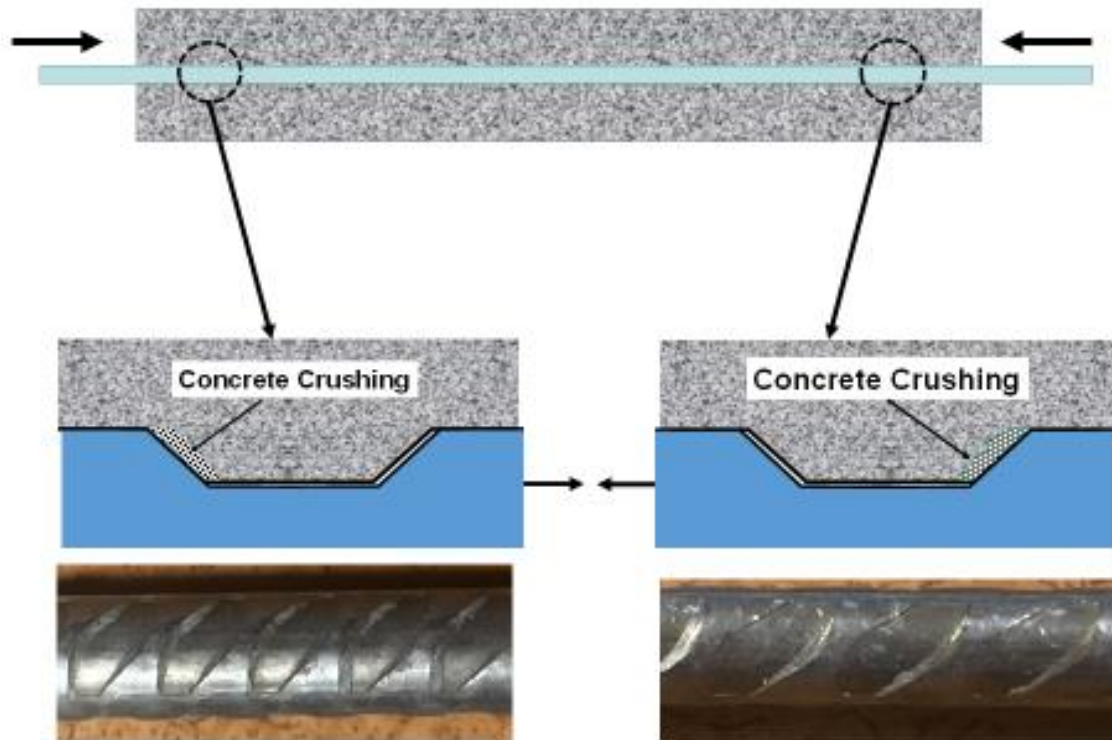


Figure 3-21: Hypothesized Sidewall Concrete Crushing (Beck, 2019)

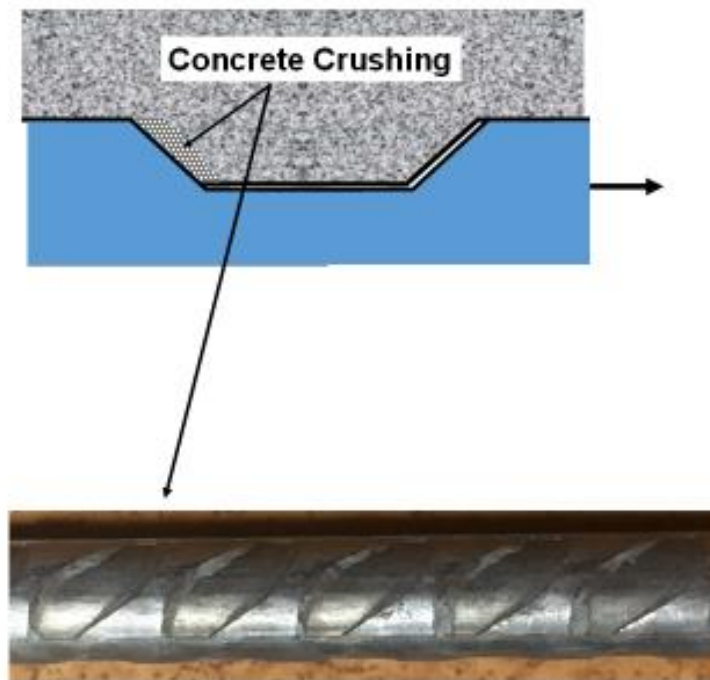


Figure 3-22: Observed Crushed Concrete Residue-Left side of the WH Wire Type (Beck, 2019)

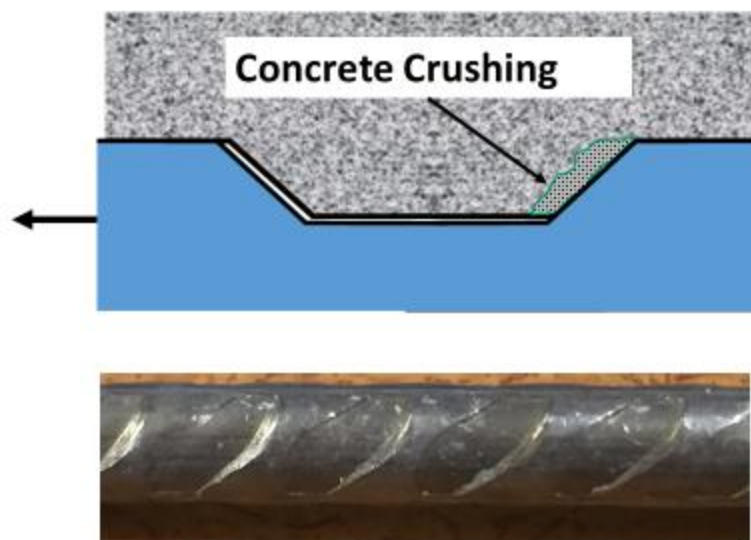


Figure 3-23: Observed Crushed Concrete Residue-Right side of the WH Wire Type
 Figure 3-22 and Figure 3-23 show the observed crushed residue for both sides of the wire.

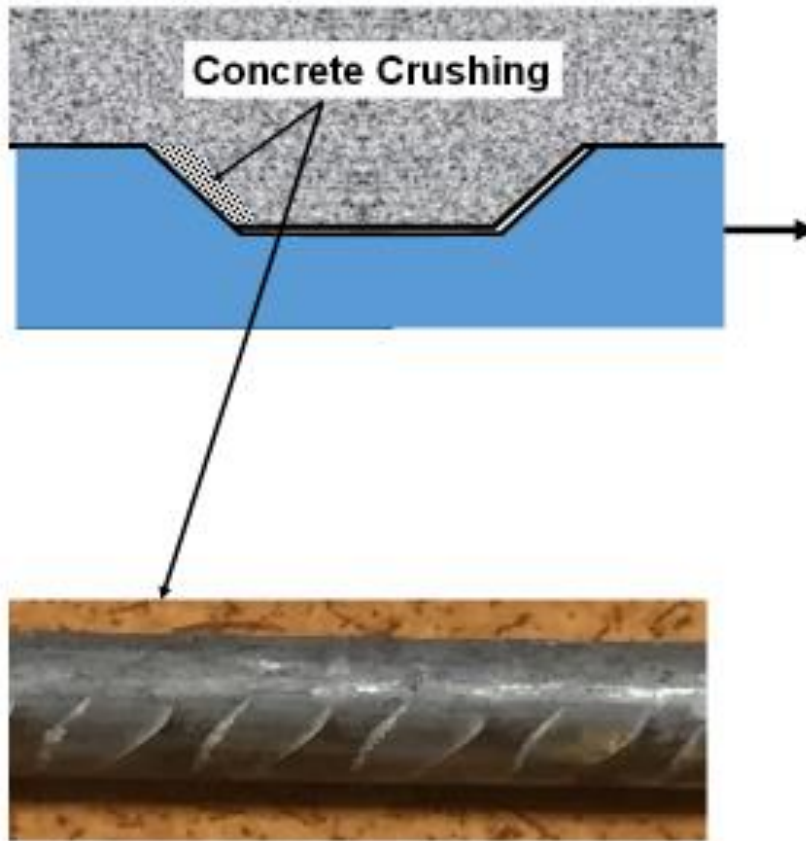


Figure 3-24: Observed Crushed Concrete Residue for Wire Type WG

3.3 Concrete Materials and Mix Design

This section will be dedicated to the materials which were used in this study.

3.3.1 Cement

Monarch Type III cement was used for all concrete mix designs used in this study. The cement was obtained from Concrete Materials Inc. in Overland Park and stored in 55-gallon drums until needed.

3.3.2 Aggregates

A crushed gravel from Tucson, Arizona with 100 % passing the $\frac{3}{4}$ in sieve for the first mixture was used for the present study (Figure 3-25 and Figure 3-26). Additionally, granite was used for the second mixture with 100% passing the $\frac{3}{8}$ in sieve (Figure 3-27), and a local pea gravel (uncrushed gravel) with a $\frac{3}{4}$ in. max-sized aggregate was used for the third mixture (Figure 3-28). A locally available natural silica sand was also used for this research (Figure 3-29). Prior to the casting operation, all of the material was dried in an oven to gain consistency in mixture proportions. The aggregates were dried in an oven at 200 deg Fahrenheit for approximately 24 hours to ensure the moisture content was zero. After drying, the aggregates were then stored

in a dry storage container until they were used for batching. Two hours before the mixing operation, the materials were weighed and stored in buckets located in a temperature-controlled room until the concrete was batched. This procedure ensured consistency in batch temperature and almost the same slump for all mixes.



Figure 3-25: Tucson Small Crushed Gravel Aggregate (CA3) used in the study



Figure 3-26: Tucson Large Crushed Gravel Aggregate (CA2) used in this study



Figure 3-27: Granite Aggregate (CA4) used in this study



Figure 3-28: Uncrushed Pea Gravel Aggregate (CA1) used in this study



Figure 3-29: Fine Aggregate (sand) used in this study

3.3.3 High-Range-Water Reducing Admixture

To achieve the desired concrete consistencies (slump) with low-water/cementitious (w/c) ratio, ADVA CAST 530 was used for all tests. This high-range-water-reducing admixture is a polycarboxylate-based superplasticizer. ADVA CAST 530 complies with ASTM C494 Type A and Type F and ASTM C1017 Type I and can produce concrete with extremely high levels of workability without segregation. ADVA CAST 530 was used to produce concrete with very low water/cement ratios with normal levels of workability. ADVA CAST 530 is ideal for use in precast and prestressed applications where concrete needs to achieve high early strength along with high levels of workability. Normally the range of using ADVA CAST 530 is from 3 to 10 fl oz/100 lbs of cement.

3.3.4 Mix-design during lab phase

Concrete for pre-tensioned concrete prisms was batched using a Mud Hog concrete mixer (Figure 3-30). Three different mixtures were used to cast concrete prisms. Tables 4-6 lists the materials which were used per ft³ in each concrete mixture. Mix-Design #1 consists of Tucson (crushed) aggregate, two type one with 3/4 in max aggregate size sieve. Mix-Design #2 consisted of granite as aggregate. Mix-Design #3 consisted of a local pea gravel (un-crushed aggregate). 1.98 ft³ of concrete was cast every time.

Table 4 presents Mix-design #1

Table 4: Mix design #1

Material	Weight (lbs.) /yd ³
Cement	813.8
Water	260.4
Large Crushed Gravel (CA2)	897.8
Small Crushed Gravel (CA3)	538.7
Sand (SSD)	1436.5
HRWR	81 fl.oz/yd ³

Table 5: Mix design #2

Material	Weight (lbs.) /yd ³
Cement	813.8
Water	260.4
Crushed Granite (CA4)	1447
Sand (SSD)	1447
HRWR	81 fl.oz/yd ³

Table 6: Mix design #3

Material	Weight (lbs.) /yd ³
Cement	780
Water	249.6
Uncrushed Pea Gravel (CA1)	1526
Sand (SSD)	1526
HRWR	81 fl.oz/yd ³



Figure 3-30: Concrete Mixer

For this study, a consistent mixture of Type III cement with a water-cement ratio of 0.32 was used for all constructed prisms except for prisms casted with WE wire. For these prisms a water/cementitious ratio of 0.38 was used for compressive strength 3500 psi, 4500 psi and 6000 psi. 12000 psi compressive strength was reached after six days and water/cementitious ratio was 0.26.

4. Methodology

4.1 Experimental Facility and Prism Casting Procedure

Original prestressed concrete prisms were fabricated at Kansas State University under a different study (Bodapati, 2018), and these prisms had a reinforcement edge distance of 1 in. Additionally, the center-to-center spacing between wires within the prism was 1.5 in. Figure 4-1 shows the cross section of a typical prism with 1 in edge distance. For the current research study, three prisms with varying cross sections were used which included a center-to-center spacing of 2.0 in. between wires with a maximum reinforcement edge distance of $\frac{3}{4}$ in. and a minimum edge distance of $\frac{1}{2}$ in. A primary difference between the original prisms developed at Kansas State University and the ones utilized in this study was the reinforcement edge distance which was reduced by 25 % to 50 % of the original dimensions. The wires in the prisms were each tensioned to 7000 lbs. The average initial compressive stress for edge distance $\frac{3}{4}$ in. was equal to: $28000 \text{ lb.} / (3.5 \text{ in.})^2 = 2285 \text{ psi}$. For prisms with a $\frac{5}{8}$ in. edge distance, the value of stress was: $28000 \text{ lb.} / (3.25 \text{ in.})^2 = 2650 \text{ psi}$ which was 59 % of the 4500 psi concrete release strength. For prisms with $\frac{1}{2}$ in. edge distance, average initial compressive stress was it was 3110 psi, which was approximately 89 % of the 4500 psi concrete release strength. This value is significantly into the nonlinear range of the concrete.

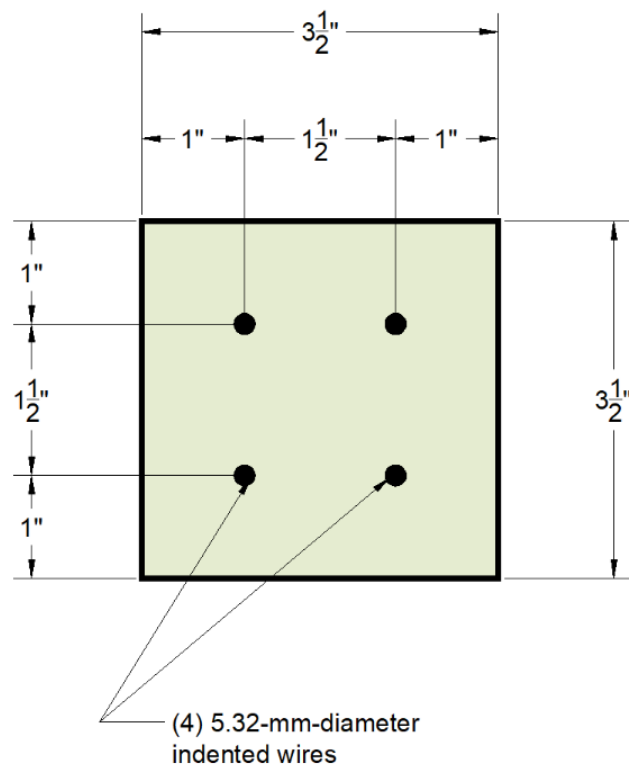


Figure 4-1: Original Pre-tensioned Concrete Prism -1in Edge distance (Bodapati, 2018)

Figure 4-2 shows the prestressing bed with three sets of steel frames, each resulting in a prism with different reinforcement edge distance. Multiple tests were conducted on pre-tensioned concrete prisms cast in these steel frames. As stated previously, four prestressing wires were symmetrically embedded into each concrete prism, resulting in a typical center-to-center wire spacing of 2.0 in.

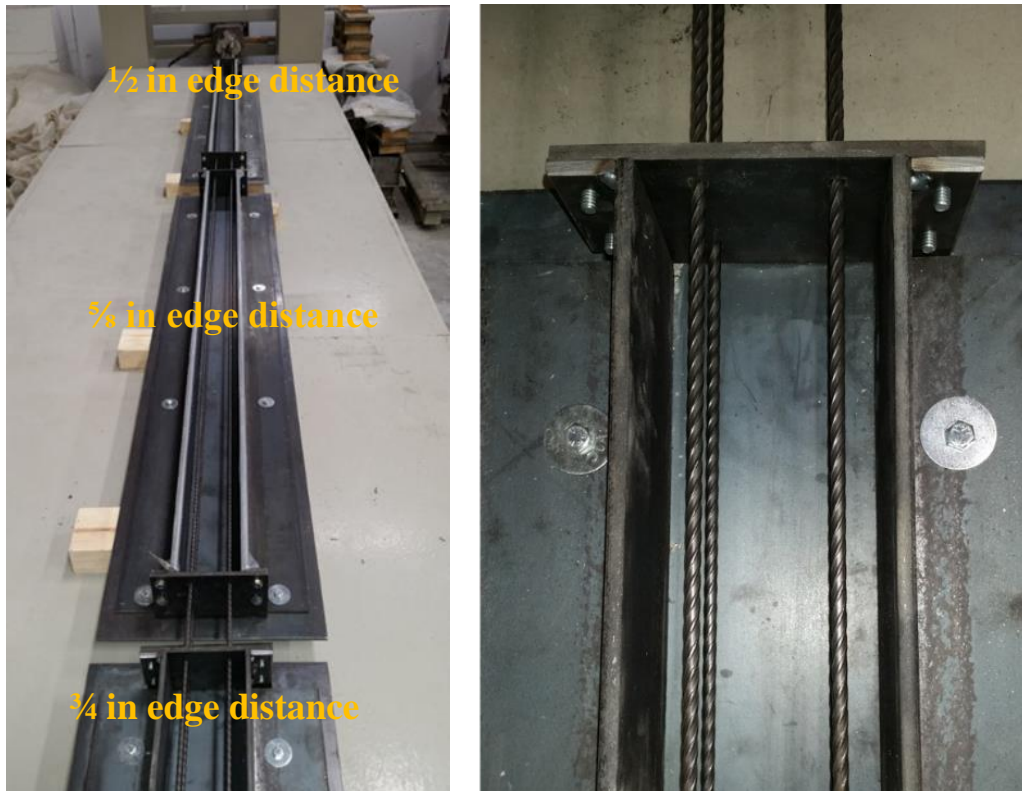
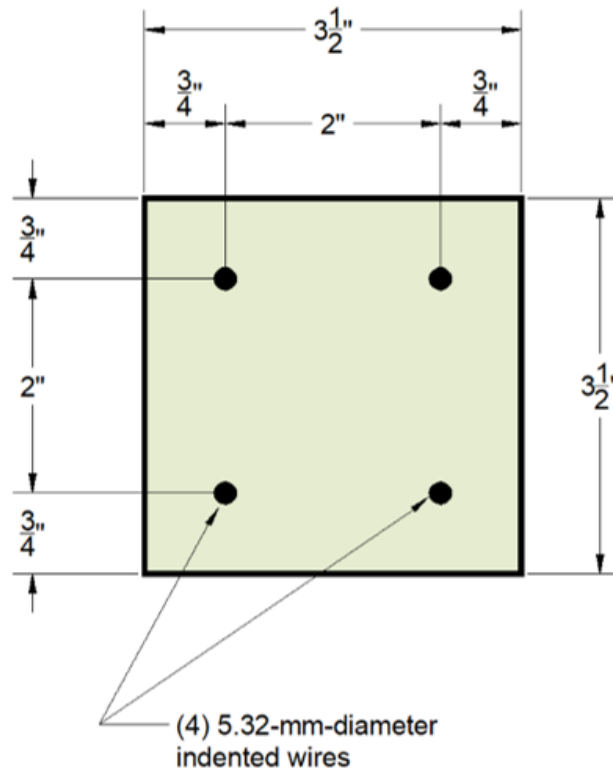
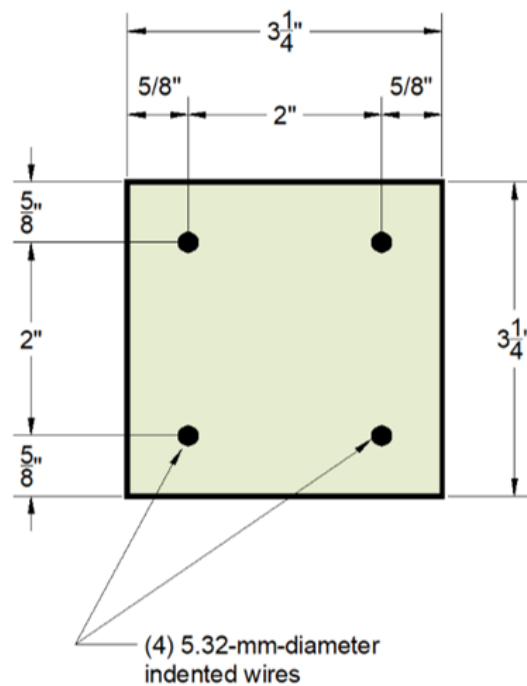


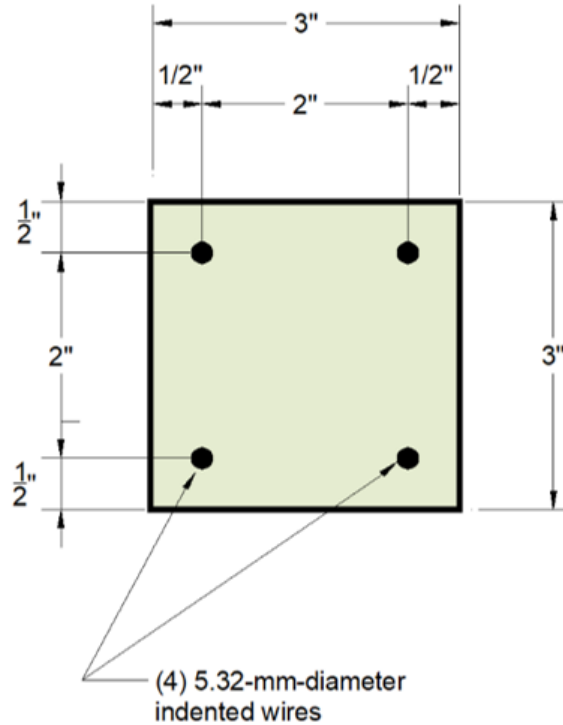
Figure 4-2: Steel Frames (Savic, 2018)



(a) Prism having $\frac{3}{4}$ in Edge Distance



(b) Prism having $\frac{5}{8}$ in Edge Distance



(c) Prism having $\frac{1}{2}$ in Edge Distance

Figure 4-3: Prisms with Different Cross Sections (Savic, 2018)

4.2 Experimental Set-up

4.2.1 Prestressing Frame and Load Cells

In the pre-tensioning frame, wires within each prism were tensioned between two abutments prior to the casting of concrete. The abutments were fixed at the ends of a prestressing frame and Figure 4-4 illustrates the pre-tensioning process that was used in this study. A special jacking assembly was also developed at Kansas State University and used for this study. The mechanical gear jack was attached to the metal frame which allowed gradual tensioning and release operations. Jacking of the steel prestressing wires occurred at the end of the steel frame referred to as the “Live End” as shown in Figure 4-6.

The live end of the prestressed bed was the end of the prestressing frame where stressing operations occurred and total jacking force was measured. However, the dead end of the prestressed bed was where individual wire forces were measured by load cells (Figure 4-5). The load cells used in this study were S-type transducers which converted force into a measurable electrical output. These strain gauge load cells had precision accuracies that were within 0.25 % of full scale. During the prestressing operation, both the total jacking force and the force in each wire were monitored as verification of the prestressing force at both ends of the prestressed bed (live and dead end) which ensured the desired stress in each prestressing tendon was achieved.

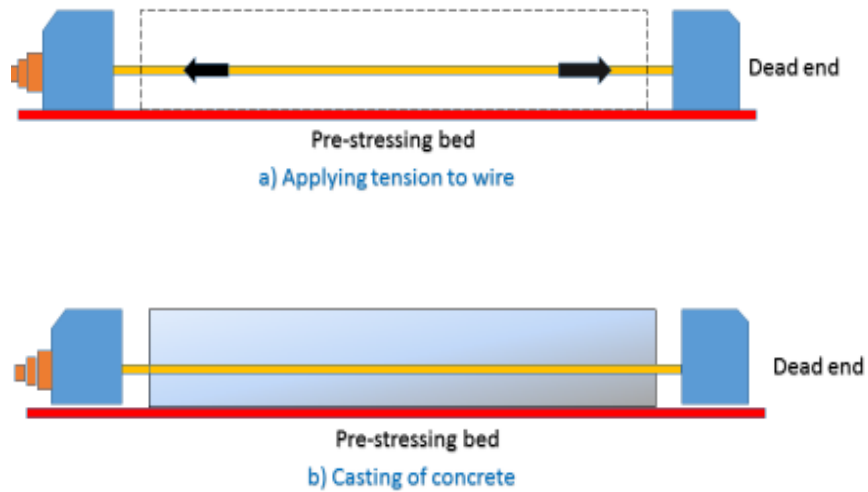


Figure 4-4: Stages of Pre-tensioning

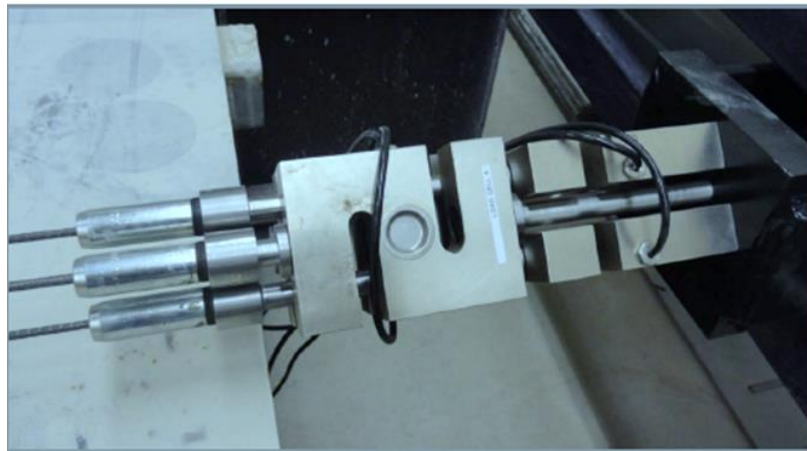


Figure 4-5: Load Cells at Dead End of Prestressing Bed



Figure 4-6: Prestressed Jacking arrangement at the Live End



Figure 4-7: Digital Display of Prestressing Forces Measured by Load cell

Figure 4-5 shows the four load cells that were used were to measure the prestressing force in each individual wire at the Dead End.

Wires WG and WH were extracted from the prisms which were cast by Bodapati, and the length of the wires were approximately 63 in. For these wires, the original setup was adjusted by inserting additional prestressing splice chucks between the first and second prisms, and between the second and third prisms. At the end of the dead end of the third prism, shorter pieces of wires were required with additional prestressing chucks as shown in Figure 4-8, Figure 4-9, and Figure 4-10.



Figure 4-8: Adjusted Setup-Additional Chucks between First and Second Prism

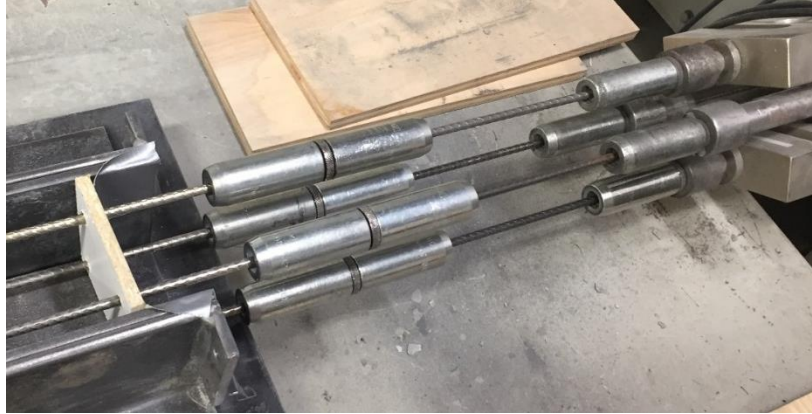


Figure 4-9: Adjusted Setup-Dead End of the Prestressed Bed

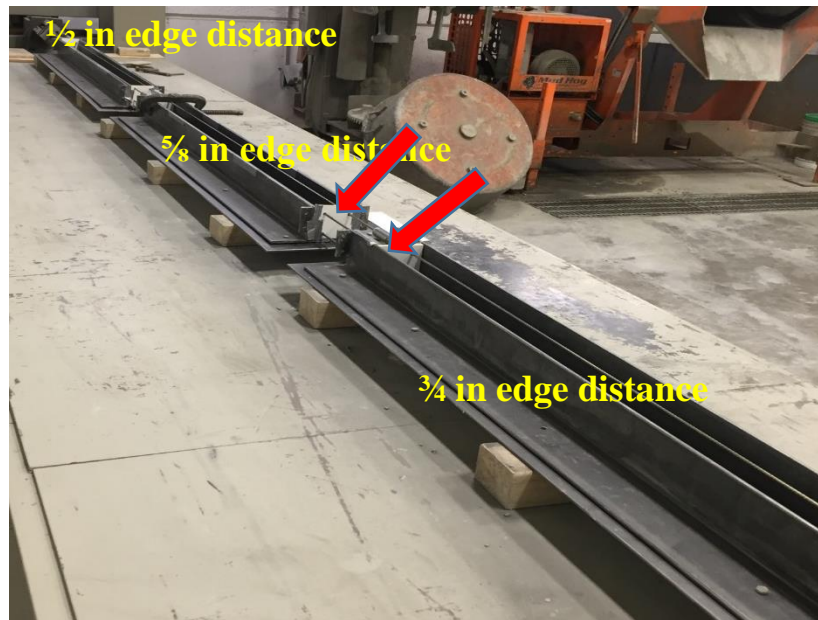


Figure 4-10: Adjusted setup of Prestressed Bed

4.3 Casting Procedure of Prisms

The casting procedure described was used for all prisms constructed during this study. All materials described in the previous chapter for concrete mix were oven dried, and weighed appropriately, and mixed in a horizontal-shaft electric concrete mixer. Typical mixtures utilized a 0.32 w/c ratio, and the desired consistency (slump) was achieved by slight adjustment of the ADVA CAST 530 dosage. Slump at the time of specimen casting was between 6 in. and 8 in, and the slump was measured prior to each casting operation. Concrete was then placed in the three-steel form on the prestressing bed and consolidated using a flexible-shaft internal vibrator with a 1in diameter head. After casting was completed, the concrete prism specimens were covered with a poly tarp to retain the internally-generated heat and increase the strength-gaining rate of the concrete. Figure 4-11 shows placement of the concrete in the steel prism.



Figure 4-11: Casting the Prestressed Concrete Prisms

4.4 Sure Cure System

In addition to casting the prisms, 12 4 in x 8 in compression strength cylinders were also cast simultaneously using the Sure Cure System which allowed the cylinders to have the same temperature as the prisms. The Sure Cure curing control system consisted of three major parts: (1) a Windows based computer; (2) USB port used to transfer data to and from the USB flash drive to a 485 converter; and (3) the I/O cabinet. The I/O cabinet contained associated cable connectors which included blue connectors for thermocouples (Type T), and black connectors was for on-off heating of cylinders. A black multi-conductor cable with green ends were used to connect between the I/O cabinet and the USB to 485 converters. The study used 6 channels to collect data from 12 cylinders.

Figure 4-12 shows 12 cylinders used for the study in a temperature-controlled environment using the Sure Cure mini controlling system. Figure 4-13 shows the typical temperature plot of prisms and cylinder specimens.



Figure 4-12: Twelve Concrete Cylinders under Temperature Control through Sure Cure Mini Controlling System

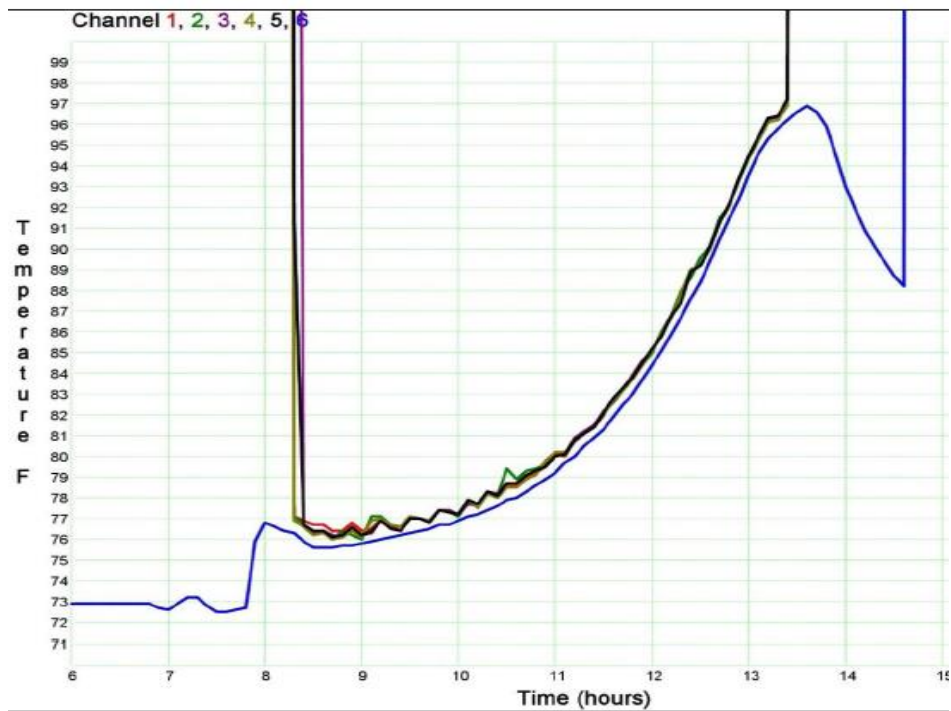


Figure 4-13: Typical Temperature (F) Plot of Prism and Cylinder Specimens

Figure 4-14 shows the example of making cylinders in-situ. All 12 cylinders developed for this study were capped and tested using a Forney 250,000-pound-capacity compression testing machine as shown in Figure 4-15.



Figure 4-14: Making the Sure-Cure Cylinders



Figure 4-15: Testing the Cylinder Using Forney machine

During the study, the Forney machine was retrofitted to include a VFD Automatic System which gathers, stores, and transmits data.

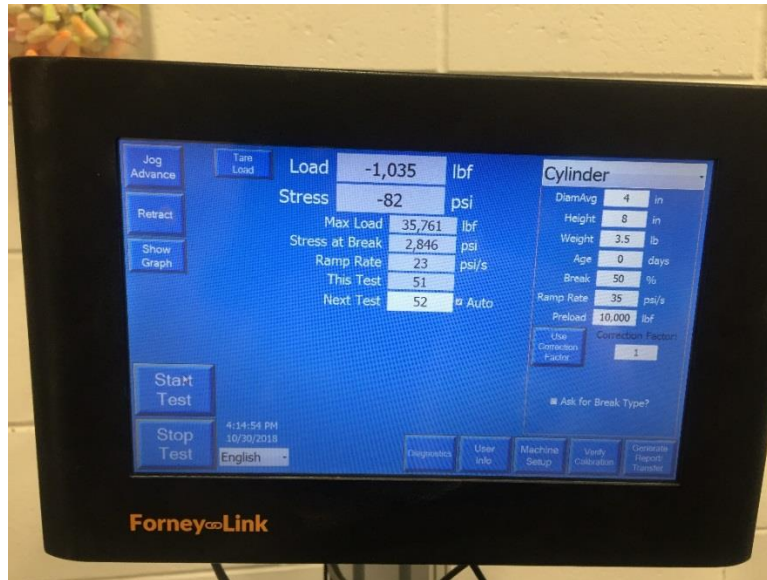


Figure 4-16: Example of Measured Compressive strength of Cylinder

As illustrated in Figure 4-16, a touchscreen was used to control and configure test set-up of the Forney machine. Five hours after casting, cylinders were tested using the Forney machine and tests were repeated every 45 minutes. The desired strength of 4500 psi was reached approximately after 8 hours and 6000 psi after 11 hours, when the process of de-tensioning commenced.

4.5 Testing procedure and Transfer length Measurement

As stated previously, four wires were embedded into each concrete prism. The spacing between wires was 2.0 in. for all three specimens cast in series on the prestressing bed. The wires were initially tensioned to 7000 lbs. and gradually de-tensioned when the desired compressive strength reached the specified prescribed values of 3500 psi, 4500 psi, 6000 psi, and 12000 psi for each casting. In addition to observing and recording cracking/splitting of prisms, measurements of longitudinal surface strain were recorded using a Continuous Scanning/Traversing (CST) strain measurement system (Beck, 2015).

In order for prestressed concrete railroad ties to function adequately in the field, and to ensure safety, the prestressing force must be fully introduced into the railroad tie at a location well before the rail load is applied. The length required to transfer the prestress force into the concrete member is well known as the “Transfer length”.

A 3D CAD drawing of Continuous Scanning/Traversing (CST) strain measurement system is shown in Figure 4-20 (Beck, 2015). This device is also called a Laser-Speckle Imaging (LSI) system. The LSI system can serve as a tool to evaluate the effect of process and material changes on prestressing steel bond. It utilized a laser-speckle imaging (LSI) principle for making the required local measurements of surface displacement, from which local strain is determined. The device has an equivalent gauge length of 6.0 in, and a strain resolution of about +/- 20 microstrain (Beck, 2010).



Figure 4-17: Laser Speckle Imaging System (Beck, 2010)

The laser-speckle device was used to scan the top surface of a concrete prism before and after de-tensioning, and automatically plot the strain profile and determine the transfer length using a least-squares algorithm (Zhao, 2012). For this purpose, the automated traversing system with translating LSI sensor was used. The system included a 24 in scan length of measurement on each end of prism end. The average time for 60 distributed strain measurement per scan was 1 minute, with around 0.010 in repeatable sensor traverse positioning accuracy. The LSI sensor and traversing system were connected to a Laptop computer. The traverse control and data acquisition, and data processing were conducted using the same Laptop computer through a LabVIEW interface (Beck, 2010).

For transfer length measurement two scans were required one prior to de-tensioning, and the second subsequent to the cutting after de-tensioning operation. Figure 4-17 shows a practical implementation of the automated traversing system (Beck, 2015). Figure 4-19 presents measuring the transfer lengths in the laboratory phase. When the raw images were captured, the surface strain was calculated and plotted automatically (Beck, 2010).

When the surface strain profile was obtained, the transfer length can be extracted using 95% Average Maximum Strain (95% AMS) method, or the Zhao-Lee least squares algorithm (Zhao, 2012). This algorithm is based on a least-squares technique and provides unbiased estimation of the transfer length. The approach of this method was to find the optimal location of the intersection point that minimizes a target function, and target function is generated by assuming the surface strain to be bilinear with the rounding effect of the gauge length of the sensor taken into account (Beck, 2010).

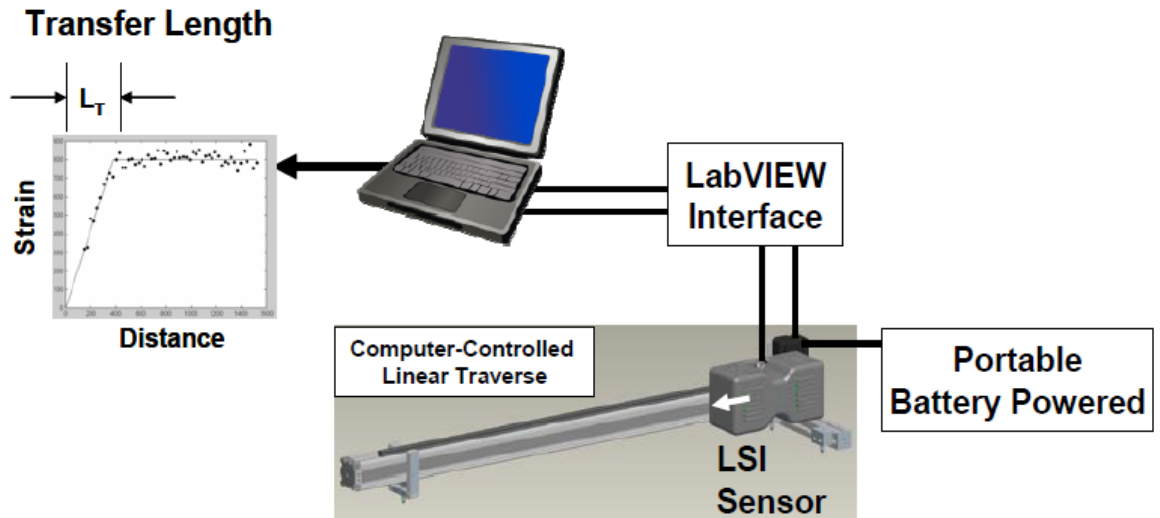


Figure 4-18: Overall Automated LSI Sensor Traversing System (Beck, 2010)



Figure 4-19: Measuring the Transfer Lengths (Savic, 2018)

A laptop computer provided USB and RS 232 communications with the traverse system and the LSI sensor. Position of the traverse control and data acquisition were in one software package, and the data processing were conducted at the same laptop (Beck, 2010). Figure 4-20 shows the traverse control and LabView data acquisition interface.

Two scans are required for transfer length measurement one prior to de-tensioning and one subsequent to the cutting operation after de-tensioning procedure. The surface strain was calculated and plotted automatically after the raw images are captured.

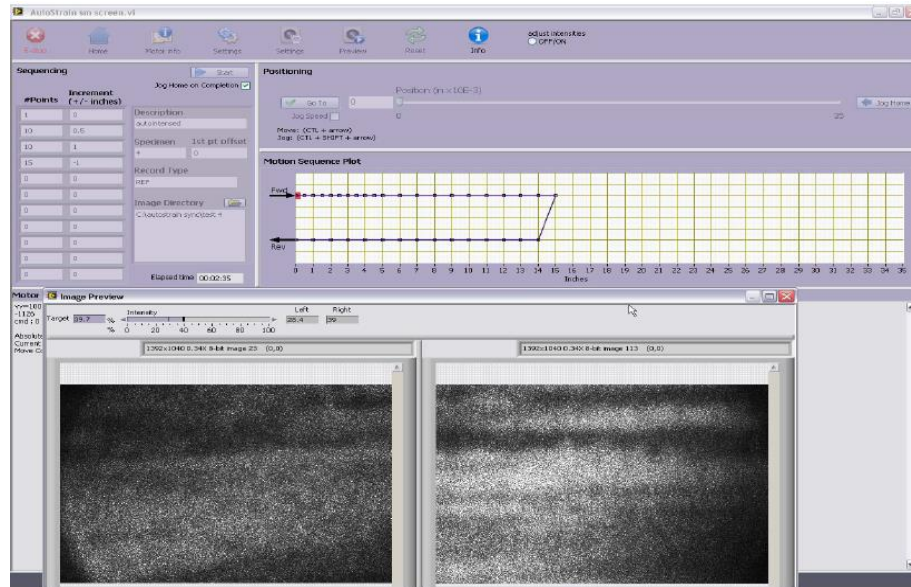


Figure 4-20: Traverse Control and LabVIEW Data Acquisition Interface (Beck, 2010)

Each prism provided two measurements of transfer lengths (live and dead end) and provided approximately eight independent splitting tests of edge distance (four wire cover tests on each end) for a given release strength.

4.6 Assessment of Prism cracking

Each prism provided eight different experimental results for assessing the effect of cover, corresponding to four wire cover tests on each end of the prism. Photographs of the prism surfaces were documented for quantitative and qualitative assessment of cracking behavior. Cracking photos show the position on the beam of each crack, bottom, front, top and back position for live end of the prism and the same for the dead end. Photographs of the prism ends, and side wall surfaces provide the location and distribution of all surface cracking phenomena.

In addition to simply specifying the number of wires that were observed to exhibit cracking out of the total of eight wires per prism, the maximum crack widths and overall crack lengths were carefully measured and documented for all prism tests as shown in Figure 4-21.


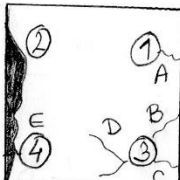
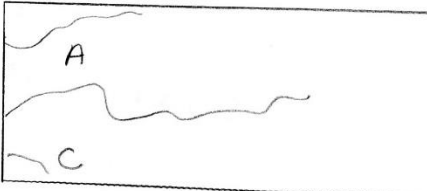

W/P	11/16/2017	6000psi	5/8 IN EDGE DISTANCE
A - WIDTH 0.010 IN CRACK LENGTH - 4.4 IN B - WIDTH - 0.010 IN CRACK LENGTH - 14.6 IN C - CRACK WIDTH 0.010 IN CRACK LENGTH 2.5 IN D - CRACK WIDTH - 0.010 IN CRACK LENGTH - 2.2 IN		DEAD END SPALLING PRODUCED BY FORM DAMAGE	
			
E - CRACK WIDTH 0.010 IN CRACK LENGTH - 2.1 IN			

Figure 4-21: Example of Crack Assessment Form

A crack Comparator similar to that shown in Figure 4-22 was used to measure maximum crack width for each observed crack. A crack Comparator can monitor cracks from 0.004 to 0.26 in. Crack length was measured by tracing out the path of a given crack with a piece of string and measuring the overall path (string) length including branches. In cases where spalling was observed, the crack width was assigned an arbitrary width value of 0.20 in. Crack area was defined as the total crack length multiplied by the maximum crack width.



Figure 4-22: Measuring Crack Width (Savic, 2018)

Figure 4-23 shows the position of cracks on each end of the prism (live and dead end), marked with the permanent red marker.



Figure 4-23: Example of Prisms and Observed Cracking ($\frac{1}{2}$ in edge distance)

Figure 4-24 shows the images which were taken after measuring the values of crack width and crack length. These images indicate the position of cracks on each side surface of the prism (TOP, BOTTOM, FRONT, BACK), shown below the corresponding live end and dead-end locations. For clear identification, the cracks were traced with permanent red marker. All prisms were investigated after three months in order to get long-term data. End-splitting cracks often formed at the time of de-tensioning operation, but some of them can develop during the first few weeks after de-tensioning procedure due to the sustained lateral stresses exerted by the prestressing tendons. The capability of the concrete to resist these bursting stresses without cracking was determined (in this study) to be primarily a function of distance from the reinforcement to the nearest parallel edge of concrete, the aggregate type and maturity of the concrete.

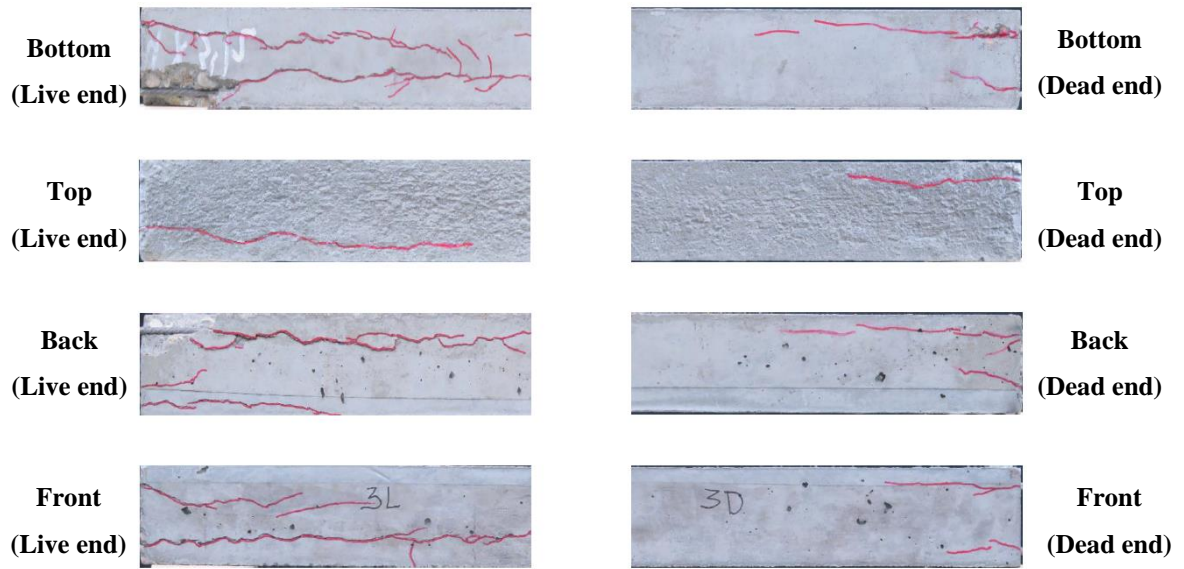


Figure 4-24: Typical Picture of Observed Cracking Live and Dead end (Savic, 2018)

5. Results

In order to determine which parameters have the most effect on longitudinal splitting between prestressing tendons and concrete, strain profiles, crack area and crack length were systematically evaluated for prisms having different release strengths of concrete and different tendon edge distances. Prisms with no cracks had a well-developed plateau region of approximately uniform strain. Prisms with observed cracking experienced loss of bond and often had non-uniform strain profiles with shorter or no strain plateaus. In addition to the number of wires that exhibited cracking, overall crack lengths were measured for each prism having a given release strength and edge distance. From this information, a representative crack area was also determined. This crack area was defined as the total crack length multiplied by the maximum measured crack width.

In addition, photographs of the dead and live end of the prisms were taken for all prisms for quantitative and qualitative assessment of cracking behavior. Photographs of the prism's side surfaces were also taken for the prisms fabricated with wire type WE, which had a spiral indentation pattern. Photographs of the prism ends and side wall surfaces (WE wire) provide the location and distribution of all surface cracking phenomena. Each prism test comprises a total of eight different experimental results for assessing the effect of edge distance, corresponding to four wire cover tests on each end of the prisms. For clear identification in photographs the cracks were traced with a permanent red marker.

Table 7 shows the number of prisms fabricated with each different type of concrete mixture, release strength and wire type. The total number of prisms fabricated and evaluated in this research program was 141.

Table 7: Number of Prisms with Each Wire Type, Concrete Mixture, and Release Strength

Wire Type	Tucson Coarse Aggregate				Granite Coarse Aggregate		Pea Gravel Coarse Aggregate	
	3500	4500	6000	12000	4500	6000	4500	6000
WA	-	-	3	-	-	-	-	-
WB	-	3	9	-	3	3	3	-
WE	3	3	3	3	-	-	-	-
WF	-	3	3	-	3	3	3	-
WG	-	3	-	-	3	-	-	-
WH	-	3	-	-	3	-	-	-
WI	-	3	3	-	3	3	3	-
WJ	-	3	3	-	3	6	3	-
WM	-	3	3	-	3	3	3	-
WP	-	3	3	-	3	3	3	-
WQ	-	3	3	-	3	3	3	-

Total: 141 prisms

5.1 Transfer lengths and Prism Cracking-Mix#1

The following data presents the results for different concrete release strength and different types of wires using the concrete mixture with crushed gravel aggregate.

5.1.1 Mix#1-WA wire type, Release strength 6000psi

The test was conducted with WA wire type with concrete release strength of 6000 psi. WA wire type performed very well with no observed cracks for $\frac{3}{4}$ in and $\frac{1}{2}$ in edge distance, and for $\frac{5}{8}$ in. edge distance a 0.04 in² crack area and a 4 in. crack length were observed as shown in Figure 5-6 and Figure 5-7. The values of transfer lengths were higher on the $\frac{3}{4}$ in edge distance than on the prisms with different types of indent. Figure 5-1, Figure 5-2, and Figure 5-3 show the longitudinal strain profiles on the prisms with $\frac{3}{4}$ in, $\frac{5}{8}$ in. and $\frac{1}{2}$ in. edge distances. Additionally, Figure 5-4 and Figure 5-5 show observed prisms and Figure 5-8 shows the number of cracks on each prism.

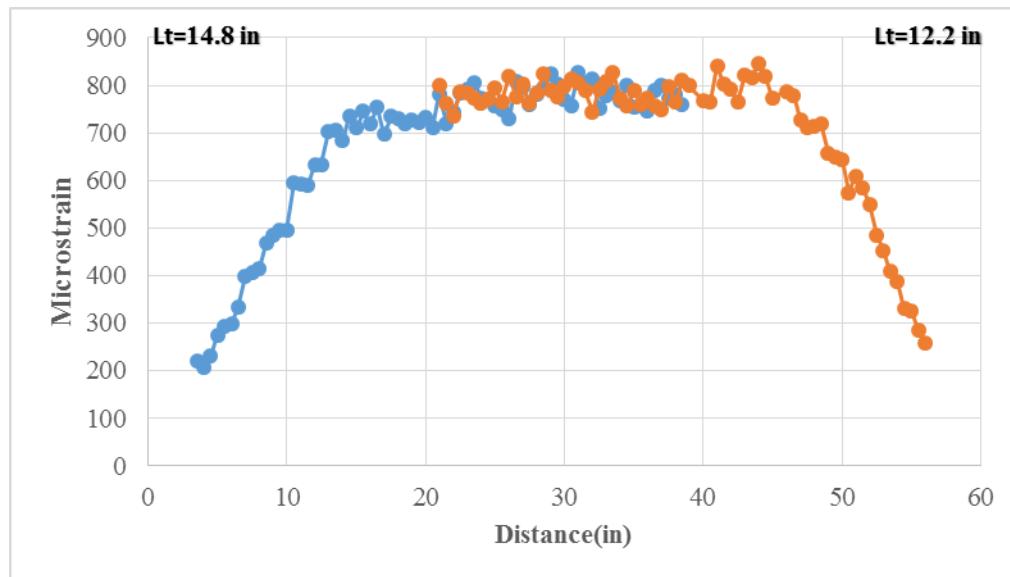


Figure 5-1: Mix#1, 6000 psi, WA, $\frac{3}{4}$ in. Edge Distance-Longitudinal Strain Profile

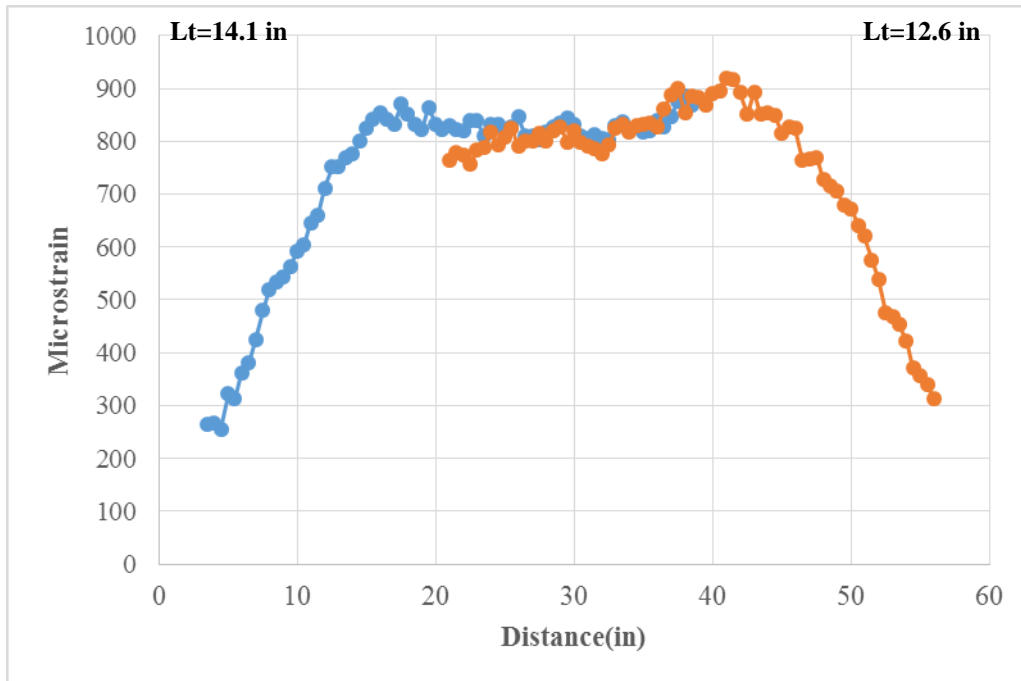


Figure 5-2: Mix#1, 6000 psi, WA, 5/8 in Edge Distance-Longitudinal Strain Profile

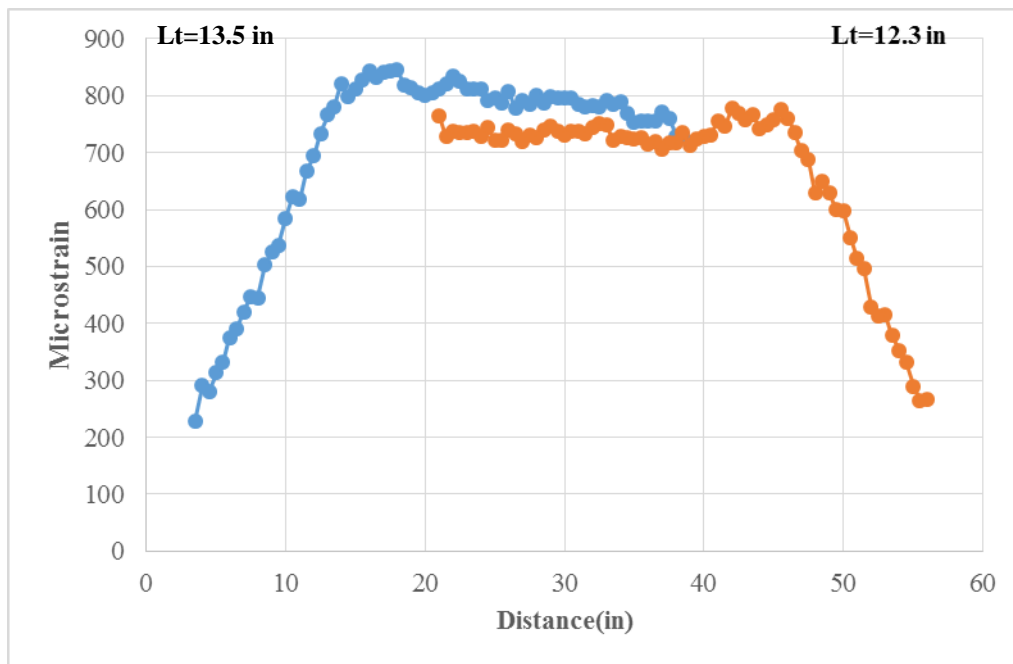


Figure 5-3: Mix#1, 6000 psi, WA, 1/2 in Edge Distance-Longitudinal Strain Profile



Figure 5-4: Mix#1, 6000psi, WA-Observed Cracking (Live End)

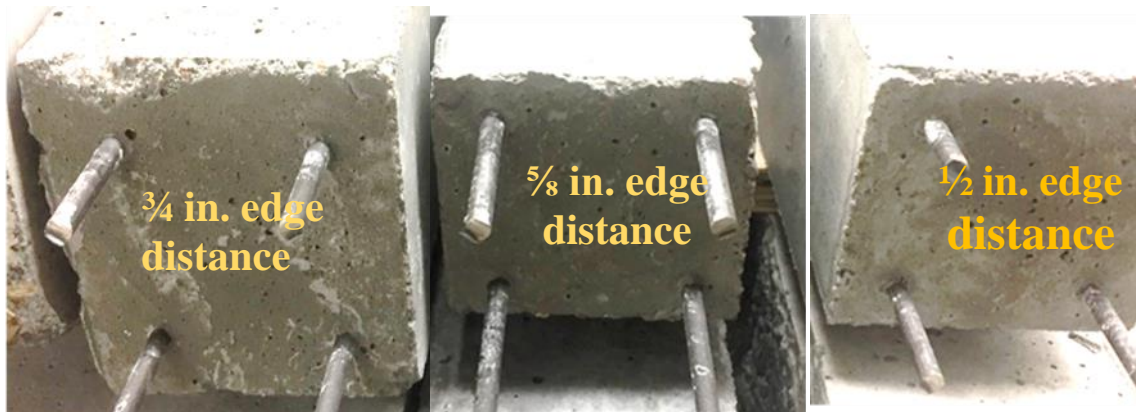


Figure 5-5: Mix#1, 6000psi, WA-Observed Cracking (Dead End)

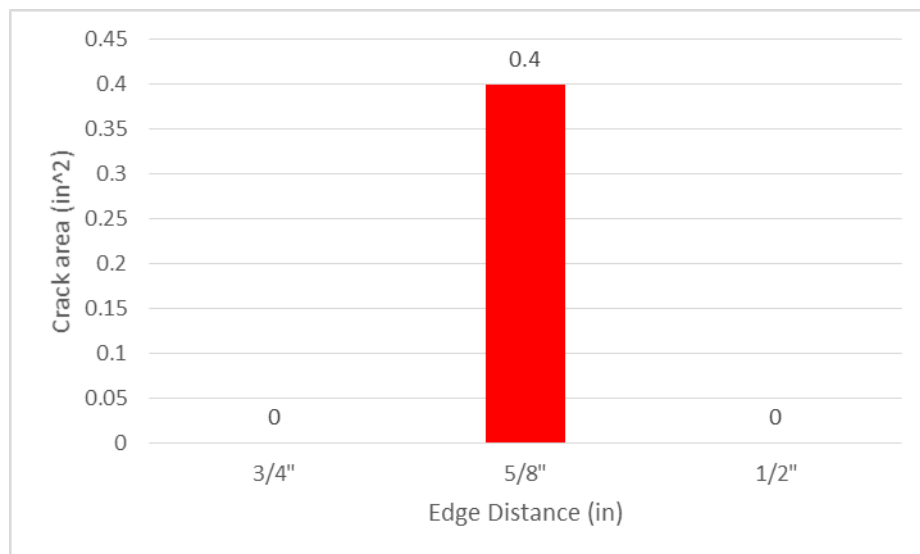


Figure 5-6: Mix#1, 6000psi, WA-Crack Area (in²)

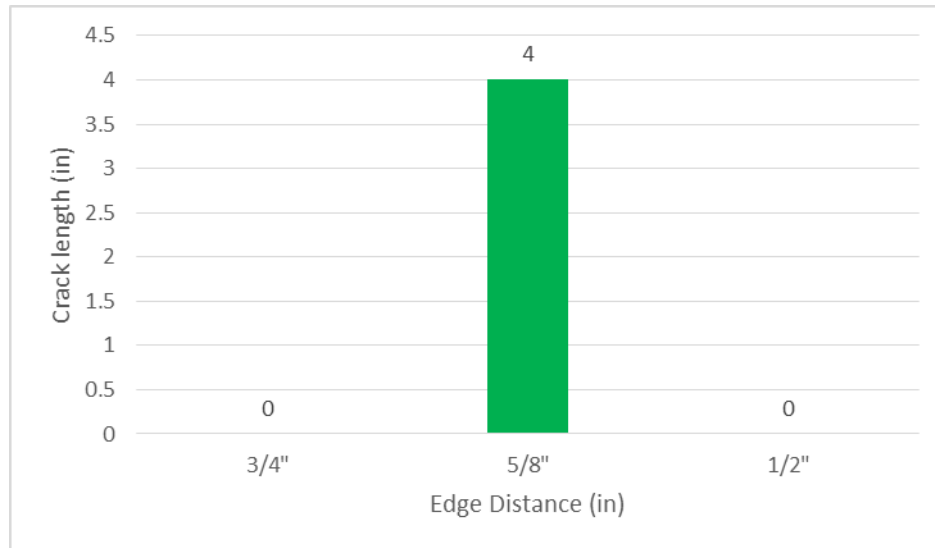


Figure 5-7: Mix#1, 6000psi, WA-Crack Length (in)

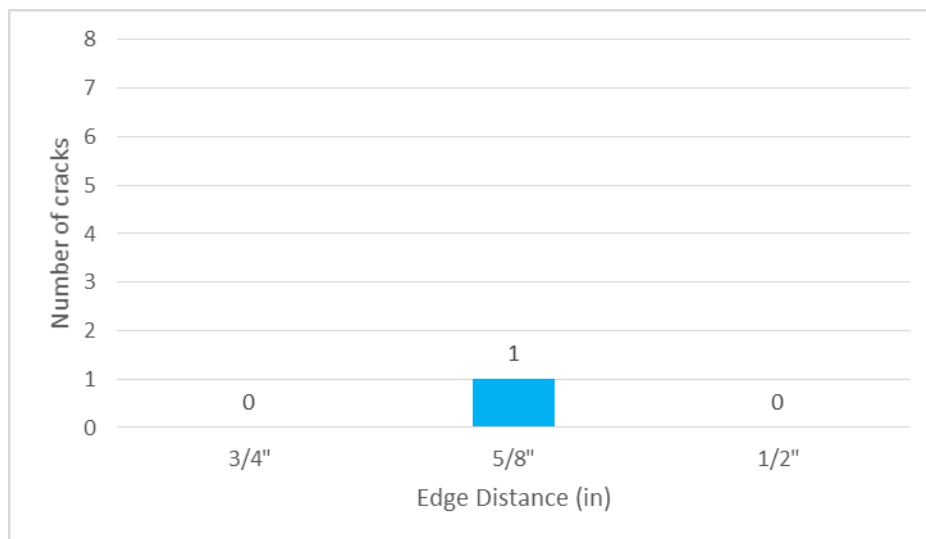


Figure 5-8: Mix#1, 6000psi, WA-Number of Cracks

5.1.2 Mix#1-WB wire type

The tests were conducted with WB type wire and concrete release strength of 4500 psi and 6000 psi. Tests were repeated three times with concrete strength of 6000 psi, and every test with WB wire performed poorly, with four cracks observed on each side of the prisms. WB wire had an average indent depth of 0.119 mm (0.004685 in.), and edge wall angle 16.45 degree.

5.1.2.1. WB-Release Strength 4500 psi

Figure 5-9 and Figure 5-10 show observed cracking of the prisms with concrete release strength of 4500 psi and the edge distances of $\frac{3}{4}$ in, $\frac{5}{8}$ in. and $\frac{1}{2}$ in. The maximum crack width on the prism with $\frac{3}{4}$ in. edge distance was 0.02 in. and the maximum crack length was 53 in. The prisms with $\frac{1}{2}$ in. edge distance indicated poor performance with evident spalling on the front side of the prism on the live end.

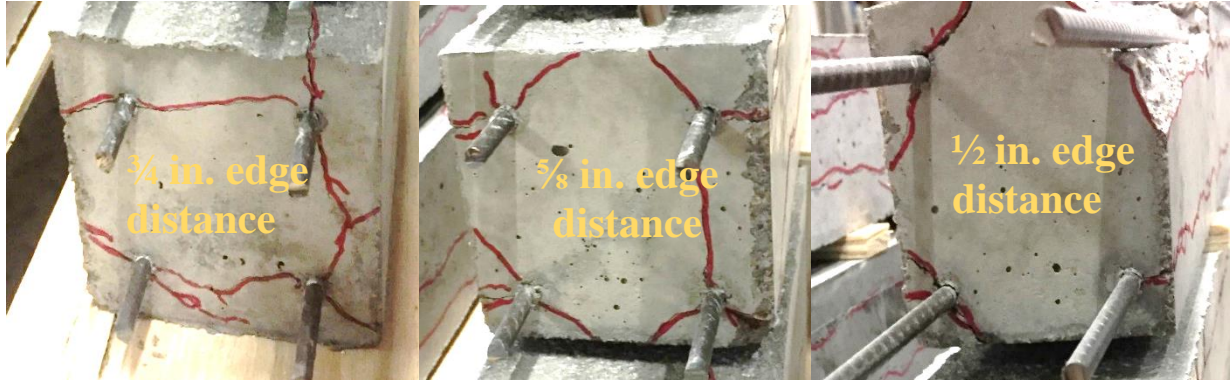


Figure 5-9: Mix#1, 4500psi, WB-Observed Cracking (Dead End)

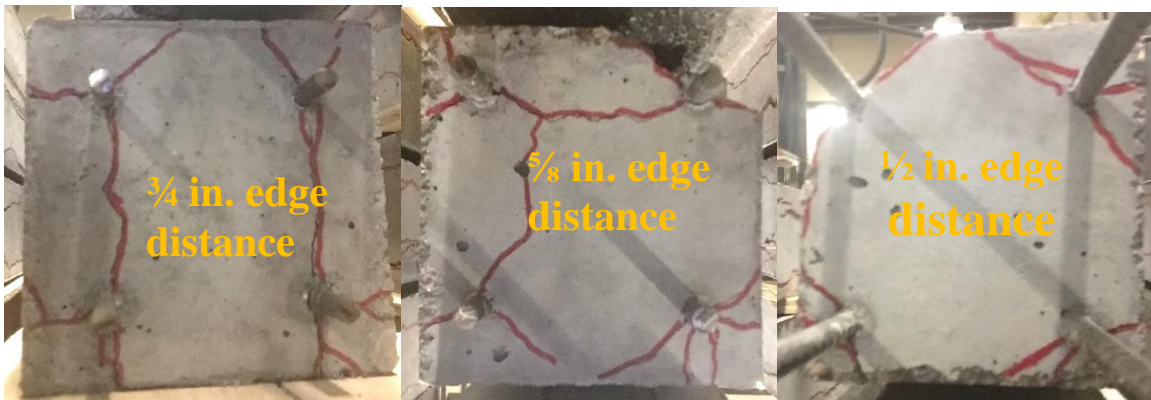


Figure 5-10: Mix#1, 4500 psi, WB-Observed Cracking (Live End)

Figure 5-11, Figure 5-12, and Figure 5-13 show crack area, crack length and number of cracks for each prism with different value of edge distance, respectively.

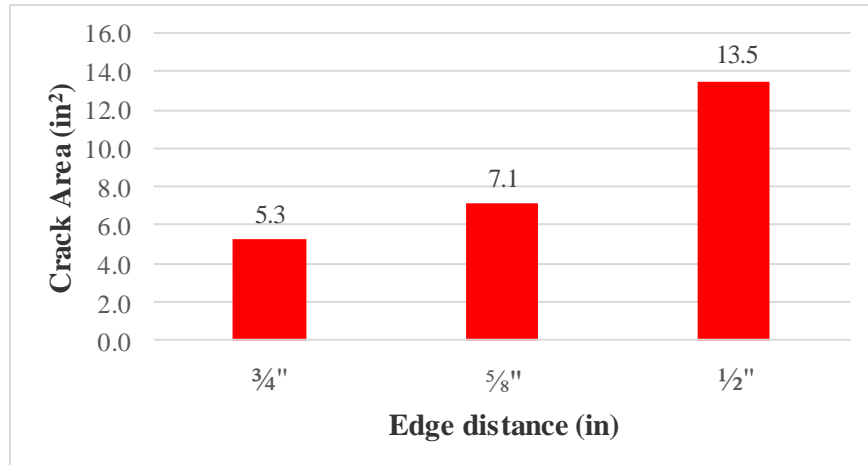


Figure 5-11: Mix#1, 4500 psi, WB-Crack Area (in²)

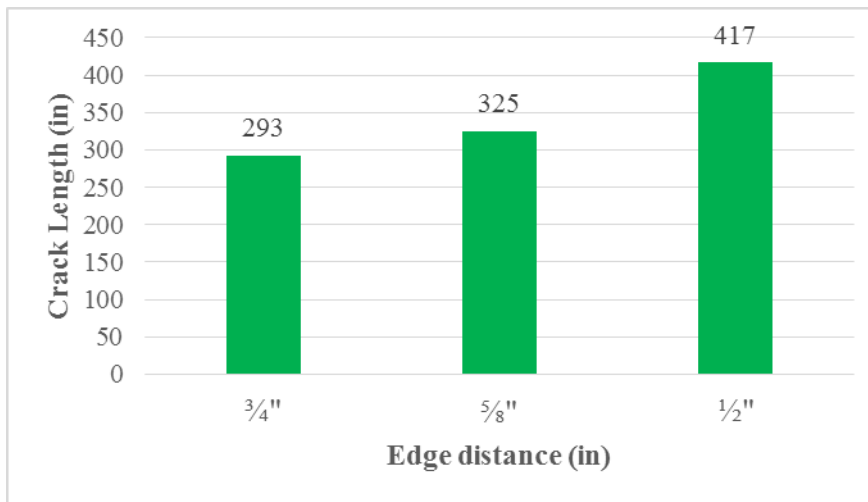


Figure 5-12: Mix#1, 4500 psi, WB-Crack Length (in)

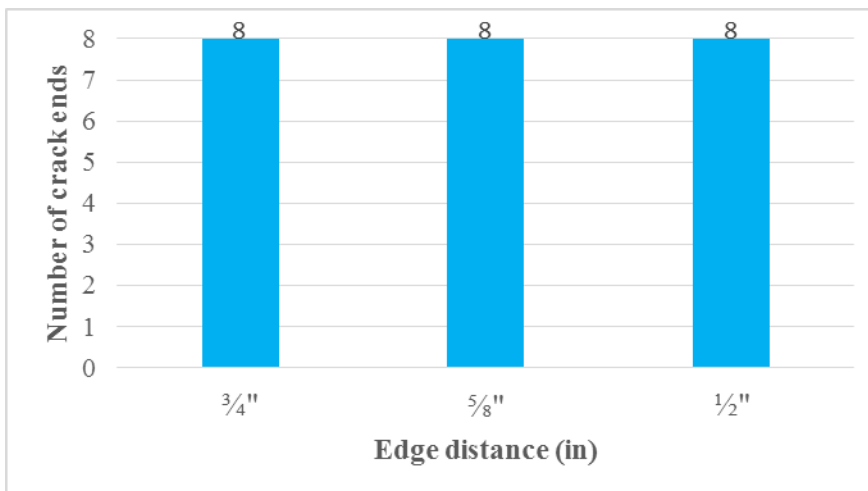


Figure 5-13: Mix#1, 4500 psi, WB-Number of Cracks

5.1.2.2. WB-Release Strength 6000psi (First Time)

Figure 5-14 and Figure 5-15 show the prisms with concrete release strength of 6000 psi, and three different edge distances. The tests were repeated with 6000 psi release strength of concrete three times. Each test with WB wire resulted in eight observed cracks on each prism as shown in Figure 5-18. Spalling was also observed on the prism with $\frac{1}{2}$ in. edge distance which indicated that bond between wire and concrete was totally lost as shown in Figure 5-14 and Figure 5-15.

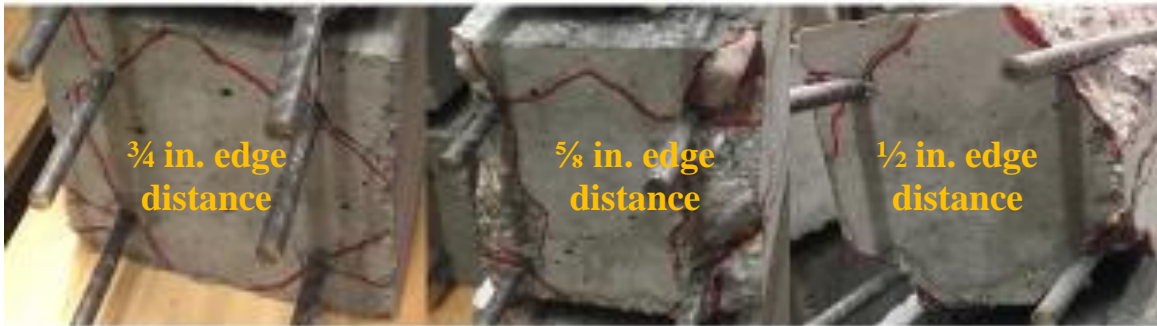


Figure 5-14: Mix#1, 6000psi, WB-Observed Cracking (Dead end)

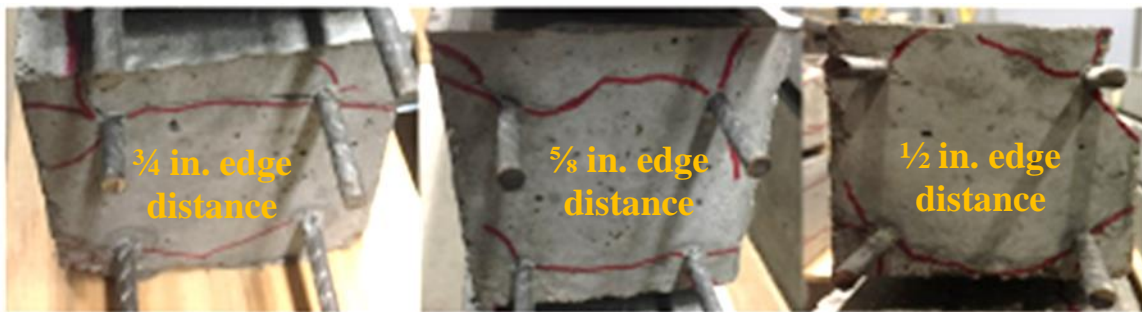


Figure 5-15: Mix#1, 6000 psi, WB-Observed Cracking (Live end)

The maximum crack width observed on the prism with $\frac{3}{4}$ in. edge distance was 0.04 in, and the maximum crack length was 57 in. With decreasing edge distance from $\frac{3}{4}$ in. to $\frac{5}{8}$ in, spalling was observed on the live end of the prism. Spalling also occurred on the front and back side of the prism with 8 in. and 6 in. in length respectively. Prism with $\frac{1}{2}$ in. edge distance performed poorly with spalling on the live end of the prism on the front, bottom and back side of the prism with 31 in, 30 in, 6 in. and 5 in. lengths respectively.

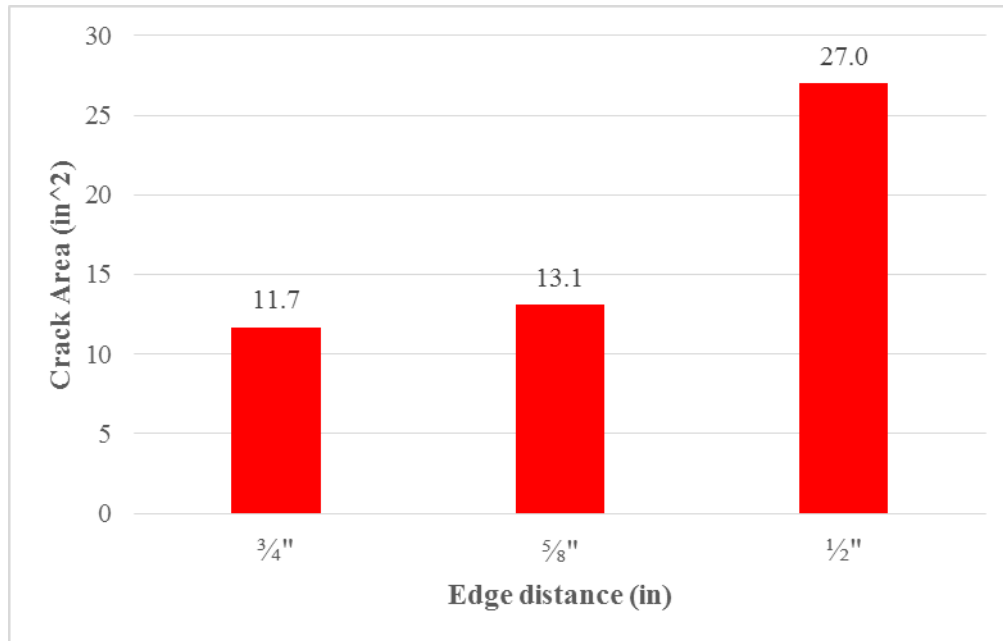


Figure 5-16: Mix#1, 6000 psi, WB-Crack Area (in²)

Figure 5-16, Figure 5-17 and Figure 5-18 show the crack area, crack length, and number of cracks as a function of edge distance, respectively. Decreasing the edge distance resulted in increasing the crack area, crack lengths and number of cracks.

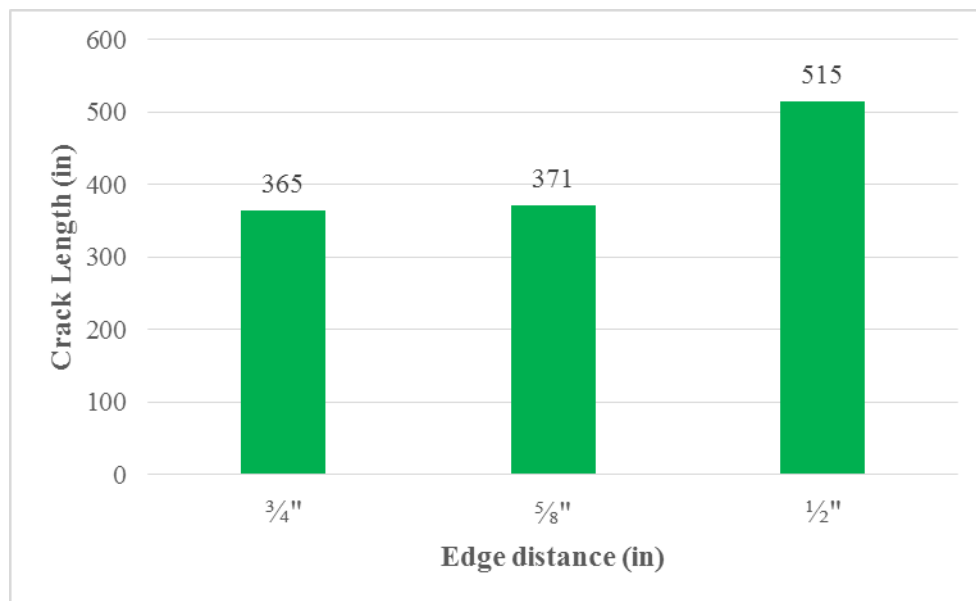


Figure 5-17: Mix#1, 6000 psi, WB-Crack Length (in)

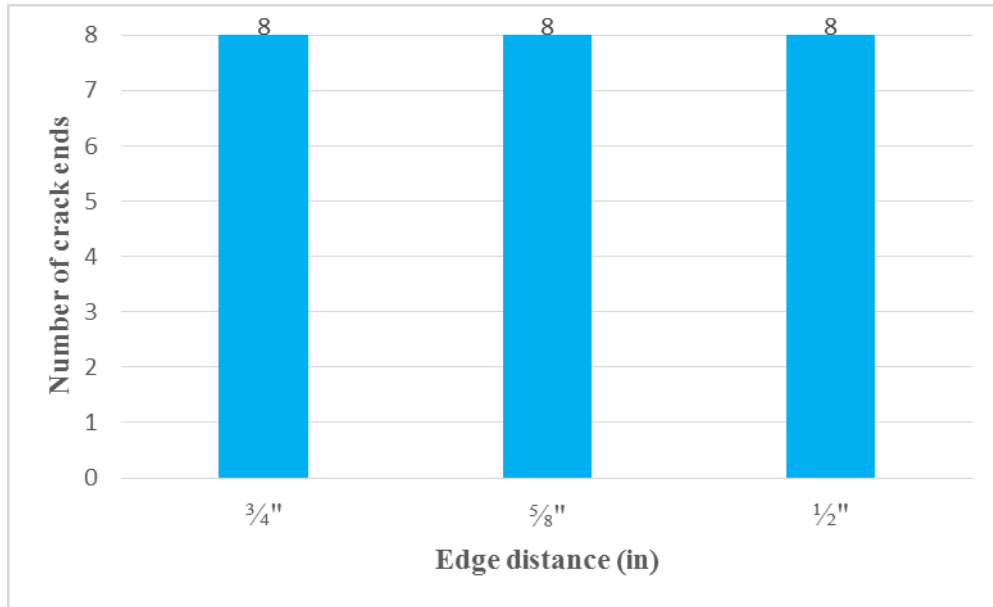


Figure 5-18: Mix#1, 6000 psi, WB-Number of Cracks

5.1.2.3. WB-Release Strength 6000 psi (Second Time)

Figure 5-19 shows the values of crack areas for the wire WB and 6000 psi release strength. WB wire performed poorly with eight cracks observed on each prism. Similar casting and curing conditions were used throughout the entire laboratory phase.

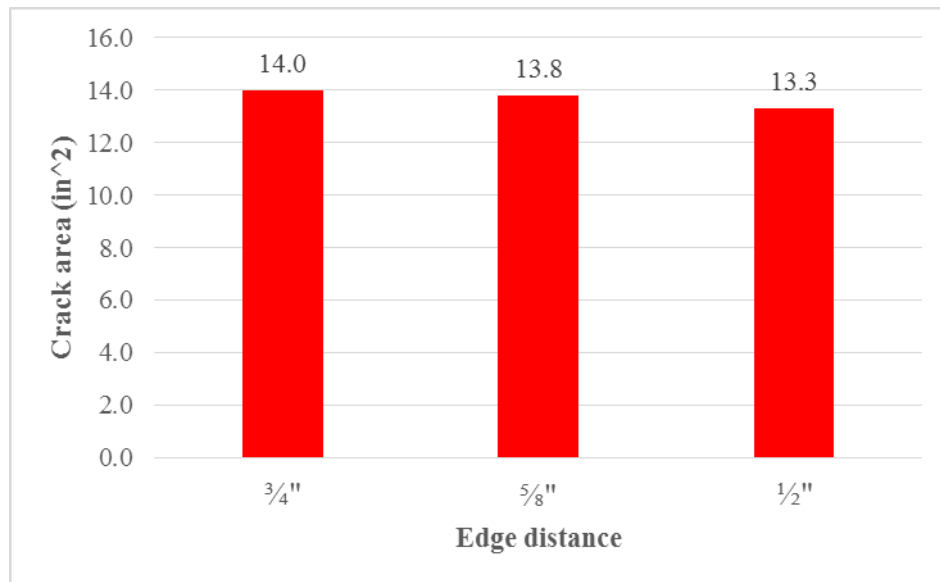


Figure 5-19: Mix#1, 6000 psi, WB second time-Crack Area (in²)

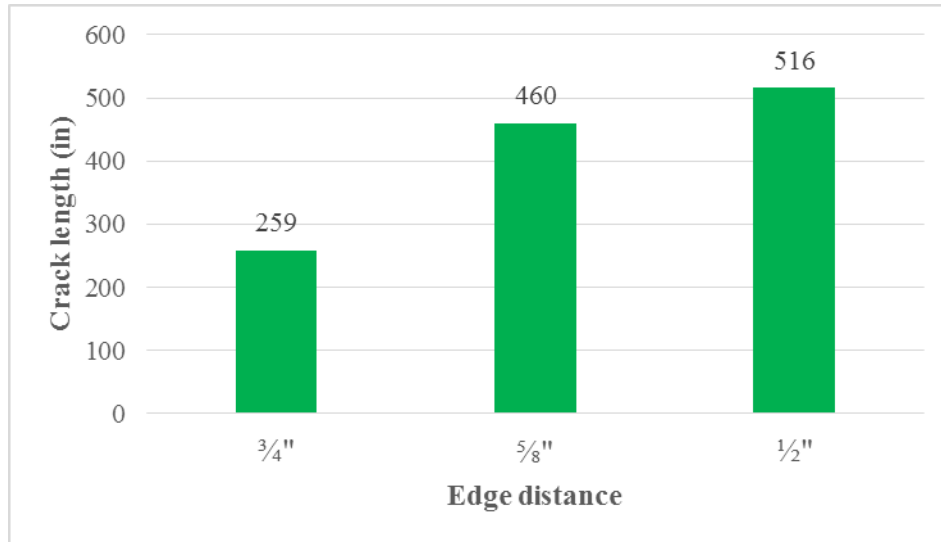


Figure 5-20: Mix#1, 6000 psi, WB second time-Crack Length (in)

Figure 5-20 presents the values of crack lengths as a function of the edge distance. The maximum crack width observed for the prism with $\frac{3}{4}$ in. cover was 0.04 in. and maximum crack length was 34 in. Decreasing the cover to $\frac{5}{8}$ in. resulted in spalling on the both sides of the prism. Additionally, the prism with $\frac{1}{2}$ in. edge distance had severe damage. Figure 5-21 shows the number of cracks as a function of edge distance.

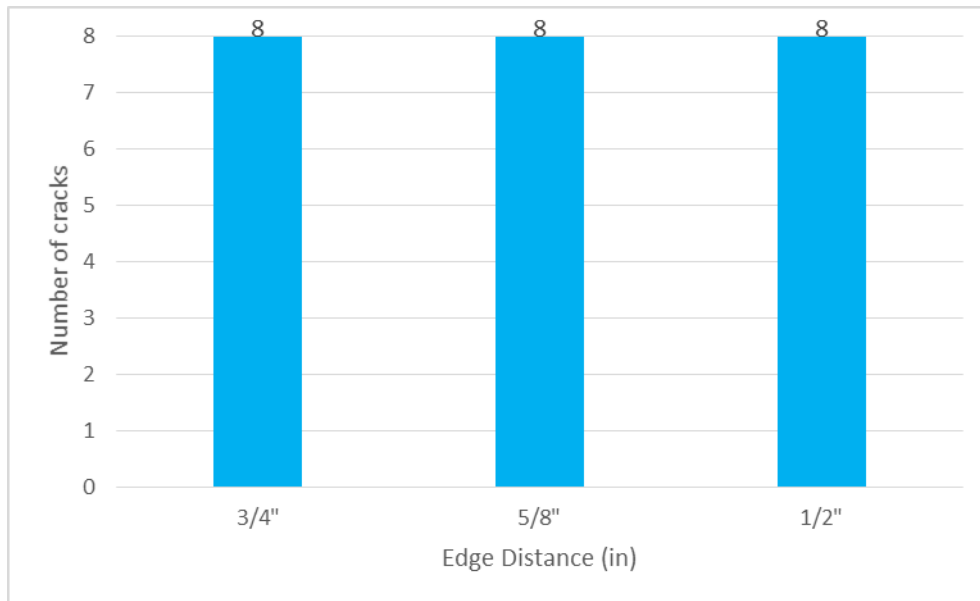


Figure 5-21: Mix#1, 6000 psi, WB second time-Number of Cracks

5.1.2.4. WB-Release Strength 6000 psi (Third time)

Figure 5-22 shows the value of crack area for WB wire. The tests with this wire were repeated three times. The conditions were the same and WB wire exhibited consistent behavior which resulted in eight cracks per prism.

The maximum crack width for the prism with $\frac{3}{4}$ in. edge distance was 0.03 in. and the maximum crack length was 46 in. The prism with $\frac{5}{8}$ in. edge distance had eight cracks, with four cracks on each side. The maximum crack width was 0.016 in. and 34 in. was the maximum crack length. The prism with $\frac{1}{2}$ in. edge distance had four cracks on each side of the prism. The maximum crack width was 0.04 in. and the maximum crack length was 59 in. As compared with previous results, with a 6000 psi release strength, eight cracks were observed on each prism with the different thicknesses of edge distances. However, spalling did not occur at any time.

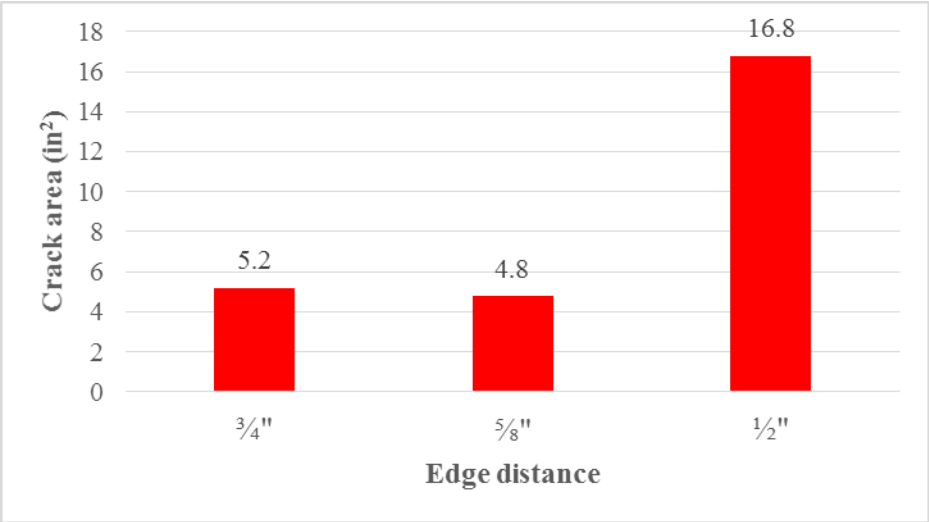


Figure 5-22: Mix#1, 6000 psi, WB third time-Crack Area (in²)

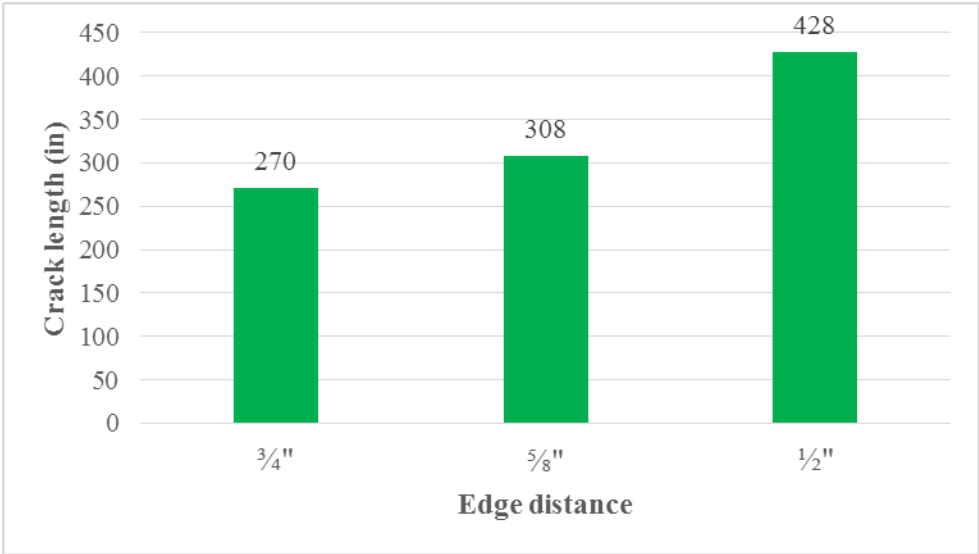


Figure 5-23: Mix#1, 6000 psi, WB third time-Crack Length (in)

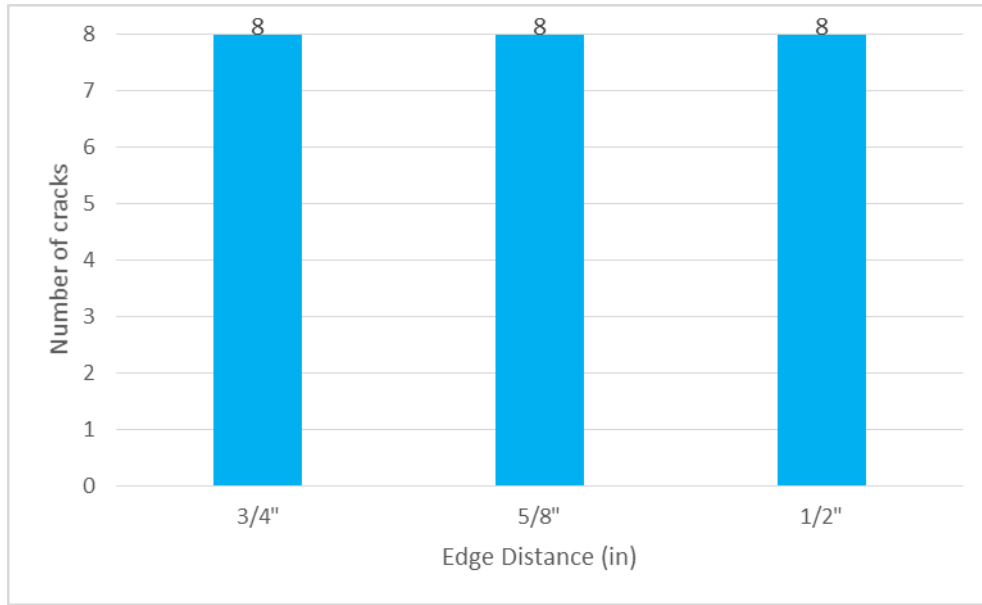


Figure 5-24: Mix#1, 6000 psi, WB third time-Number of Cracks

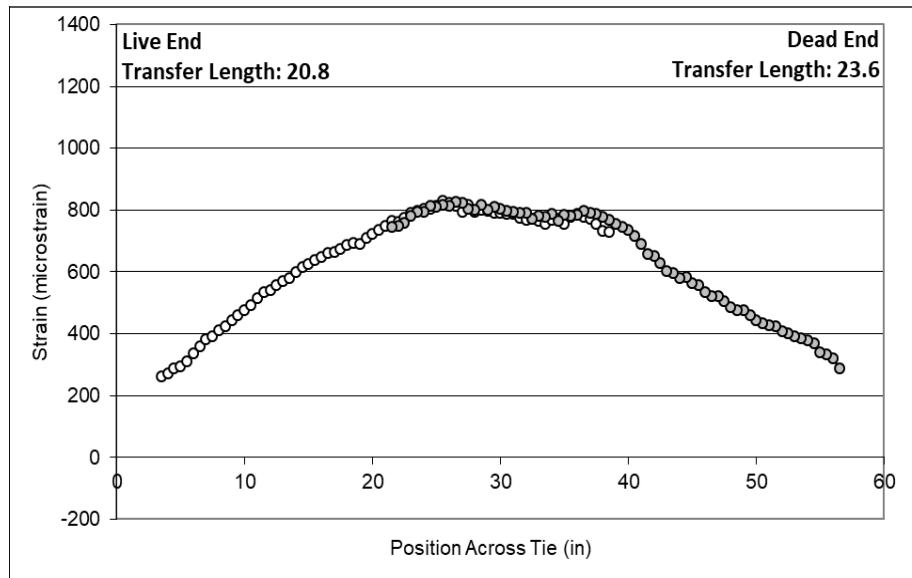
Figure 5-22, Figure 5-23 and Figure 5-24 show the crack area and crack lengths, respectively. The high values of crack lengths indicated poor performance of WB wire type.

5.1.3 Mix#1-WE wire type

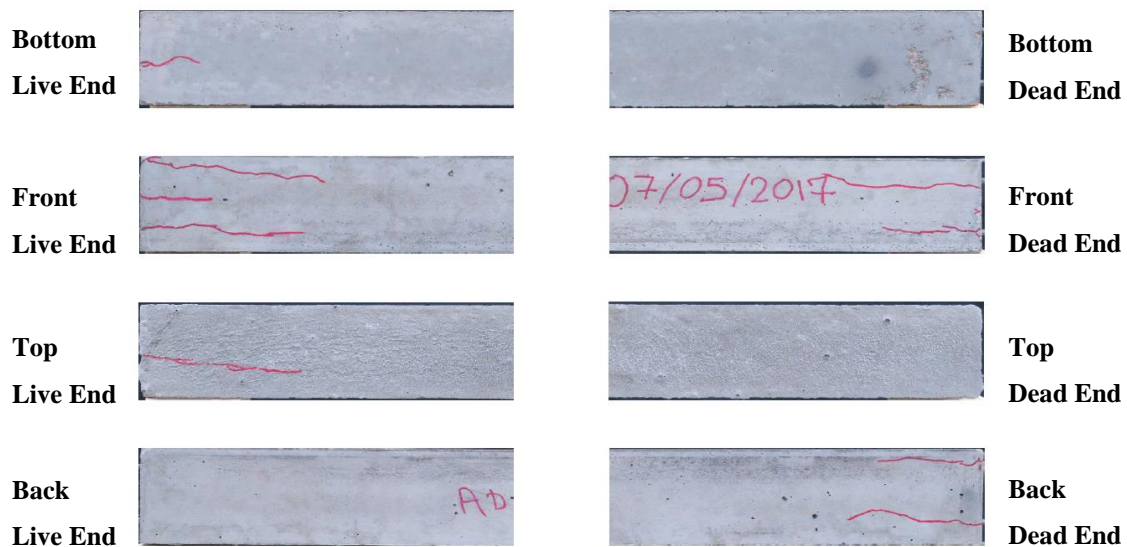
WE wire is a spiral type of wire with an average rib depth of 0.259 mm (0.010197 in.), an average width of 6.164 mm (0.24268 in.) and edge wall angle of 15.1 degrees as reported by Haynes.

5.1.3.1. WE-Release Strength 3500 psi

Figure 5-25 shows the longitudinal strain profile and observed cracking for the prism with 3500 psi concrete release strength and with $\frac{3}{4}$ in. edge distance. In Figure 5-25 (a) the strain profile across the prism is shown, along with the values of the transfer lengths on each end of the prism. Also shown is an image of the cracking on each end of the prism (Figure 5-25b)



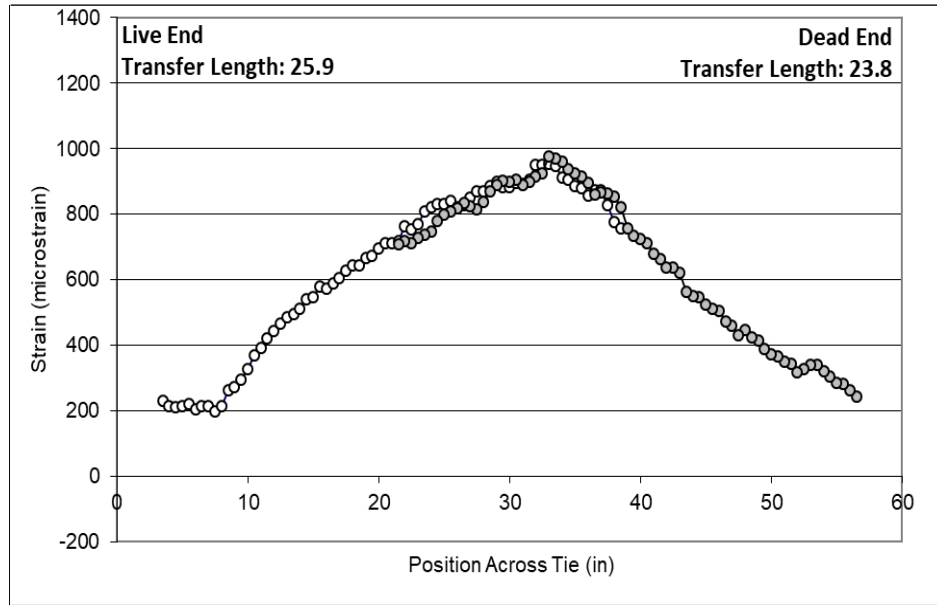
(a) Longitudinal Strain Profile



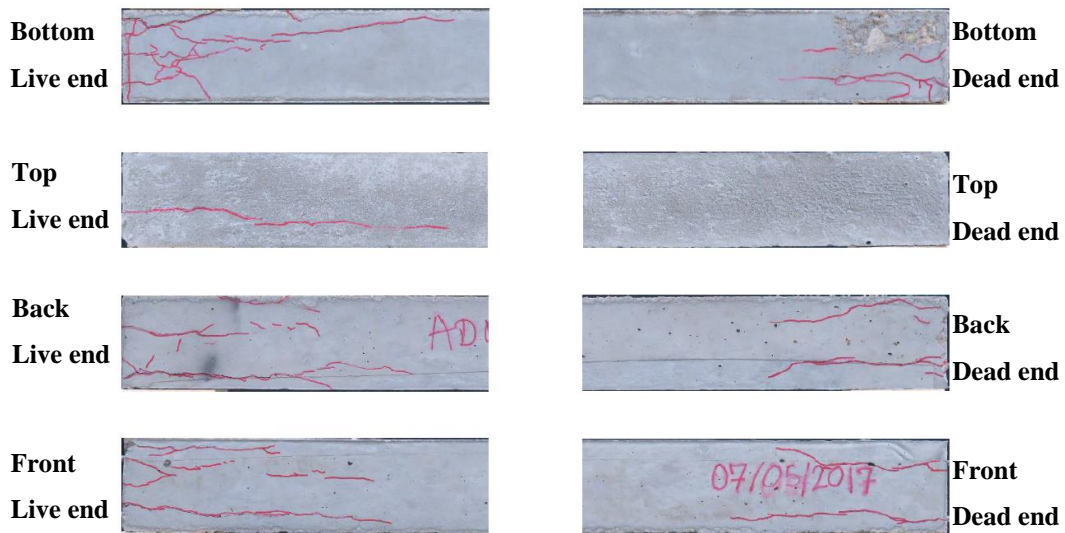
(b) Observed Cracking

Figure 5-25: Mix#1, 3500 psi, WE, $\frac{3}{4}$ in. Edge distance (Savic, 2018)

As shown in Figure 5-25 (b), the position of cracks on each end (live end and dead end), on the bottom, front, top and back of the prism were given. Figure 5-26 shows the longitudinal strain profile for a concrete release strength of 3500 psi, and $\frac{5}{8}$ in. edge distance. According to these graphs it is noticeable that with reducing the value of edge distance transfer lengths are longer, and cracks are larger.



(a) Longitudinal Strain Profile



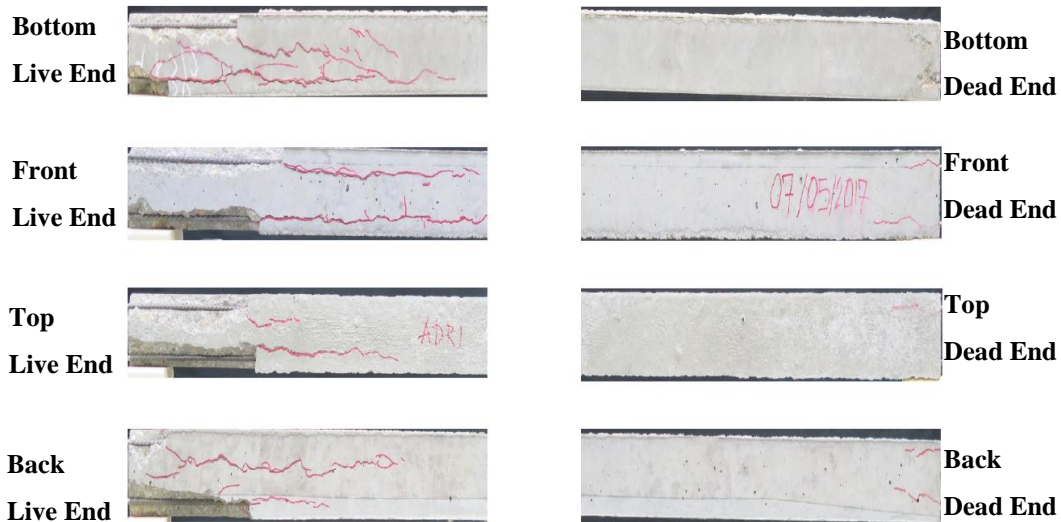
(b) Observed Cracking

Figure 5-26: Mix#1, 3500 psi, WE, $\frac{5}{8}$ in. Edge distance (Savic, 2018)

Figure 5-27 shows the longitudinal strain profile for a concrete release strength of 3500 psi, and $\frac{1}{2}$ in. edge distance. As the edge distance decreased from $\frac{3}{4}$ in. to $\frac{5}{8}$ in. and finally to $\frac{1}{2}$ in, more cracks were observed.



(a) Longitudinal Strain Profile

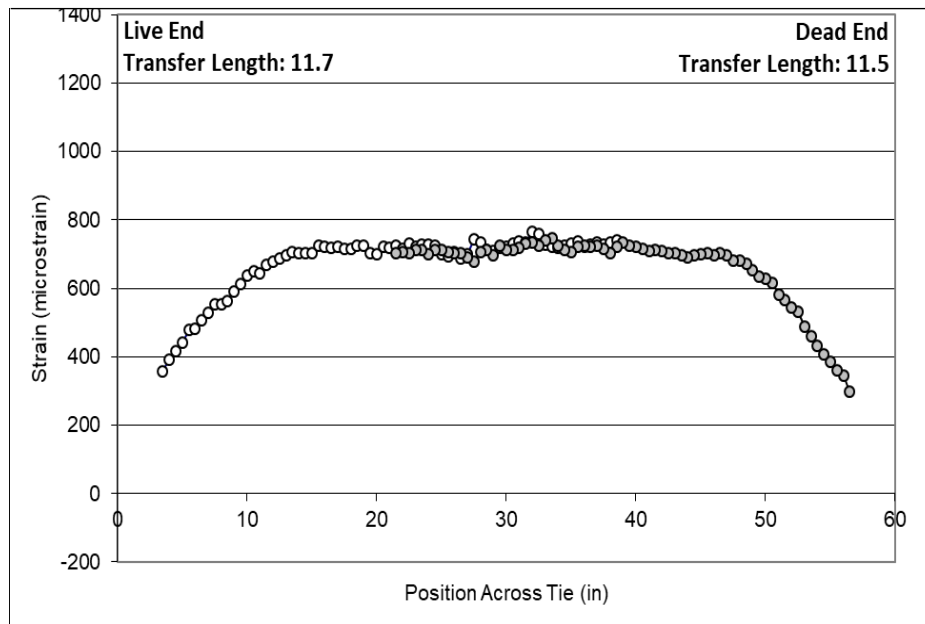


(b) Observed Cracking

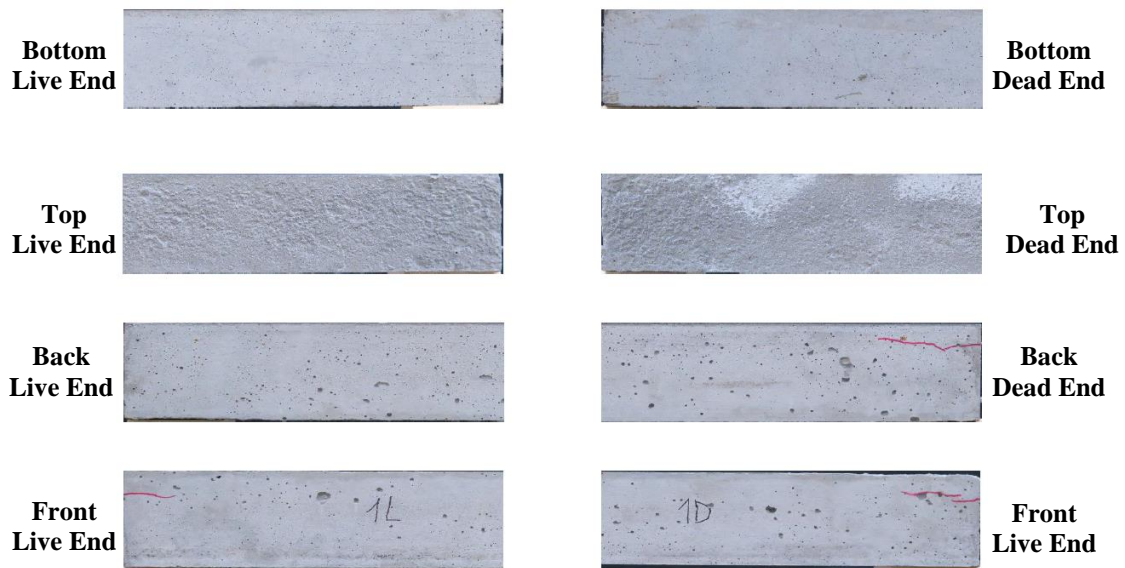
Figure 5-27: Mix#1, 3500 psi, WE, ½ in. Edge distance (Savic, 2018)

5.1.3.2. WE-Release Strength 4500 psi

Figure 5-28 shows the longitudinal strain profile for a concrete release strength of 4500 psi, and ¾ in. edge distance. As shown in this image, it was observed that with a higher concrete release strength and the same cover, less cracking occurred. Transfer lengths were shorter and on the live end of the prism at the front only one crack occurred, whereas on the dead-end cracks it appeared on both, the back and on the front.

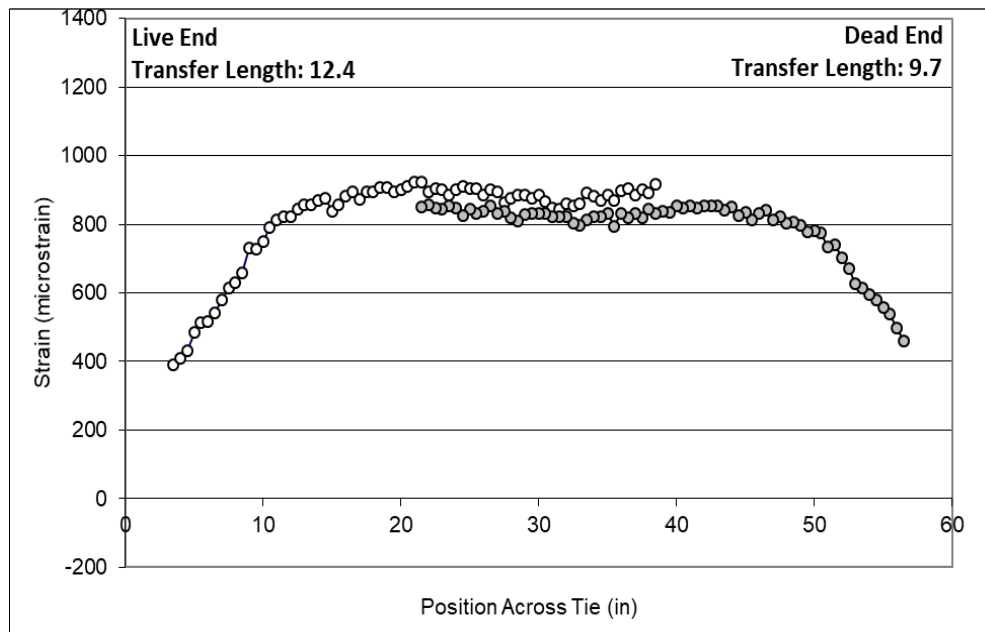


(a) Longitudinal Strain Profile

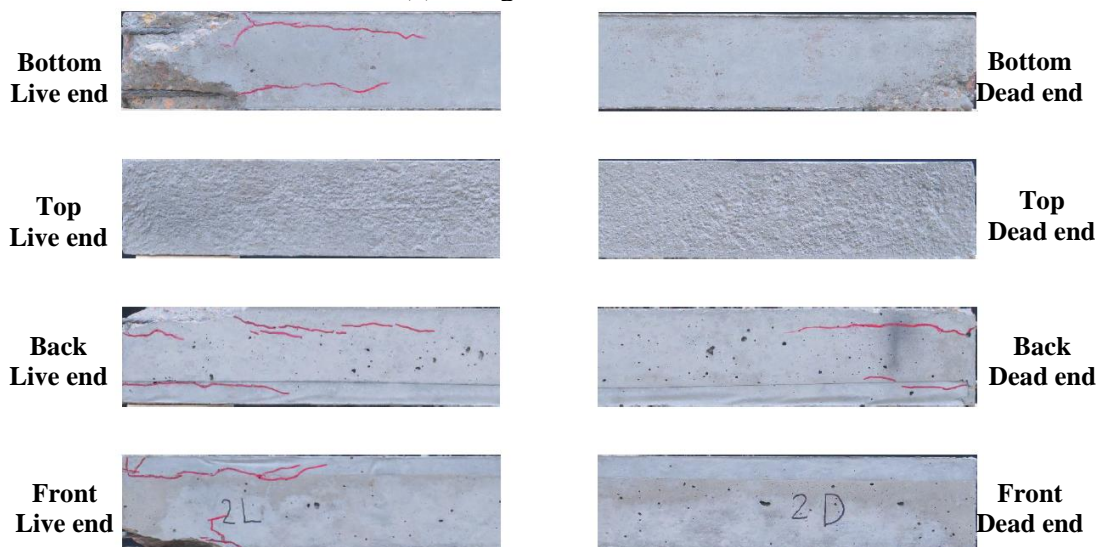


(b) Observed Cracking

Figure 5-28: Mix#1, 4500 psi, WE, $\frac{3}{4}$ in. Edge distance (Savic, 2018)



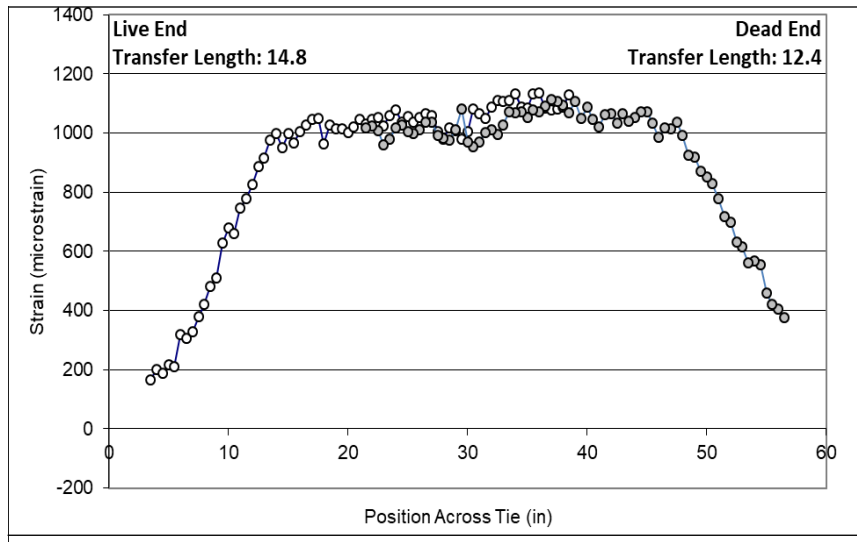
(a) Longitudinal Strain Profile



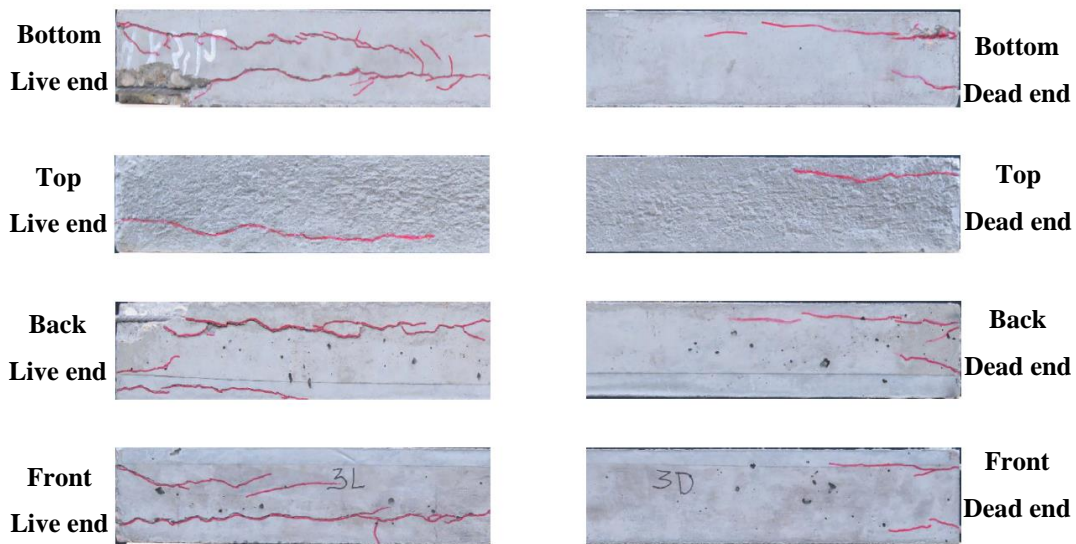
(b) Observed Cracking

Figure 5-29: Mix#1, 4500 psi, WE, $\frac{5}{8}$ in. Edge distance (Savic, 2018)

Figure 5-29 shows the longitudinal strain profile for a concrete release strength of 4500 psi, and $\frac{5}{8}$ in. edge distance. Figure 5-30 shows the longitudinal strain profile for a concrete release strength of 4500 psi, and $\frac{1}{2}$ in. edge distance.



(a) Longitudinal Strain Profile



(b) Observed Cracking

Figure 5-30: Mix#1, 4500 psi, WE, ½ in. Edge distance (Savic, 2018)

5.1.3.3. WE-Release Strength 6000 psi

Figure 5-31, Figure 5-32, and Figure 5-33 show the longitudinal strain profile and cracking observations for a concrete release strength of 6000 psi, as the amount of cover is reduced from ¾ in. to ½ in.

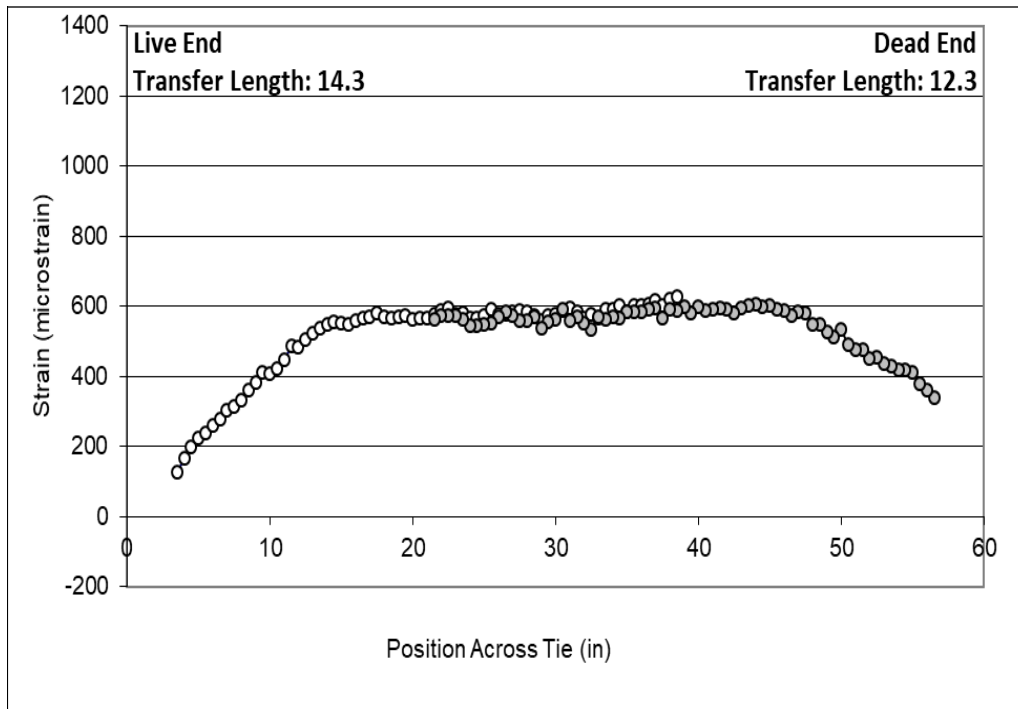


(a) Longitudinal Strain Profile

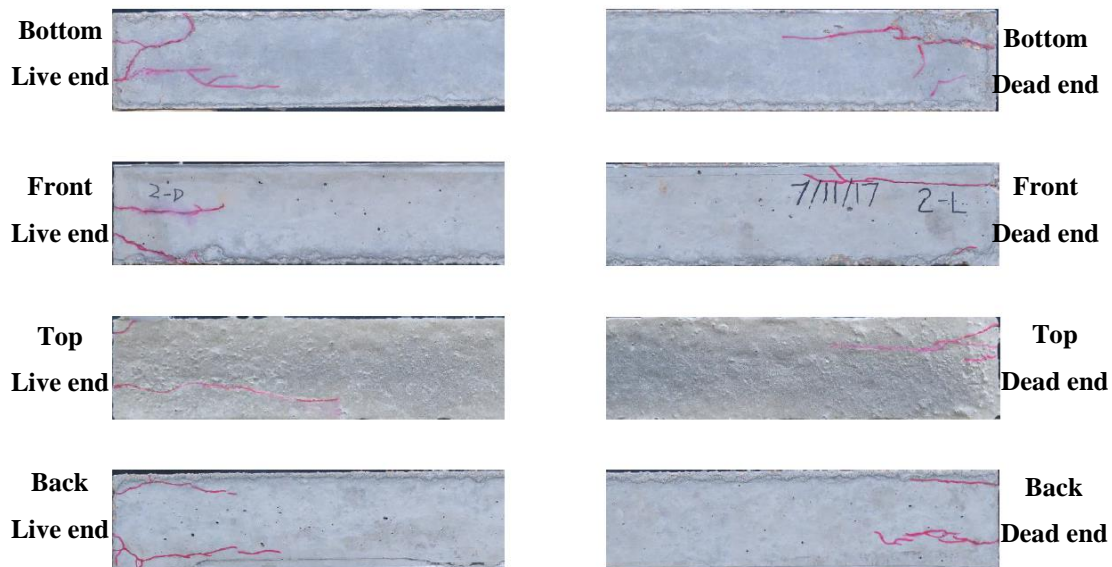


(b) Observed Cracking

Figure 5-31: Mix#1, 6000 psi, WE, $\frac{3}{4}$ in. Edge distance (Savic, 2018)



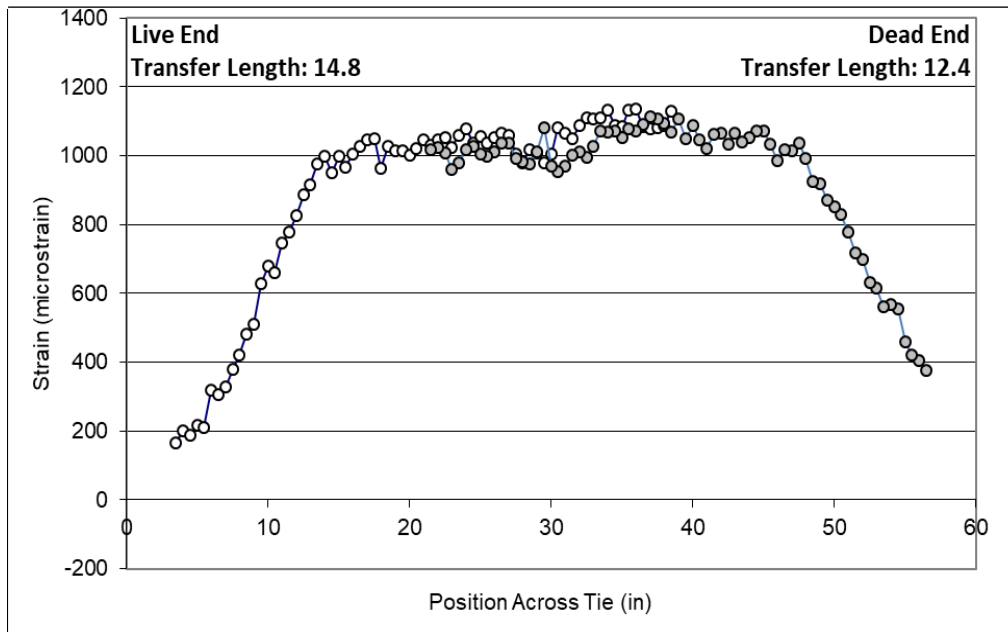
(a) Longitudinal Strain profile



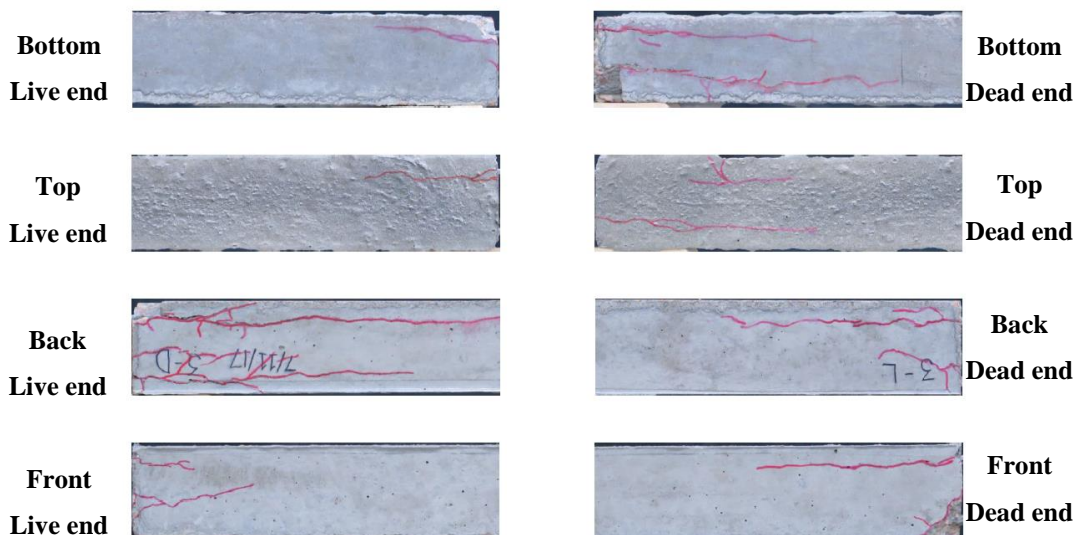
(b) Observed Cracking

Figure 5-32: Mix#1, 6000 psi, WE, 5/8 in. Edge distance (Savic, 2018)

The strain profiles exhibited well-established plateaus and the transfer length values were generally small. The amount of cracking appeared to have been reduced; however, as the cover was reduced to 1/2 in. there was again a significant increase in the observed cracking behavior.



(a) Longitudinal Strain Profile



(b) Observed Cracking

Figure 5-33: Mix#1, 6000 psi, WE, ½ in. Edge distance (Savic, 2018)

5.1.3.4. WE-Release Strength 12000 psi

In addition to the above cases with the release strengths of 3500 psi, 4500 psi and 6000 psi, a set of prism tests were conducted with an extreme release strength of 12000 psi. This was done to test a popular hypothesis that too high of a release strength could result in increased splitting due to the increased brittleness of concrete resulted. For the concrete release strength of 12000 psi, the w/c ratio of concrete mix was 0.26. The appropriate strength was reached after six days, after which de-tensioning commenced. Enlarged images of the prism ends for ¾ in. cover showed no evidence of any cracking, as shown in Figure 5-34 for the live end and for the dead end.

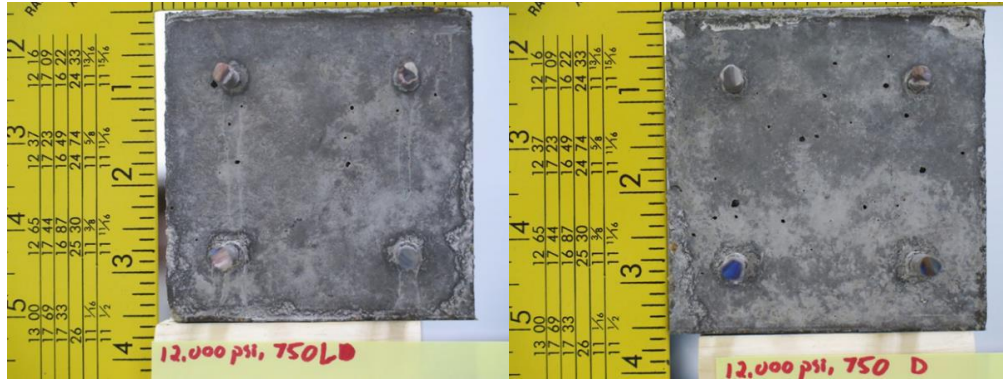


Figure 5-34: Mix#1, 12000 psi (82.74MPa), WE, $\frac{3}{4}$ in. Edge distance- Live and Dead End

Approximately 40 minutes after de-tensioning, there was a loud “popping” sound that corresponded to the initial of a crack on the prism with $\frac{1}{2}$ in. edge distance. This confirmed that splitting cracks do not always occur at the time of de-tensioning.

Overall, it was observed that with a release concrete strength of 3500 psi, transfer lengths were large on both sides of the prisms and a significant amount of cracking was observed. The concrete release strength of 4500 psi performed better, yielding shorter transfer lengths with greater established strain profiles having well-defined plateau regions, and cracks less noticeable. With a concrete release strength of 6000 psi, the strain profile across the prisms resulted in almost ideal bilinear behavior for cover $\frac{3}{4}$ in. The concrete release strength of 12000 psi was found to provide the best results, and the first cracks appeared on the prism with $\frac{5}{8}$ in. Contrary to the popular conjecture, the higher release strength improved the longitudinal splitting resistance of the prisms.

In addition to the number of wires that were found to exhibit cracking, overall crack length was observed for a given prism test at a given release strength and amount of edge distance. From data collected, a representative crack area was also found. Figure 5-35 shows the number of cracks as a function of the edge distance and release strength of concrete.

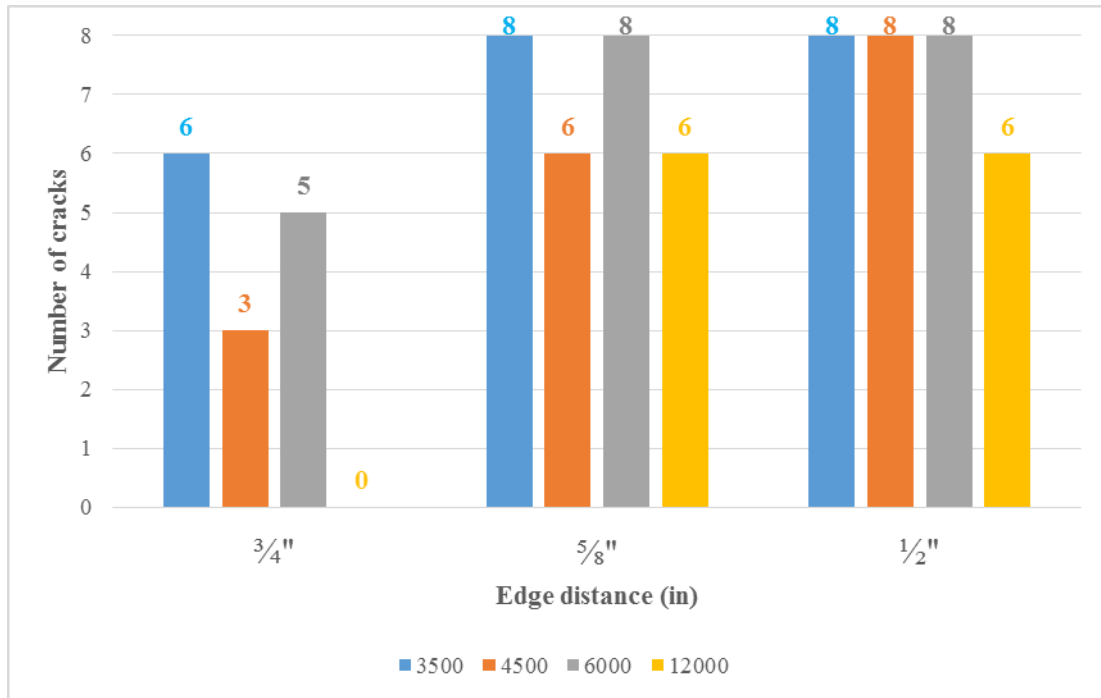


Figure 5-35: Mix#1, WE-Number of Cracks

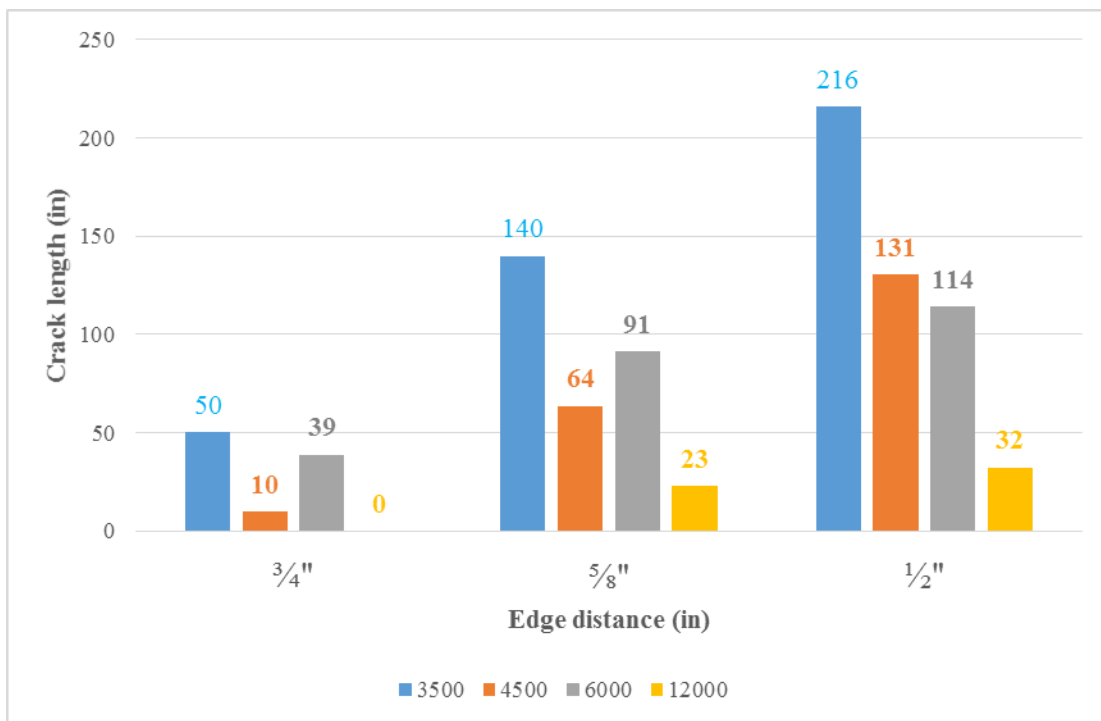


Figure 5-36: Mix#1, WE-Crack Length (in)

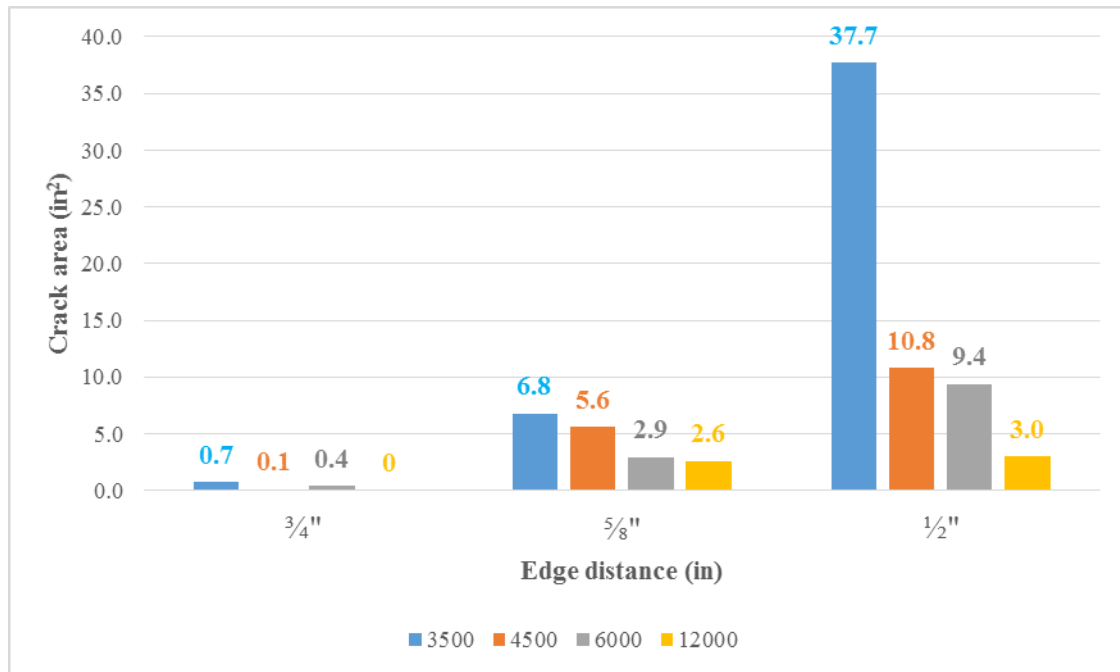


Figure 5-37: Mix#1, WE-Crack Area (in²)

Figure 5-36 shows the total crack length as a function of different edge distance and concrete compressive strength. Figure 5-36 also shows as the edge distance is reduced, the total length of cracking was consistently observed to increase, and for all levels of release strength. Furthermore, there was a general tendency for the total crack length to decrease as the release strength was increased.

Figure 5-37 shows the total crack area for the prisms as a function of the amount of edge distance from 3/4 in. to 1/2 in. which resulted in a consistent increase in total area of cracks.

6. Comparison Charts

6.1 Concrete Mixture-Mix#1

6.1.1 Release Strength 4500 psi

In order to understand which parameters were the most significant that could affect the longitudinal splitting between steel and concrete, crack area, and crack length, an investigation targeting these parameters as a function of the edge distance were undertaken. As stated previously, crack area was defined as the total crack length multiplied by the maximum crack width. Figure 6-1, Figure 6-2 and Figure 6-3 show the crack area for a release strength of 4500 psi and three different values of edge distances ($\frac{3}{4}$ in, $\frac{5}{8}$ in, and $\frac{1}{2}$ in). As shown in these Figures, reducing the cover from $\frac{3}{4}$ in. to $\frac{1}{2}$ in. for a given release strength led to an increase in the extent of cracking and therefore an increase in total crack area. Also stated previously, wire WF wire type was a deep chevron type of wire and showed the formation of very large crack areas (37 in^2 and 59 in^2) for $\frac{5}{8}$ in. and $\frac{1}{2}$ in. the edge distances. Wire types WG, WJ, WM, WP and WQ indicate no cracks on the prism having $\frac{3}{4}$ in. edge distance.

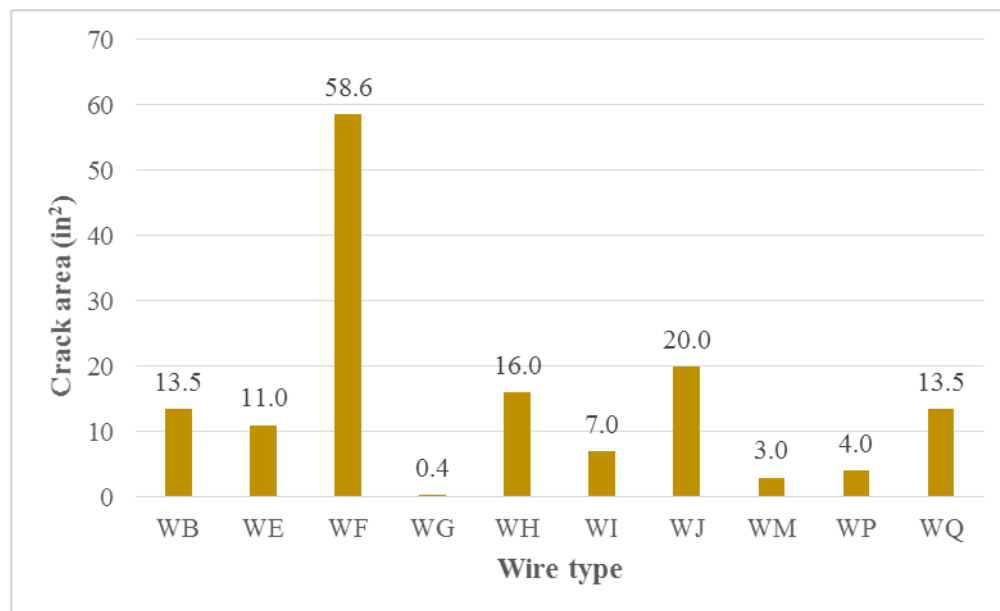


Figure 6-1: Mix#1, 4500 psi, $\frac{1}{2}$ in. Edge Distance-Crack Area (in²)

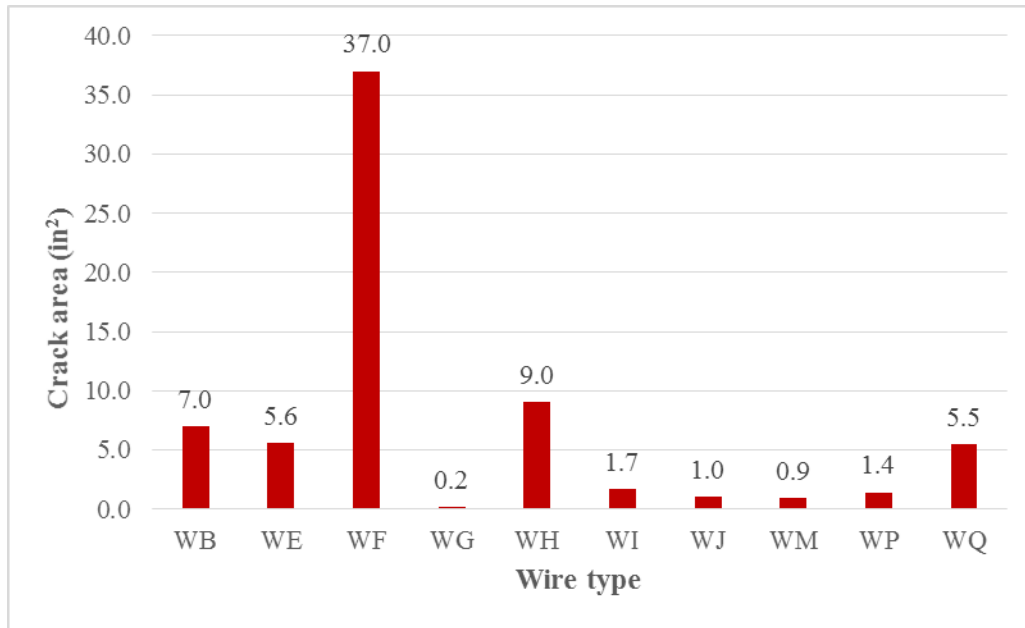


Figure 6-2: Mix#1, 4500 psi, $\frac{5}{8}$ in. Edge Distance-Crack Area (in²)

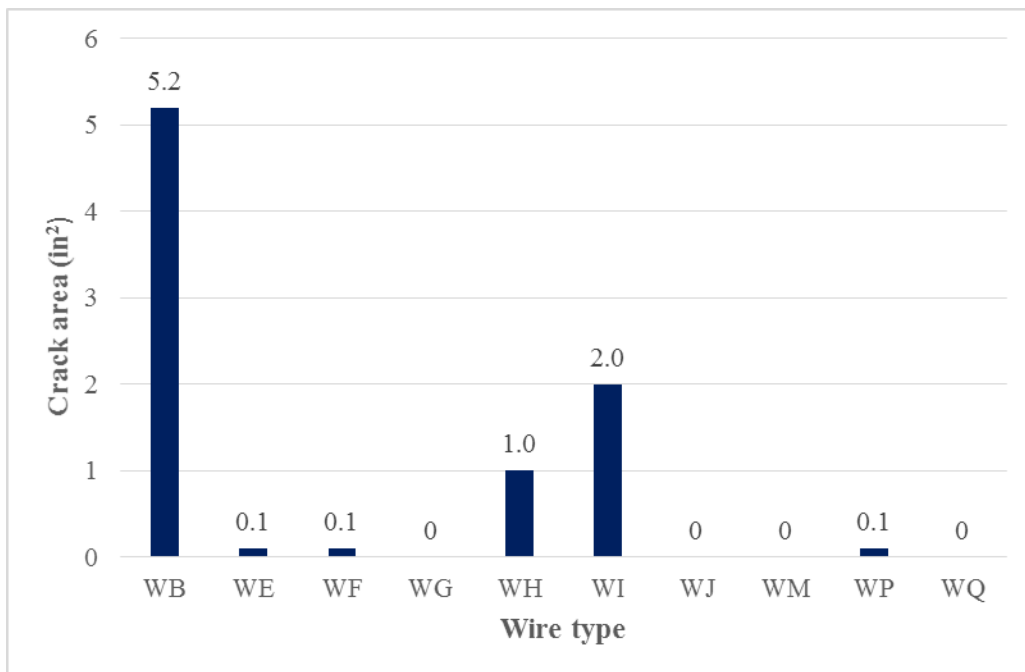


Figure 6-3: Mix#1, 4500 psi, $\frac{3}{4}$ in. Edge Distance-Crack Area (in²)

Figure 6-4, Figure 6-5 and Figure 6-6 show the crack length for a 4500 psi release strength of concrete and the three different thicknesses of edge distance. As shown in these figures, WB wire type indicated poor performance for all three values of edge distances $\frac{3}{4}$ in, $\frac{5}{8}$ in. and $\frac{1}{2}$ in. Additionally, wire types WJ, WM, WG and WQ performed very well for $\frac{3}{4}$ in. edge distance and were found to have very short crack lengths for the $\frac{5}{8}$ in. edge distance.

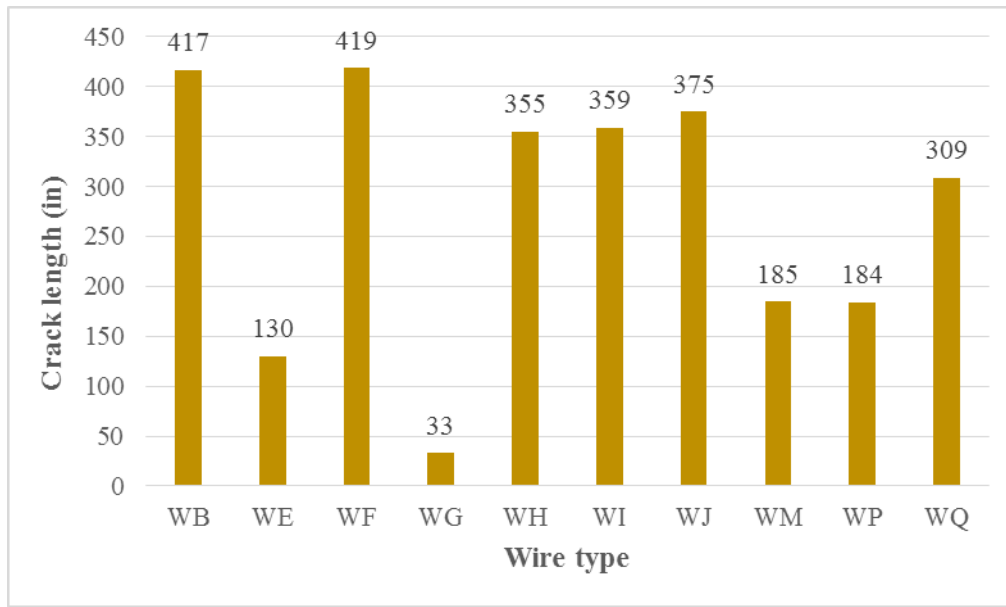


Figure 6-4: Mix#1, 4500 psi, 1/2 in. Edge Distance-Crack Length (in)

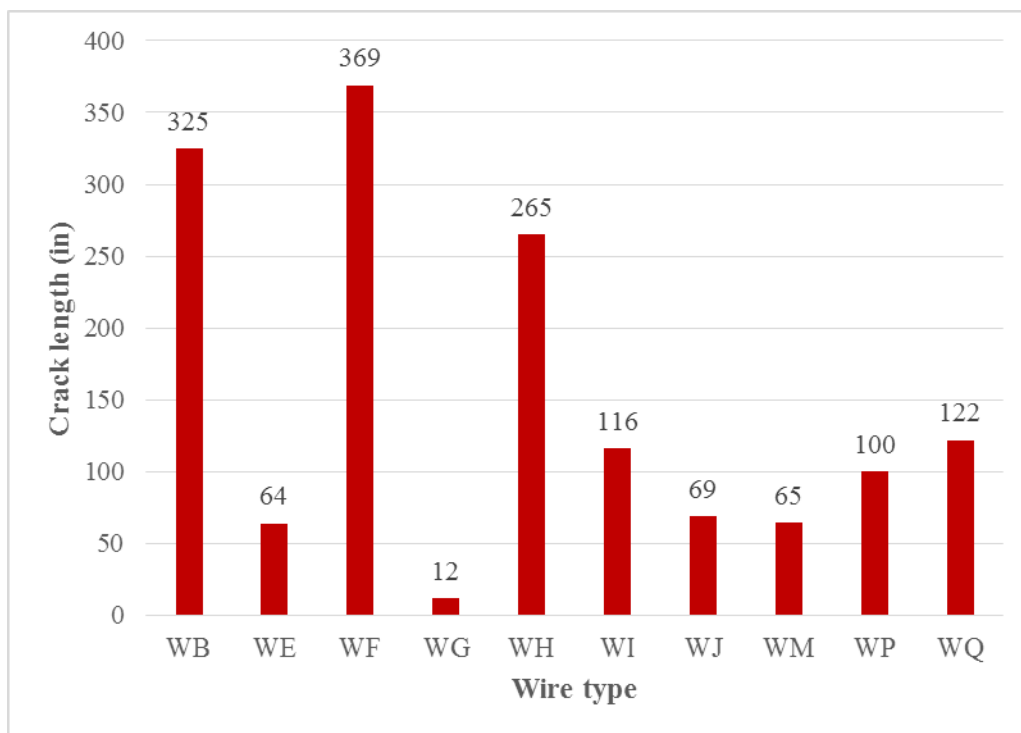


Figure 6-5: Mix#1, 4500 psi, 5/8 in. Edge Distance-Crack Length (in)

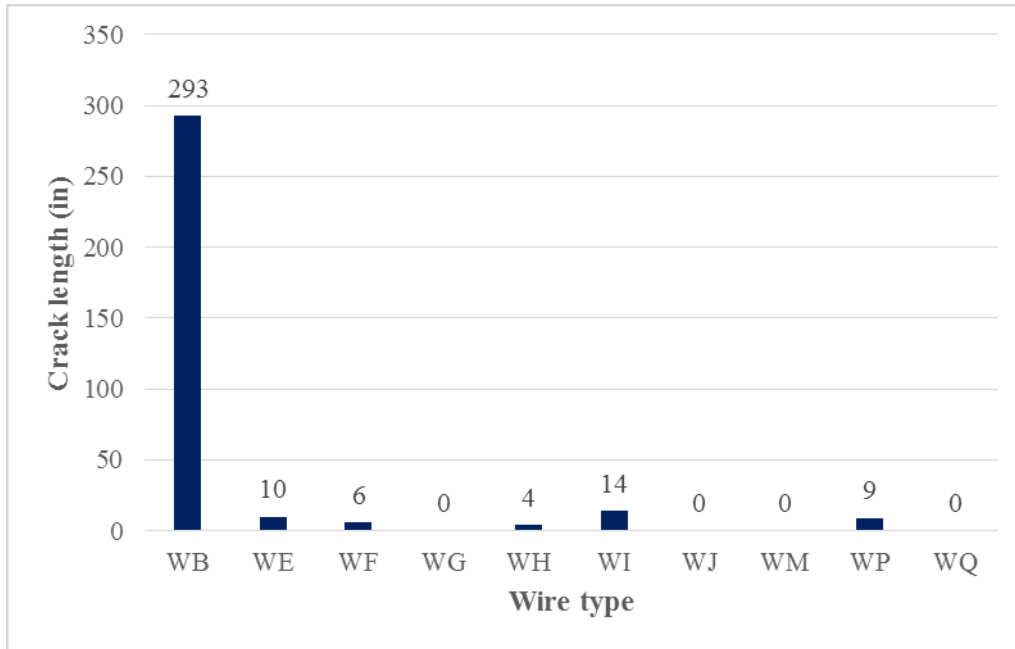


Figure 6-6: Mix#1, 4500 psi, ¾ in. Edge Distance-Crack Length (in)

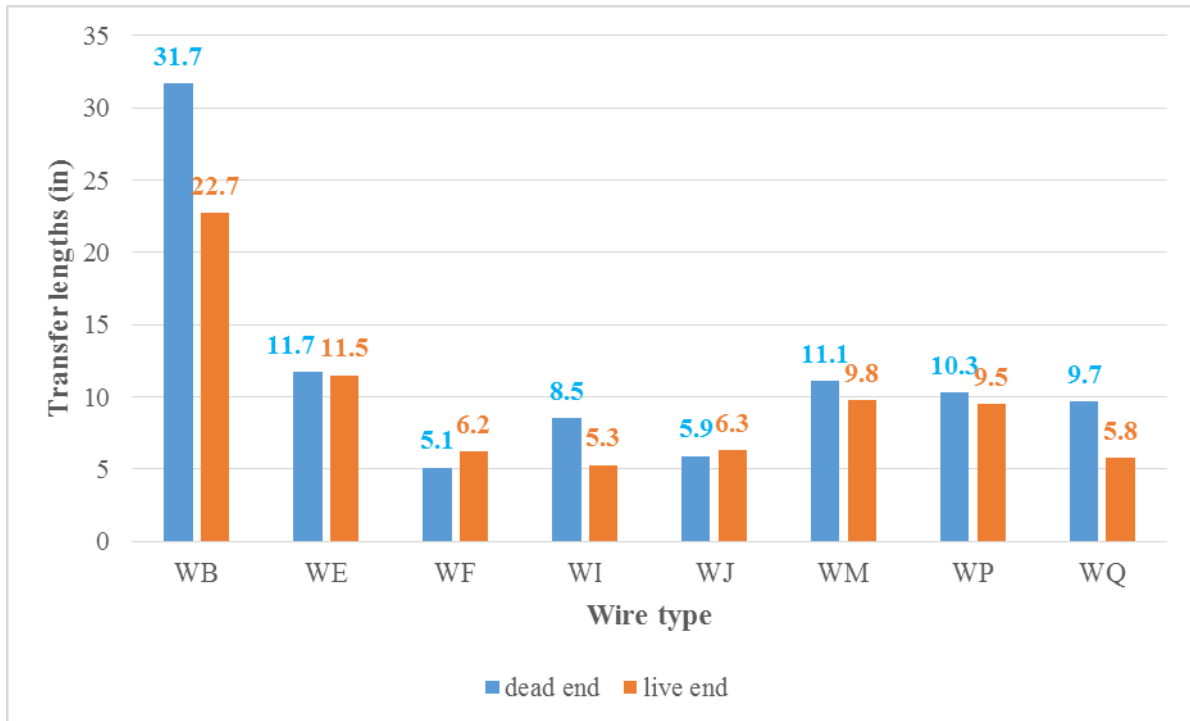


Figure 6-7: Mix#1, 4500 psi, ¾ in. Edge Distance-Transfer Lengths (Dead and Live end)

Figure 6-7 shows the values of transfer length for each wire on both dead and live ends. The values of transfer lengths for WB wire type were found to be large. This resulted from the larger magnitudes of longitudinal surface strain that accompanied the longitudinal splitting of the prism. This also indicated that wire type WB exhibited poor performance which resulted in the maximum number of eight cracks on each prism.

In addition to the number of wires that exhibited cracking, Figure 6-8 shows the number of wires observed to crack (out of eight per prism) as a given as a function of edge distance for the different levels of concrete release strength tested. As the extent of the edge distance was reduced, the tendency was for all ten wire types to crack with ½ in. edge distance for all compressive strengths. Figure 6-8 shows the number of wires ends with splitting cracks for a compressive strength of 4500 psi.

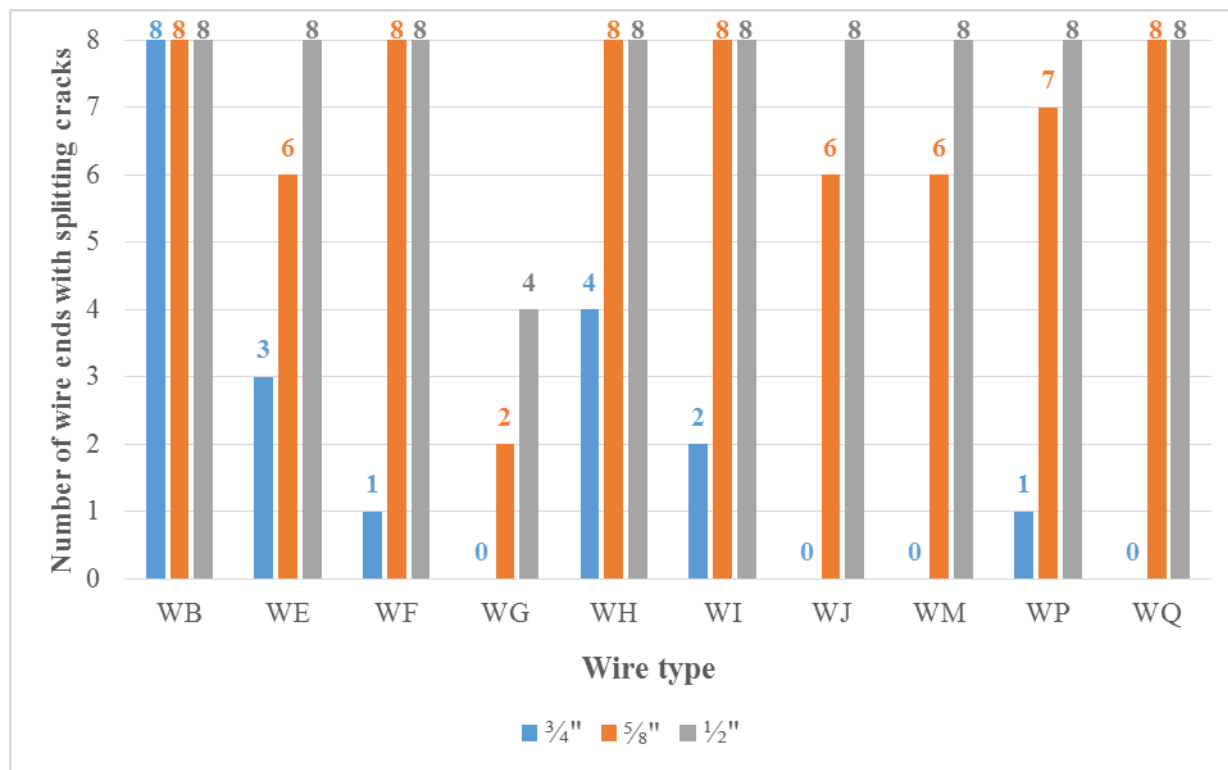


Figure 6-8: Mix#1, 4500 psi-Number of Wires Ends with Splitting Cracks

6.1.2 Release Strength 6000 psi

Figure 6-9, Figure 6-10 and Figure 6-11 show the crack area for a 6000 psi release strength. As shown in these Figures, it was found that increasing the release strength of concrete from 4500 psi to 6000 psi resulted in a decreased crack area. WB wire type indicated poor performance and resulted in the appearance of cracking in all three prisms. WF wire type also performed poorly with prisms having ½ in. and 5/8 in. edge distances resulting in 37.5 in² and 17.4 in² crack areas respectively. Chevron types of wire (WI, WJ, WM, WP and WQ) indicated good performance with prisms having 3/4 in edge distance, and with a decrease in the edge distance to 5/8 in. the values of crack areas were found to increase. The highest level of crack area was observed for the ½ in. edge distance. For a release strength 6000 psi, tests were also performed with smooth wire WA. WA wire type performed very well with no crack appearing for the prisms having 3/4 in. and ½ in. the edge distance, and for the prism having 5/8 in. edge distance a 0.04 in² crack area and a 4 in. crack length were observed.

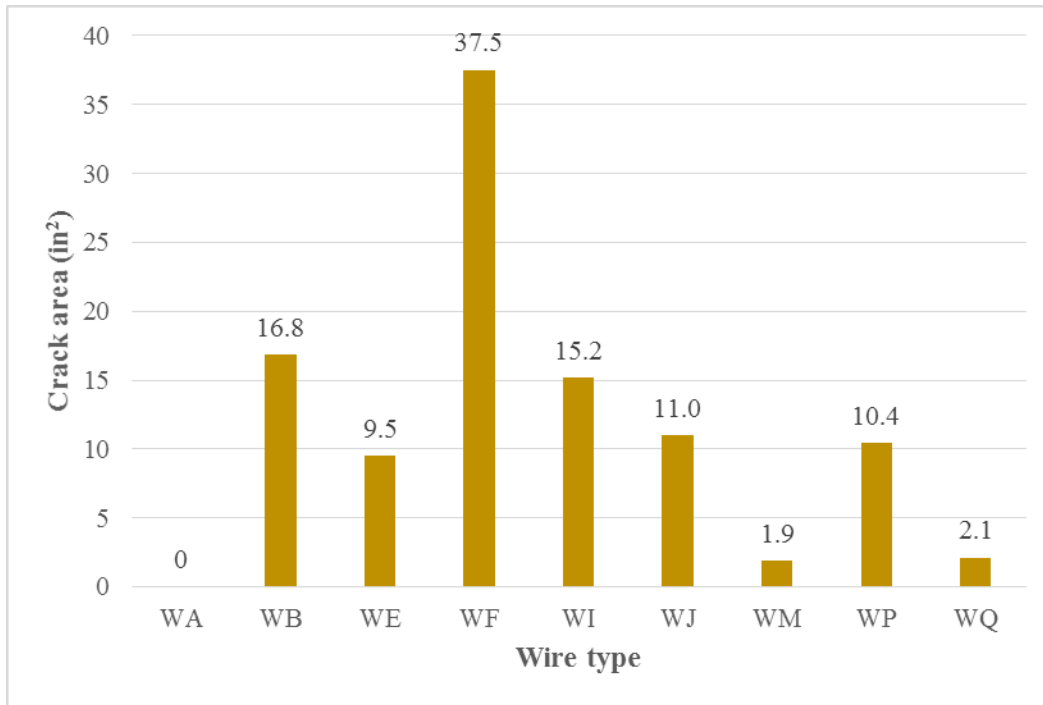


Figure 6-9: Mix#1, 6000 psi, 1/2 in. Edge Distance-Crack Area (in²)

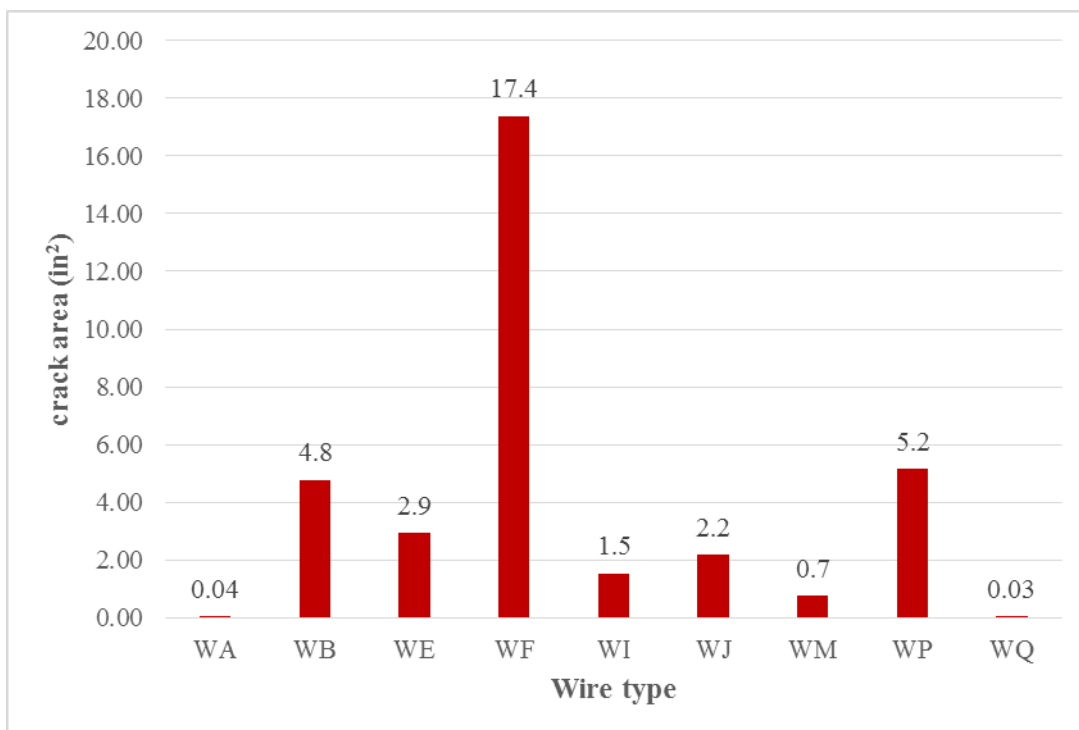


Figure 6-10: Mix#1, 6000 psi, 5/8 in. Edge Distance-Crack Area (in²)

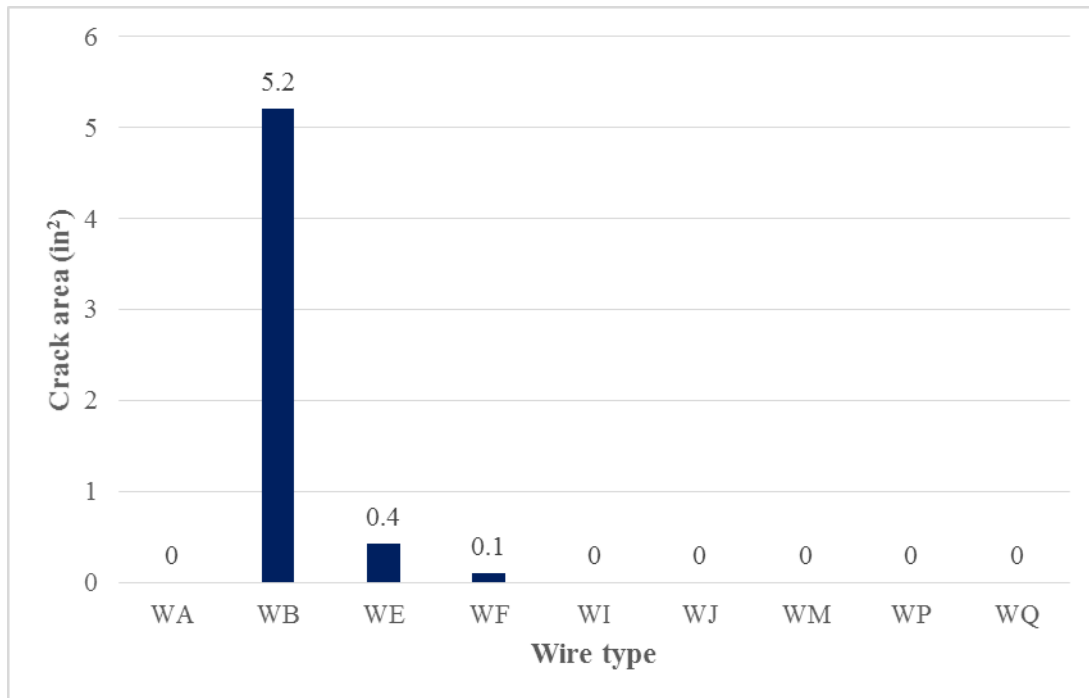


Figure 6-11: Mix#1, 6000 psi, $\frac{3}{4}$ in. Edge Distance-Crack Area (in²)

Figure 6-12, Figure 6-13 and Figure 6-14 show the variation of crack lengths as a function of concrete release strength and the value of the edge distance. The values of crack length were the highest for WB and WF type wires, which belong to the deep chevron type of wire. The shortest length observed was for WQ wire type which indicated the best behavior. It was found that the values of crack lengths increased upon decreasing the edge distance. Wire types WI, WJ, WM, WP and WQ performed well with prisms having $\frac{3}{4}$ in. edge distance.

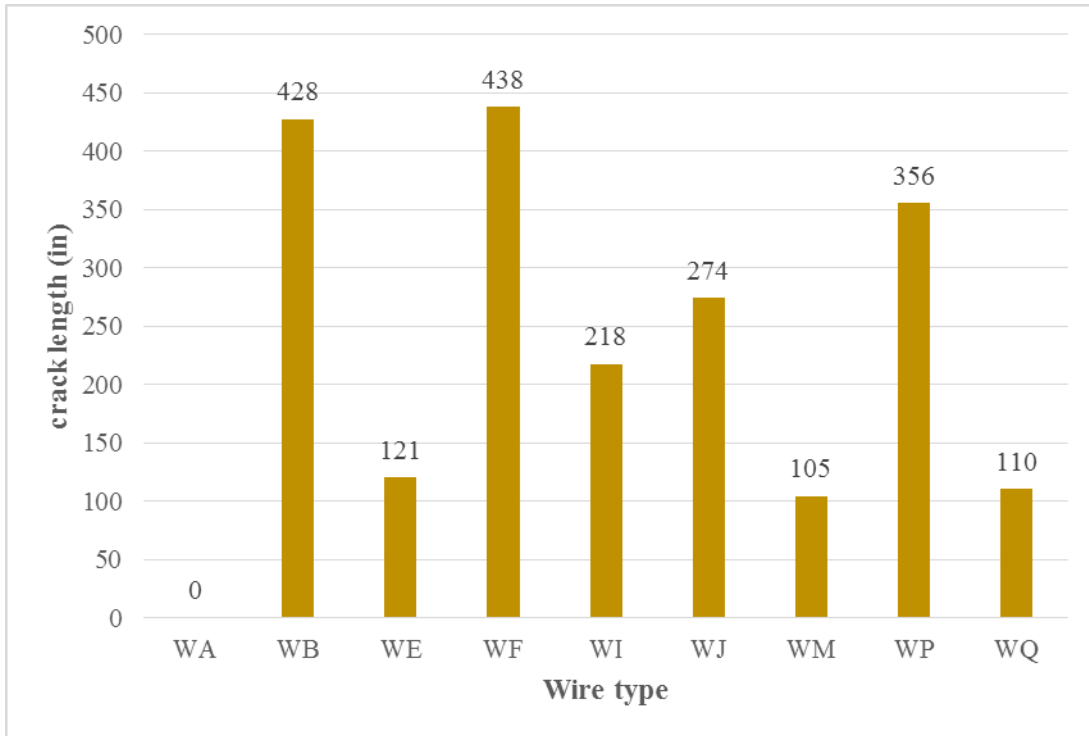


Figure 6-12: Mix#1, 6000 psi, 1/2 in. Edge Distance-Crack Length (in)

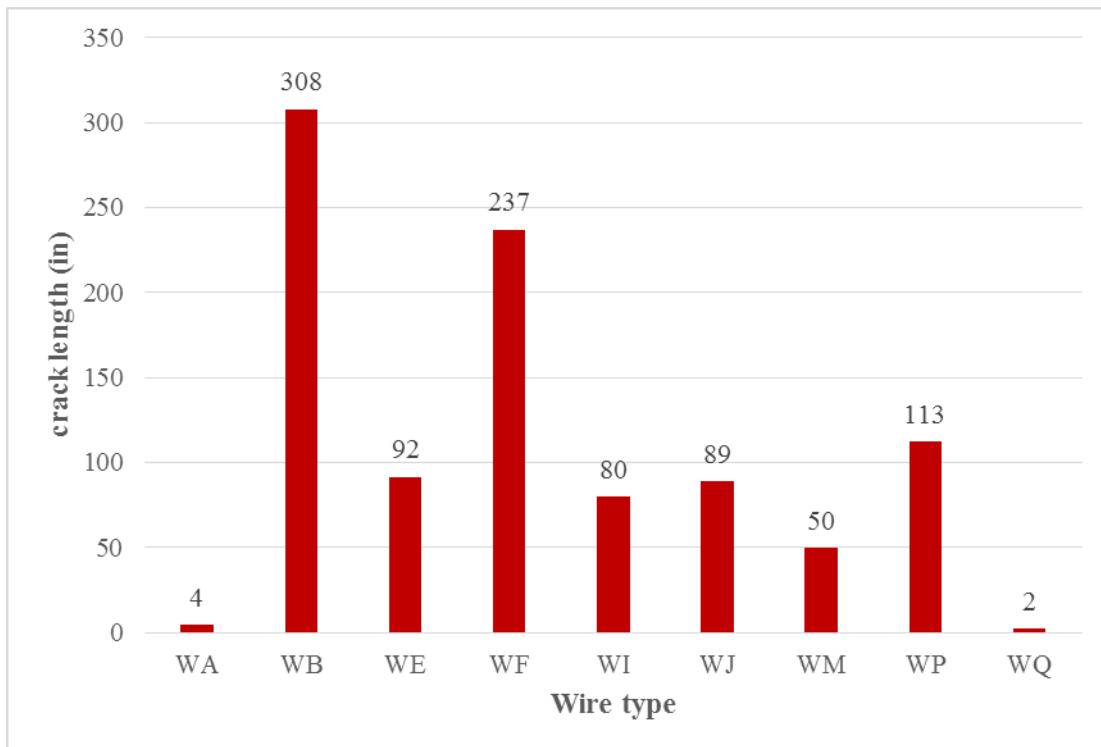


Figure 6-13: Mix#1, 6000 psi, 5/8 in. Edge Distance-Crack Length (in)

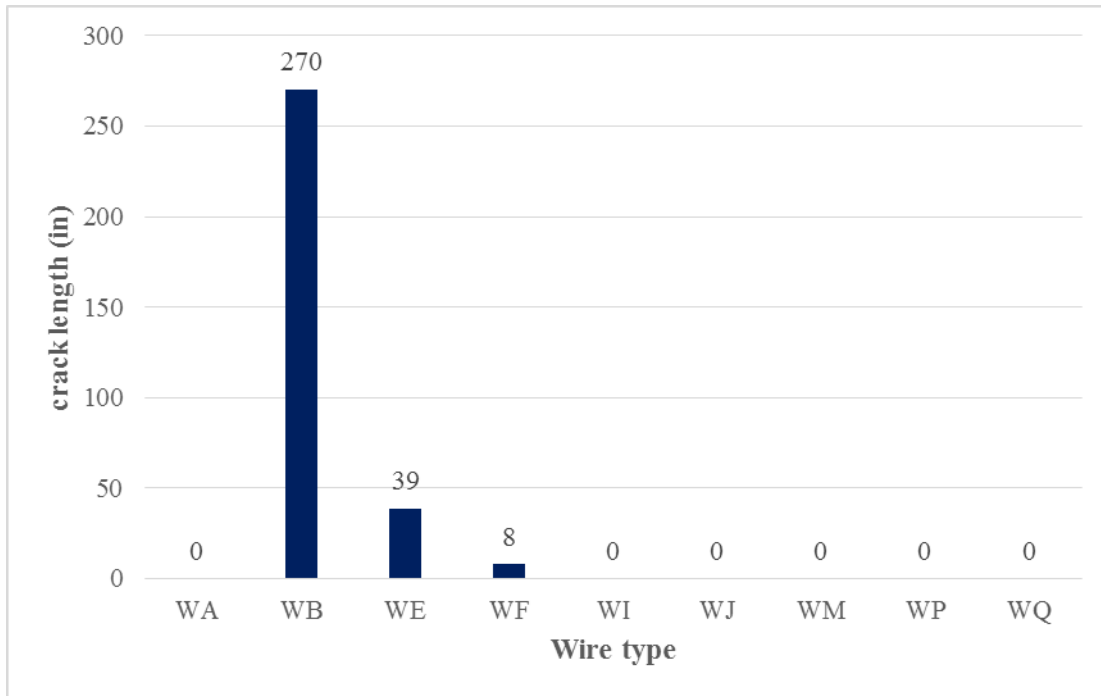


Figure 6-14: Mix#1, 6000 psi, $\frac{3}{4}$ in. Edge Distance-Crack Length (in)

Figure 6-15 shows the number of wires ends with splitting cracks for 6000 psi release strength. As shown in Figure 6-15 decreasing the edge distance resulted in increasing the number of cracks. WB wire type indicated poor performance with eight cracks on each prism. Smooth wire type WA indicated good performance, with no crack appearance for the prisms having $\frac{3}{4}$ in. and $\frac{1}{2}$ in. edge distances and only one crack on $\frac{5}{8}$ in. edge distance. The corresponding value of crack length was 4 in. WQ wire type indicated the best behavior, showing no cracks for the prism with $\frac{3}{4}$ in. edge distance and only three cracks on the prism with $\frac{5}{8}$ in. edge distance.

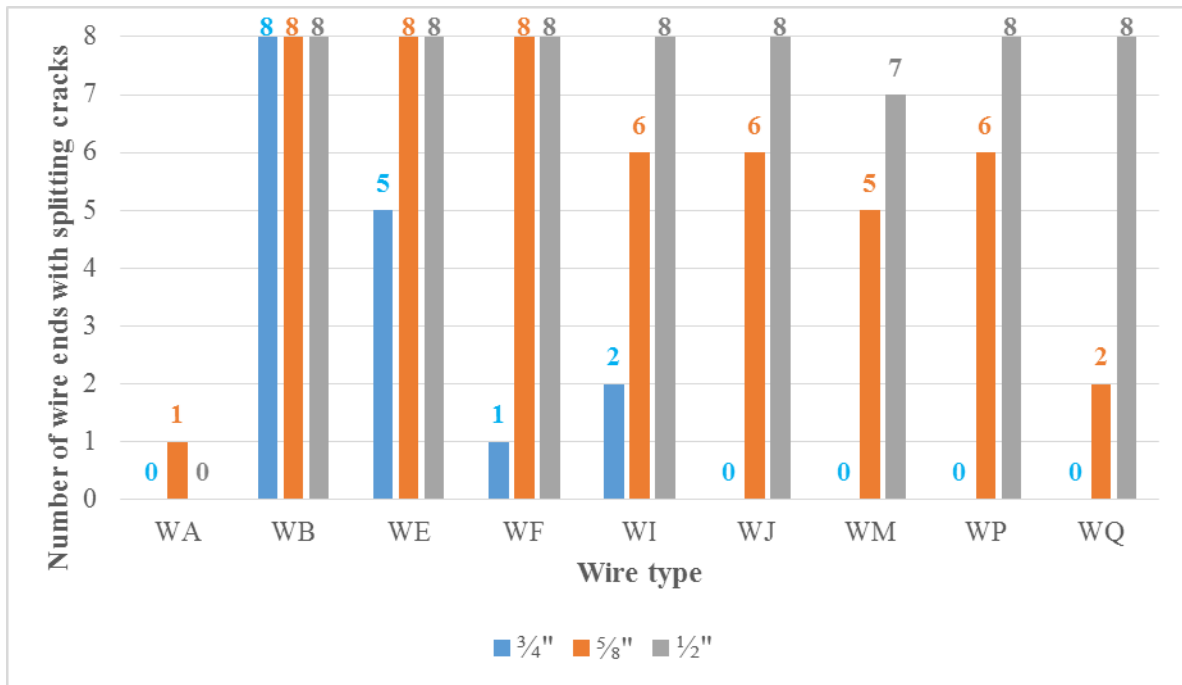


Figure 6-15: Mix#1, 6000 psi-Number of Wires Ends with Splitting Cracks

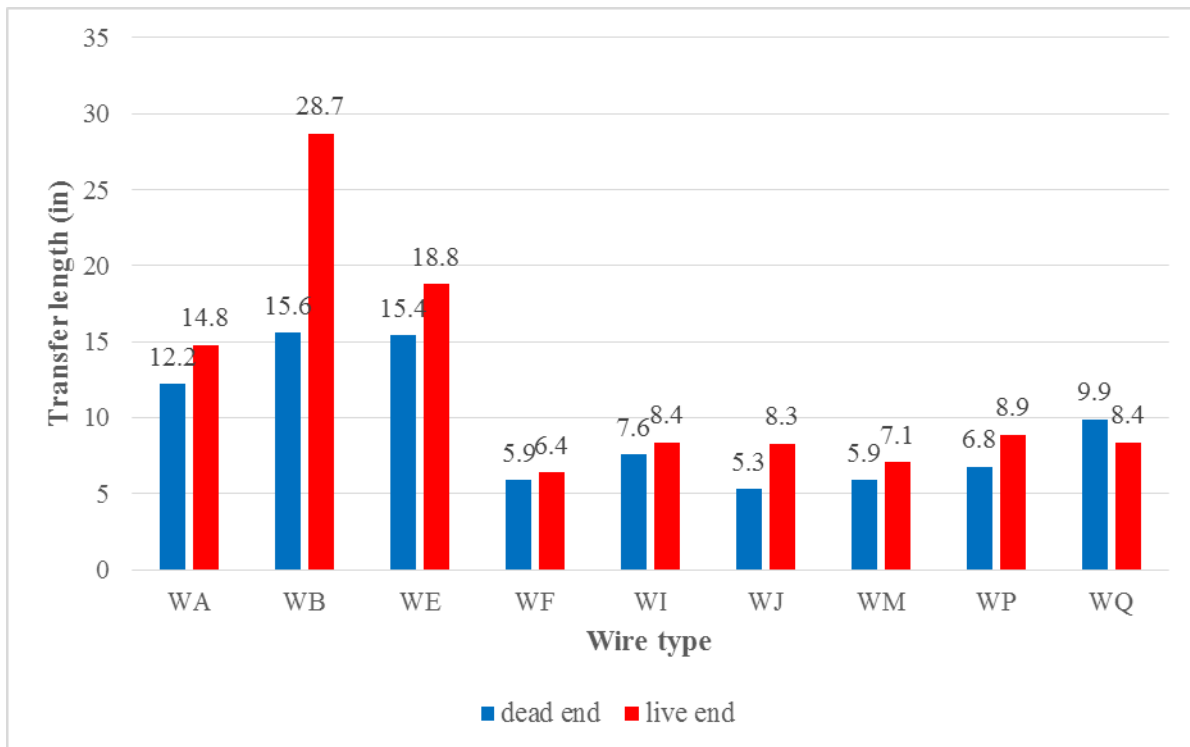


Figure 6-16: Mix#1, 6000 psi-Transfer Lengths (Dead end and live end)

Figure 6-16 shows the values of transfer length for a release strength 6000 psi where it was found that values for transfer length decreased. The values for transfer length for WB wire type had the highest values due to the higher observed magnitudes of longitudinal surface strain. This indicated longitudinal splitting/cracking of the prism and poor performance resulting in a maximum number of eight cracks on each prism.

6.1.3 4500psi Release Strength Versus 6000 psi Release Strength

Figure 6-17 shows the crack length as a function of varying release strengths and the values of edge distances. For the first prism with $\frac{3}{4}$ in. edge distance, the difference between crack lengths for the two-release strengths was found to be 5.8 %. For the second prisms in the series, it was found that this difference increased to 44 %. The third prisms in series showed a crack length difference of 35 % for different release strengths.

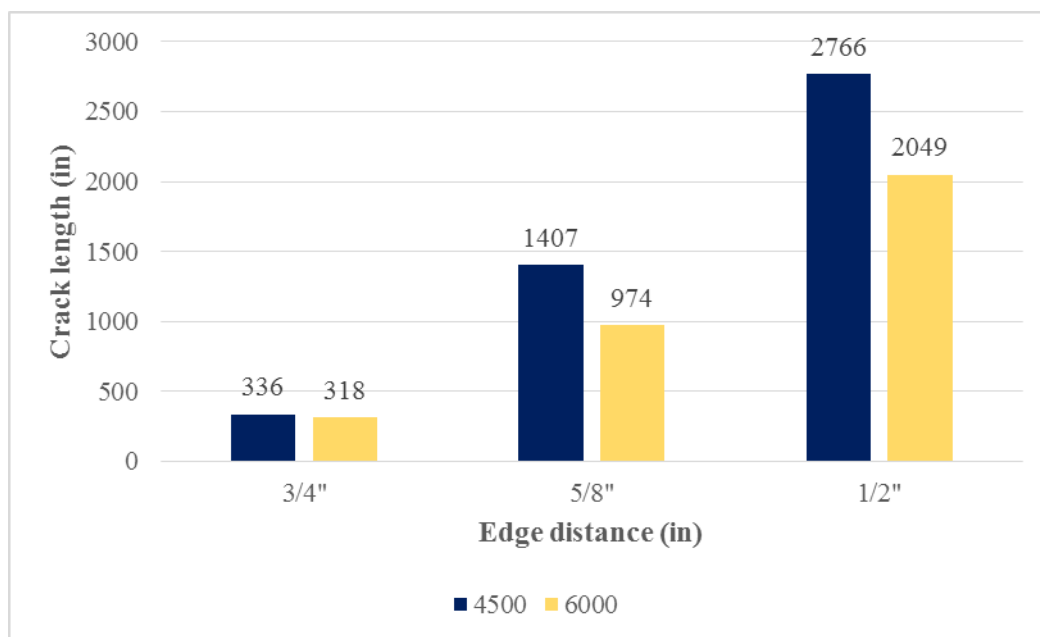


Figure 6-17: Mix#1-4500 psi vs 6000 psi

The overall crack length for all the prisms done with 4500 psi release strength were 4508 in, and 3340 in. for the prisms done with 6000 psi release strength.

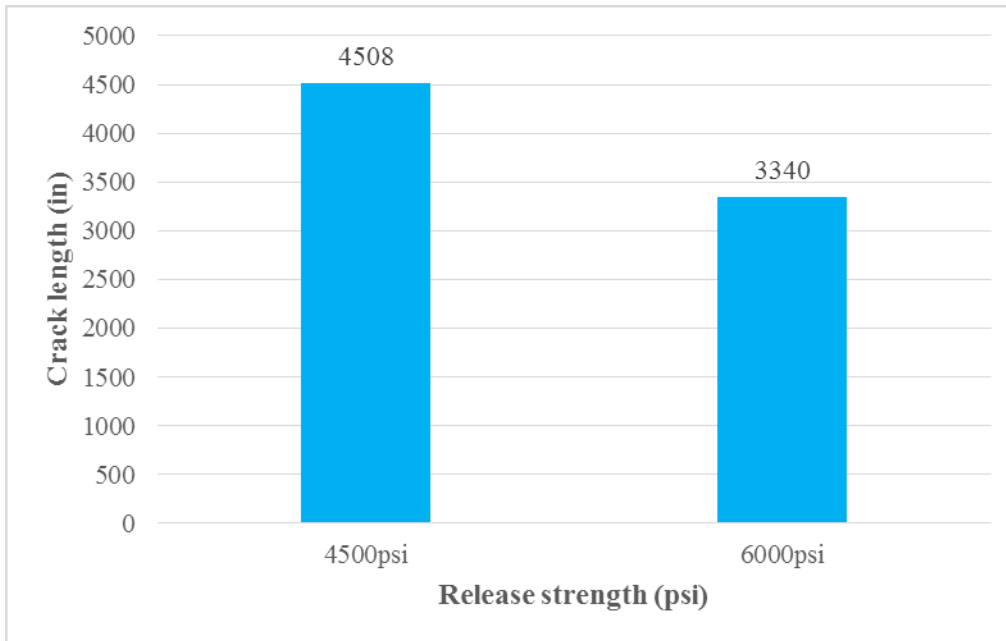


Figure 6-18: Mix#1-Total Crack Lengths-4500 psi vs 6000 psi

6.2. Concrete Mixture-Mix#2

6.2.1. Release strength 4500 psi

Figure 6-19 through Figure 6-21 show the overall crack area for the prisms constructed with granite aggregates. Chevron wire types (WG, WI, WJ, WM, WP and WQ) indicated good performance with prisms having a $\frac{3}{4}$ in edge distance. Deep chevron wire types performed poorly resulting in crack areas of 3.6 in^2 for WB, 1.4 in^2 for WF and 0.1 in^2 for WH type wires for the prisms having a $\frac{3}{4}$ in. edge distance. When the edge distance was reduced from $\frac{3}{4}$ in. to $\frac{5}{8}$ in. it was observed that more cracks appeared; consequently, these crack areas were larger. The highest values of crack areas were for WB and WF type wires. WJ type wire performed very well with prism having a $\frac{5}{8}$ in. edge distance which resulted in no cracks appearing on the prism. Shallow chevron wire types performed better than deep chevron, and the average crack area was approximately 0.3 in^2 for WM, WG, WQ and WP type wires.

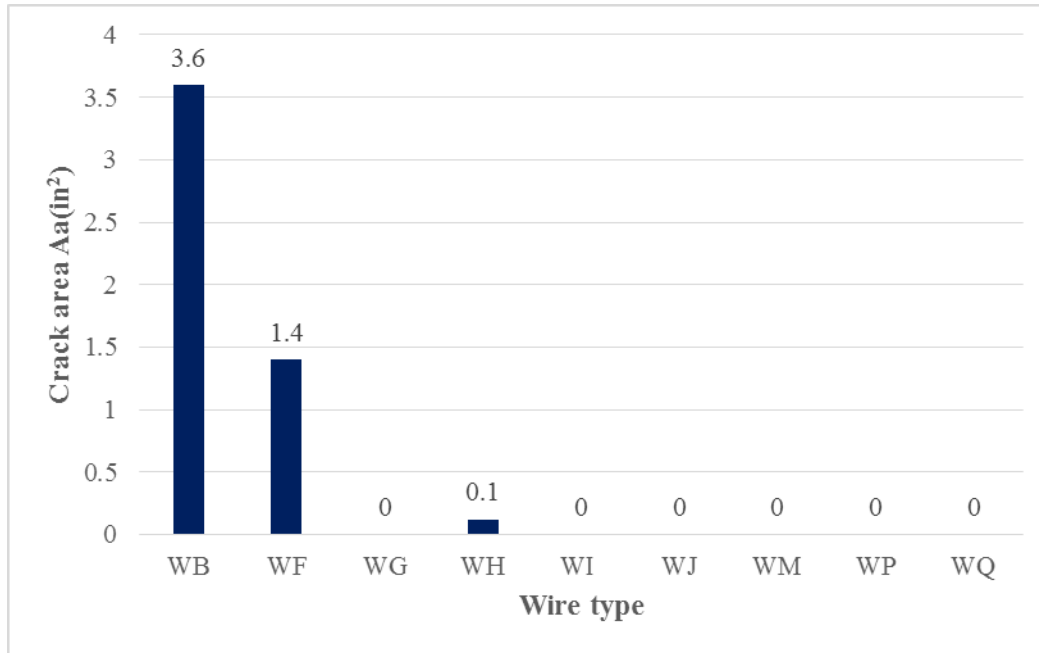


Figure 6-19: Mix#2, 4500 psi, ¾ in. Edge Distance-Crack Area (in²)

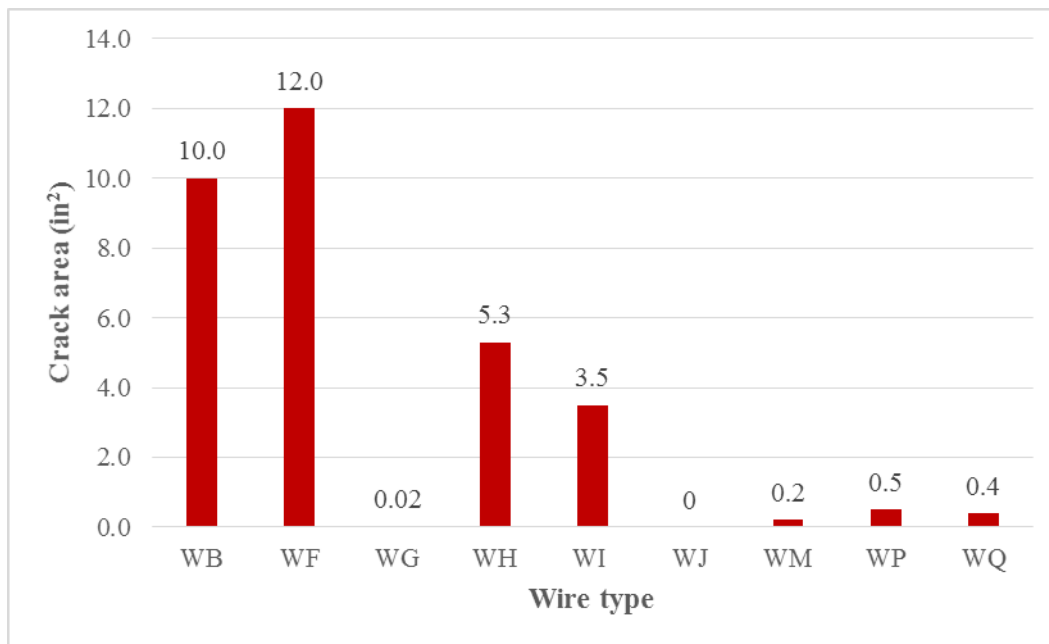


Figure 6-20: Mix#2, 4500 psi, 5/8 in. Edge Distance-Crack Area (in²)

Prisms having ½ in. edge distance performed poorly resulting in larger crack areas especially for WF and WJ wire type exhibited crack areas of 59.4 in² and 49.1 in² respectively. WG wire type was found to have the smallest crack area as shown in Figure 6-21.

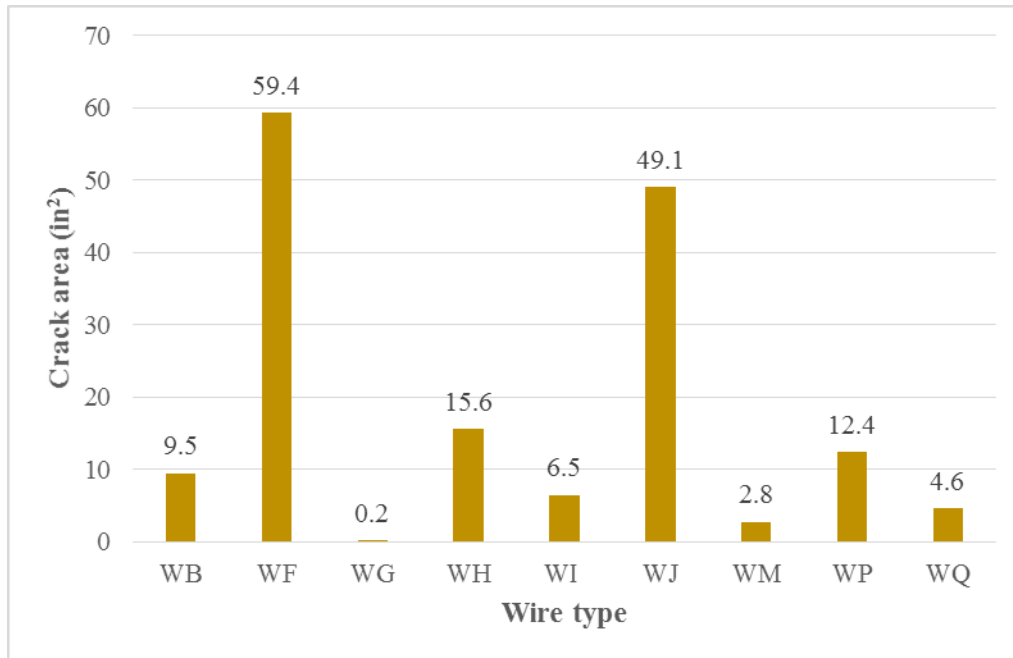


Figure 6-21: Mix#2, 4500 psi, ½ in. Edge Distance-Crack Area (in²)

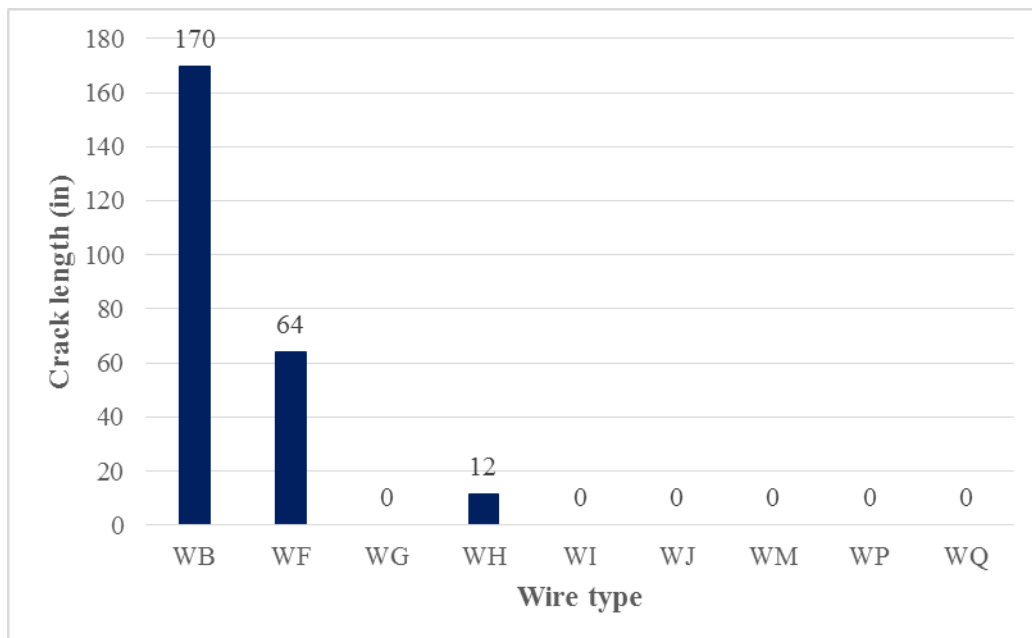


Figure 6-22: Mix#2, 4500 psi, ¾ in. Edge Distance-Crack Length (in)

Additionally, as seen in Figure 6-22, Figure 6-23, and Figure 6-24, similar crack patterns was found with crack lengths. The highest value of crack length was found for WB type wire which was 170 in. on the prism with ¾ in. edge distance. Decreasing the values of edge distances, resulted in an increase in crack lengths for almost every wire type except for WJ for prisms with ⅝ in. edge distance. Prisms having ½ in. edge distance showed that deep chevron type wires had the poorest behavior (WF, WH, WB wire type), and WG had the best behavior with only 23 in

crack lengths observed. Figure 6-25 shows the number of wires ends with splitting cracks for 4500 psi release strength.

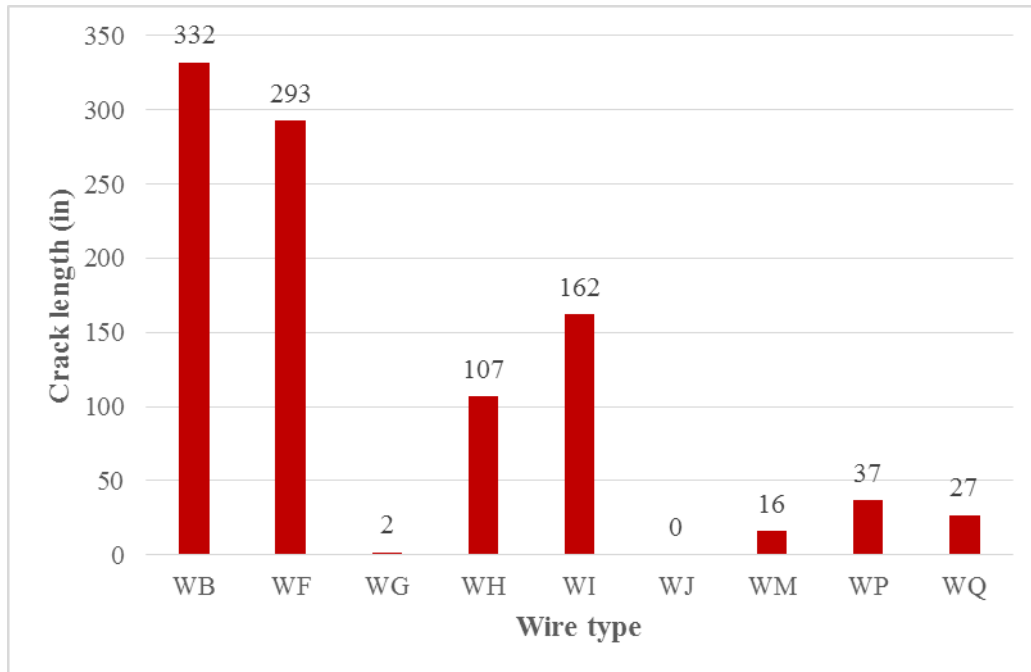


Figure 6-23: Mix#2, 4500 psi, $\frac{5}{8}$ in. Edge Distance-Crack Length (in)

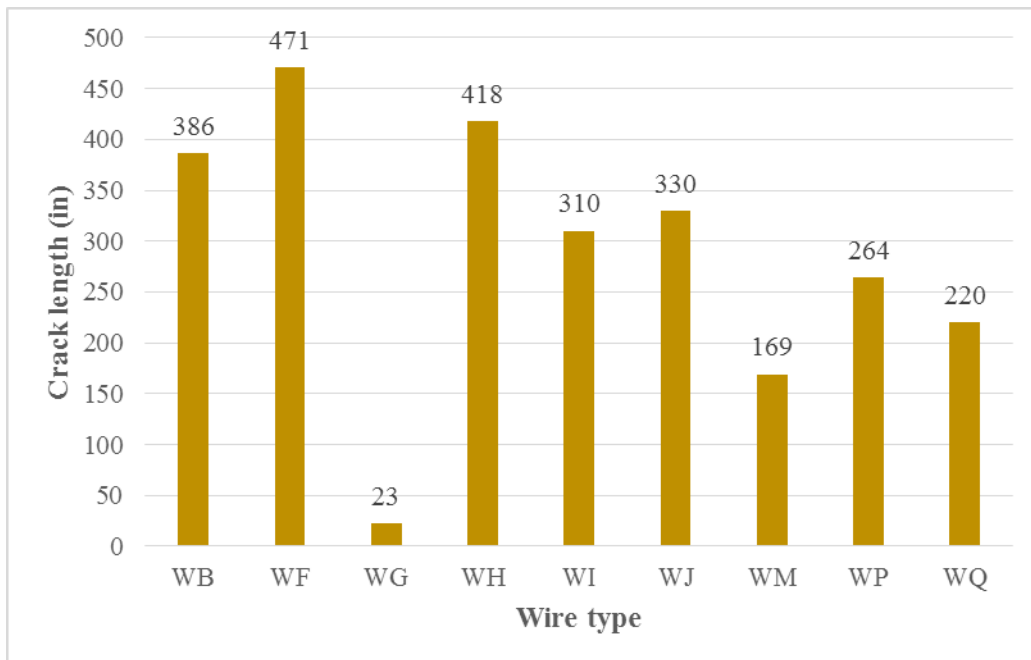


Figure 6-24: Mix#2, 4500 psi, $\frac{1}{2}$ in. Edge Distance-Crack Length (in)

Figure 6-25 shows the influence of edge distance on cracking propensity.

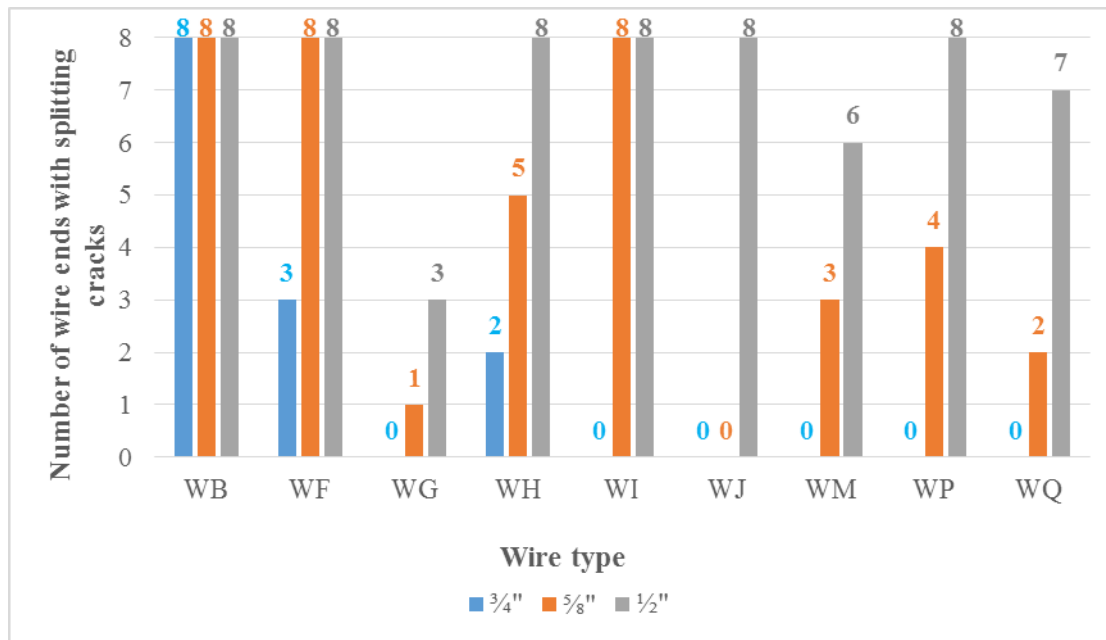


Figure 6-25: Mix#2, 4500 psi-Number of Wires Ends with Splitting Crack

6.2.2 Release strength 6000 psi

Increasing the release strength, resulted in crack areas that were smaller for all types of wires as shown in Figure 6-26, Figure 6-27, and Figure 6-28. Wire types WJ, WM and WQ did not have any cracks on the prism with 3/4 in. value of edge distance, and WB wire type showed poor behavior having 1.9 in² crack area.

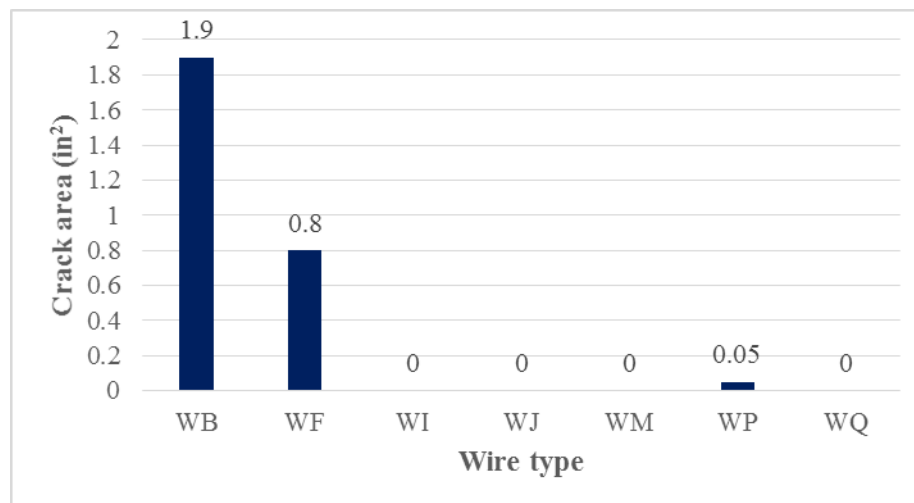


Figure 6-26: Mix#2, 6000 psi, 3/4 in. Edge Distance-Crack Area (in²)

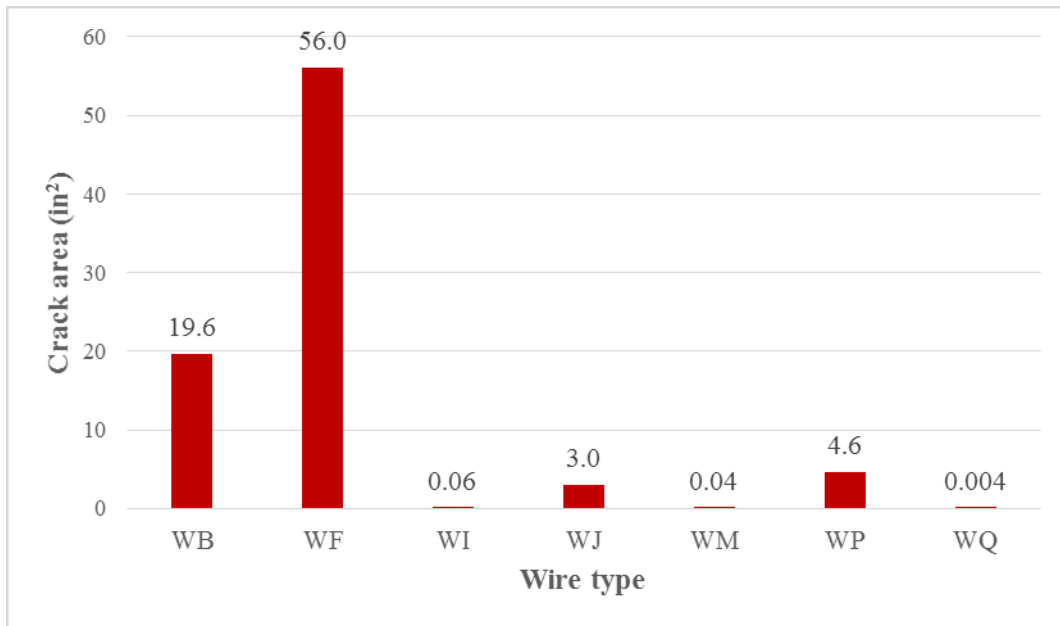


Figure 6-27: Mix#2, 6000 psi, 5/8 in. Edge Distance-Crack Area (in²)

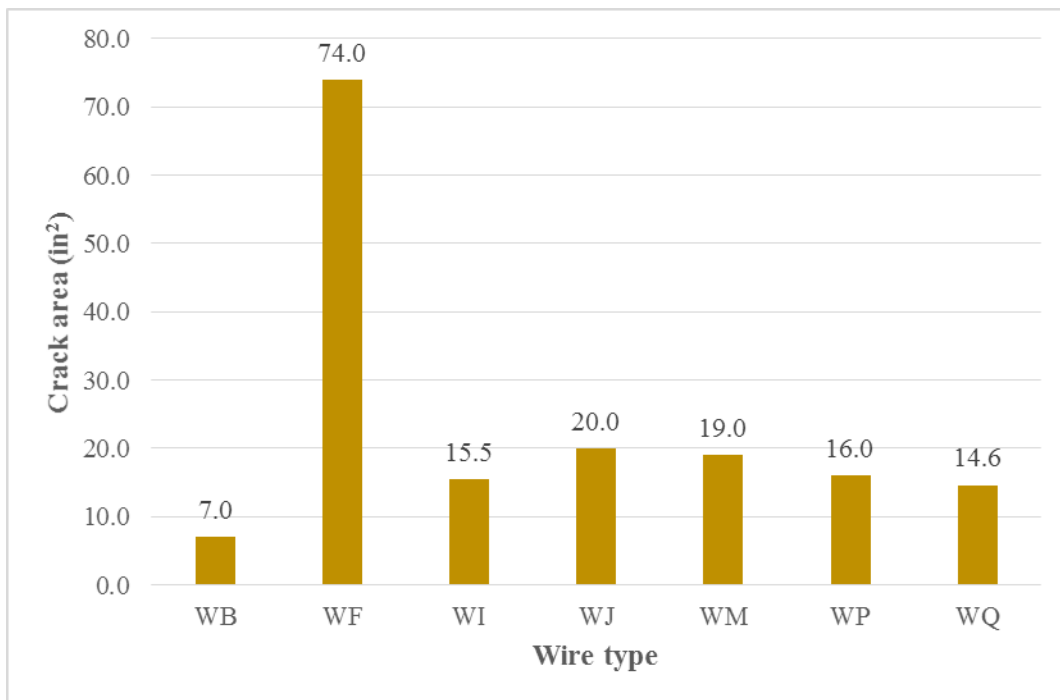


Figure 6-28: Mix#2, 6000 psi, 1/2 in. Edge Distance-Crack Area (in²)

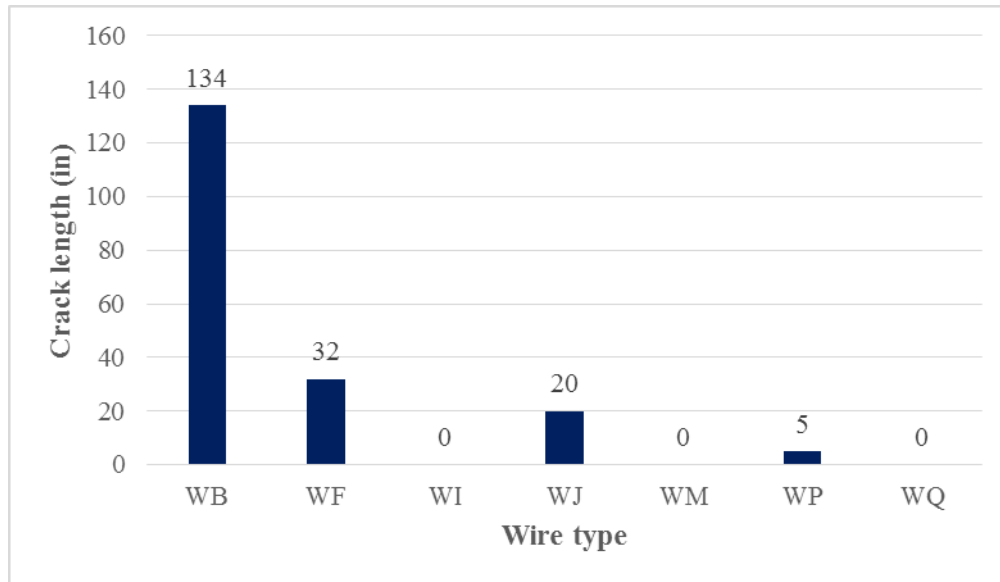


Figure 6-29: Mix#2, 6000 psi, $\frac{3}{4}$ in. Edge Distance-Crack Length (in)

It was found that decreasing the edge distance resulted in additional cracks, which were observed on the prisms with $\frac{1}{2}$ in. edge distance. All wire types exhibited poor performance with the prisms having a $\frac{1}{2}$ in edge distance. WF wire type was found to have the largest crack area for both prisms with values of $\frac{5}{8}$ in. and $\frac{1}{2}$ in. edge distances and the values observed were 56.0 in² and 74.0 in² respectively. Additionally, the values of crack areas also indicated that bond between steel and concrete was destroyed.

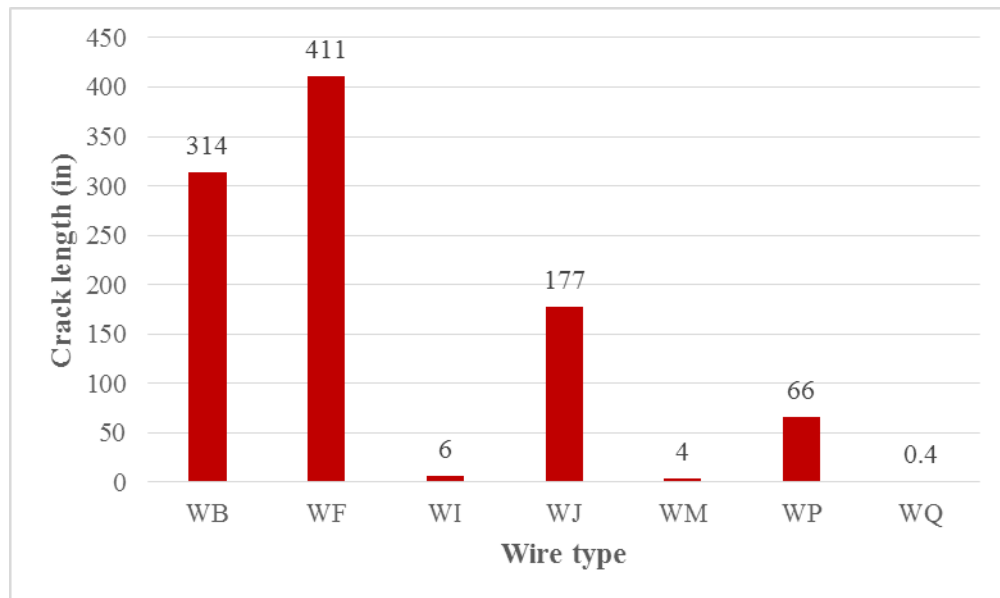


Figure 6-30: Mix#2, 6000 psi, $\frac{5}{8}$ in. Edge Distance-Crack Length (in)

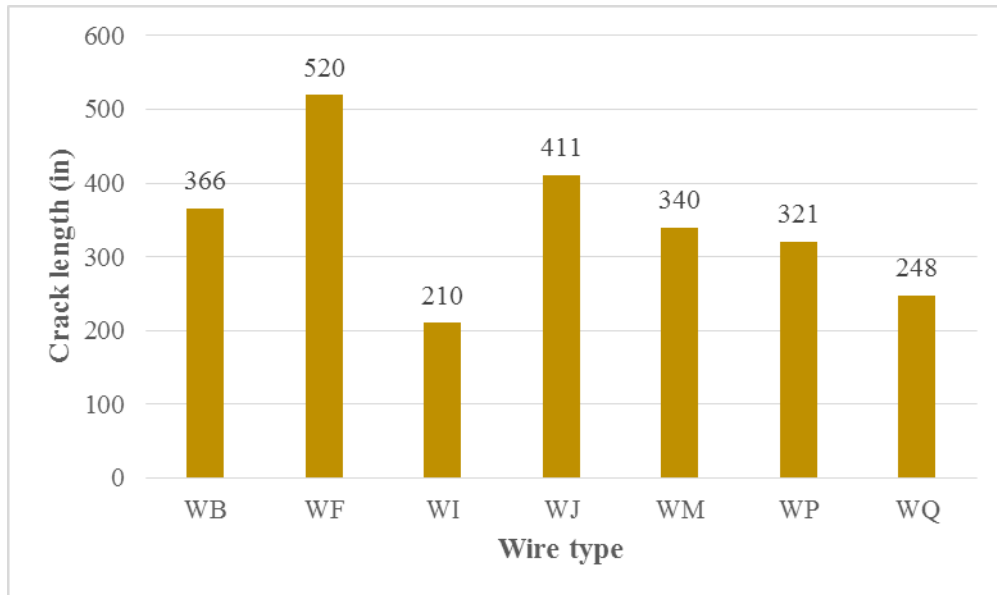


Figure 6-31: Mix#2, 6000 psi, 1/2 in. Edge Distance-Crack Length (in)

The values of crack lengths are shown in Figure 6-29 to Figure 6-31, and these values were found to increase with reducing the cover. The same cracking pattern was repeated with WF wire type, which indicated the worst behavior for the values of 5/8 in. and 1/2 in. edge distances. WQ wire type performance was found to be excellent with this mixture. Figure 6-32 shows the number of wires ends with splitting cracks as a function of edge distance.

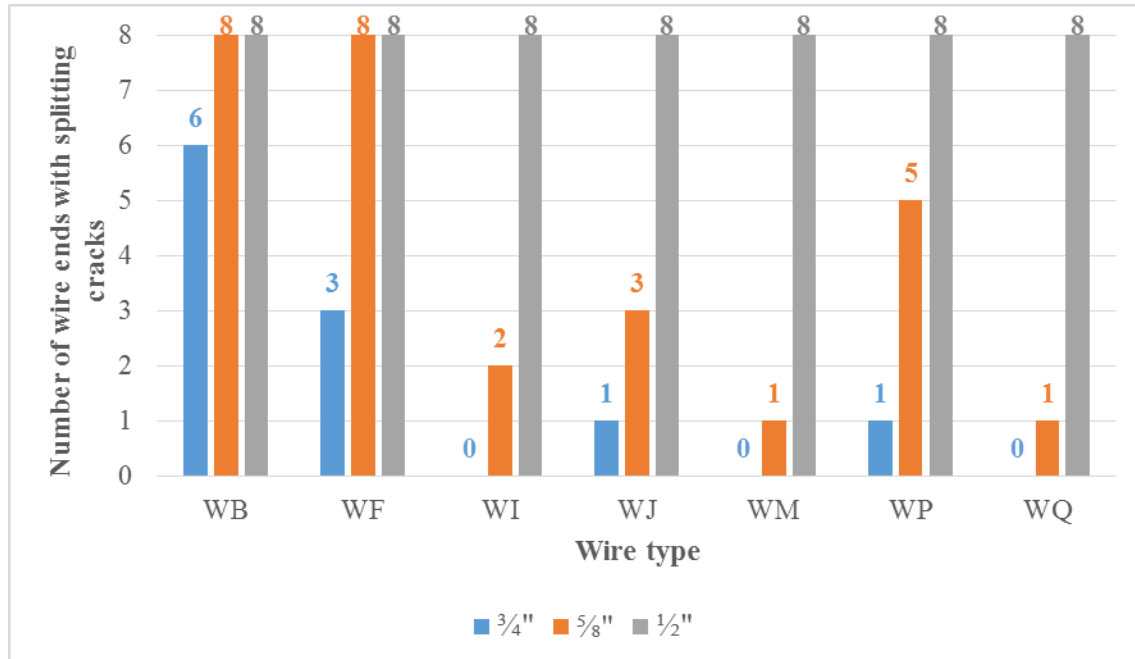


Figure 6-32: Mix#2, 6000 psi-Number of Wires Ends with Splitting Cracks

6.2.3. 4500psi release strength versus 6000 psi release strength

The difference between crack lengths for the two release strengths 4500 psi and 6000 psi is shown in Figure 6-33. The prism with $\frac{3}{4}$ in. edge distance performed better with the higher release strength resulting in a difference of 28 %. The prism with $\frac{5}{8}$ in. edge distance performed approximately 0.3 % better for the 6000 psi release strength. The third prism in series had approximately 0.7 % better performance with the 6000 psi release strength. The overall crack length for 4500 psi release strength was 3812 in. and for 6000 psi release strength was 3585 in, which results in a difference of 6.0 % as shown in Figure 6-34. As shown by these results, the release strength played an important role for the prisms with $\frac{3}{4}$ in. edge distance. Additionally, reducing the cover resulted in a decrease in the influence of release strength. The reason for this decrease in the influence of release strength was found to be a tendency for prisms to crack with the smaller amount of cover.

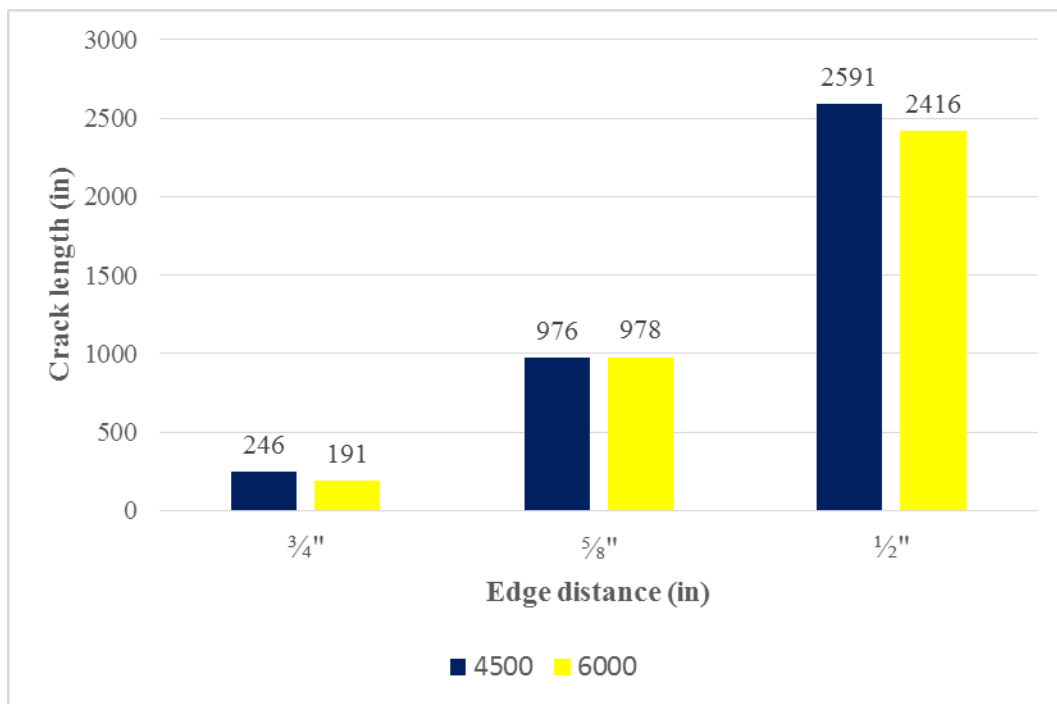


Figure 6-33: Mix#2-4500 psi vs 6000 psi

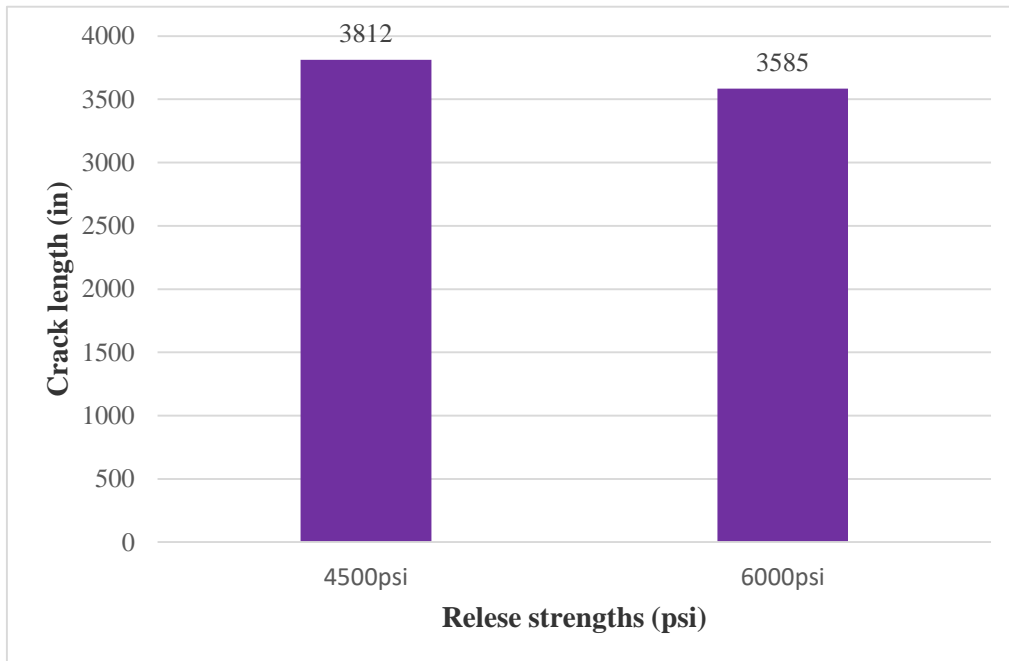


Figure 6-34: Mix#2, Crack Lengths (in)-4500 psi vs 6000 psi

6.3. Concrete Mixture-Mix#3

The third mixture was made of uncrushed pea-gravel aggregate and was found to have poor performance with almost all wires tested. Wire type WQ performed very well with the prism having a $\frac{3}{4}$ in. edge distance. As shown in Figure 6-35 wire type WQ performed the best. All other wires showed a predisposition to split on the first prism with $\frac{3}{4}$ in. edge distance. The largest crack area was for wire type WB which exhibited the worst performance among all wires tested.

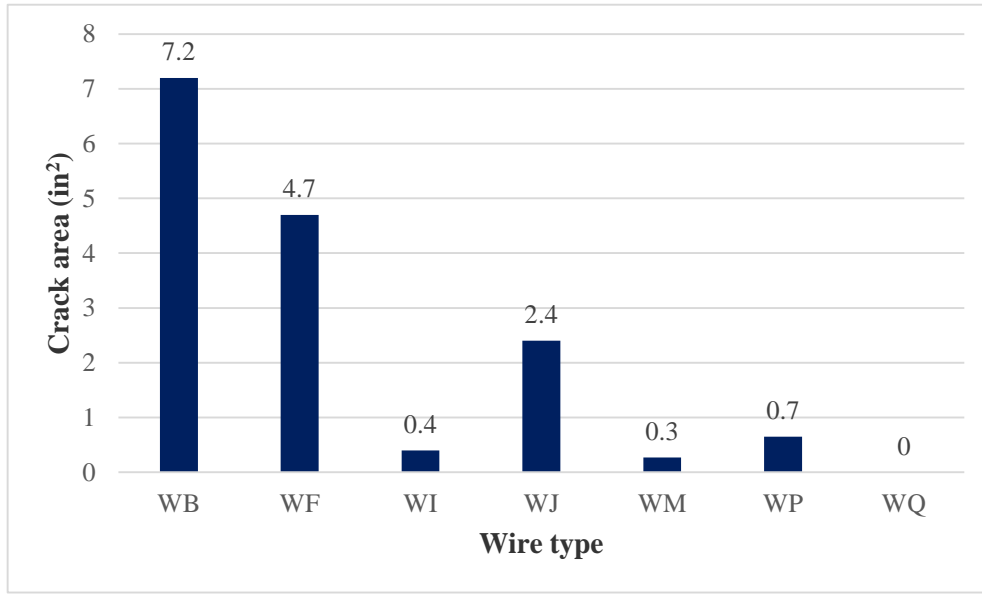


Figure 6-35: Mix#3, 4500 psi, ¾ in. Edge Distance-Crack Area (in²)

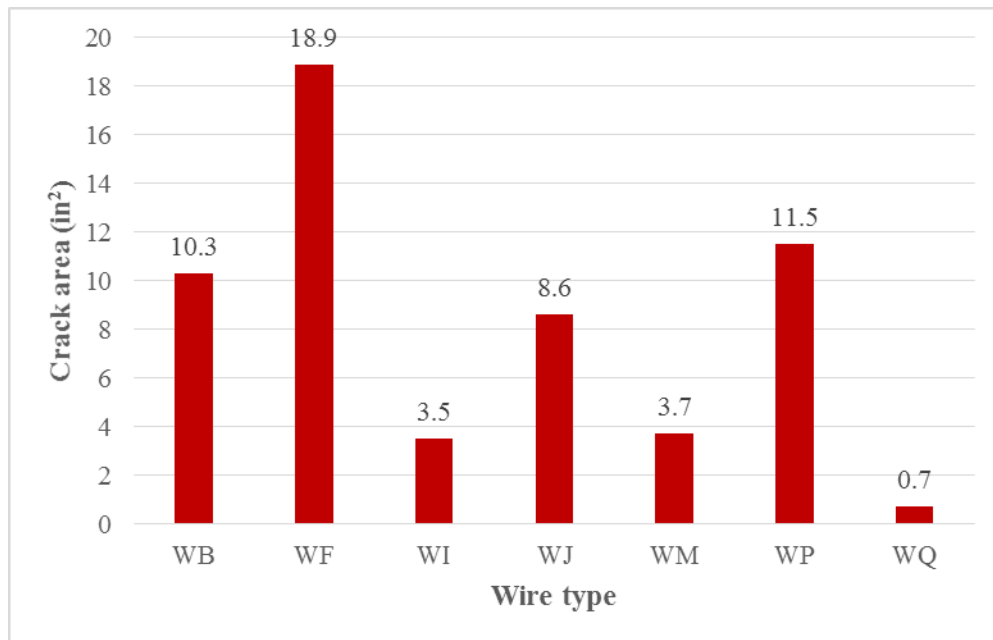


Figure 6-36: Mix#3, 4500 psi, 5/8 in. Edge Distance-Crack Area (in²)

With a decrease in the cover, all wires showed poor behavior as shown in Figure 6-36 and Figure 6-37. WF wire type was found to have the largest crack area. WQ wire type exhibited the best behavior with three cracks on the prisms with 5/8 in. edge distance. The same crack pattern was also shown for the prism with 1/2 in. edge distance.

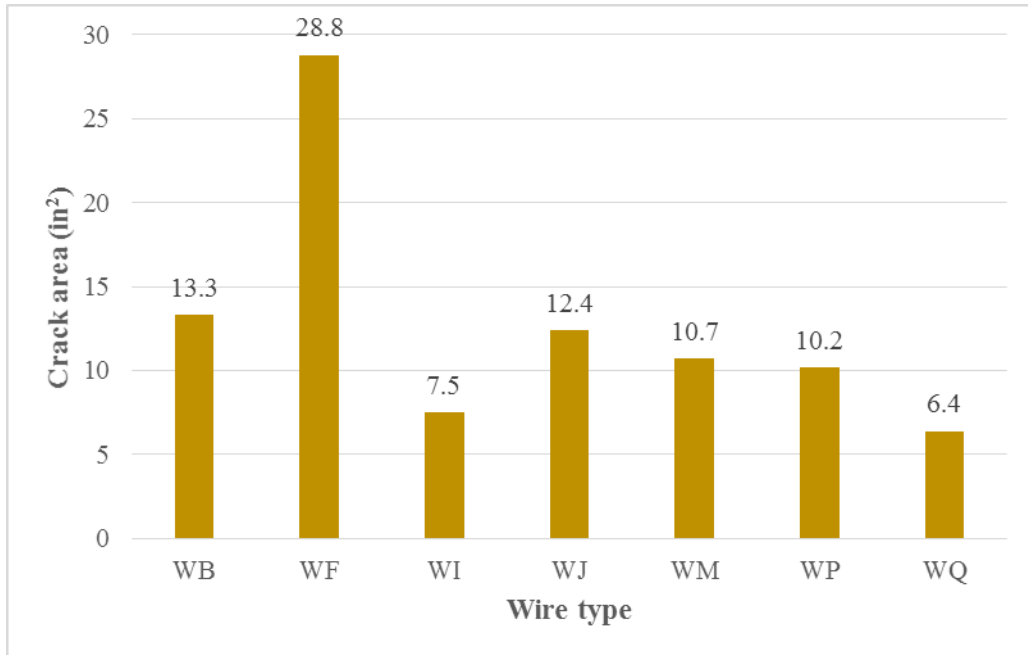


Figure 6-37: Mix#3, 4500 psi, 1/2 in. Edge Distance-Crack Area (in²)

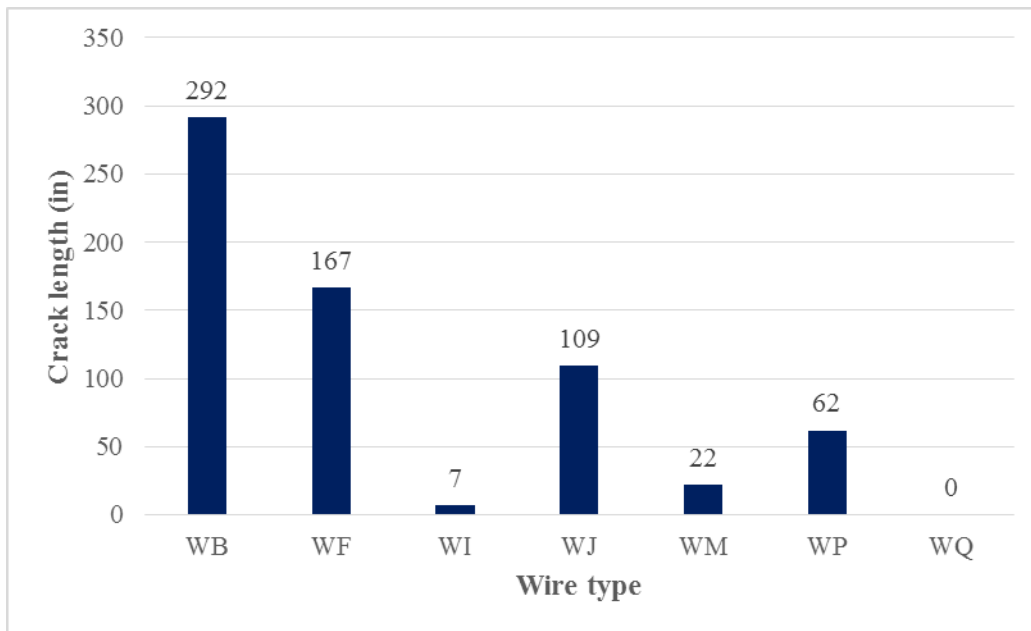


Figure 6-38: Mix#3, 4500 psi, 3/4 in. Edge Distance-Crack Length (in)

Figure 6-38 shows crack length given as a function of wire type for the 3/4 in. edge distance. WB type wire had the largest value of crack length. Comparing with the other mixtures, the value of crack length was highly increased for Mix#3 for almost all the type of wires.

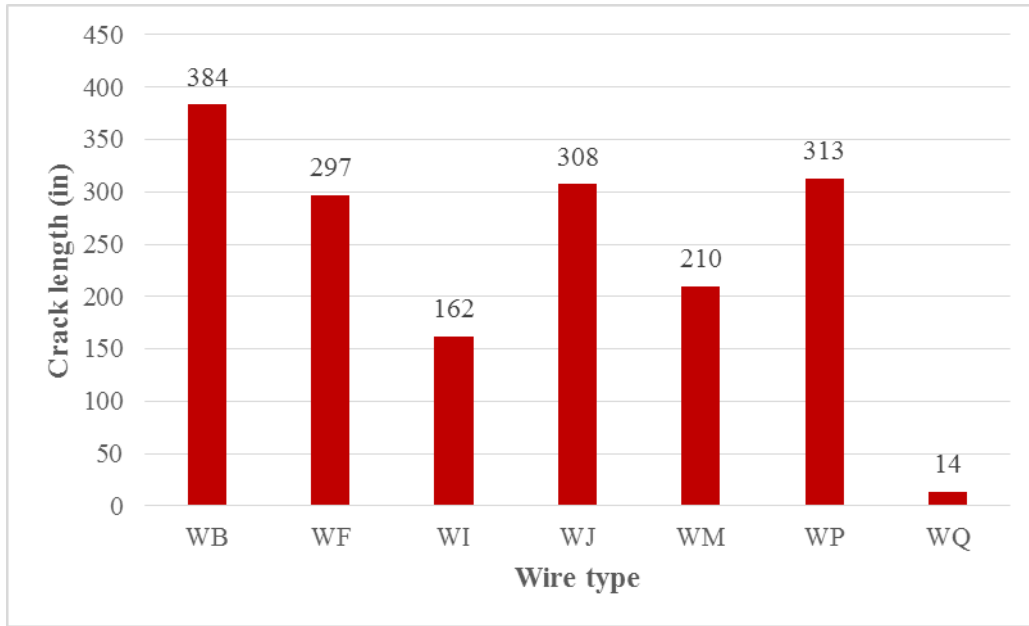


Figure 6-39: Mix#3, 4500 psi, 5/8 in. Edge Distance-Crack Length (in)

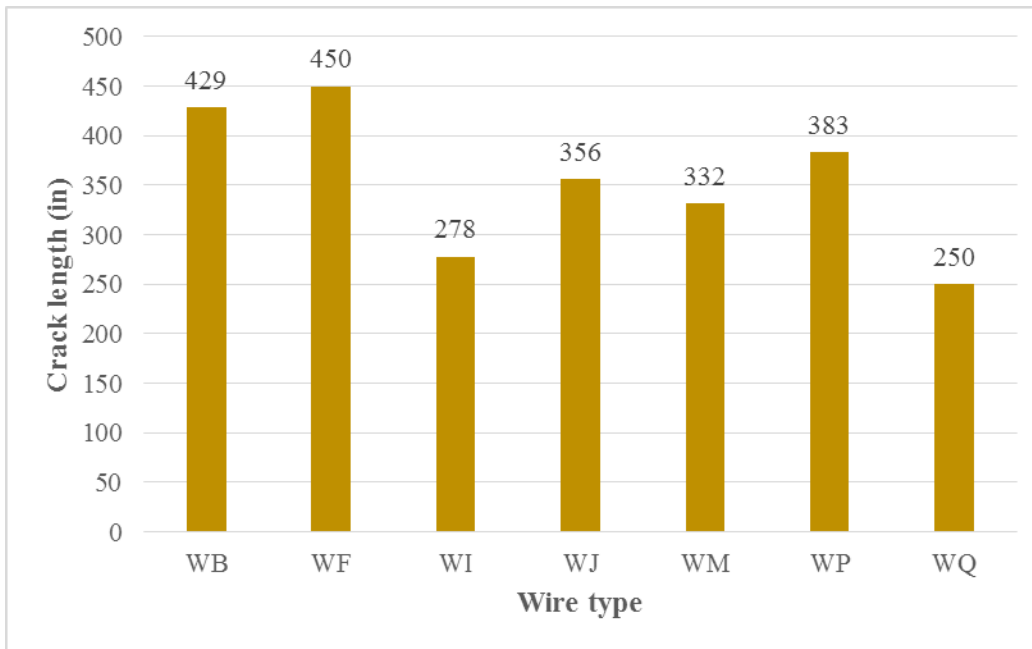


Figure 6-40: Mix#3, 4500 psi, 1/2 in. Edge Distance-Crack Length (in)

Figure 6-38, Figure 6-39, Figure 6-40 and Figure 6-41 illustrate the influence of edge distance on the bond behavior between steel and concrete. Decreasing the value of edge distance resulted in larger values of crack lengths. Wire types WB and WF (deep chevron type of wire) exhibited poor behavior.

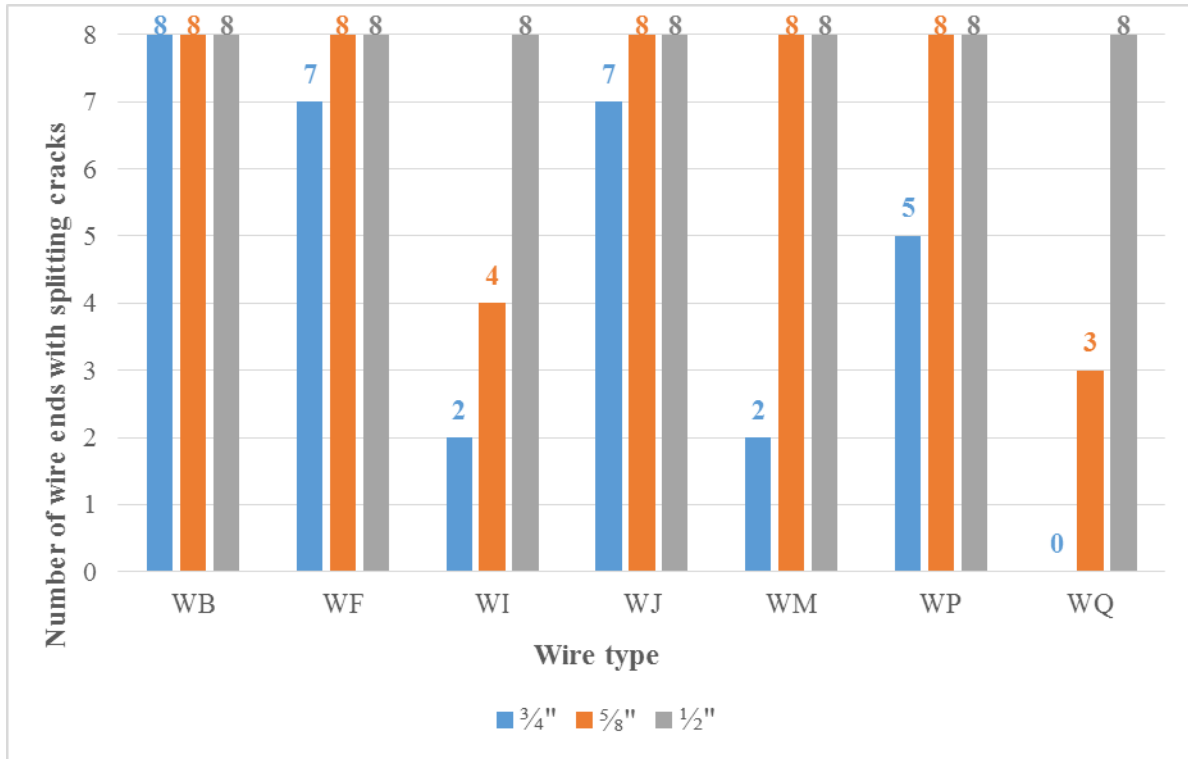


Figure 6-41: Number of Wires Ends with Splitting Cracks

6.4. Mix#1 versus Mix#2

6.4.1. Release Strength 4500psi

Figure 6-42 shows a comparison chart for the prisms with 3/4 in. edge distance using two different types of mixtures. The first type of mixture used crushed aggregate (Tucson aggregate) and the second used granite as aggregate. The different types of wires that were studied including “WB”, “WF”, “WG”, “WH”, “WI”, “WJ”, “WM”, “WP” and “WQ”. Prisms with granite aggregate performed better resulting in smaller crack areas, except for WF wire. WP and WI type wires did not exhibit any cracks with the granite mixture, and with the Tucson aggregate the crack areas were 0.1 in² and 2.0 in² respectively. WH type wire had a 0.1 in² crack area for the mixture using granite aggregate and had a crack area of 1.0 in² using the Tucson aggregate, WI wire showed no cracking with Granite aggregate but had 2 in² crack area with crushed gravel (Tucson aggregate).

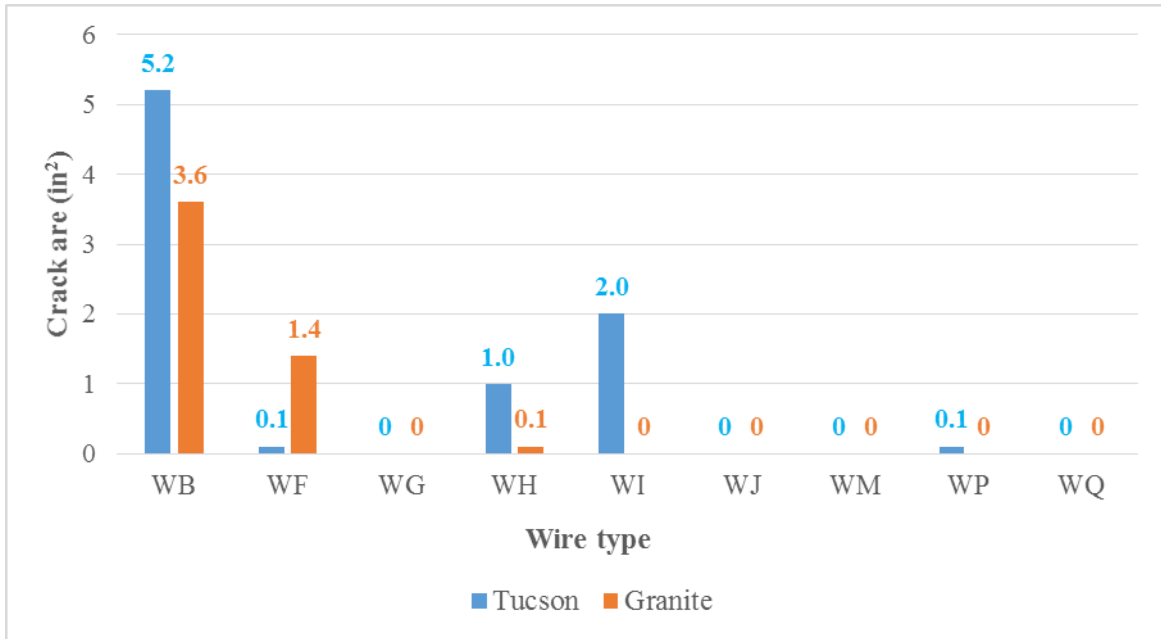


Figure 6-42: Mix#1 vs Mix#2, 4500 psi, ¾ in. Edge Distance-Crack Area (in²)

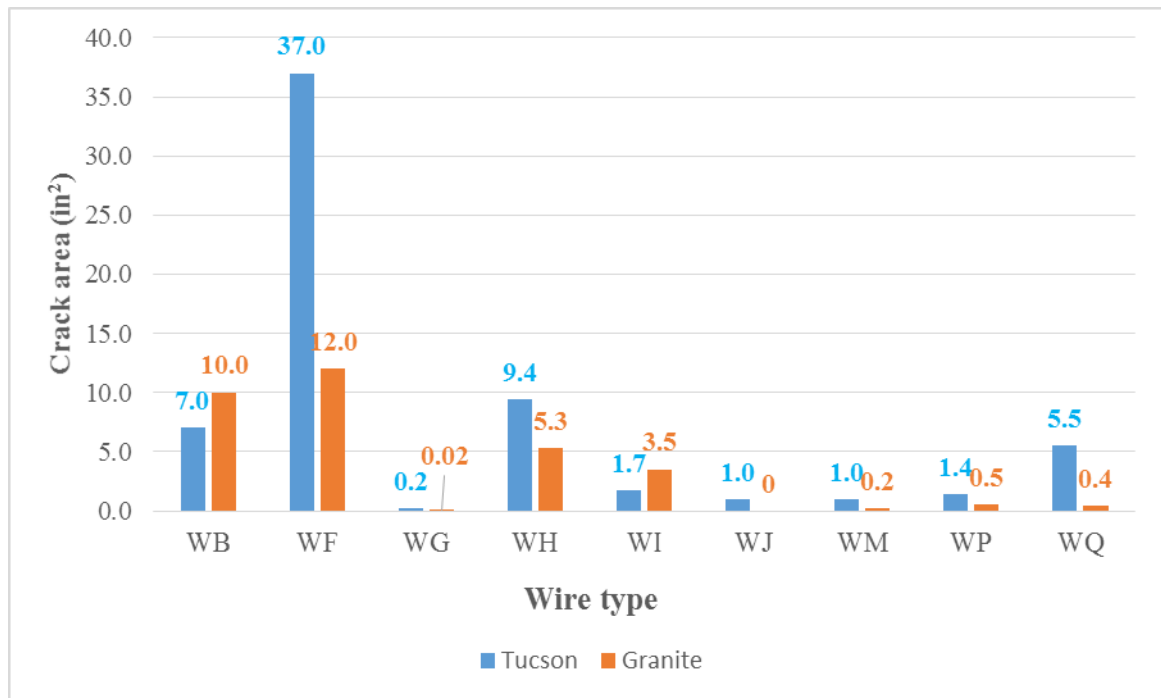


Figure 6-43: Mix#1 vs Mix#2, 4500 psi, 5/8 in. Edge Distance-Crack Area (in²)

Decreasing the edge distance to 5/8 in. made it obvious that wires performed better with the Granite aggregate as shown in Figure 6-43. Decreasing the edge distance to 1/2 in. all prisms had tendency to crack as shown in Figure 6-44.

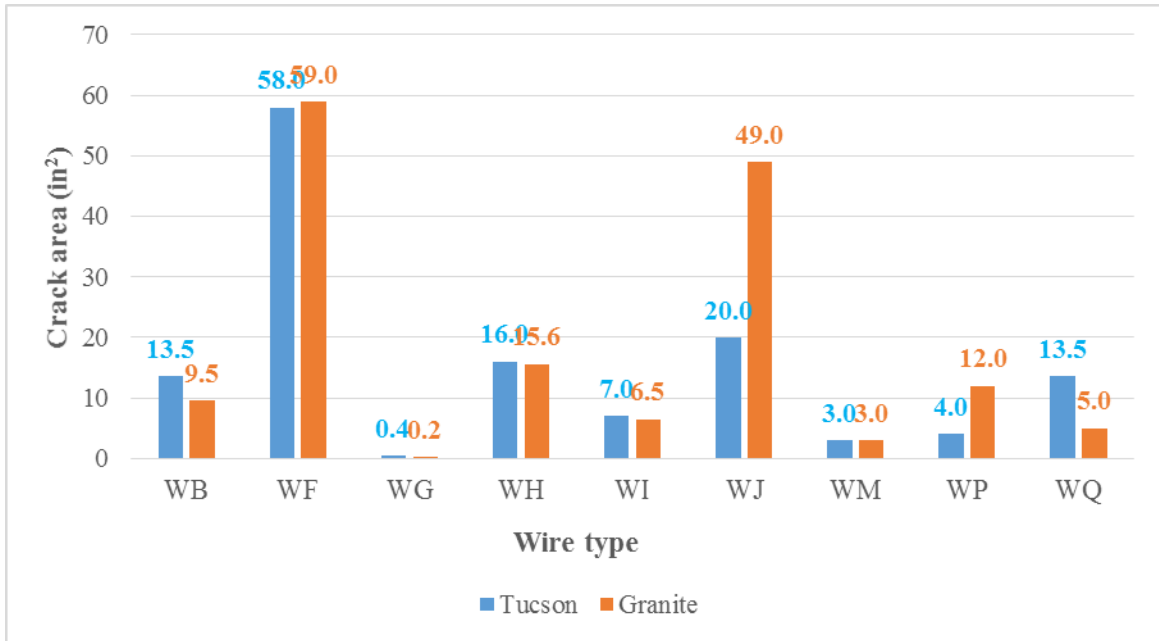


Figure 6-44: Mix#1 vs Mix#2, 4500 psi, ½ in. Edge Distance-Crack Area (in²)

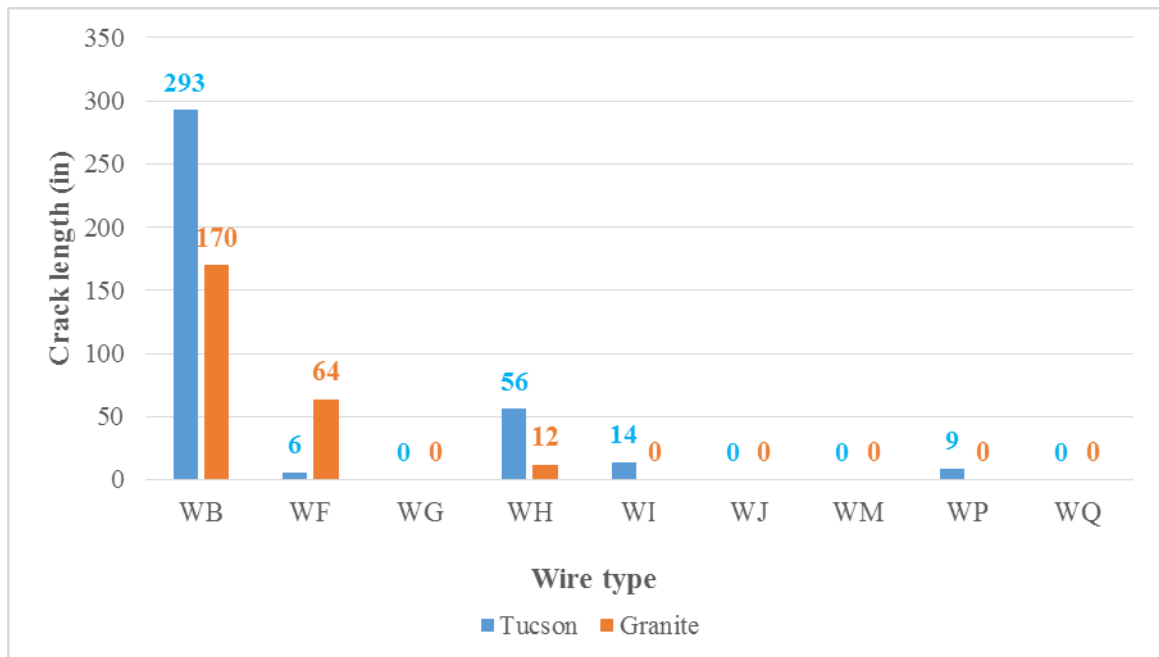


Figure 6-45: Mix#1 vs Mix#2, 4500 psi, ¾ in. Edge Distance-Crack Length (in)

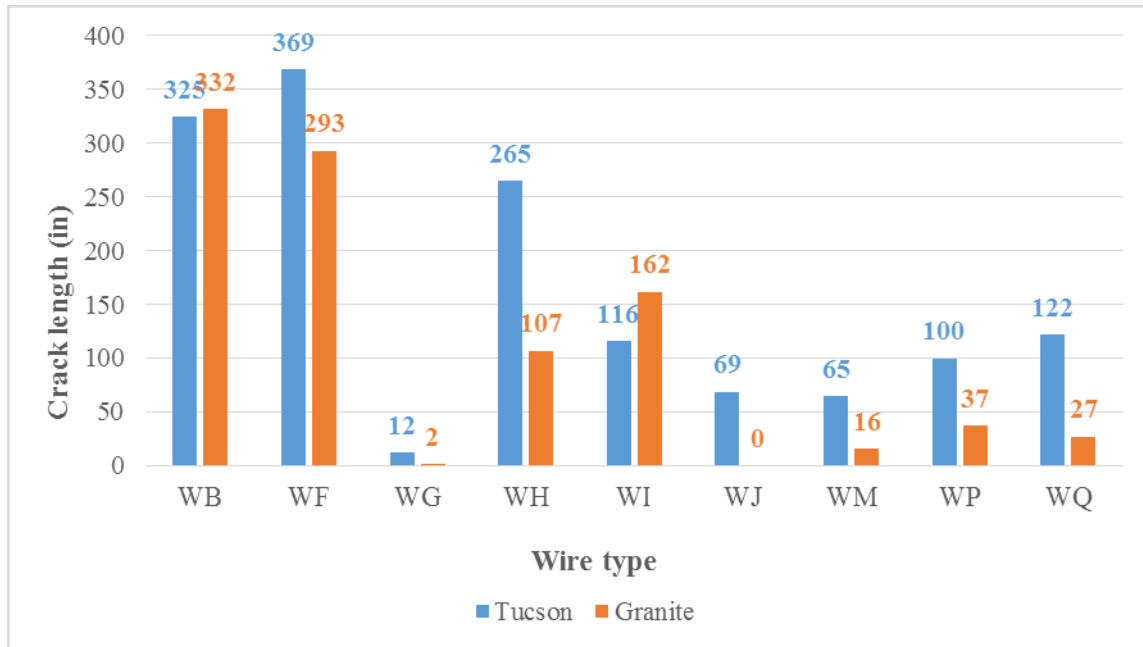


Figure 6-46: Mix#1 vs Mix#2, 4500 psi, 5/8 in. Edge Distance-Crack Length (in)

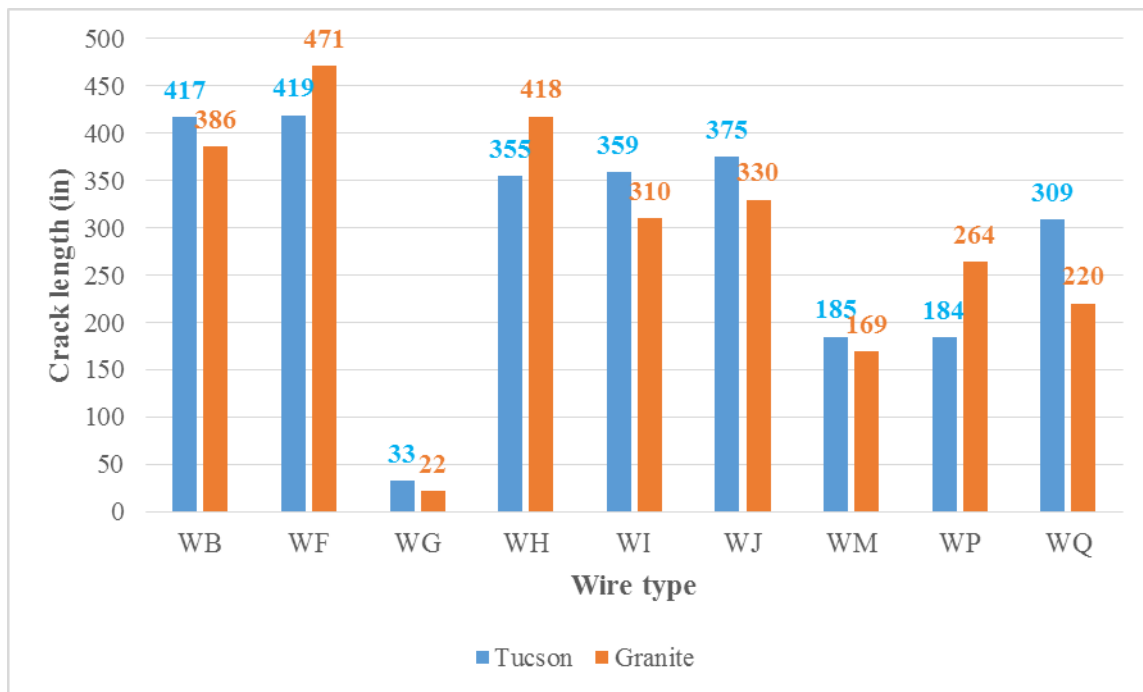


Figure 6-47: Mix#1 vs Mix#2, 4500 psi, 1/2 in. Edge Distance-Crack Length (in)

Figure 6-45 to Figure 6-47 show the crack length for two different mixtures (Mix#1 and Mix#2) and three different values of edge distances. All chevron types of wires were found to have smaller crack lengths with Granite aggregate and all wires which belong to the deep chevron type were found to have better performance with the Tucson aggregate.

Figure 6-48 to Figure 6-50 show the number of wires ends with splitting cracks for two different mixtures (Mix#1 and Mix#2) and three different values of edge distances.

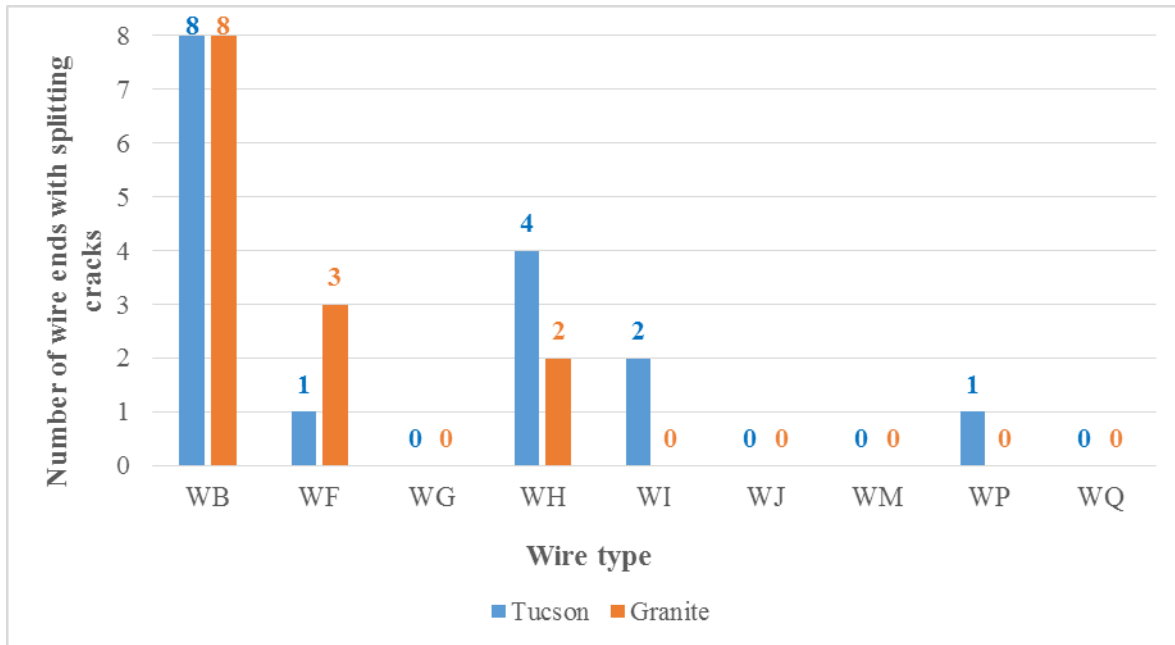


Figure 6-48: Mix#1 vs Mix#2, 4500 psi, $\frac{3}{4}$ in. Edge Distance-Number of Wires Ends with Splitting Cracks

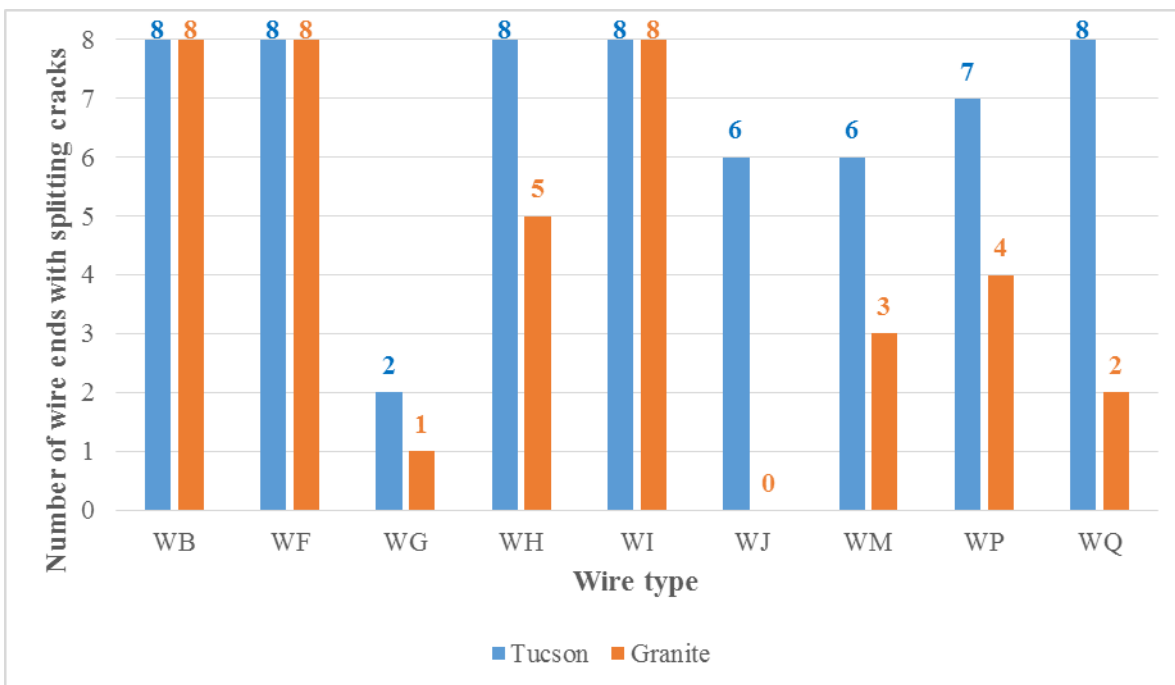


Figure 6-49: Mix#1 vs Mix#2, 4500 psi, $\frac{5}{8}$ in. Edge Distance-Number of Wires Ends with Splitting Cracks

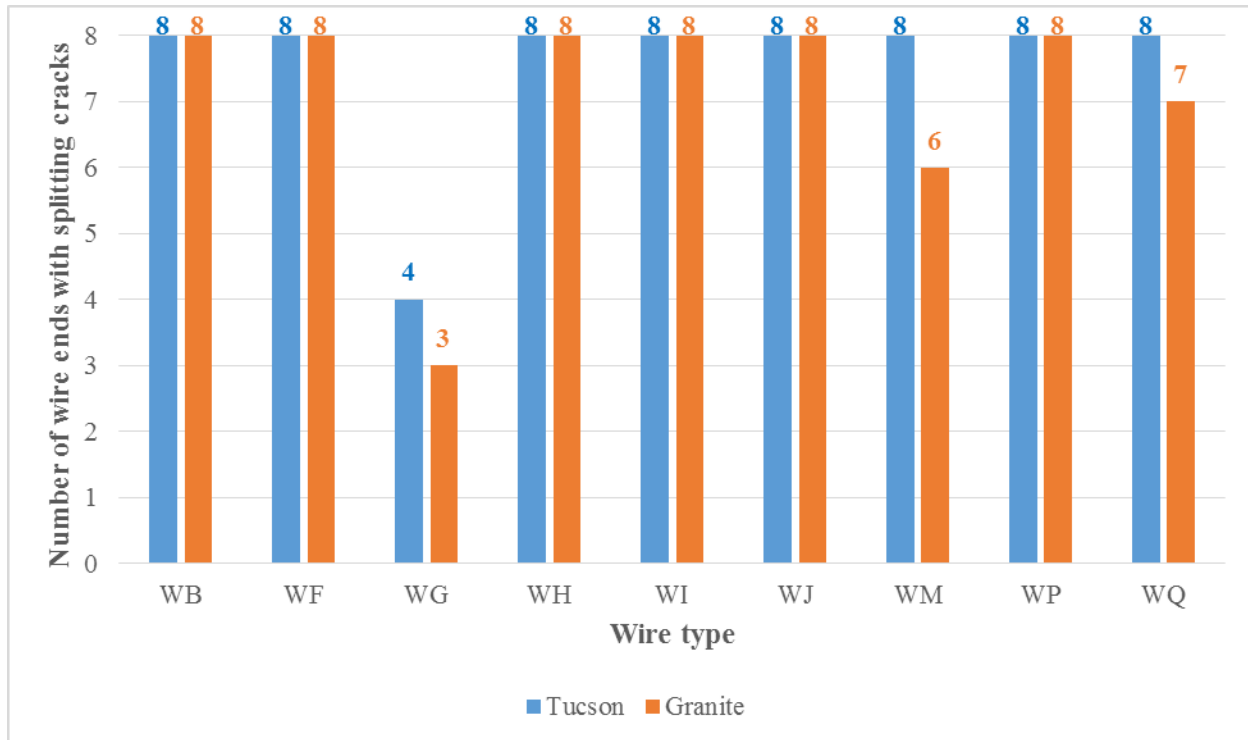


Figure 6-50: Mix#1 vs Mix#2, 4500 psi, ½ in. Edge Distance-Number of Wires Ends with Splitting Cracks

6.4.2. Release Strength 6000 psi

Increasing the release strength to 6000 psi resulted in a decrease in crack areas in most cases, except for wire type WB. Comparing two different mixtures, wires with Granite aggregate tend to perform better. WB wire type with crushed Tucson aggregate had a 12.0 in² crack area and with Granite 2.0 in² crack area as shown in Figure 6-51. Decreasing the value of edge distance to ⅝ in. gave WQ wire type a 0.004 in² crack area with Granite, and 0.03 in² crack area with crushed gravel (Tucson aggregate) as shown in Figure 6-52. Wire types WM, WQ and WI had lower crack areas with Granite aggregate than with crushed gravel. Decreasing the value of edge distance to ½ in, resulted in higher crack areas for the prisms constructed with Granite aggregate. The largest value of crack area was for WF type wire which was 74 in² as shown in Figure 6-53. Crack lengths followed the same crack pattern as crack areas as presented in Figure 6-54, Figure 6-55, and Figure 6-56. Higher crack lengths were found for prisms which were cast with Granite aggregate and had ½ in. edge distance (Figure 6-56).

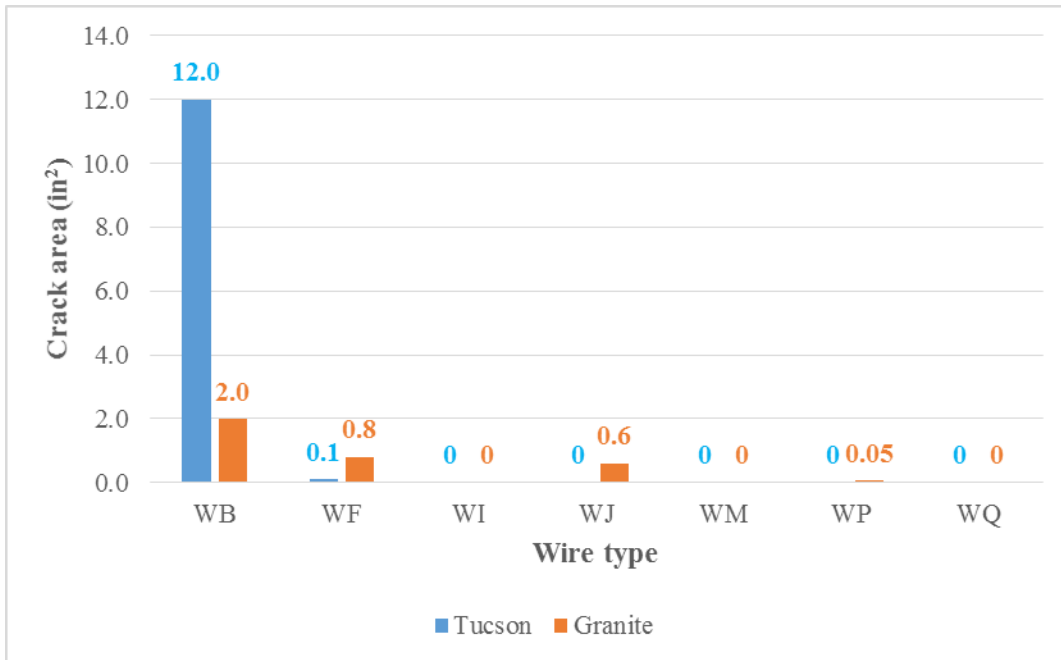


Figure 6-51: Mix#1 vs Mix#2, 6000 psi, ¾ in. Edge Distance-Crack Area (in²)

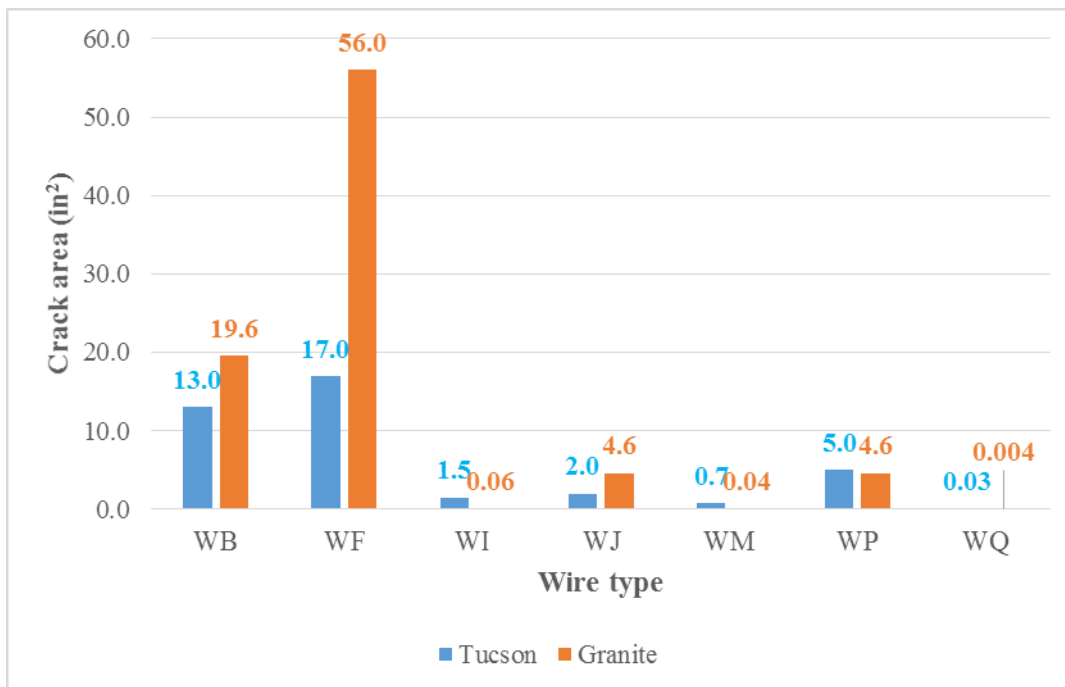


Figure 6-52: Mix#1 vs Mix#2, 6000 psi, 5/8 in. Edge Distance-Crack Area (in²)

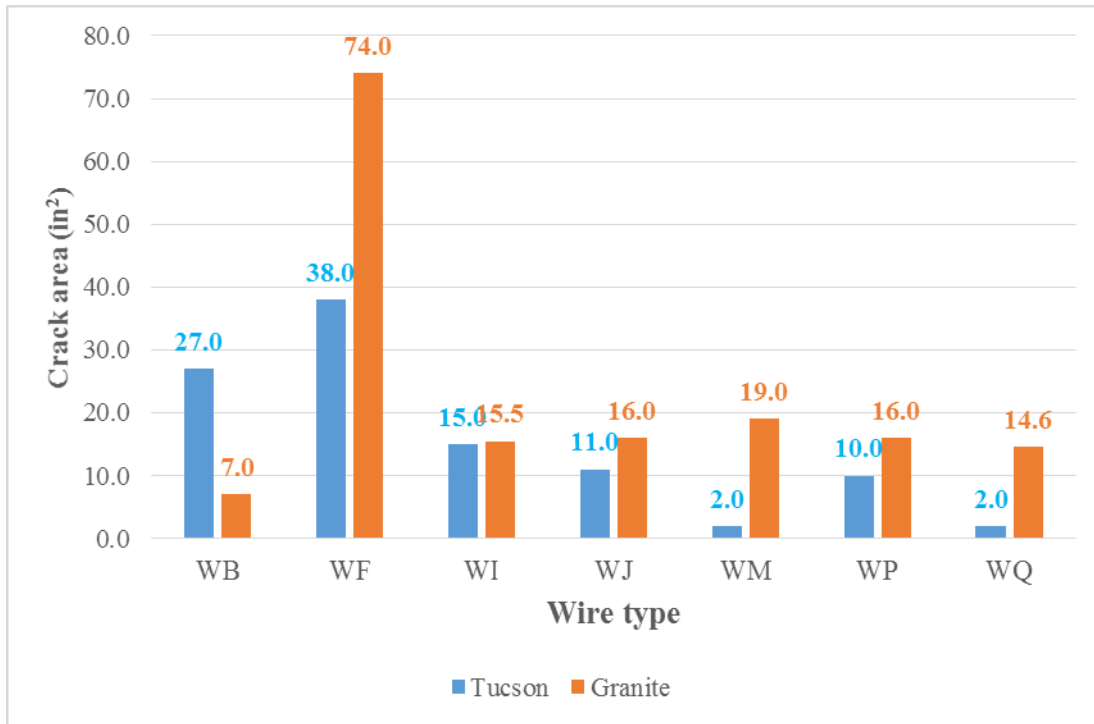


Figure 6-53: Mix#1 vs Mix#2, 6000 psi, ½ in. Edge Distance-Crack Area (in²)

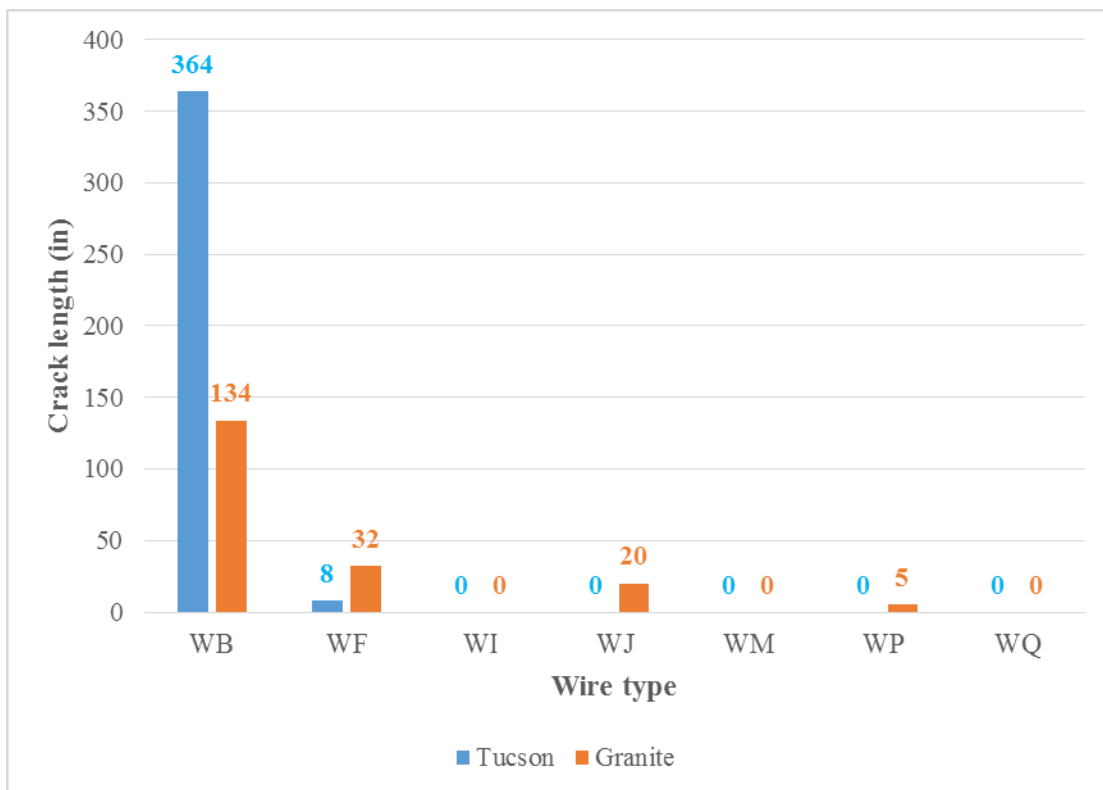


Figure 6-54: Mix#1 vs Mix#2, 6000 psi, ¾ in. Edge Distance-Crack Length (in)

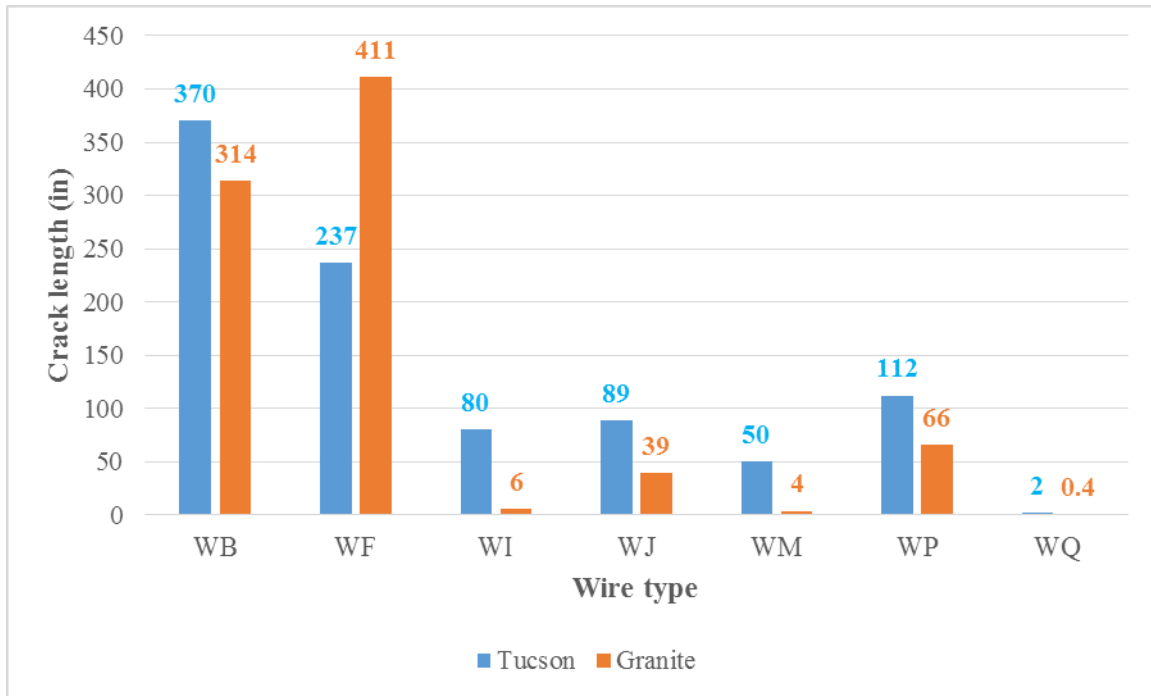


Figure 6-55: Mix#1 vs Mix#2, 6000 psi, 5/8 in. Edge Distance-Crack Length (in)

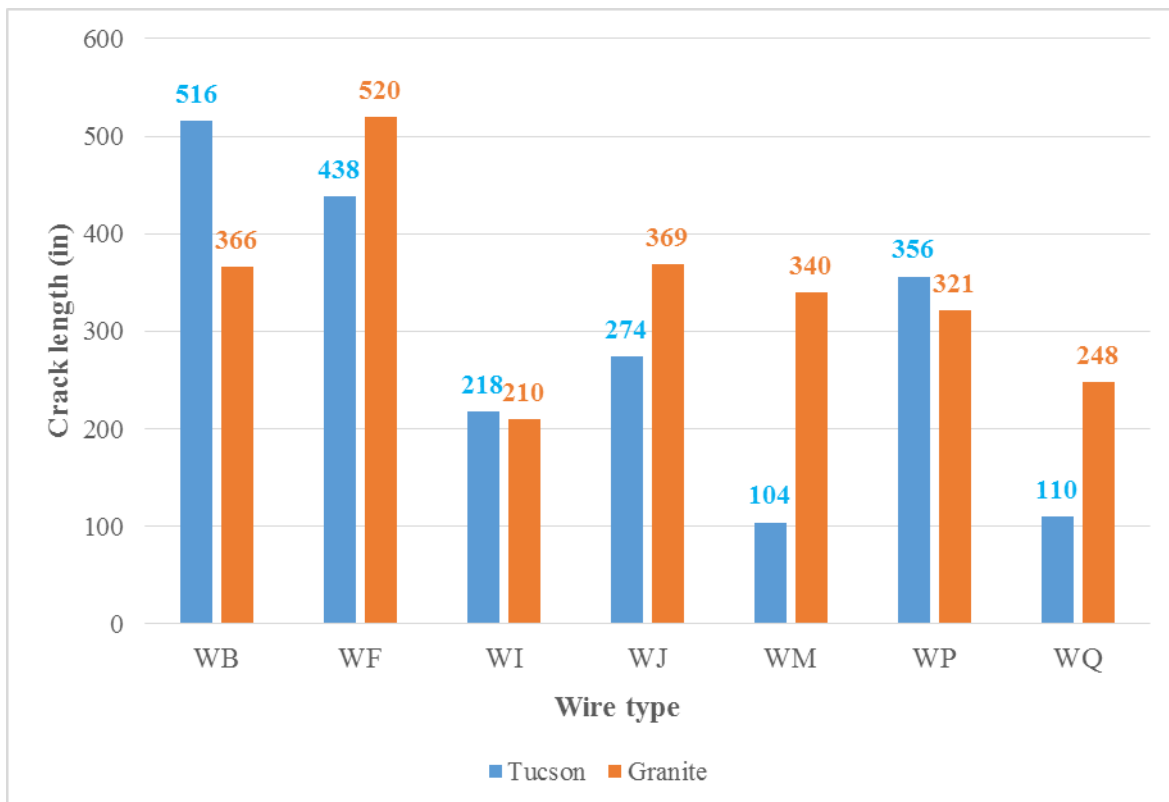


Figure 6-56: Mix#1 vs Mix#2, 6000 psi, 1/2 in. Edge Distance-Crack Length (in)

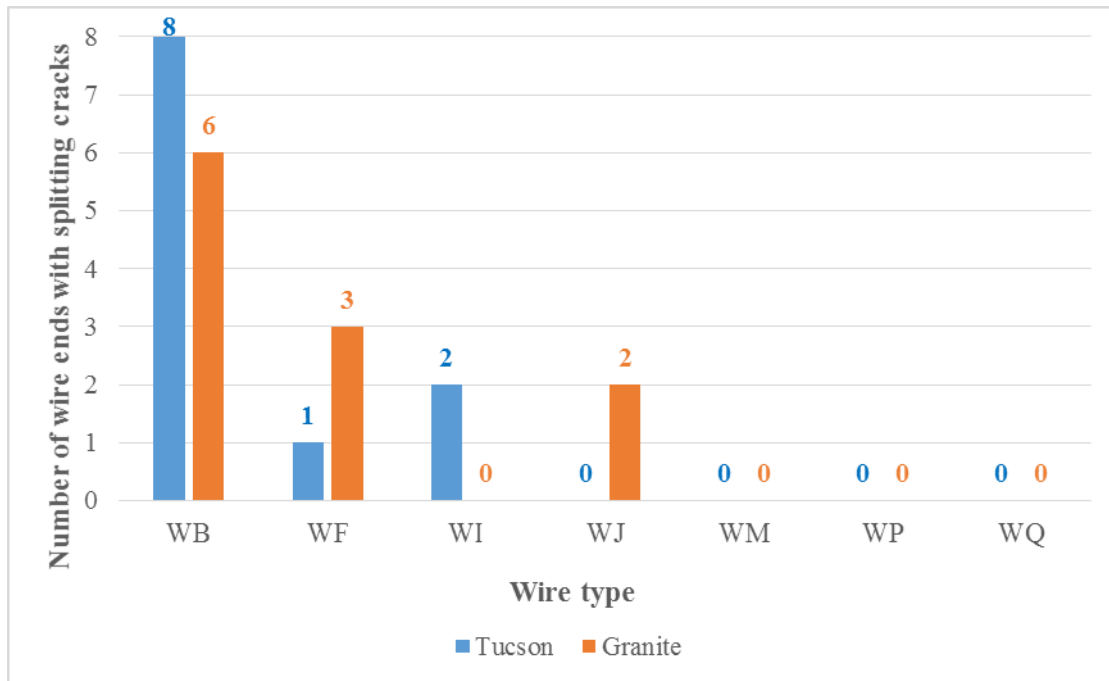


Figure 6-57: Mix#1 vs Mix#2, 6000 psi, $\frac{3}{4}$ in. Edge Distance-Number of Wires Ends with Splitting Cracks

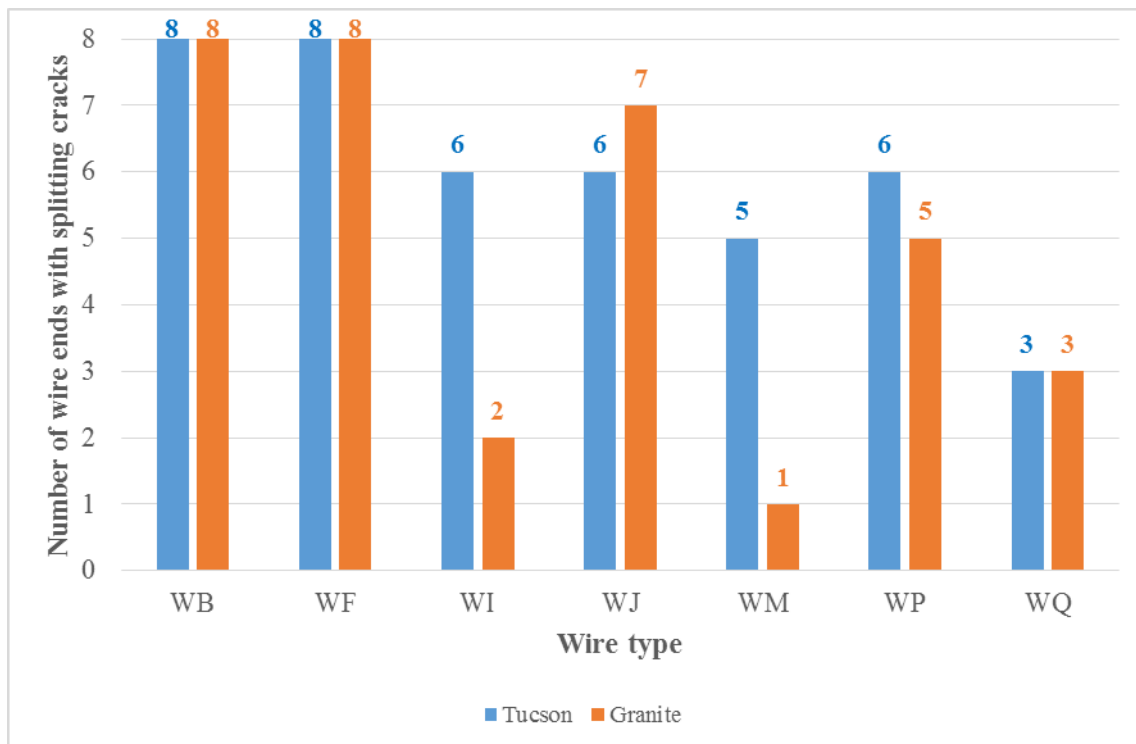


Figure 6-58: Mix#1 vs Mix#2, 6000 psi, $\frac{5}{8}$ in. Edge Distance- Number of Wires Ends with Splitting Cracks

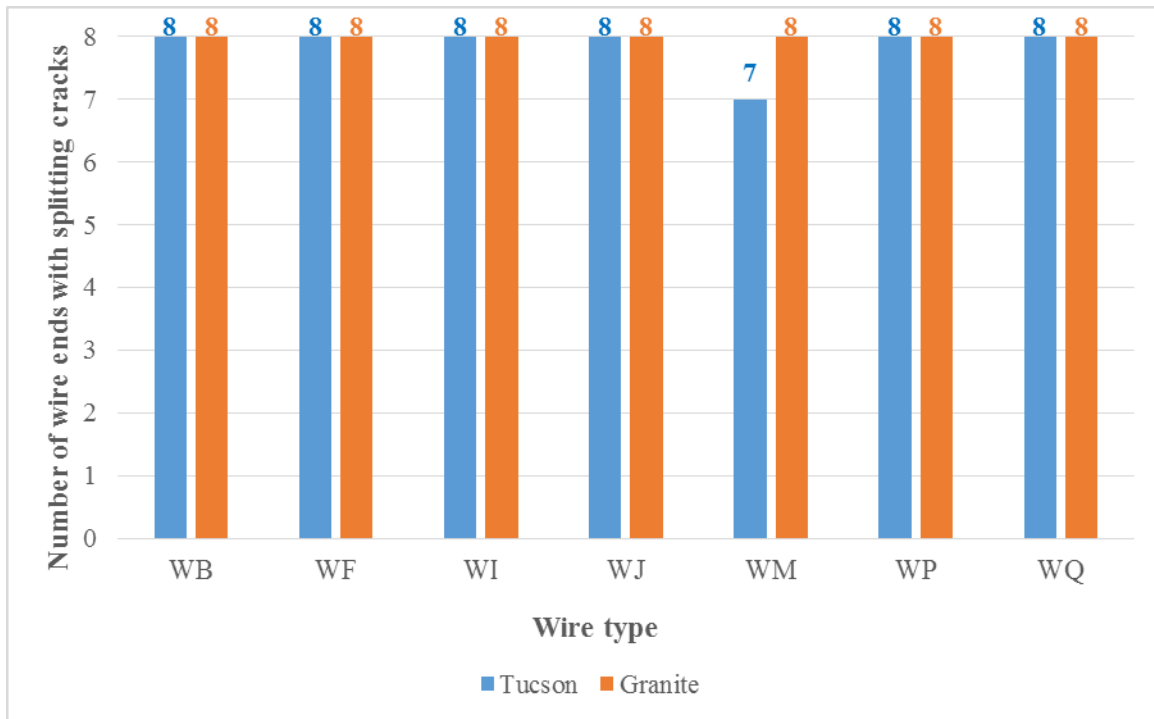


Figure 6-59: Mix#1 vs Mix#2, 6000 psi, ½ in. Edge Distance-Number of Wires end With Splitting Cracks

Figure 6-57, Figure 6-58, Figure 6-59 show the number of wires ends with splitting cracks. Prism with WJ and WF wire types performed better using crushed gravel as aggregate and having ¾ in. edge distance. Prisms with WB, WI had better performance using Granite as aggregate on the prisms having ¾ in. edge distance. Decreasing the edge distance to ⅝ in, prisms performed better using Granite as aggregate as shown in Figure 6-58. Reducing the edge distance to ½ in. all prisms had tendency to crack (Figure 6-59).

6.5 Mix#1 versus Mix#2 versus Mix#3

6.5.1 Release Strength 4500 psi

The influence of concrete mixture was clearly indicated in the figures presented in this section. Figure 6-60 and Figure 6-61 show the overall crack length (the sum of all crack lengths for the prisms having the same edge distance and the same concrete mixtures) used in the study including all wires as a function of edge distance. The maximum crack length for the prism with ¾ in. edge distance using granite as aggregate was 234 in. Overall, crack length for mixture using crushed gravel (Tucson) aggregate was 322 in. The mixture using local uncrushed aggregate (pea gravel) had a 659 in. overall crack length. The mixture using granite was found to be better than Tucson for approximately 38 % less value of crack lengths, and Granite was better than uncrushed gravel (pea gravel) for 282 % less value of crack lengths. Decreasing the edge distance to ⅝ in. resulted in an increase in crack length. Prisms using granite aggregate had an 866 in crack length, crushed gravel (Tucson) had 1178 in. and uncrushed (pea gravel) had a 1688 in. The overall crack length for the third prisms in series with ½ in edge distance was 2150 in. for Granite, 2248 in. for Tucson and 2478 in. for pea-gravel aggregate.

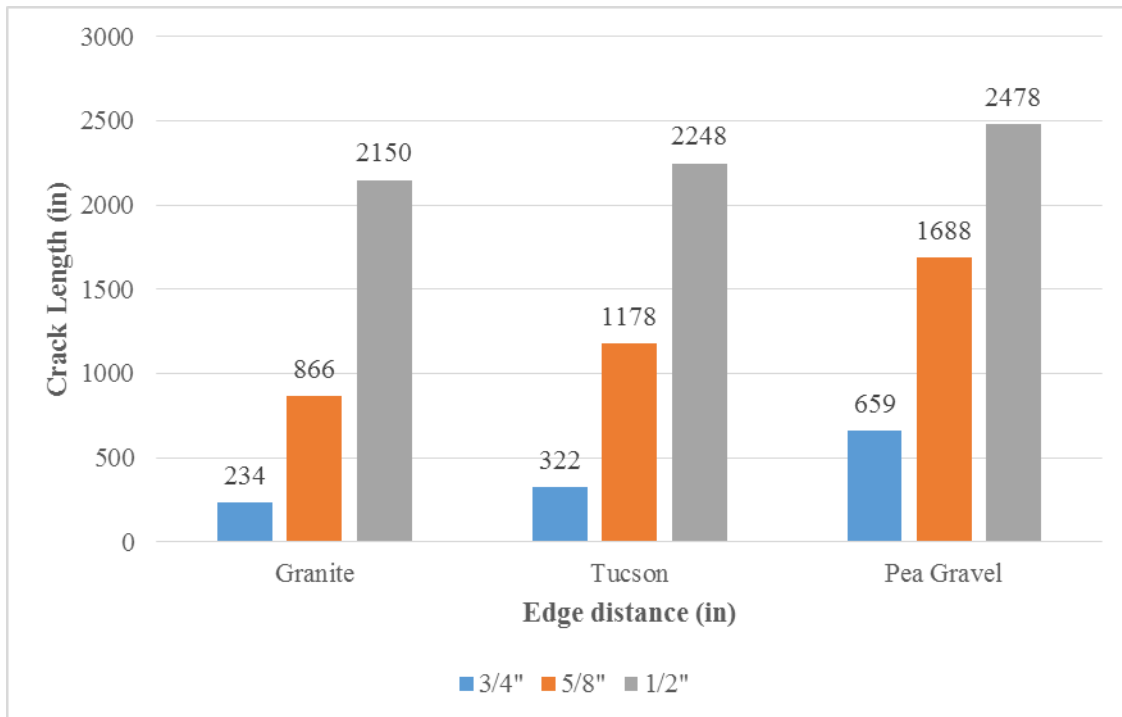


Figure 6-60: Mix#1, Mix#2, Mix#3-Effect of Cover on End-Splitting

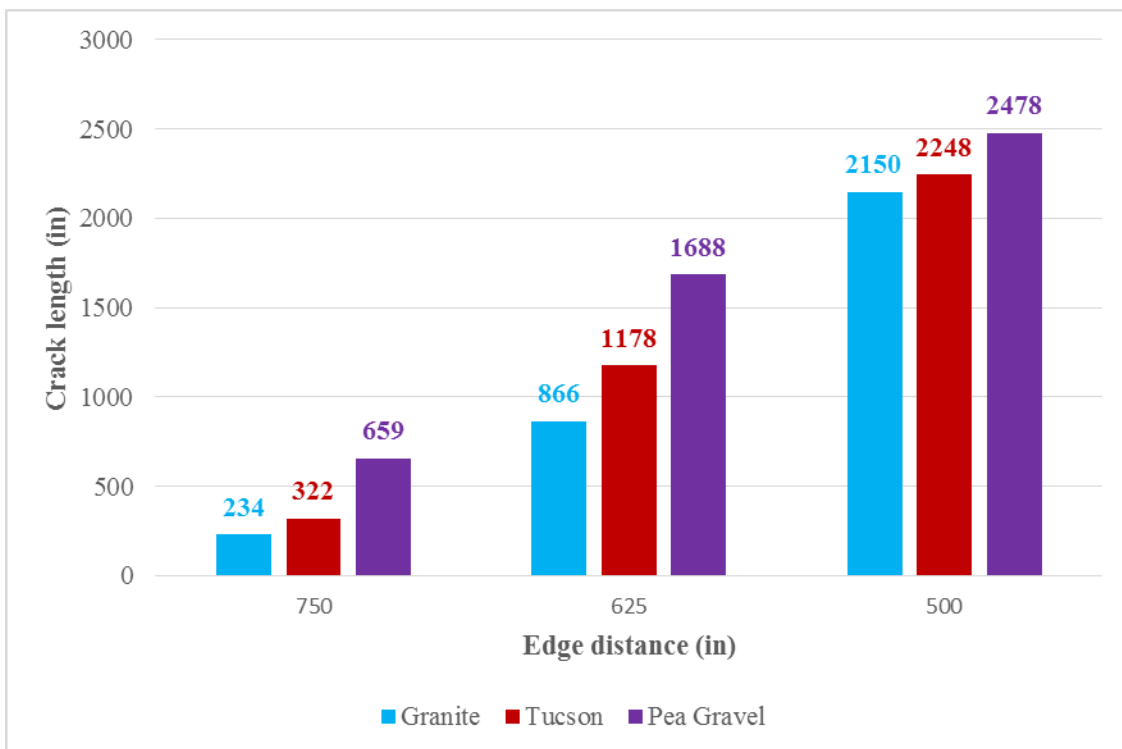


Figure 6-61: Mix#1 vs Mix#2 vs Mix#3-Crack Length (in)

Figure 6-62 shows the overall crack length (the value of crack length for prisms having three different values of edge distances and having the same concrete mixture) for each type of mixtures and all wires used in these experiments including all three thicknesses of edge distance. Prisms having Granite as aggregate was found to have a 3250 in. crack length, prisms having crushed gravel (Tucson) had a 3748 in. crack length and prisms having uncrushed gravel (pea Gravel) had 4825 in. crack length. Prisms having Granite performed better than prisms having crushed gravel having the value of crack lengths less for approximately 15 %. Prisms having Granite performed better than prisms having uncrushed gravel having the value of crack lengths less for 49 %.

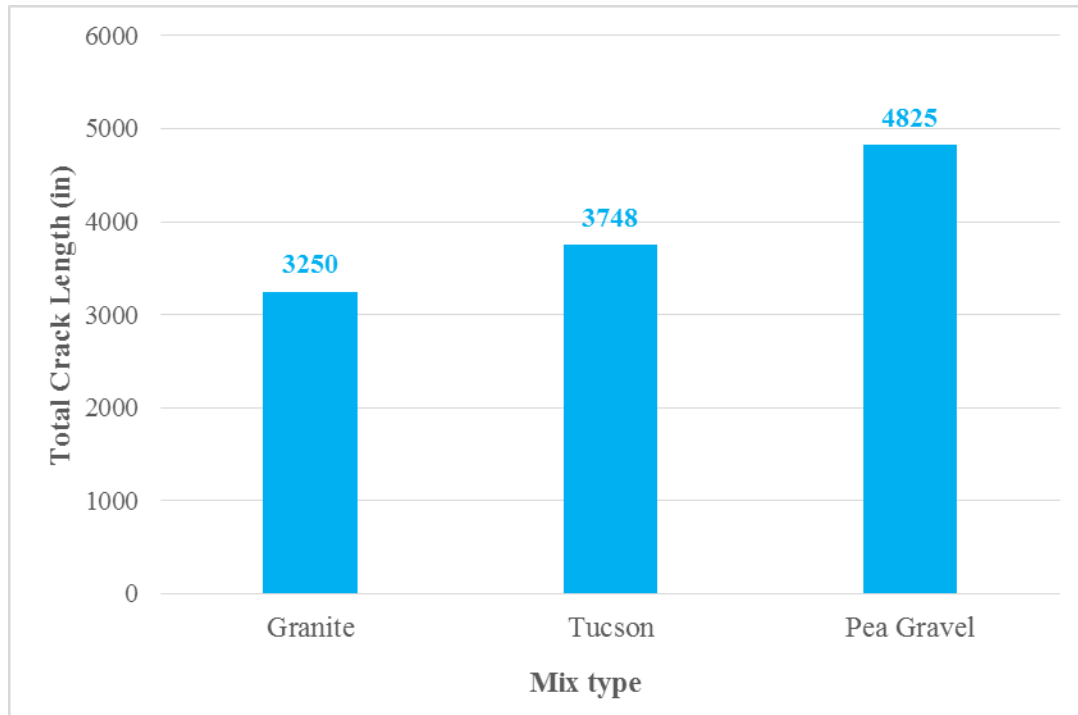


Figure 6-62: Mix#1 vs Mix#2 vs Mix#3-The Overall Crack Length (in)

The highest effectiveness of mix type was observed for the prism with $\frac{3}{4}$ in. and $\frac{5}{8}$ in. values of edge distances. It was also found that decreasing the edge distance resulted in a lower overall performance. Prisms that had a $\frac{1}{2}$ in. edge distance were found to tend to lose the bond between steel and concrete.

7. Proposed Qualification Test for Arema Manual for Railway Engineering

Based on the work completed on pre-tensioned concrete prisms presented in Chapters 3-6, the following Qualification test is recommended to identify ties that may be susceptible to end-splitting cracks.

7.1. Resistance to End-Splitting

End-splitting cracks along tendons in prestressed concrete ties can occur unless adequate confinement of the lateral “bursting” stresses caused by the prestressing reinforcement is achieved. In the case of pre-tensioned concrete ties, these lateral bursting stresses are caused by several factors including the Hoyer effect (change in diameter of the prestressing tendons due to Poisson’s Ratio), the jacking force in the tendons, and the rate of bond development in the tie, and the overall geometric features and indent characteristics of the prestressing tendons.

End-splitting cracks can form at the time of de-tensioning, but they can also develop during the first few weeks after de-tensioning due to sustained lateral stresses exerted by the prestressing tendons. The ability of the concrete to resist these bursting stresses without cracking is primarily a function of distance from the reinforcement to the nearest parallel edge of concrete (cover), the aggregate type, and maturity of the concrete at de-tensioning.

The most important concrete characteristic affecting splitting resistance is the amount of cover provided over exterior prestressing tendons. Larger, angular coarse aggregates tend to provide more splitting resistance than smaller, rounded aggregates. For concrete compressive strengths above 3500psi, increased concrete maturity at the time of de-tensioning provides additional splitting resistance. However, for a given concrete mixture, higher compressive strengths at transfer of prestress also correspond to a higher Modulus of Elasticity (MOE). The higher MOE causes increased lateral stresses and serves to diminish much of the benefit aspect of the increased tensile strength.

7.1.1 System Qualification Test

The test purpose was to identify tie designs that may be susceptible to end-splitting cracks. Since the splitting resistance of a given tie design is a complex function of the prestressing reinforcement geometry, initial force per tendon, the edge distance, concrete mixture, and the maturity of the concrete at de-tensioning, the system Qualification test will serve to identify tie designs that have an increased risk of developing end-splitting cracks.

The System Qualification Test involves six pre-tensioned concrete prisms with the same prestressing tendons and concrete mixture that is used in the concrete ties, except that the edge distance for the prisms is reduced by approximately 25 percent. If this reduction in edge distance results in longitudinal splitting cracks along the prestressing tendons, then the system (tie design and material selection) may be susceptible to concrete end-splitting cracks. In this case, changes to the design and/or material selection should be made prior to mass production of ties.

7.1.2 Determination of Prism Parameters

This section provides a step-by step procedure to calculate System Qualification Test prism parameters based on a given tie design.

- (a) Determine the total number of prestressing tendons in the actual tie
- (b) Determine the prestress jacking force (P) per tendon
- (c) Determine the smallest cross-sectional area (A) located anywhere in the tie
- (d) Determine the smallest possible edge distance (D) for an individual tendon within 12 in of the tie end. This distance is measured from the center axis of the tendon to the nearest concrete surface minus allowable placement tolerances.
- (e) Calculate the reduced edge distance (RD) to be used for the prisms where $RD = 0.75 \times D$. This number may be rounded down to the nearest 1/16 in for convenience.
- (f) Calculate the dimensions of the square cross-section (S x S), where $S = \sqrt{\frac{4A}{n}}$ rounded to the nearest 1/8 in.

7.1.3 Prism Fabrication

Cast six pre-tensioned concrete prisms having a square cross-section with dimensions S x S and tendon edge distance RD. The dimensional tolerances for prism fabrication are $\pm 1/8$ in. for cross-section dimension S and $\pm 1/32$ in. for edge distance RD. The prisms should have a minimum length of 59.5 in. When fabricating the prisms, use similar prestressing tendons, jacking force per tendon (P), concrete mixture, and placement, vibration, curing and de-tensioning procedures that are used for the actual concrete ties. Temperature-match cure the prisms and de-tension at the minimum allowable de-tensioning strength for the ties ± 200 psi. The prisms may be fabricated directly by the tie producer or by an experienced lab capable of meeting the above criteria. If a shorter prestressing bed is used to fabricate the prisms than is used to manufacture the actual ties, excessive chuck seating losses could significantly reduce tendon tension and thereby skew the test in a more favorable way. In this case, one or more in-line load cells should be used to verify proper tendon tension is achieved after lock-off.

7.1.4 Additional Sampling of Prestressing Tendons

At the time of prism fabrication, cut twelve 36 in samples of the prestressing tendons and save these in a clean, sealed container. These tendons can then be benchmarked using appropriate ASTM bond tests (ASTM A1096 for wires, ASTM A1081 for strands). Benchmarking tendon bond according to the current ASTM standards will enable prestressing tendons with similar-bonding characteristics to be specified in future purchase orders.

7.1.5 Prism Inspection and Storage

Within eight hours of de-tensioning, inspect all twelve prism ends (both ends of six prisms) for cracking at each location where the prestressing tendon enters the concrete (48 locations total). Inspection should be done using a bright light, alcohol spray, and 5x magnification. Note any visible cracks by drawing a line adjacent to the crack using a fine-point permanent marker. The line should be drawn along the entire length of any visible cracks. Measure and record the total length of each crack that runs parallel along the tendon. Note, cracks that appear on the ends of

the prism but do not propagate to the sides of the prism along the wire line have a length of zero. All initial cracks should additionally be documented by photographs.

The prisms should be stored indoors and in the dry condition (not moist or wet cured) for at least 90 days. Storing the ties in the dry condition will maximize drying shrinkage and enhance the conditions for cracking.

After 90 days, the ties should be re-inspected using a similar procedure as above. All new cracks and/or any crack growth should be noted with a different-colored fine point-permanent marker and the total longitudinal length of each crack should be measured and recorded. All cracks should again be documented by photographs.

7.1.6 Interpretation of Results

After 90 days, if the summation of all longitudinal crack lengths initiating from the 48 tendon entry locations is less than 6 in, then the proposed tie design and selected materials have a demonstrated factor of safety to resist early-age bursting forces without cracking.

7.1.7 Suggestions for Corrective Action in the Event of System Qualification Test Failure

If the summation of longitudinal crack lengths after 90 days is more than 6 in, this is an indication that the tie design may have an increased risk of end-splitting due to insufficient cover for the prestressing tendons and concrete mixture selected. Careful measurements of tendon edge distances should be made to determine if the prisms were fabricated correctly, and all test documentation should be reviewed to ensure the proper mixture and release strength was obtained. If the test was conducted correctly then appropriate adjustments should be made to the design parameters and the System Qualification Test repeated to obtain a more resilient design.

The most direct way to provide increased splitting resistance is to increase the concrete cover for exterior prestressing tendons in the design. Other ways to reduce splitting propensity include using prestressing tendons with different indent characteristics and/or lower inherent bond, using larger and/or more angular coarse aggregates, and increasing concrete strength at the de-tensioning.

A minimum prestressing edge distance of 4 diameters and a minimum center-to center tendon spacing of 8 diameters is recommended to reduce the risk of splitting.

7.1.8 Flexural Load Tests to Failure

In addition to end-splitting that occur during the first few weeks after de-tensioning, end-splitting of ties can also result from extreme overloads. This occurs when tendon end-slippage (bond slip) occurs due to additional tensile demands produced by flexural and/or shear cracking. End-splitting during load tests indicates that the concrete mixture and prestressing tendon system is incapable of remaining intact during extreme overloads. Since concrete end-splitting is an undesirable failure mode, plants are encouraged to frequently bend test full-strength concrete ties to failure to ensure there will not be end-splitting.

8. Theoretical Lateral Stresses Due to Hoyer Effect

The influence of edge distance, release strength of concrete and concrete mixture on lateral bursting stresses is explored analytically for the wires used. Wires with 5.32 mm (0.21 in.) diameter were investigated.

Using the analytical model (Brier, 2012), the evaluation of the radial and tangential stresses between wire and concrete considering Poisson's effect, thickness of the edge distance and the mechanical properties of the materials was done. The 5.32-mm-diameter prestressing wires used in this study were tensioned to 7000 lbs. (31.14 kN) corresponding to an average stress of 203.17 ksi. The modulus of elasticity of the prestressing steel was assumed to be 28,500 ksi and the Poisson's ratio for the steel was assumed to be 0.30. The modulus of elasticity for concrete was estimated to be 3780 ksi corresponding to a release strength of concrete 6000 psi. Poisson's ratio for concrete was assumed to be 0.17. The edge distance was given as a function of diameter of wire (D) and for the edge distance 1.0 in this corresponds to 4.77D. Decreasing the edge distances to $\frac{3}{4}$ in, $\frac{5}{8}$ in and $\frac{1}{2}$ in correspond to 3.58D, 2.98D and 2.39D respectively. The tangential pressure at the interface was obtained from analysis by Briere, 2012. From the interface pressure, the radial and tangential stresses can be expressed as a function of the radial distance from the wire axis.

$$\sigma_r = \frac{-p(\frac{1}{c^2} - \frac{1}{r^2})}{(\frac{1}{c^2} - \frac{1}{R^2})} \quad 8-1$$

$$\sigma_\theta = \frac{-p(\frac{1}{c^2} + \frac{1}{r^2})}{(\frac{1}{c^2} - \frac{1}{R^2})} \quad 8-2$$

Where: σ_r = radial stress

p = radial pressure at pretensioning tendon-concrete interface

c = distance from center of tendon to concrete edge

r = radial distance from axis of prestressing tendon

R = radius of prestressing tendon

σ_θ = circumferential (tangential stress)

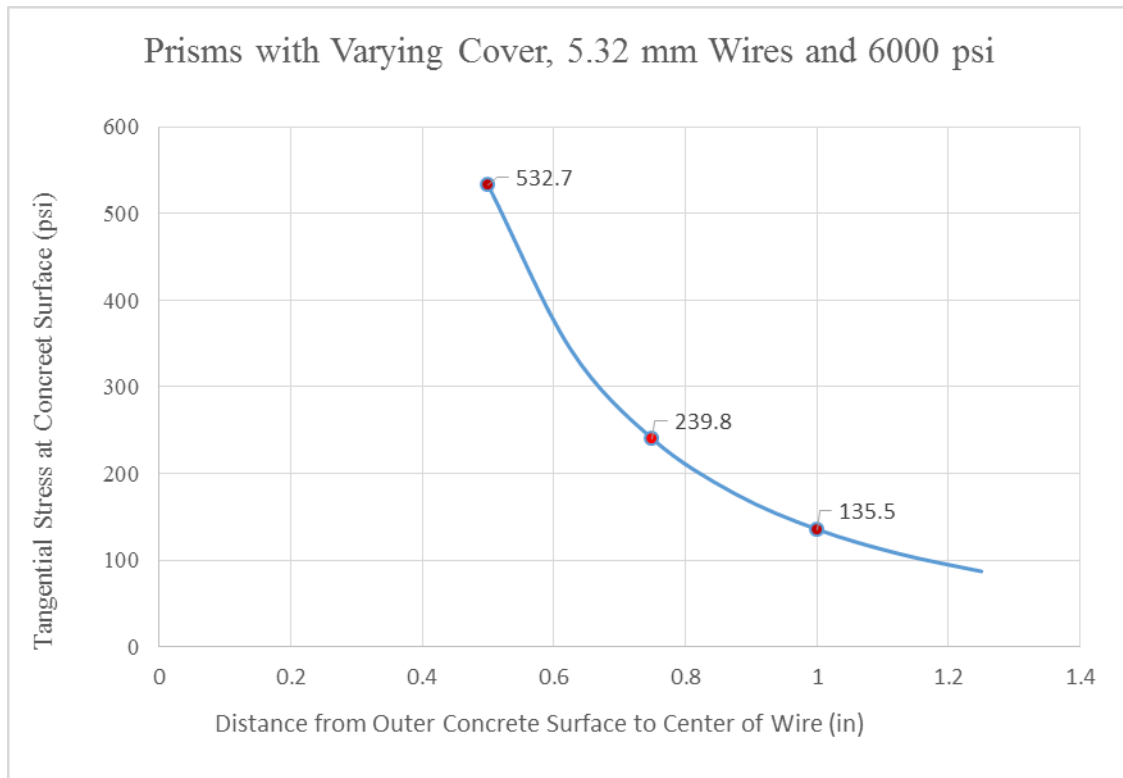


Figure 8-1: Tangential Stress in Concrete (psi)

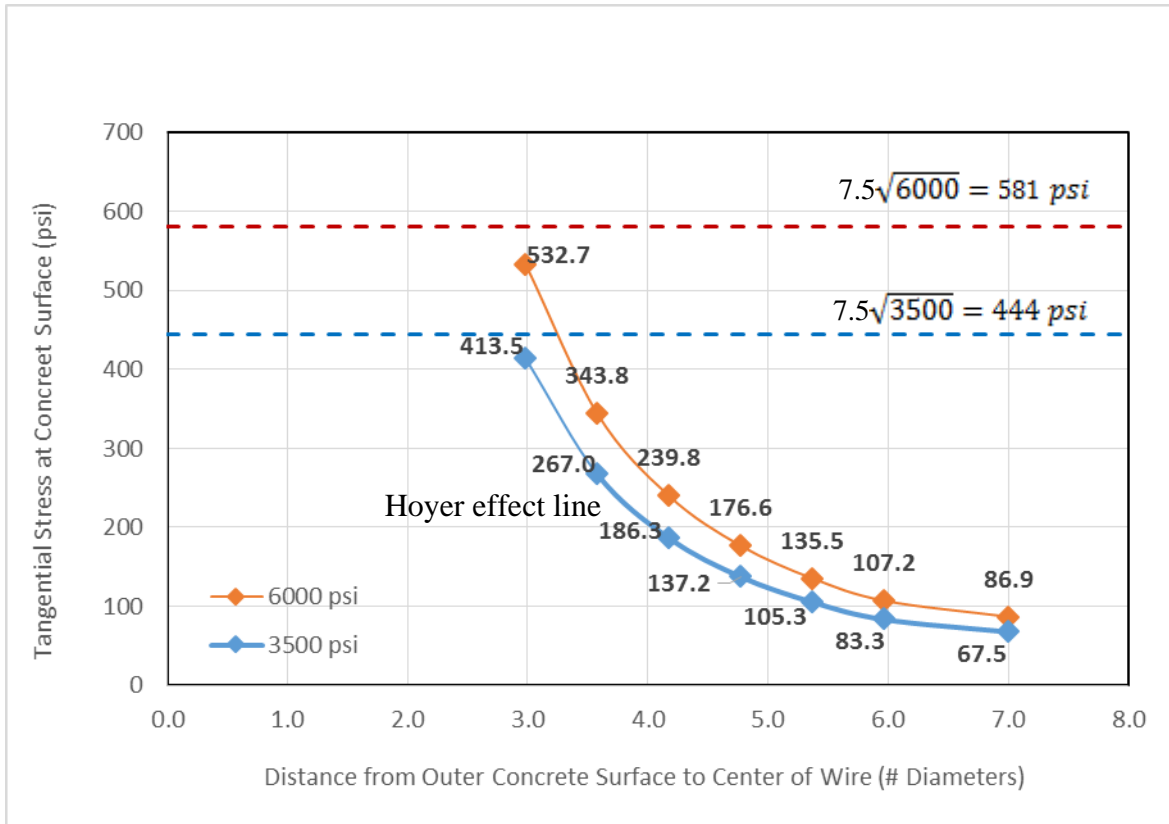


Figure 8-2: Prisms with Varying Cover and Release Strength (Based on # of Tendon Diameters)

The splitting resistance for 6000 psi release concrete strength is 581 psi and for 3500 psi is 444 psi as given in Figure 8-2. For concrete compressive strengths above 3500 psi, increased concrete maturity at the time of de-tensioning provides additional splitting resistance. However, for a given concrete mixture, higher compressive strengths at transfer of prestress also correspond to a higher Modulus of Elasticity (MOE). The higher MOE causes increased lateral stresses and serves to diminish much of the benefit aspect of the increased tensile strength.

This analysis is useful for understanding the significance of concrete cover on longitudinal splitting propensity. From Figure 8-1, the tangential (tensile) stress varies approximately as a function of $1/c^2$, where “c” is the distance from the prestressing tendon center to the nearest edge. With an edge distance of $\frac{3}{4}$ in, the theoretical tensile stress at the concrete surface is 240 psi so there would not be any cracking due to the Hoyer Effect alone.

It is hypothesized that there are additional tensile stresses that arise as the prestressing tendons slip and concrete that was originally located within the indent portions is displaced outward. In this way, wires with deeper indentations would displace more concrete thereby producing higher tensile stresses and longitudinal splitting.

Also, from Figure 8-1, at an edge distance of $\frac{1}{2}$ in, the theoretical tensile stress at the concrete surface is 533 psi, which is close to the theoretical tensile capacity of the concrete. At this edge distance, all prisms split except for the prism with smooth wire WA.

9. Conclusions and Recommendations

9.1. Conclusions

Based on the results of this study, the following four primary conclusions are drawn.

1. Tendon edge distance is the most significant parameter affecting longitudinal splitting along pretensioned concrete tendons. For any given release strength, the number of wires where longitudinal cracks formed increased as the amount of edge distance was reduced. Therefore, the most direct way to provide increased splitting resistance is to increase the edge distance for exterior prestressing tendons in the design.
2. The second important parameter affecting longitudinal splitting was wire indent geometry. Based on the analysis of data collected, it was determined that the shallow chevron type of wires performed better than deep chevron type of wire.
3. The third important parameter affecting longitudinal splitting was the type of concrete mixture used for each prism test. The concrete mixtures containing a crushed granite performed better than mixtures with crushed gravel (Tucson) and pea gravel aggregates.
4. The least significant parameter affecting longitudinal splitting was the concrete release strength. The amount of longitudinal splitting, as evaluated by total crack length and total crack area, reduced by only 8-10% when the release strength was increased from 4500 to 6000 psi.

Additional conclusions related to specific wire types, concrete mixtures, and release strengths are listed below.

- Total crack lengths in prisms containing crushed (Tucson aggregate) were 1.37 times longer than crack lengths in prisms with granite at a release strength of 4500 psi and edge distance of $\frac{3}{4}$ in.
- Total crack lengths in prisms containing un-crushed pea gravel were 2.82 times longer than crack lengths in prisms with granite at a release strength of 4500 psi and edge distance of $\frac{3}{4}$ in.
- All prisms containing Mix#3 with un-crushed pea gravel (CA1) and a wire edge distance of $\frac{3}{4}$ in. had longitudinal splitting cracks except the prism containing wire type WQ. All prisms with pea gravel and edge distances of $\frac{5}{8}$ in. and $\frac{1}{2}$ in. resulted in eight longitudinal cracks.
- Prisms using Mix#1 (crushed gravel CA2 and CA3) and Mix#2 (crushed granite CA4) and shallow chevron wire types (WG, WQ, WM and WJ) did not have any longitudinal splitting cracks at $\frac{3}{4}$ in. edge distance and 4500 psi release strength. The prism with wire type WM using crushed gravel aggregate (CA2 and CA3) and $\frac{3}{4}$ in edge distance had one crack at 6000 psi release strength. The prism with wire type WJ using granite aggregate and $\frac{3}{4}$ in. edge distance had one crack at 6000 psi release strength. Prisms with wire types WG and WQ having $\frac{3}{4}$ in. edge distance did not have any visible cracks at 6000 psi release strength.
- Total crack area for wire type WF (deep chevron) was the greatest for all three types of mixtures having $\frac{5}{8}$ in. and $\frac{1}{2}$ in. thicknesses of edge distance. This cracking resulted in a total loss of bond between the WF wires and concrete.

- Prisms manufactured with wire type WB typically had longitudinal cracks initiating at all eight wire-end locations. The only exception was the prism using granite aggregate, 6000 psi release strength, and $\frac{3}{4}$ in. edge distance where the total number of observed cracks was six.
- Prisms manufactured with wire type WA (smooth wire) having 6000 psi release strength performed very well with only one observed crack on the prism having $\frac{5}{8}$ in. edge distance. Prisms with wire type WA had the largest values of transfer length.
- Prisms manufactured with wire type WJ indicated very good performance with Mix#2 (crushed granite CA4) as aggregate and a release strength of 4500 psi. Prisms having $\frac{3}{4}$ in. and $\frac{5}{8}$ in. edge distances did not have any visible cracks.
- Prisms manufactured with wire type WQ indicated very good performance in all three mixtures and both release strengths 4500 psi and 6000 psi. There were no observed cracks on the prisms having $\frac{3}{4}$ in. edge distance.
- The theoretical analysis shows evaluation of the tangential stresses between wire and concrete, taking into account Poisson's effect, the edge distance, and the mechanical properties of the material. It is hypothesized that there are additional tensile stresses that arise as the prestressing tendons slip and concrete that was originally located within the indent portions is displaced outward. In this way, wires with deeper indentations would displace more concrete thereby producing higher tensile stresses and longitudinal splitting.
- Based on the current research, concrete release strength of 4500 psi and 6000 psi and edge distances of $\frac{5}{8}$ in and $\frac{1}{2}$ in using the 5.32 mm diameter of wire are not recommended for the manufacturing of pretensioned concrete members. Furthermore, the test results indicate that $\frac{3}{4}$ in. edge distance is the minimum cover to achieve crack-free members with shallow chevron types of wire. In this case, a 1 in. edge distance would provide a reasonable factor of safety against splitting cracks from a design standpoint. The Qualification Test presented in Chapter 7 may be used to establish minimum cover requirements for other reinforcement types and concrete mixtures.

10. References

1. Bond of Reinforcement in Concrete [Book]/State-of-art report prepared by Task Group Bond Models// August 2000
2. Bond and Splitting Action of Prestressing Strand [Journal] / auth. Den Ujl Ja, Riga, Latvia, October 15-17, 1992 // pp: 145-170, OCLC-32077098
3. Bond modelling of Prestressed concrete During the Prestressing Force Release [Journal] / Auth. Jose M. Benitez, Jaime Galvez // Materials and Structures 12 May 2010
4. Development of a Standard Bond test for Indented Prestressing wires [Conference] / auth. Matthew L. Arnold, Robert J. Peterman, Naga Narendra B. Bodapatti, B. Terry Beck and Chih-Hang (John) Wu // Joint Rail Conference paper no. JRC2013-2461, pp. V001T01A009, Knoxville, Tennessee, April 2013
5. Dilation Behavior of Seven-wire Prestressing strand-The Hoyer effect [Journal] / auth. Vincent Briere Kent A. Harries, Jarret Kasan, Charles Hager // Construction and Building Materials, December 2012
6. Theoretical Analysis of Transfer Lengths in Pretensioned Prestressed concrete members [Journal] / Auth. Byung Hwan Oh, M. ASCE, Eui Sung Kim and Young Cheol Choi // Journal of Engineering Mechanics, vol. 132, issue 10, October 2006
7. Cracking of edge distance along anchored deformed reinforcing bars [Journal] / auth. Ralejs Tepfers // Magazine of concrete research volume 31, issue 106, pp 3-12, 1979
8. Nature of Bond in Pre-tensioned prestressed concrete [Journal] / auth. Jack R. Janney // Journal Proceedings, volume 50, issue 5, pp 713-736 May 1954
9. Bond Between smooth Prestressing wires and Concrete: Finite element model and Transfer Lengths analysis for pretensioned concrete crossties / auth. Hailing Yu, David Y. Jeong // ASCE Structures Congress 2014
10. Characteristics of Pretensioned Strand [Journal] / auth/ Abrishami H.H, Mitchell D // ACI Materials Journal/ May-June, pp 228-235
11. Steel Encased Pull Through and Push-in tests of Indented Three-wire Strands [Report] / Auth. R. Gustavson // Concrete structures, Chalmers University of Technology, Goteborg, 2001, 183p
12. Splitting Failure of Precast Prestressed Concrete during the Release of the Prestressing Force J.C Galvez, J.M. Benitez, B. Tork, M.J.Casati, D.A.Cendon, Engineering Failure Analysis Volume 16, December 2009, pp 2618-2634
13. In-Plant Testing of a new Multi-Camera Transfer Length Measurement System for Monitoring Quality of Railroad Crosstie Production [Conference] / auth. Beck, B. Terry, Peterman Robert J., Wu Chih-Hang (John) // Proceedings of the 2015 Joint Rail conference, March 23-26, 2015, san Hose, CA, USA
14. Effects of Cover, Compressive strength and Wire type on Bond performance in

- Prismatic Prestressed concrete members [Conference] / auth. Adrijana Savic, b. Terry Beck, Aaron Robertson, Robert J. Peterman, J. Clark, Chih-hang Wu // Proceedings of 2018 ASME Joint Rail Conference, April 18-20, 2018, Pittsburgh, PA, USA
15. Effect of Strand Blanketing on performance of pretensioned girders [Journal] / auth. Kaar P., D. Magura // PCI Journal, V.10, No. 6, December 1965, pp. 20-34.
 16. Determining the Transfer Length in Prestressed Concrete Railroad Ties Produced in The United States [Master Thesis] //Robert Lawrence, Kansas State University 2012, Manhattan, KS, USA
 17. Non-Contact Measurement of Wire Indent Profiles on Prestressing Reinforcement Steel [Conference] / Auth. Mark Haynes, John C-H Wu, B. Terry Beck, Robert Peterman // Proceedings of the 2012 AREMA Conference, Sept. 16-19, 2012, Chicago Illinois, USA
 18. Suitability and Variability of Non-Destructive Testing Methods for Concrete Railroad Tie Inspection [Conference] / auth. Aref Shafiei, Kyle Riding, Robert J. Peterman, Chris Christensen, B. Terry Beck // Proceedings of the 2016 Joint Rail Conference, April 12-15, 2016, Columbia, SC, USA
 19. Effect of Prestressing Wire Type on the Development Length and Flexural Capacity of Pre-tensioned Concrete Crossties [Conference] / auth. Amir Farid Momeni, Robert J. Peterman, B. Terry Beck, Chih-Hang John Wu, Naga Narendra B. Bodapati // Paper Number JRC2015-5739, Proceedings of the 2015 Joint Rail Conference JRC2015, March 23-26, San Jose, California, USA
 20. PCI Design Handbook [Book] / auth. Precast/Prestressed Concrete Institute. - Chicago IL: [s.n], 2010
 21. Prestressed Concrete Ties for North American Railroads [Journal] / auth. Hanna Amir N // PCI -Sept. – Oct. 1979. – pp. 32-61
 22. Standard Test Method for Compressive Strength of Cylindrical Concrete Specimens [Journal] / Auth. ASTM C39 / C39M-12a // ASTM International. – West Conshohocken, PA: [s.n.], 2012
 23. Standard Test Method for Splitting Tensile Strength of Cylindrical Concrete Specimens [Journal] / Auth. ASTM C496 / C496M-11 // ASTM International. – West Conshohocken, PA: [s.n.], 2010
 24. Standard Test Method for Static Modulus of Elasticity and Poisson's Ration of Concrete In Compression [Journal] / auth. ASTM C469/C469M-10 // ASTM International. – West Conshohocken, PA: [s.n.], 2010
 25. Standard Transfer Lengths in Full Scale AASHTO Prestressed Concrete Girders [Journal] / Auth. Shahawy Mohsen A, ISSA Moussa and Bachelor Barrington deV //PCI Journal. – 1992. – 3: Vol. 37. -pp.84-96
 26. Un-tensioned Pull-Out Tests to Predict the Bond Quality of Different Prestressing Reinforcements Used in Concrete Railroad Ties [Report] / auth. Arnold Matthew Lukas / Department of Civil Engineering. – Manhattan, KS: Kansas State University, 2013
 27. ADVA Cast 530 Data Sheet [Online] / auth. W. R. Grace & Co. – Conn. // GCP applied

- Technologies (Grace Construction & packing). – 2007.-
31D_ADVA_Cast_530_11_15_07.pdf.
28. ASTM A1096 Standard Test Method for Evaluating Bond of Individual Steel Wire, Indented or Plain, for Concrete Reinforcement [Report]. - West Conshohocken, PA: ASTM International, 2015
 29. Building Code Requirements for Structural Concrete [Report] / auth. ACI 318-11. - [s.l.]: American Concrete Institute, 2011.
 30. Capacity optimization of a prestressed concrete railroad tie [Report]: Master's Thesis / Auth. Lutch Russell H / Department of Civil and Environmental Engineering; Michigan Technological University. - 2009.
 31. Concrete Crossties in the United States [Journal] / auth. Weber J W // PCI JOURNAL. – February 1969. - 1: Vol. 14. - pp. 46-61.
 32. Determining the transfer length in prestressed concrete railroad ties produced in the United States [Report]: Master's thesis / auth. Murphy Robert Lawrence / Department of Civil Engineering; Kansas State University. - 2012.
 33. Effects of concrete composition on transmission length of prestressing strands [Journal] / Auth. Marti-Vargas J R [et al.] // Construction and Building Materials. - February 2012. - 1: Vol. 27. - pp. 350-356.
 34. Evaluation of As-Cast Strand-Depth on transfer and Development Length in Concrete Mixes with Different Fluidity [Report]: Draft Final Report submitted to PCI / auth. Peterman Robert J / RJ Peterman & Associates, Inc. - January 2012.
 35. Experimental Assessment of Factors Affecting Transfer Length [Journal] / auth. Barnes Robert W, Grove J W and Burns N H // ACI Structural Journal. - Nov-Dec 2003. - Vol. 100. - pp. 740-748
 36. Flexural Bond Tests of Pre-tensioned Prestressed Beams [Journal] / auth. Hanson Norman W and Kaar Paul H // ACI Journal. - 1959. - 1: Vol. 55. - pp. 783-802.
 37. LRFD Bridge Design Specifications [Book] / auth. AASHTO. - Washington, DC: American Association of State Highway and Transportation Officials, 2014.
 38. Experimental determination of prestressing wire bond and splitting propensity Characteristics Through tensioned pullout tests [report] / auth. Joseph Robert Holste // Kansas State University 2014.
 39. Effect of concrete properties and prestressing steel indentation types on the Development Length and flexural capacity of pre-tensioned concrete members [Report] / auth. Momeni Amir // Kansas State University, May 2016
 40. A comprehensive study of prestressing steel and concrete variables affecting transfer Length in Pre-tensioned concrete crossties [Report] / auth. Naga Narednra Babu Bodapati // Kansas State University 2018.
 41. Experimental determination of prestressing wire bond and splitting propensity Characteristics through tensioned pullout tests [report]/ auth. Joseph Holste // Kansas State University 2015.

42. Improving Prestressed reinforcement for concrete Railroad ties via geometrical Dimensioning and tolerancing [report] /auth. Mark Haynes //Kansas State University 2015.
43. A High-Resolution Automated Prestressing Wire Indent Profiling System for Verification of Wire-Concrete Mix Compatibility [conference]/ auth. B.T.Beck, A. Robertson, R.J.Peterman, K. Ryding, Savic A.//JRC2019-1269, April 2019
44. Sure Cure [manual] by Products Engineering, 30735 Bryant Drive, Unit 606 Evergreen, Colorado 80439
45. Forney machine [manual] by Forney LP 2050 Jackson's Pointe Court Zelienople, PA 16063, USA

Appendix Calculation of System Qualification Test Prism Parameters

A.

The generic prestressed concrete tie section in Figure 10-1, located near the end of a tie, has fifteen 0.25 in diameter prestressing tendons that are initially tensioned to 9200 lbs. each. The smallest nominal edge distance of any tendon within 12 in of the tie is determined to be 1.40 in. The tendon placement has tolerances $\pm 1/8$ in. The smallest cross-sectional area of the tie is known to be 81.5 in².

Determine the parameters of the System Qualification Test prisms.

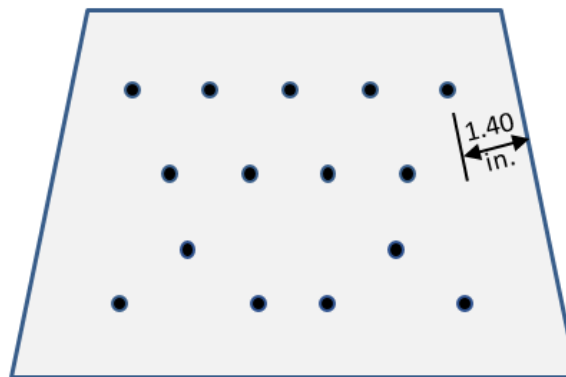


Figure 10-1: Generic Tie Cross-Section

The average initial compressive stress in the tie (neglecting losses) is calculated as:

$$\frac{(15 \text{ wires}) \left(\frac{9200 \text{ lb}}{\text{wire}} \right)}{81.5 \text{ in}^2} = 1693 \text{ psi}$$

10-1

The minimum permissible edge distance, D, is 1.40 in. (nominal)-0.125 in. (tolerance)=1.275 in. The reduced distance, RD, is then determined as 0.75 x 1.275 in.=0.956 in. This may be rounded to 15/16 in for convenience or kept at 0.956 in.

The side dimensions of the square prism are then calculated as $\sqrt{\frac{(4)(81.5 \text{ in}^2)}{(15)}} = 4.66 \text{ in.}$ Rounding to the nearest 1/8 in.=4 5/8 in. Therefore, use the prism cross-section shown in Figure 10-2.

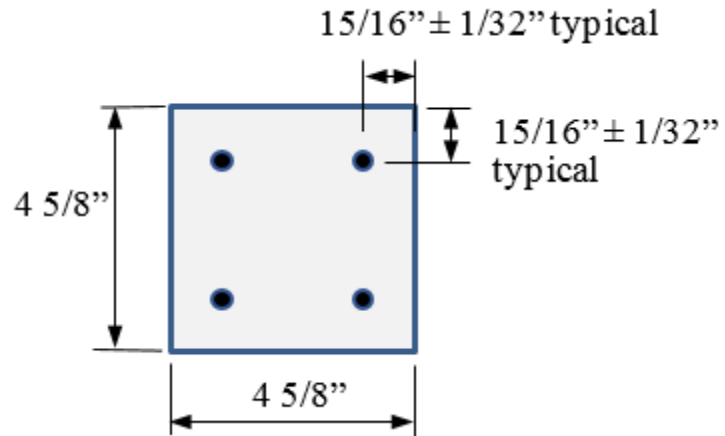


Figure 10-2: System Qualification Test Prism Cross-Section

The average initial compressive stress in the System Qualification Test Prism (neglecting losses) is calculated as:

$$\frac{(4 \text{ wires}) \left(\frac{9200 \text{ lb}}{\text{wire}} \right)}{(4.625 \text{ in})^2} = 1720 \text{ psi}$$

The prism has approximately the same compressive stress as the tie cross-section. The slight difference is due to rounding of dimensions.

Appendix B. Results

Mix#1-WA wire type

Release strength 6000psi

The test was conducted with WA wire type with concrete release strength of 6000 psi. WA wire type performed very well with no observed cracks for $\frac{3}{4}$ in and $\frac{1}{2}$ in edge distance, and for $\frac{5}{8}$ in. edge distance a 0.04 in² crack area and a 4 in. crack length were observed as shown in Figure 10-8 and Figure 10-9. The values of transfer lengths were higher on the $\frac{3}{4}$ in. edge distance than on the prisms with different types of indent, Figure 10-3, Figure 10-4 and Figure 10-5, and show the longitudinal strain profiles on the prisms with $\frac{3}{4}$ in, $\frac{5}{8}$ in. and $\frac{1}{2}$ in edge distances. Additionally, Figure 10-6 and Figure 10-7 show observed prisms and Figure 10-10 shows the number of cracks on each prism.

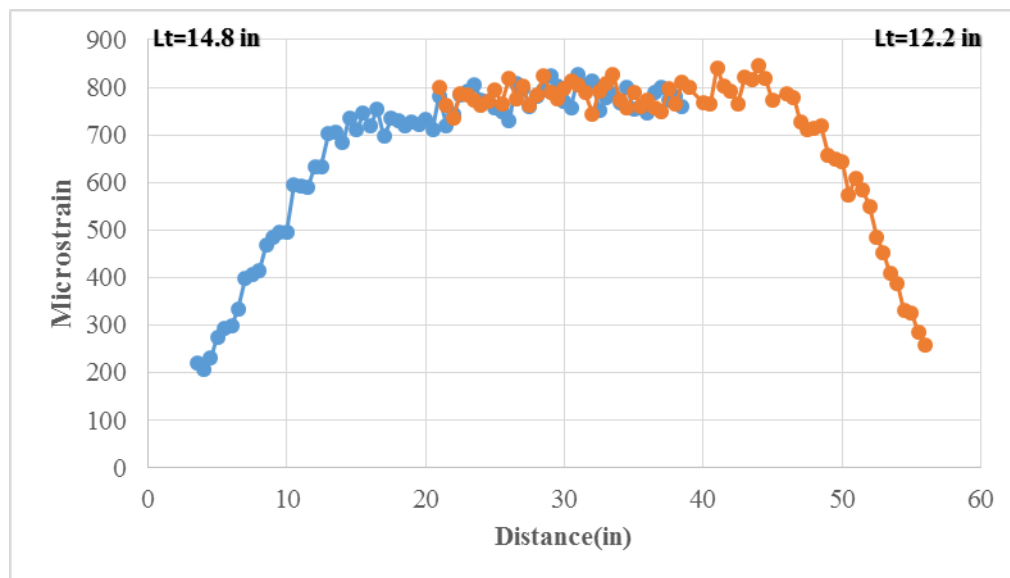


Figure 10-3: Mix#1, 6000 psi, WA, $\frac{3}{4}$ in. Edge Distance-Longitudinal Strain Profile

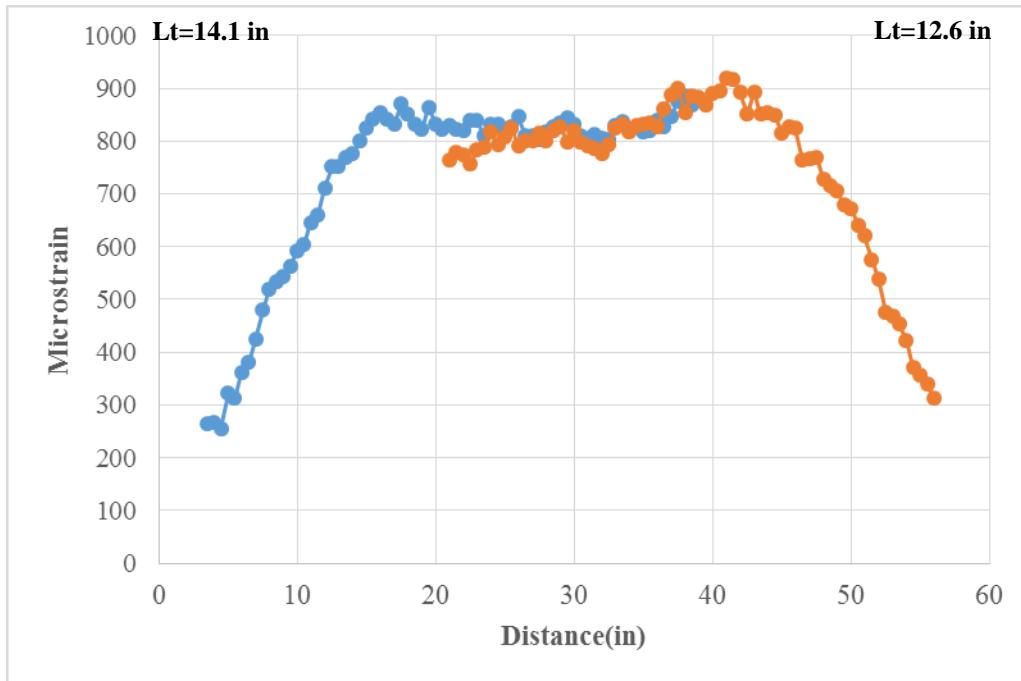


Figure 10-4: Mix#1, 6000 psi, WA, 5/8 in. Edge Distance-Longitudinal Strain Profile

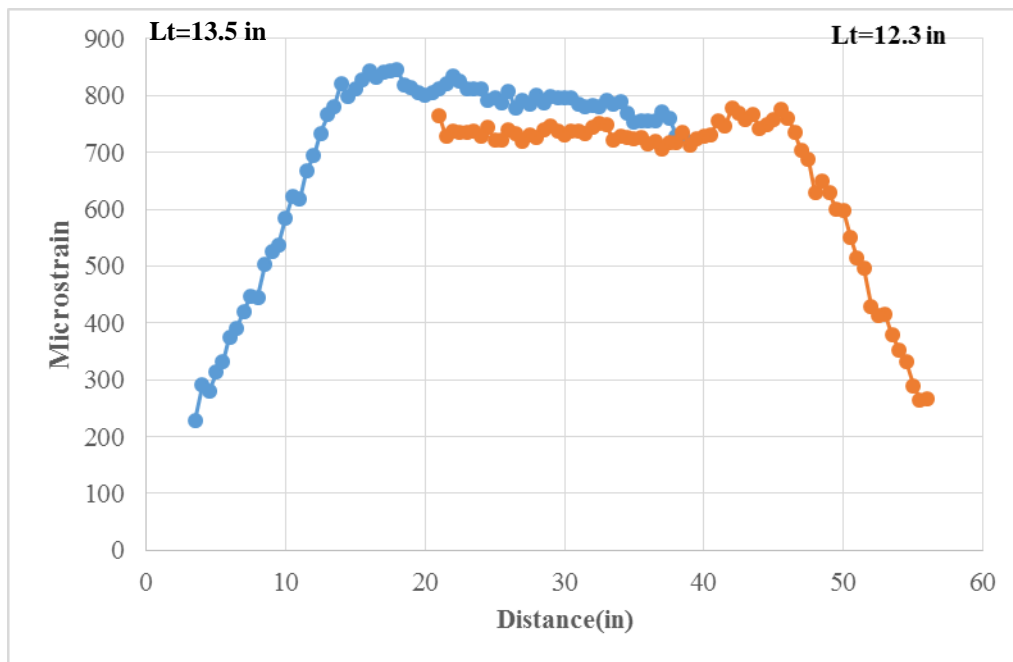


Figure 10-5: Mix#1, 6000 psi, WA, 1/2 in. Edge Distance-Longitudinal Strain Profile

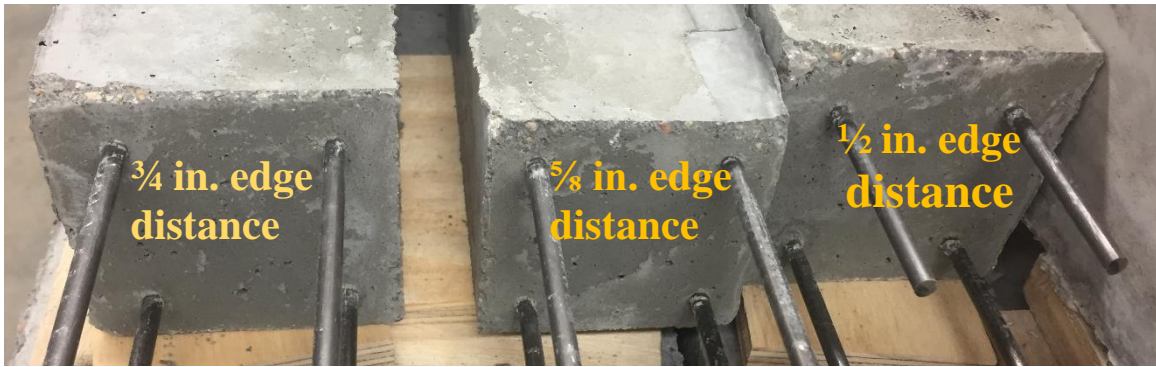


Figure 10-6: Mix#1, 6000psi, WA-Observed Cracking (Live End)

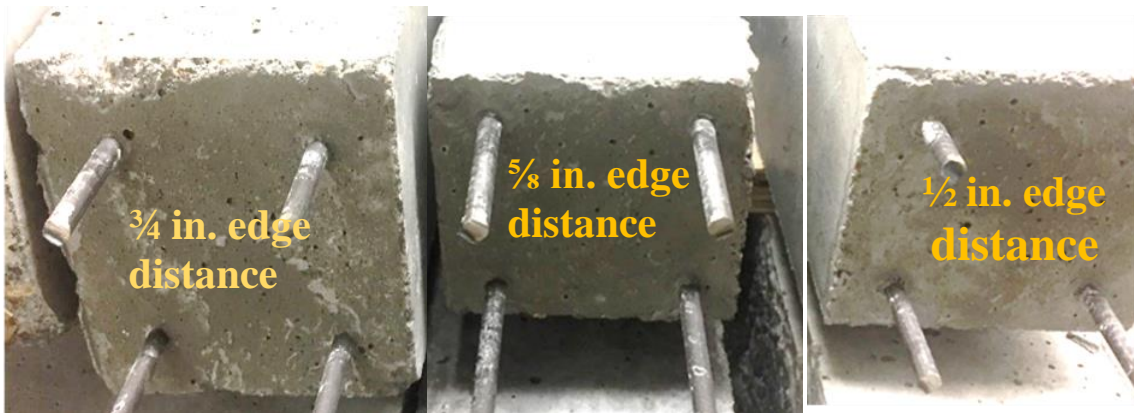


Figure 10-7 : Mix#1, 6000psi, WA-Observed Cracking (Dead End)

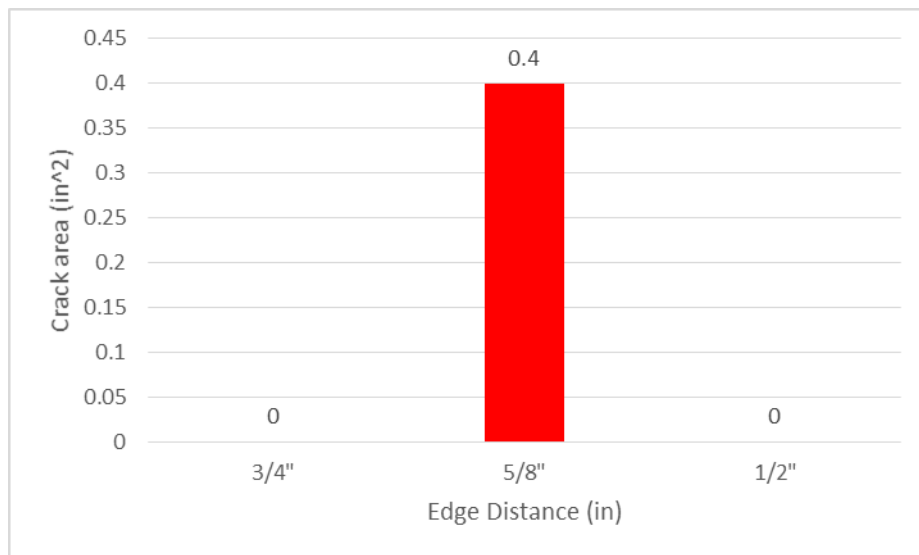


Figure 10-8: Mix#1, 6000psi, WA-Crack Area (in²)

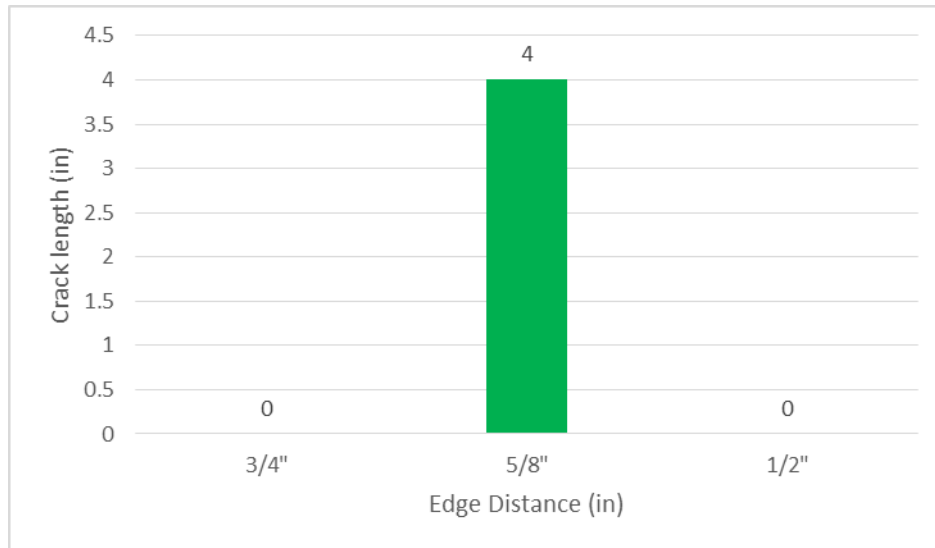


Figure 10-9: Mix#1, 6000psi, WA-Crack Length (in)

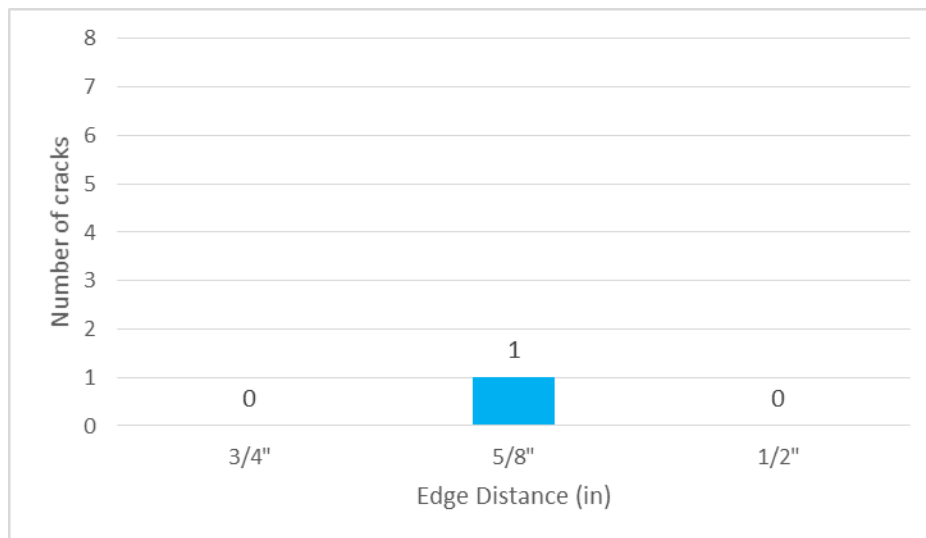


Figure 10-10: Mix#1, 6000psi, WA-Number of Cracks

Mix#1-WB wire type

The tests were conducted with WB type wire and concrete release strength of 4500 psi and 6000 psi. Tests were repeated three times with concrete strength of 6000 psi, and every test with WB wire performed poorly, with four cracks observed on each end of the prisms. WB wire had an average indent depth of 0.119 mm (0.004685 in.), and edge wall angle 16.45 degree.

WB-Release Strength 4500 psi

Figure 10-11 and Figure 10-12 show observed cracking of the prisms with concrete release strength of 4500 psi and the edge distances of $\frac{3}{4}$ in, $\frac{5}{8}$ in. and $\frac{1}{2}$ in. The maximum crack width on the prism with $\frac{3}{4}$ in. edge distance was 0.02 in and the maximum crack length was 53 in. The prisms with $\frac{1}{2}$ in. edge distance indicated poor performance with evident spalling on the front side of the prism on the live end. Figure 10-13, Figure 10-14, and Figure 10-15 show crack area, crack length and number of cracks for each prism with different value of edge distance, respectively.

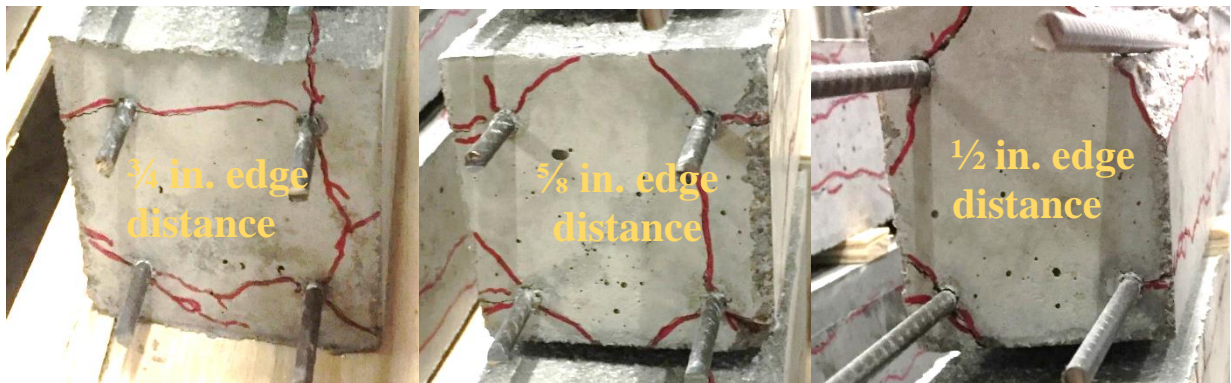


Figure 10-11: Mix#1, 4500psi, WB-Observed Cracking (Dead End)

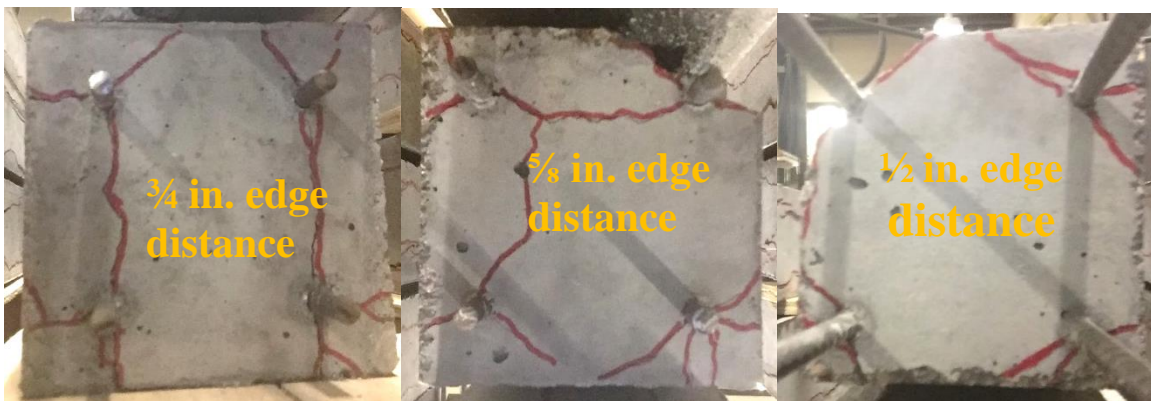


Figure 10-12: Mix#1, 4500 psi, WB-Observed Cracking (Live End)

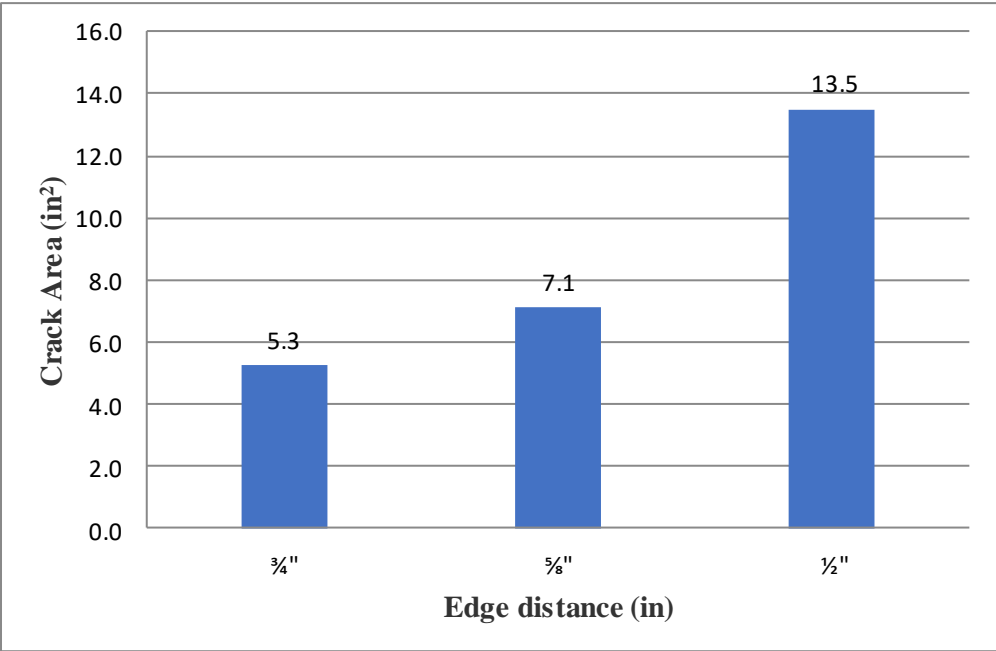


Figure 10-13: Mix#1, 4500 psi, WB-Crack Area (in²)

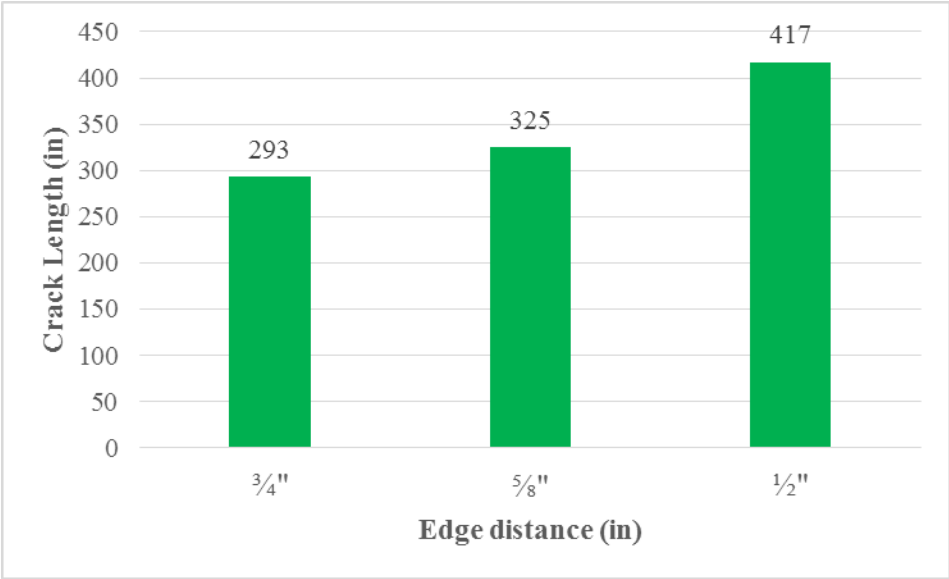


Figure 10-14: Mix#1, 4500 psi, WB-Crack Length (in)

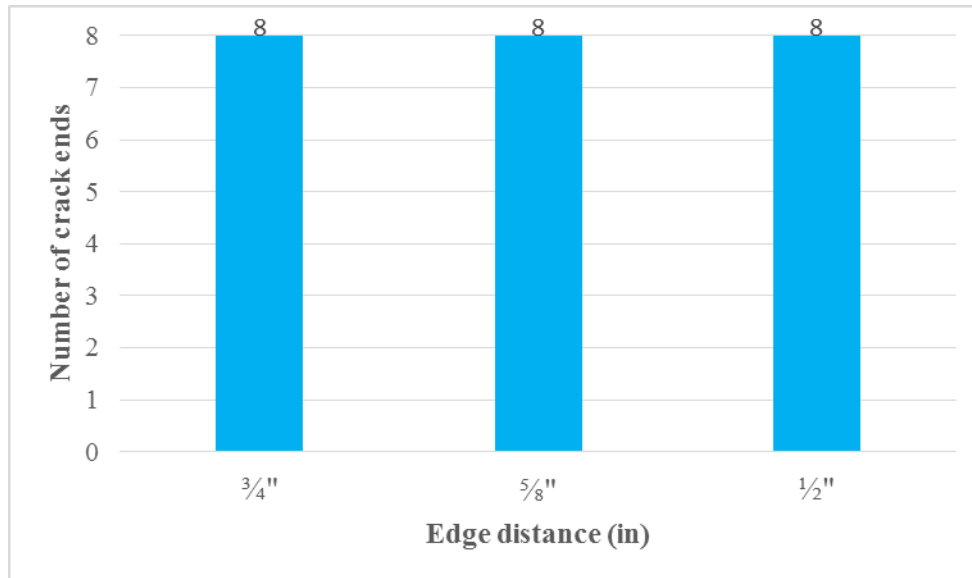


Figure 10-15: Mix#1, 4500 psi, WB-Number of Cracks

WB-Release Strength 6000psi (First Time)

Figure 10-16 and Figure 10-17 show the prisms with concrete release strength of 6000 psi, and three different edge distances. The tests were repeated with 6000 psi release strength of concrete three times. Each test with WB wire resulted in eight observed cracks on each prism as shown in Figure 10-20. Spalling was also observed on the prism with $\frac{1}{2}$ in. edge distance which indicated that bond between wire and concrete was totally lost as shown in Figure 10-18 and Figure 10-19.

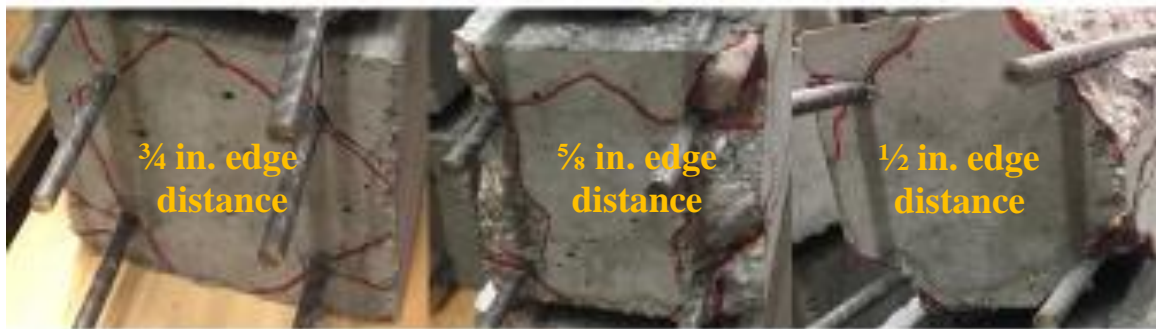


Figure 10-16: Mix#1, 6000psi, WB-Observed Cracking (Dead end)

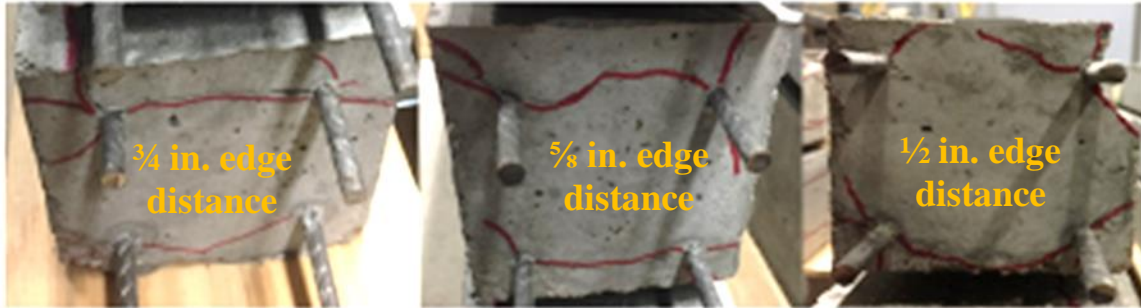


Figure 10-17: Mix#1, 6000 psi, WB-Observed Cracking (Live end)

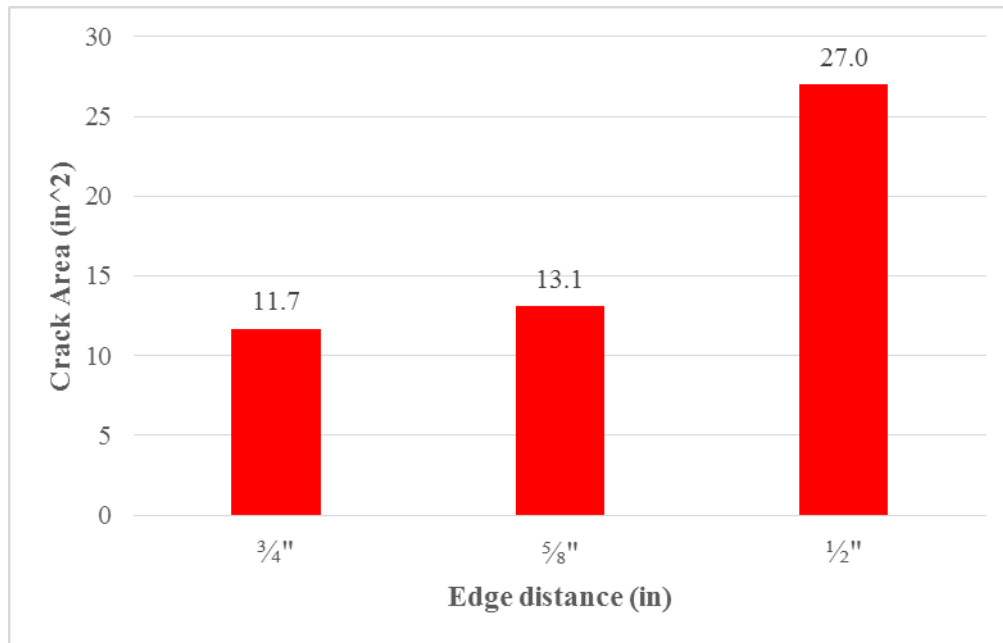


Figure 10-18: Mix#1, 6000 psi, WB-Crack Area (in²)

Figure 10-18 and Figure 10-19 show the crack area and crack length, respectively. Decreasing the edge distance resulted in increasing the crack area and crack lengths.

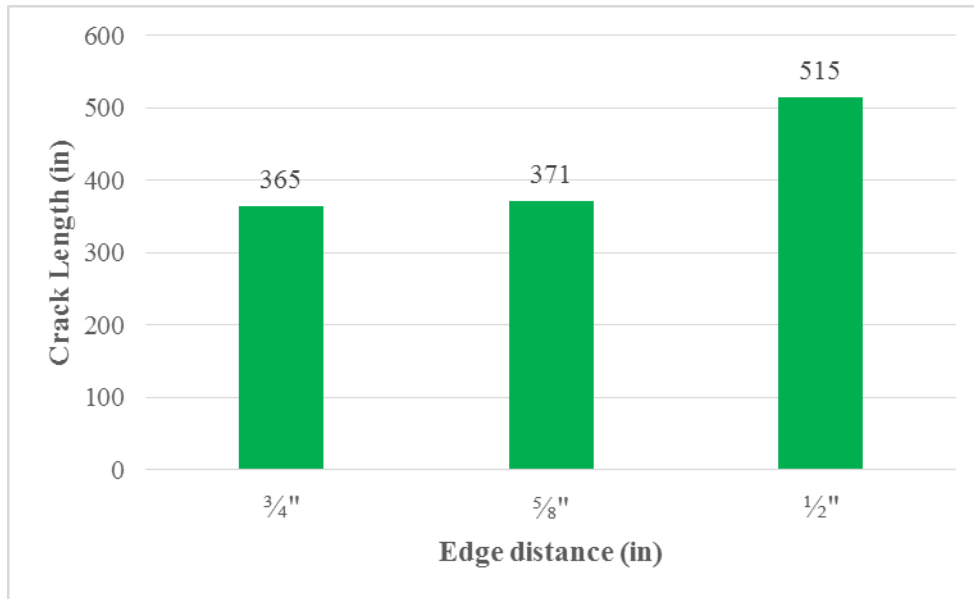


Figure 10-19: Mix#1, 6000 psi, WB-Crack Length (in)

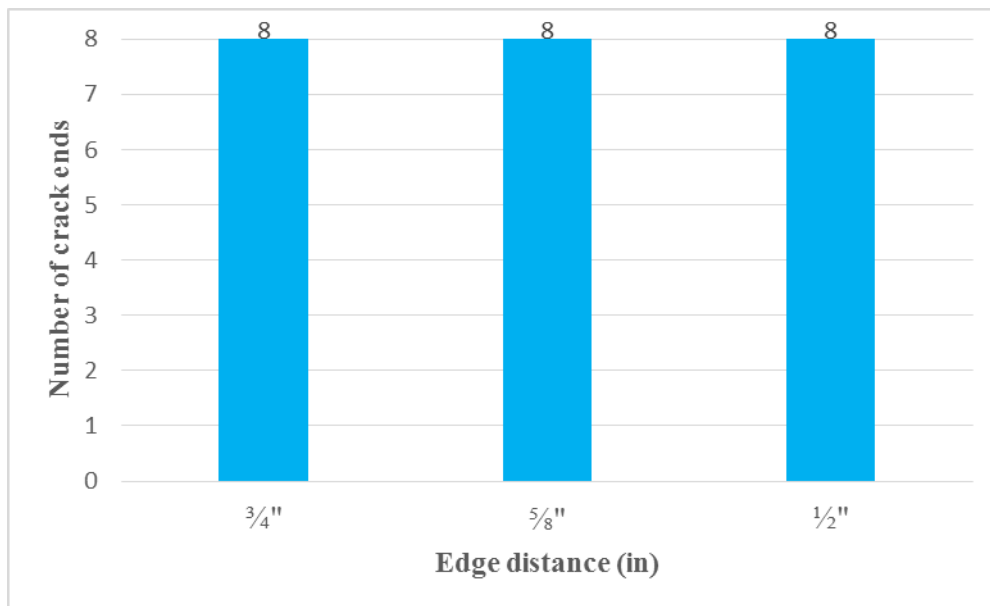


Figure 10-20: Mix#1, 6000 psi, WB-Number of Cracks

The maximum crack width observed on the prism with $\frac{3}{4}$ in. edge distance was 0.04 in, and the maximum crack length was 57 in. With decreasing the edge distance from $\frac{3}{4}$ in. to $\frac{5}{8}$ in. spalling was observed on the live end of the prism. Spalling also occurred on the front and back side of the prism with 8 in. and 6 in. in length respectively. Prism with $\frac{1}{2}$ in. edge distance performed poorly with spalling on the live end of the prism on the front, bottom and back side of the prism with 31 in, 30 in, 6 in and 5 in. lengths respectively.

WB-Release Strength 6000 psi (Second Time)

Figure 10-21 shows the values of crack areas for the wire WB and 6000 psi release strength. WB wire performed poorly with eight cracks observed on each prism. Similar casting and curing conditions were used throughout entire the laboratory phase.

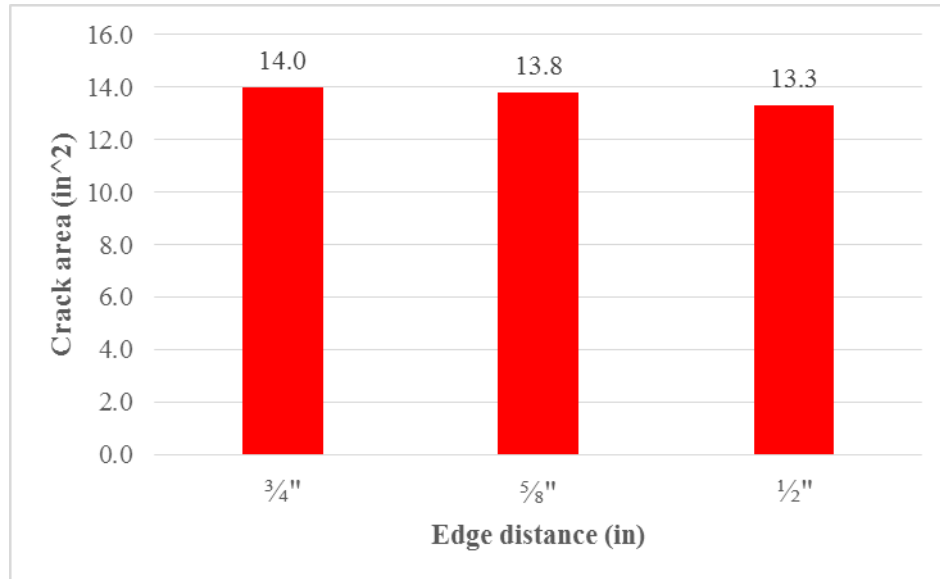


Figure 10-21: Mix#1, 6000 psi, WB second time-Crack Area (in²)

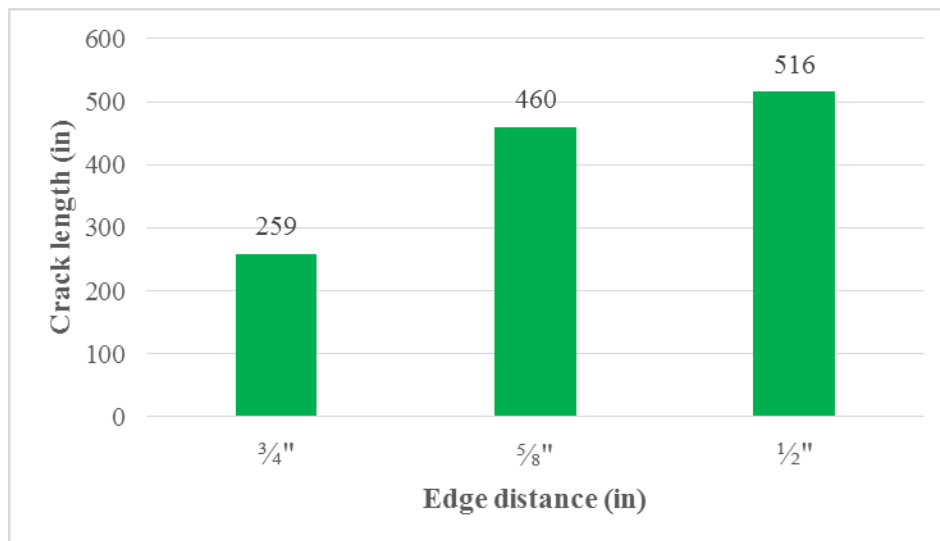


Figure 10-22: Mix#1, 6000 psi, WB second time-Crack Length (in)

Figure 10-22 presents the values of crack lengths as a function of the edge distance. The maximum crack width observed for the prism with 3/4 in. cover was 0.04 in. and maximum crack length was 34 in. Decreasing the cover to 5/8 in. resulted in spalling on the both sides of the prism. Additionally, the prism with 1/2 in. edge distance had severe damage.

WB-Release Strength 6000 psi (Third time)

Figure 10-23 shows the value of crack area for WB wire. The tests with this wire were repeated three times. The conditions were the same and WB wire exhibited consistent behavior which resulted in eight cracks per prism.

The maximum crack width for the prism with 3/4 in. edge distance was 0.03 in. and the maximum crack length was 46 in. The prism with 5/8 in. edge distance had eight cracks, with four cracks on each side. The maximum crack width was 0.016 in. and 34 in. was the maximum crack length. The prism with 1/2 in. edge distance had four cracks on each side of the prism. The maximum crack width was 0.04 in. and the maximum crack length was 59 in. As compared with previous results, with a 6000 psi release strength, eight cracks were observed on each prism with the different thicknesses of edge distances. However, spalling did not occur at any time.

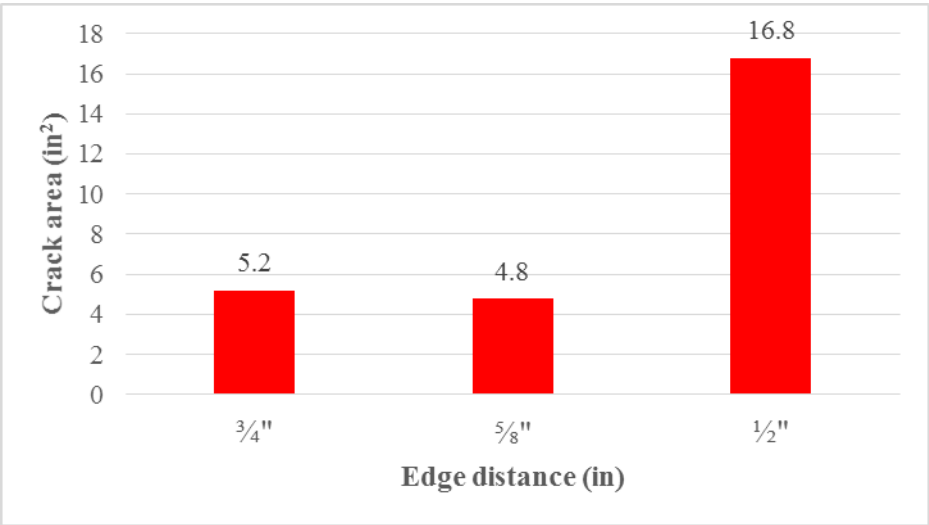


Figure 10-23: Mix#1, 6000 psi, WB third time-Crack Area (in²)

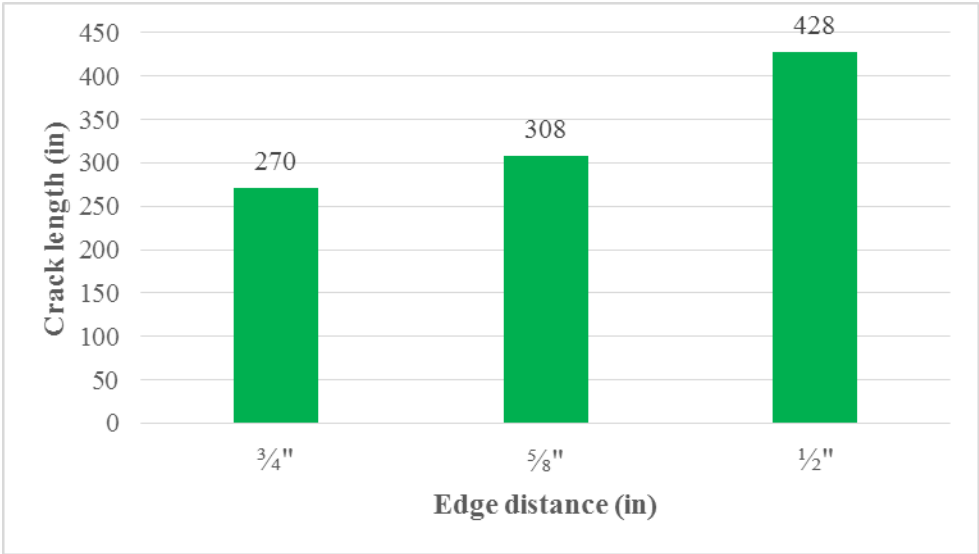


Figure 10-24: Mix#1, 6000 psi, WB third time-Crack Length (in)

Mix#1-WF wire type

WF wire had a depth of 0.163 mm (0.006417 in), and edge wall angle of 28.07 degrees with standard deviation more than 10 %. As stated previously, WF wire is considered a deep chevron type of wire.

WF-Release Strength 4500 psi

End-splitting cracks on the prism with $\frac{3}{4}$ in. edge distance did not form at the time of de-tensioning, they developed during the first month after de-tensioning due to sustained lateral stresses. The longitudinal strain profile was measured immediately after the process of de-tensioning. Transfer length on the live end was 5.9 in. and on the dead end was 6.2 in. One month after the process of de-tensioning, one crack appeared on the live end of the prism with $\frac{3}{4}$ in. edge distance. The crack width was less than 0.01 in. and the crack length was 5 in. Figure 10-25 shows the longitudinal strain profile on the prism with cover $\frac{3}{4}$ in. alongside with the values of transfer lengths. Figure 10-26 and Figure 10-27 present detected cracking on the dead end and live end of the prisms in series.

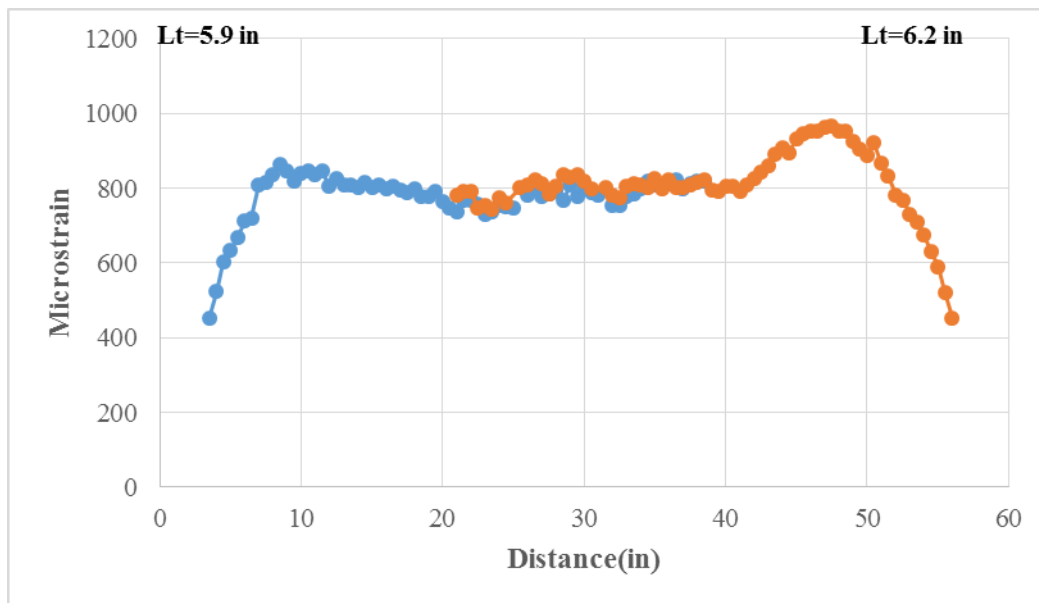


Figure 10-25: Mix#1, 4500 psi, WF, $\frac{3}{4}$ in. Edge Distance-Longitudinal Strain Profile

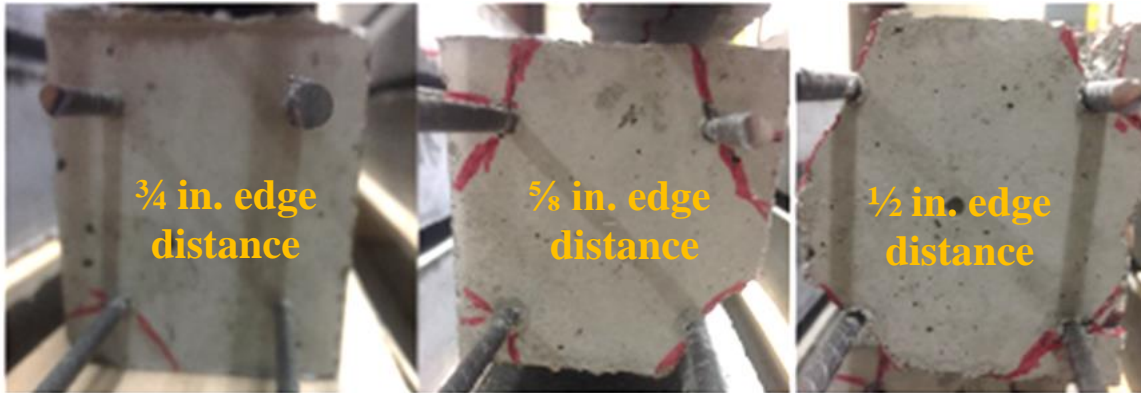


Figure 10-26: Mix#1, 4500psi, WF-Observed Cracking (Dead end)

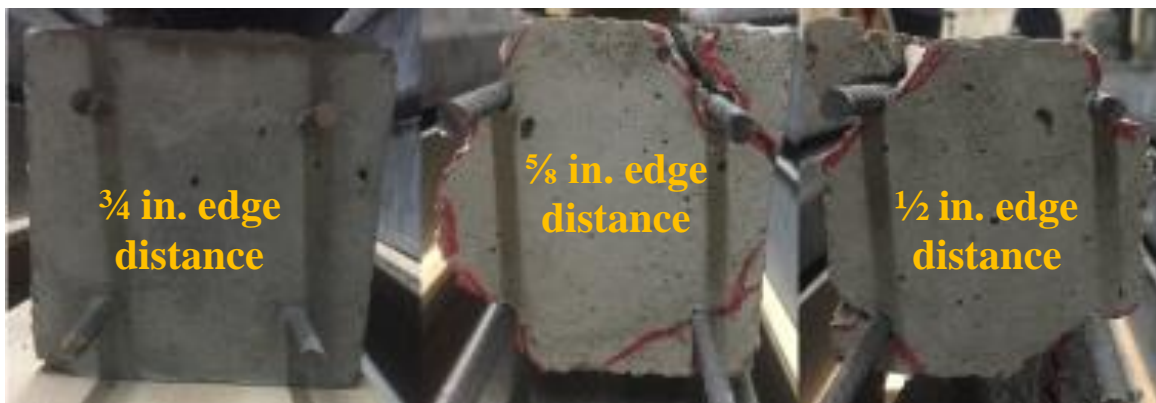


Figure 10-27: Mix#1, 4500 psi-Observed Cracking (Live end)

Figure 10-28 and Figure 10-29 show that with the reduction the edge distance from $\frac{3}{4}$ in. to $\frac{5}{8}$ in. to $\frac{1}{2}$ in. more cracks appeared. Spalling also occurred on the prism with $\frac{5}{8}$ in. cover on the dead end with the maximum length of 62 in, and on the live end with the maximum length of 13 in. On the third prism, with $\frac{1}{2}$ in. cover, spalling occurred on the both sides of the prism with maximum length of 31 in. on the live end and 55 in. on the dead end.

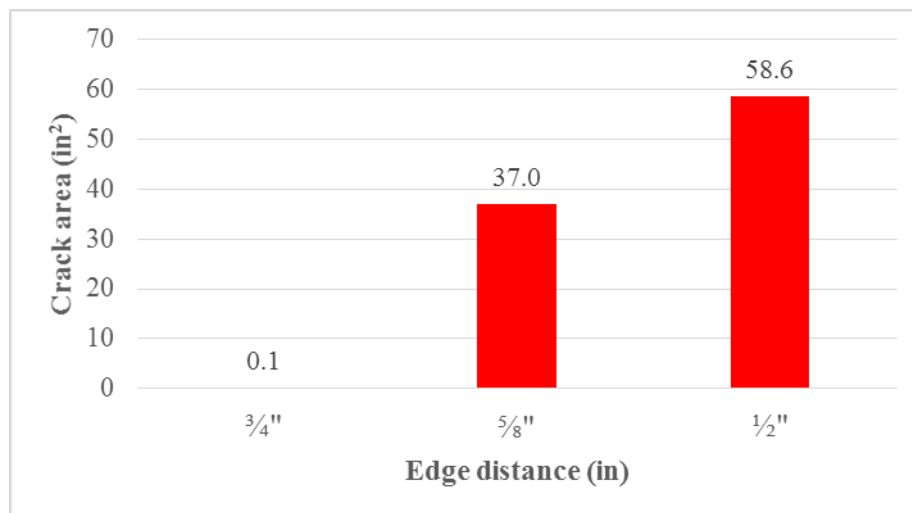


Figure 10-28: Mix#1, 4500 psi, WF-Crack Area (in²)

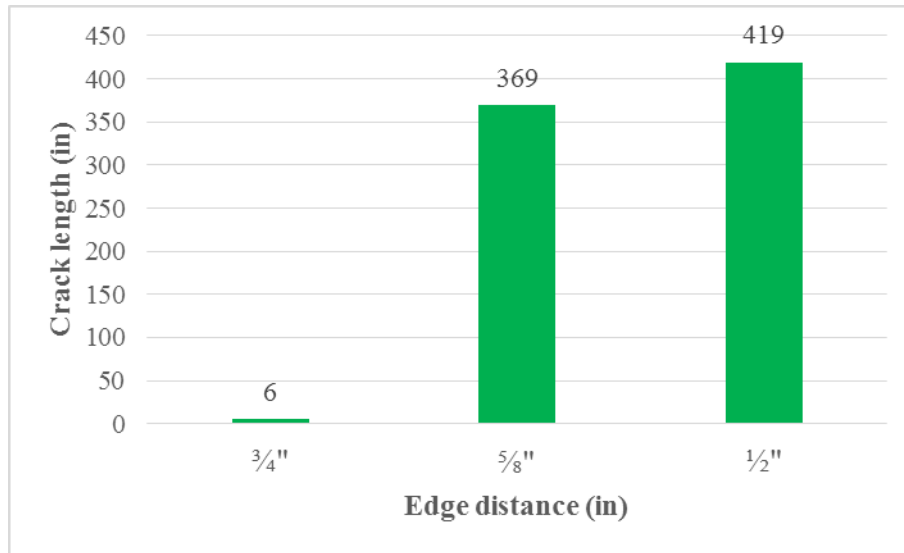


Figure 10-29: Mix#1, 4500 psi, WF-Crack Length (in)

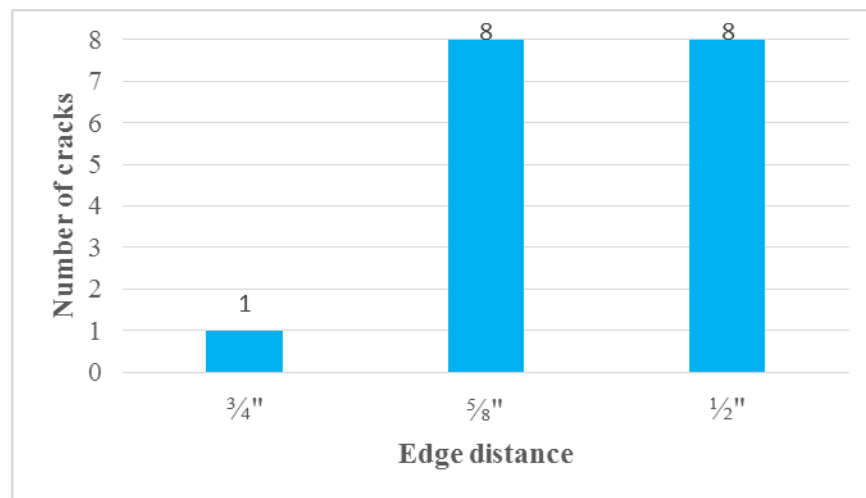


Figure 10-30: Mix#1, 4500 psi, WF-Number of Cracks

According to Figure 10-30 it was evident that with decreasing the cover, more cracks appeared. The WF wire was also tested by Bodapati (2018) with an edge distance of 1 in, which was found to perform very well with no crack appearing. With decreasing the edge distance to $\frac{3}{4}$ in. one crack appeared and decreasing the edge distance to $\frac{5}{8}$ in. and $\frac{1}{2}$ in. the values of crack areas were 37.0 in^2 and 59.0 in^2 , respectively.

WF-Release Strength 6000 psi

Figure 10-31 shows the prism strain profile of WF type wire and $\frac{3}{4}$ in. edge distance.

Figure 10-32 and Figure 10-33 show the observed cracking on the dead end and live end of the prisms.

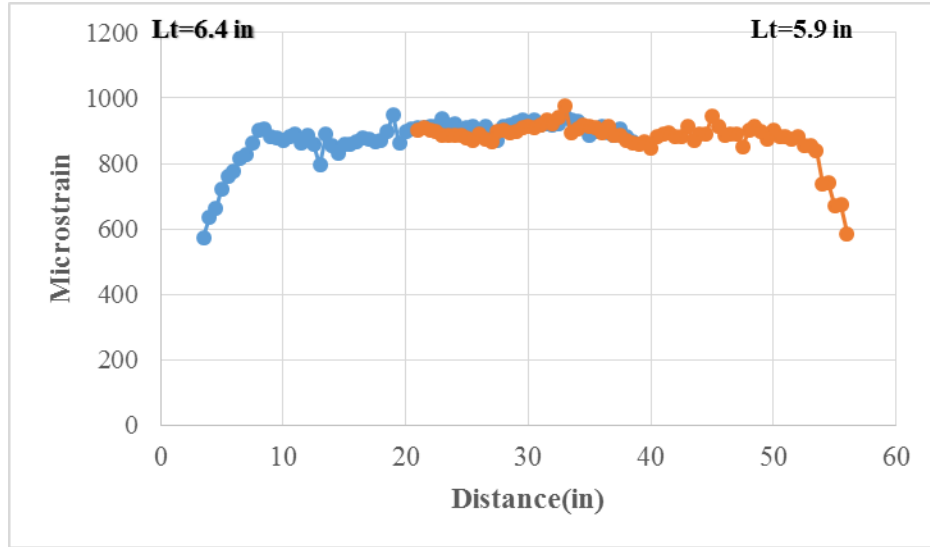


Figure 10-31: Mix#1, 6000 psi, WF, $\frac{3}{4}$ in. Edge Distance-Longitudinal Strain Profile



Figure 10-32: Mix#1, 6000 psi, WF-Observed Cracking (Dead End)

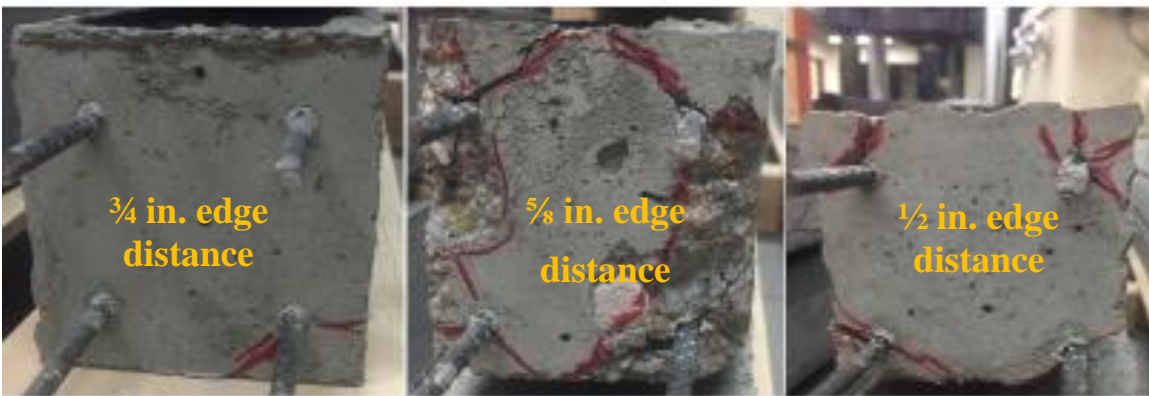


Figure 10-33: Mix#1, 6000 psi, WF-Observed Cracking (Live End)

According to Figure 10-34, Figure 10-35 and Figure 10-36, with decreasing the edge distance from $\frac{3}{4}$ in. to $\frac{5}{8}$ in. to $\frac{1}{2}$ in. more cracks systematically appeared. One visible crack was noticed on the $\frac{3}{4}$ in. edge distance and eight on the two prisms with thicknesses $\frac{5}{8}$ in. cover and $\frac{1}{2}$ in. cover.

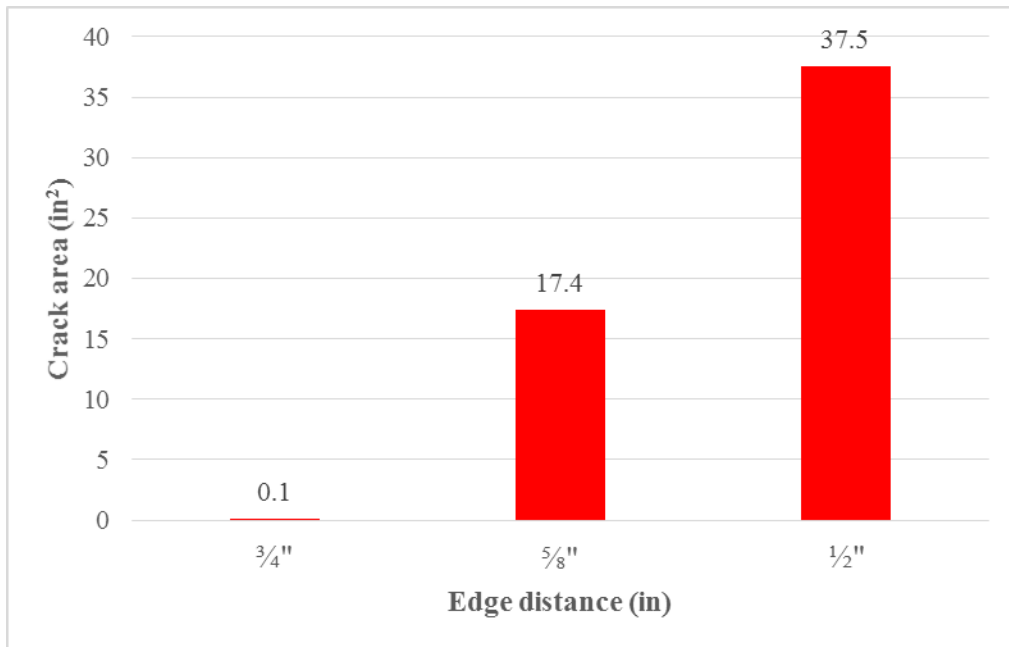


Figure 10-34: Mix#1, 6000 psi, WF-Crack Area (in²)

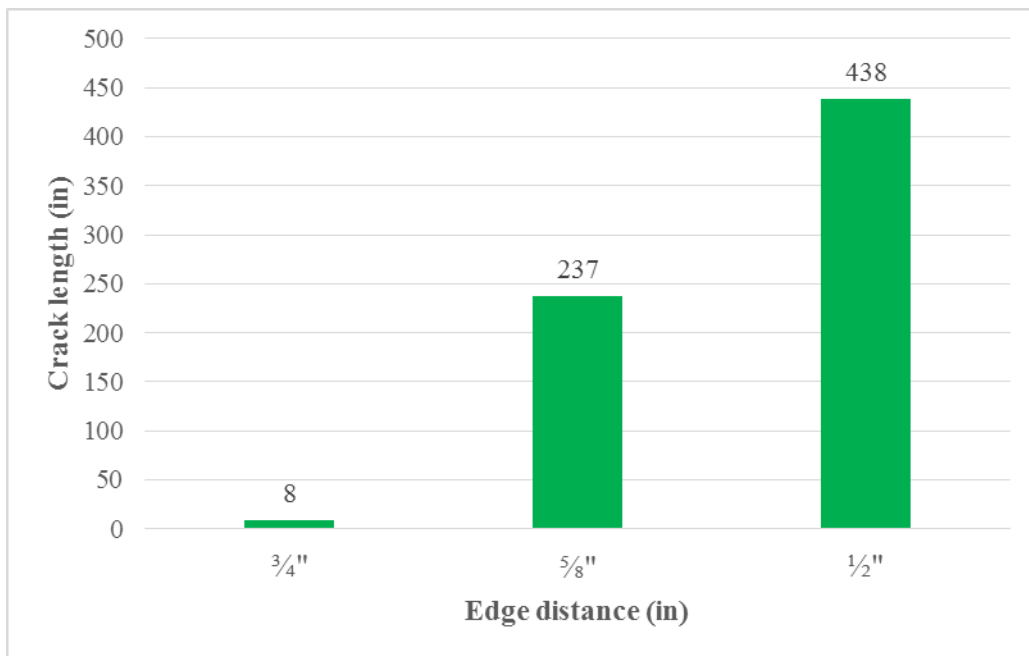


Figure 10-35: Mix#1, 6000 psi, WF-Crack Length (in)

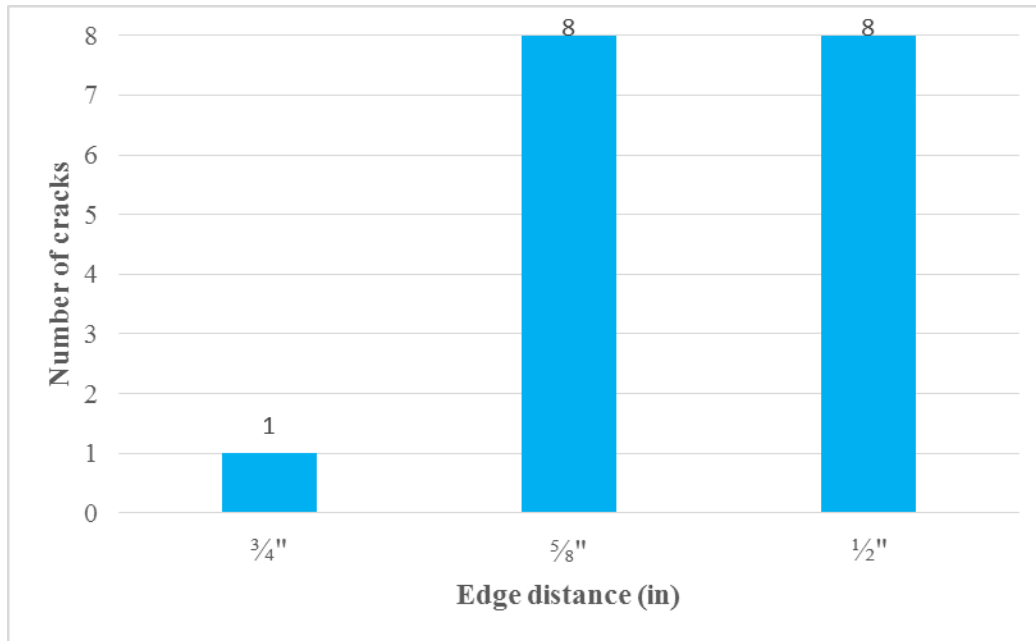


Figure 10-36: Mix#1, 6000 psi, WF-Number of Cracks

Figure 10-34, Figure 10-35 and Figure 10-36 show the values of crack areas, crack lengths and the number of cracks as a function of edge distance, respectively.

Mix#1-WG wire type

WG-Release Strength 4500 psi

WG wire has average indent depth of 0.066 mm (0.002598 in.) and edge wall angle 10.56 degrees.

WG wire was performed with 4500 psi release strength of concrete. WG belongs to shallow chevron type of wire and performed very well. There were no visible cracks observed on the prism with $\frac{3}{4}$ in. the edge distance, two cracks on the prism with $\frac{5}{8}$ in. the edge distance and three cracks on the $\frac{1}{2}$ in. the edge distance.

Figure 10-37 and Figure 10-38 show the position of the cracks on the live end and dead end for each side of the prism.



Figure 10-37: Mix#1, 4500psi, WG-Observed Cracking (Dead end)

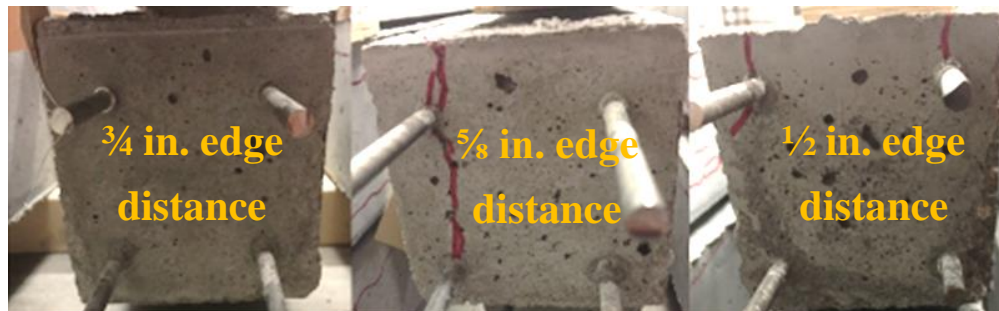


Figure 10-38: Mix#1, 4500 psi-Observed Cracking (Live end)

Figure 10-39 and Figure 10-40 show the crack area as a function of the edge distance, and crack length as a function of the edge distance. Reducing the values of the edge distance from $\frac{3}{4}$ in. to $\frac{5}{8}$ in. and $\frac{1}{2}$ in. more cracks appeared as shown in Figure 10-41.

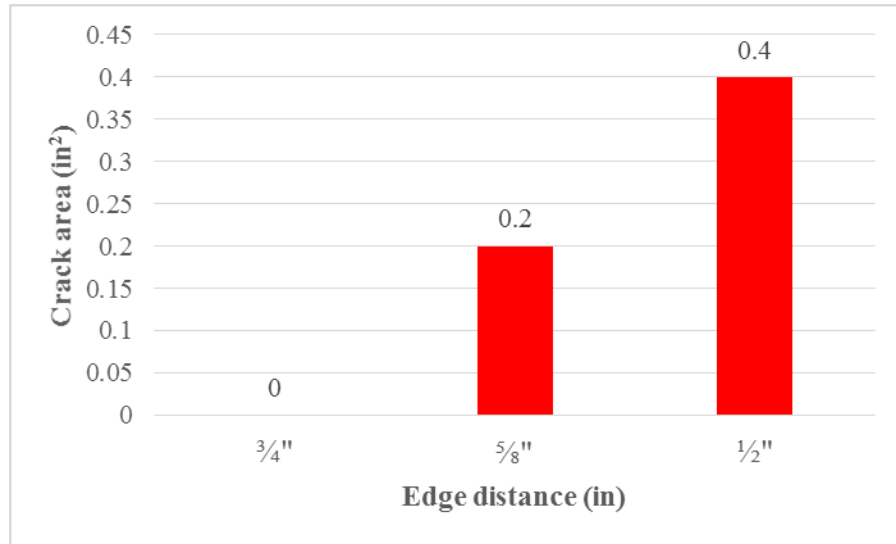


Figure 10-39: Mix#1, 4500 psi, WG-Crack Area (in²)

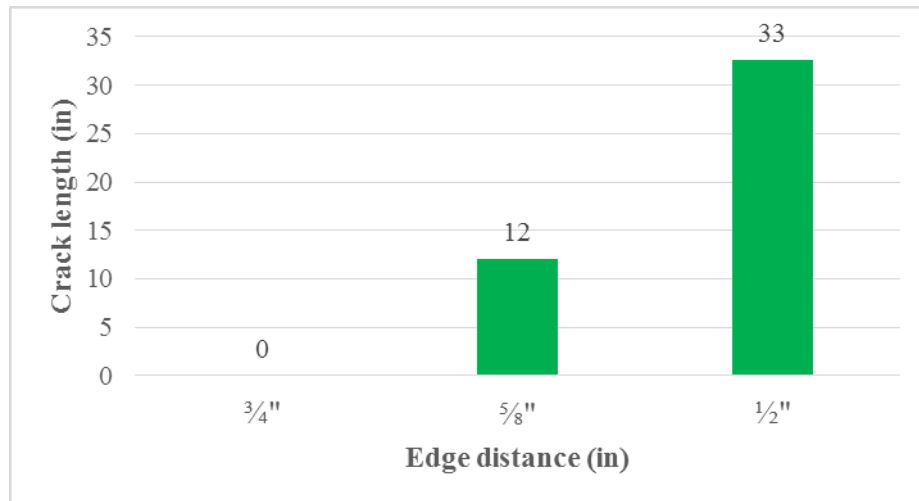


Figure 10-40: Mix#1, 4500 psi, WG-Crack Length (in)

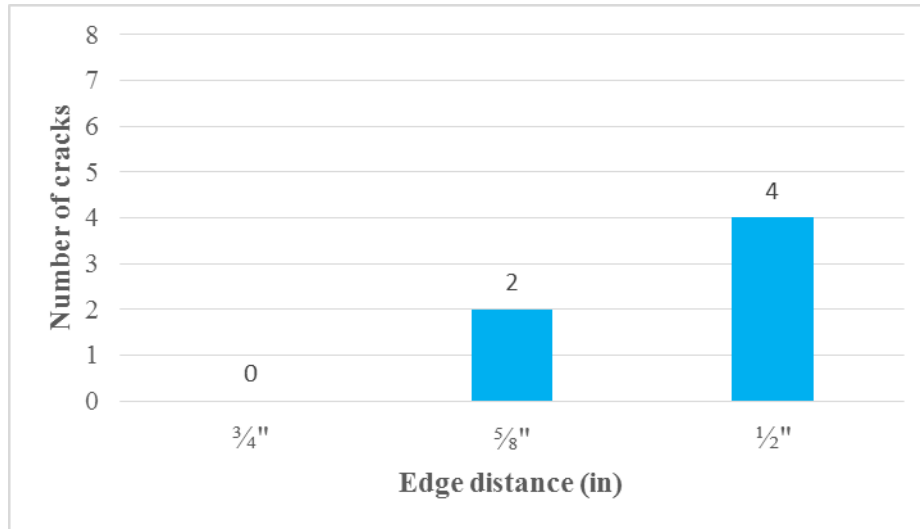


Figure 10-41: Mix#1, 4500 psi, WG-Number of Cracks

Prism with a $\frac{5}{8}$ in. edge distance had two cracks on the live end. The maximum crack width was 0.02 in. and the maximum crack length was 8 in. Prism with a $\frac{1}{2}$ in. edge distance had four cracks. The maximum crack width on the live end was 0.013 in. with the maximum crack length of 12 in. On the dead end the maximum crack width was 0.013 in. and the maximum crack length was 13 in.

Mix#1-WH wire type

WH-Release Strength 4500 psi

WH wire is deep chevron type of wire with an average indent depth of 0.164 mm (0.006457 in.), and edge wall angle of 16.27 degrees. Three prisms were cast with this wire and release concrete strength was 4500 psi. The first prism with $\frac{3}{4}$ in. the edge distance had three cracks on the live end with the maximum crack width of 0.016 in. and the maximum crack length of 16 in. Dead end of the prism had two cracks with the maximum width of 0.02 in. and the maximum crack length of 11 in. Spalling was observed on the second prism in series on the both sides of the prism. Length of spalling on the live end was 1 in. and 14 in. on the dead end. Spalling was occurred on the live end in the length of 23 in. on the prism having a $\frac{1}{2}$ in. edge distance. On the dead end four cracks appeared with the maximum crack width of 0.08 in. and the maximum crack length of 28 in. The positions of the cracks at the live end and dead end of the prism are given in the Figure 10-42 and Figure 10-43.



Figure 10-42: Mix#1, 4500 psi, WH-Observed Cracking (Dead End)

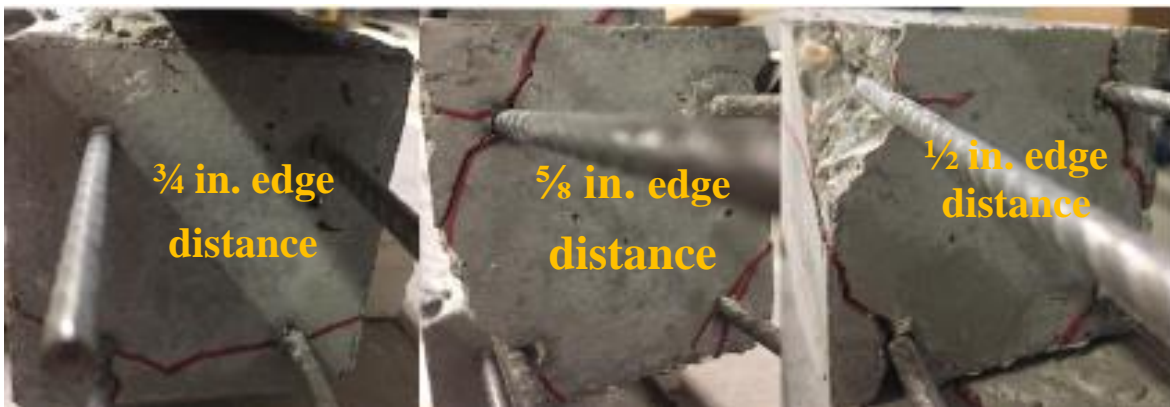


Figure 10-43: Mix#1, 4500 psi, WH-Observed Cracking (Live End)

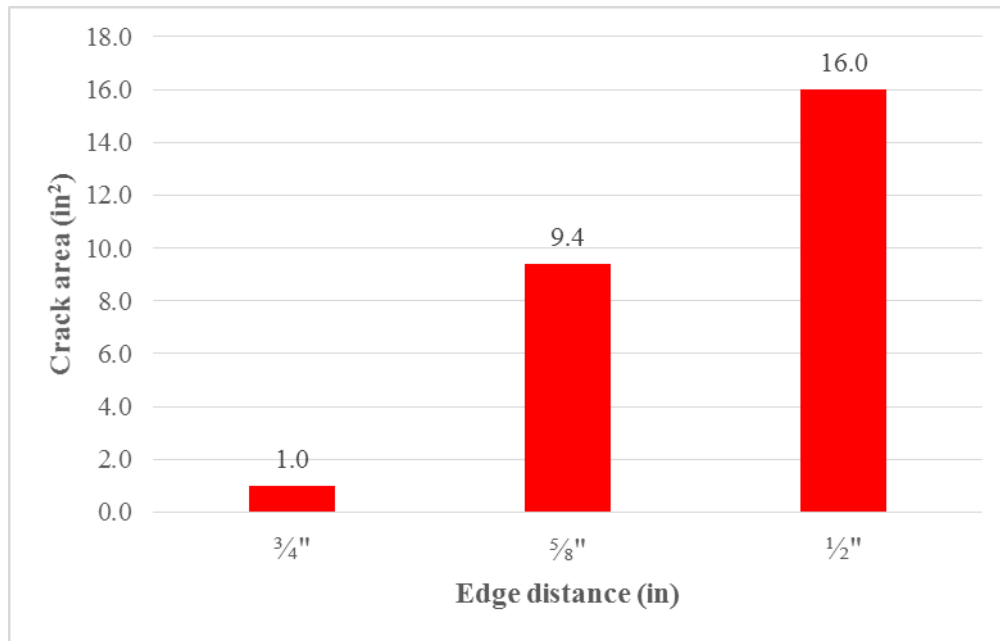


Figure 10-44: Mix#1, 4500 psi, WH-Crack Area (in²)

Figure 10-44, Figure 10-45 and Figure 10-46 show the values of crack area and crack length and number of cracks as a function of edge distance.

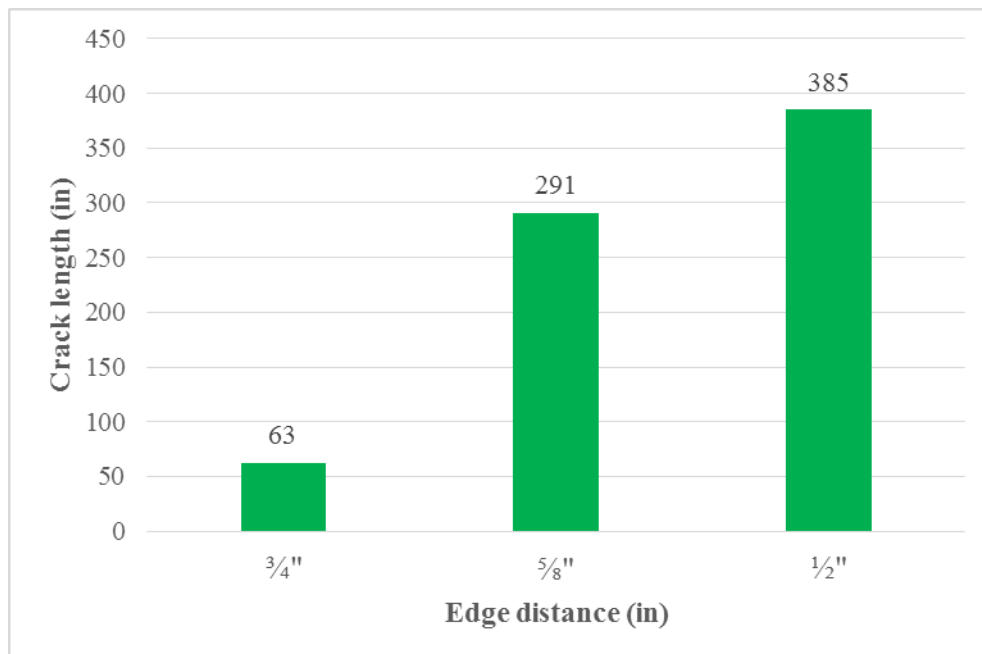


Figure 10-45: Mix#1, 4500 psi, WH-Crack Length (in)

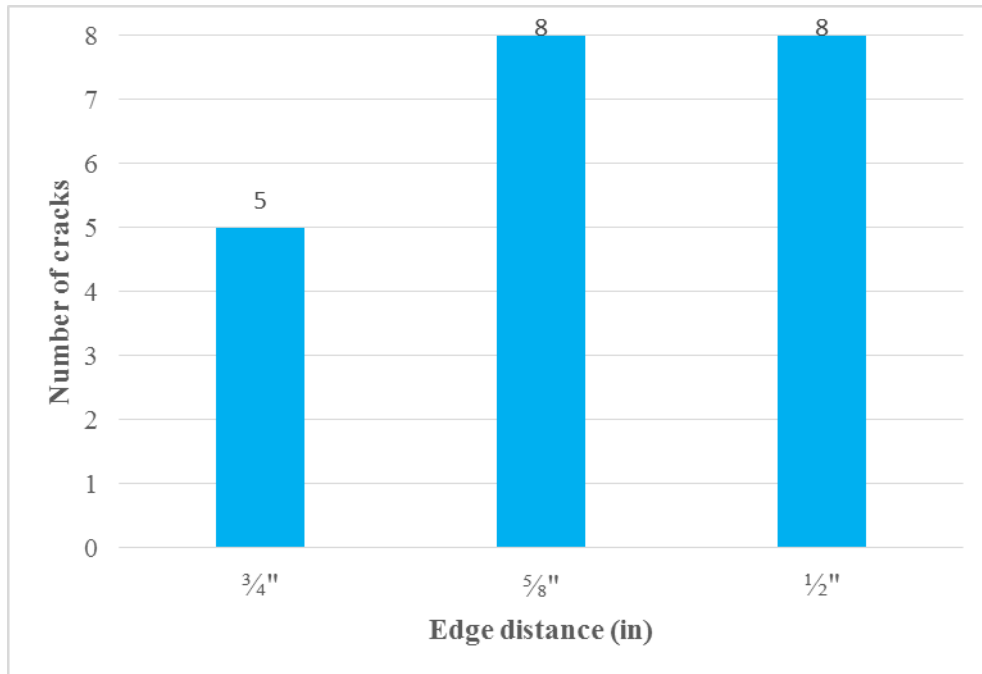


Figure 10-46: Mix#1, 4500 psi, WH-Number of Cracks

Mix#1-WI wire type

WI wire is a chevron type of wire with 0.094 mm (0.0037 in.) average indent depth, and edge wall angle 11.02 degrees. The concrete release strength was 4500 psi and 6000 psi.

WI-Release Strength 4500 psi

The longitudinal strain profile point to that transfer length on the live end of the prism was longer than the transfer length on the dead end due to cracking on the live end of the prism. Spalling was identified on the dead end of the prism with $\frac{5}{8}$ in. edge distance. Figure 10-47 shows the longitudinal strain profile for the prism with $\frac{3}{4}$ in. edge distance along with the values of transfer lengths. The value of the transfer length on the dead end was larger which indicates crack appearance.

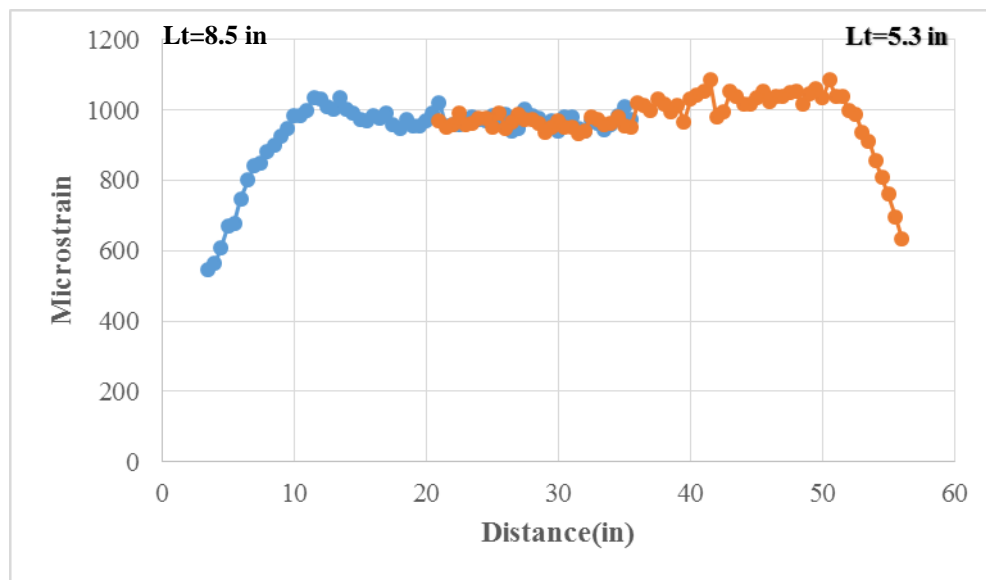


Figure 10-47: Mix#1, 4500 psi, WI, $\frac{3}{4}$ in. Edge Distance-Longitudinal Strain Profile

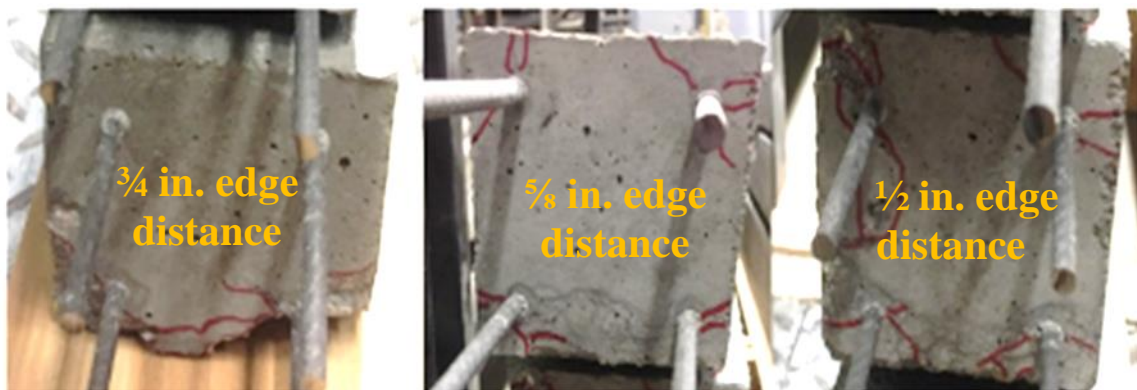


Figure 10-48: Mix#1, 4500 psi, WI-Observed Cracking (Dead End)

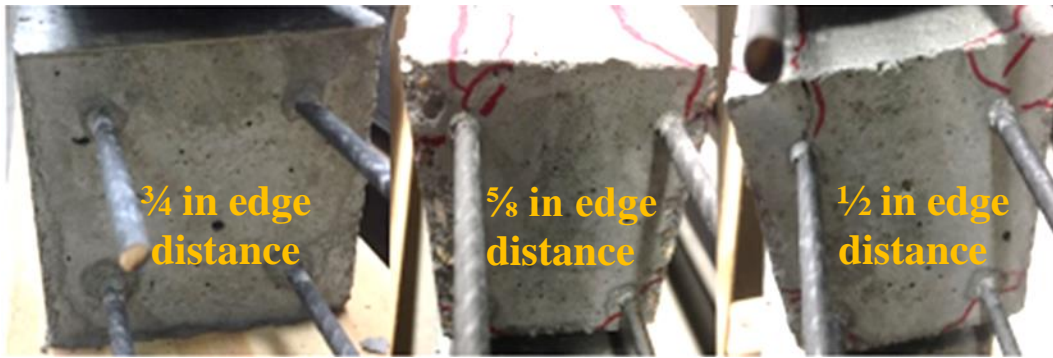


Figure 10-49: Mix#1, 4500 psi, WI-Observed Cracking (Live End)

Figure 10-48 and Figure 10-49 show observed cracking on the both sides of the prisms (Live and Dead end).

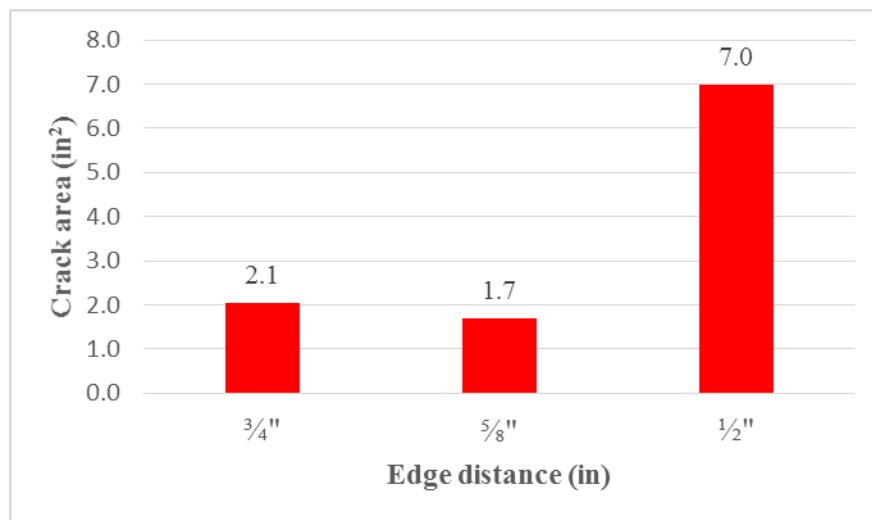


Figure 10-50: Mix#1, 4500 psi, WI-Crack Area (in²)

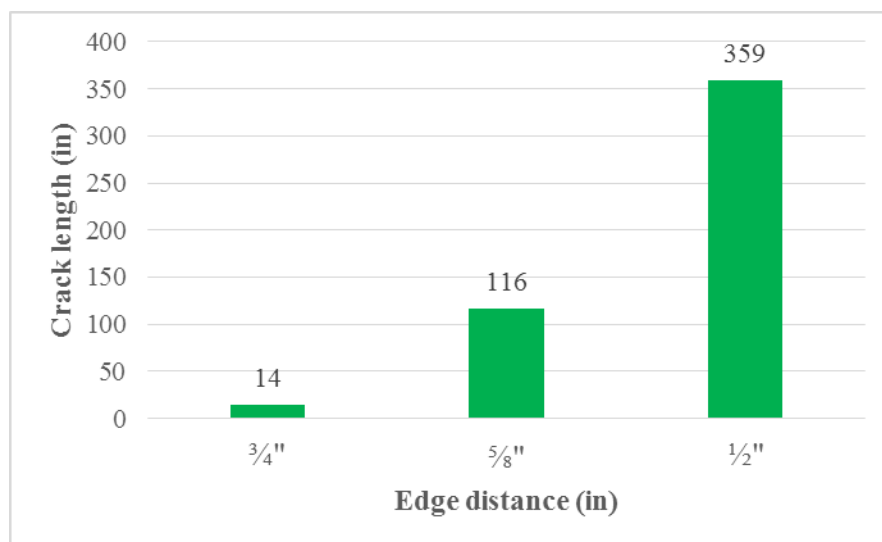


Figure 10-51: Mix#1, 4500 psi, WI-Crack Length (in)

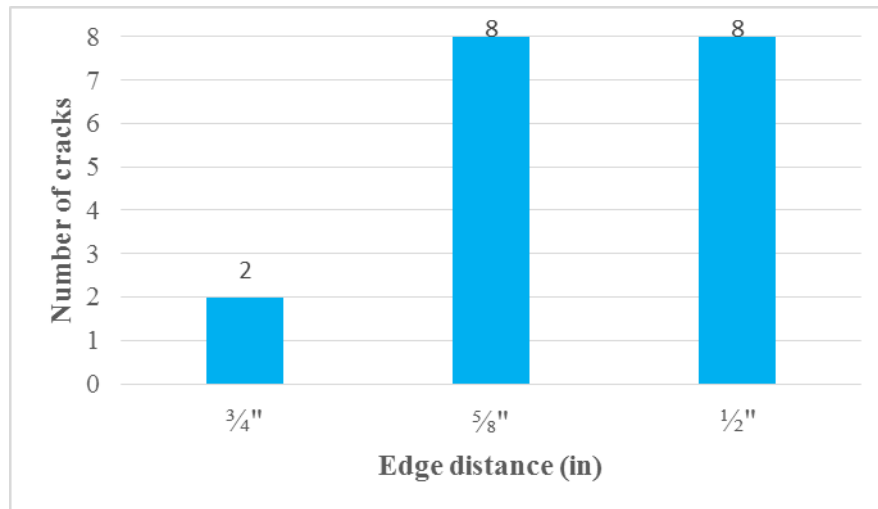


Figure 10-52: Mix#1, 4500 psi, WI-Number of Cracks

The prism with 5/8 in. edge distance had the maximum crack width of 0.02 in. and the maximum crack length of 14 in. The prism with 1/2 in. edge distance had four cracks on each side of the prism with maximum crack width of 0.03 in. and 49 in. crack length. Figure 10-50, Figure 10-51 and Figure 10-52 show crack area, crack lengths and number of cracks as a function of edge distance.

WI-Release Strength 6000 psi

Figure 10-53 shows the longitudinal strain profile and values of the transfer lengths. It was evident that the transfer length on the live end had larger value due to crack which appeared after de-tensioning procedure.

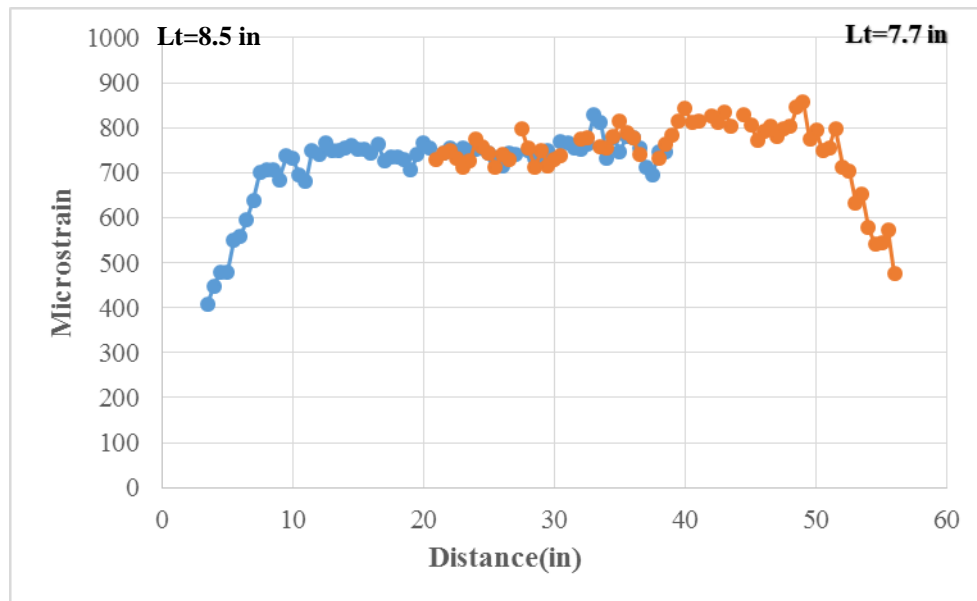


Figure 10-53: Mix#1, 6000 psi, WI, 3/4 in. Edge Distance-Longitudinal Strain Profile

With increasing the release strength to 6000 psi, one crack appeared on the live end of the prism with $\frac{3}{4}$ in edge distance. The crack had width of 0.02 in and crack length of 6 in. The values of crack areas decreased using higher release strength of concrete. However, for a given concrete mixture, higher compressive strength at transfer of prestress correspond to a higher Modulus of Elasticity. The higher Modulus of Elasticity causes increased lateral stresses.

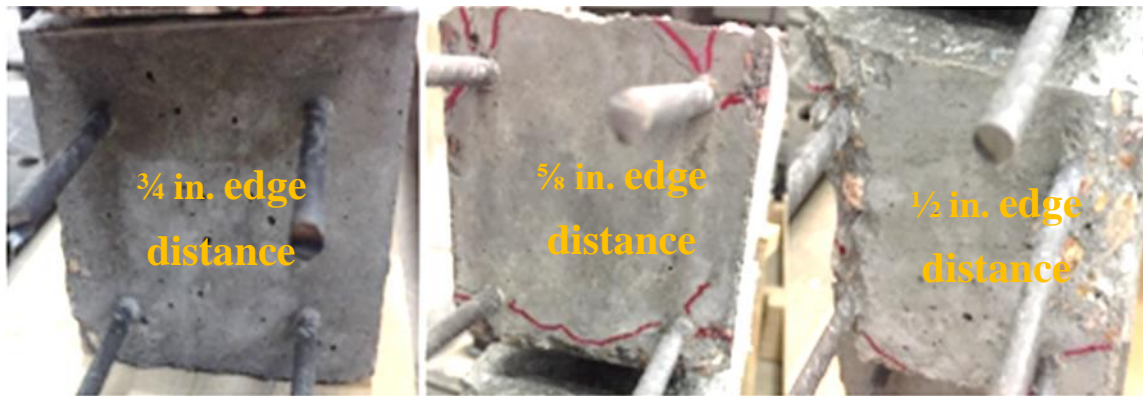


Figure 10-54: Mix#1, 6000 psi, WI-Observed Cracking (Dead end)



Figure 10-55: Mix#1, 6000 psi, WI-Observed Cracking (Live end)

Figure 10-54 and Figure 10-55 illustrate the performance of WI wire with different edge distances. It was visible that with decreasing the edge distance from $\frac{3}{4}$ in. to $\frac{5}{8}$ in. to $\frac{1}{2}$ in, more cracks started to appear. One crack on the $\frac{3}{4}$ in. edge distance was observed, six on the $\frac{5}{8}$ in. cover and eight cracks on $\frac{1}{2}$ in. thickness of the edge distance. The average crack width for the prism with $\frac{5}{8}$ in. thickness of the edge distance was 0.02 in. and the maximum crack length was 18 in.

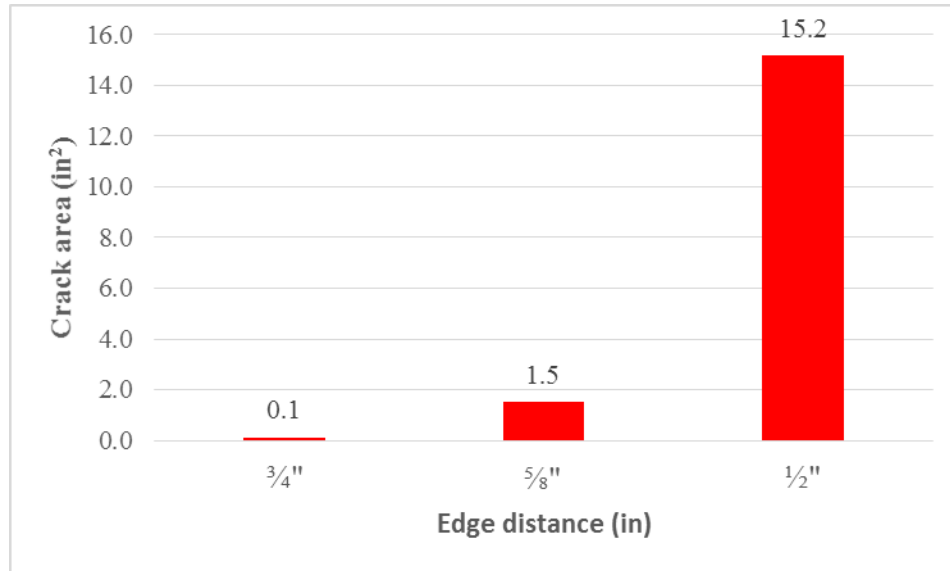


Figure 10-56: Mix#1, 6000 psi, WI-Crack Area (in²)

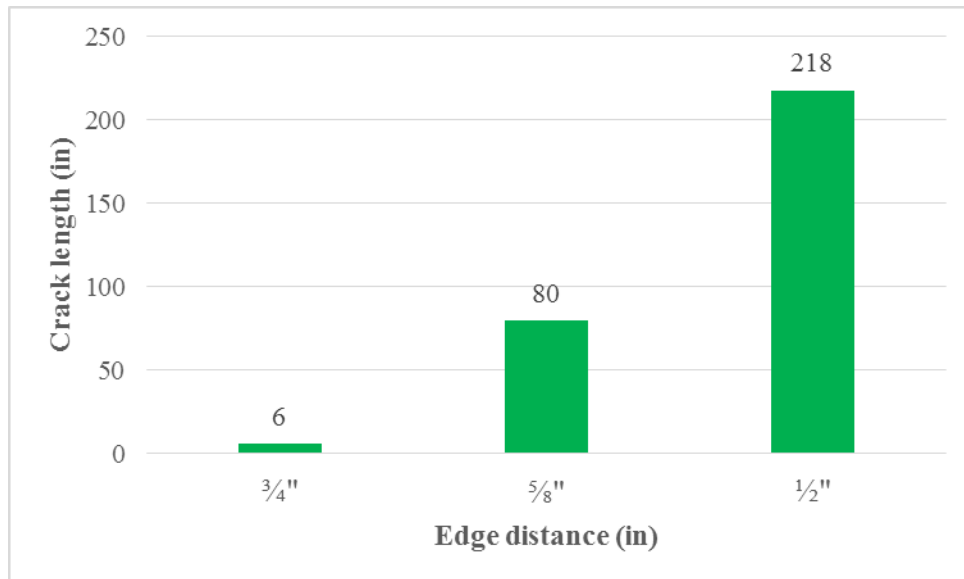


Figure 10-57: Mix#1, 6000 psi, WI-Crack Length (in)

Prism with $\frac{1}{2}$ in. edge distance had four cracks on each side of the prism. Maximum crack length on the live end of the prism was 35 in. and the maximum crack width was 0.02 in. On the dead end of the prism, maximum crack width was 0.04 in. and maximum crack length was 24 in. Figure 10-56, Figure 10-57, and Figure 10-58 show crack area, crack lengths and number of cracks, respectively. WI wire chevron type with original test and prisms having 1 in. edge distance (Bodapati 2018) performed very well, with decreasing the cover to $\frac{3}{4}$ in. one crack was observed and spalling on the prism with $\frac{5}{8}$ in. edge distance.

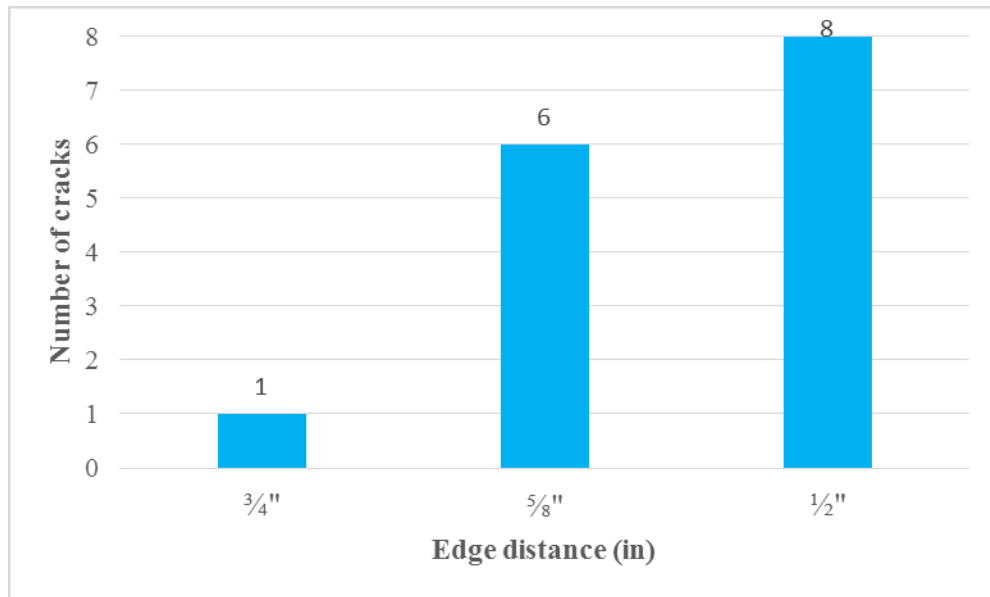


Figure 10-58: Mix#1, 6000 psi, WI-Number of Cracks

Mix#1-WJ wire type

WJ wire is a chevron type of wire with an average indent depth of 0.123 mm (0.00484 in), and edge wall angle 11.52 degrees.

WJ-Release Strength 4500psi

Figure 10-59 shows the longitudinal strain profile along with the values of the transfer lengths for the prism having $\frac{3}{4}$ in. edge distance. Average transfer length for the prism having a $\frac{3}{4}$ in. edge distance was approximately 6 in. There were no visible cracks on the surface on the observed prism.

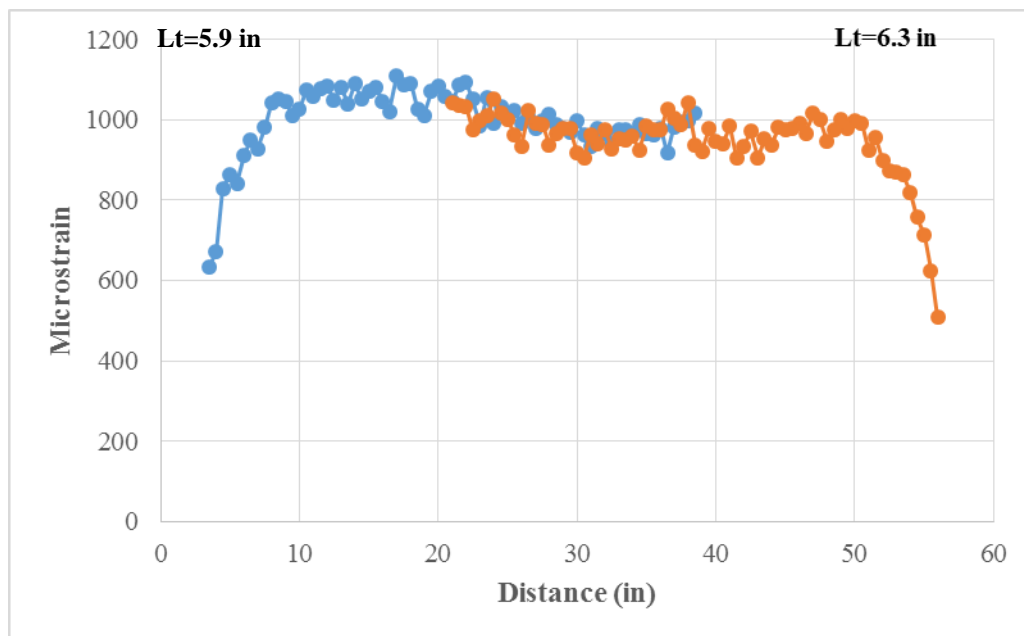


Figure 10-59: Mix#1, 4500 psi, WJ, $\frac{3}{4}$ in. Edge Distance-Longitudinal Strain Profile

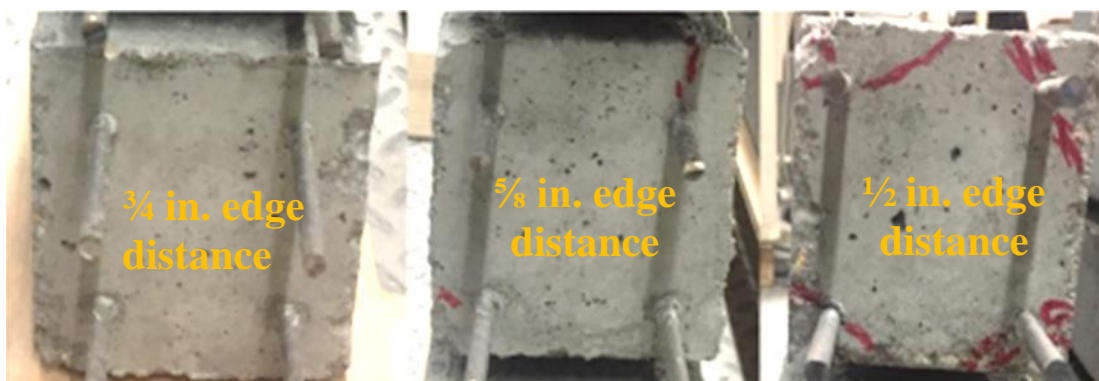


Figure 10-60: Mix#1, 4500psi, WJ-Observed Cracking (Dead End)

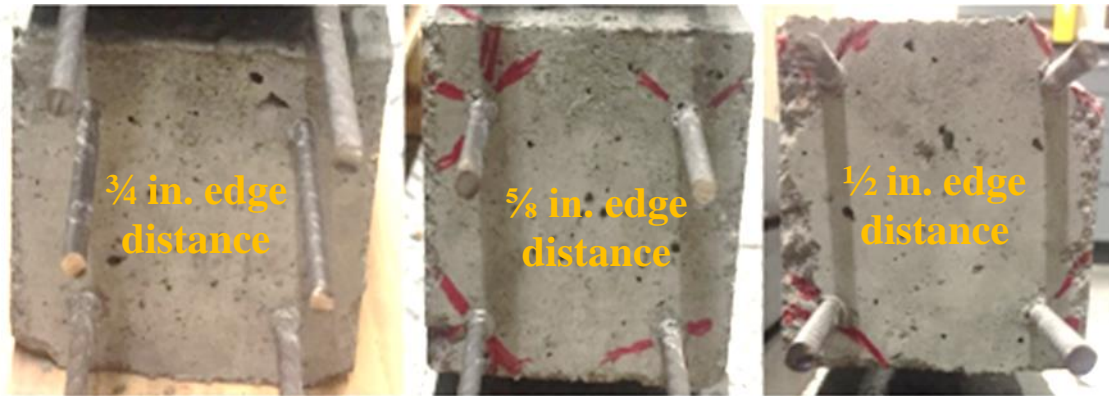


Figure 10-61: Mix#1, 4500psi, WJ-Observed Cracking (Live End)

Figure 10-60 and Figure 10-61 show observed cracking for all three prisms casted in series. Reducing the thickness of the edge distance more cracks appeared.

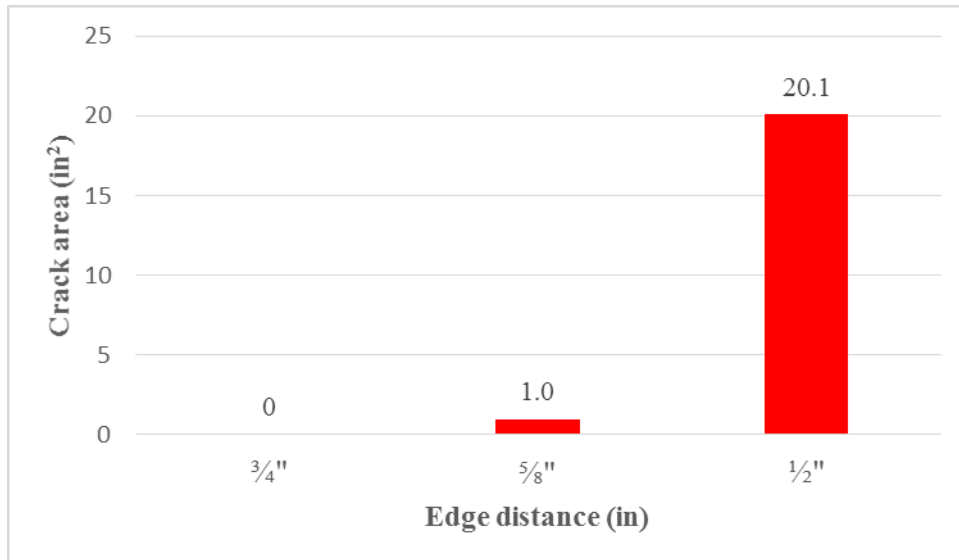


Figure 10-62: Mix#1, 4500 psi, WJ-Crack Area (in²)

Prism with a $\frac{5}{8}$ in. edge distance had two cracks on the dead end with the width of 0.01 in. and crack length of 3 in. On the live end four cracks appeared with a maximum crack width of 0.02 in. and a maximum crack length of 10 in. Spalling was observed on the prism with $\frac{1}{2}$ in. edge distance on the live end with a maximum length of 28 in. Four cracks were indicated on the dead end of the prism with a maximum crack width of 0.04 in. and a maximum crack length of 31 in.

Figure 10-62, Figure 10-63, and Figure 10-64 show crack area, crack length and number of cracks as a function of edge distance, respectively.

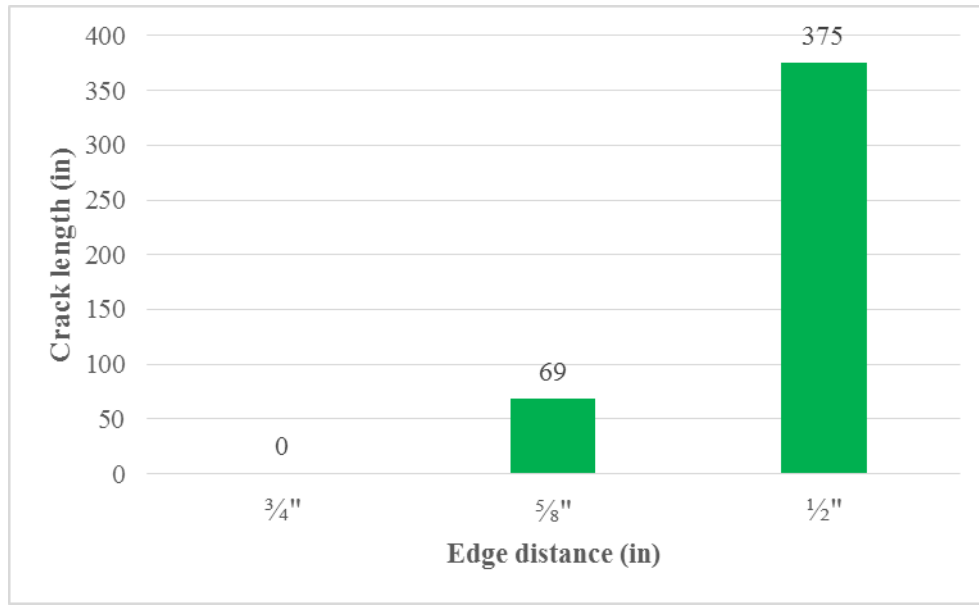


Figure 10-63: Mix#1, 4500 psi, WJ-Crack Length (in)

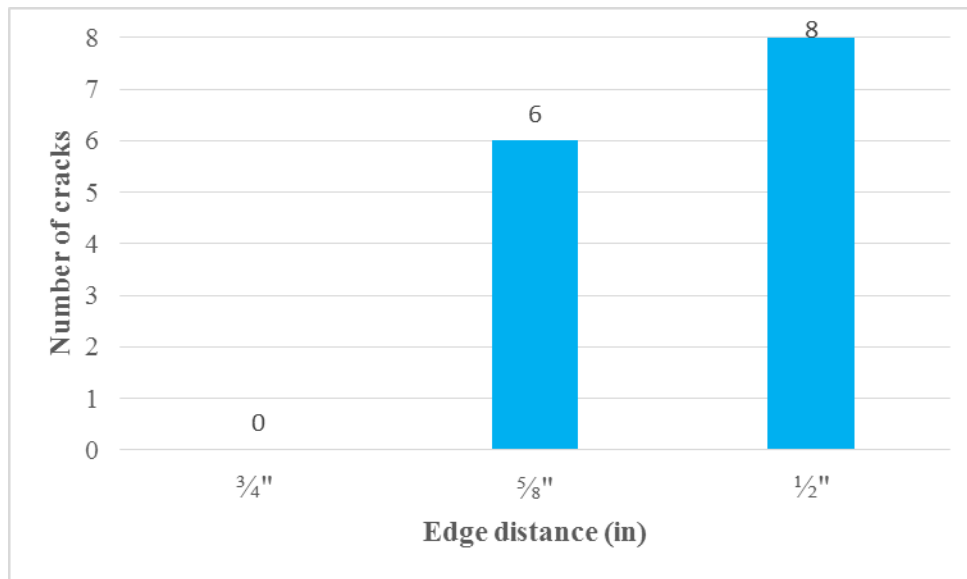


Figure 10-64: Mix#1, 4500 psi, WJ-Number of Cracks

WJ-Release Strength 6000 psi

With increase in the release strength to 6000 psi, the values of transfer lengths were 8.30 in. on the dead end and 5.30 in. on the live end respectively as shown in Figure 10-65. There were no visible cracks on the prism with $\frac{3}{4}$ in. edge distance.

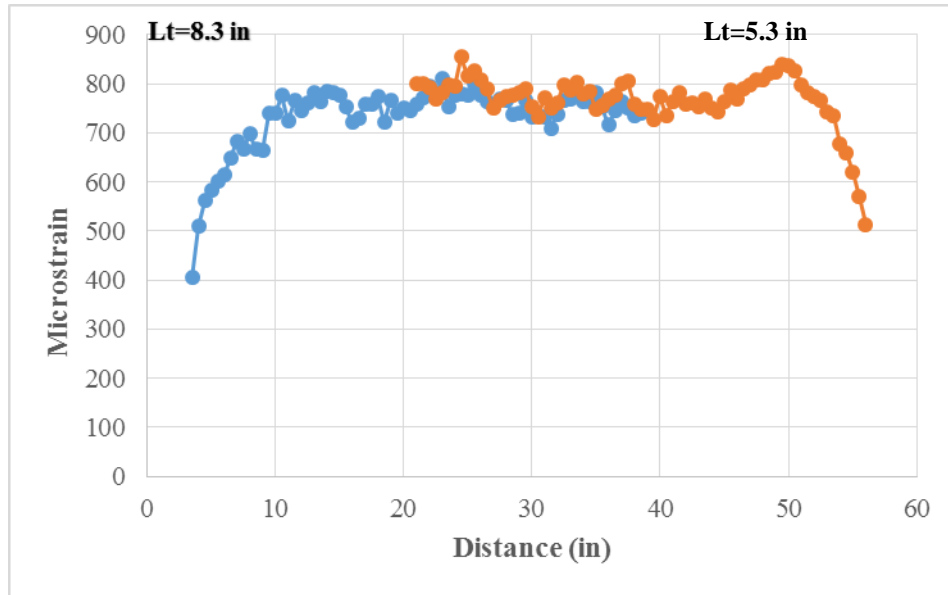


Figure 10-65: Mix#1, 6000 psi, WJ, $\frac{3}{4}$ in. Edge Distance-Longitudinal Strain Profile

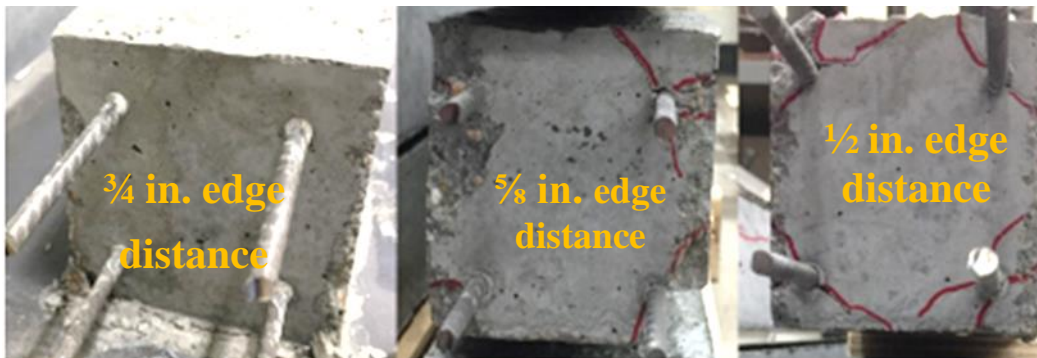


Figure 10-66: Mix#1, 6000 psi, WJ-Observed Cracking (Dead end)

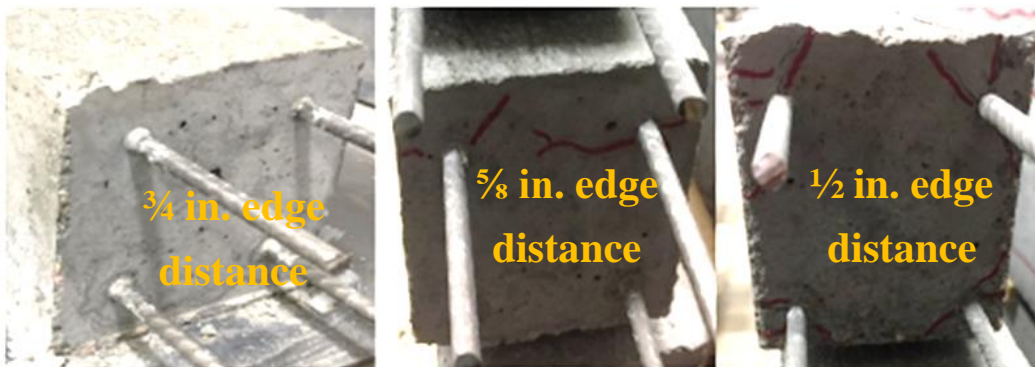


Figure 10-67: Mix#1, 6000 psi, WJ-Observed Cracking (Live end)

Reducing the value of edge distance from $\frac{3}{4}$ in. to $\frac{5}{8}$ in. to $\frac{1}{2}$ in, more cracks appeared. Prism with a $\frac{3}{4}$ in. edge distance had no cracks, $\frac{5}{8}$ in. cover prism had five cracks and $\frac{1}{2}$ in. cover prism had eight cracks as shown in Figure 10-66 and Figure 10-67.

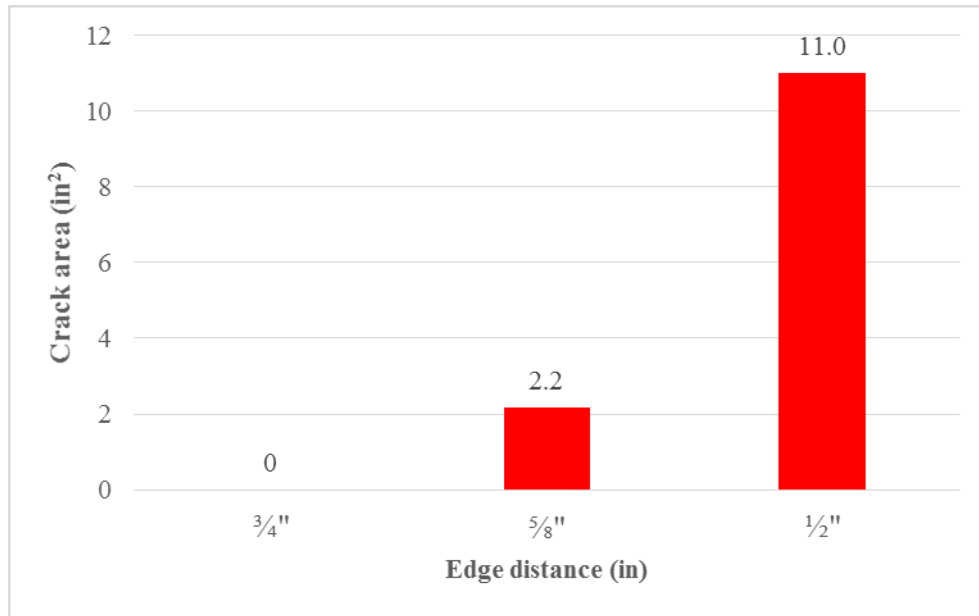


Figure 10-68: Mix#1, 6000 psi, WJ-Crack Area (in²)

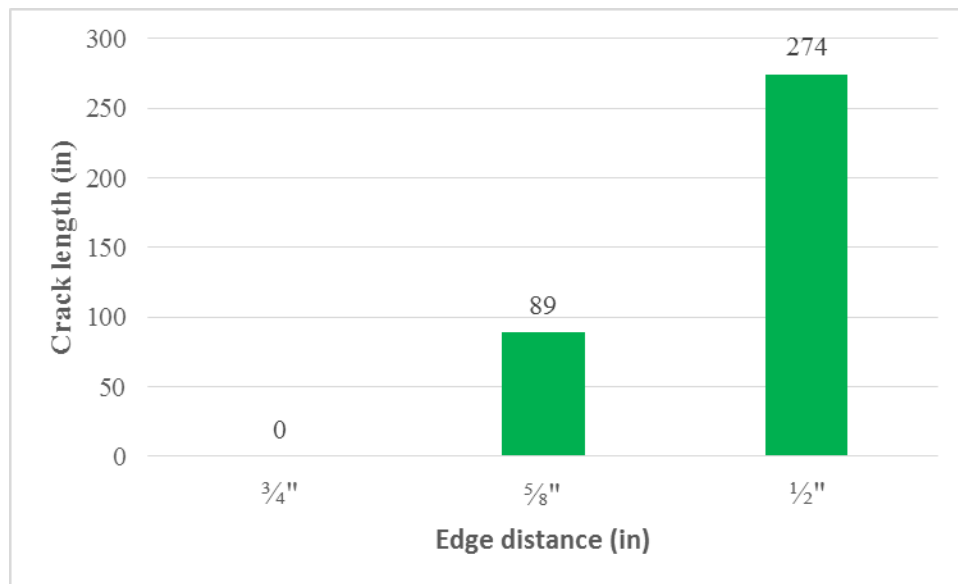


Figure 10-69: Mix#1, 6000 psi, WJ-Crack Length (in)

The second prism in series performed poorly with six cracks. Two cracks appeared on the back and front side of the live end of the prism and four cracks on the dead end of the prism. The maximum crack width on the live end was 0.02 in. and the maximum crack length was 7 in. The maximum crack width on the dead end was 0.03 in. with crack length of 20 in. The third prism had four cracks on each side of the prism with average crack width of 0.03 in. and the maximum crack length of 36 in. Figure 10-68, Figure 10-69, and Figure 10-70 show crack area, crack lengths and number of cracks as a function of edge distance.

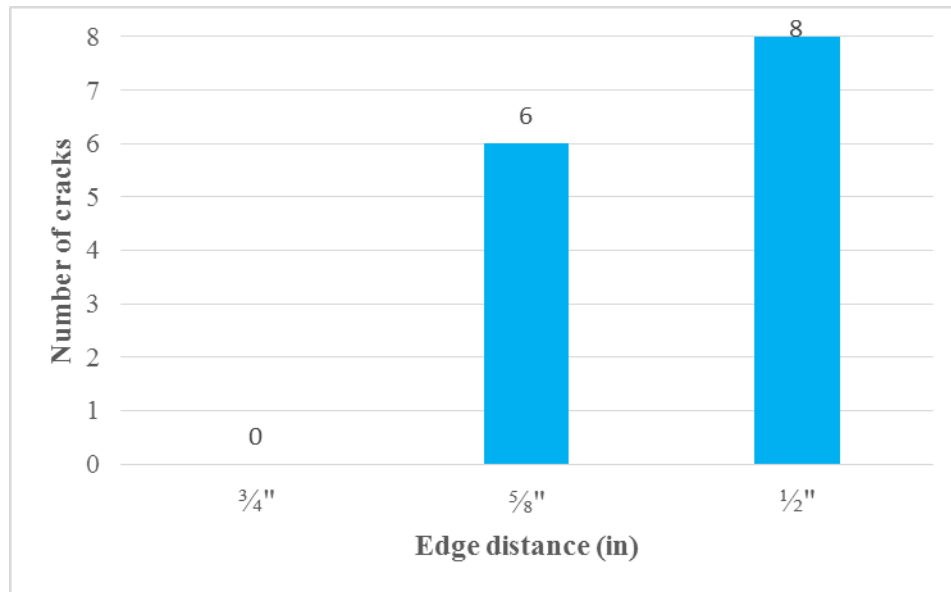


Figure 10-70: Mix#1, 6000 psi, WJ-Number of Cracks

Mix#1-WM wire type

WM wire has an average indent depth of 0.101mm (0.00397 in) and edge wall angle 16.41 degrees. Release strengths of concrete for these prisms were 4500 psi and 6000 psi. The experiments with WM wire showed very well performance at the time when de-tensioning commenced, without cracks on the prism having $\frac{3}{4}$ in. the edge distance and only one crack on the prism having $\frac{5}{8}$ in. the edge distance. The values for longitudinal strain profiles were given after the process of de-tensioning. Due to lateral sustained stresses cracks appeared after three months of de-tensioning procedure, consequently, the values of crack areas and crack lengths increased.

WM-Release Strength 4500 psi

Figure 10-71 shows the longitudinal strain profile for the prism having $\frac{3}{4}$ in. the edge distance along with the values of transfer lengths. The average value of transfer length was approximately 10.5 in.

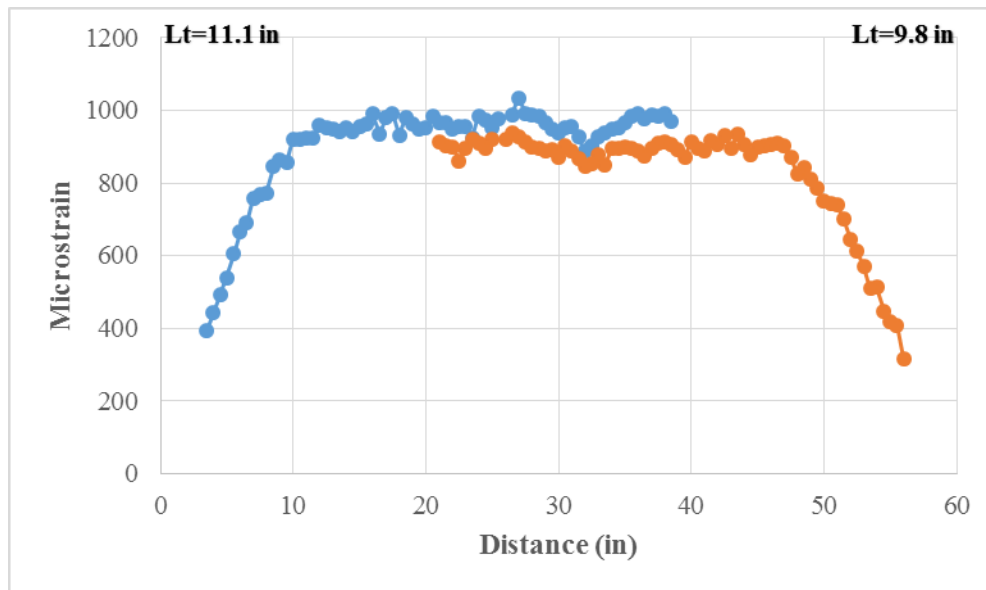


Figure 10-71: Mix#1, 4500 psi, WM, $\frac{3}{4}$ in. Edge Distance-Longitudinal Strain Profile

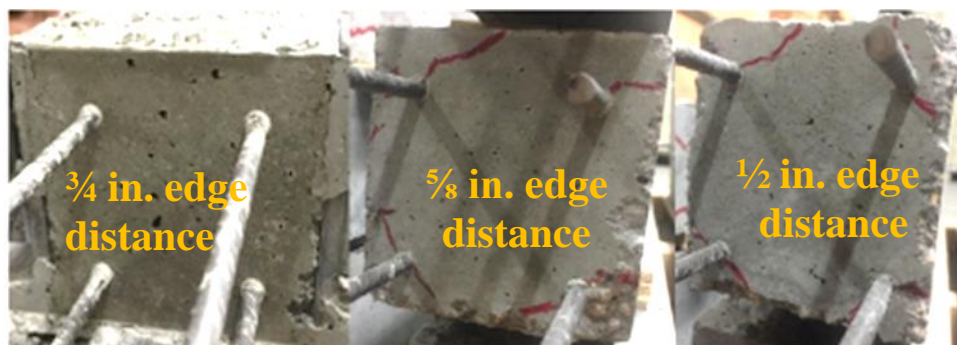


Figure 10-72: Mix#1, 4500psi, WM-Observed Cracking (Dead End)

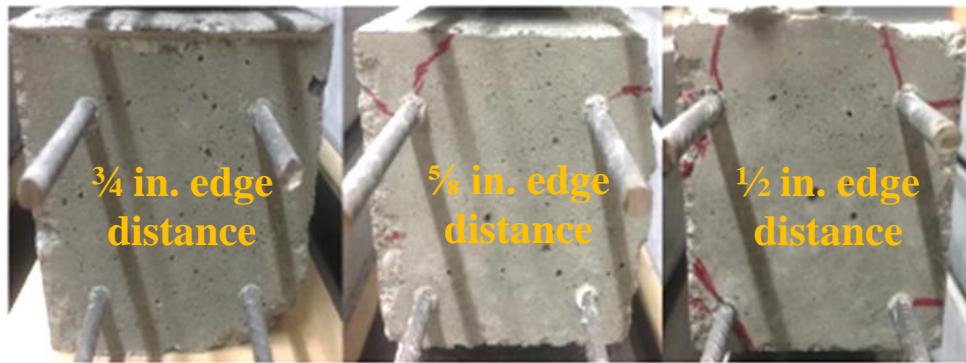


Figure 10-73: Mix#1, 4500 psi, WM-Observed Cracking (Live End)

Figure 10-72 and Figure 10-73 show the performance of WM wire with different values of edge distances. The number of cracks increased with decreasing the edge distance, from zero on the prism with $\frac{3}{4}$ in. thickness of the edge distance to six on the prism with $\frac{5}{8}$ in. thickness of the edge distance and to eight cracks on the prism with $\frac{1}{2}$ in. thickness of the edge distance.

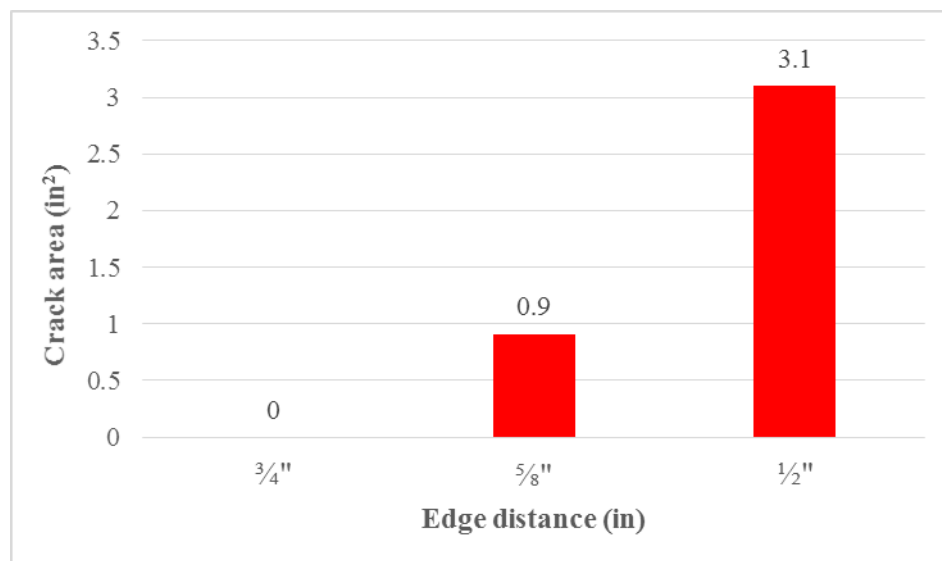


Figure 10-74: Mix#1, 4500 psi, WM-Crack Area (in²)

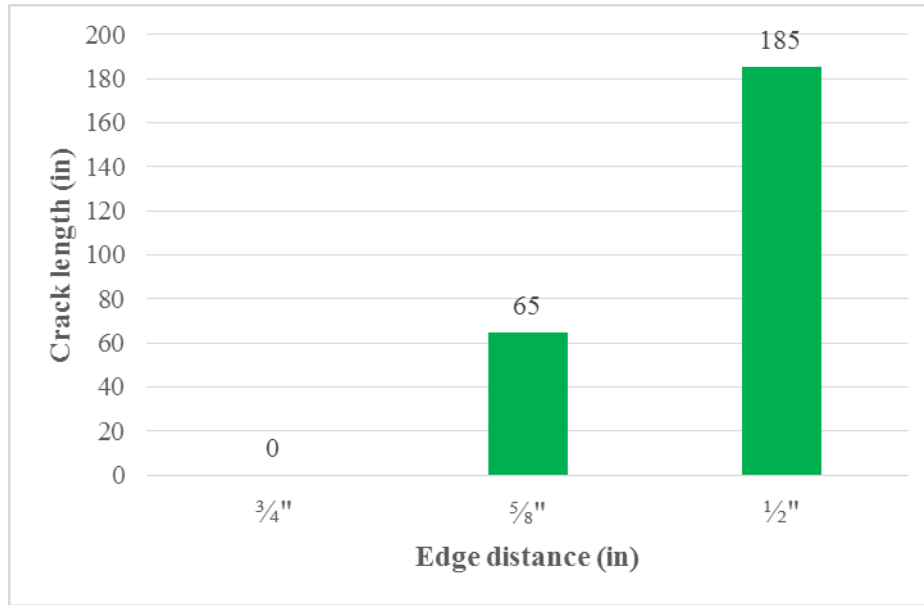


Figure 10-75: Mix#1, 4500 psi, WM-Crack Length (in)

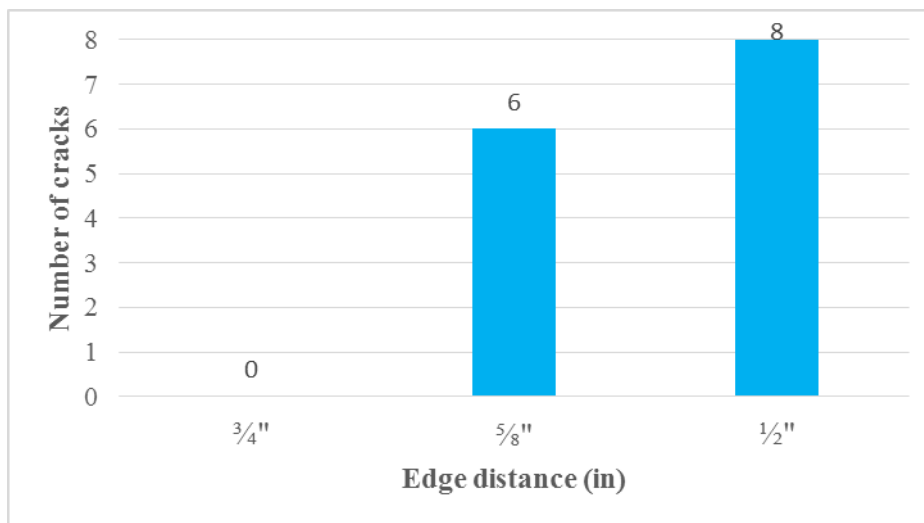


Figure 10-76: Mix#1, 4500 psi, WM-Number of Cracks

Figure 10-74, Figure 10-75, and Figure 10-76 show crack area, crack length and number of cracks as a function of edge distance.

WM-Release Strength 6000 psi

Figure 10-77 shows the longitudinal strain profile for the prism having $\frac{3}{4}$ in. the edge distance along with the values of transfer lengths. After de-tensioning procedure there were no visible cracks on the prism with a $\frac{3}{4}$ in. edge distance, and only three cracks on the prism with $\frac{5}{8}$ in. edge distance. Due to lateral sustained stresses after three month's one crack appeared on the prism with $\frac{3}{4}$ in. the edge distance and five cracks on the prism with $\frac{5}{8}$ in. the edge distance. Figure 10-78 shows longitudinal strain profile along with the values of transfer lengths for the prism having $\frac{5}{8}$ in. edge distance.

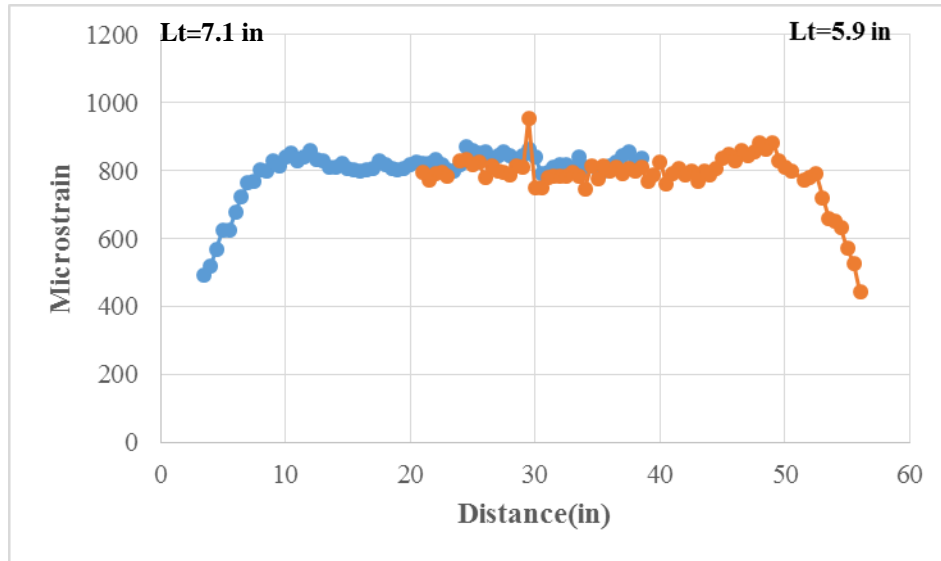


Figure 10-77: Mix#1, 6000 psi, WM, $\frac{3}{4}$ in. Edge Distance-Longitudinal Strain Profile

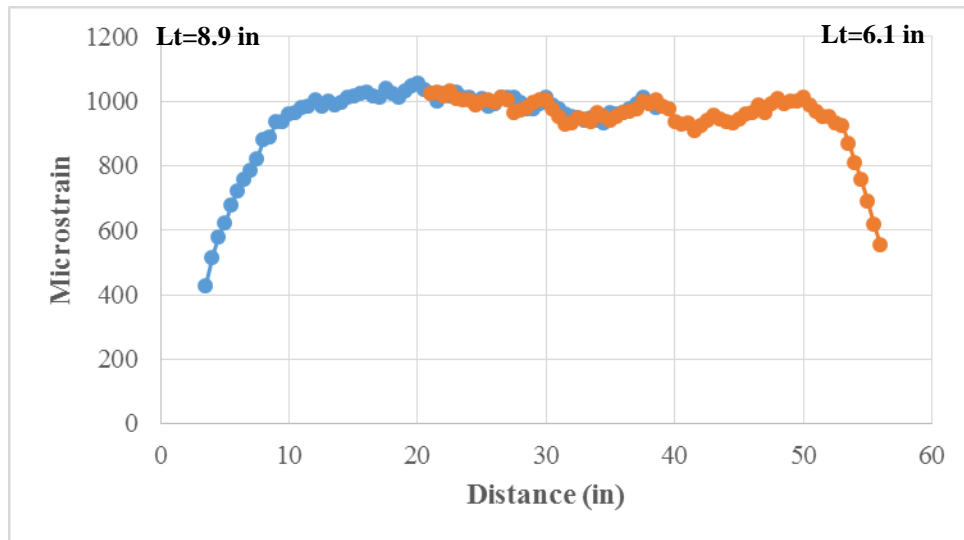


Figure 10-78: Mix#1, 6000 psi, WM, $\frac{5}{8}$ in. Edge Distance-Longitudinal Strain Profile

With increase in the concrete release strength from 4500 psi to 6000 psi it was noticed that prisms with a $\frac{5}{8}$ in. and a $\frac{1}{2}$ in. the edge distances performed better. Prism with a $\frac{3}{4}$ in. edge distance and 4500 psi release strength had improved performance than prism with 6000 psi release strength. When cover was reduced, the number of cracks increased as shown in Figure 10-81, Figure 10-82 and Figure 10-83.



Figure 10-79: Mix#1, 6000 psi, WM-Observed Cracking (Dead End)



Figure 10-80: Mix#1, 6000 psi, WM- Observed Cracking (Live End)

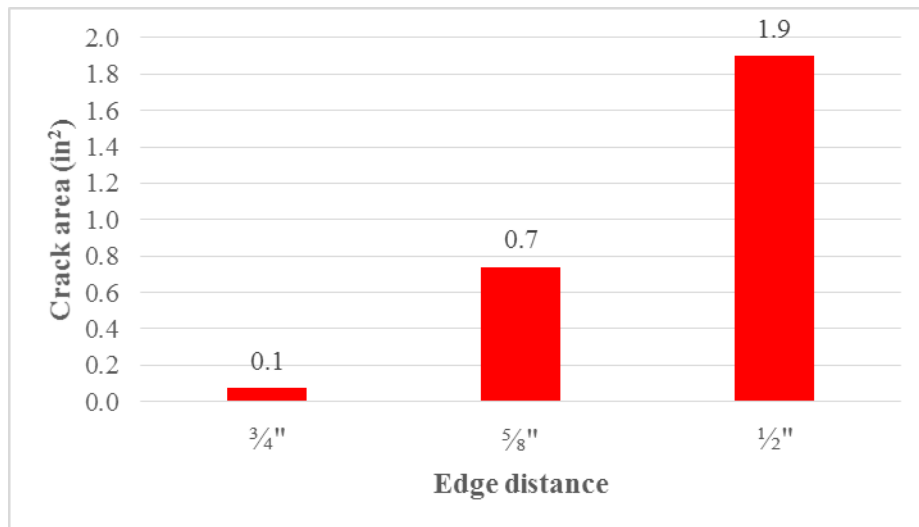


Figure 10-81: Mix#1, 6000 psi, WM-Crack Area (in²)

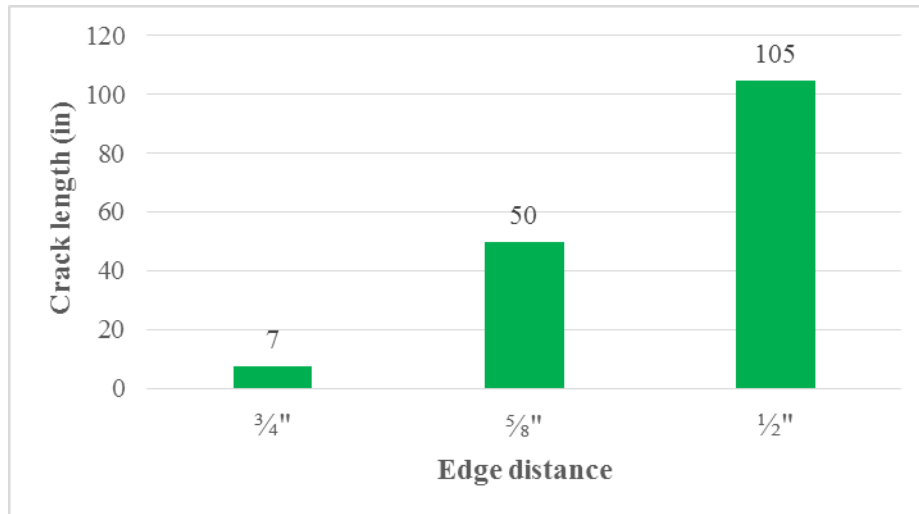


Figure 10-82: Mix#1, 6000 psi, WM-Crack Length (in)

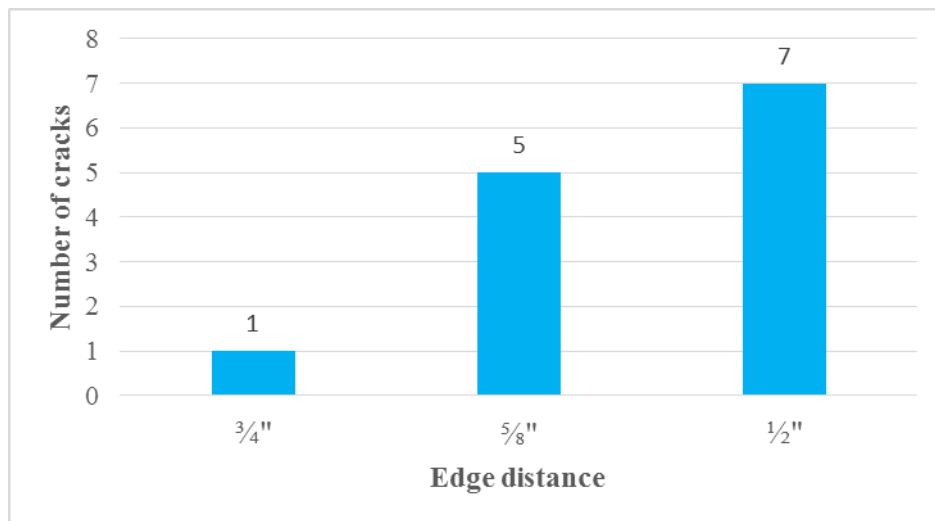


Figure 10-83: Mix#1, 6000 psi, WM-Number of Cracks

Mix#1-WP wire type

WP is a chevron type of wire. Two different concrete release strength 4500 psi and 6000 psi was investigated using this wire type. The average indent depth is 0.117 mm (0.004606 in.) with edge wall angle 29.00 degrees.

WP-Release Strength 4500 psi

Figure 10-84 shows the longitudinal strain profile along with the values of transfer lengths for the prism having a $\frac{3}{4}$ in the edge distance.

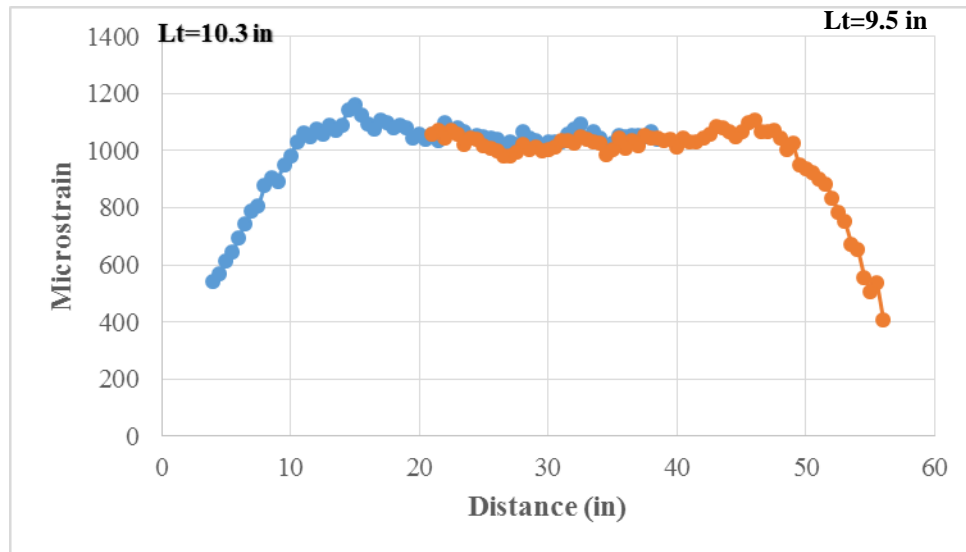


Figure 10-84: Mix#1, 4500 psi, WP, $\frac{3}{4}$ in. Edge Distance-Longitudinal Strain Profile

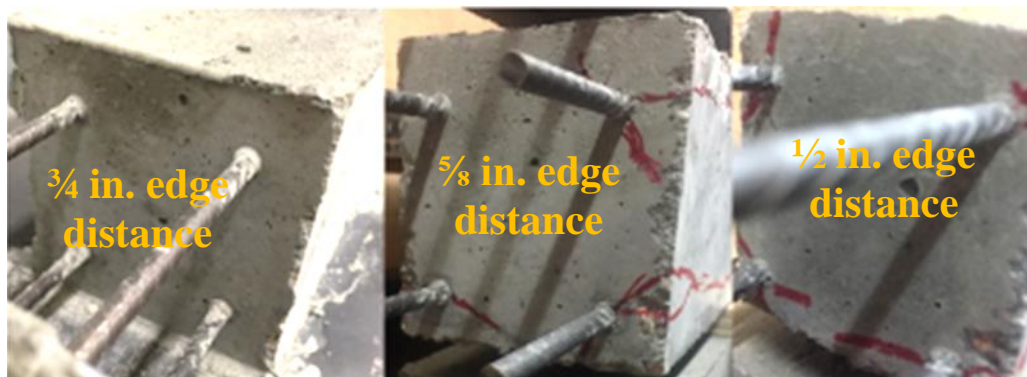


Figure 10-85: Mix#1, 4500 psi, WP-Observed Cracking (Dead End)



Figure 10-86: Mix#1, 4500 psi, WP-Observed Cracking (Live End)

Figure 10-85 and Figure 10-86 show the appearance of cracking, which increased with decreasing the value of the edge distance. The total crack area for the prism having $\frac{3}{4}$ in. the edge distance was 0.1 in^2 and with reducing the cover to $\frac{5}{8}$ in. the value of crack area increased to 1.4 in^2 as shown in Figure 10-87.

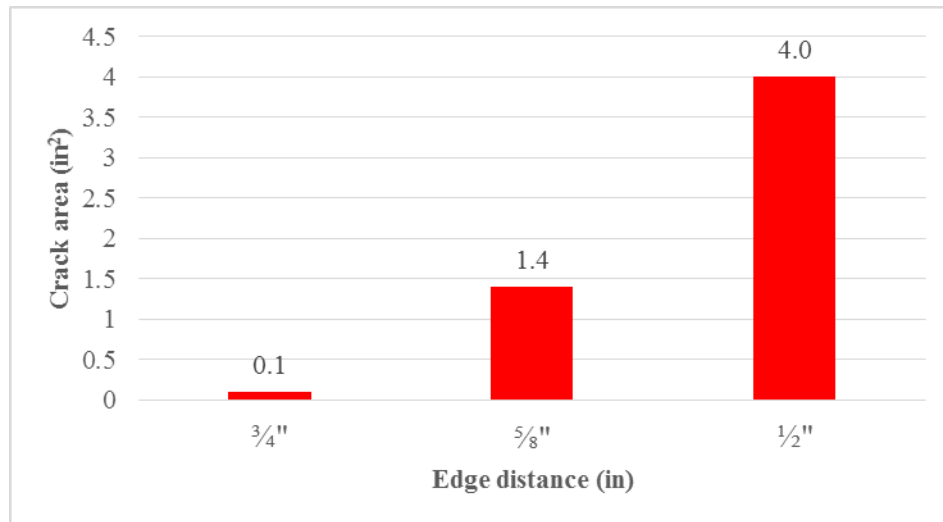


Figure 10-87: Mix#1, 4500 psi, WP-Crack Area (in²)

Prism with a $\frac{1}{2}$ in edge distance had the largest value of crack area. The value of crack area was 4.0 in^2 . When the thickness of the edge distance was reduced, the values of crack length increased on the both prisms with thicknesses of $\frac{5}{8}$ in. and $\frac{1}{2}$ in. edge distance as shown in Figure 10-88. Figure 10-89 shows the number of cracks as a function of edge distance.

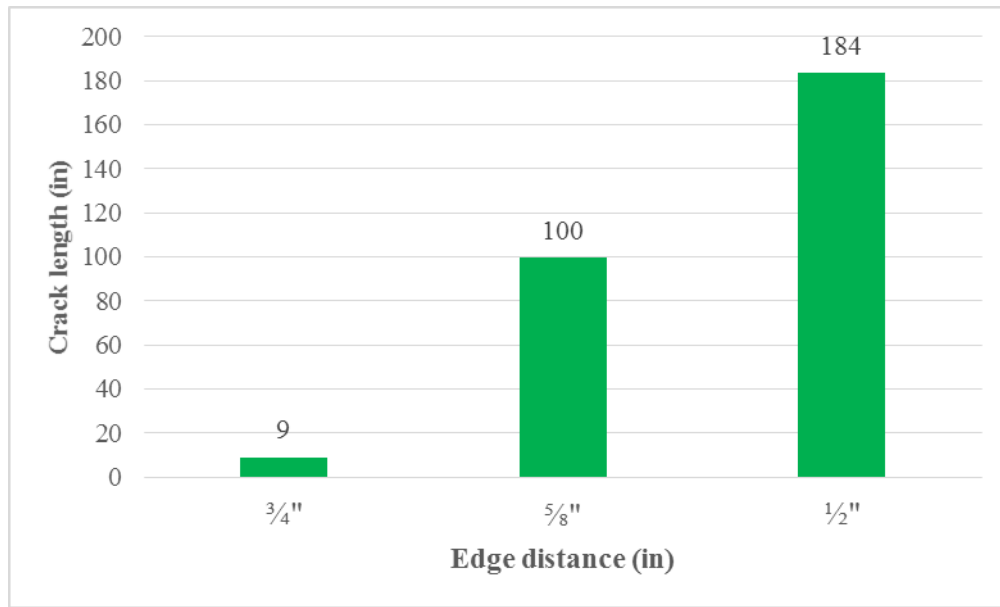


Figure 10-88: Mix#1, 4500 psi, WP-Crack Length (in.)

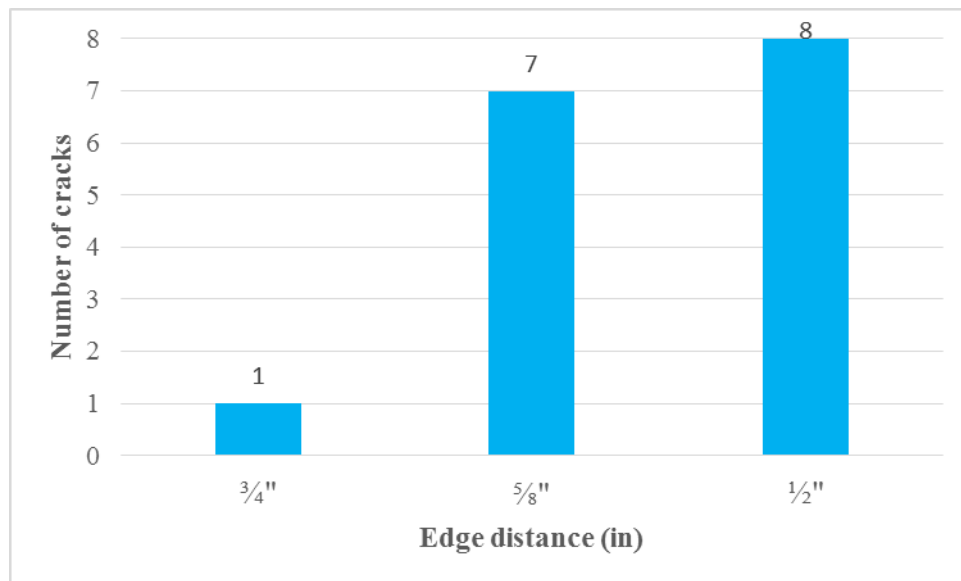


Figure 10-89: Mix#1, 4500 psi, WP-Number of Cracks

WP-Release Strength 6000 psi

With increasing the concrete release strength from 4500 psi to 6000 psi, the values of transfer lengths on both ends of the prism having $\frac{3}{4}$ in. edge distance decreased. Figure 10-90 shows the longitudinal strain profile for the prism having a $\frac{3}{4}$ in. the edge distance along with the values of transfer lengths. Figure 10-91 and Figure 10-92 show observed cracking on the Dead and Live end of the prism.

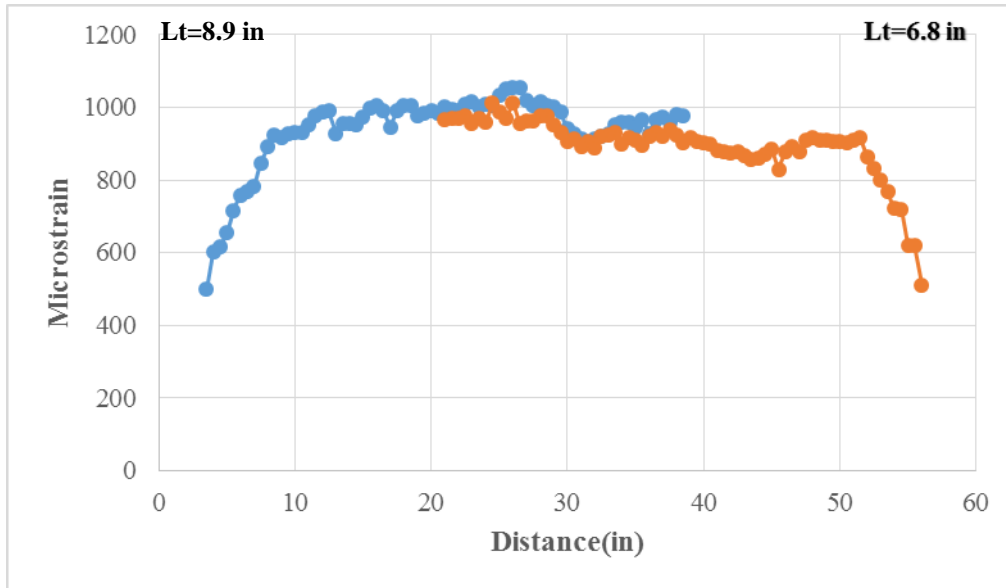


Figure 10-90: Mix#1, 6000 psi, WP, $\frac{3}{4}$ in. Edge Distance-Longitudinal Strain Profile



Figure 10-91: Mix#1, 6000 psi, WP-Observed Cracking (Dead End)

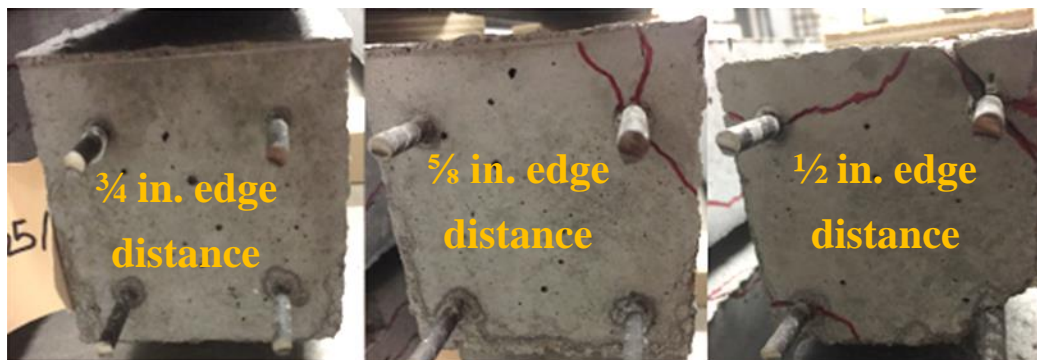


Figure 10-92: Mix#1, 6000 psi, WP-Observed Cracking (Live End)

Prism having a $\frac{1}{2}$ in. the edge distance had four cracks on each side of the prism. The maximum crack width was 0.04 in. with crack length of 22 in. on the dead end, and spalling occurred on the live end of the prism. Prism with a $\frac{5}{8}$ in. edge distance had spalling on the dead end with four cracks and two cracks on the live end of the prism. The maximum crack width on the live end was 0.01 in. and maximum crack length was 5 in.

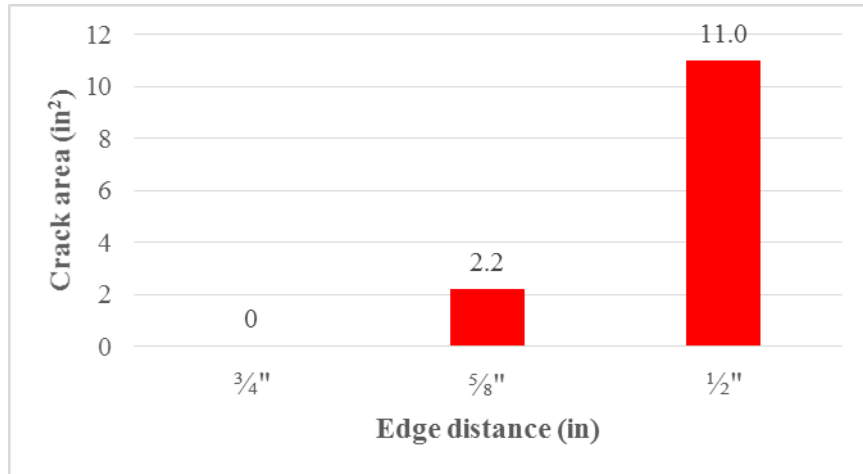


Figure 10-93: Mix#1, 6000 psi, WP-Crack Area (in²)

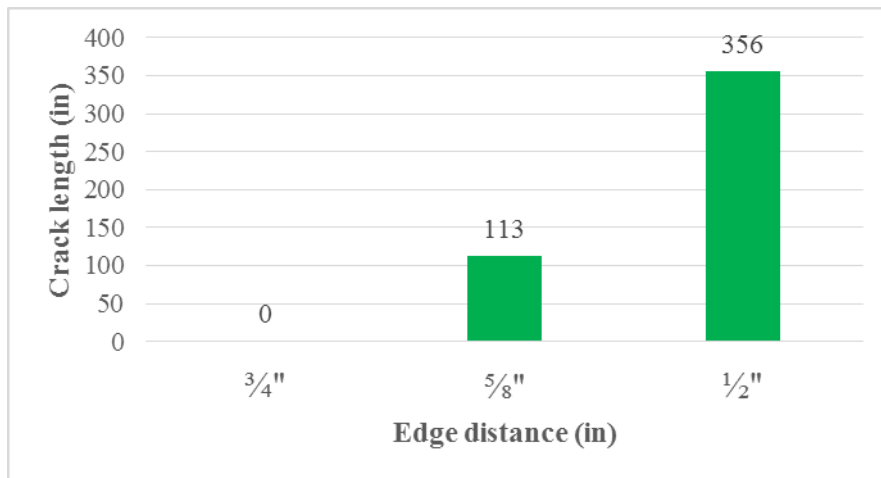


Figure 10-94: Mix#1, 6000 psi, WP-Crack Length (in)

Figure 10-93, Figure 10-94, and Figure 10-95 show crack area, crack lengths and number of cracks as a function of the edge distance.

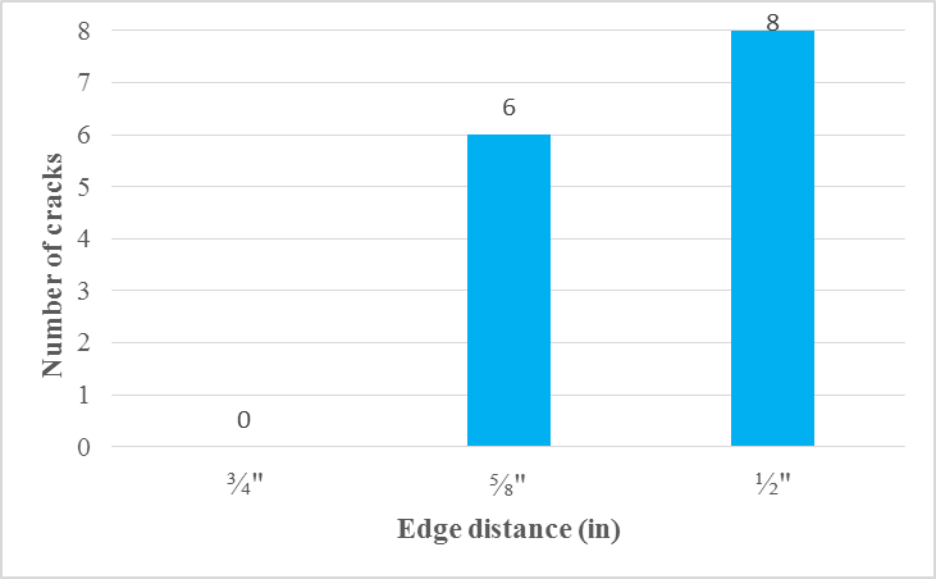


Figure 10-95: Mix#1, 6000 psi, WP-Number of Cracks

Mix#1-WQ wire type

WQ wire belongs to chevron type of wire with 0.067 mm (0.002638 in.) average indent depth and 11.58-degrees edge wall angle.

WQ-Release Strength 4500 psi

The test was conducted with WQ wire which belongs to chevron wire type. Two different release strengths of concrete were investigated 4500 psi and 6000 psi. Figure 10-96 shows the longitudinal strain profiles along with the values of transfer lengths. Prism having a $\frac{3}{4}$ in. the edge distance did not have visible cracks on the surface on both the sides of the prism. Prism having a $\frac{5}{8}$ in. thickness of the edge distance had four cracks on the live end of the prism with the spalling on the bottom, back and front side of the prism as shown in Figure 10-97 and Figure 10-98. On the dead end of the prism, four cracks were observed with the maximum crack width of 0.016 in and the maximum crack length of 5 in. The third prism in series performed poorly with spalling on the dead end, and four cracks on the live end of the prism. The maximum crack width on the live end was 0.02 in. and the maximum crack length was 31 in.

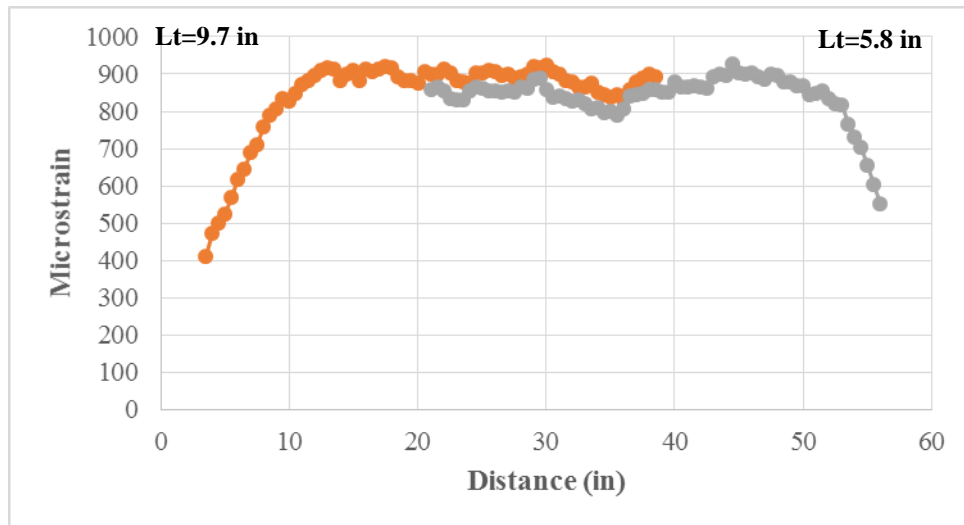


Figure 10-96: Mix#1, 4500 psi, WQ, $\frac{3}{4}$ in. Edge Distance-Longitudinal Strain Profile

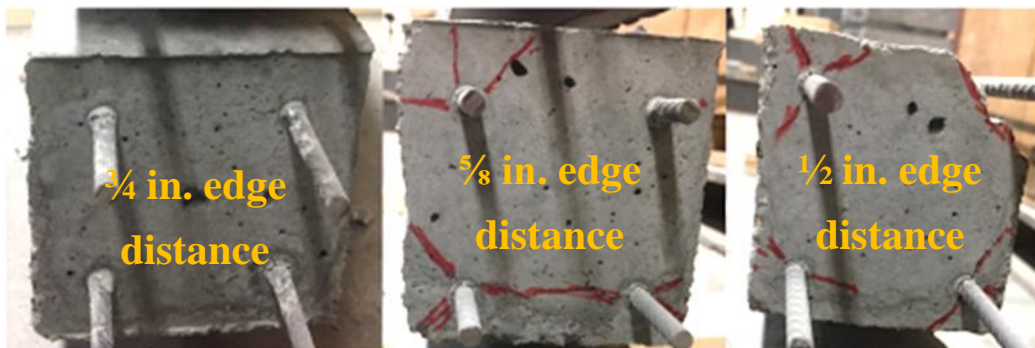


Figure 10-97: Mix#1, 4500 psi, WQ-Observed Cracking (Dead End)

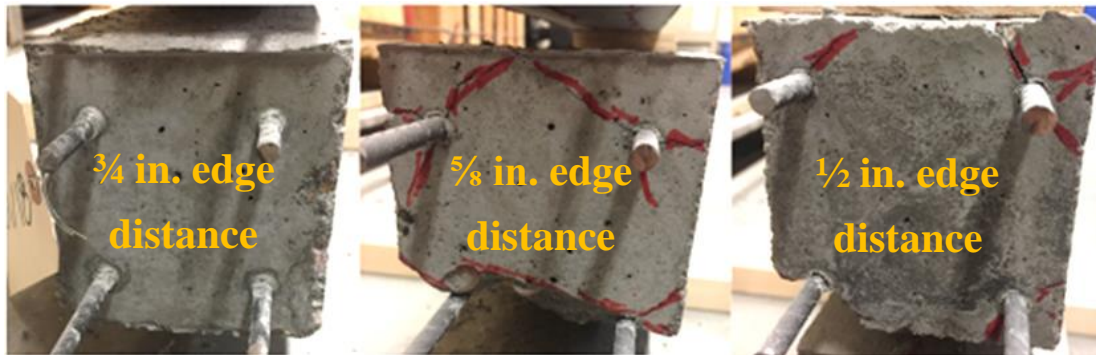


Figure 10-98: Mix#1, 4500 psi, WQ-Observed Cracking (Live End)

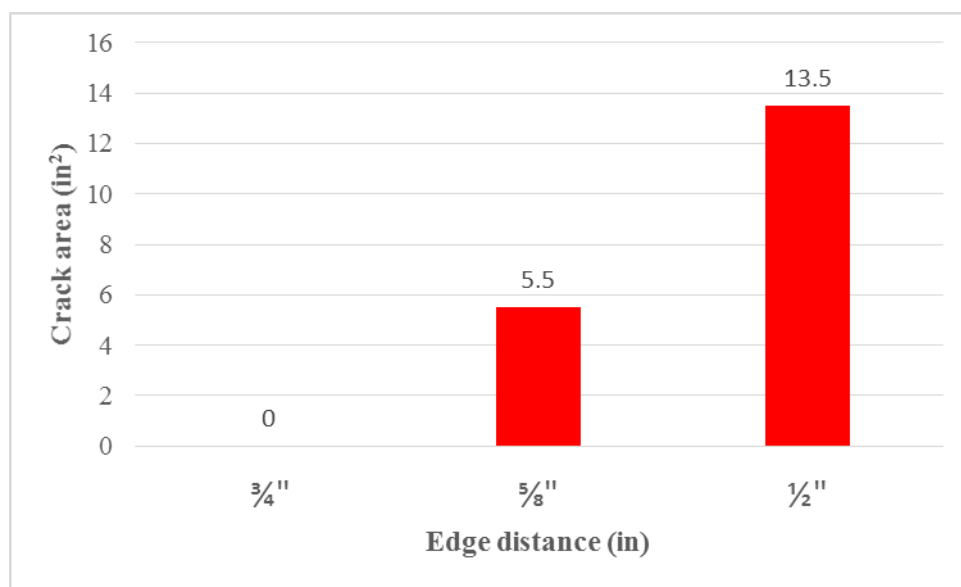


Figure 10-99: Mix#1, 4500 psi, WQ-Crack Area (in²)

According to Figure 10-99, Figure 10-100 and Figure 10-101 the values of crack areas increased with reducing the thickness of the edge distance, from zero for prism with a $\frac{3}{4}$ in. edge distance to 13.5 in² for prism with a $\frac{1}{2}$ in. the edge distance.

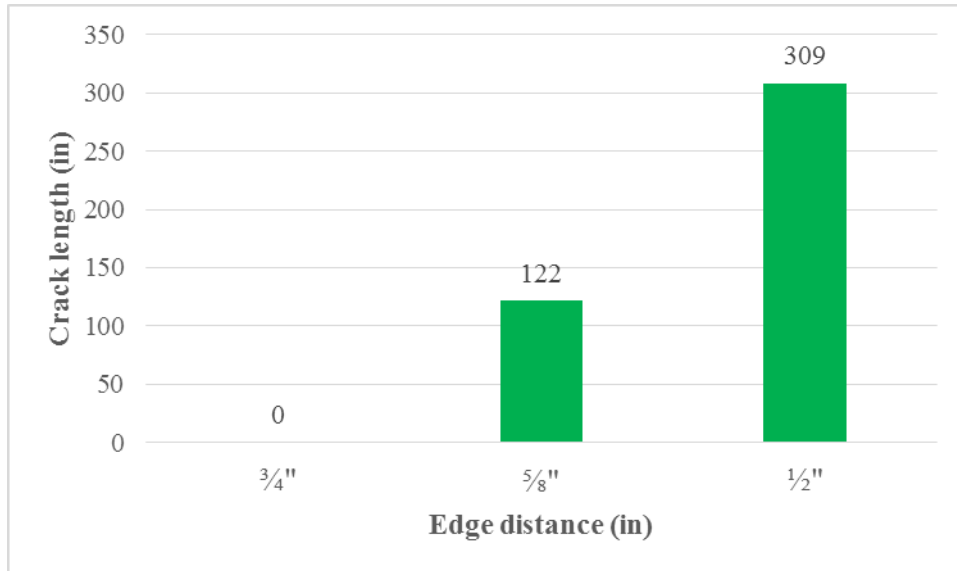


Figure 10-100: Mix#1, 4500 psi, WQ-Crack Length (in)

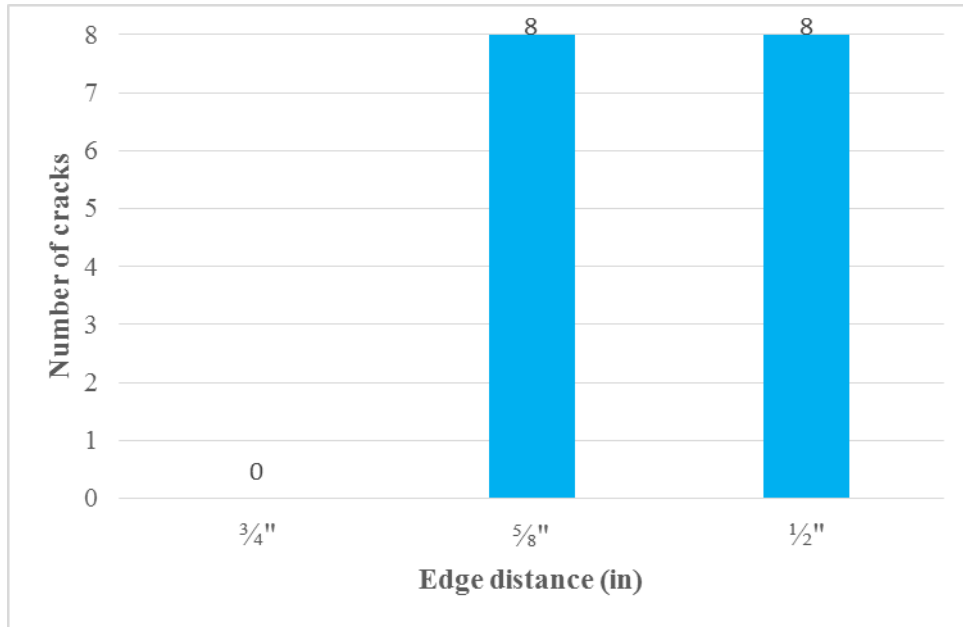


Figure 10-101: Mix#1, 4500 psi, WQ- Number of Cracks

WQ-Release Strength 6000 psi

Figure 10-102 and Figure 10-103 show the longitudinal strain profiles along with the values of transfer lengths. The average value of transfer length for the prism having a $\frac{3}{4}$ in. the edge distance was approximately 7.3 in. and the average value of transfer length for the prism with $\frac{5}{8}$ in. the edge distance was approximately 6.8 in. The longitudinal strain profiles were measured immediately after de-tensioning procedure.

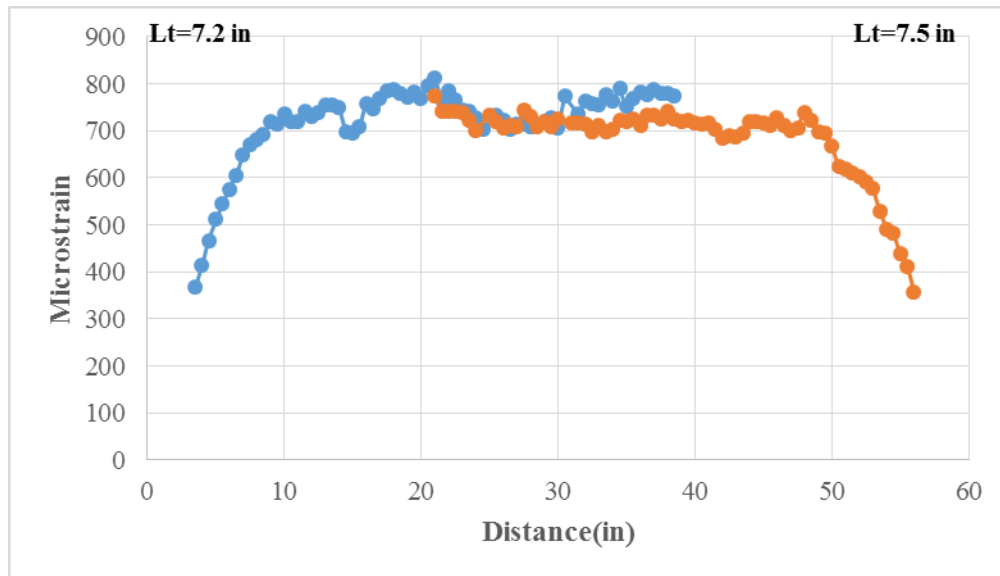


Figure 10-102: Mix#1, 6000 psi, WQ, $\frac{3}{4}$ in. Edge Distance-Longitudinal Strain Profile

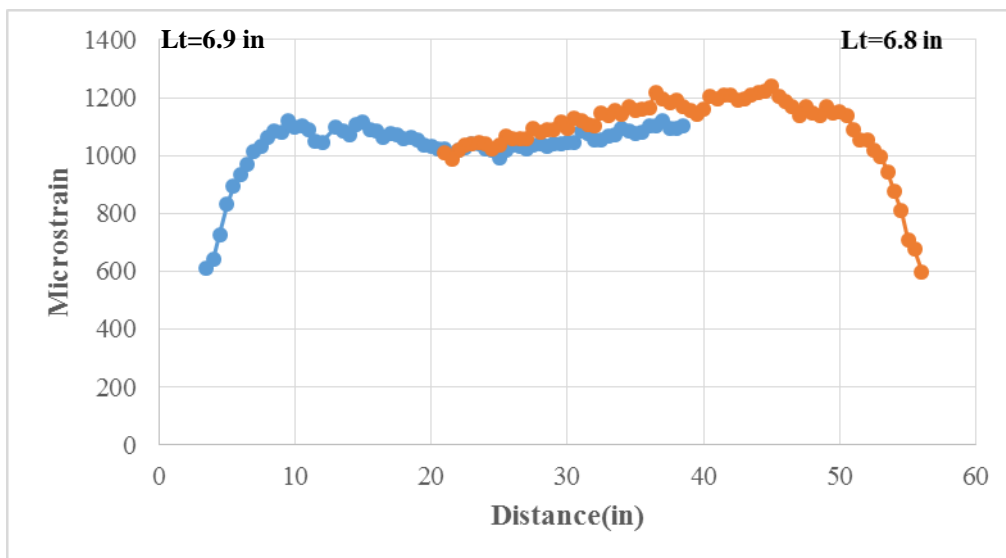


Figure 10-103: Mix#1, 6000 psi, WQ, $\frac{5}{8}$ in. Edge Distance-Longitudinal Strain Profile

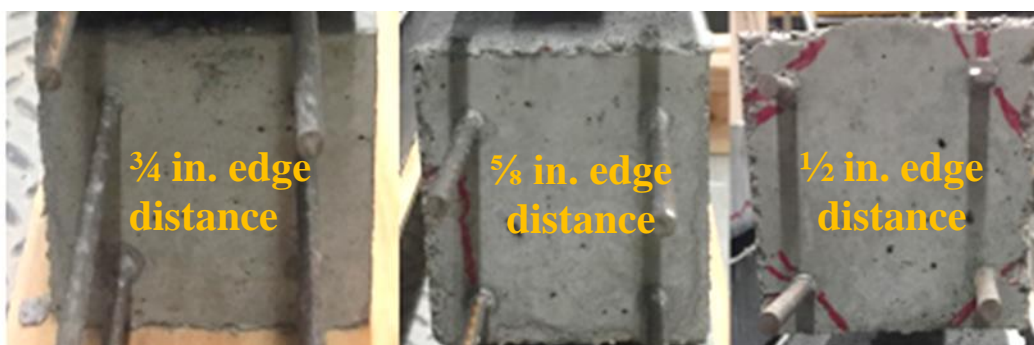


Figure 10-104: Mix#1, 6000 psi, WQ- Observed Cracking (Dead End)

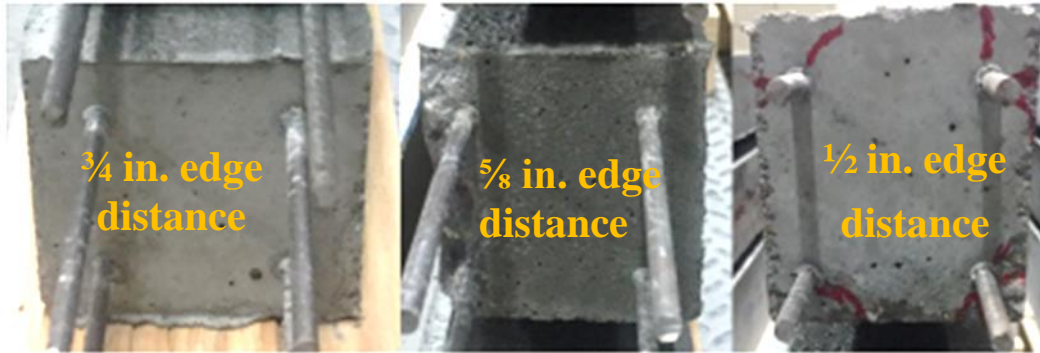


Figure 10-105: Mix#1, 6000 psi, WQ-Observed Cracking (Live End)

The first prism in series did not have any visible cracks on the surface on both the sides of the prism. With reducing the edge distance to a $\frac{5}{8}$ in. only one crack appeared with the width of 0.013 in. and 1 in. crack length. The third prism in series had four cracks on each side of the prism. The maximum crack width on the live end was 0.02 in. and the maximum crack length was 13 in. The maximum crack width on the dead end was 0.03 in. with crack length of 11 in. (Figure 10-104 and Figure 10-105). Figure 10-106, Figure 10-107, and Figure 10-108 show crack area, crack length and number of cracks as a function of edge distance, respectively.

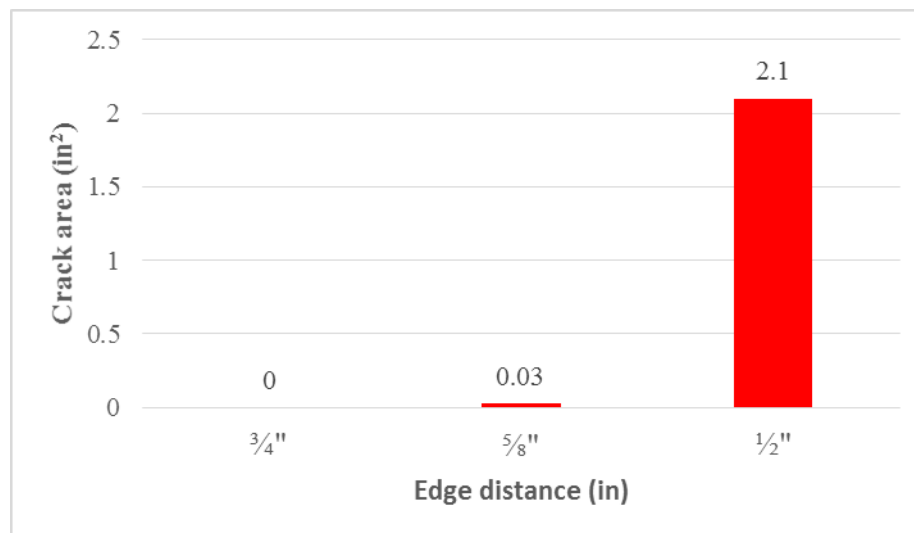


Figure 10-106: Mix#1, 6000 psi, WQ-Crack Area (in²)

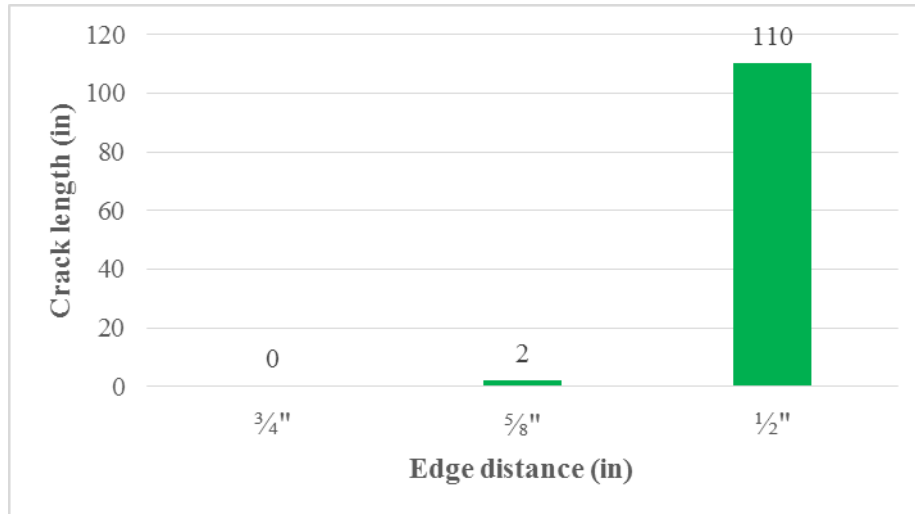


Figure 10-107: Mix#1, 6000 psi, WQ-Crack Length (in)

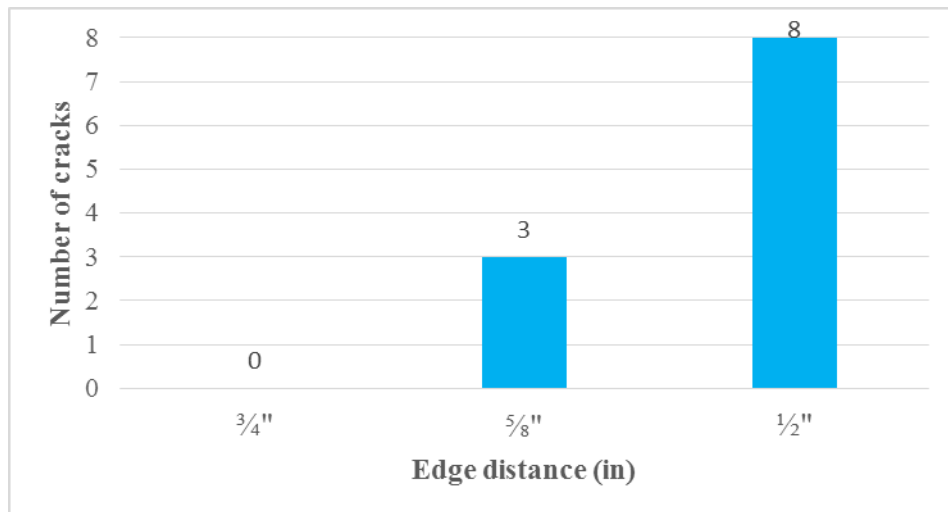


Figure 10-108: Mix#1, 6000 psi, WQ-Number of Cracks

Mix#2-WB wire type

WB-Release Strength 4500 psi

Figure 10-109 shows longitudinal strain profile for the prism with a $\frac{3}{4}$ in. edge distance. The values for transfer lengths are tremendous. This result from the large magnitudes of longitudinal surface strain that go along with longitudinal splitting of the prism. The values of transfer lengths indicate that wire type WB exhibits poor performance, resulting in the maximum number of eight cracks on each prism as shown in Figure 10-114.

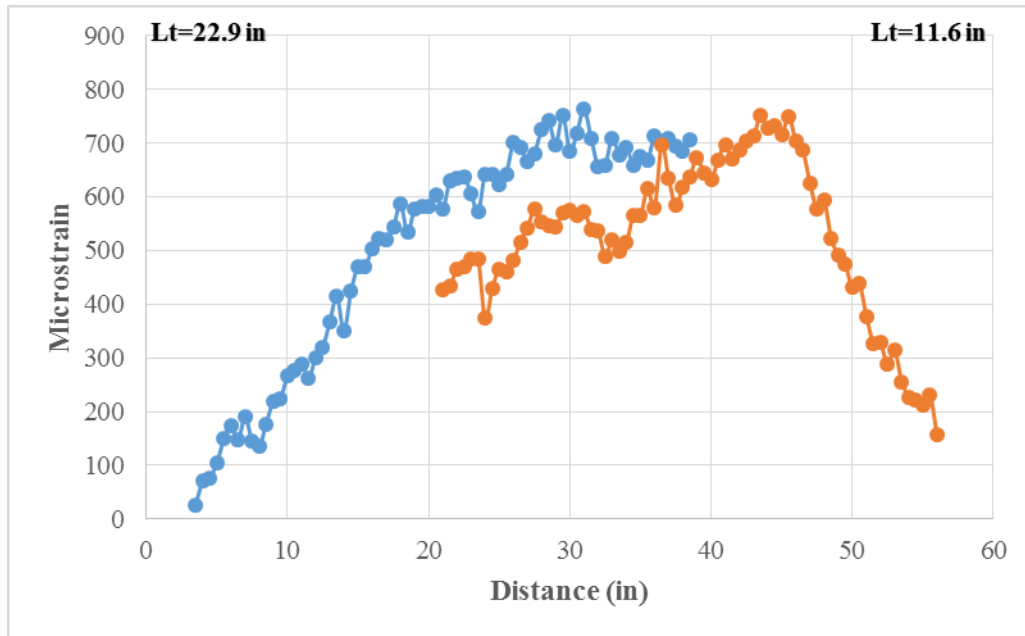


Figure 10-109: Mix#2, 4500 psi, WB, $\frac{3}{4}$ in. Edge Distance-Longitudinal Strain Profile



Figure 10-110: Mix#2, 4500psi, WB-Observed Cracking (Dead End)

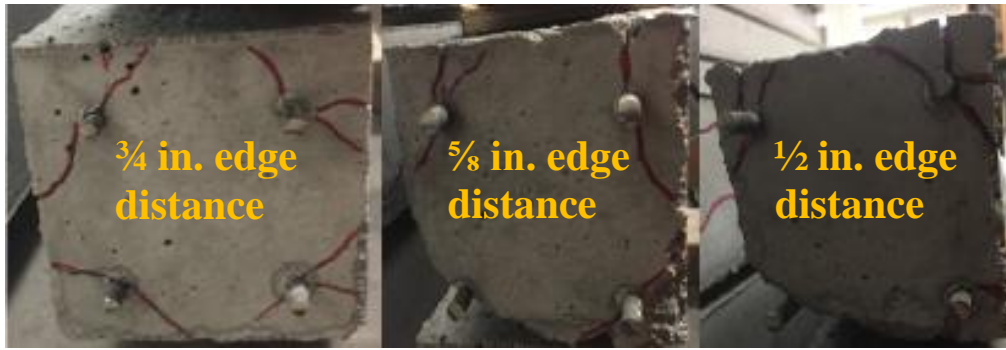


Figure 10-111: Mix#2, 4500 psi, WB-Observed Cracking (Live End)

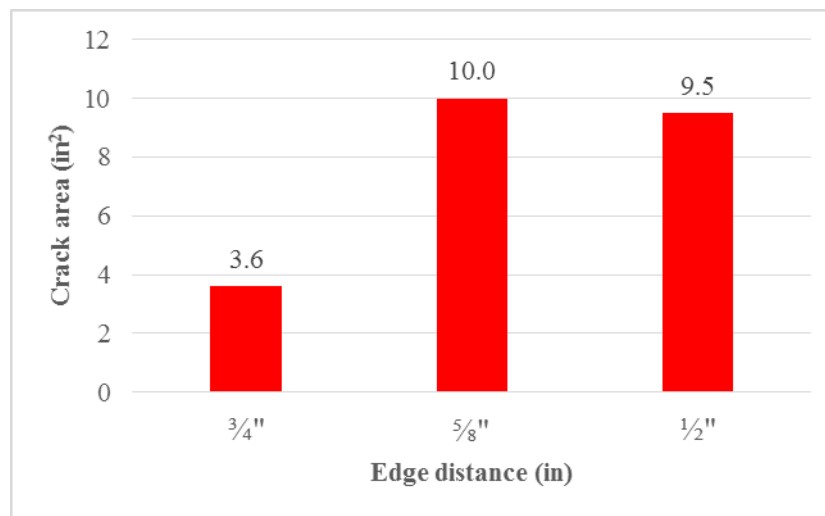


Figure 10-112: Mix#2, 4500 psi, WB-Crack Area (in²)

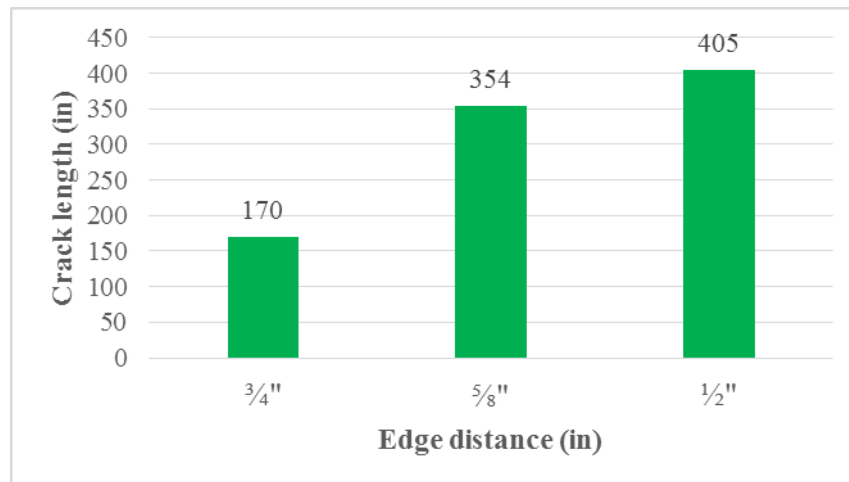


Figure 10-113: Mix#2, 4500 psi, WB-Crack Length (in)

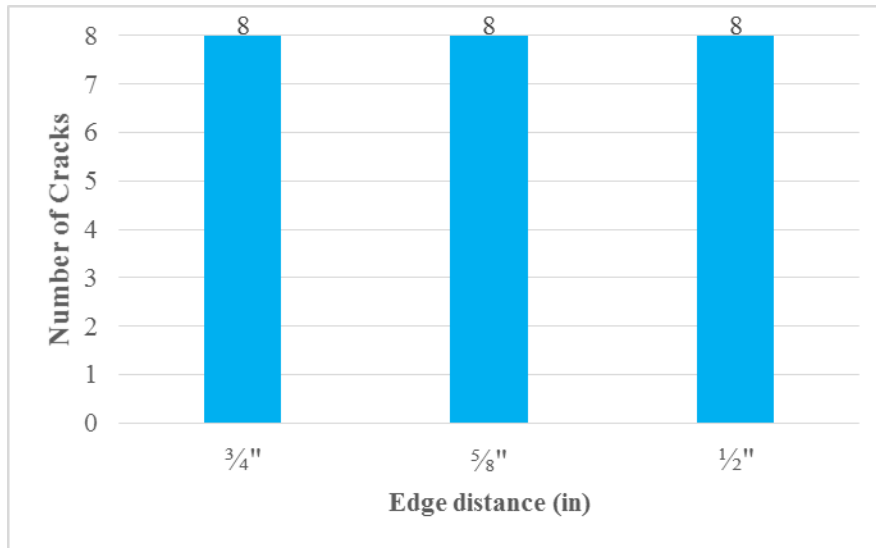


Figure 10-114: Mix#2, 4500 psi, WB-Number of cracks

According to Figure 10-112 it is visible that crack area for $\frac{3}{4}$ in. prism was greater than any other wire type. Average crack width was 0.02 in. and the average crack length was approximately 15 in. Cracks appeared on each side of the prism. With decreasing the values of the edge distance, the magnitude of the crack area was increased. Spalling was observed on the both prisms in series with $\frac{5}{8}$ in. and $\frac{1}{2}$ in. thicknesses of edge distance on the live end and dead end of the prism.

WB-Release Strength 6000 psi

Figure 10-115 shows longitudinal strain profile for $\frac{3}{4}$ in. edge distance. Eight cracks on each prism affected the values of transfer lengths. The values of transfer lengths are high due to splitting/cracking which indicated poor performance of the wire.

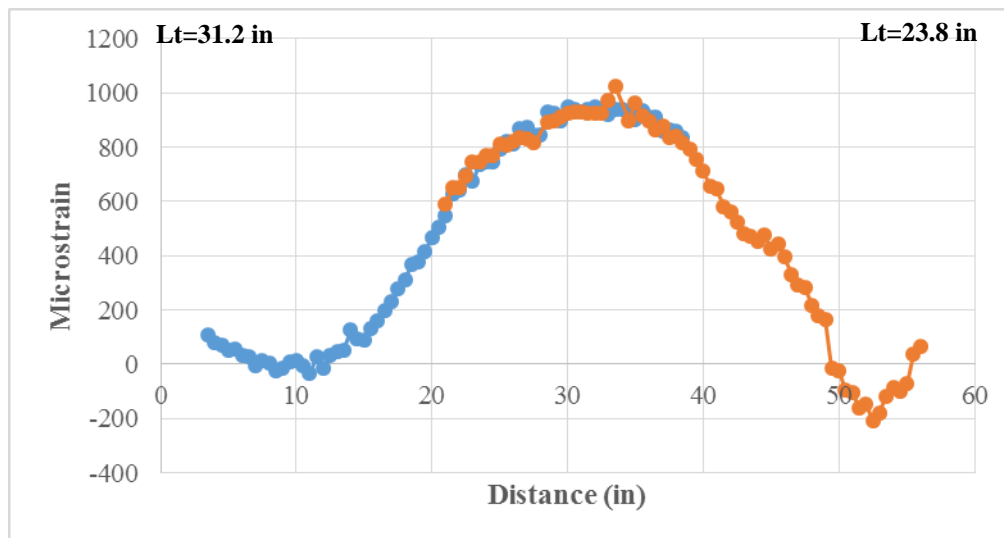


Figure 10-115: Mix#2, 6000 psi, WB, $\frac{3}{4}$ in. Edge Distance-Longitudinal Strain Profile



Figure 10-116: Mix#2, 6000 psi, WB-Observed Cracking (Dead End)



Figure 10-117: Mix#2, 6000 psi, WB-Observed Cracking (Live End)

Prism with a $\frac{3}{4}$ in. edge distance had three cracks on the live end of the prism. Maximum crack width was 0.013 in. and the maximum crack length was 21 in. On the dead end of the prism three cracks were observed with maximum crack width of 0.016 in. and maximum crack length of 15 in. On the second prism in series spalling was noticed in the length of 46 in. The dead end of the prism indicated better performance without spalling, but four cracks were observed with a maximum crack length of 21 in. Prism with $\frac{1}{2}$ in. edge distance had spalling on both the sides of the prism (Figure 10-116 and Figure 10-117). Consequently, the bond between steel and prestressed concrete was destroyed, without the possibility of transferring the stresses between the two materials.

Figure 10-118, Figure 10-119 and Figure 10-120 show crack area, crack length and number of cracks as a function of edge distance.

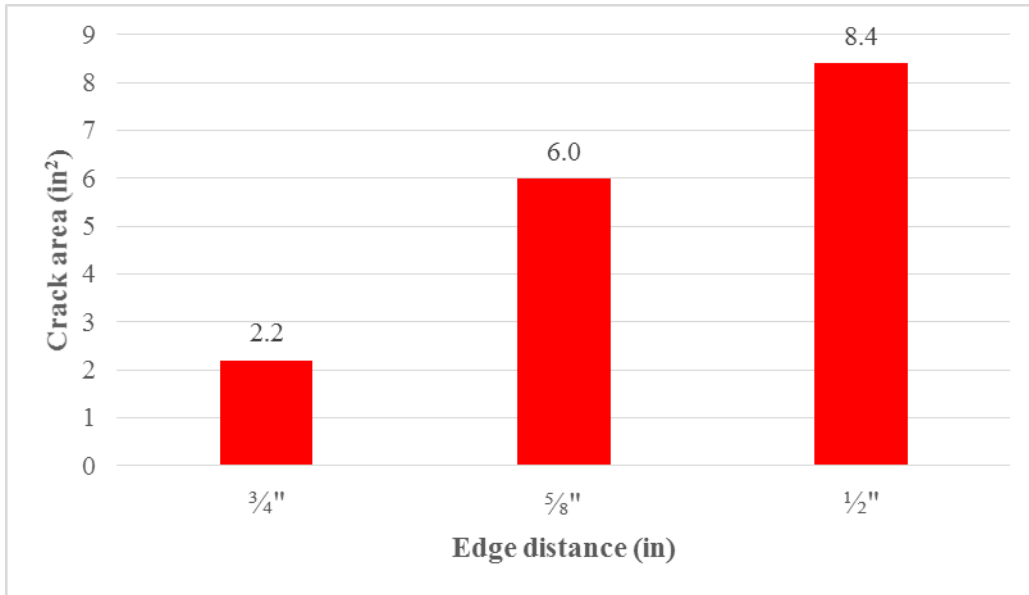


Figure 10-118: Mix#2, 6000 psi, WB-Crack Area (in²)

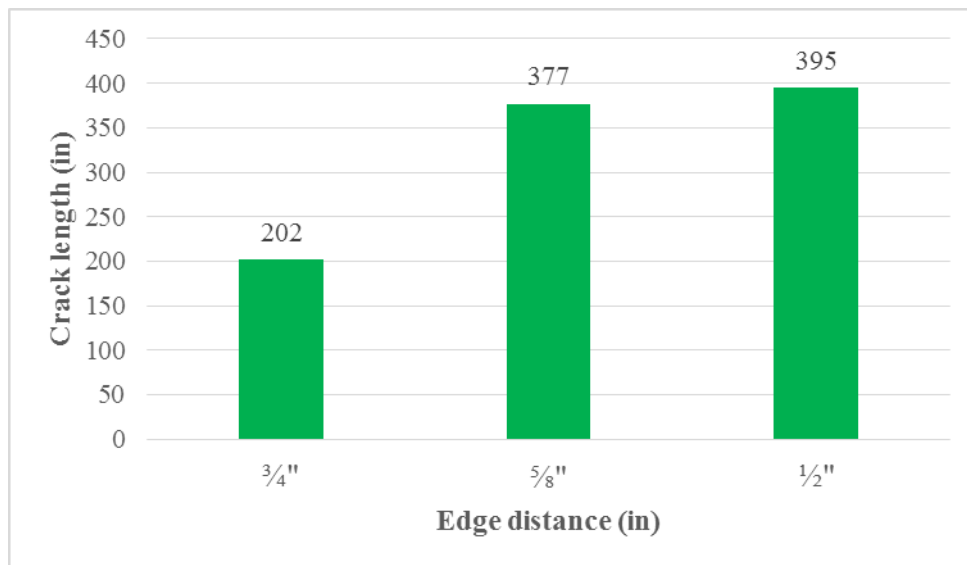


Figure 10-119: Mix#2, 6000 psi, WB-Crack Length

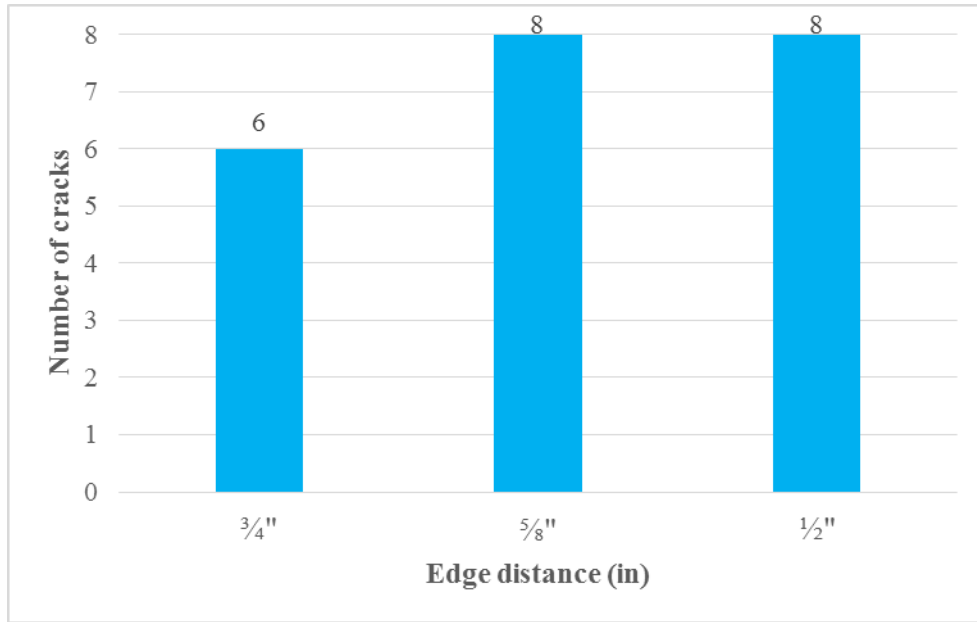


Figure 10-120: Mix#2, 6000 psi, WB- Number of Cracks

Mix#2-WF wire type

WF-Release Strength 4500 psi

WF wire performed poorly with concrete mixture used granite as aggregate, resulting in three cracks on the prism with $\frac{3}{4}$ in. edge distance and eight cracks for both prisms with $\frac{5}{8}$ in. and $\frac{1}{2}$ in. the edge distance. The longitudinal strain profile was measured immediately after the process of de-tensioning. One crack appeared on the prism with $\frac{3}{4}$ in. edge distance after the process of de-tensioning. Due to lateral stresses after two months of the process of de-tensioning two more cracks appeared.

Figure 10-121 presents longitudinal strain profile for $\frac{3}{4}$ in. edge distance along with the values of transfer lengths.

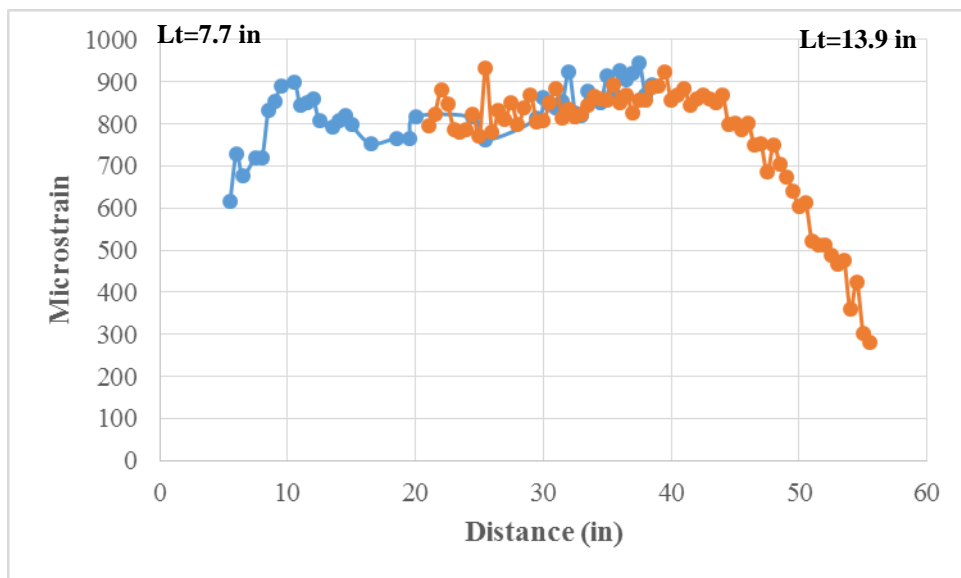


Figure 10-121: Mix#2, 4500 psi, WF, $\frac{3}{4}$ in. Edge Distance-Longitudinal Strain Profile

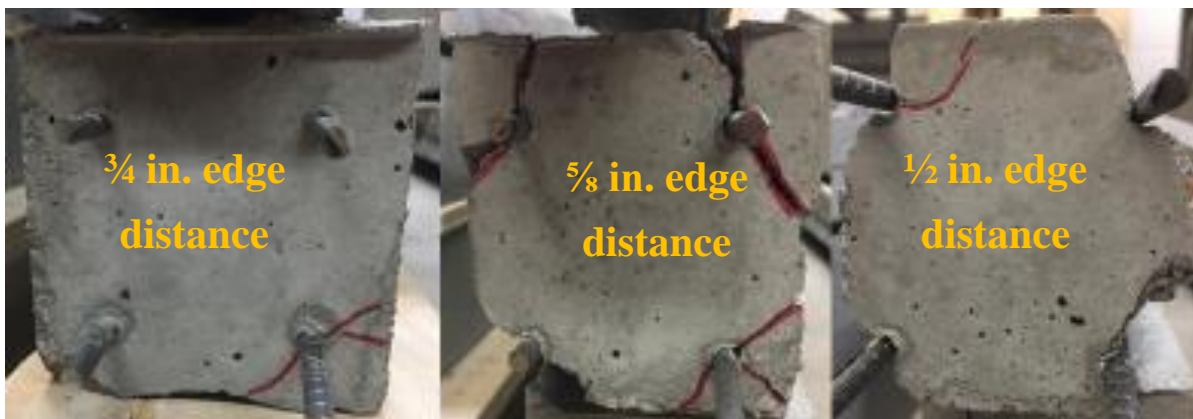


Figure 10-122: Mix#2, 4500 psi, WF-Observed Cracking (Dead End)

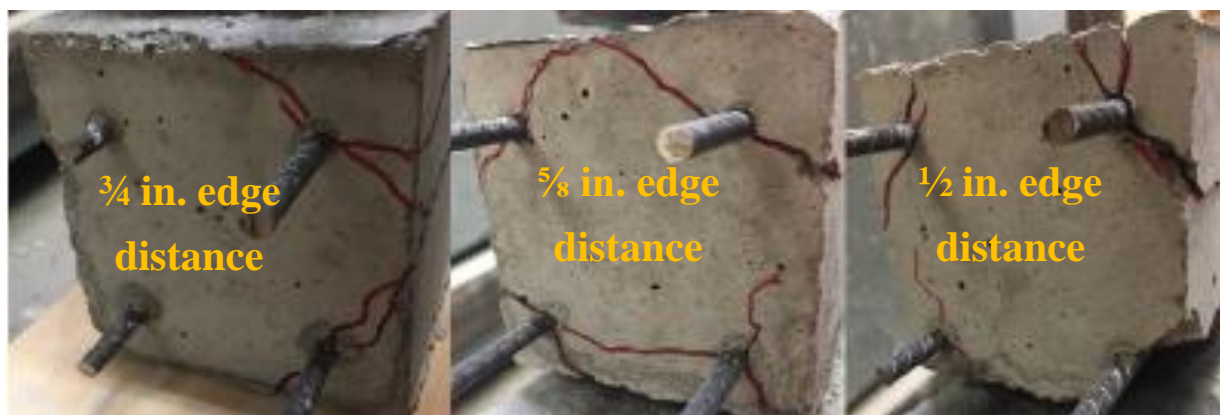


Figure 10-123: Mix#2, 4500 psi, WF-Observed Cracking (Live End)

Figure 10-122 and Figure 10-123 show observed cracking (dead and live end). Two cracks appeared on the dead end of the prism with a $\frac{3}{4}$ in. edge distance with maximum crack width of 0.04 in. and maximum crack length of 18 in. One crack appeared on the live end of the prism having a $\frac{3}{4}$ in. edge distance with average crack width of 0.01 in. With decreasing the edge distance spalling was observed on the live end of the prism with a $\frac{5}{8}$ in. edge distance in the length of 17 in. Prism with $\frac{1}{2}$ in. thickness had spalling on both the sides of the prisms which indicated that the bond between steel and concrete was completely destroyed.

Figure 10-124, Figure 10-125, and Figure 10-126 show crack area, crack length and number of cracks as a function of edge distance.

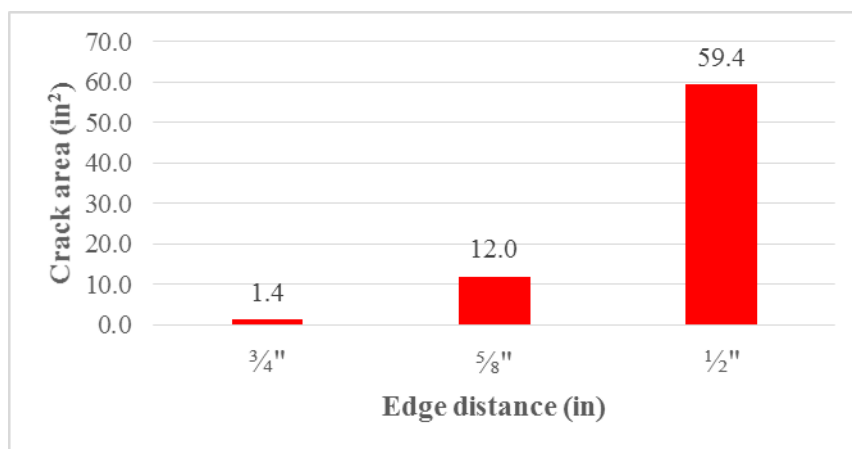


Figure 10-124: Mix#2, 4500 psi, WF-Crack Area (in²)

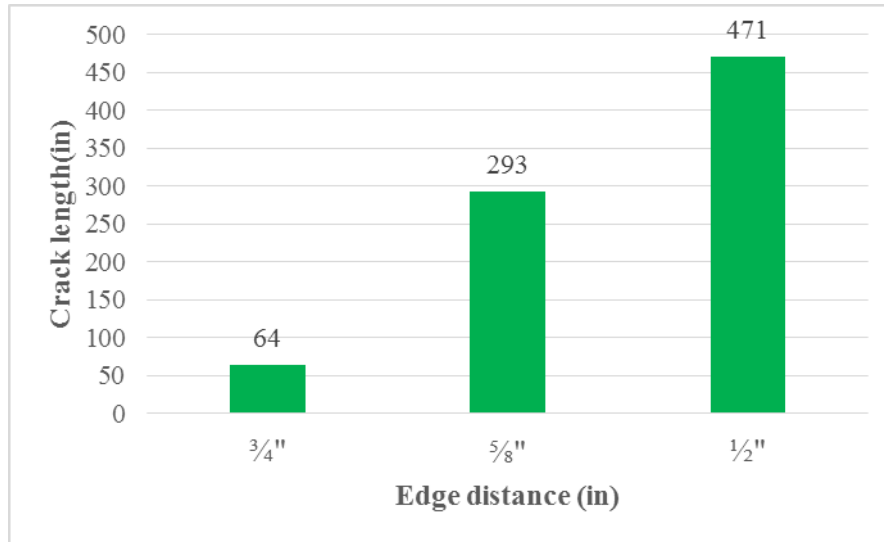


Figure 10-125: Mix#2, 4500 psi, WF-Crack length (in)

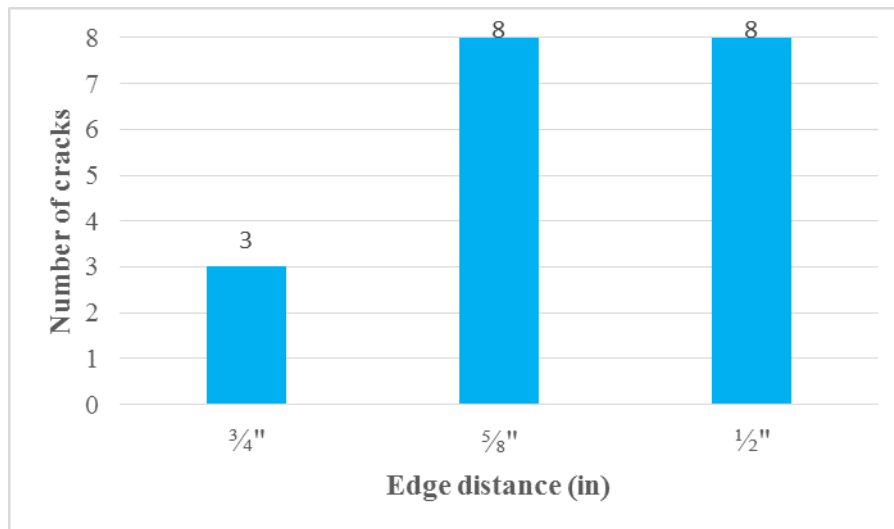


Figure 10-126: Mix#2, 4500 psi, WF-Number of Cracks

WF-Release Strength 6000 psi

With increasing the release concrete strength to 6000 psi, WF wire had three cracks on the prism with a $\frac{3}{4}$ in. edge distance, and eight cracks on the prisms with $\frac{5}{8}$ in. and $\frac{1}{2}$ in. edge distances.

Figure 10-127 shows the longitudinal strain profile along with the values of transfer lengths for the prism having a $\frac{3}{4}$ in. thickness of the edge distance.

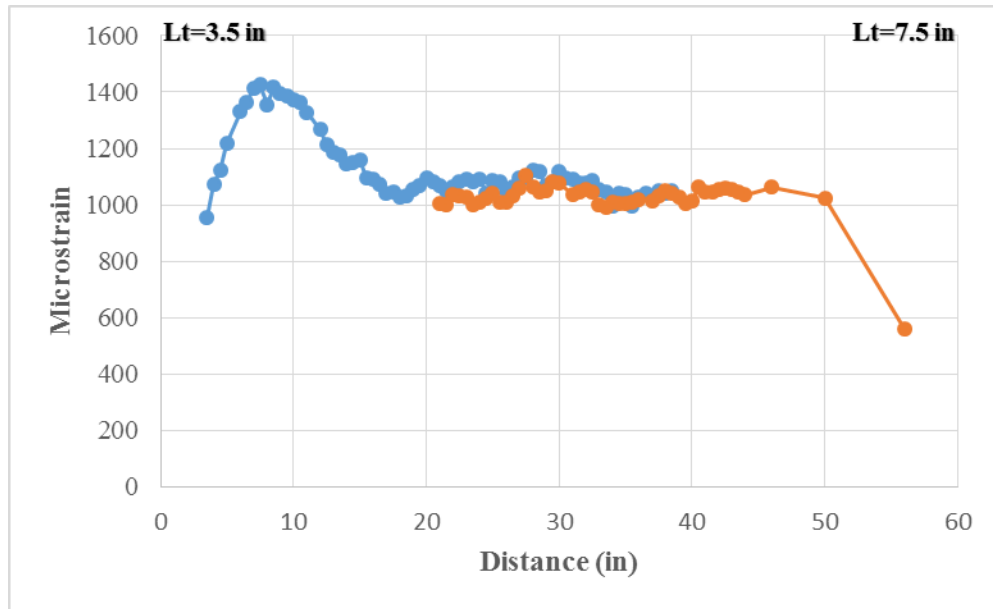


Figure 10-127: Mix#2, 6000 psi, WF, $\frac{3}{4}$ in. Edge Distance-Longitudinal Strain Profile

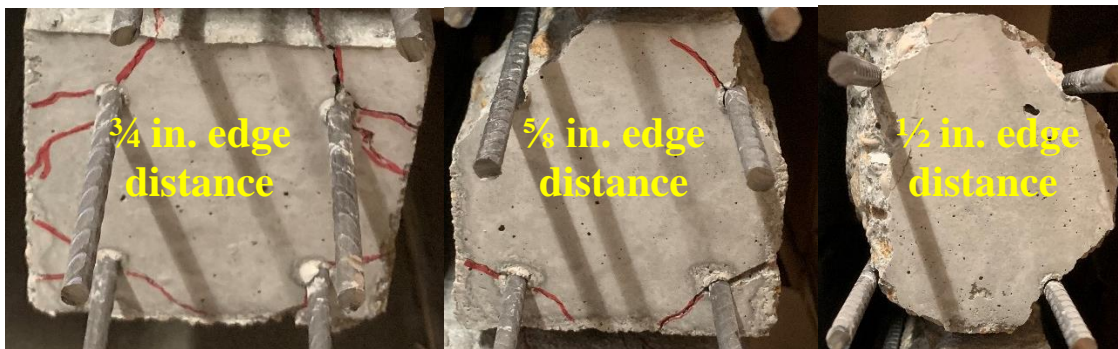


Figure 10-128: Mix#2, 6000 psi, WF-Observed Cracking (Dead End)

Figure 10-128 shows observed cracking on the dead end. Two cracks appeared on the live end of the prism with $\frac{3}{4}$ in. edge distance, the maximum crack width was 0.04 in. and the maximum crack length was 13 in. On the dead end of the prism, one crack appeared with crack width of 0.01 in. and maximum crack length of 3 in. With reducing the edge distance to $\frac{5}{8}$ in. and $\frac{1}{2}$ in. spalling was observed. The values of crack areas were very large which indicates poor bond performance.

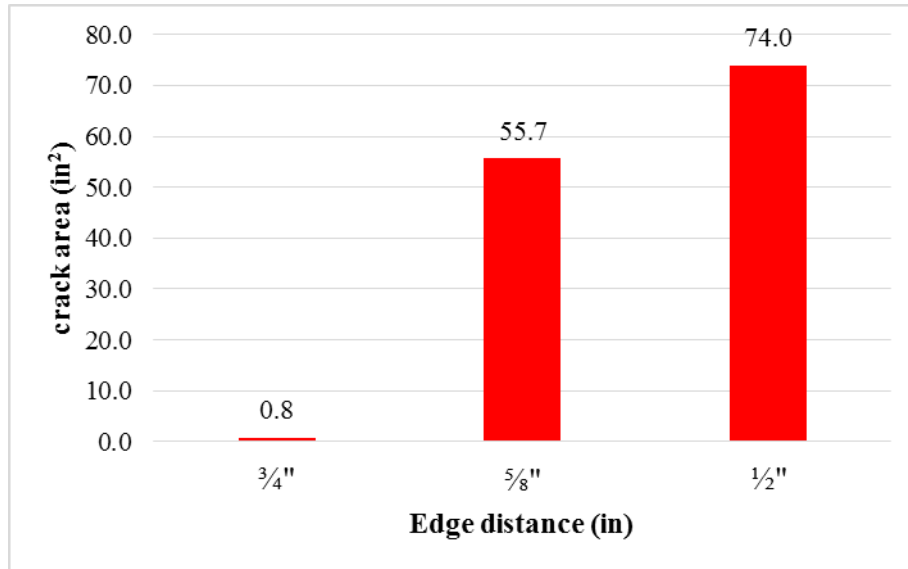


Figure 10-129: Mix#2, 6000 psi, WF-Crack Area (in²)

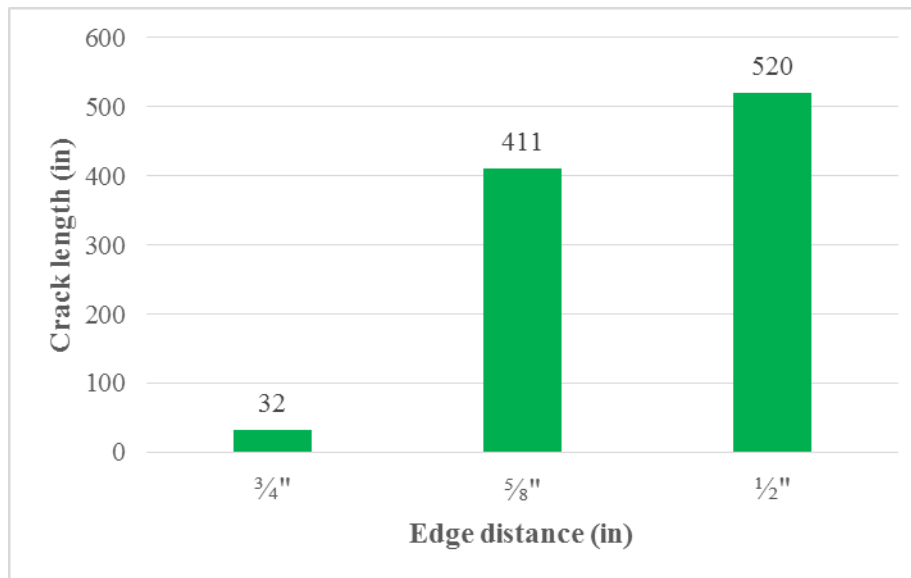


Figure 10-130: Mix#2, 6000 psi, WF-Crack-Length

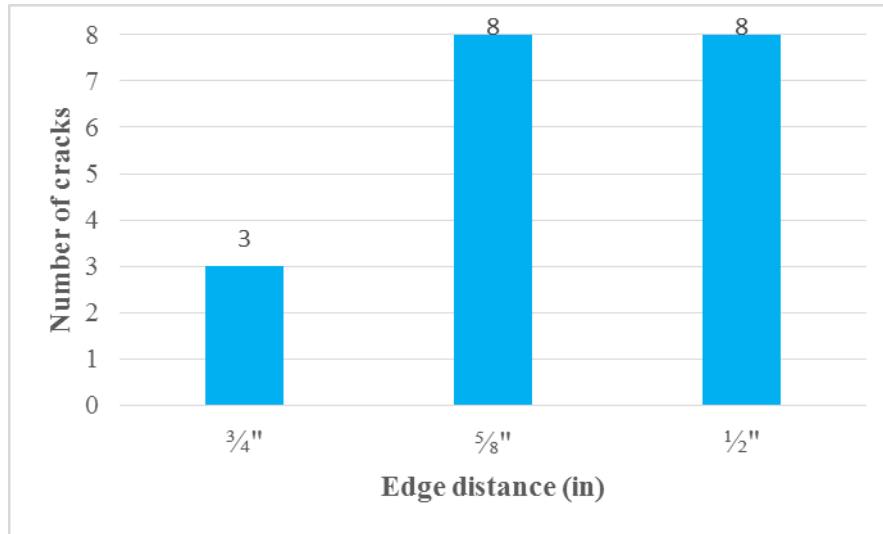


Figure 10-131: Mix#2, 6000 psi, WF-Number of Cracks

Figure 10-129, Figure 10-130, and Figure 10-131 present total crack area, crack length and number of cracks.

Mix#2-WG wire type

WG-Release Strength 4500 psi

WG wire was extracted from the prisms which were done at the beginning of this project. WG wire belongs to chevron type of wire and indicated very good performance. The longitudinal strain profiles were measured along with the values of transfer lengths for all the three prisms. Approximately the value of transfer length for the prisms was approximately 13 in. Figure 10-132, Figure 10-133, and Figure 10-134 present the longitudinal strain profiles along with the values of transfer lengths.

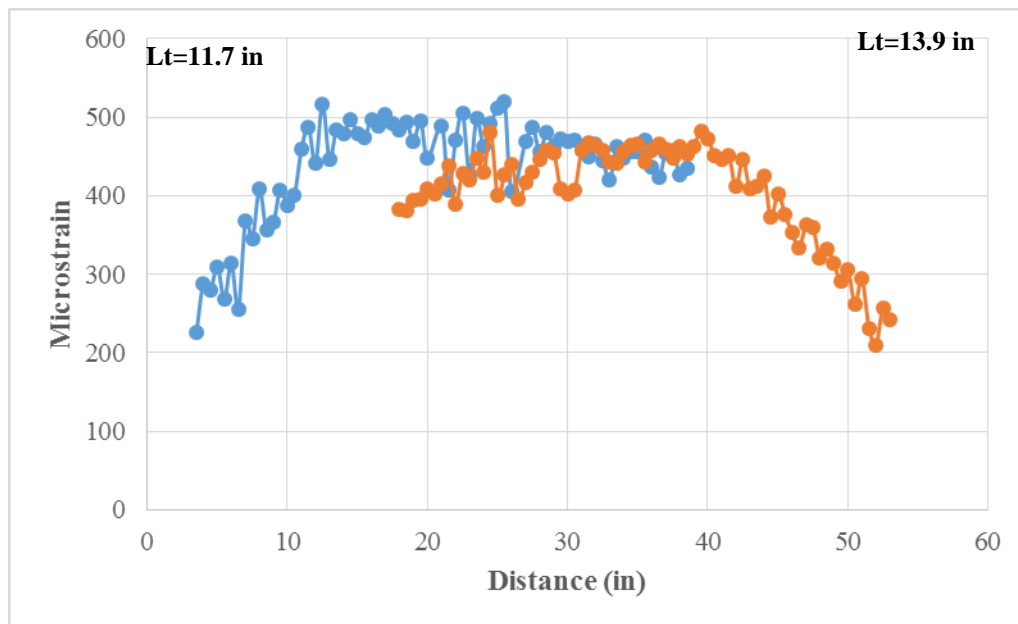


Figure 10-132: Mix#2, 4500 psi, WG, $\frac{3}{4}$ in. Edge Distance-Longitudinal Strain Profile

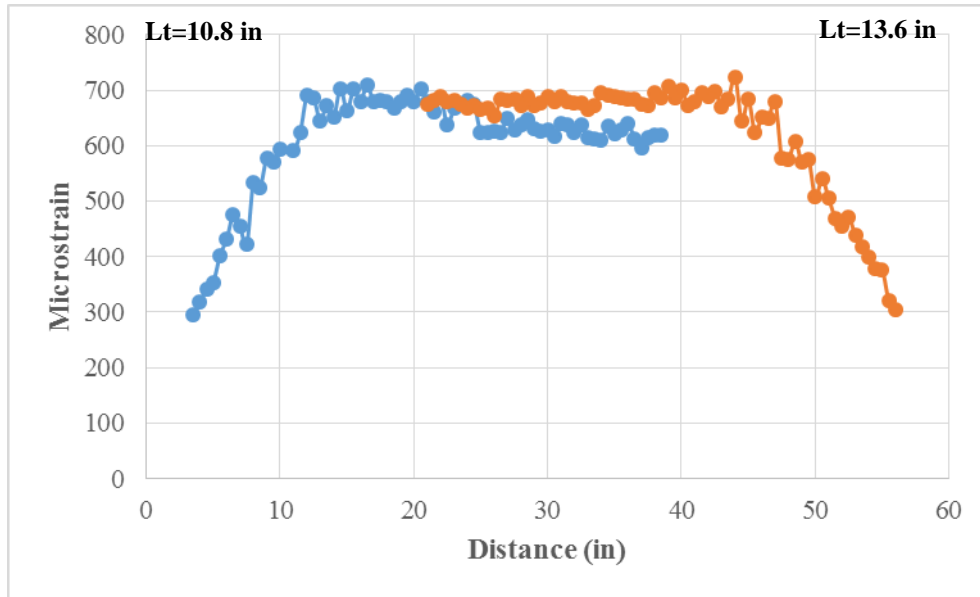


Figure 10-133: Mix#2, 4500 psi, WG, 5/8 in. Edge Distance-Longitudinal Strain Profile

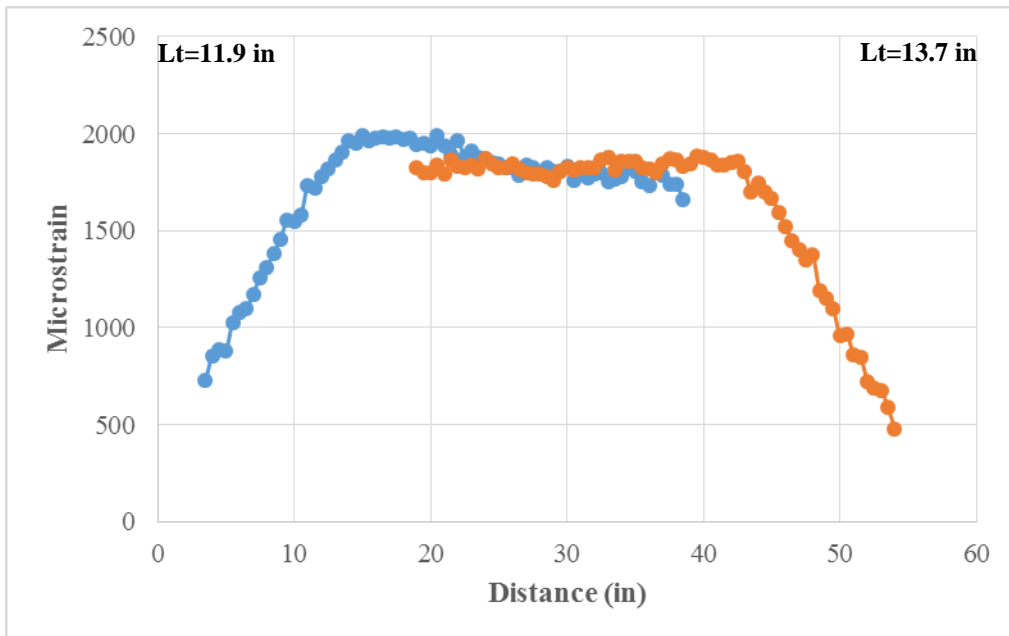


Figure 10-134: Mix#2, 4500 psi, WG, 1/2 in. Edge Distance-Longitudinal Strain Profile



Figure 10-135: Mix#2, 4500 psi, WG-Observed Cracking (Dead End)



Figure 10-136: Mix#2, 4500 psi, WG-Observed Cracking (Live End)

Figure 10-135 and Figure 10-136 show observed cracking on the dead and live end. On the prisms with $\frac{3}{4}$ in. edge distance, no visible cracks on the surface appeared. On the prism with $\frac{1}{2}$ in. edge distance, three cracks were observed with length less than 5 in. and with crack width of 0.01 in.

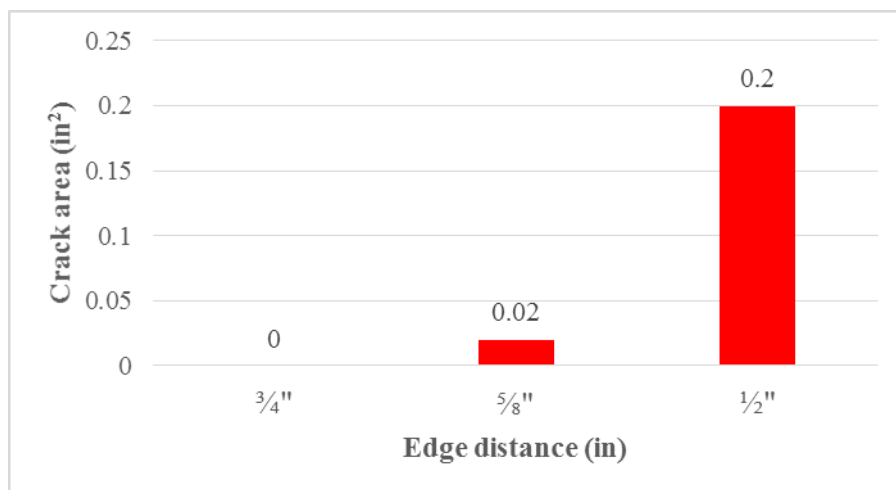


Figure 10-137: Mix#2, 4500 psi, WG-Crack Area (in²)

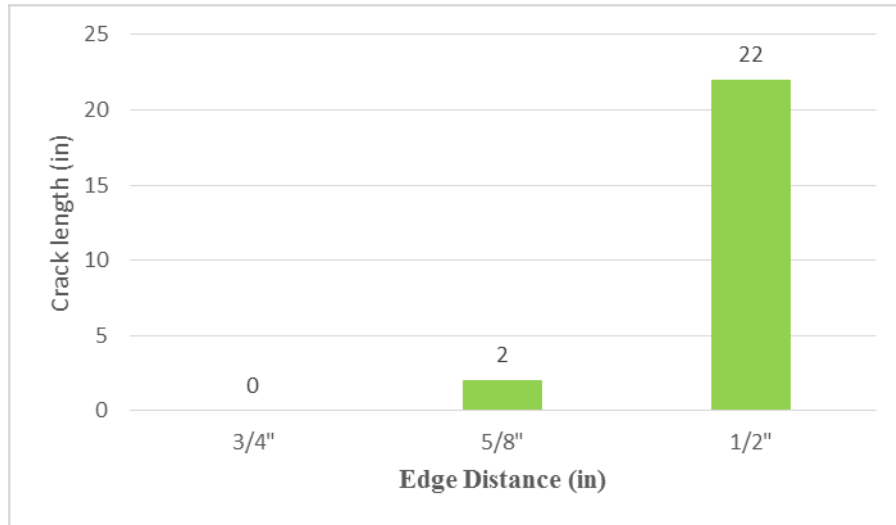


Figure 10-138: Mix#2, 4500 psi, WG-Crack Length (in)

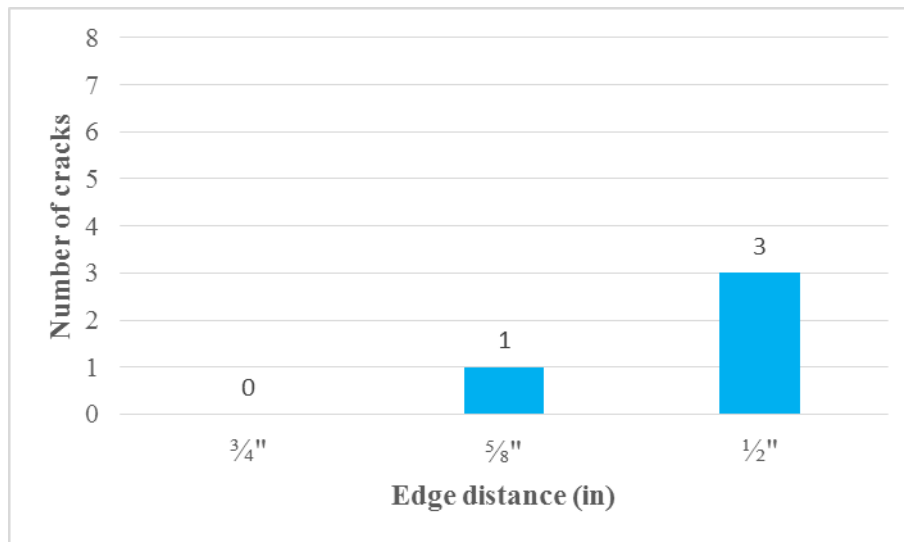


Figure 10-139: Mix#2, 4500 psi, WG-Number of Cracks

WG wire performed very well with no cracks on the prism with a $\frac{3}{4}$ in. the edge distance, one crack on the $\frac{5}{8}$ in. edge distance with 0.02 in^2 crack area and 2 in. crack length. Third prism in series with a $\frac{1}{2}$ in. edge distance had three cracks, with the value of crack area approximately 0.2 in^2 and average crack length of 23 in.

Figure 10-137, Figure 10-138, and Figure 10-139 show crack area, crack length and number of cracks as a function of edge distance, respectively.

Mix#2-WH wire type

WH-Release Strength 4500 psi

WH wire as WG wires were extracted from the existing prism. For this test the length of the wires was shorter and adjusted setup was used to conduct this experiment. WH wire which belongs to deep chevron type of wire with an average indent depth of 0.164 mm (0.00646 in.) and 16.27-degrees edge wall angle performed poorly resulting in two cracks on the live end of the prism with $\frac{3}{4}$ in. edge distance and with the maximum crack length of 5 in. These two-cracks on the prism with a $\frac{3}{4}$ in. edge distance had 0.01 in. maximum crack width. Cracks were observed on the back and front side of the prism. On the dead end, there were no visible cracks on the surface.



Figure 10-140: Mix#2, 4500 psi, WH-Observed Cracking (Dead End)



Figure 10-141: Mix#2, 4500 psi, WH-Observed Cracking (Live End)

The second prism in series performed poorly with spalling in the maximum length of 5 in. on the live end of the prism, and maximum crack length of 4 in. on the dead end. Figure 10-140 and Figure 10-141 demonstrate observed cracking on all three prisms. The images gave the clarity that the third prism performed the worst with four cracks on each side of the prism. Maximum crack width on the live end was 0.08 in. and the maximum crack length was 42 in. The dead end of the prism with $\frac{1}{2}$ in. edge distance had four cracks with maximum crack width of 0.04 in. and maximum crack length of 40 in. According to charts for crack area and crack length, a clear image of effectiveness of edge distance on the bond performance between steel and concrete was provided.

Figure 10-142, Figure 10-143 and Figure 10-144 present crack area, crack length and number of cracks as a function of edge distance, respectively.

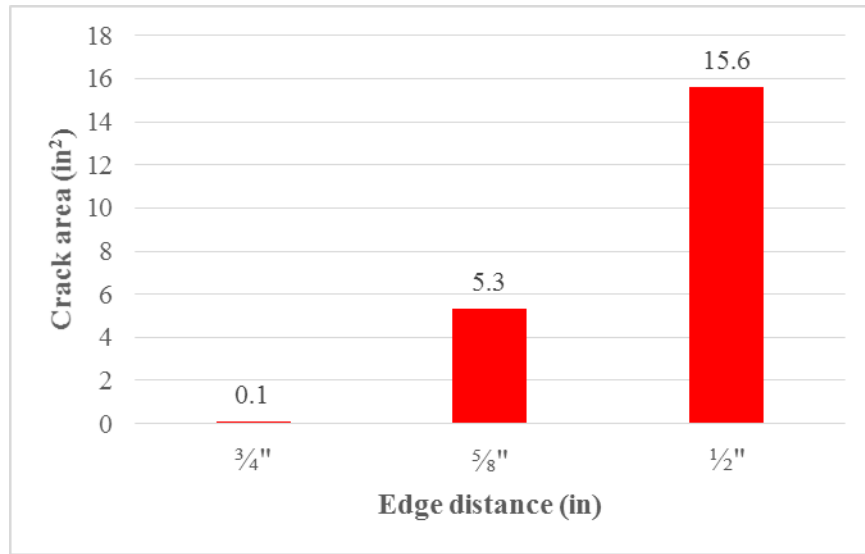


Figure 10-142: Mix#2, 4500 psi, WH-Crack Area (in²)

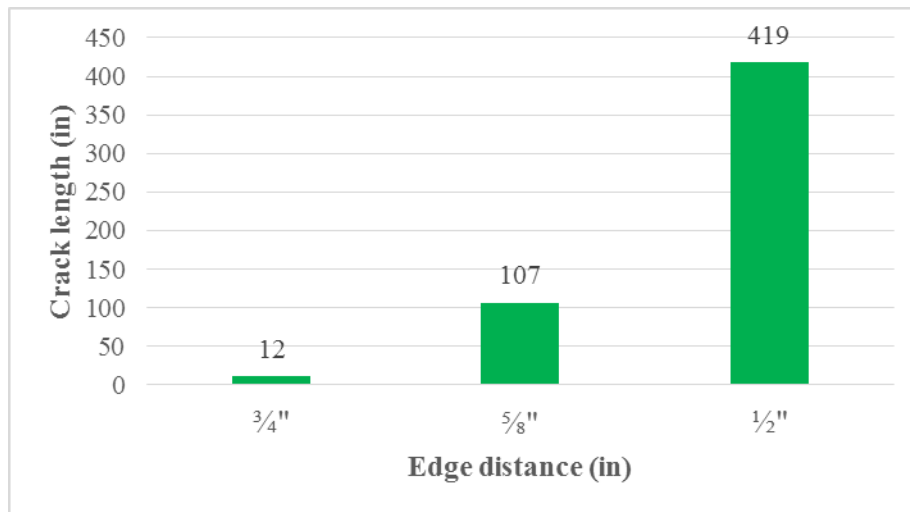


Figure 10-143: Mix#2, 4500 psi, WH--Crack Length (in)

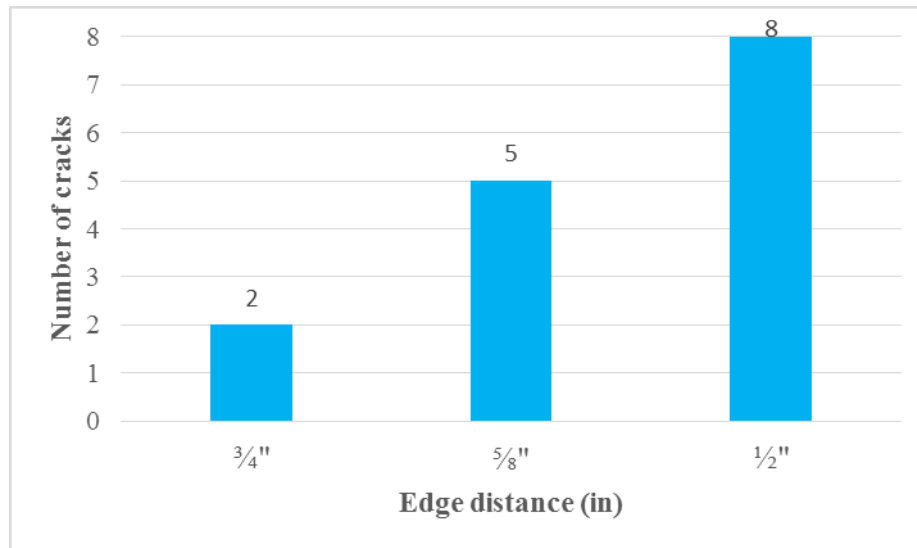


Figure 10-144: Mix#2, 4500 psi, WH-Number of Cracks

Mix#2-WI wire type

WI-Release Strength 4500 psi

WI wire belongs to chevron type of wire. This wire performed well with a $\frac{3}{4}$ in. edge distance in resulting no cracks appearance and eight cracks on $\frac{5}{8}$ in. and $\frac{1}{2}$ in. thicknesses of edge distance. Figure 10-145 shows the longitudinal strain profile. The average value of transfer length was 8.9 in.

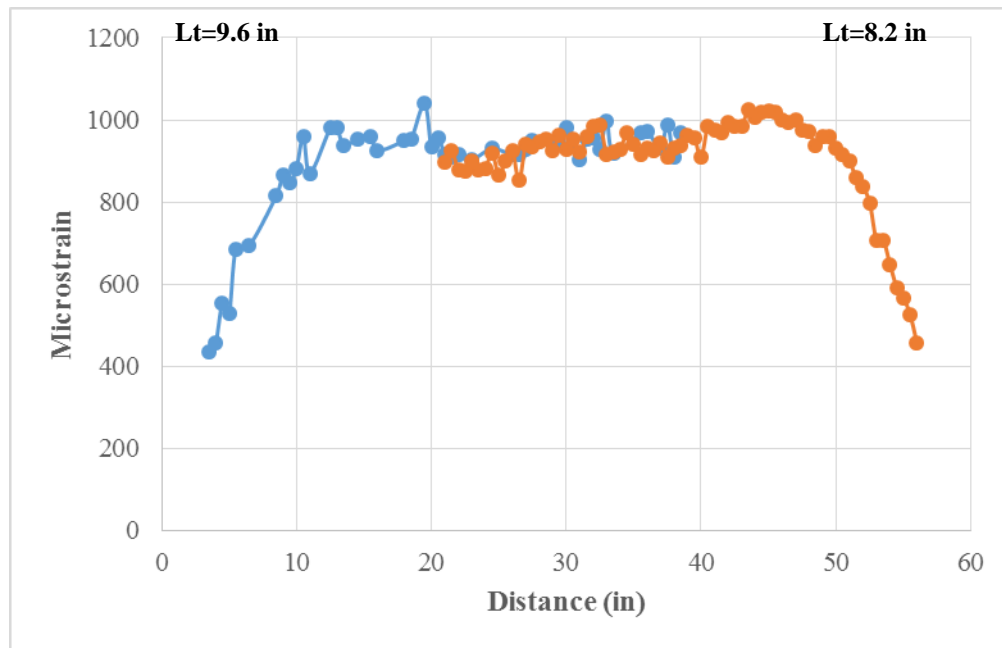


Figure 10-145: Mix#2, 4500 psi, WI, $\frac{3}{4}$ in. Edge Distance-Longitudinal Strain Profile

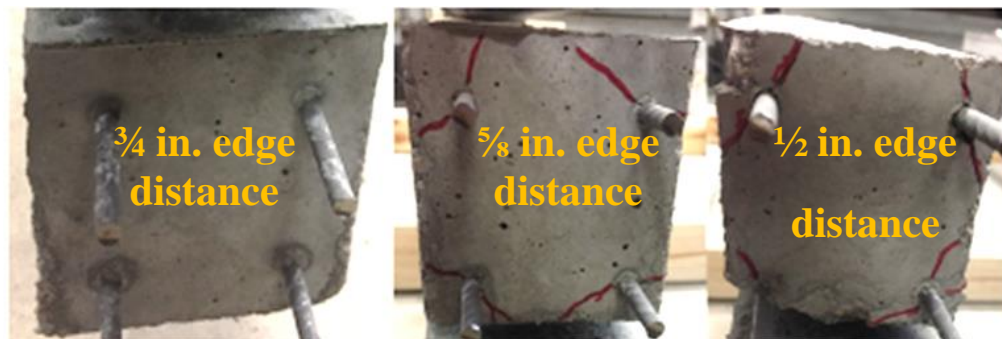


Figure 10-146: Mix#2, 4500 psi, WI-Observed Cracking (Dead End)

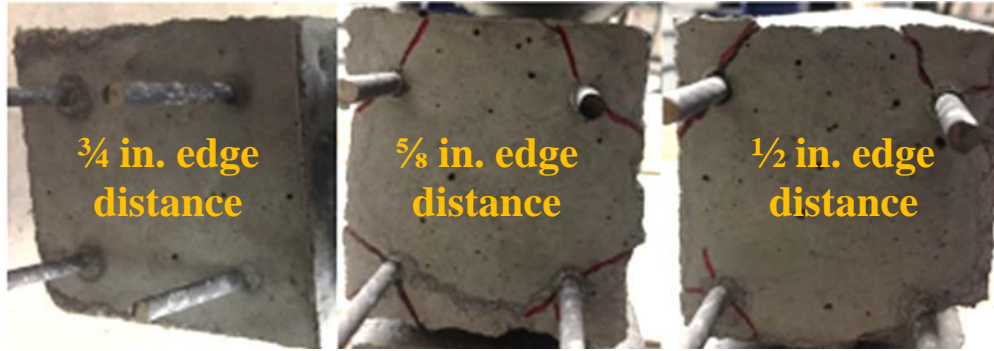


Figure 10-147: Mix#2, 4500 psi, WI-Observed Cracking (Live End)

Prism with $\frac{5}{8}$ in. edge distance had four cracks on each side of the prism. Maximum crack width was 0.04 in on the live end and maximum crack length was 20 in. When the edge distance was decreased to $\frac{1}{2}$ in. spalling was observed on both the sides of the prisms. (Figure 10-146 and Figure 10-147)

Figure 10-148, Figure 10-149 and Figure 10-150 show crack area, crack length and number of cracks as a function of edge distance, respectively.

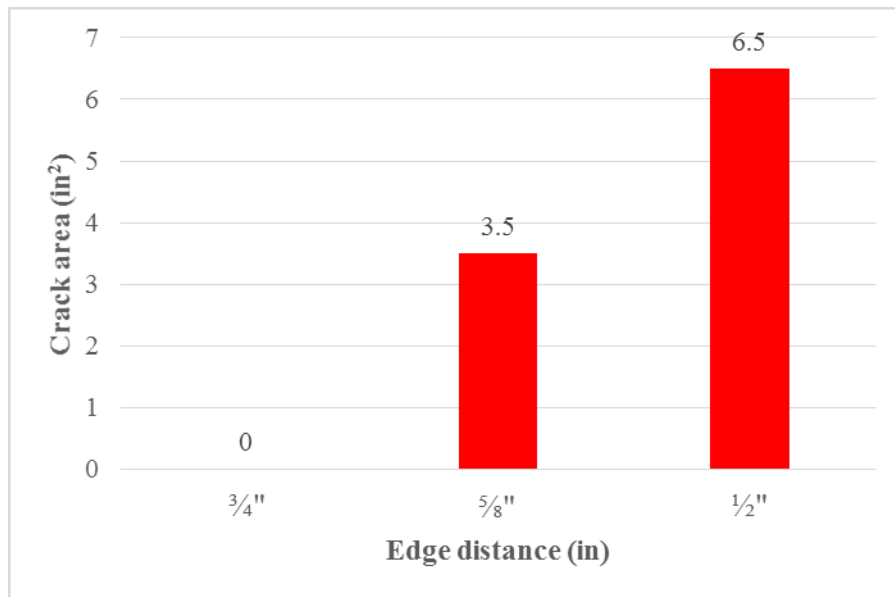


Figure 10-148: Mix#2, 4500 psi, WI-Crack Area (in²)

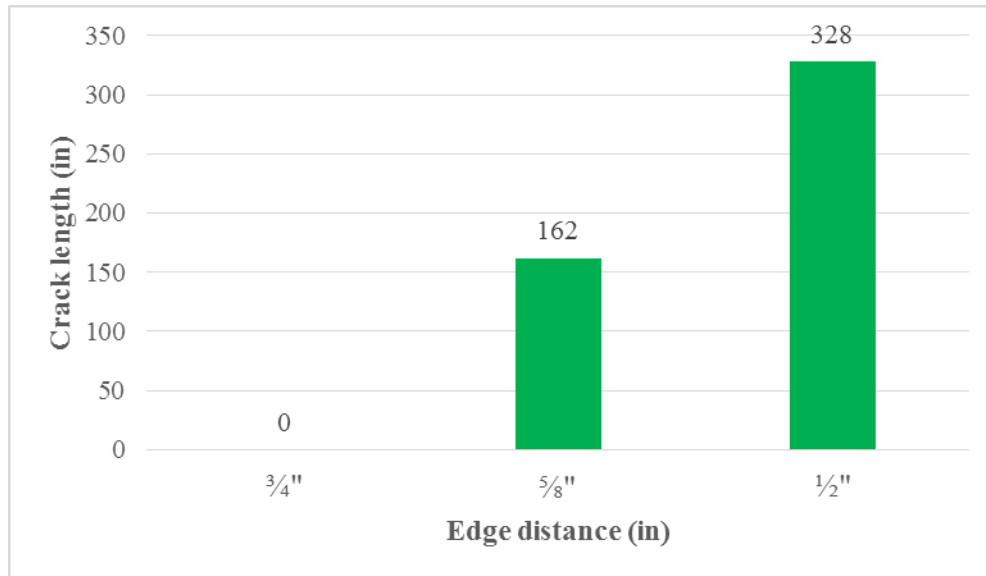


Figure 10-149: Mix#2, 4500 psi, WI-Crack Length (in)

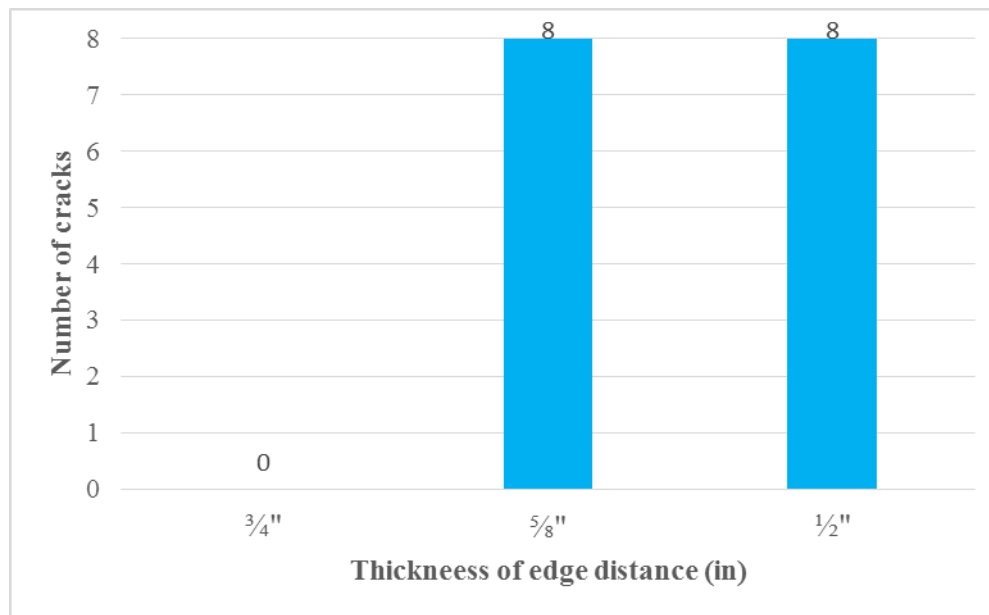


Figure 10-150: Mix#2, 4500 psi, WI- Number of Cracks

WI-Release Strength 6000 psi

WI wire was done with 6000 psi, and with increasing the release strength this wire performed very well in resulting no crack appearance on the prism with a $\frac{3}{4}$ in. the edge distance. When the de-tensioning procedure commenced, no visible cracks were observed on the prisms with $\frac{3}{4}$ in. and $\frac{5}{8}$ in. the edge distances in series. Longitudinal strain profiles, along with the values of transfer lengths were given for both prisms (Figure 10-151 and Figure 10-152). After de-

tensioning there was no visible cracks on the prism with $\frac{5}{8}$ in the edge distance, after three months, due to lateral stresses one crack appeared on both the sides of the prism. These cracks had a length of 2 in. and width of 0.01 in. on the dead end and length of 2 in. and crack width of 0.01 in. on the live end. (Figure 10-153 and Figure 10-154)

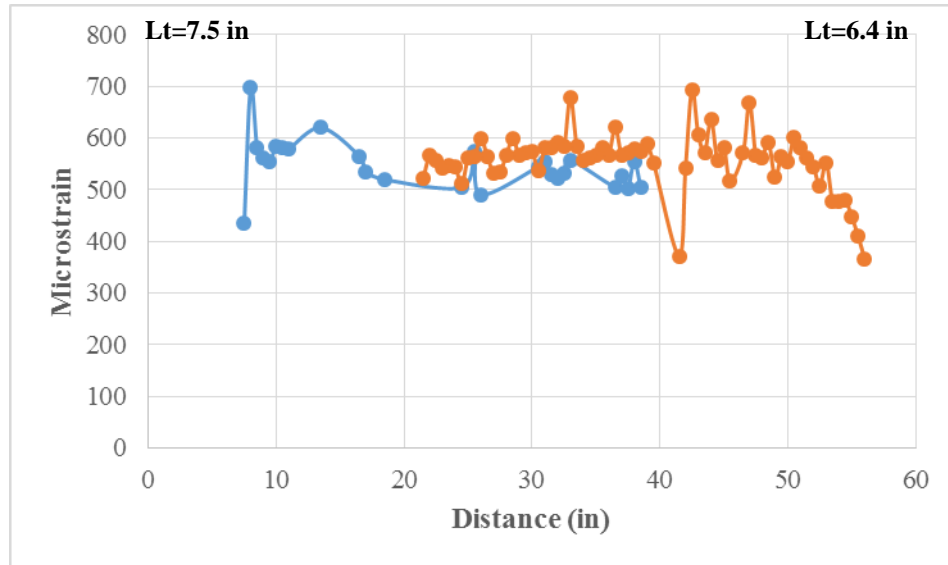


Figure 10-151: Mix#2, 6000 psi, WI, $\frac{3}{4}$ in. Edge Distance-Longitudinal Strain Profile

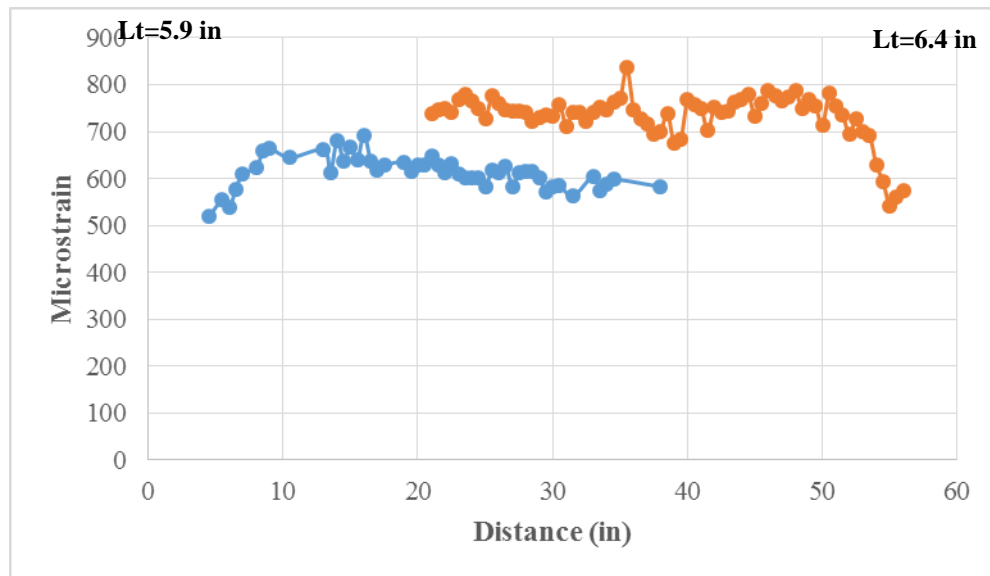


Figure 10-152: Mix#2, 6000 psi, WI, $\frac{5}{8}$ in. Edge Distance-Longitudinal Strain Profile

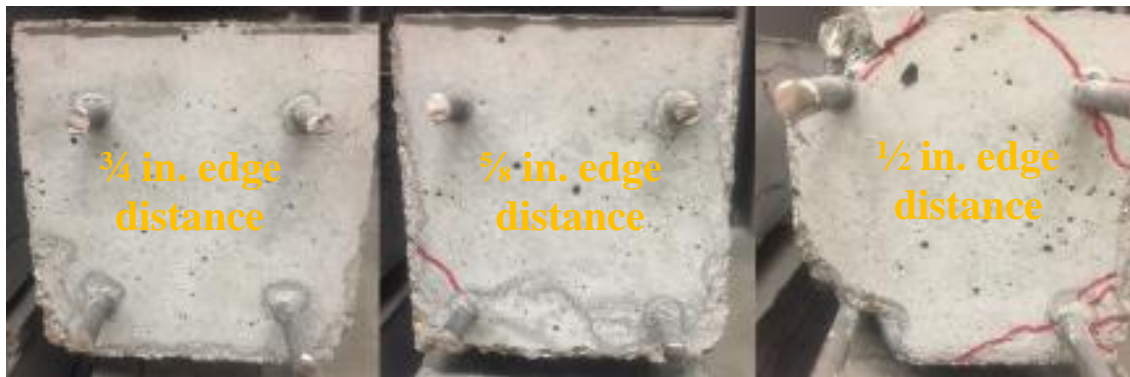


Figure 10-153: Mix#2, 6000 psi, WI-Observed Cracking (Dead End)



Figure 10-154: Mix#2, 6000 psi, WI-Observed Cracking (Live End)

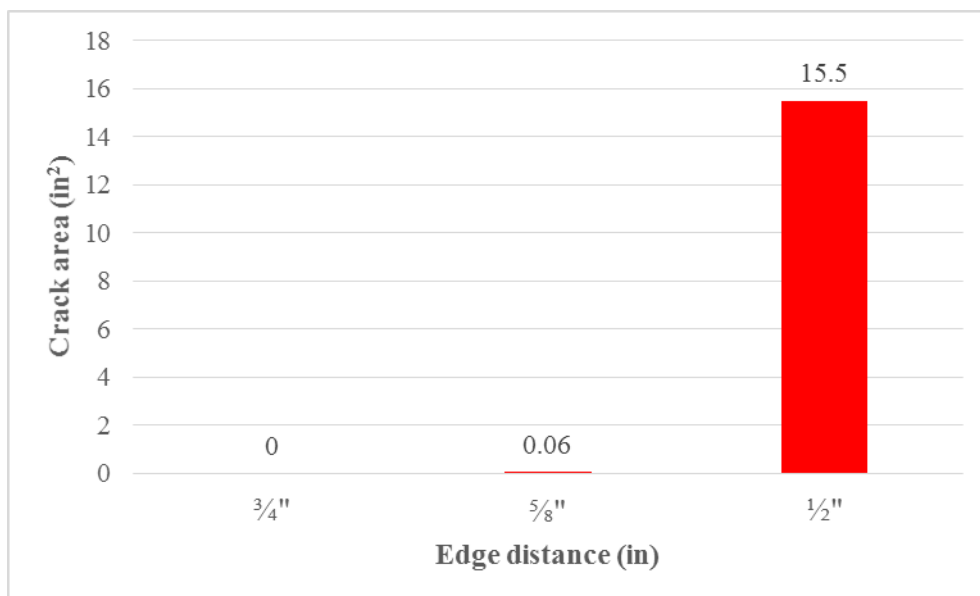


Figure 10-155: Mix#2, 6000 psi, WI- Crack Area (in²)

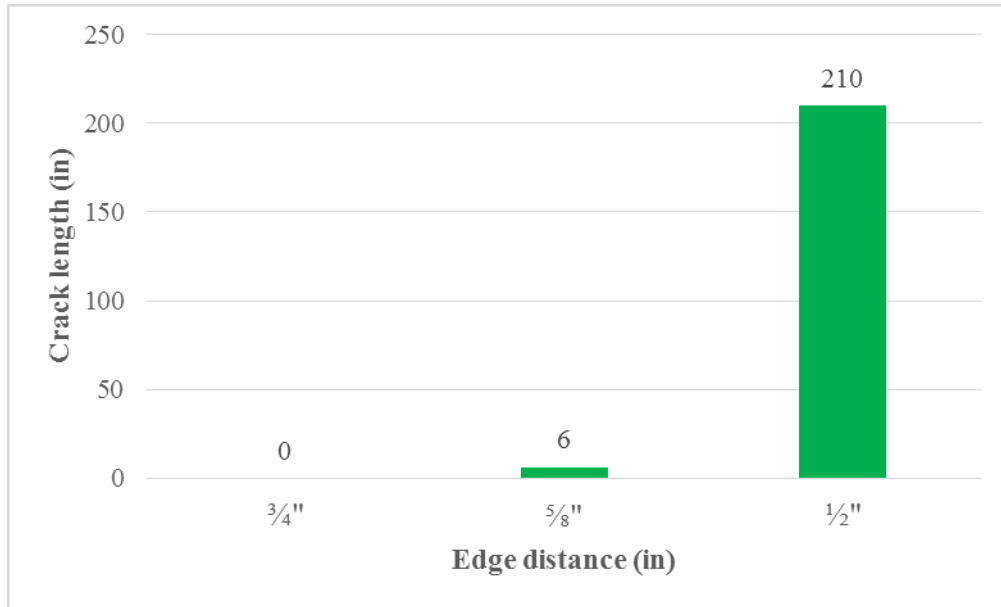


Figure 10-156: Mix#2, 6000 psi, WI-Crack Length (in.)

According to Figure 10-155, Figure 10-156, and Figure 10-157 third prism performed the worst with spalling, which occurred on the live end of the prism in the length of 6 in. and 20 in. on the dead end.

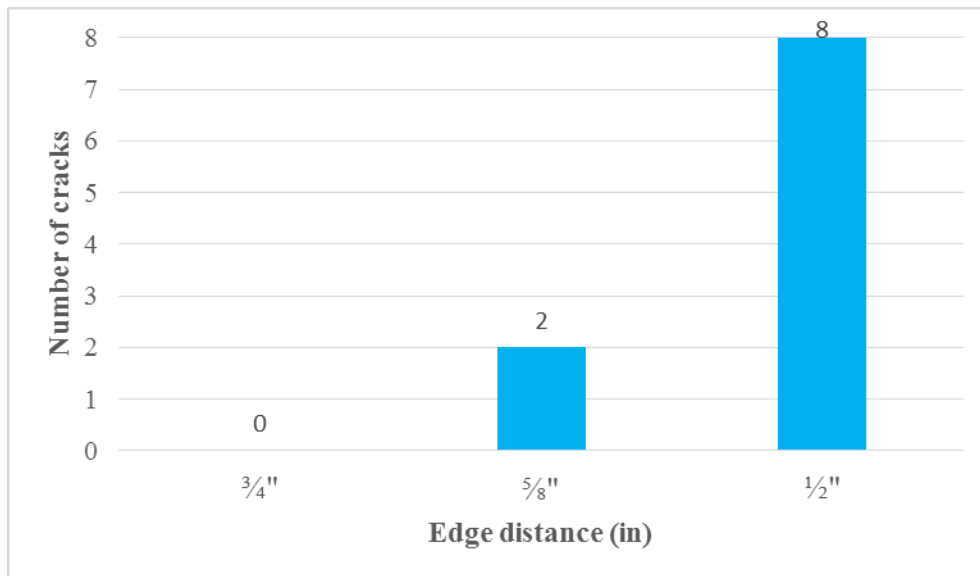


Figure 10-157: Mix#2, 6000 psi, WI-Number of Cracks

Mix#2-WJ wire type

WJ-Release Strength 4500 psi

WJ wire with the 4500 psi release strength and the second type of mixture performed very well. There were no visible cracks on both prisms with $\frac{3}{4}$ in. edge distance and $\frac{5}{8}$ in. the edge distance. Reducing the edge distance to $\frac{1}{2}$ in. eight cracks appeared. Increasing the number of cracks due to the edge distance point out the significance of the value of the edge distance in prestressed concrete.

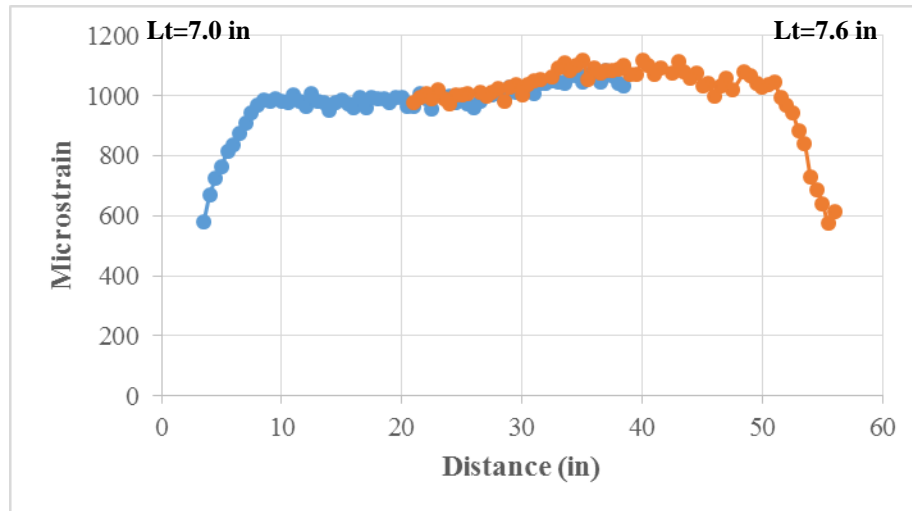


Figure 10-158: Mix#2, 4500 psi, WJ, $\frac{3}{4}$ in. Edge Distance-Longitudinal Strain Profile

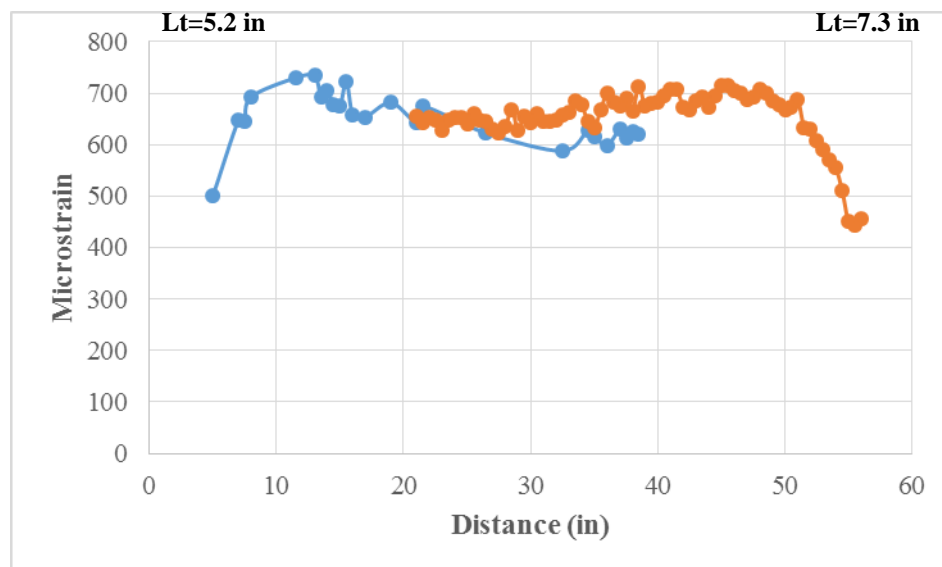


Figure 10-159: Mix#2, 4500 psi, WJ, $\frac{5}{8}$ in. Edge Distance-Longitudinal Strain Profile

Figure 10-158 and Figure 10-159 show the longitudinal strain profiles along with the values of transfer lengths on both the sides of the prisms. The average value of transfer lengths for the prism with $\frac{3}{4}$ in. edge distance was 7.3 in. and 6.5 in. for the prism with $\frac{5}{8}$ in. edge distance.

This wire indicated very well performance with no cracks on the first two prisms and eight cracks on $\frac{1}{2}$ in. edge distance. Spalling was observed on both the sides of the prism, and a maximum length of spalling was 33 in. on the live end and 27 in. on the dead end.



Figure 10-160: Mix#2, 4500 psi, WJ-Observed Cracking (Dead End)

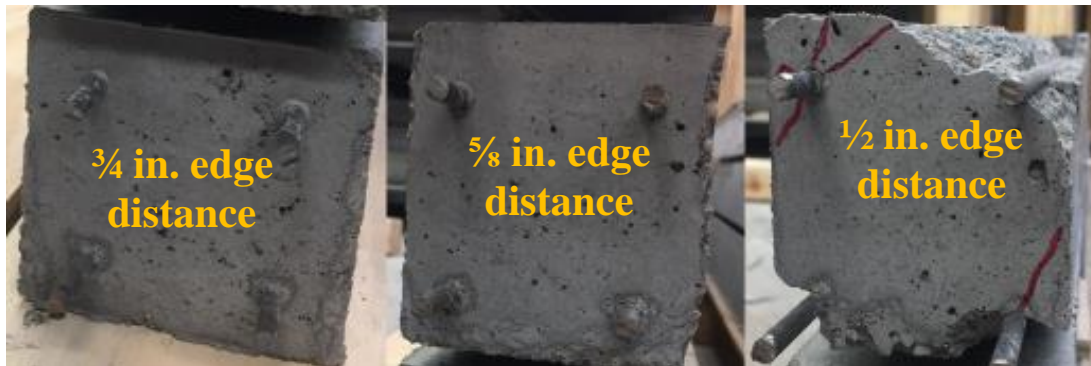


Figure 10-161: Mix#2, 4500 psi, WJ-Observed Cracking (Live End)

Figure 10-162, Figure 10-163 and Figure 10-164 show the magnitudes of crack areas, crack lengths and number of wires which had the tendency to crack.

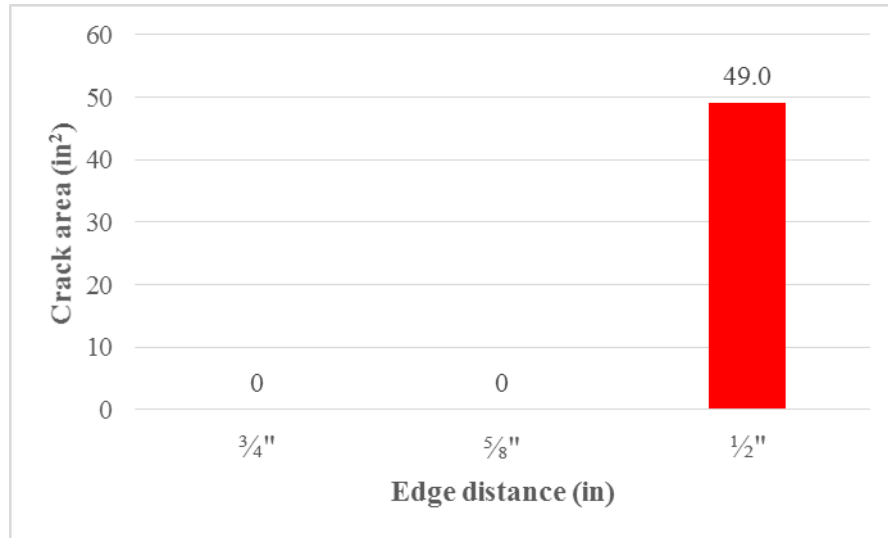


Figure 10-162: Mix#2, 4500 psi, WJ-Crack Area (in²)

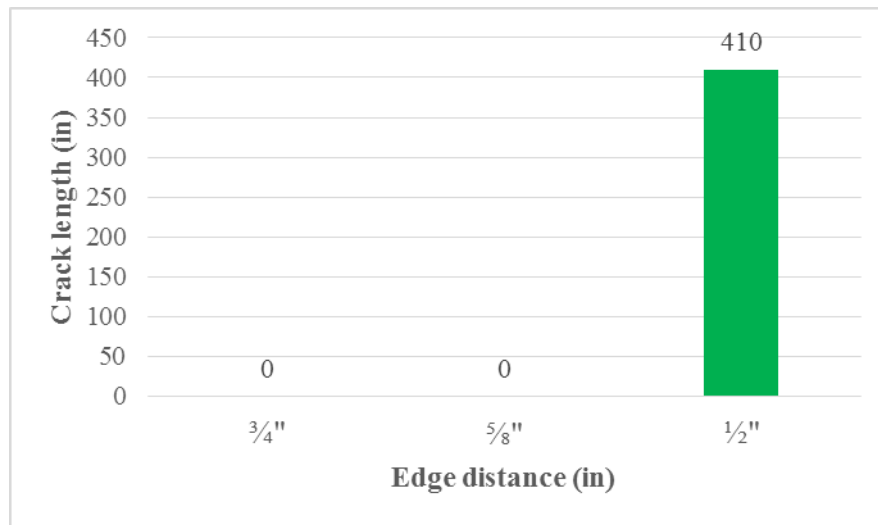


Figure 10-163: Mix#2, 4500 psi, WJ-Crack Length (in)

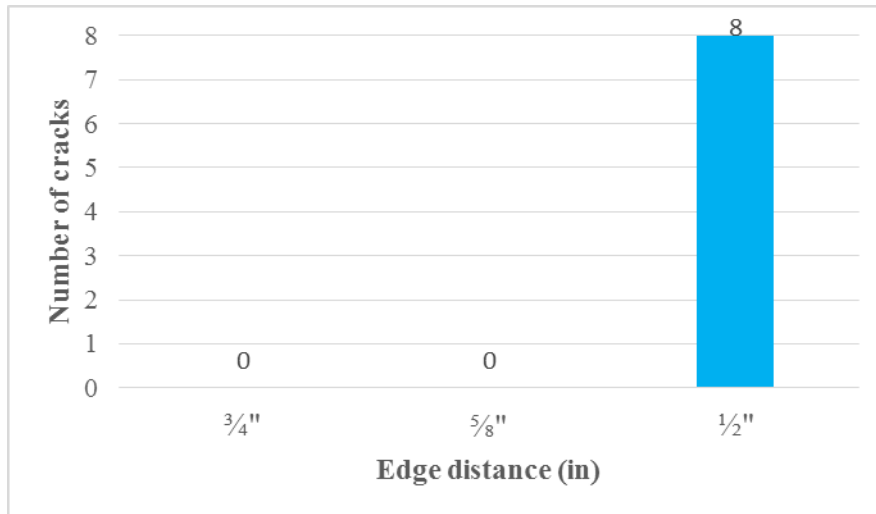


Figure 10-164: Mix#2, 4500 psi, WJ-Number of Cracks

WJ-Release Strength 6000 psi

With increase in the release strength from 4500 psi to 6000 psi, WJ wire indicated worse behavior in resulting two cracks on the prism with a $\frac{3}{4}$ in. the edge distance, seven cracks on a $\frac{5}{8}$ in. edge distance prism and eight cracks on the prism with a $\frac{1}{2}$ in. the edge distance. Since the results for 6000 psi release strength of concrete indicated worse behavior than with 4500 psi release concrete strength, WJ wire with 6000 psi was performed one more time. This second testing indicated improved wire performance, but still WJ wire with release strength 4500 psi performed better. In the second testing there was one crack on the prism having $\frac{3}{4}$ in. the edge distance, three cracks on $\frac{5}{8}$ in. and eight cracks on the prism having $\frac{1}{2}$ in. the edge distance. The values of transfer lengths were shorter with 6000 psi release concrete strength. The following charts present the longitudinal strain profiles for each testing, crack area, crack length and number of cracks for each prism.

Figure 10-165 shows the longitudinal strain profile along with the values of transfer lengths for the prism with a $\frac{3}{4}$ in. thickness of the edge distance.

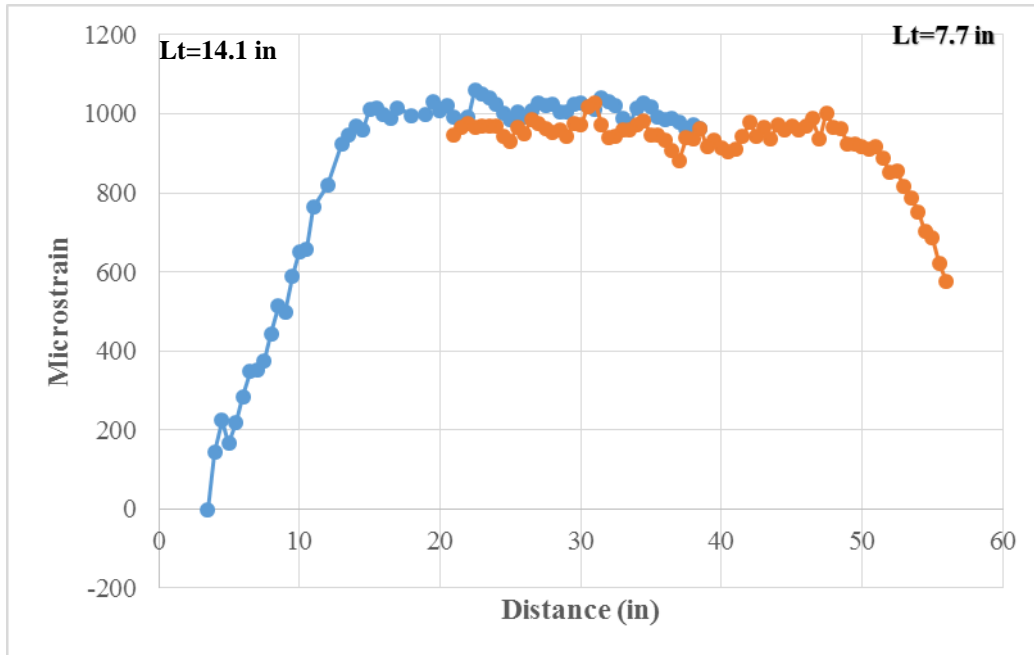


Figure 10-165: Mix#2, 6000 psi, WJ, $\frac{3}{4}$ in. Edge Distance-Longitudinal Strain Profile

The value of transfer length on the live end was 14.1 in. results from the large magnitudes of longitudinal surface strain that accompany with two cracks on the prism.

Figure 10-166 and Figure 10-167 show observed cracking on the dead and live end.



Figure 10-166: Mix#2, 6000 psi, WJ-Observed Cracking (Dead End)

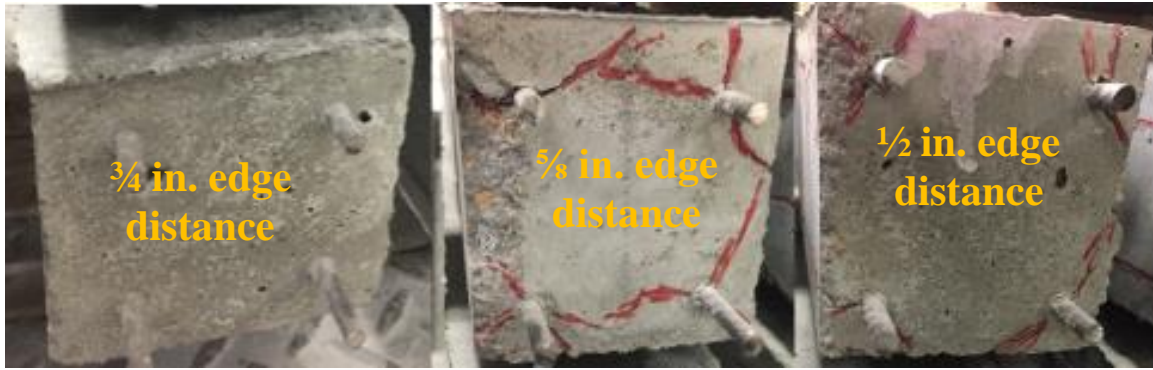


Figure 10-167: Mix#2, 6000 psi, WJ-Observed Cracking (Live End)

Figure 10-168, Figure 10-169 and Figure 10-170 present the crack area, crack length and number of cracks as a function of the edge distance for these three prisms. The results indicated that with the higher release of concrete strength the more cracks appeared. After approximately three months this test was repeated with the same release strength of 6000 psi.

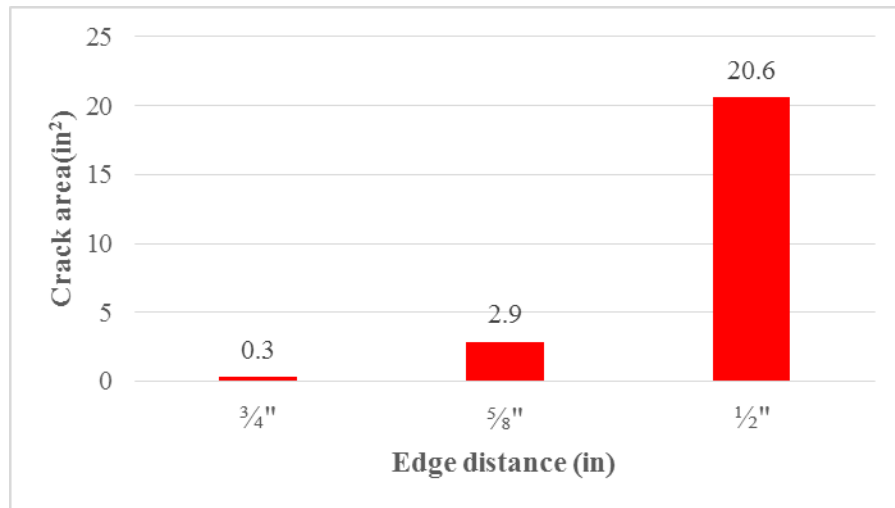


Figure 10-168: Mix#2, 6000 psi, WJ-Crack Area (in²)

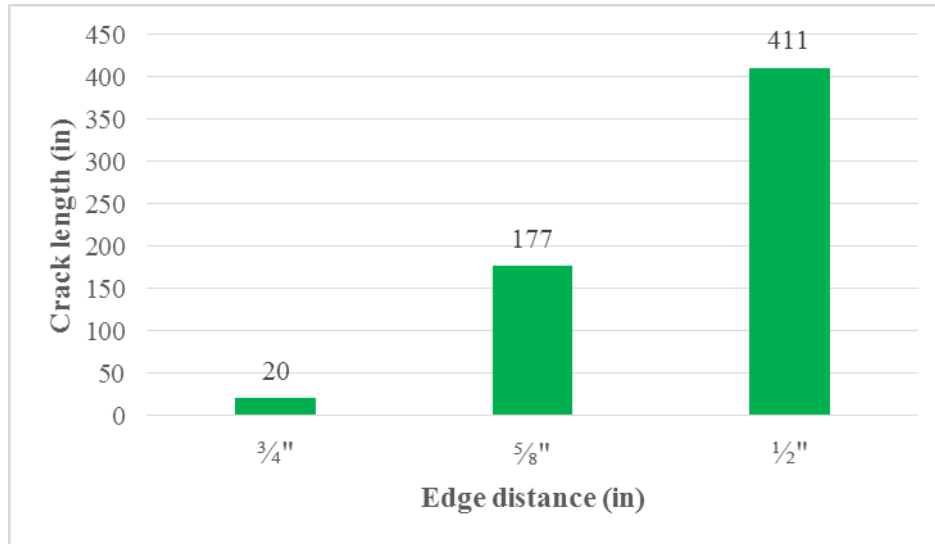


Figure 10-169: Mix#2, 6000 psi, WJ-Crack Length (in)

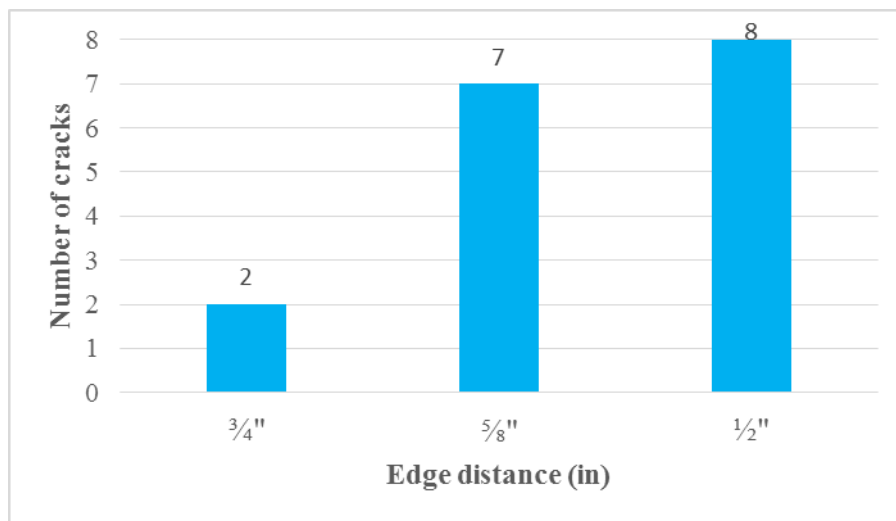


Figure 10-170: Mix#2, 6000 psi, WJ-Number of Cracks

WJ-Release Strength 6000 psi (Second Time)

Figure 10-171 shows the longitudinal strain profile along with values of transfer lengths. The approximate value of transfer length was approximately 6.5 in. One crack appeared on the live end after two months due to the sustained lateral stresses, on the prism with a $\frac{3}{4}$ in. the edge distance. Transfer lengths were determined after de-tensioning procedure when no cracks appeared on this prism.

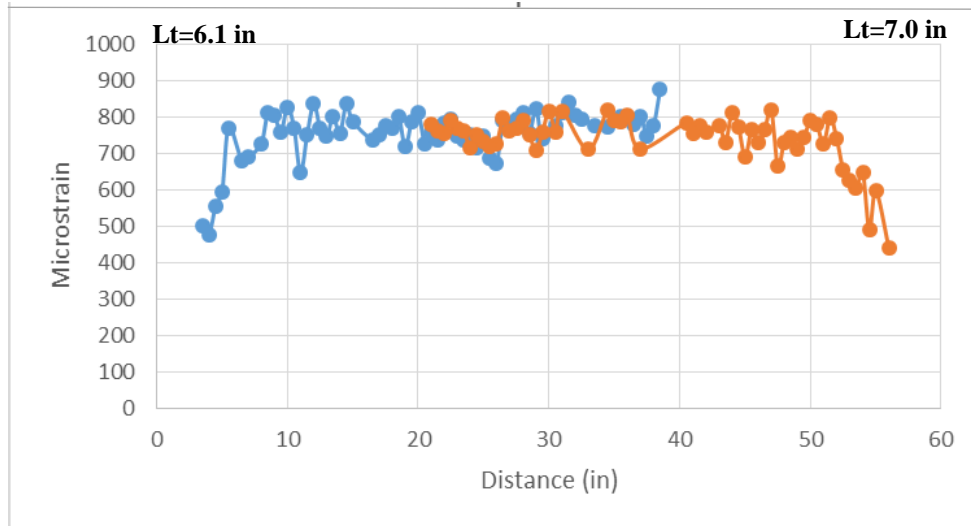


Figure 10-171: Mix#2, 6000 psi, WJ second time, $\frac{3}{4}$ in. Edge Distance-Longitudinal Strain Profile

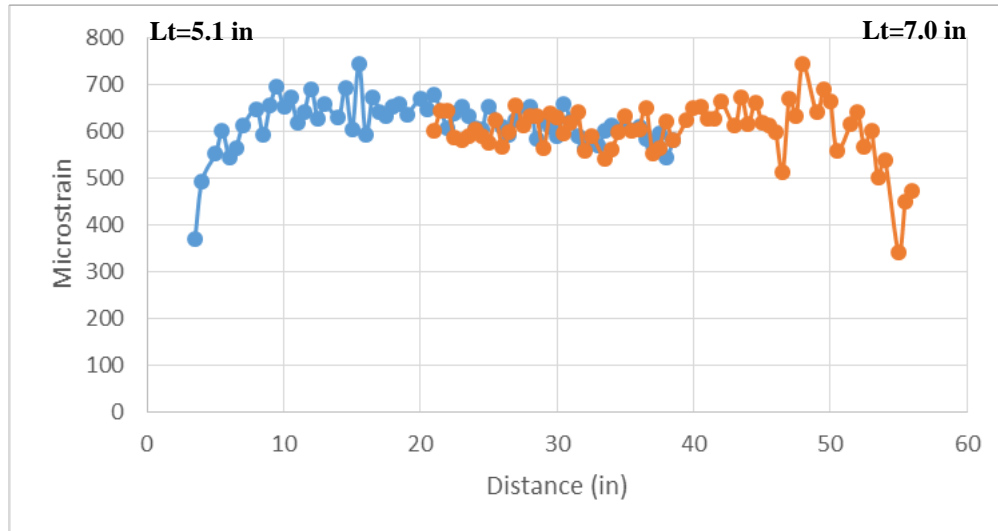


Figure 10-172: Mix#2, 6000 psi, WJ second time, $\frac{5}{8}$ in. Edge Distance-Longitudinal Strain Profile

Figure 10-172 shows the longitudinal strain profile for prism with $\frac{5}{8}$ in. the edge distance. The values of transfer lengths were 5.1 in. and 7.0 in. respectively. At the time of de-tensioning procedure there were no visible cracks on the surface of this prism and after approximately two months three cracks appeared. Average crack width was approximately 0.01 in. and the average crack length was approximately 6 in. For prism with $\frac{1}{2}$ in. edge distance spalling occurred on the dead end, on front and bottom side of the prism, in approximately 20 in. length. For spalling arbitrary value of crack width was 0.2 in.

Figure 10-173, Figure 10-174, and Figure 10-175 show crack area, crack length and number of cracks as a function of edge distance, respectively.

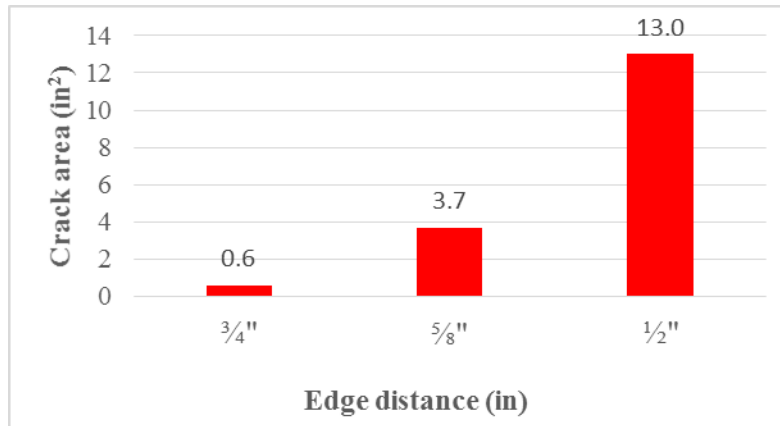


Figure 10-173: Mix#2, 6000 psi, WJ second time-Crack Area (in²)

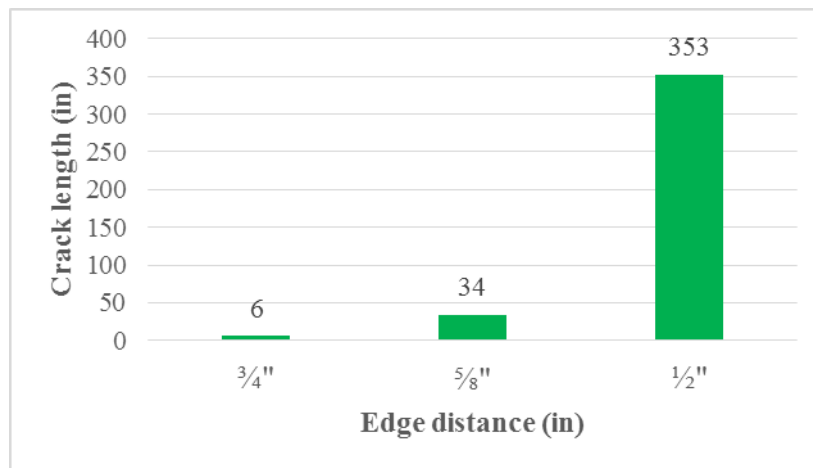


Figure 10-174: Mix#2, 6000 psi, WJ second time-Crack Length (in)

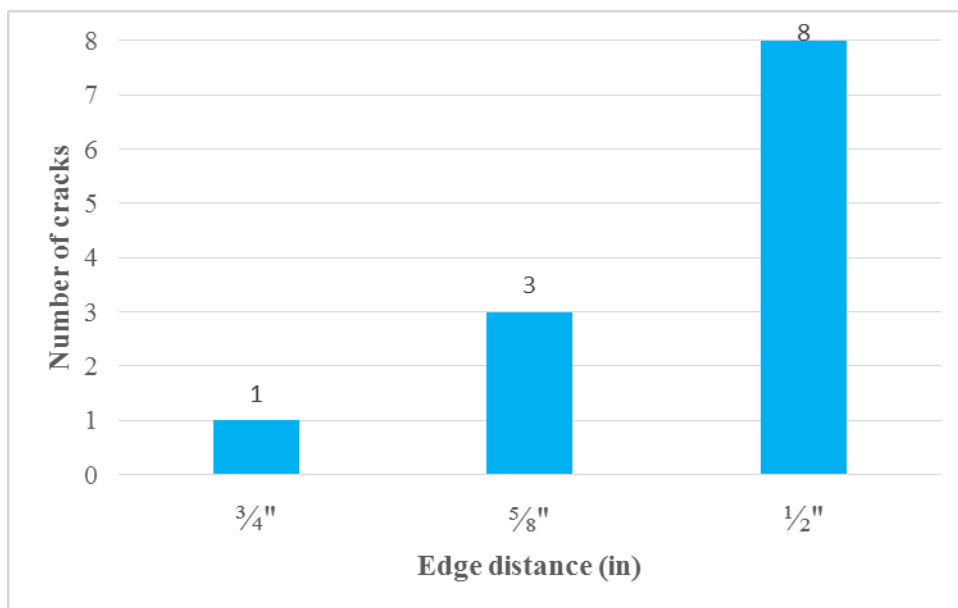


Figure 10-175: Mix#2, 6000 psi, WJ second time-Number of Cracks

Mix#2-WM wire type

WM-Release Strength 4500 psi

WM wire with release strength of 4500 psi performed very well with no cracks on the first prism. Three cracks were observed on the second prism and six cracks on the third prism. After de-tensioning procedure there was only one crack on the second prism but during the time of three months the number of cracks increased to three. Figure 10-176 and Figure 10-177 present the longitudinal strain profiles for first two prisms along with the values of transfer lengths.

Figure 10-178 and Figure 10-179 show observed cracking on the dead and live end. Average crack width for the prism with a $\frac{5}{8}$ in. edge distance was approximately 0.013 in. and the average crack length was approximately 4 in. Two cracks appeared on the live end of the prism and one of the dead-end with 0.01 in. crack width and 4 in. crack length on the prism with a $\frac{5}{8}$ in. the edge distance. The average crack width for prism with $\frac{1}{2}$ in. edge distance was approximately 0.02 in. and the average crack length was approximately 13 in.

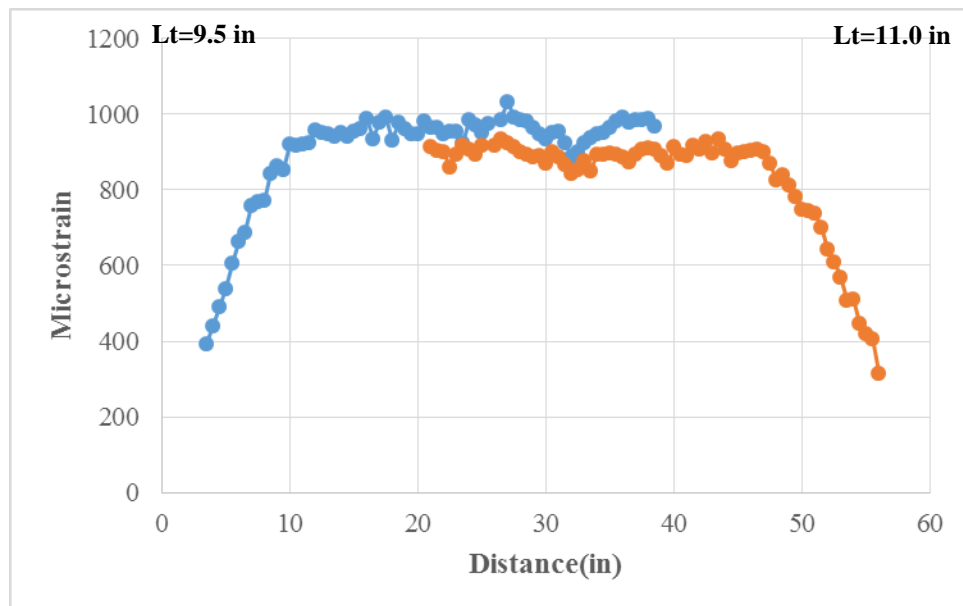


Figure 10-176: Mix#2, 4500 psi, WM, $\frac{3}{4}$ in. Edge Distance-Longitudinal Strain Profile

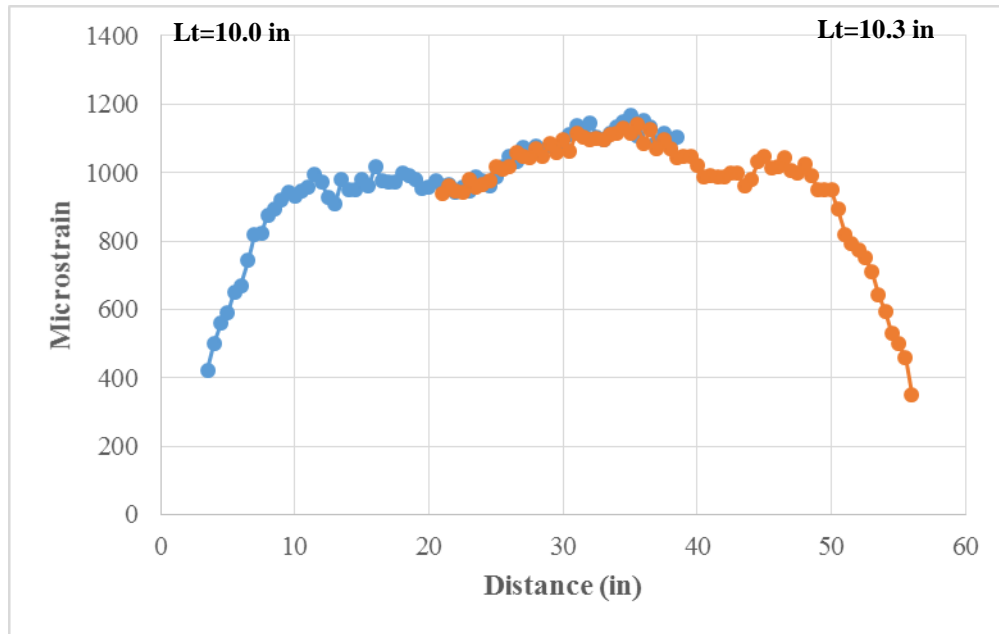


Figure 10-177: Mix#2, 4500 psi, WM, $\frac{5}{8}$ in. Edge Distance-Longitudinal Strain Profile

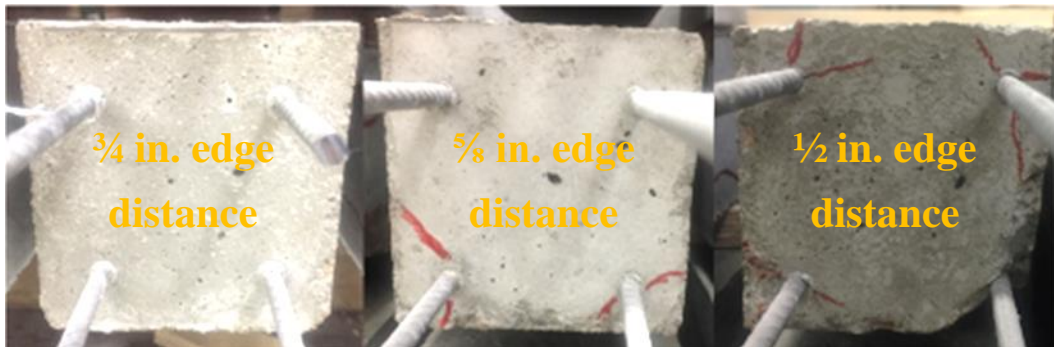


Figure 10-178: Mix#2, 4500 psi, WM-Observed Cracking (Dead End)



Figure 10-179: Mix#2, 4500 psi, WM-Observed Cracking (Live End)

Values of crack areas for prisms with $\frac{5}{8}$ in. and $\frac{1}{2}$ in. edge distances were small 0.2 in^2 and 2.8 in^2 respectively as shown in Figure 10-180. Figure 10-181 and Figure 10-182 show crack length and number of cracks as a function of edge distance, respectively.

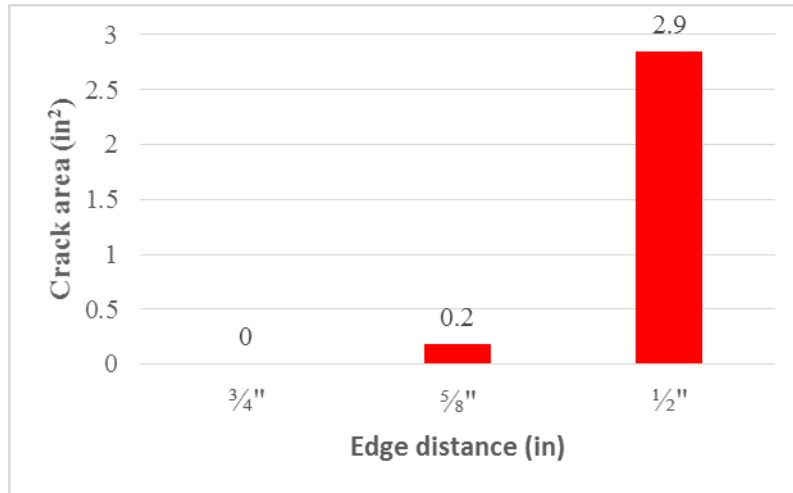


Figure 10-180: Mix#2, 4500 psi, WM-Crack Area (in²)

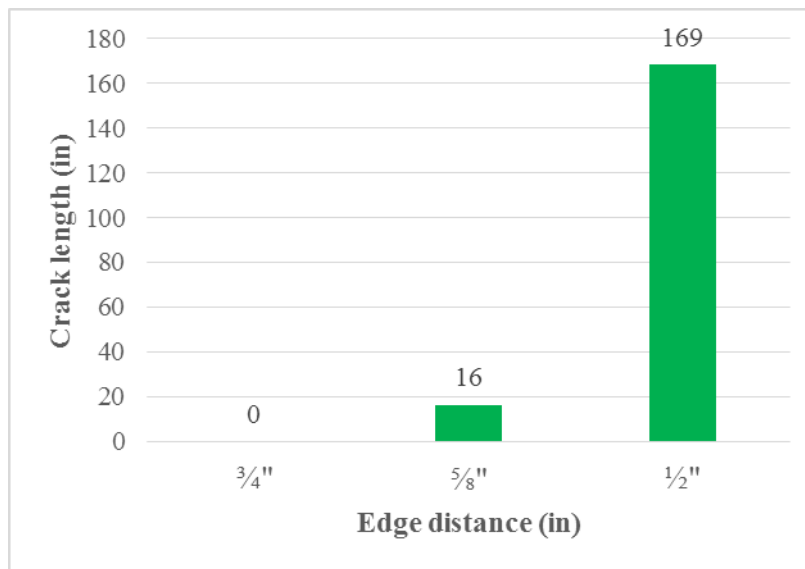


Figure 10-181: Mix#2, 4500 psi, WM-Crack Length

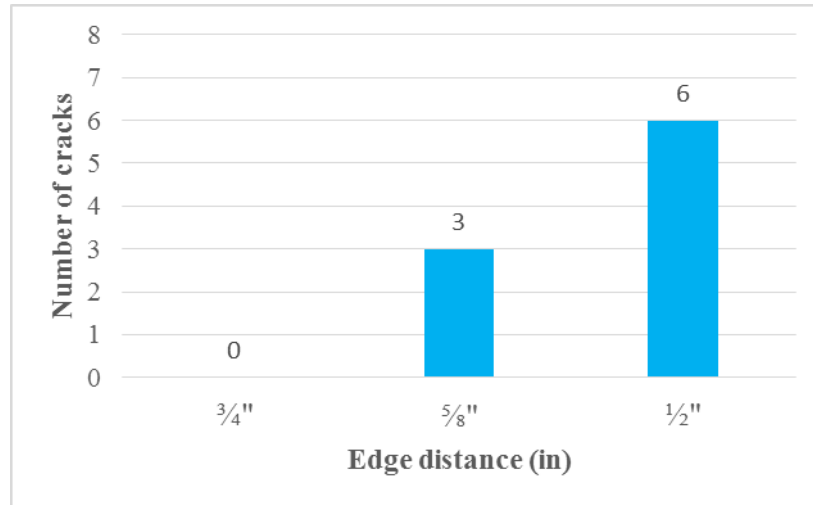


Figure 10-182: Mix#2, 4500 psi, WM-Number of Cracks

WM-Release Strength 6000 psi

The longitudinal strain profile indicated bilinear performance with average values of transfer lengths 8.2 in for the prism with a $\frac{3}{4}$ in. edge distance and 7.7 in. for the prism with a $\frac{5}{8}$ in. the edge distance. Figure 10-183 and Figure 10-184 present the longitudinal strain profiles for the first two prisms in series.

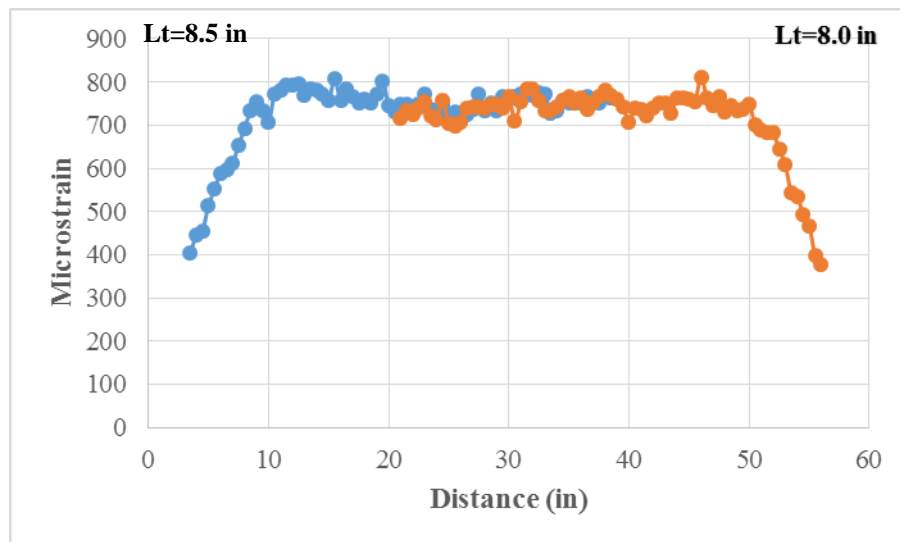


Figure 10-183: Mix#2, 6000 psi, WM, $\frac{3}{4}$ in. Edge Distance-Longitudinal Strain Profile

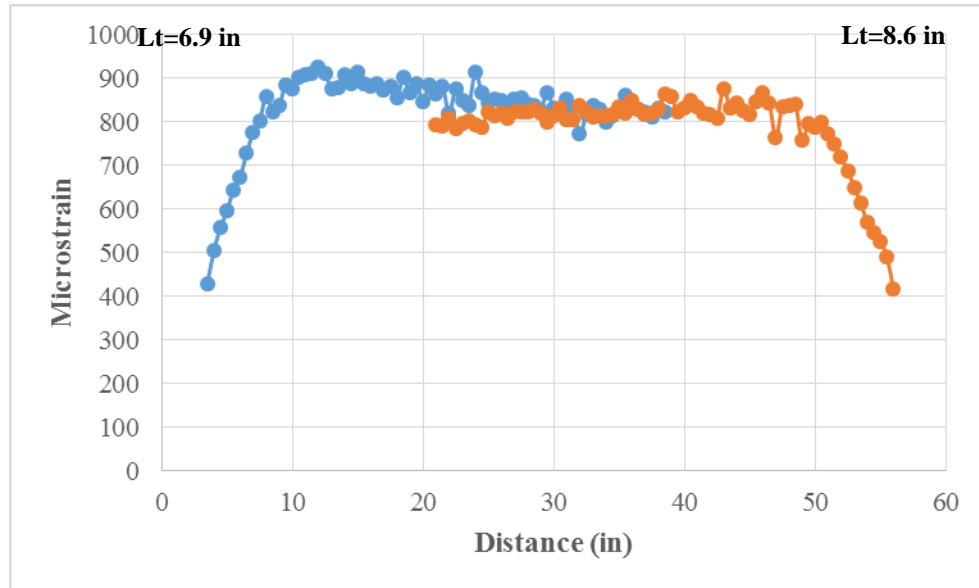


Figure 10-184: Mix#2, 6000 psi, WM, $\frac{5}{8}$ in. Edge Distance-Longitudinal Strain Profile

WM with release strength 6000 psi and granite concrete mixture performed very well in results no cracking appearance at the $\frac{3}{4}$ in. edge distance and one crack on the live end on the prism with $\frac{5}{8}$ in. edge distance (Figure 10-185 and Figure 10-186). Crack width was 0.01 in. and the total length of the cracks was 0.6 in. on the live end. On the dead end of the prism there were no visible cracks around the wire, but one crack appeared on the side of the prism in the length of 3 in. and crack width 0.01 in. The third prism in the series indicated poor performance. Spalling occurred on the live end with a maximum length of 30 in. and four cracks on the dead end with a maximum width of the crack 0.07 in. and maximum crack length of 16 in.



Figure 10-185: Mix#2, 6000 psi, WM-Observed Cracking (Dead End)

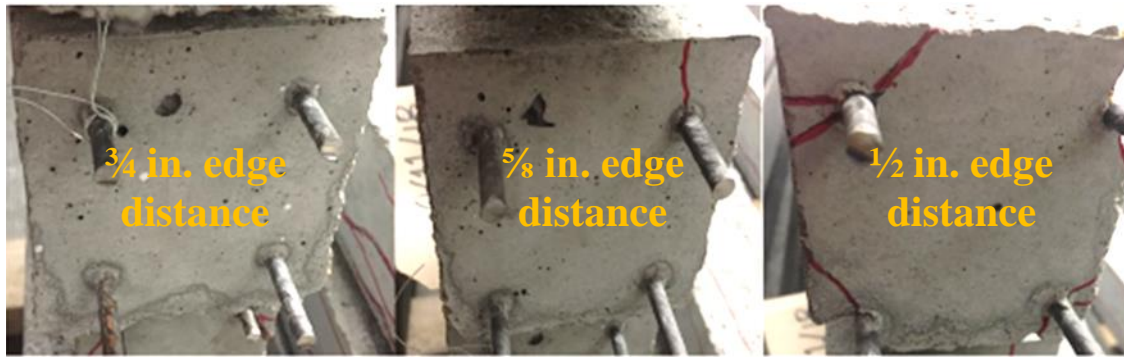


Figure 10-186: Mix#2, 6000 psi, WM-Observed Cracking (Live End)

Figure 10-187, Figure 10-188, and Figure 10-189 present crack area, crack length and number of cracks as a function of edge distance, respectively.

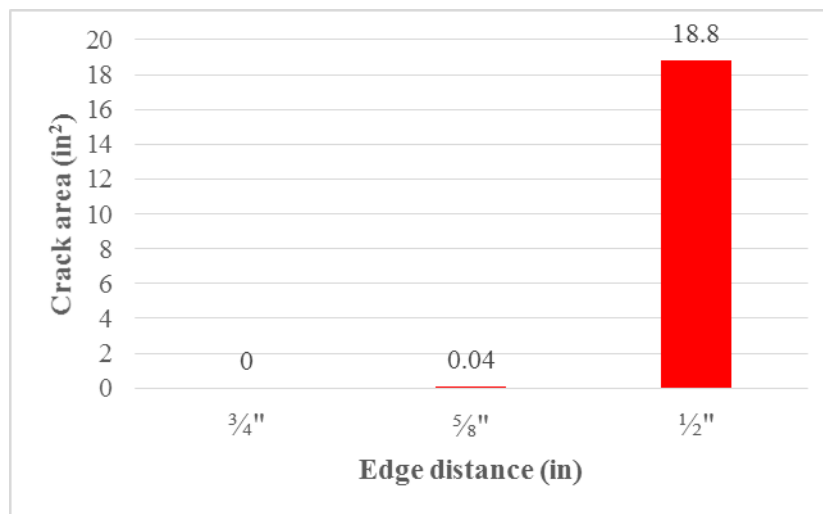


Figure 10-187: Mix#2, 6000 psi, WM-Crack Area (in²)

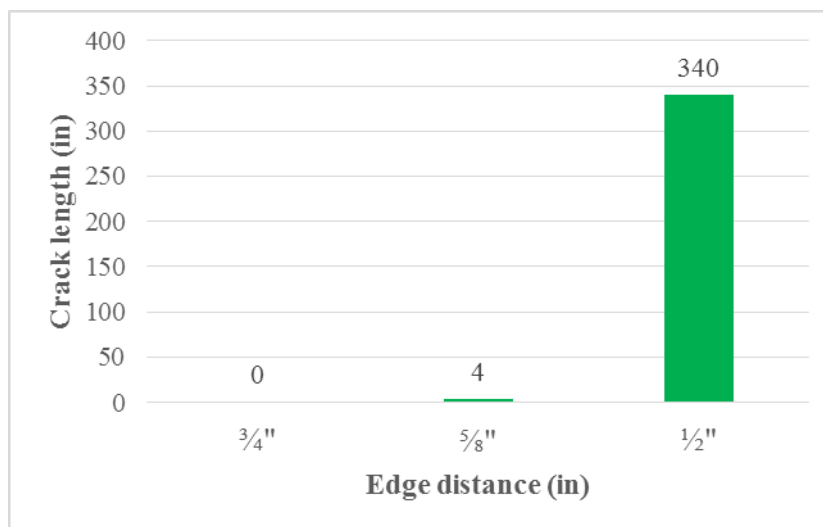


Figure 10-188: Mix#2, 6000 psi, WM-Crack Length (in)

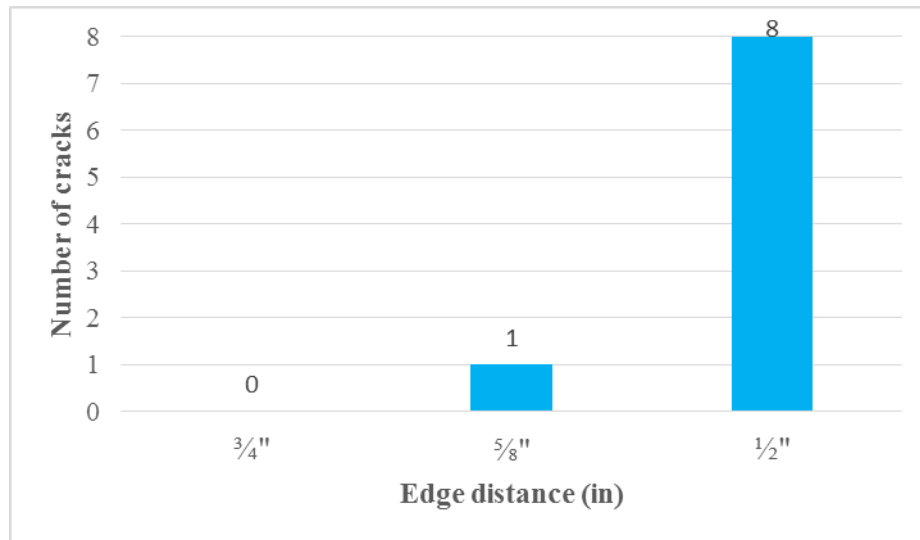


Figure 10-189: Mix#2, 6000 psi, WM-Number of Cracks

Mix#2-WP wire type

WP-Release Strength 4500 psi

WP wire performed better with the concrete mixture using granite as aggregate. No visible cracks on the prism with $\frac{3}{4}$ in. edge distance, four on $\frac{5}{8}$ in. and eight on the $\frac{1}{2}$ in. edge distance. Figure 10-190 and Figure 10-191 show the longitudinal strain profiles for the first two prisms with the values of transfer lengths on both the sides of the prism. The average value of transfer length was approximately 8.0 in.

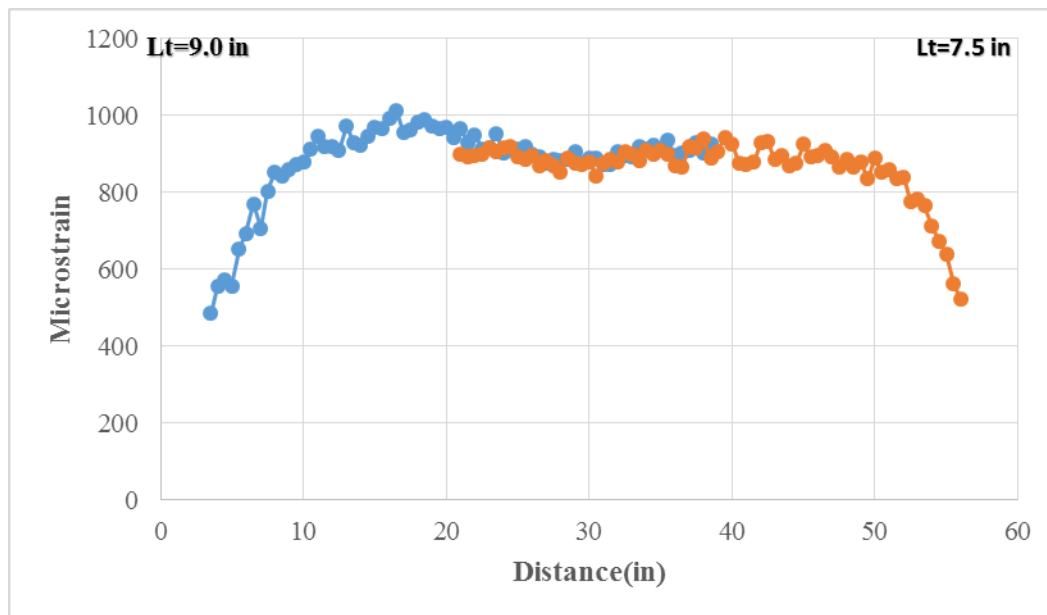


Figure 10-190: Mix#2, 4500 psi, WP, $\frac{3}{4}$ in. Edge Distance-Longitudinal Strain Profile

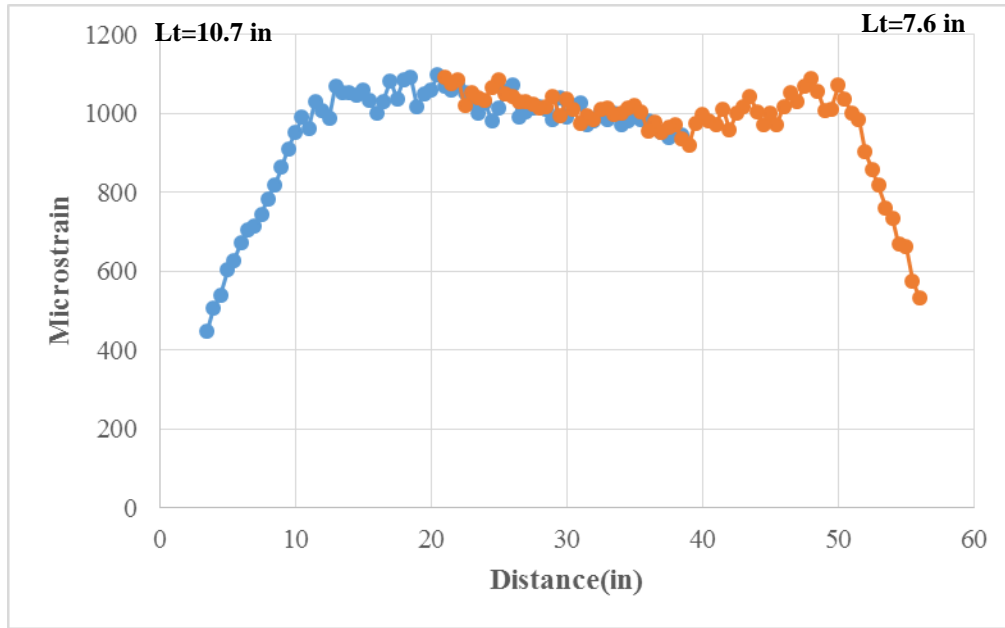


Figure 10-191: Mix#2, 4500 psi, WP, $\frac{5}{8}$ in. Edge Distance-Longitudinal Strain Profile

Figure 10-192 and Figure 10-193 show observed cracking for the dead and live end. The average crack width for the prism with a $\frac{5}{8}$ in. edge distance was 0.01 in. and the average crack length was 6 in. Prism with $\frac{1}{2}$ in. thickness had spalling on the dead end of the prism in length of 33 in. on the front and bottom side of the prism.

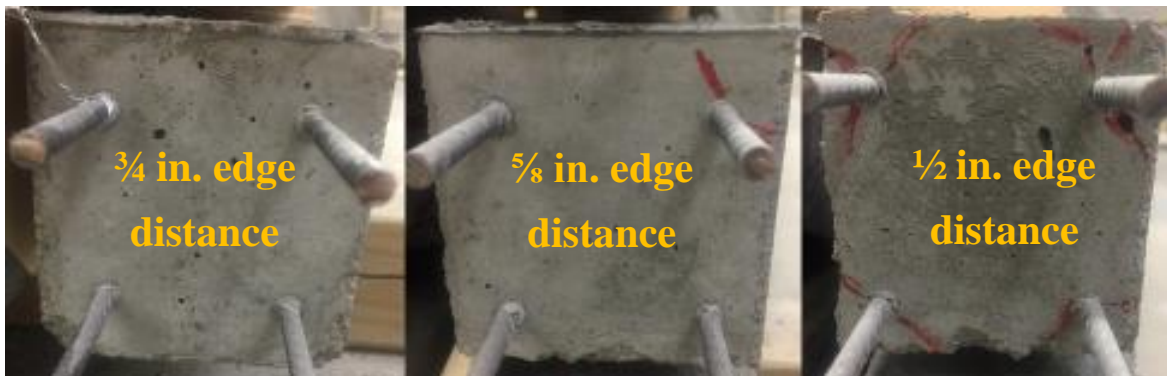


Figure 10-192: Mix#2, 4500 psi, WP-Observed Cracking (Dead End)



Figure 10-193: Mix#2, 4500 psi, WP-Observed Cracking (Live End)

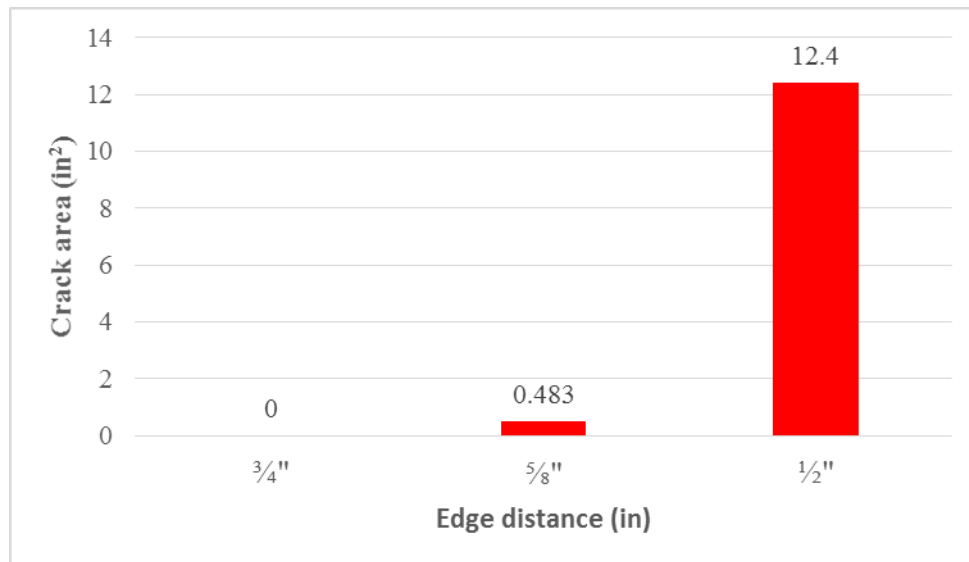


Figure 10-194: Mix#2, 4500 psi, WP-Crack Area (in²)

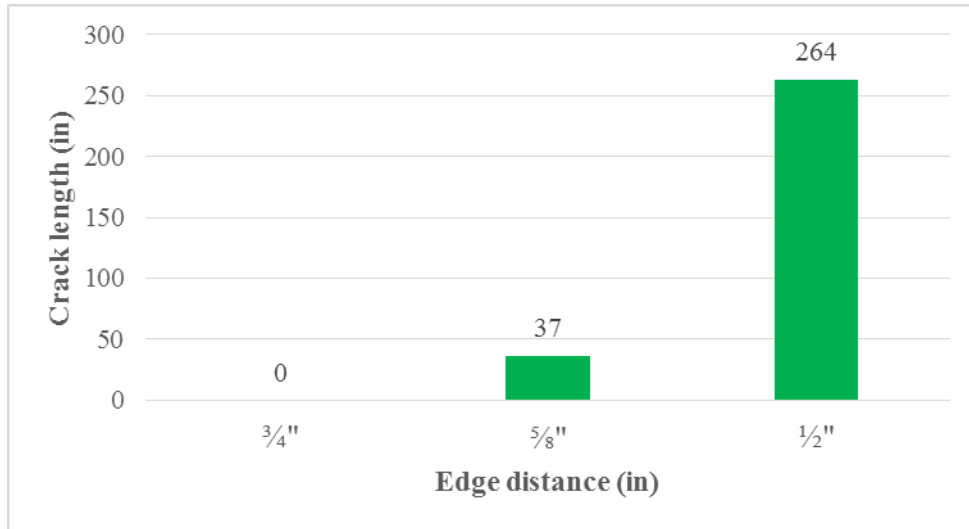


Figure 10-195: Mix#2, 4500 psi, WP-Crack Length (in)

Figure 10-194 and Figure 10-195 show the crack area and crack length for the prisms done with WP wire. WP wire performed very well with the larger value of the edge distance, and the number of cracks increased with $\frac{5}{8}$ in. and $\frac{1}{2}$ in. edge distances from four to eight cracks as shown in Figure 10-196. The value of the crack area for the prism with $\frac{5}{8}$ in. was not large, which indicates that the width of crack was small and crack lengths were short.

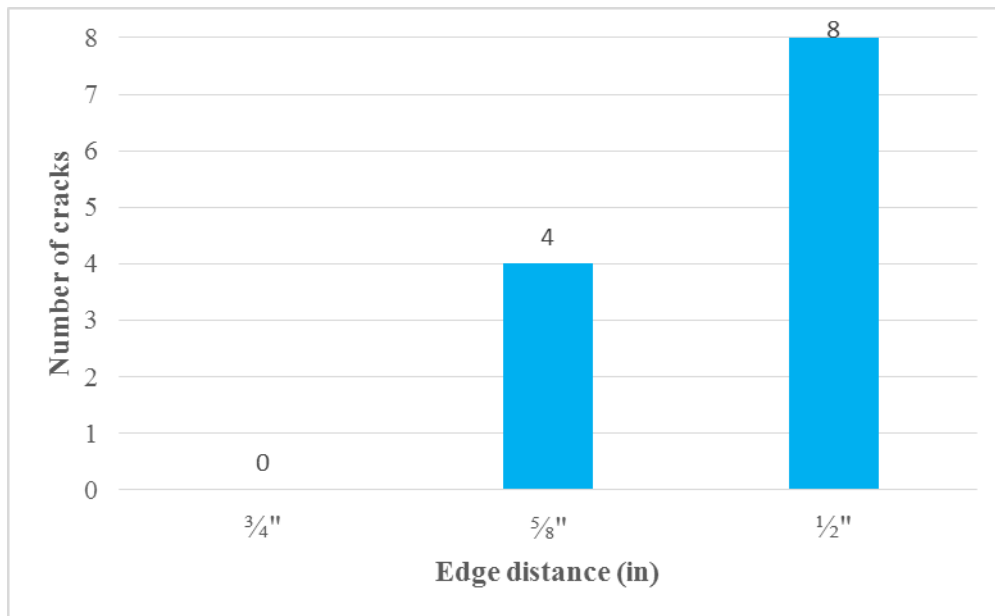


Figure 10-196: Mix#2, 4500 psi, WP-Number of Cracks

WP-Release Strength 6000 psi

WP wire performed poorly with granite mixture on 6000 psi release strength of concrete. Figure 10-197 shows longitudinal strain profile along with the value of transfer lengths. One crack was observed on the dead end of the prism having a $\frac{3}{4}$ in. the edge distance. The average width was 0.01 in. and the maximum crack length was 3 in. Figure 10-197 shows the longitudinal strain

profile along with the values of transfer length, 11.2 in. on the live end and 10.1 in. for the dead end.

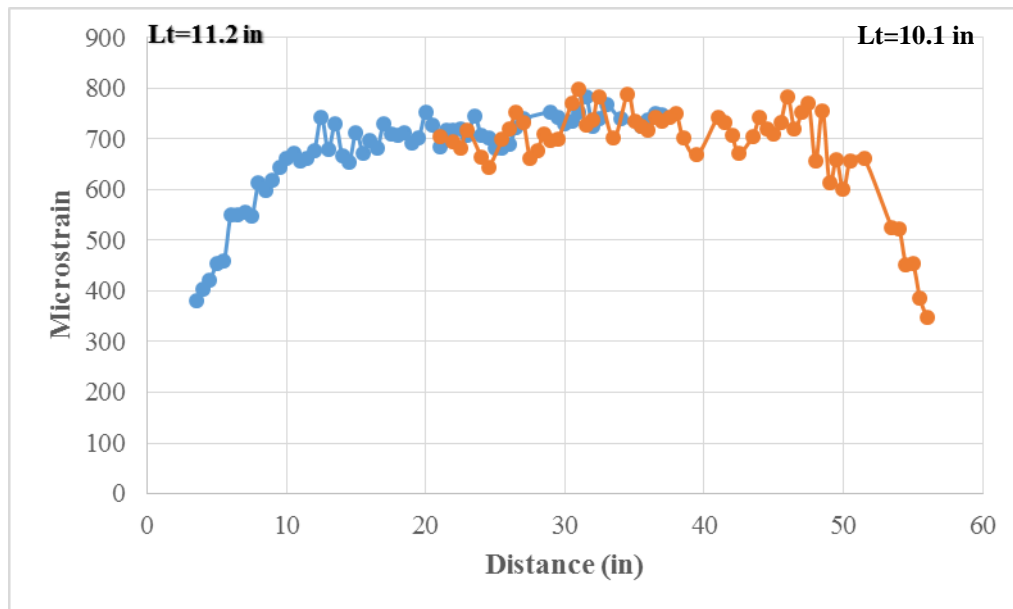


Figure 10-197: Mix#2, 6000 psi, WP, $\frac{3}{4}$ in. Edge Distance-Longitudinal Strain Profile

Figure 10-198 and Figure 10-199 show observed cracking. The second prism in series had one crack on the dead end with maximum crack width of 0.016 in. and maximum crack length of 7 in. and observed spalling on the live end of the prism. Spalling had a length of 10 in. Prism with the thinnest edge distance had poor behavior with spalling on the live end in the maximum length of 27 in. and maximum crack width of 0.02 in. on the dead end and maximum crack length of 28 in. on the live end.



Figure 10-198: Mix#2, 6000 psi, WP-Observed Cracking (Live End)

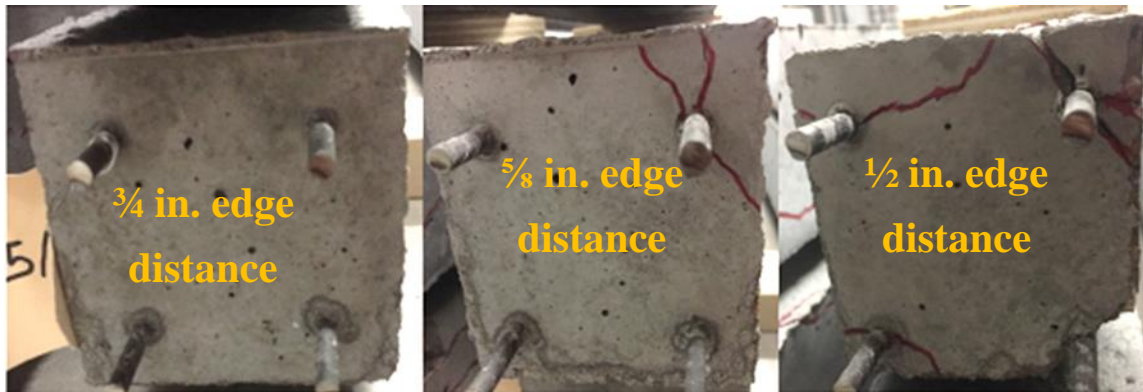


Figure 10-199: Mix#2, 6000 psi, WP-Observed Cracking (Dead End)

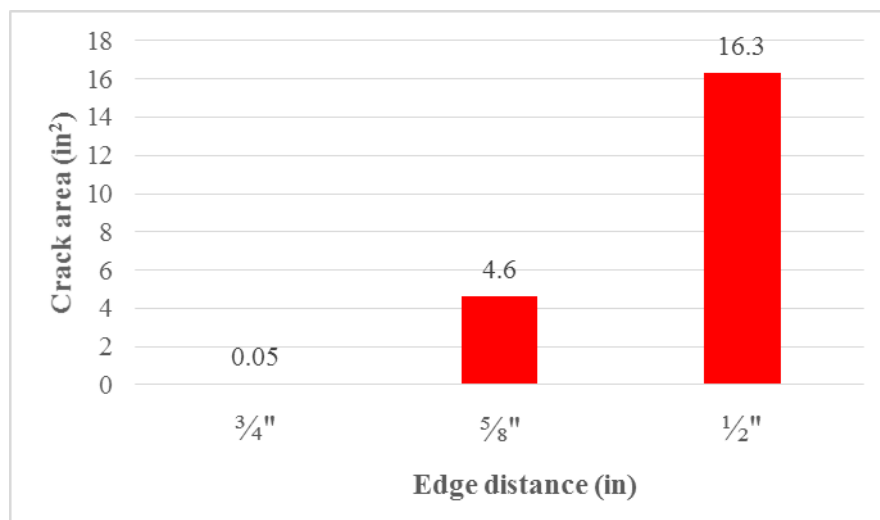


Figure 10-200: Mix#2, 6000 psi, WP-Crack Area (in²)

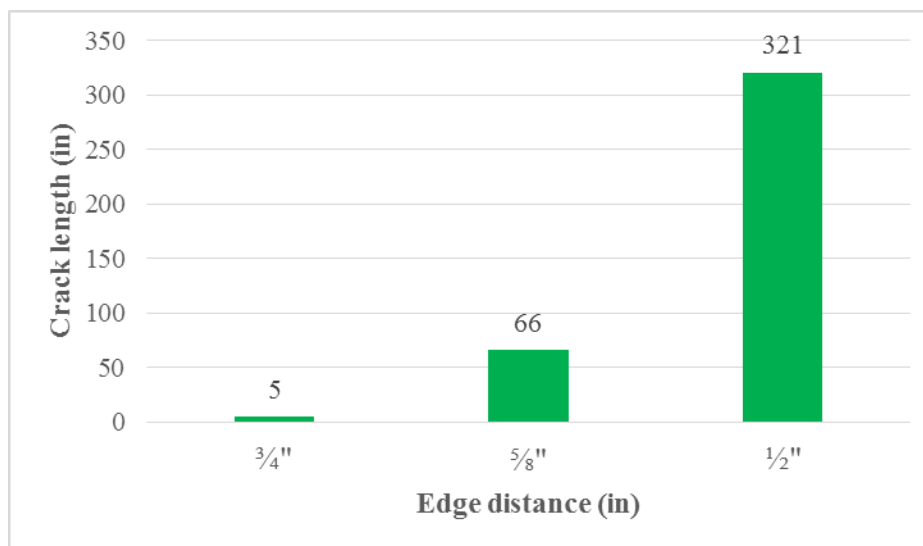


Figure 10-201: Mix#2, 6000 psi, WP-Crack Length (in)

Figure 10-200, Figure 10-201, and Figure 10-202 show crack area, crack length and the number of cracks as a function of edge distance, respectively.

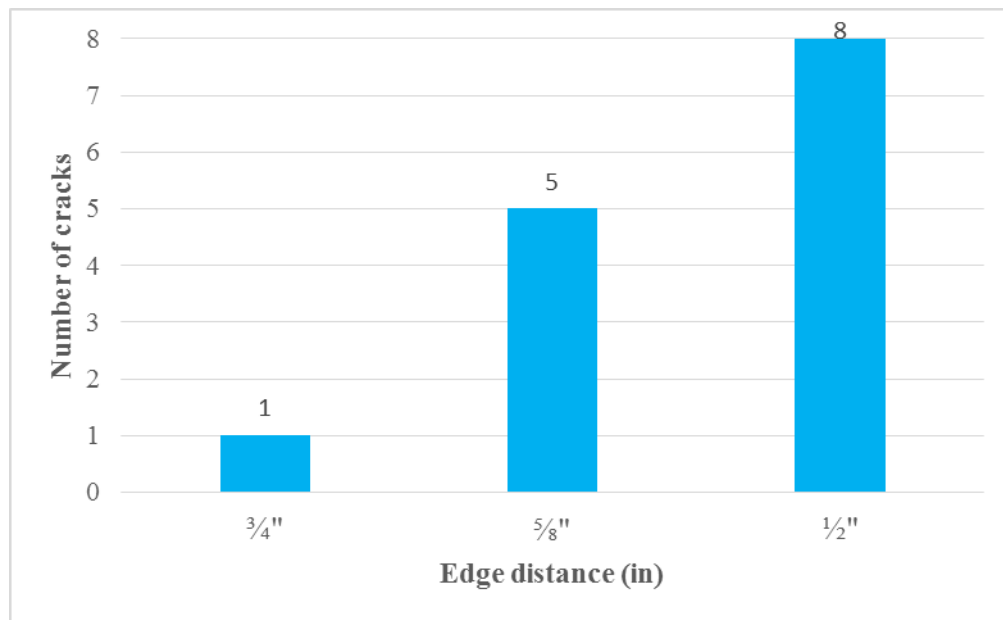


Figure 10-202: Mix#2, 6000 psi, WP-Number of Cracks

Mix#2-WQ wire type

WQ-Release Strength 4500 psi

WQ wire shows very good performance with the concrete mixture using granite as aggregate. Figure 10-203 and Figure 10-204 show the longitudinal strain profiles for the two first prisms along with the values of transfer lengths on both sides of the prism. The values of transfer lengths were approximately 8.5 in.

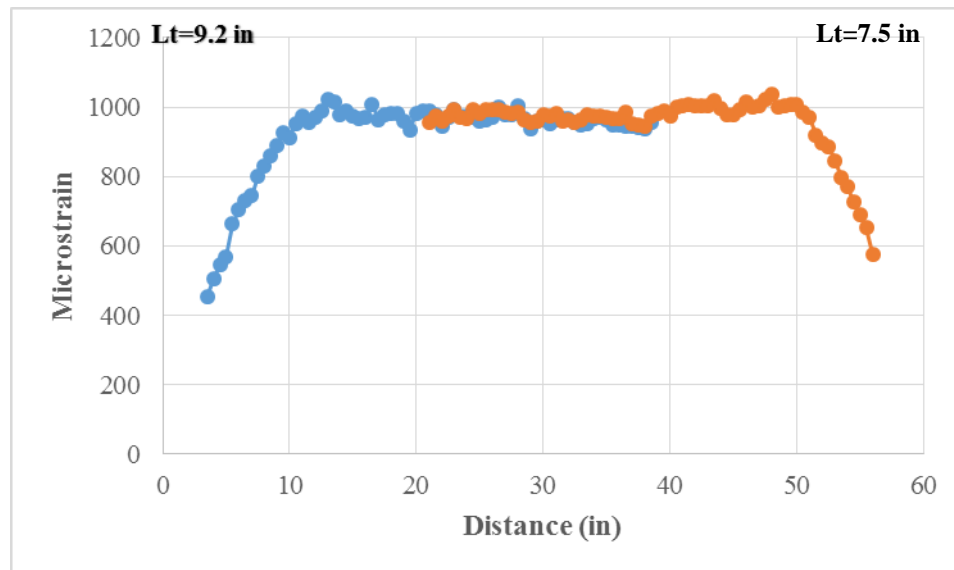


Figure 10-203: Mix#2, 4500 psi, WQ, 3/4 in. Edge Distance-Longitudinal Strain Profile

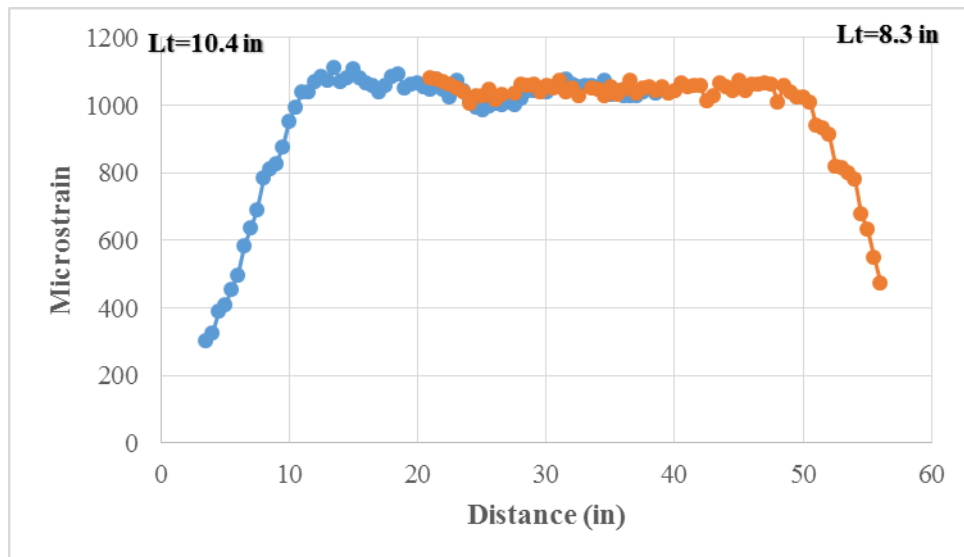


Figure 10-204: Mix#2, 4500 psi, WQ, 5/8 in. Edge Distance-Longitudinal Strain Profile

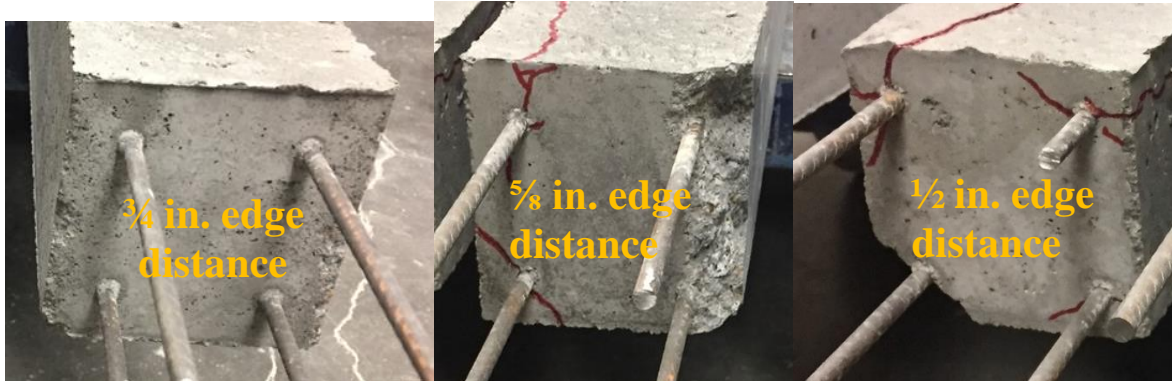


Figure 10-205: Mix#2, 4500 psi, WQ-Observed Cracking (Live End)

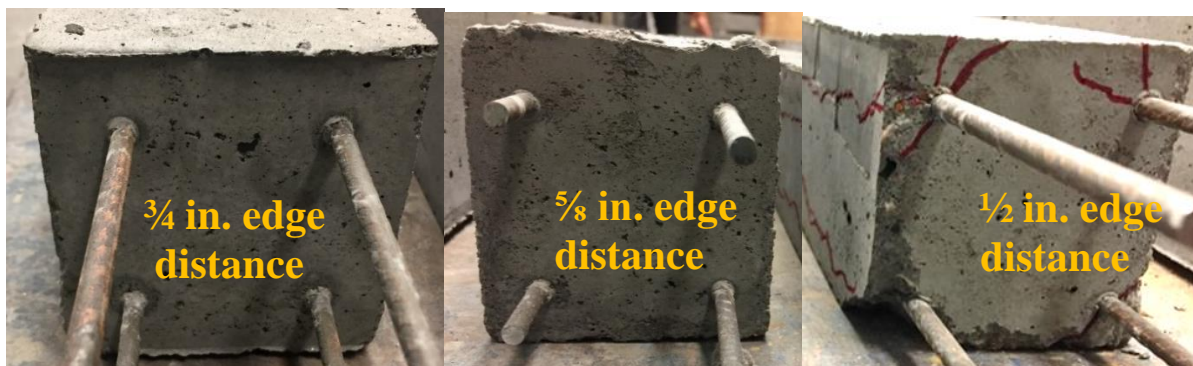


Figure 10-206: Mix#2, 4500 psi, WQ-Observed Cracking (Dead End)

Figure 10-205 and Figure 10-206 show observed cracking on each side of the prisms. Prism with a $\frac{3}{4}$ in. edge distance performed very well with no crack appearance, two cracks were observed on the $\frac{5}{8}$ in. edge distance and seven cracks on the third prism in series.

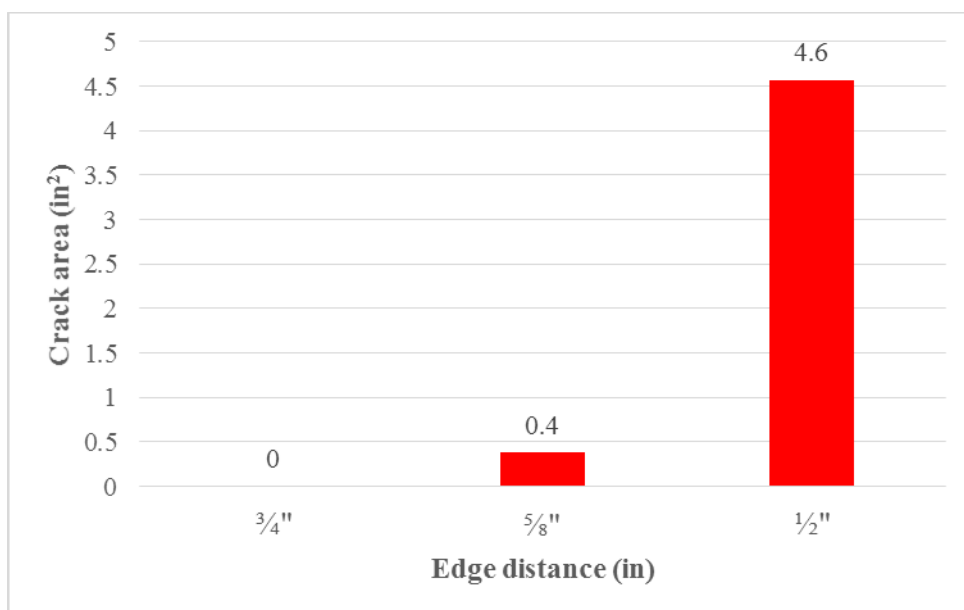


Figure 10-207: Mix#2, 4500 psi, WQ-Crack Area (in²)

According to Figure 10-207 with reducing the cover crack area increased from zero to 0.38 in^2 for the prism having $\frac{5}{8}$ in. edge distance and 4.57 in^2 for the prism having $\frac{1}{2}$ in. edge distance. Figure 10-208 shows the values of crack lengths which increased with decreasing the edge distance from zero for prism having $\frac{3}{4}$ in. edge distance to 27 in. for the prism having $\frac{5}{8}$ in. edge distance and 220 in. for the prism having $\frac{1}{2}$ in. thickness of the edge distance. Figure 10-209 shows the number of cracks as a function of edge distance.

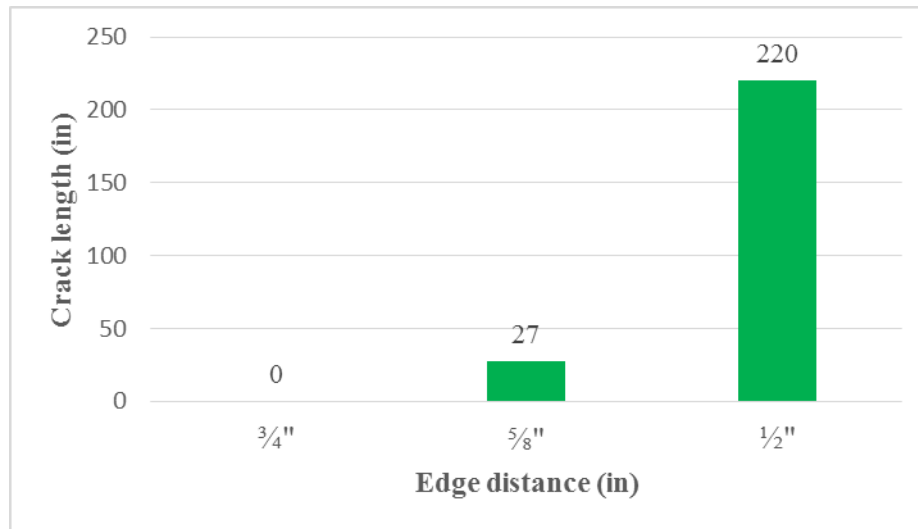


Figure 10-208: Mix#2, 4500 psi, WQ-Crack Length (in)

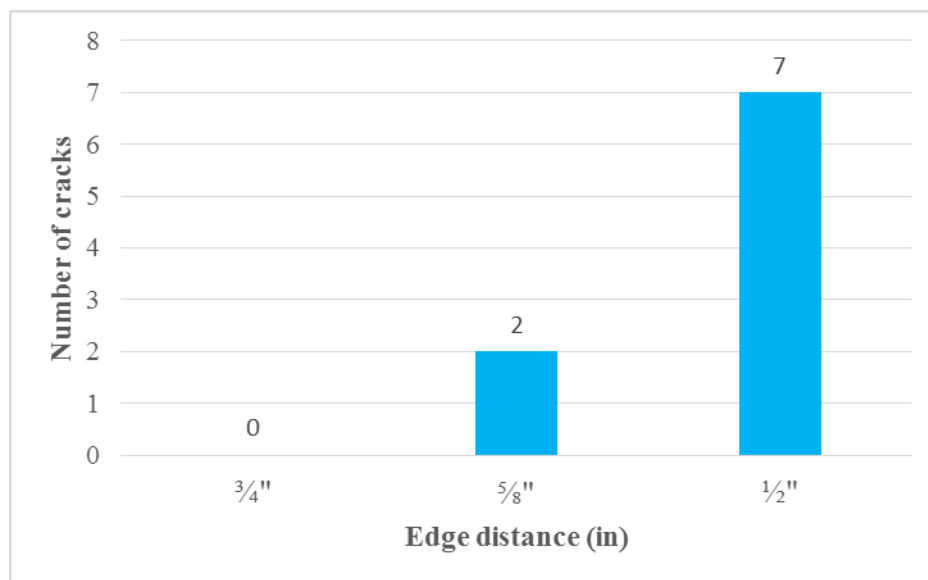


Figure 10-209: Mix#2, 4500 psi, WQ-Number of Cracks

WQ-Release Strength 6000 psi

Figure 10-210 and Figure 10-211 show the longitudinal strain profiles for the prisms with a $\frac{3}{4}$ in. edge distance and $\frac{5}{8}$ in. edge distance along with the values of transfer lengths. Transfer lengths were shorter in comparison with the mixture using crushed gravel as aggregate, and the average value of transfer length was approximately 8.5 in.

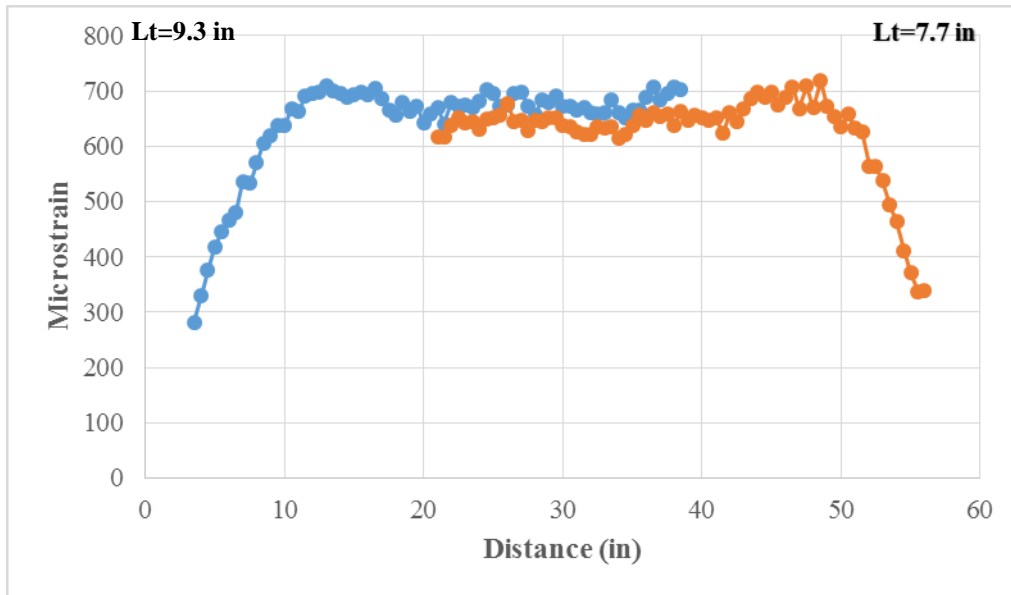


Figure 10-210: Mix#2, 6000 psi, WQ, $\frac{3}{4}$ in. Edge Distance-Longitudinal Strain Profile

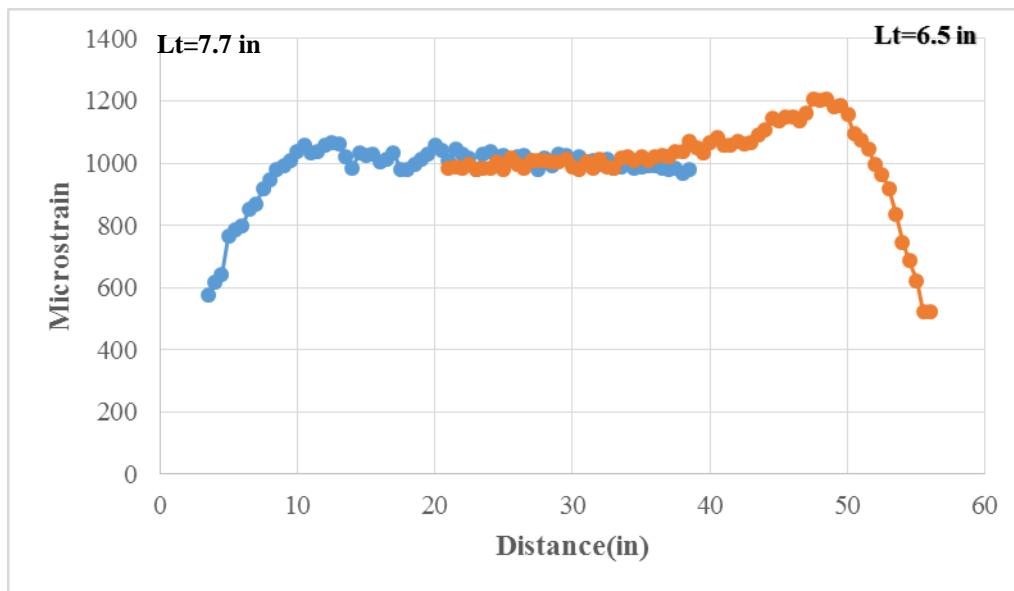


Figure 10-211: Mix#2, 6000 psi, WQ, $\frac{5}{8}$ in. Edge Distance-Longitudinal Strain Profile

Figure 10-212 and Figure 10-213 show observed cracking on the dead and live end of the prism. The first prism in series did not have any visible surface cracks on both the sides of the prism. Prism with a $\frac{5}{8}$ in. edge distance had one crack on the live end, with crack width of 0.01 in. and crack length of 0.4 in. There were no visible surface cracks on the dead end. Prism with a $\frac{1}{2}$ in. edge distance indicated poor performance. Spalling was observed on the live end in the maximum length of 34 in, and four cracks on the dead end. The maximum crack width on the dead end was 0.03 in. and the maximum crack length was 22 in.

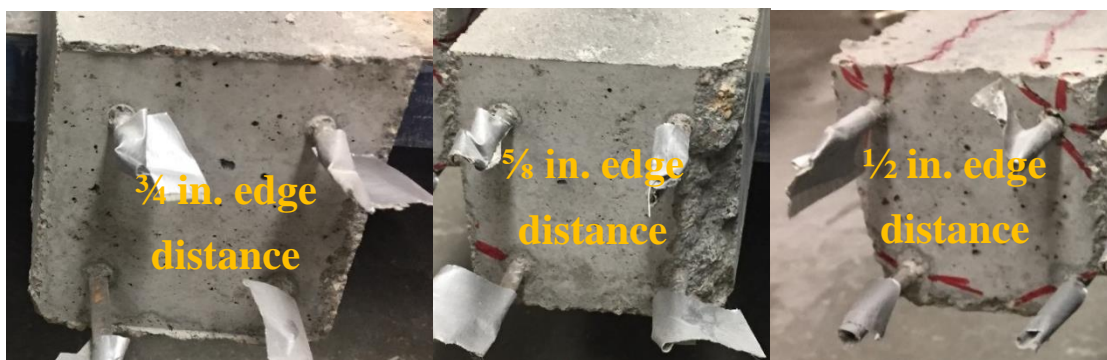


Figure 10-212: Mix#2, 6000 psi, WQ-Observed Cracking (Live End)



Figure 10-213: Mix#2, 6000 psi, WQ-Observed Cracking (Dead End)

WQ wire type performed very well with release strength of 6000 psi. The crack area had a value of 0.004 in² for the prism with a 5/8 in. the edge distance and with the values of transfer lengths approximately 8.5 in. for the prism having 3/4 in. the edge distance as shown in Figure 10-214. Figure 10-215 and Figure 10-216 show crack length and number of cracks as a function of edge distance, respectively.

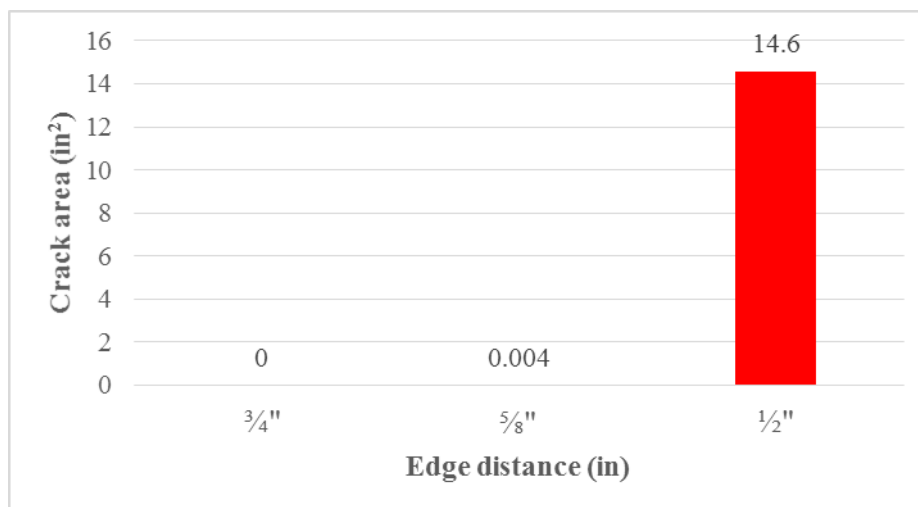


Figure 10-214: Mix#2, 6000 psi, WQ-Crack Area (in²)

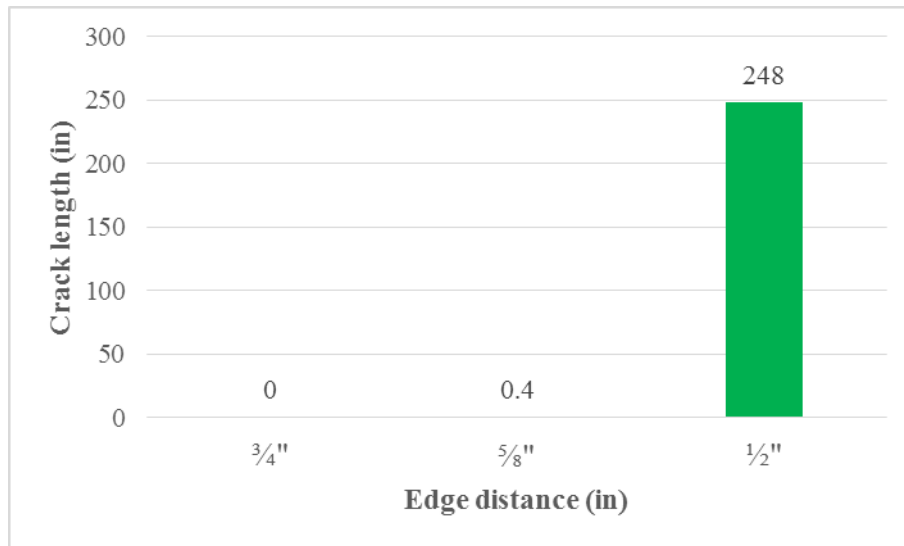


Figure 10-215: Mix#2, 6000 psi, WQ-Crack Length (in)

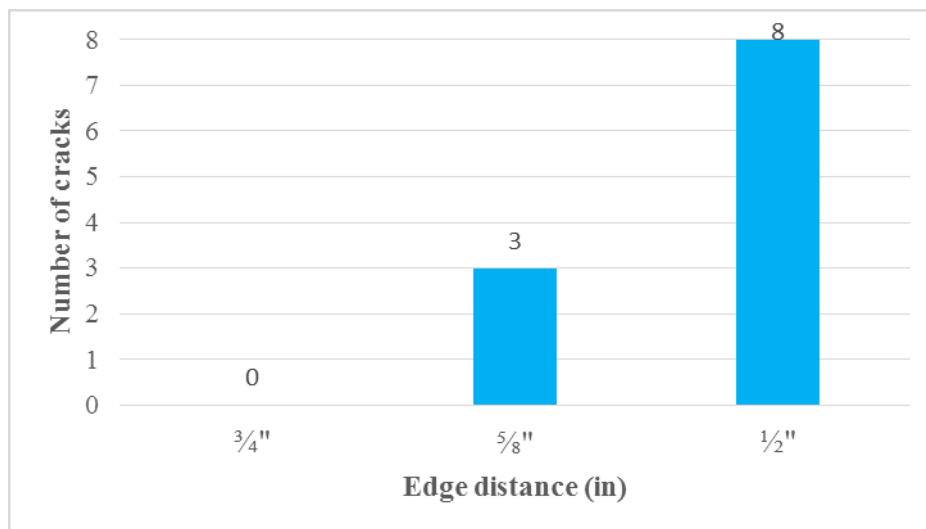


Figure 10-216: Mix#2, 6000 psi, WQ-Number of Cracks

Mix#3-WB wire type

WB-Release Strength 4500 psi

WB wire performed poorly resulting eight cracks on each prism. Figure 10-217 and Figure 10-218 show the marked cracks on each side of the prism, live end and dead end. The maximum crack width on the live end of the prism with a $\frac{3}{4}$ in. edge distance was 0.05 in. and the maximum crack length was 32 in. On the other side, maximum crack width was 0.04 in. and maximum crack length was 27 in. Spalling was observed on the dead end of the prism with $\frac{5}{8}$ in. edge distance in the maximum length of 10 in. On the live end maximum crack width was 0.020 in. and the maximum crack length was 23 in. Spalling was observed on the live end on the prism with a $\frac{1}{2}$ in. edge distance in the maximum length of 2 in. Maximum crack width on the dead end of the prism with $\frac{1}{2}$ in. cover was 0.06 in. and the maximum crack length was 48 in.

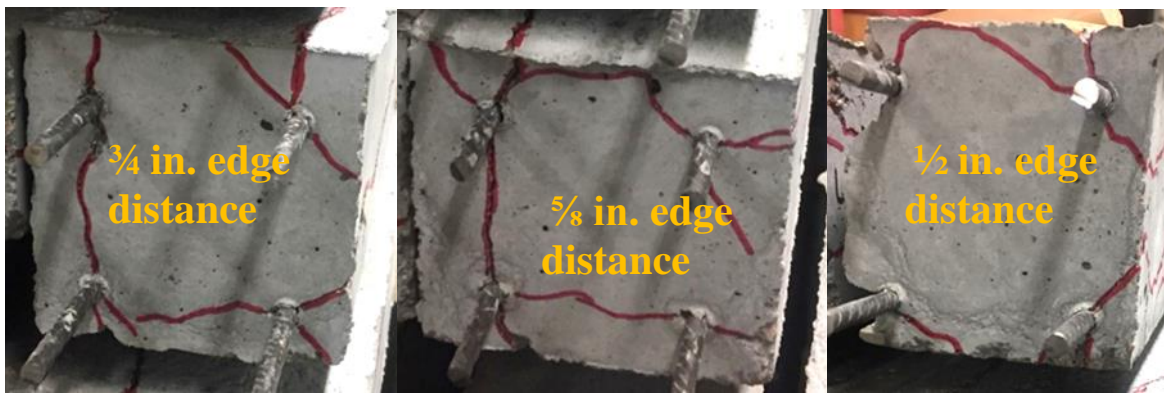


Figure 10-217: Mix#3, 4500 psi, WB-Observed Cracking (Live End)

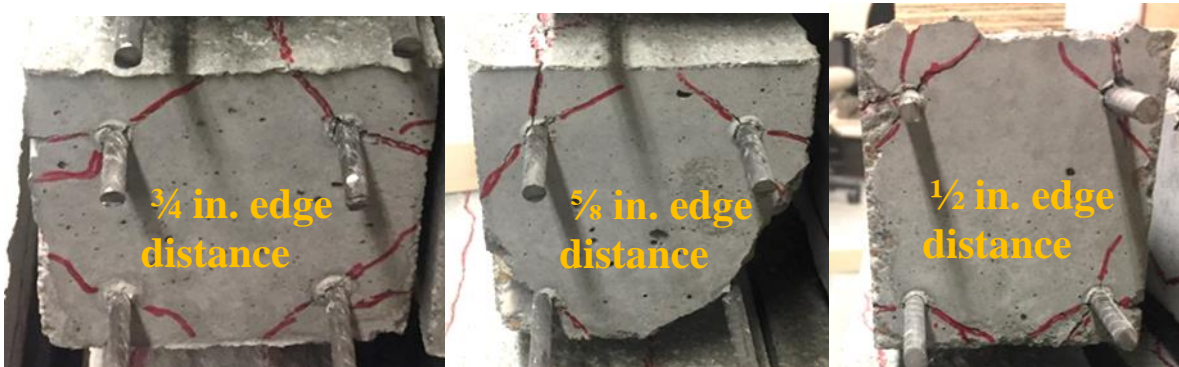


Figure 10-218: Mix#3, 4500 psi, WB-Observed Cracking (Dead End)

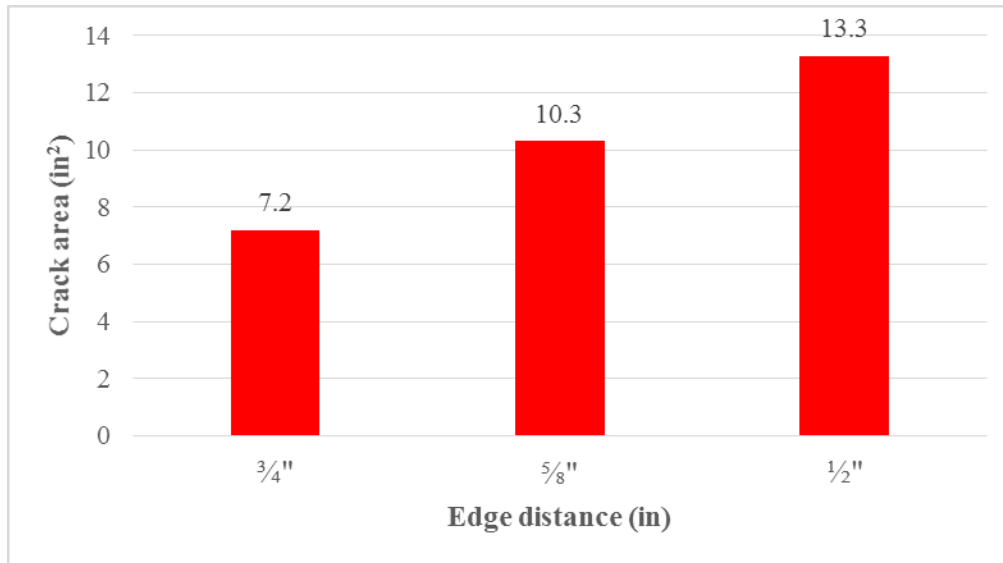


Figure 10-219: Mix#3, 4500 psi, WB-Crack Area (in²)

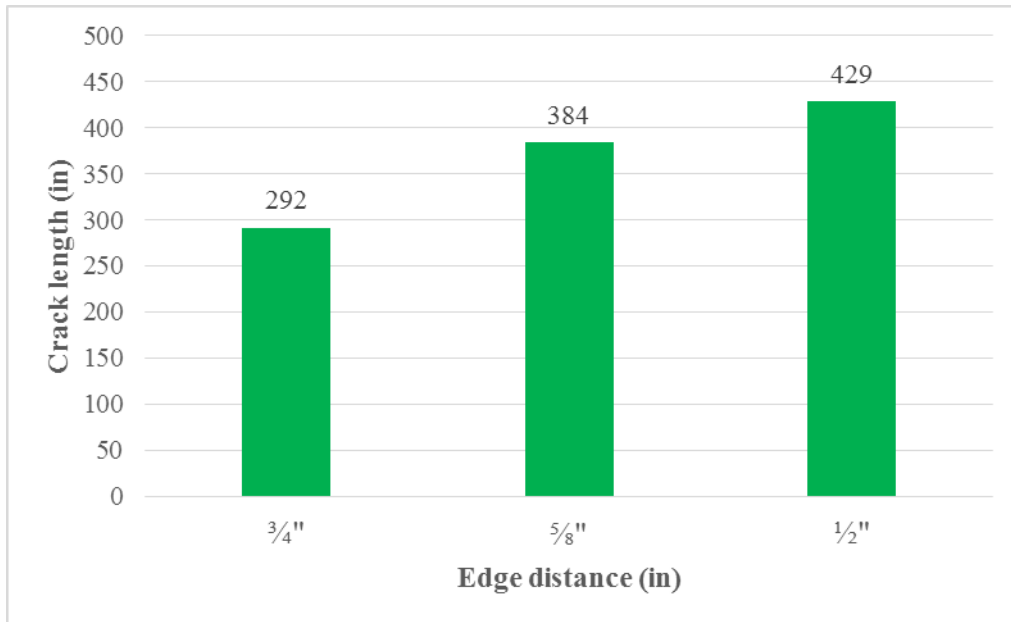


Figure 10-220: Mix#3, 4500 psi, WB-Crack Length (in)

Even though spalling which occurred on the prism with a $\frac{5}{8}$ in. edge distance had larger length than prism with $\frac{1}{2}$ in. the edge distance, the overall crack area was bigger for the prism with a $\frac{1}{2}$ in. the edge distance. The crack length was also larger on the prism with $\frac{1}{2}$ in. edge distance. This wire performed poorly with all three thicknesses, but with reducing the cover more damage appeared. Figure 10-219, Figure 10-220, and Figure 10-221 show crack area, crack length and number of cracks as a function of edge distance, respectively.

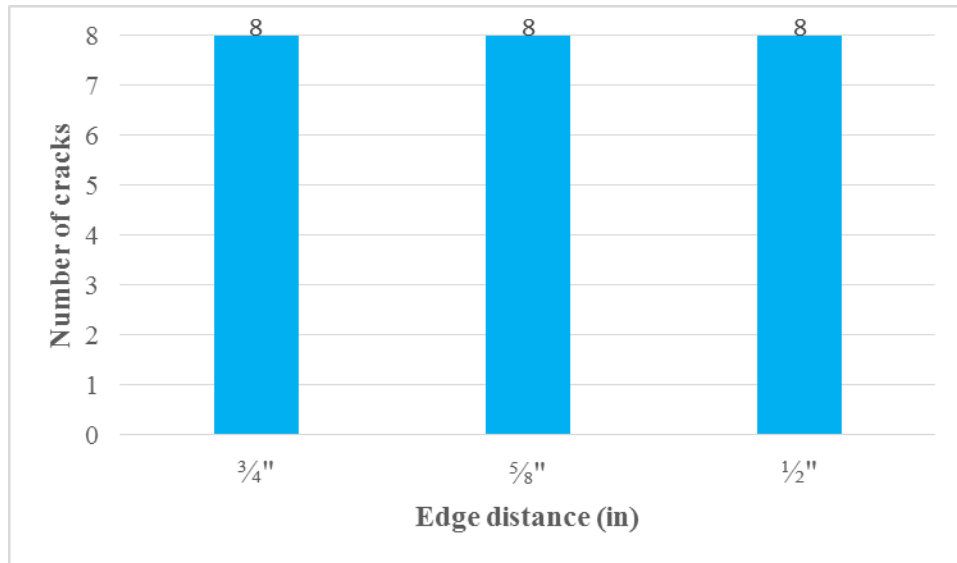


Figure 10-221: Mix#3, 4500 psi, WB-Number of Cracks

Mix#3-WF wire type

WF-Release Strength 4500 psi

WF type wire with this type of concrete mixture performed poorly with a crack appearance in every prism. On the prism with $\frac{3}{4}$ in. edge distance spalling was observed in the length of 7 in. on the live end. The maximum crack width on the dead end was 0.04 in. and the maximum crack length was 21 in. The second prism in series exhibited poor behavior with spalling on the live end, in the length of 4 in. and 36 in. on the dead end. The maximum crack area on the second prism was 18.9 in² as shown in Figure 10-224. The third prism with $\frac{1}{2}$ in. edge distance had spalling on the live end in the maximum length of 29 in. and 21 in. on the dead end. The maximum crack area was 28.8 in² as shown in Figure 10-224.

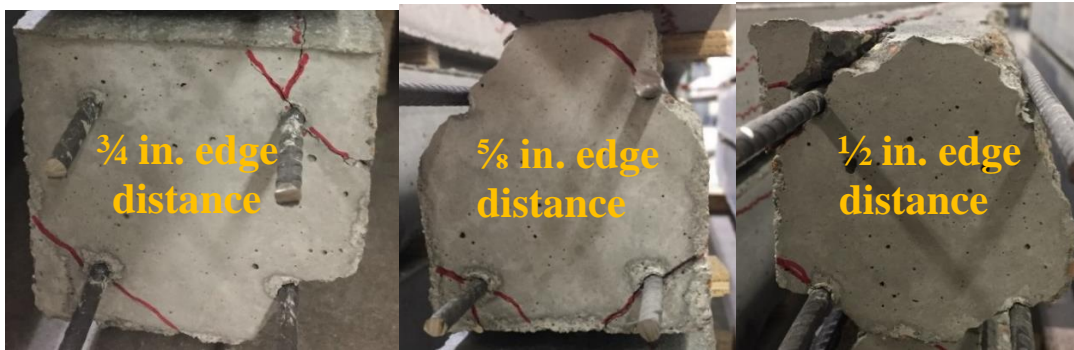


Figure 10-222: Mix#3, 4500 psi, WF-Observed Cracking (Dead End)

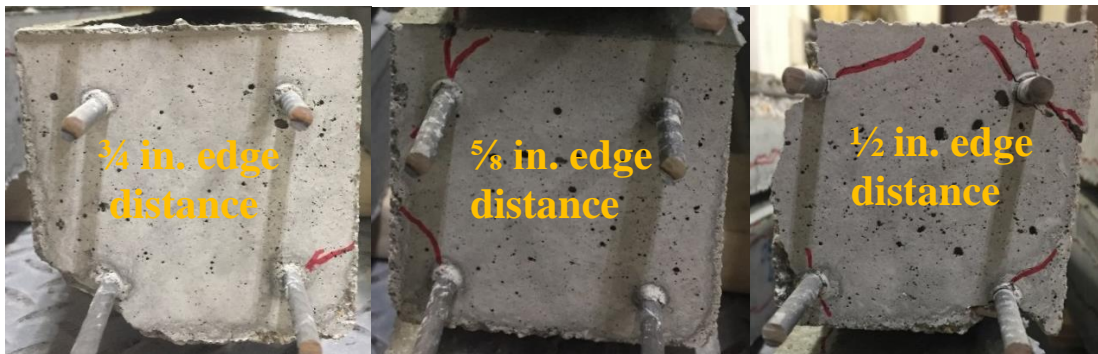


Figure 10-223: Mix#3, 4500 psi, WF-Observed Cracking (Live End)

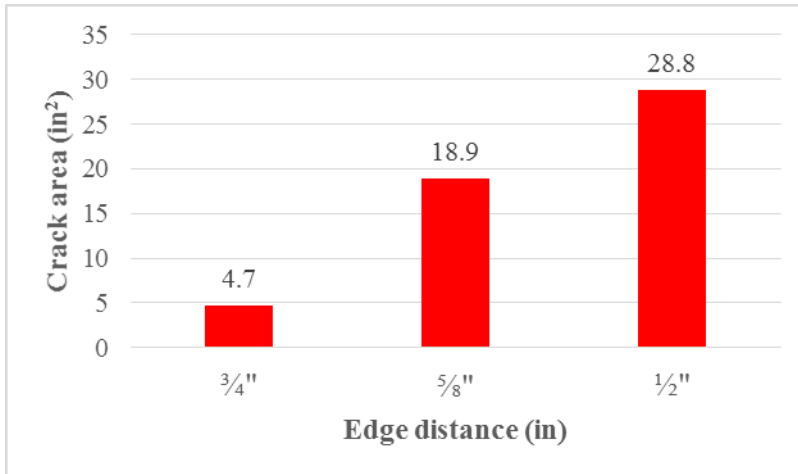


Figure 10-224: Mix#3, 4500 psi, WF-Crack Area (in²)

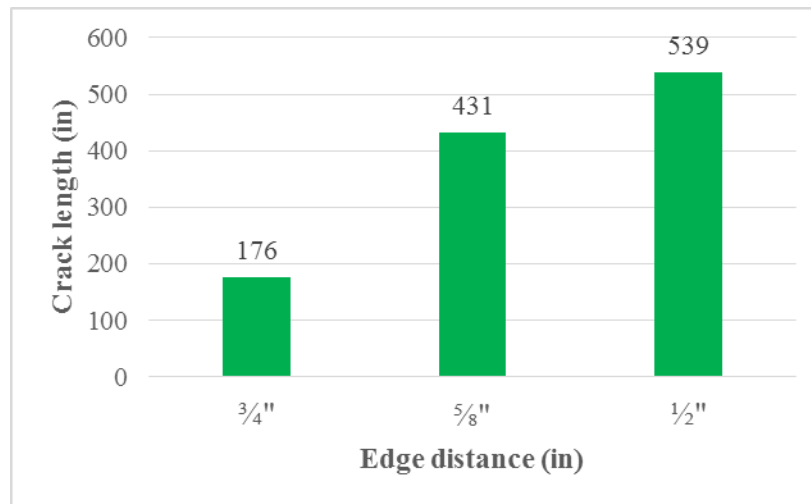


Figure 10-225: Mix#3, 4500 psi, WF-Crack Length (in)

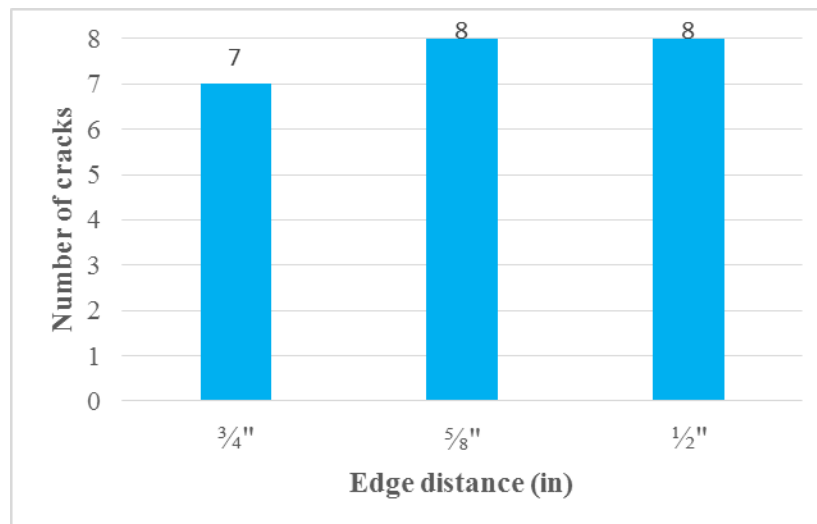


Figure 10-226: Mix#3, 4500 psi, WF-Number of Cracks

According to Figure 10-225 and Figure 10-226 it was noticeable that WF type wire exhibited critical behavior with this type of mixture using locally available pea gravel (uncrushed) aggregate. WF wire belongs to deep chevron type of wire and according to all these results mentioned above, existing spalling indicated that bond between steel and concrete was completely destroyed.

Mix#3-WI wire type

WI-Release Strength 4500 psi

Figure 10-227 and Figure 10-228 show the position of the cracks on the dead end and live end of the prism. Prism with a $\frac{3}{4}$ in. edge distance on the live end had no visible cracks on the surface. Spalling in the length of 2 in. was observed on the dead end and one crack with a width of 0.01 in. and the total length of 5 in. The second prism in series had two cracks on the live end with crack width of 0.01 in. and maximum crack length of 5 in. On the dead end two cracks were detected with maximum crack width of 0.016 in. and maximum crack length of 5 in. The third prism in series exhibited poor performance with spalling in the maximum length of 7 in. on the live end and spalling on the dead end in the length of 3 in.

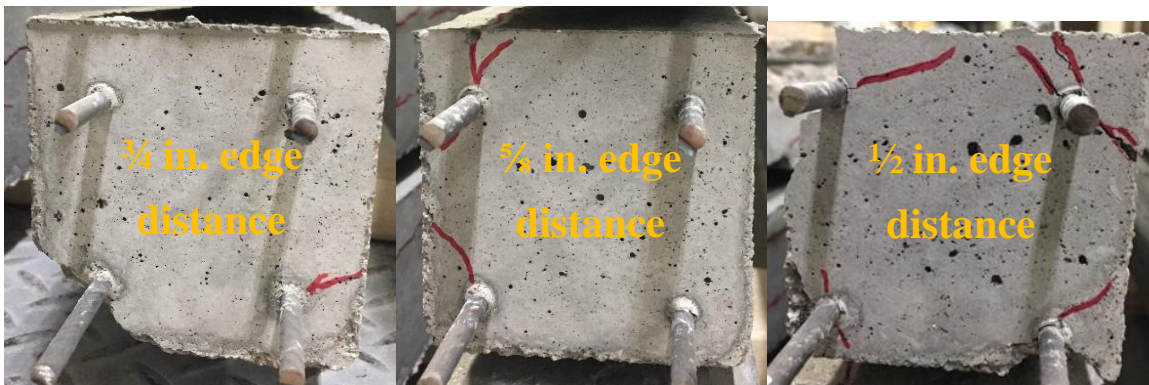


Figure 10-227: Mix#3, 4500 psi, WI-Observed Cracking (Dead End)



Figure 10-228: Mix#3, 4500 psi, WI-Observed Cracking (Live End)

According to Figure 10-229, Figure 10-230, and Figure 10-231 it was observed that with reducing cover the values of crack areas, crack length and number of cracks increased.

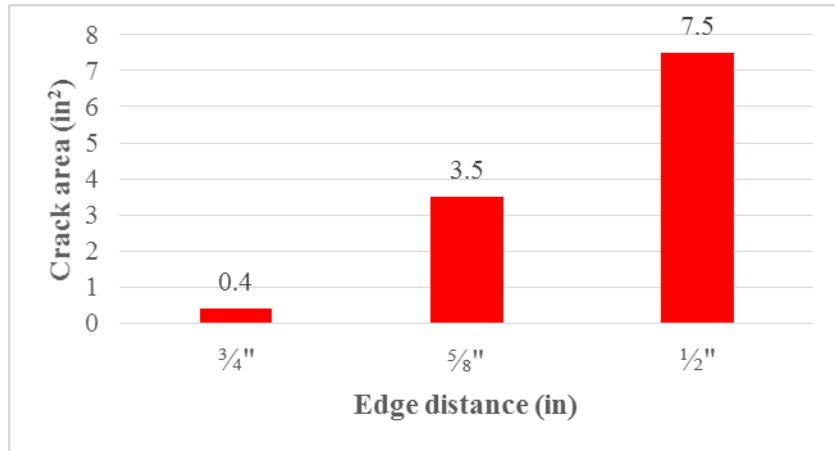


Figure 10-229: Mix#3, 4500 psi, WI-Crack Area (in²)

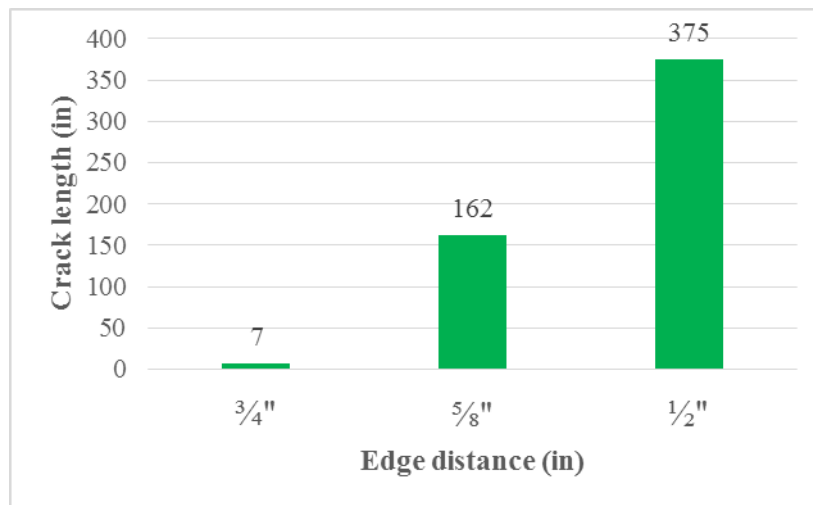


Figure 10-230: Mix#3, 4500 psi, WI-Crack Length (in)

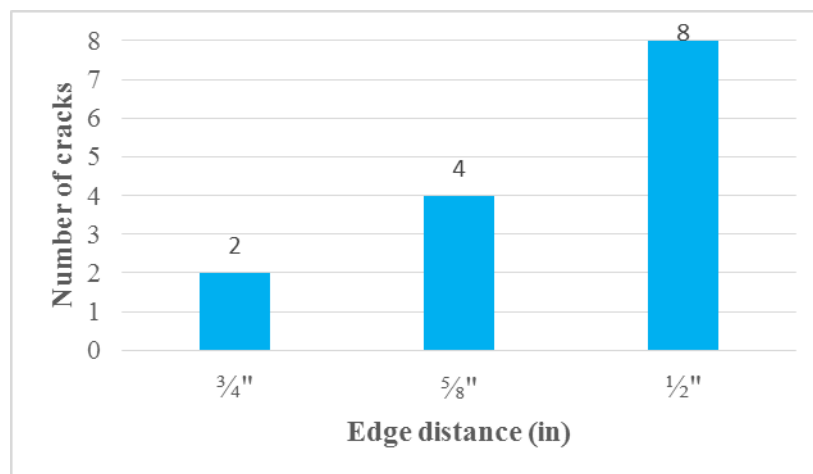


Figure 10-231: Mix#3, 4500 psi, WI-Number of Cracks

Mix#3-WJ wire type

WJ-Release Strength 4500 psi

WJ wire with the third type of mixture performed poorly in resulting seven cracks on the prism with $\frac{3}{4}$ in edge distance, eight cracks on $\frac{5}{8}$ in. and eight cracks on the $\frac{1}{2}$ in. the edge distance as shown in Figure 10-232, Figure 10-233, and Figure 10-236. Concrete mixture using uncrushed local aggregate provided poor results with seven cracks on the prism having $\frac{3}{4}$ in. edge distance and eight on the second and third prism in series.

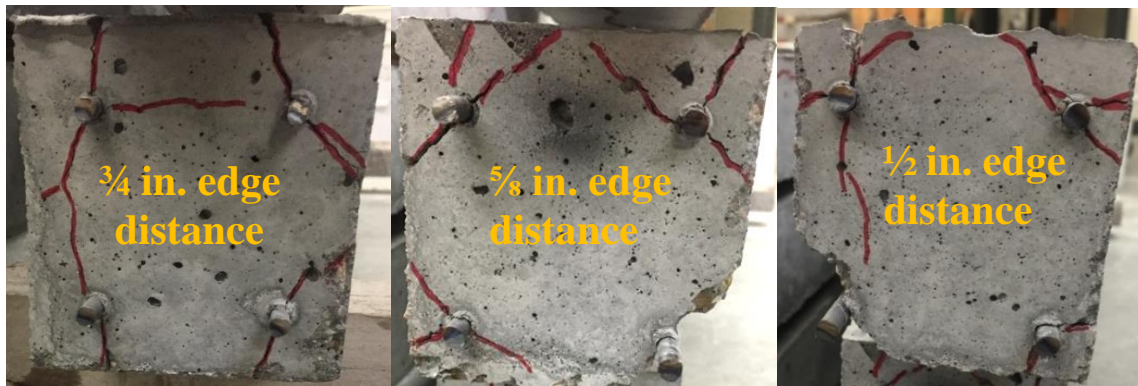


Figure 10-232: Mix#3, 4500 psi, WJ-Observed Cracking (Live End)

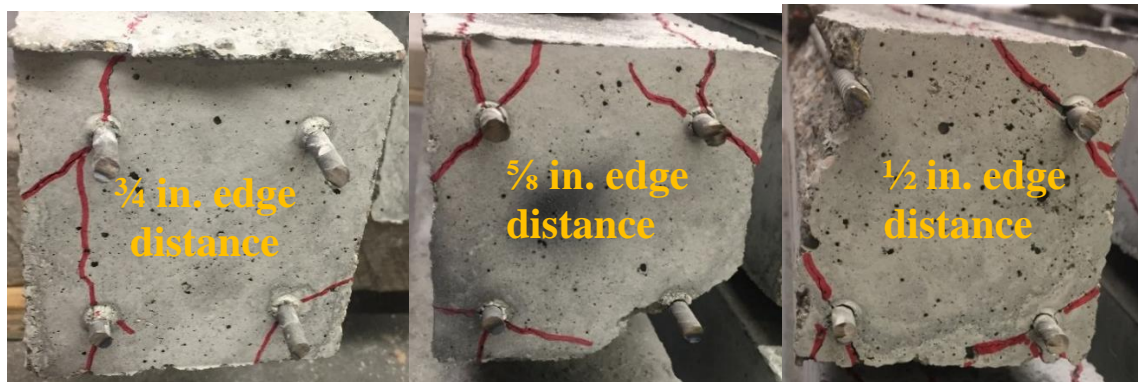


Figure 10-233: Mix#3, 4500 psi, WJ-Observed Cracking (Dead End)

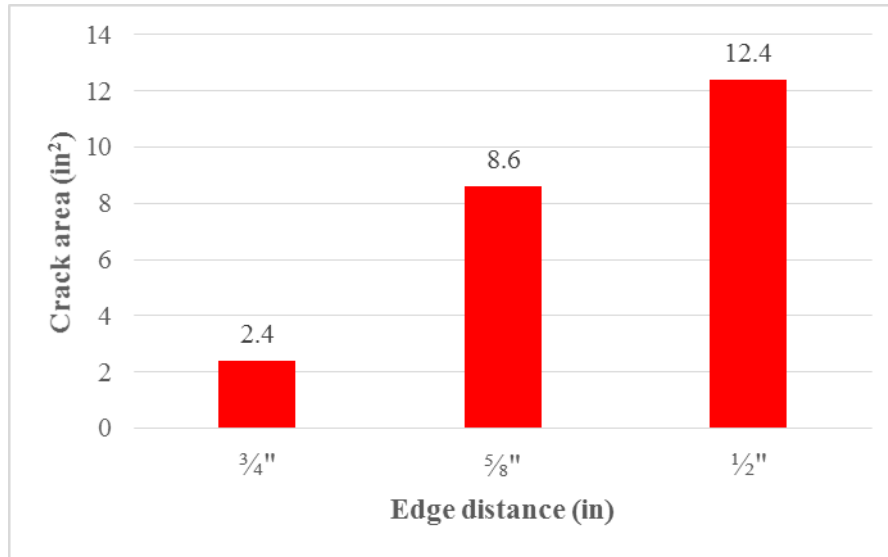


Figure 10-234: Mix#3, 4500 psi, WJ-Crack Area (in²)

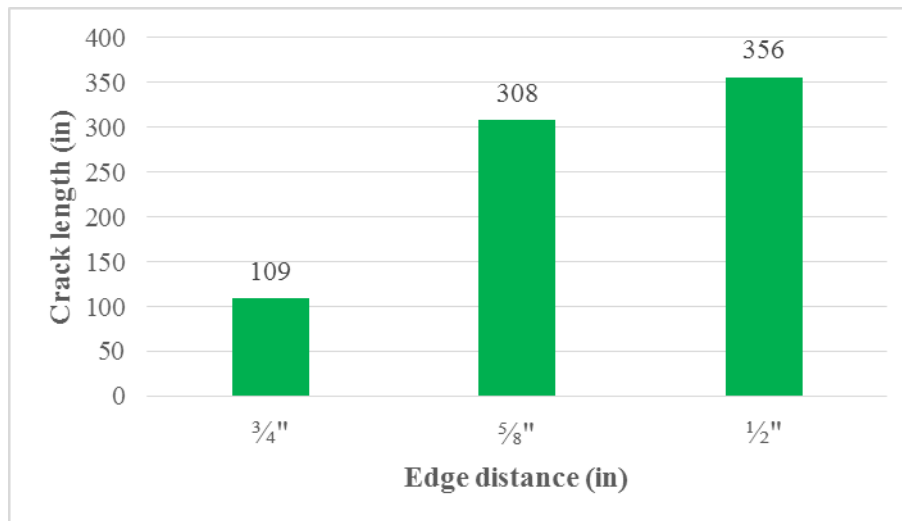


Figure 10-235: Mix#3, 4500 psi, WJ-Crack Length (in)

Prism with a $\frac{3}{4}$ in. edge distance had seven cracks, with three cracks on the live end and four cracks on the dead end. The maximum crack width was 0.04 in. and the maximum crack length was 12 in. The second prism in the series had eight cracks. Spalling occurred on both the sides of the prism, on the live end in the length of 5 in and on the dead end in the length of 6 in. Prism with a $\frac{1}{2}$ in. edge distance had more damage with spalling on the live end in the length of 10 in. and on the dead end in the length of 6 in. Figure 10-234, Figure 10-235, and Figure 10-236 show crack area, crack length and number of cracks as a function of edge distance, respectively.

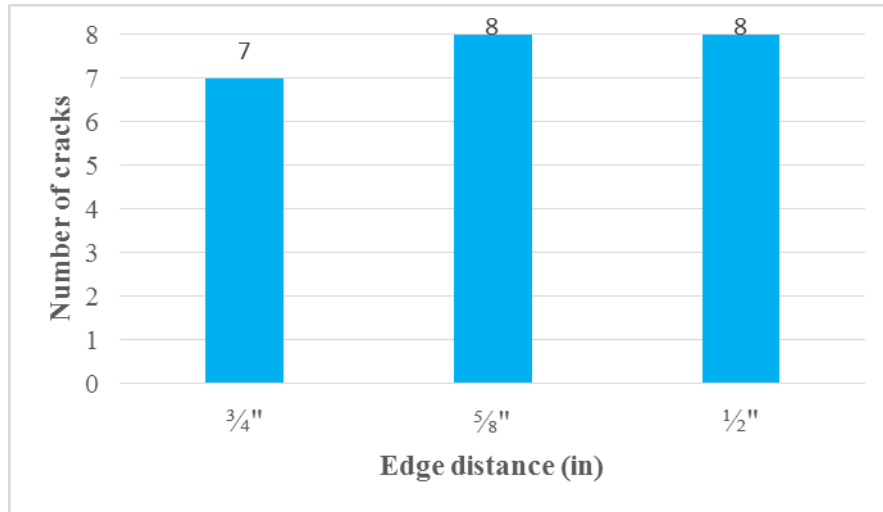


Figure 10-236: Mix#3, 4500 psi, WJ-Number of Cracks

Mix#3-WM wire type

WM-Release Strength 4500 psi

WM wire with a mixture which included local uncrushed aggregate (pea gravel) performed worse than mixture with crushed aggregate (Tucson aggregate) and Granite. Figure 10-237 shows the longitudinal strain profiles along with the values of transfer lengths.

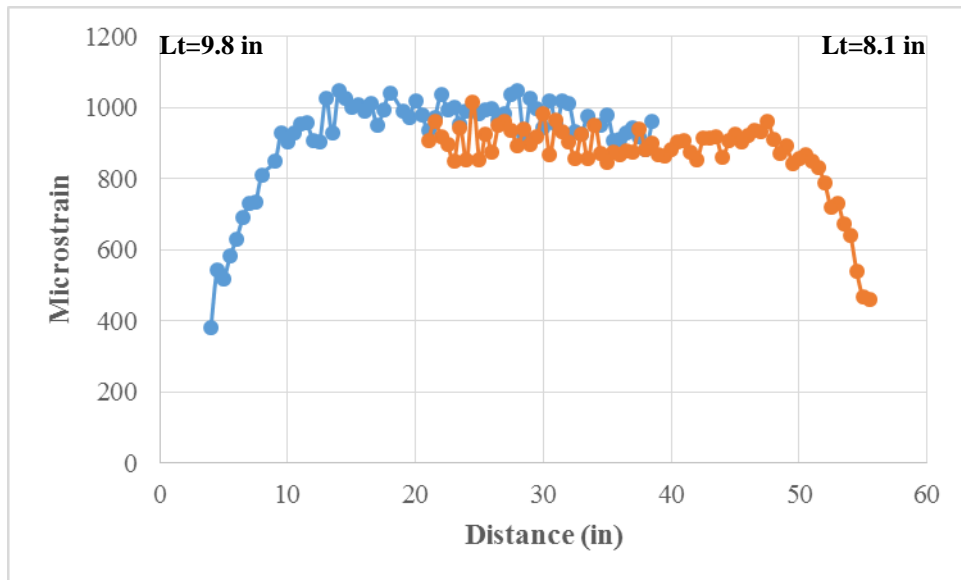


Figure 10-237: Mix#3, 4500 psi, WM, $\frac{3}{4}$ in. Edge distance- Longitudinal Strain Profile

Figure 10-238 and Figure 10-239 show observed cracking on the dead and live end of the prisms. Two cracks appeared on the prism with a $\frac{3}{4}$ in. the edge distance on the live end with average width of 0.012 in. and maximum crack length of 9 in. Prism with a $\frac{5}{8}$ in. edge distance had four cracks on each side of the prism. Spalling in the length of 2 in. appeared on the dead end. Prism with a $\frac{1}{2}$ in. edge distance performed poorly with spalling on both sides of the prism. Spalling appeared in the length of 14 in. on the live end and 6 in. on the dead end.



Figure 10-238: Mix#3, 4500 psi, WM-Observed Cracking (Live End)

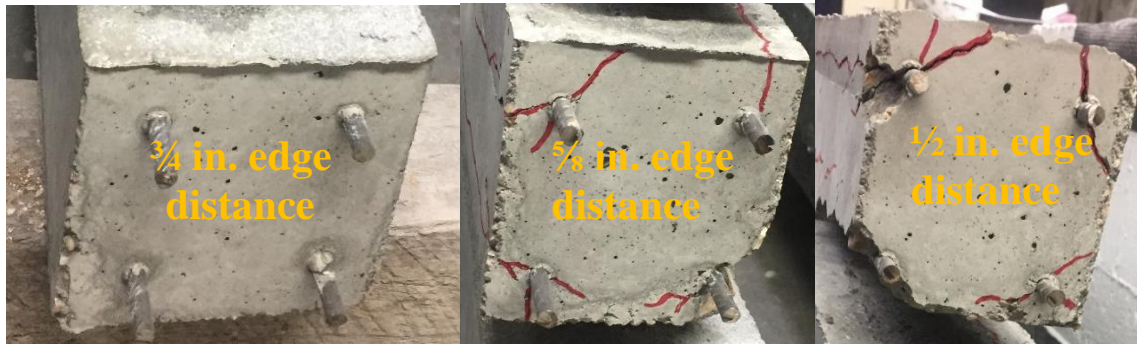


Figure 10-239: Mix#3, 4500 psi, WM-Observed Cracking (Dead End)

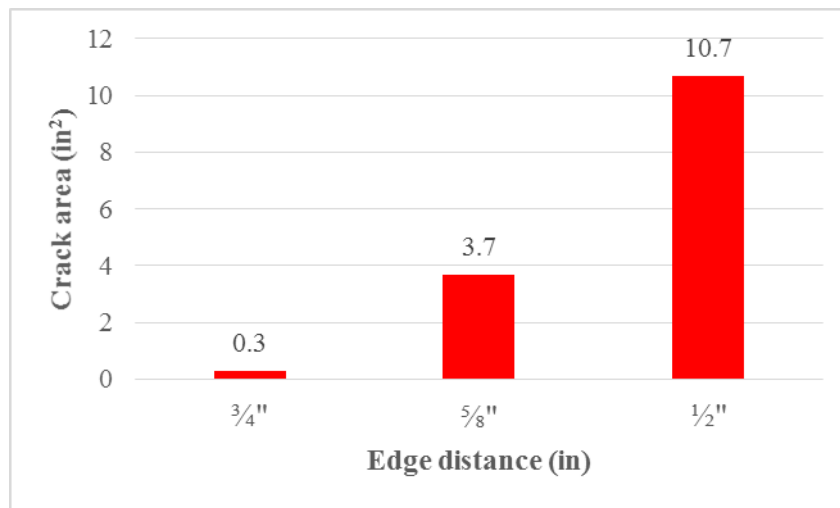


Figure 10-240: Mix#3, 4500 psi, WM-Crack Area (in²)

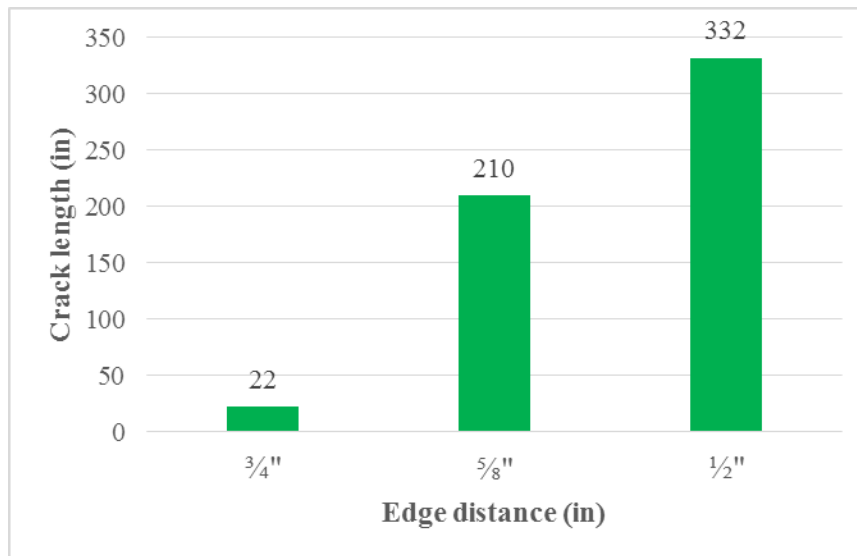


Figure 10-241: Mix#3, 4500 psi, WM-Crack Length

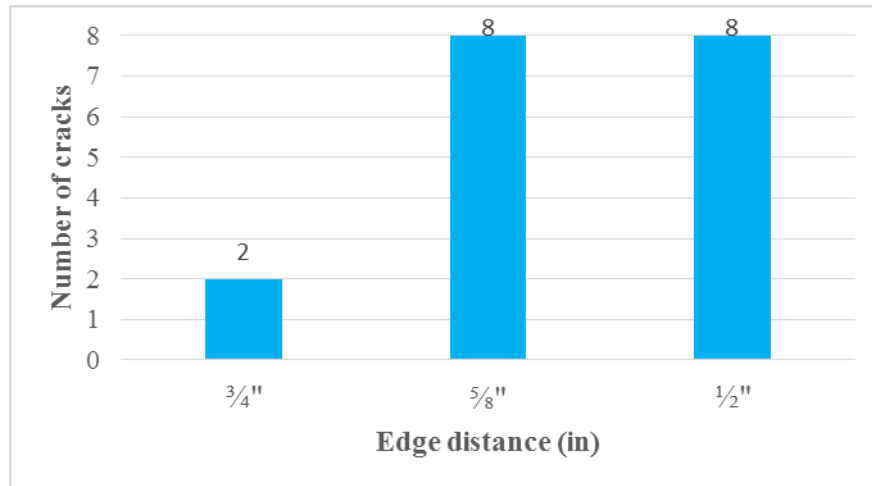


Figure 10-242: Mix#3, 4500 psi, WM- Number of Cracks

The crack area indicated that cracks appeared on all three prisms, and in comparison, with a mixture which was done with crushed gravel aggregate (Tucson aggregate) and granite aggregate the values of the crack areas were higher as shown in Figure 10-240.

Figure 10-240, Figure 10-241, and Figure 10-242 show crack area, crack length and number of cracks as a function of edge distance, respectively.

Mix#3-WP wire type

WP-Release Strength 4500 psi

Figure 10-243 and Figure 10-244 show the position of the cracks on each side of the prism live end and dead end. Prism with $\frac{3}{4}$ in. edge distance had one crack with the width of 0.01 in. and maximum crack length of 5 in. on the live end. On the other side of the prism four more cracks appeared and maximum crack width was 0.02 in. with maximum crack length 16 in. Spalling was observed on the prism with $\frac{5}{8}$ in. edge distance, on the live end spalling occurred in the maximum length of 16.0 in. On the dead-end spalling occurred in the length of 2 in. Spalling was indicated on the prism with $\frac{1}{2}$ in. edge distance in the length of 2 in. on the live end and maximum length of spalling 3 in. on the dead end.



Figure 10-243: Mix#3, 4500 psi, WP-Observed Cracking (Live End)



Figure 10-244: Mix#3, 4500 psi, WP-Observed Cracking (Dead End)

Figure 10-245, Figure 10-246, and Figure 10-247 show crack area, crack length and number of cracks as a function of edge distance, respectively.

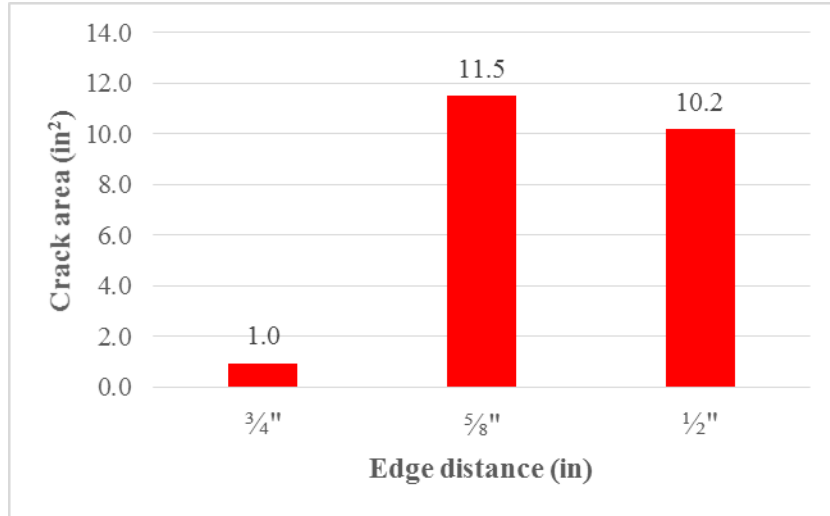


Figure 10-245: Mix#3, 4500 psi, WP-Crack Area (in²)

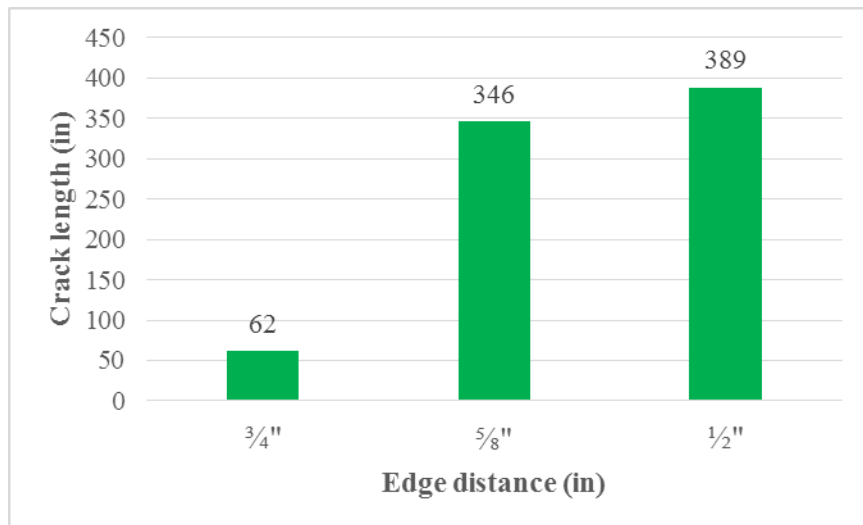


Figure 10-246: Mix#3, 4500 psi, WP-Crack Length (in)

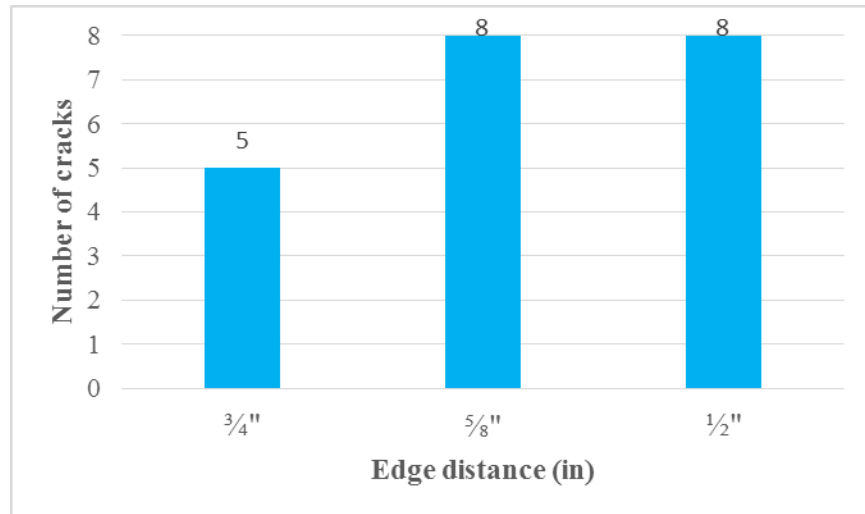


Figure 10-247: Mix#3, 4500 psi, WP-Number of Cracks

Mix#3-WQ wire type

WQ-Release Strength 4500 psi

WQ wire with this type of mixture performed very well, in resulting no cracking appearance for prisms with $\frac{3}{4}$ in. and $\frac{5}{8}$ in. edge distances, and eight cracks on the prism with a $\frac{1}{2}$ in. the edge distance as shown in Figure 10-254. The average values of transfer lengths for the first and second prism were 9.6 in. and 8.8 in. respectively (Figure 10-248 and Figure 10-249).

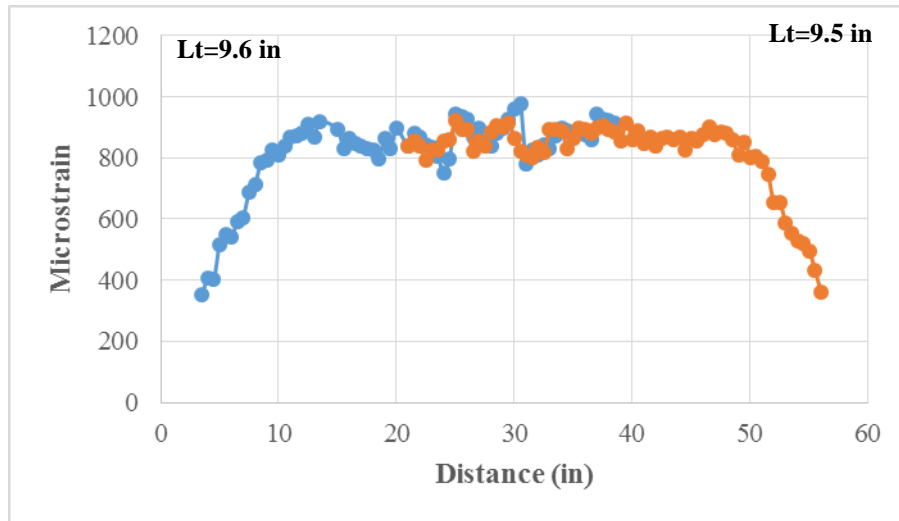


Figure 10-248: Mix#3, 4500 psi, WQ, $\frac{3}{4}$ in. Edge Distance-Longitudinal Strain Profile

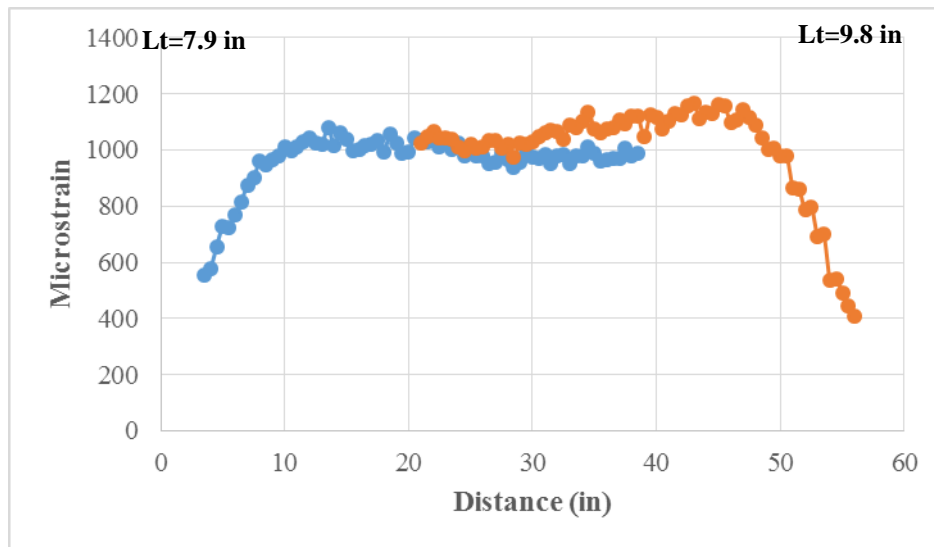


Figure 10-249: Mix#3, 4500 psi, WQ, $\frac{5}{8}$ in. Edge Distance-Longitudinal Strain Profile



Figure 10-250: Mix#3, 4500 psi, WQ-Observed Cracking (Live End)

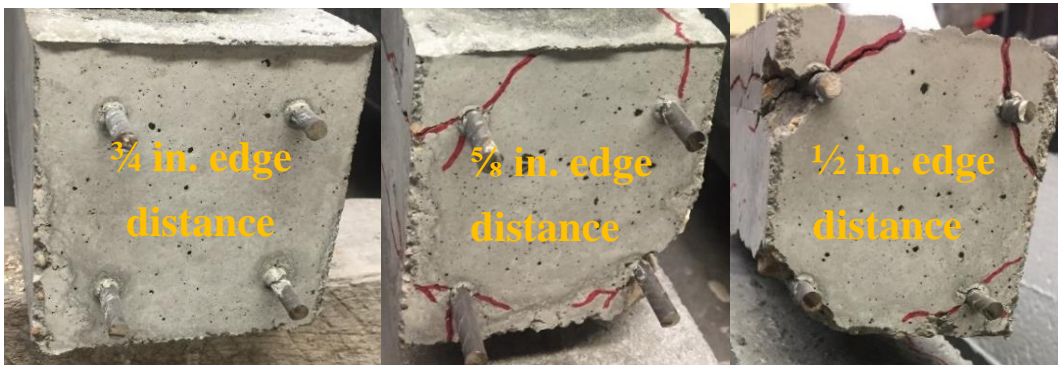


Figure 10-251: Mix#3, 4500 psi, WQ-Observed Cracking (Dead End)

Figure 10-250 and Figure 10-251 present observed cracking for each prism. It is clear that WQ wire performed very well with this type of mixture and results no crack appearance on the prism with $\frac{3}{4}$ in. edge distance. Prism having $\frac{5}{8}$ in. edge distance had one crack on the live end of the prism and spalling on the dead end with the length of 2 in.

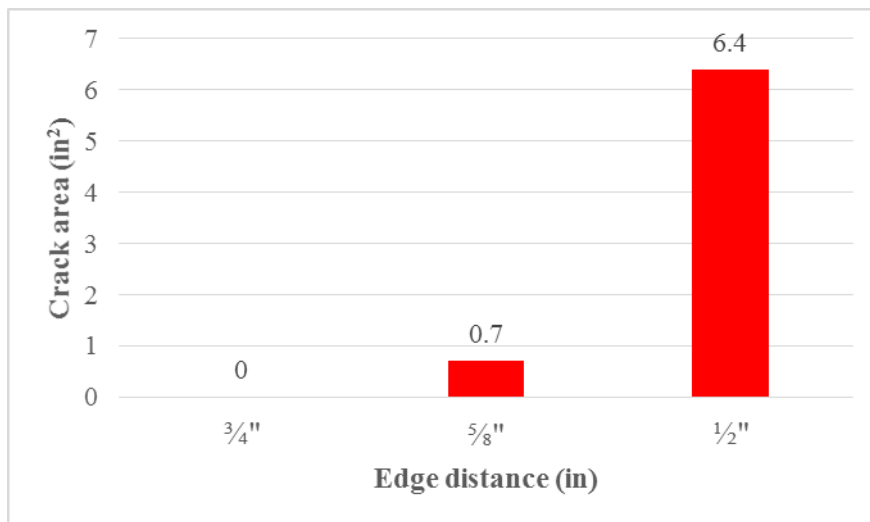


Figure 10-252: Mix#3, 4500 psi, WQ-Crack Area (in²)

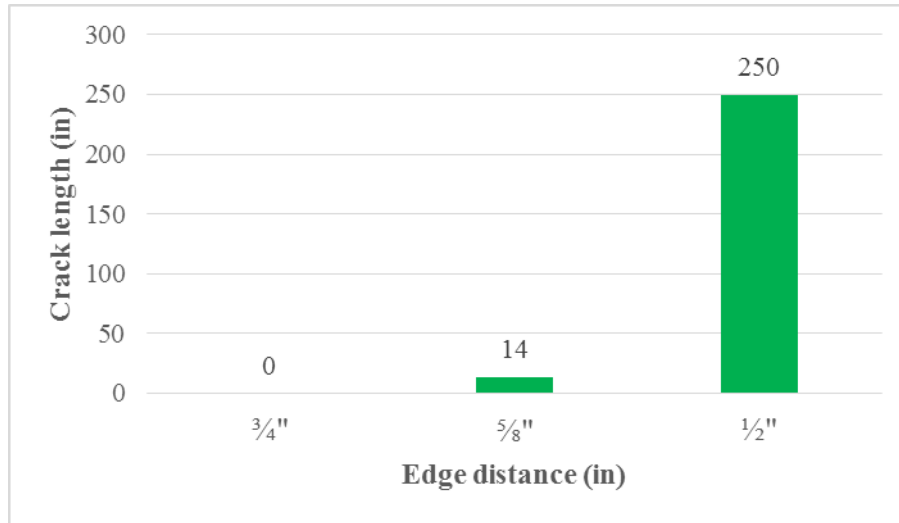


Figure 10-253: Mix#3, 4500 psi, WQ-Crack Length

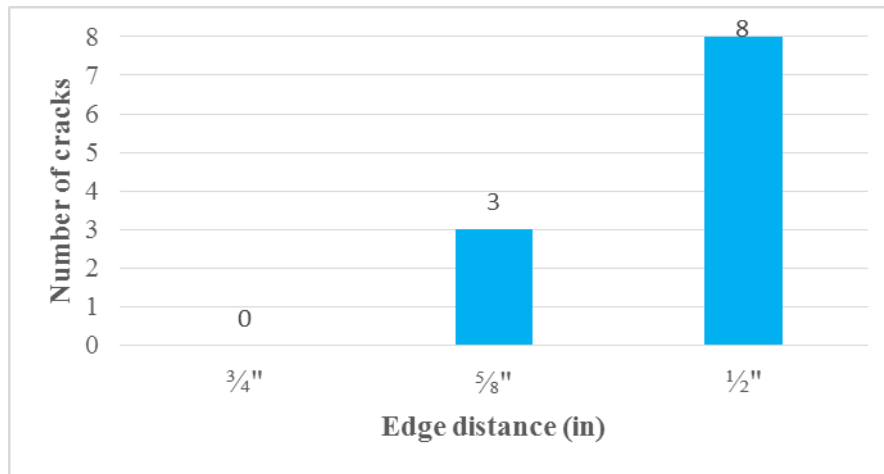


Figure 10-254: Mix#3, 4500 psi, WQ-Number of Cracks

Crack area for the prism having $\frac{5}{8}$ in. edge distance was 0.7 in^2 and 6.4 in^2 for prism having $\frac{1}{2}$ in. edge distance as shown in Figure 10-252. According to these results WQ wire using uncrushed gravel aggregate performed better than mixture having crushed gravel-Tucson aggregate. Spalling in the maximum length of 3 in. was observed on the third prism in series. On the live end of the prism having $\frac{1}{2}$ in. edge distance, maximum crack width was 0.02 in. and the maximum crack length was 26 in. Figure 10-253 shows crack length as a function of edge distance.